Georgia Tech

THE GEORGE W. WOODRUFF SCHOOL OF
MECHANICAL ENGINEERING

Georgia Institute of Technology
Atlanta, Georgia 30332-0405

ME 4182

Mechanical Design Engineering

NASA/UNIVERSITY

ADVANCED DESIGN PROGRAM

LUNAR DEEP DRILL APPARATUS

June 1989

Jill Harvey, Editor

Professor: Mr. J. W. Brazell

FOREWORD

This report represents the combined effort of 49 students from the Georgia Institute of Technology's School of Mechanical Engineering Senior Design class. Although this report describes a conceptual design, it serves two purposes. First it serves to teach the design process. Second, it provides NASA with a general conceptual design of a Lunar Drilling Apparatus capable of many drilling and sampling tasks.

The students of ME 4182 were organized into nine groups of five and one group of four. Each group was given a part of the Lunar Drilling Apparatus to design as best they could in a period of eight weeks. Each group met with Professor Brazell once a week for advisement and accountability. Four weeks into the project, each group made an oral presentation of their progress and built a quarter-scale model. This report served as a source of communication between the groups. Students were required to provide weekly written progress reports with graphics to serve as communication between the groups.

Students were encouraged to use any resources available to them, including, but not limited to vendors, the Georgia Tech library, handbooks, imagination, and similar terrestrial designs. Databases, NASA documents, and long distance phone service were made available as well.

The Lunar Drilling Apparatus (LDA) is a part of a larger design for a previously designed three-legged lunar rover named "SKITTER". SKITTER should be able operate from a lunar base and be commanded from the earth. It will go from the base to given locations to drill holes for samples and other scientific and engineering purposes.

The design itself is conceptual and should be checked for engineering credibility. Experimental testing and detailed analysis should be completed before this design could be considered functional. Students' time was limited by the overall time frame of the project and other class requirements.

CONTRIBUTORS

Agin, Arthur Harlan	Section 4.2
Avery, Robert Eugene	Section 4.8
Black, Angela Michelle	Section 4.2
Blair, Dwight Nelson	Section 4.5
Blam, Thomas Franz Alfred	Section 4.10
Bourcier, Mark Allen	Section 4.3
Bowden, Allen Kenneth	Section 4.5
Bridges, Timothy Scott	Section 4.5
Bruzzano, Marco Anthony	Section 4.10
Collins, Robert Jackson	Section 4.4
Cooper, Jeffrey Allan	Section 4.6
Donahue, David Philip	Section 4.7
Dyer, John Francis	Section 4.6
Fortson, Reginald Darnell	Section 4.10
Gargour, Farid Gilbert	Section 4.1
Halferty, John Peter	Section 4.6
Harper, Ronald James	Section 4.8
Headley, Frank Anthony, Jr.	Section 4.7
Hurst, Mark Edward	Section 4.6
Hutto, James Douglass	Section 4.7
Jennings, Scott Patrick	Section 4.3
Kennedy, John Douglas	Section 4.4
Kinney, Jody Tilmon	Section 4.8
Klima, Gerald Gregory, Jr.	Section 4.4
Kuster, James Robert	Section 4.1
Marsh, William Hill	Section 4.10
Martin, James Stephen	Section 4.2
McBrayer, Michael Sean	Section 4.7
McDaniels, Robert Dale	Section 4.9
McGinn, Patrick Laun	Section 4.9
Miller, Scott Edward	Section 4.8
Moy, Jennifer Ann	Section 4.7
Murphy, Christopher Browning	Section 4.1
Powell, Barry Edward	Section 4.10
Ridlehoover, Kathryn Elizabeth	Section 4.6
Rosario-Cuevas, Edward	Section 4.2
Rush, Phillip Joseph	Section 4.1
Saxon, Gregory Bruce	Section 4.9
Seckinger, Cheryl Ann	Section 4.3
Sheiner, Jeffrey Stuart	Section 4.3
Sherrard, Roger Scott	Section 4.9
Sobel, Bradley Paul	Section 4.4
Stelzenmuller, Gregory Brennan	Section 4.9
Stewart, Chilton Taylor	Section 4.3
Waldee, Timothy L	Section 4.5
Wielbruda, Richard Frank	Section 4.5
Williams, Margaret Crecelius	Section 4.4
Willingham, James Thomas, Jr.	Section 4.1
Wolfe, Charles Vincent	Section 4.8

LIST OF FIGURES

LIST OF TABLES

LIST OF ABBREVIATIONS

a	coefficient of thermal expansion
A	area
AISI	American Institute of Steel and Iron
Al	aluminum
amp	ampere
BTU	British Thermal Unit
C (deg)	Celsius
CCW	counter clockwise
cm	centimeter
CRS	Cutting Removal System
CSM	Curvo-Synchronous Motor
CW	clockwise
D,d	diameter
deg	degree(s)
e	ductility
E	Young's modulus
F	force
F (deg)	Fahrenheit
FH	fence height
FT	number of fences per turn
ft	foot
g	gram
g	acceleration due to gravity
G	Giga (10^9)
h	height
Hp	horsepower
I	moment of inertia
in	inch
J	angular moment of inertia
kg	kilogram
kW	kilowatt
L,l	length

λ	wavelength
lb	pound
LDA	Lunar Drill Apparatus
LDDA	Lunar Deep Drill Apparatus
m	meter
M	Mega (10^6)
μ	viscosity
max	maximum
MCR	Macro Core Retrieval
MIRS	Motor Interface Rod Section
mm	millimeter
MMC	Metal Matrix Composite
MMI	Magnetic Motor Interface
n	efficiency
N	Newton
NASA	National Aeronautics and Space Administration
NiCad	Nickel Cadmium
P	pitch
π	pi (3.14159...)
PLC	Programmable Logic Controller
PTS	Power Transfer System
q	heat transfer
ρ	density
R,r	radius
RAM	Random Access Memory
RIM	Rod Interface Mechanism
RPM,rpm	revolutions per minute
σ_y	yield strength
σ_{ut}	ultimate tensile strength
SAE	Society of Automotive Engineers
sec	second
SKITTER	Spatial Kinematic Inertial Translatory Tripod Extremity Robot
Sn	tin
STD	standard
T	temperature

Ti	titanium
v	velocity
V	volts
VRA	Vertically Reciprocating Auger
w	width
W	Watt
ω	radial frequency
wt	weight

1.0 EXECUTIVE SUMMARY

The scope of this project is to design a self contained, mobile drilling and coring system to operate on the Lunar surface and be controlled remotely from earth. The system will use SKITTER as its foundation and produce Lunar core samples two meters long and fifty millimeters in diameter.

The drill bit used for this is composed of 30 per carat diamonds in a sintered tungsten carbide matrix. The bit assembly is 2 m long. Because high temperatures will accelerate bit wear and 70% of the heat generated from drilling will be held in the cuttings, a stepped auger will be used to bring the chips away from the bit and up out of the hole. The auger will be accelerated vertically upward by a cam-follower mechanism which will convert the rotational motion of the rotary drive into a vertically reciprocating motion.

To drill up to 50 m depths, the bit assembly will be attached to a drill string made from 2 m rods which will be carried in racks on SKITTER. The rods will be retrieved by a mechanical arm system which will place them into the drill string. This mechanical arm system allows two degrees of freedom: rotational and rotary movement. The drive will be detached during rod addition of removal, so the footplate will be used to support the drill string at these times. This device is stored in the drive via an adaptor and is placed onto the Lunar surface at the drill site first. Its support mechanism consists of an aluminum lithium spring locking device similar to an automotive speed washer. The spring is deflected by a battery powered motor to open it during drilling.

Rotary power for drilling will be supplied by a Curvo - Synchronous motor. This motor has only one moving part, can operate at temperatures up to 350 F , and is 92% efficient. The motor will be powered by a hydrogen oxygen fuel cell which has an output

of 2 to 12 kilowatts. Heat generated by the motor will be transferred to a thermal radiator oriented towards deep space through a system of three heat pipes.

SKITTER is to support this system through a hexagonal shaped structure which will contain the drill motor and the power supply. This structure will be made from silicon carbide aluminum and it will attach to SKITTER with three actuator latches.

A micro-coring drill will be used to remove a preliminary sample 5 mm in diameter and 20 mm long from the side of the core. This drill utilizes one motor for rotational movement and one for vertical translation. Finally, after all drilling, the core will be removed in 2 m sections by cutting the sample with the macro core retriever. The samples will be cataloged and placed in a protective storage cell.

This whole system is to be controlled from Earth. This is carried out by a continuously monitoring PLC onboard the drill rig. A touch screen control console allows the operator on Earth to monitor the progress of the operation and intervene if necessary.

2.0 PROBLEM STATEMENT.

In future exploration of the lunar surface, drilled holes and core samples will be required for various applications in the initial phases of outpost habitation. Drilling holes for the emplacement of scientific instruments, setting of structural anchors, and the acquisition of geological samples for analysis are but a few of the potential uses of a drilling apparatus. The drilling will be conducted by a device attached to a three-legged walker called SKITTER (Spatial Kinematic Inertial Translatory Tripod Extremity Robot).

The lunar environment is different from the terrestrial environment, therefore terrestrial methods of drilling may not be directly applied. Characteristics of the lunar environment which need to be considered include lunar dust, reduced gravity, lack of atmosphere, micrometeorite bombardment, extreme temperature gradients, radiation,and the 14-day diurnal cycle.

2.1 Performance Objectives.

The drill will be remotely controlled and will be attached to the bottom of SKITTER. The system must be firmly anchored and braced to avoid movement during the drilling operation. It should be light enough so that SKITTER can easily transport it to the desired drill site and position it. The device should also be detachable so that SKITTER can disengage and walk away from it if necessary.

A downward force must be used to effectively drill into the lunar surface. A minimum downward force of 200 pounds is required with a rotational speed of 300 RPM. The drill bit must be able to drill a hole into sandy or solid basalt and must be able to complete a 50 meter hole without being replaced. About 80 percent of the heat created by the bit during drilling will be retained in the

cuttings. To prevent the bit from overheating, these cuttings must be removed from the bottom of the hole periodically.

The drilling implement will include enough rods to drill a hole up to 50 meters deep. The diameter of the hole may range from 50 millimeters to 100 millimeters. Drilling angles of up to 20 degrees from vertical must be accommodated. Core samples must be removed and stored periodically during drilling. The removal process must occur with minimal damage and disturbance to the samples. Cataloged storage will facilitate later testing and analysis. The storage system must be able to hold all the core samples which are removed from a 50 meter hole.

A power supply must be able to allow the drilling of a hole up to 50 meters deep without recharging. Effective heat dissipation from the apparatus is necessary so that drilling will be possible anytime during the 14-day lunar day or night. Control of SKITTER and the drilling apparatus will be coordinated from Earth. After the successful completion of drilling, the device will disengage from the drill hole and return to a base so that core samples can be deposited and fresh batteries retrieved. The absence of human operators makes it necessary for the design to be fully maintained robotically. This will be best accomplished by having the least number of moving parts and striving for the least complex design possible.

2.2 Constraints.

Size and weight limitations due to transportation have not been specified. Taking into account the estimated $20,000/lb price tag for lunar freight, the design should be as light as possible.

The drilling device will be attached to the triangular base plate on the bottom of SKITTER which is equilateral with each side measuring 1.5 meters. SKITTER's clearance of one meter, minimum, and four meters, maximum, must be included in the design. When

retracted, the apparatus should be as non-intrusive as possible to allow clearance of the legs for "walking".

Temperature extremes and vacuum environment prevent the use of fluids for cooling of the drill bit and removal of cuttings. Heat management must be accomplished by the use of conduction and radiation. Cuttings will be removed from the drill hole by use of a vertical accelerator and stepped auger. Another characteristic of the lunar surface which will affect the bit is the constant temperature (minus 50 degrees C) which exists at a depth of 80 centimeters or more .

Lunar dust is abundant and tends to adhere to all exposed surfaces. This can cause problems for moving parts. It may also reduce the effectiveness of radiation panels. The dust will also adhere to the stored core samples, so a micro-coring device must be designed to extract small core samples from the drill hole and protect them from the lunar dust.

Since the moon has no protective atmosphere, solar radiation and micrometeorite bombardment must be considered in the selection of materials. Material strength is important due to the high drilling forces that will be necessary to penetrate the basaltic lunar crust which has properties close to that of granite.

Reduced gravity on the moon must also be considered in the design of the drill. Since a lightweight apparatus is desired and the moon's gravity is only one-sixth of that on Earth, some type of downward force must be provided for drilling.

A specific control problem arising from the remote operation of the drill is the 2.6 second communications delay between Earth and the moon. Visual monitoring of the system may not be practical, and lack of audible transmission will also make control more difficult.

3.0 GENERAL ARRANGEMENT

THE SKITTER (Spatial Kinematic Inertial Translatory Tripod Extremity Robot) has been developed as a tool in lunar exploration and in the initial phase of outpost habitation. Projected duties planned for the robot are drilling, mining, site preparation and benefication of lunar soil prior to pilot-plant oxygen extraction and other soil processing techniques.

The drilling implement is one of a series of interchangeable implements whose individual use will be intermittent. The drill's uses will include obtaining soil samples for scientific analysis, mineral locations, foundation analysis and hole preparation for scientific instrument placement, structural anchors, excavation explosives and mining methods. The drill is designed to take advantage of the lunar environment while operating within the constraints imposed by that environment.

Figures 3.1 and 3.2 at the end of this section show the general arrangement of the drilling implement as described below.

The drilling implement connects to SKITTER via the structural platform and interfacing latches. Three latches mounted in the underside of SKITTER are designed so that the structure can be engaged and disengaged from controllers on Earth. The space-frame platform supports all parts of the drilling implement including the power system, robot arm and rod holders, rods and associated devices, and control box.

The drill motor and power system (consisting of pressure vessels and fuel cell) sit inside the platform. The motor shaft

protrudes through the underside of the structure where it connects to the drill string. Heat generated from the motor is transferred away by use of heat pipes. A rejection panel (not shown) is mounted on the outside of the structure. This is the primary power system for the main drilling operation.

A rotating plate, supporting a robot arm, is mounted underneath the structure. The rotating plate allows the two-degree-of-freedom arm to reach up and grab the rods from the rod holders and connect them to the motor shaft and the sunk drill string.

A footplate will hold the drill string while the robot arm connects another rod or device. The rod holders extend out from the structure in between SKITTER'S legs and use clips to attach the rods. Approximately thirty rods and associated devices can be held at a time. The 25 rods that make up the drill-string are hollow and contain a helically-stepped auger which serves to collect the broken outer rock for removal by the vertical accelerator. The rods have specially designed connections for attachment to the motor shaft, periphery devices, drill bit, and each other. The full set of rods and devices can drill to a depth of 50 meters.

Several associated devices will fit in the rod racks and are integral to the drilling operation. The vertical accelerator shakes the rods to force the broken rock up the auger and out of the rods. It is manufactured in the shape of a rod and is oscillated vertically by a rotary driven cam. Thus, it attaches and operates identically to the drill string. The macro-core retrieval device is implemented after the vertical accelerator clears the small chips away. Its purpose is to break off and remove the cylindrical rock section left in the center of the bit. The micro-core retrieval device is implemented after the hole is drilled and cleared. Its purpose is to remove core samples from different shaft depths for analysis. Manufactured in the

shape of the rods, the device contains its own power source, drive train, drill, retrieval and storage devices.

The drill bit has a diamond cutting face consisting of 54 facial diamonds. The maximum downward drill force required is 250 pounds at 300 revolutions per minute. This force required still leaves ample weight on SKITTER for good traction between the lunar surface and SKITTER's legs.

A preliminary controls scenario has been designed for the entire drilling procedure. This scenario is for Earth-based control and considers the three second time lag between Earth and the moon, the desired sequence of operation, and the actuators needed to trigger the individual operations. A carefully detailed sequence of operation is presented in the controls section of this report.

The basic sequence of the drilling operation begins with the SKITTER squatting down and engaging the structure, supporting and containing all drilling devices, via the latches. The drilling process initiates with the robot arm placing the footplate on the lunar surface. The arm then obtains the drill bit rod from the rod holders and attaches it to the motor shaft. Drilling occurs as SKITTER slowly squats down to a specified level. The footplate then clamps the drill bit rod so the rod can be disconnected from the motor shaft. Once this is done, SKITTER stands up, the robot arm retrieves the vertical accelerator apparatus from the rod rack and connects it to the motor and the sunk drill string. The broken rock is shaken out. The robot arm and footplate then work to place the vertical accelerator and drill bit rod back in the rod racks. The macro-core retrieval device is then used to clear the drilled shaft of the unbroken rock. The drill bit rod is then placed back in the cleared shaft and held by the footplate. An additional drill string rod is attached to the shaft and drill bit rod. SKITTER slowly squats down, drilling to the next level. This process is

repeated until the desired drill depth is reached. At each rod change or addition, the footplate is used to hold the drill string already in the shaft so new rods can be put in place. After the drilling is completed, the micro-core retrieval device is used, along with rods to extend to desired depth, to obtain off-hole samples.

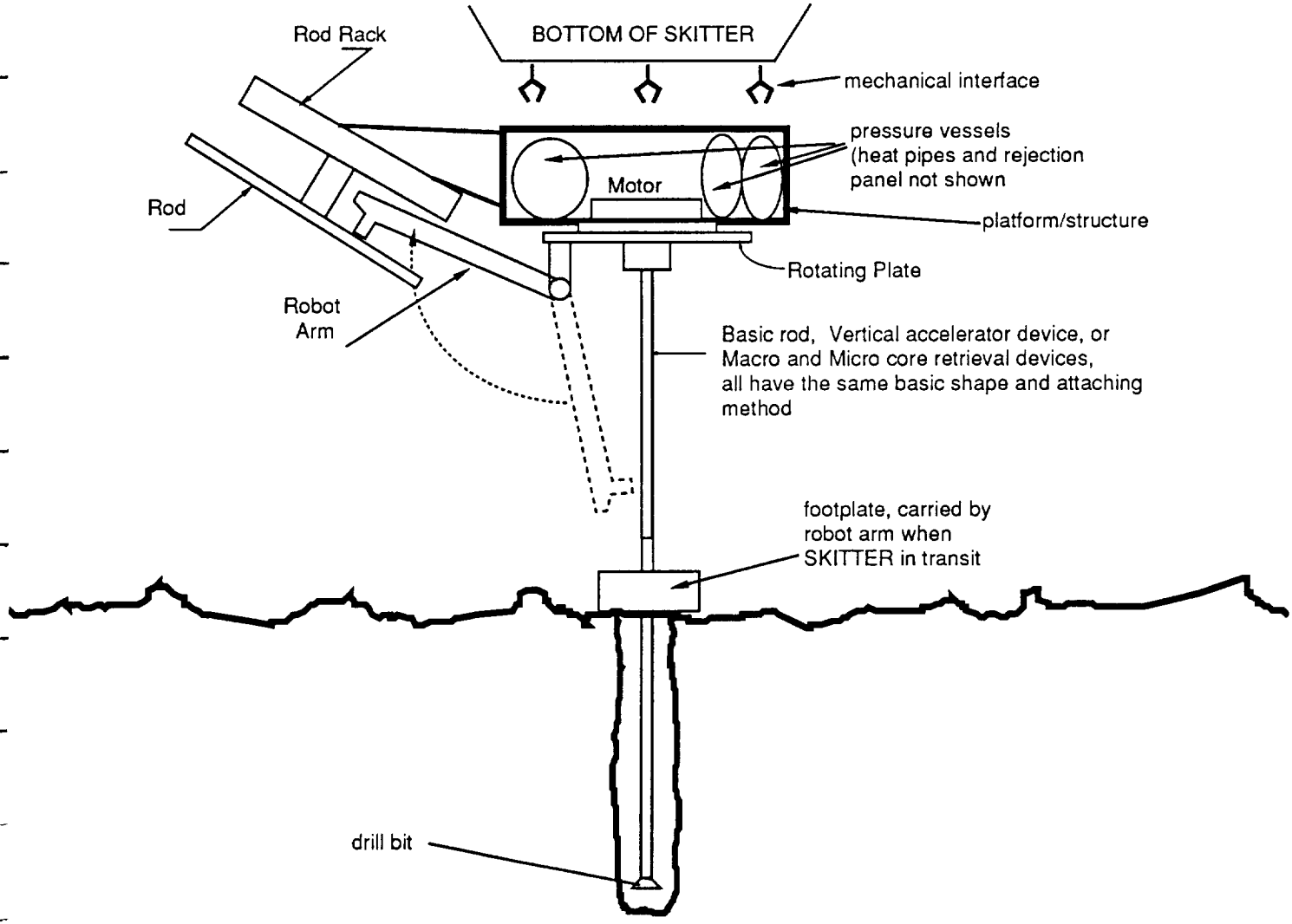

Figure 3.0.1 - side view of drilling implement

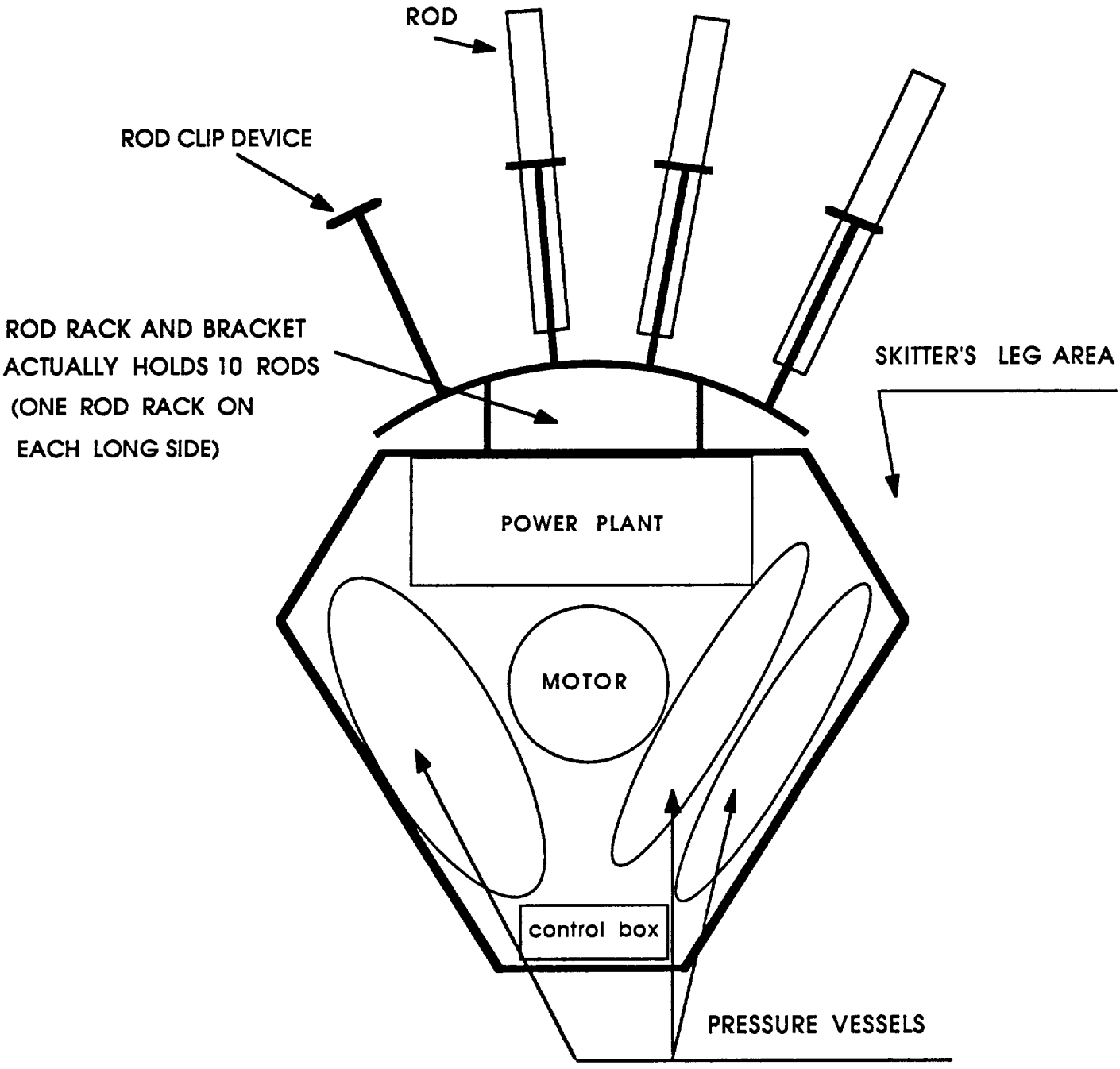

Figure 3.0.2 - top view of drilling platform

4.0 DEEP DRILL APPARATUS SYSTEMS DESIGN

4.1 BIT CUTTING LOADING INTO STEPPED AUGER

4.1.1 Cutting Teeth

In this design, diamonds were selected as the cutting teeth due to their extreme hardness. Diamonds were also chosen as the cutting teeth because they require less thrust than other cutting materials. The teeth will consist of Type IA diamonds, 30 per carat, having a dodecahedron shape. Past research has shown that cutting teeth having these characteristics provide the best results. The diamonds will be bonded to the bit by a powder matrix material infiltrate tested by Kennametal Corporation in Latrobe, Pennsylvania [Ref 4.1.1] The test results from this corporation showed that Type 4 powder metal would be the best at holding the diamonds in place.

There will be a total of 54 facial diamonds of which 12 of them will be inside or outside cutting diamonds. An additional 12 diamonds will be used to ream the 100mm hole to 104mm. This larger hole will allow space for the bit to turn without rubbing the side of the hole. These diamonds will be placed on the drill bit as shown in figure 4.1.1.1 in Appendix D. The diamonds are mounted on small ridges with a negative rake angle of 7.5 degrees to insure smooth particle flow around the teeth and into the shovel apparatus. These ridges are at 15 degree angles to push the particles to the outside of the bit and to prevent them from obstructing the teeth.

For this bit design, the maximum downward force and bit speed will be 250 pounds and 300 revolutions per minute, respectively. The reason for using only half of the available downward force SKITTER can provide, is to insure that SKITTER is able to have traction on the surface. The bit speed was selected to keep the heat generated to a minimum. From calculations in

Appendix A, assuming steady state and continuous drilling, the temperature of the cutting teeth would only reach 1092 degrees F. However, this design will not be continuously drilling which should lead to a bit temperature of approximately 800 degrees F to 900 degrees F. This temperature is well below the critical temperature of 952 degrees F, at which there is a build up of carbon on the diamonds. This is called graphitization or oxidation. When this happens, the cutting ability of the diamond is nullified.

With a maximum cutting depth of 0.2mm for each diamond, the expected drilling rate will be approximately 61mm per minute calculated from the following formula:

CUTTING RATE = RPM * CUTTING DEPTH

The teeth will produce a maximum torque of 41.689 N-m as calculated in Appendix A. From this torque and the additional torque from the bit dragging on the side of the hole, a set of power requirements was calculated. These calculations show that the worst case power requirements of 9.81 kW (13.2 Hp) will be sufficient to do the cutting. However, in normal drilling, the entire drill string should not rub the side of the hole. In this case, the power requirement is 2.8 kW (2.9 Hp).

This drill bit will not be operating continuously for the entire 50m of drilling. The bit will only drill 8mm before the intermediate holding device is filled. After filling the holding device, the drill bit will be raised from the bottom of the hole and vibrated up and down to advance the cut particles up the stepped auger. During this cycle, the cutting teeth will have time to radiate approximately 50 degrees F which will help increase the life of the bit.

4.1.2 Shovel Apparatus

The purpose of the shovel apparatus shown in drawing 4.1.2.1 is to scoop the loose particles from the bottom of the bit to the holding device inside the bit. There will be two shovel mechanisms to feed both storage devices at the foot of the double helical auger. The shovel will be made of tungsten carbide instead of diamonds. The reason for not putting diamonds on the shovel is because its primary use is to scoop up the loose particles, rather than to actually do any actual cutting. The front of the shovel is designed to come to a point in order to remove even the smallest particles cut.

The shovel path has a rectangular cross sectional area of 100 mm^2 that will provide a steady flow of loose particles to the holding chamber. In order to maximize the size of the holding chamber, the shovels will be placed at an angle of 40 degrees as shown in drawing 4.1.2.1 in appendix d. These shovels will span the entire width of the drill face and the reaming teeth in order to remove all of the loose particles. Only 19.9 Newtons will be placed on these shovels, which is low enough to guarantee long life. Also the shovels are designed to last as long as the cutting teeth last. As the cutting teeth wear down the shovels will wear down and remain functional.

4.1.3 Intermediate Holding Device

The holding device is an intermediary step between the removal of the cuttings from the teeth and shaking the cuttings up the stepped auger (Drawing 4.1.3.1). The shovel will dump some of these cuttings directly onto the stepped auger, which will begin at the edge of the device, and the remainder into the holding device. Thus its main purpose will be to prevent the cuttings from falling back down the shovel and onto the teeth.

The need for this device arises due to the fact that about 80% of the heat to which the teeth will be subjected is contained within the cuttings themselves. The "hot" cuttings must be kept out of contact with the teeth as much as possible in order to avoid thermal failure. Grinding of the teeth over cuttings that have fallen back into the hole is also avoided.

Due to uncertainty as to how much of the cuttings will travel directly onto the auger and how much of them will need to be contained in the holding device, it has been designed as large as possible, restricted only by the size of the drill bit and the positions of the holes.

The device will be made from ferritic steel with a high chromium content; which was chosen to match expansion factors with interfacing parts.

Calculations show that if the intermediate holding device was required to hold all of the cuttings, it would be full after drilling approximately five millimeters. This was arrived at with an expansion factor of three from solid rock to cuttings.

The possibility of insulating this device from the bottom of the drill bit and the teeth has been considered. There will be a vacuum gap between the bottom of the holding compartment and the upper surface of the section of the bit holding the teeth; which will prevent heat flow from the cuttings back down to the teeth.

4.1.4 Structural Design

The entire drill bit is 2 meters in length. The overall dimensions for the bit are given in Drawing 4.1.4.1. The upper section of the bit from the connection to the upper shafts down to the splined connection is referred to as the upper bit. The lower 2.5 cm

section containing the cutting teeth and shovel mechanism make up the lower bit. These two sections are separate and removable from one another. The combined mass of the two sections is 16.4 kg. This separation is beneficial because it allows for the replacement of the cutting teeth without disposing of the entire upper bit. The spatial separation between the lower bit and the holding device minimizes the heat transfer from the cuttings back down to the teeth. The life of the cutting teeth is extended by decreasing this downward heat flux.

The primary responsibility of the spline connection between the two sections [Drawing 4.1.4.2] is the transference of the torsional load to the cutting teeth. The downward force on the bit is not transferred via the two retaining screws in the splined section. Rather, the end of the spline on the upper bit rests directly on the lower bit transferring this force. The length of the spline connection between the retaining screws and the flange on the lower bit was minimized the shear force on the retaining screws resulting from slight differences in the thermal expansion between the two sections. By removing the two screws from the inside shaft the lower bit can be removed and replaced after it has sustained sufficient wear.

The shovel mechanism described in Section 4.1.2 is two separate pieces -- one embedded in the lower bit, the other extending from the front of the holding device on the upper bit. The scoop which actually lifts the cuttings from the bottom of the hole extends up into the lower bit to a vertical height of 15 mm. This results in a hole through the lower bit for removal of the cuttings.

The scoop extension from the upper bit mates with this hole when the two bit sections are connected. The assembled structure results in a channel from the cutting teeth to the holding mechanism. To help seal the channel connection the upper bit scoop extension fits into a small vertical protrusion from the lower bit. This will restrict the leakage of cuttings from the channel between the two bit sections.

The choice of overall bit dimensions was somewhat arbitrary. It was decided that a core sample of 50 mm in diameter was desirable. Thus, a maximum of 25 mm in radial length remained for containment of the auger. The decision to use the maximum outside diameter of 100 mm was based on allowing for optimum efficiency of the stepped auger. However, the major drawback to using such a large diameter is the high amount of work required to drill as compared to drilling a small diameter hole. Due to the restrictions of the project an optimum outside diameter for the drill bit was not analytically determined.

4.1.5 Material Selection

The extreme operating conditions necessitate close examination of the material requirements of the core drill bit. In the lower bit, the material must be wear resistant and capable of retaining strength at temperatures approaching 500°C. The upper bit is responsible for transfer of torsional load from the upper connecting shafts to the lower bit.

Tungsten is highly recommended for drilling in rock as hard as basalt. Thus, a straight tungsten carbide with 10% cobalt is most suitable for the lower bit. This sintered carbide will provide sufficient high temperature strength (Rockwell A > 80) at temperatures of 530°C. The addition of 10% Co will improve the impact properties which are of some importance in the design. Other beneficial effects of using the tungsten carbide are its relatively high thermal conductivity (150 - 180 W/m·°C) and its low coefficient of thermal expansion (5.9 micro inches/inch).

The upper bit is not exposed to the extremes in temperature as in the lower section. Therefore, the use of tungsten carbide is unnecessary as well as impractical from a fabrication standpoint. A

material with a low coefficient of thermal expansion is necessary in the upper bit because the lower section also will not change significantly with temperature. AISI-SAE H11 is recommended as the material in the upper bit. This hot work tool steel provides a low coefficient of thermal expansion and high temperature strength which is of importance in the splined connection. Its low cobalt and molybdenum content give this steel desirable impact properties as well. The wear resistance of H11 is qualitatively fair which is sufficient for the operating conditions in the upper bit.

4.1.6 Bit Life

The life of the drill bit has been approximated using experimental data from reference one. Comparing the parameters of the bit in this reference to those under which the bit being designed is operating, an estimation of the life can be made. The drill bit in reference one was tested in basalt in the quarries at Dresser, Wisconsin, simulating the worst conditions of lunar drilling. From these tests the bit was found to have a life of ten feet (roughly three meters), when drilling continuously at 1,000 RPM with up to 400 lb. downward thrust. The speed at which these tests were conducted and the fact that the drilling was continuous, are the two major factors determining the bit life. The bit designed in this report will not be running continuously, allowing for a cool-off period. It will also not exceed 300 RPM in operation. From the above it can be concluded that the life of the drill bit in this paper will be at least three times the life of the bit in reference one, probably even several times that number. This corresponds to a drilling depth of at least 30 ft. (about 10 meters), if drilling were continuous. Building and testing the bit would provide more accurate figures.

4.1.7 Stepped Auger

The stepped auger is double helical and will operate by jumping the cuttings up over a series of steps. After reaching the top of this two meter section, they will travel onto a similar auger in the next section. For details on the augers see section 4.2.8.

4.1.8 Bit and Rod Interface

The bit and rod interface is the mechanism that will allow the travel of cuttings between two meter auger sections. It may effect as much as a 70% reduction in the cutting's flow. It will be a variation on the collar interface design (section 4.2.4), and is detailed in section 4.2.9.

4.2 RODS, AUGER, AND STEPPED AUGER

4.2.1 Introduction

A system for lunar deep drilling requires a method for power transference from the surface to the bit and a method for the transport of cuttings form the bottom of the hole back to the surface. Conventional earthbound technology is insufficient for these purposes because component mass, interfacing requirements, and the need for a substantial fluid reservoir to flush cuttings from the hole do not suit the moon environment.

Several constraints in addition to those imposed by the moon environment must be accommodated by the power transfer system (PTS) and the cutting removal system (CRS) (See Fig.4.2.1.1). Some constraints are imposed on the PTS and CRS by the other systems which are to be designed to support lunar drilling operations. These systems require that a 100 mm diameter hole be drilled in two meter increments, that the interfacing of drill train components be performed by robots remotely operated from the earth, and that a variety of arrangements of in-hole components (rods, augers, and stepped augers) be possible. Specific constraints are the power and compressive force needed for bit operation (which have been set at 50 ft-lb torque, 150 rpm, and 200 lb), the number of degrees of freedom of the rod changer which must perform the interfacing operation (which has been set at two), and the load carrying ability of the rod changer and footplate clamp (which is not expected to exceed 200 lb).

4.2.2 Design Considerations

Aside from effectiveness and durability in their designated tasks, the PTS and CRS were designed with the goal of optimizing specific properties. Foremost among these properties was the

minimization of system mass and thus feasibility for transport to the moon. Secondary considerations were the desire to minimize energy and articulation requirements for component interfacing, the desire for overall design simplicity with a minimum of moving parts and potential failure modes.

Work has been done in the past at the Georgia Institute of Technology on the design of a stepped auger, or vertically reciprocating auger (VRA), for the removal of granular material during lunar drilling. Because of the availability of information on this design and its potential for effectiveness, it was decided to use a VRA as the primary component for the CRS. The other component which was required for this system was a device to remove loose material from the uppermost portion of the lunar surface as a prerequisite to the insertion of the bit for drilling hard rock. For this purpose a simple helical auger similar to those used in soft soil on the earth was chosen.

For the PTS a system of rods and interfaces was chosen as the most practical method for the mechanical transfer of the compressive and torsional forces needed for bit operation and the tensional and compressive forces required to drive the VRA. Since the number of CRS components in the hole at any given time must be determined by the geological conditions in the drilling region, it was necessary to design all interfaces to correspond with those of the VRA and the auger. If hard rock is encountered near the surface, there may be only one CRS component in the hole. Therefore, all in-hole CRS components not only functioned as PTS components in their prescribed tasks, but also could be used to operate as rods in the PTS if necessary.

4.2.3 Material Selection

Because the strength requirements for each component were similar and because the extreme operating temperature range made it preferable for all components to have the same coefficient of

thermal expansion to prevent interface seizures, all the components of the PTS and CRS should be constructed of the same material. Since none of the physical dimensions for any component were dictated by its function alone (with the exception of the outside diameters of the auger and VRA), it was decided to minimize weight by the selection of a material with a high strength to weight ratio and the reduction of component dimensions wherever stress analysis proved this to be feasible. For this purpose titanium alloys were considered and a Ti-5 Al-2.5 Sn alloy was chosen. Since this alloy is classified as a refractory metal, there should be no significant loss of properties at operating temperatures up to 800 degrees Fahrenheit in air and up to a somewhat higher temperature in space where oxygen embrittlement will not be a significant problem. Data contained in NASA SP-5012 indicates that there is consistency in material properties of Ti-5 Al-2.5 Sn down to -300 degrees Fahrenheit. This means components constructed from the alloy should be functional at any low temperature conditions which might me encountered on the moon. Some properties of this alloy are listed below:

Elastic modulus.....128×10^4 MPa
Yield Strength.....827 MPa
% Elongation.....10 %
Fracture Toughness (at -300 F).....0.8
Density.....4500 kg/m^3

Power Transfer System Component Designs

4.2.4 Interface Design

The interface design which was decided upon incorporates a solid inner cylindrical cutout in the form of a dovetail connected to an outer cylinder which constitutes the body of the component which contains the interface (rod, auger, or VRA). The interface to be oriented toward the surface end of the hole has a tapered male dovetail design (See Fig.4.2.4.1) and the lower interface has the female counterpart to this configuration (See Fig.4.2.4.4). At the

upper interface there is a bistable collar which surrounds the component and slides on a diametrically opposed set of C-shaped grooves (See Fig.4.2.4.5) such that in its lower position it surrounds the upper end of the component but sits clear of the interface. In its upper position the collar surrounds a portion of the component, the entire interface, and a portion of the second component to which the first will be coupled. This design allows for a connection operation as follows:

(1) The footplate clasps the lower rod by the collar with the collar in its lower stable position.
(2) The rod changer brings a new rod in from the side such that the dovetail is fitted into place.
(3) The new rod is rotated, depressed, and rotated again to bring the collar to its upper stable position covering the interface.
(4) The motor is connected to the upper rod (see the section 4.2.6 on the motor interface for a detailed description of this operation).
(5) The footplate releases the collar and drilling is resumed.

The same set of operations is performed in reverse for the disconnection of the rod coupling.

The nature of the rod interface design can be seen in Figures 4.2.2.1 through 4.2.2.4.

A stress analysis was performed on this design. The cases of failure which were considered:

- shearing through the weakest horizontal and vertical planes in either end
- gross plastic deformation due to axial forces
- plastic deformation of the collar due to interface flexure

The case of collar deformation due to radial forces from the footplate was not considered. In view of the current footplate design this type of failure is a probable failure mode and warrants further analysis.

4.2.5 Rod Design

The design of connecting rods for the drilling operation was dictated primarily by the interface requirements at either end. The rod itself is simply a titanium tube which is externally identical to the VRA and the auger (See Fig.4.2.5.1). The outer diameter of the rods was chosen to be the maximum which the 100 mm hole size and interface collar requirements would permit. This allowed for a maximum resistance to failure in torsion and column buckling with a minimum of rod weight. For this purpose the outer rod diameter was chosen to be 98 mm, and the inner diameter was chosen to 96 mm. A stress analysis was performed on the rod cross section. The failure modes which were considered were:

- column buckling
- shear yielding in torsion
- compressive yielding
- tension yielding
- fatigue due to tensile forces exerted by the vertical accelerator

4.2.6 Motor Interface Design

The motor interface will utilize two permanent magnets coated with a protective layer of paper. The contact force of these magnets would be approximately 45 Newtons. The surface of the magnets will be textured to prevent rotational slipping through a surface gear arrangement. This contour will work better than a flat arrangement since it would be held by the material instead of the frictional relationship.

There will be a female section of the Magnet Motor Interface (MMI) permanently attached to the shaft below the vertical accelerator. It will have an additional sheath for alignment and shielding purposes. This sheath will produce a recessed appearance.

A special rod section will be required having a male MMI at the top and an RIM at the bottom. It will also be equipped with an auger for use during the first two meters of soil. This assumes that the hard rock will not be encountered until two meters of loose material has been removed. This Motor Interface Rod Section (MIRS) will always be the top rod section on a rod string.

The MIRS will be completely out of the hole at the start of a two meter drilling period. At the end of the two meters, the MIRS will be fully inserted in the hole. The diameter of the MMI will be larger in diameter than the hole to prevent the rod string from accidentally falling into the hole.

The connection process is as follows:

(1) Rod string is lowered to maximum depth
(2) Footplate grips coupler
(3) Rod changer grips MIRS
(4) RIM is engaged
(5) SKITTER lowers onto the magnet
(6) Drilling begins

The disconnection process is as follows:

(1) SKITTER raises MIRS until the footplate can grip the coupler
(2) Footplate grips the coupler
(3) SKITTER raises up with 45 Newtons
(4) RIM is disconnected
(5) MIRS is returned to rack

There are several problems with this interface design. Initial component insertion is difficult, and adding or removing components from the rod string requires that two operations be performed per component. Furthermore, no suitable magnetic material could be found to implement this design.

4.2.7 Vertically Reciprocating Auger Description

The VRA or stepped auger is similar in appearance to an ordinary helical auger. The VRA, however, has a series of steps comprised of vertically oriented fences along its its windings (See Fig.4.2.8.2). These fences create small compartments that retain dirt. In operation the VRA is unlike conventional augers. It is not rotated but instead reciprocates along its axis. In its initial upward movement the soil particles retained on the steps obtain a significant upward velocity. When the VRA is then accelerated downward, the particles are deflected from the upper helical surface in a direction consistent with their progression up the windings. The particles are then prevented from sliding back to their original position by the subsequent fences of the VRA.

4.2.8 Vertically Reciprocating Auger Design

The design of the VRA began with a careful study of the optimization program developed by an ME 4182 group in the spring of 1988. The parameter for which this program was designed to optimize was VRA volumetric throughput. For the purposes of this design a high throughput was desirable, but additional consideration had to be given to the volume retention of the VRA. The VRA was the most practical in-hole storage device for cuttings as well as the mechanism for transport of these cuttings. However, the VRA is incapable of moving cuttings beyond its uppermost step for deposit into a more appropriate storage device. Thus the geometric constraints of the hole preclude efficient storage of cuttings outside of the VRA.

The VRA throughput-optimization program was modified to calculate retained volume in addition to throughput. The input mode to the program was altered to vary only those parameters which current design constraints permitted. The number of helices (N) was permanently set at two to facilitate the transport of cutting from the bit to the first stage of the VRA and through the VRA interfaces. The number of fences (FT) was set at six since this had proven to yield a substantial throughput with a minimal number of particle-fence collisions in the previous VRA study. Calculations of the retained volume were performed based on the assumption that the pitch angle did not vary with the radius. Although the pitch actually varies in inverse proportion to the radius, this assumption was a reasonable engineering approximation since the majority of cuttings are retained at the outer edge of the VRA helix and in the VRA core.

From the modified optimization program it was determined that the most effective VRA configuration was one with a pitch of about 4/5 of the VRA outer radius. Although the throughput of this configuration was much lower than might have been obtained with a steeper pitch, and the energy loss through particle interaction was relatively high, this design provided the advantages of high VRA volume retention and low energy input per stroke requirements. Based on this design and an estimated three-to-one expansion of cut rock, it was determined that once the hole is sufficiently deep for the insertion of nine VRA segments, all of the cuttings produced by two meters of drilling may be stored in the VRA string.

The final VRA configuration is as follows:

Inner diameter	52 mm	
Outer diameter	96 mm	
Pitch	81 mm	
Fence height	18 mm	(45%)
Number of fences per winding	6	
Total height	2 m	
Volume throughput	48.6 cm^3/stroke	

Volume retention..... 5,350 cm^3/segment

A VRA was designed within these parameters. The interface for this component had to be modified from the basic interface design to allow for the passage of cuttings through the interface.

A stress analysis was performed on the VRA design. The principle load bearing portion of this structure was considered to be the outer casing. Therefore, the analysis for VRA failures resulting from its use as a PTS component were separated from those resulting from its use in the CRS. The failure cases which were considered were:

- gross plastic deformation from tensile loading
- plastic deformation due to torsional shear
- column buckling

These analyses were identical to those performed on the rod cross section. The analysis of failures resulting from the interface modification was not performed. The only modes of failure which this could effect were compressive yielding, where the inner core of the VRA would provide additional support not available for the rod interface, and shearing, where the cross section carrying the torsional load was not significantly reduced.

4.2.9 Vertically Reciprocating Auger Interface Design

The VRA interface was modified from the basic interface design by the removal of the transverse plate. Torsion was transferred from the core to the sheath through the last two half windings of the VRA helix which were reinforced for this purpose (See item B in Fig.4.2.9.1). The steps of the helix near the interface were cut flush with the termination of the sheath so that these would not interfere with coupling and decoupling operations (See item D in Fig.4.2.9.1). Ports were added to the steps just below the interface so

that particles could drop from these steps into the VRA core for storage (See item A in Fig.4.2.9.1).

When the VRA is in operation, cuttings will be transported to the interface by a normal VRA progression. Upon reaching the interface, the particles will be thrown past the lower helical surface off of which they had been rebounding and will instead be deflected by the lower surface of a winding in the next VRA segment. A percentage of these particles will then be picked up in one of the first steps of the upper VRA segment and begin their progression up this segment on the following stroke. In this interface the coupling collar functions to prevent material from dropping off the sides back into the hole. A net reduction in throughput will occur at the interfaces due to the relatively large distance which particles must traverse in order to reach the upper winding and due to the reduced fence height on the final steps of the lower helix. A conservative estimate of this reduction was calculated by the input of a variety of similar geometries into the VRA design program. This estimate was that as much as a 70% reduction may be expected.

Clearly the VRA interface will result in a substantial waste of energy since particles will be sliding back to steps in the lower VRA segment which they have already traversed. Most of this energy loss will occur at the interface between the lowest VRA segment and the bit segment since all other VRA segments will have the same throughput reduction at both ends. This effect might be reduced by the selection of a steeper pitched VRA to be incorporated in the bit segment. This VRA design would have to have reduced fence heights to match the throughput of the interface and a sufficiently steep pitch to maximize particle contact with the windings of the upper VRA without requiring a greater input of energy than the vertical accelerator can provide or than the upper VRA can make efficient use.

4.2.10 Auger Description

The auger functions to remove loose material from the hole at the start of drilling operations. It is a piece of technology borrowed directly from conventional earthbound drilling in soft soil. The function of the auger in lunar drilling is essentially identical to its function on the earth with lower gravity and soil adhesion being the only relevant environmental differences. The auger moves material upward as a result of its rotation and downward progression just as a screw does in soft wood or soap. Two types of auger segment were needed for this purpose. The first was a 2 m auger with a cutting edge at the lower end and an interface above. This segment was to be used to begin the hole. The second was a 2 m auger with two interfaces (See Fig.4.2.10.1). This type was to be inserted behind the first segment. Although is is unlikely the material would be displaced from the bottom of the hole beyond the first auger segment, the upper auger segments could function to catch soil dislodged from the sides of the hole and transport it upward.

All auger interfaces were required to mesh with the drive motor and the connecting rods. The rod-auger connection will be necessary if the depth of loose material exceeds the combined length of the auger segments available. Since the auger interfaces were designed to match the rod interfaces, the augers may also function as rods. This connection provides an overall weight savings in the PTS by reducing the number of rods necessary for the drilling operation.

The parameter of auger design which was of primary concern was pitch. An auger with an extremely steep pitch would require an impractically large driving torque. An auger with too low a pitch angle would not provide a suitable throughput and would run the risk of clogging if it were to encounter large particles. Since the output torque of the system's driving motor was known to have a maximum of 50 ft-lb of torque and the depth of loose material was a variable dependant on the selected drilling location, it was decided to select a single helix auger with a pitch which was comparable to its

diameter. This configuration has proved effective in earthbound drilling operations. This auger provided the additional advantage of having a high retention of material within the auger windings (See Fig.4.2.10.2). Thus, if the depth of loose material is greater than the ability of the auger to transport material, the auger may be drawn directly upward after a stall condition is reached; emptied by agitation, inclination, or reverse rotation; and then reinserted for further drilling.

4.2.11 Design of Vertically Reciprocating Auger Emptying Device

The design of the VRA emptying device can only considered from a conceptual standpoint since there is not sufficient capability in either the current rod changer or footplate designs to empty the VRA. The recommendation for the design is as follows:

(1) The stepped auger is detached from the motor.
(2) The auger is swung upward until it hangs at a sufficiently steep angle for soil to slide along the helix winding.
(3) The auger may be either spun or shaken.
(4) The cuttings will fall into the 2-wheeled dump truck or an intermediate storage device and be carted away.

4.2.12 Component Fabrication

The fabrication of the components for the CRS and the PTS was not considered in depth. The titanium alloy specified may be welded using an inert gas technique and can be shaped by most standard machining operations. Titanium alloys similar to the one specified are commercially available in the forms of bar and sheet. Where applicable in stress calculations, the presence of weldments with penetration depths comparable to the thickness of the smaller member was assumed. To construct the specified components, cores, sheaths, and collars may be reduced from bar stock by lathing. Fences and helix windings may be cut and drawn from sheets. The

fabrication of the interface geometry will be difficult, but a series of lathing and milling operations should be capable of producing it. All connections may then be welded. These weldments should be inspected for defects by X-ray or ultrasound techniques.

FIGURE 4.2.1.1

ROLE OF PTS AND CRS IN LUNAR DRILLING

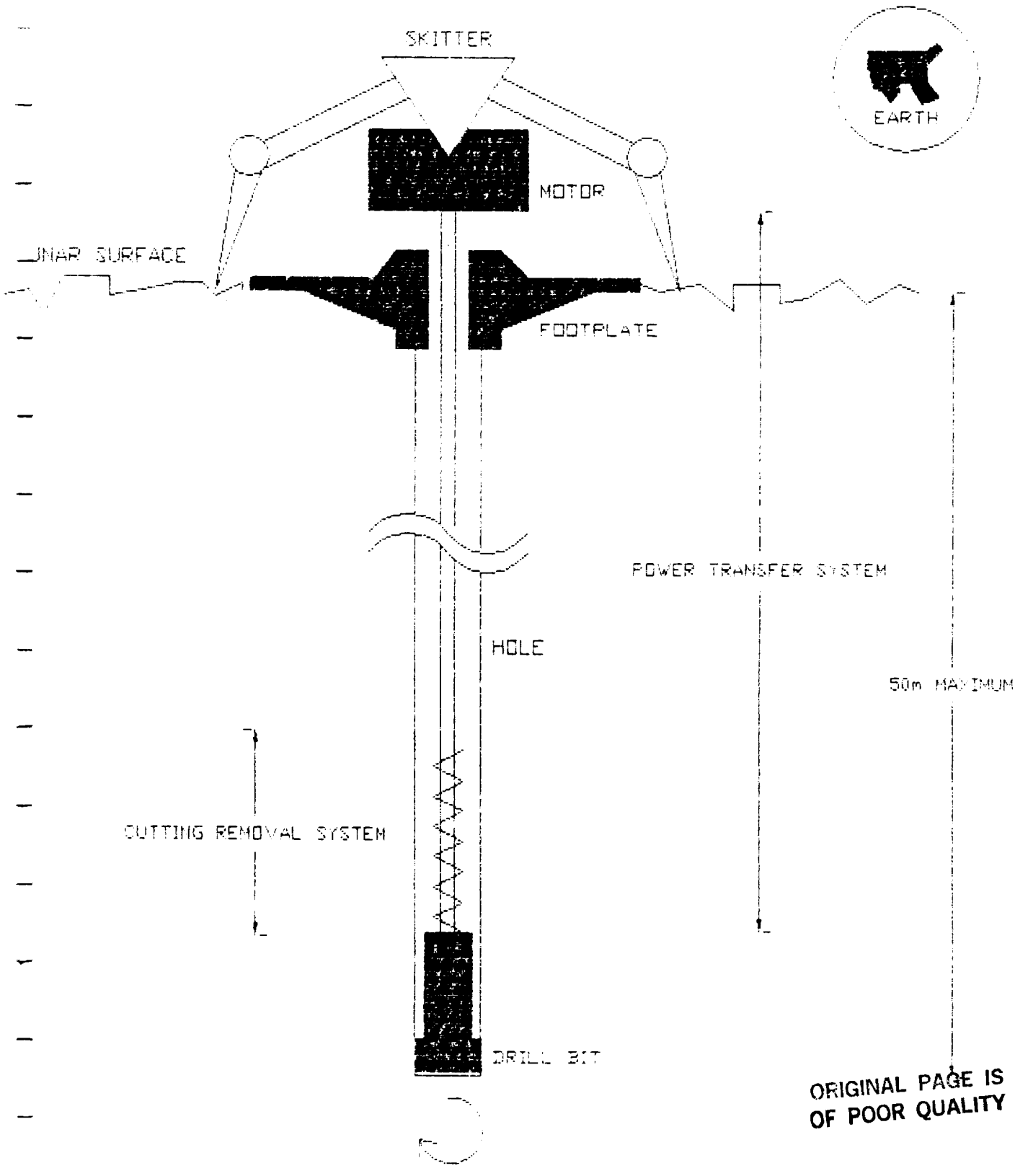

FRONT VIEW OF MALE INTERFACE AND BACK VIEW OF FEMALE INTERFACE

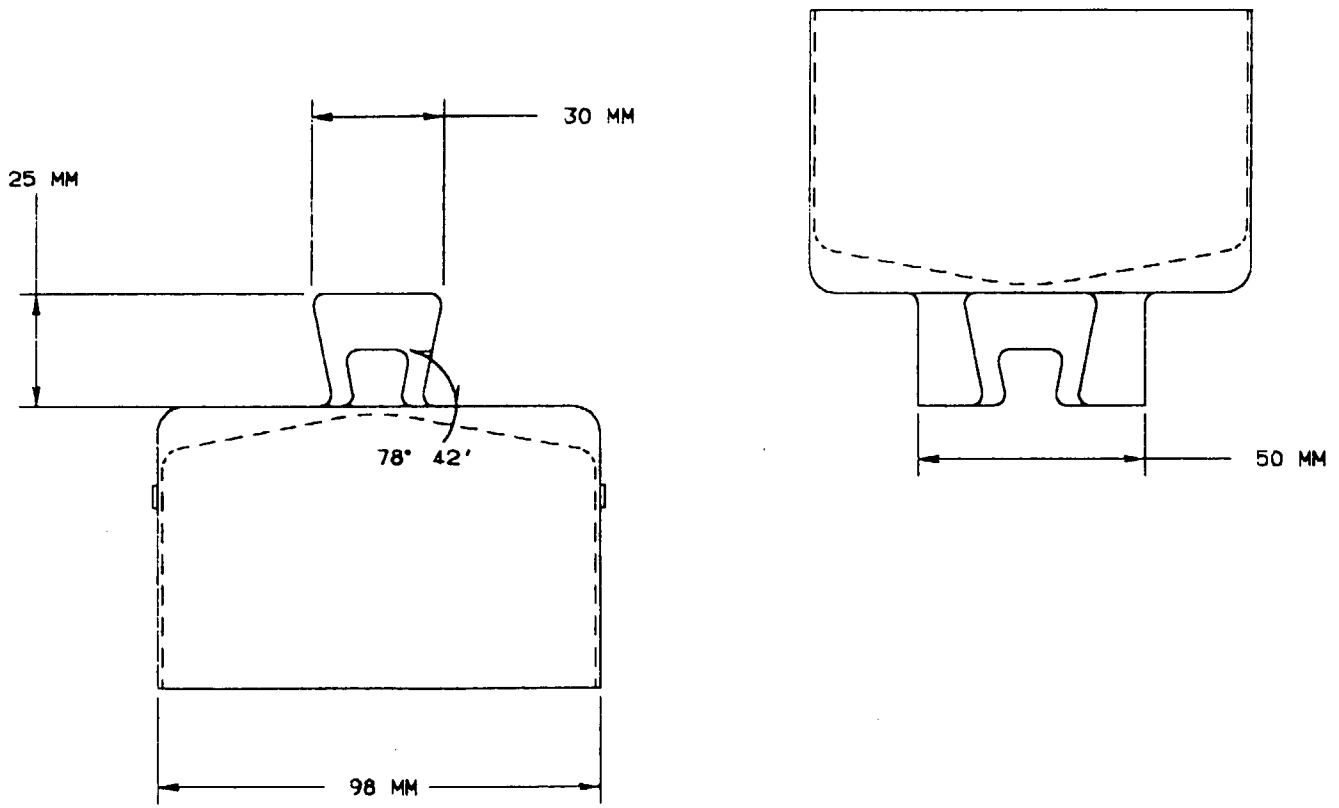

FIGURE 4.2.4.1

SIDE VIEWS OF MALE AND FEMALE INTERFACES

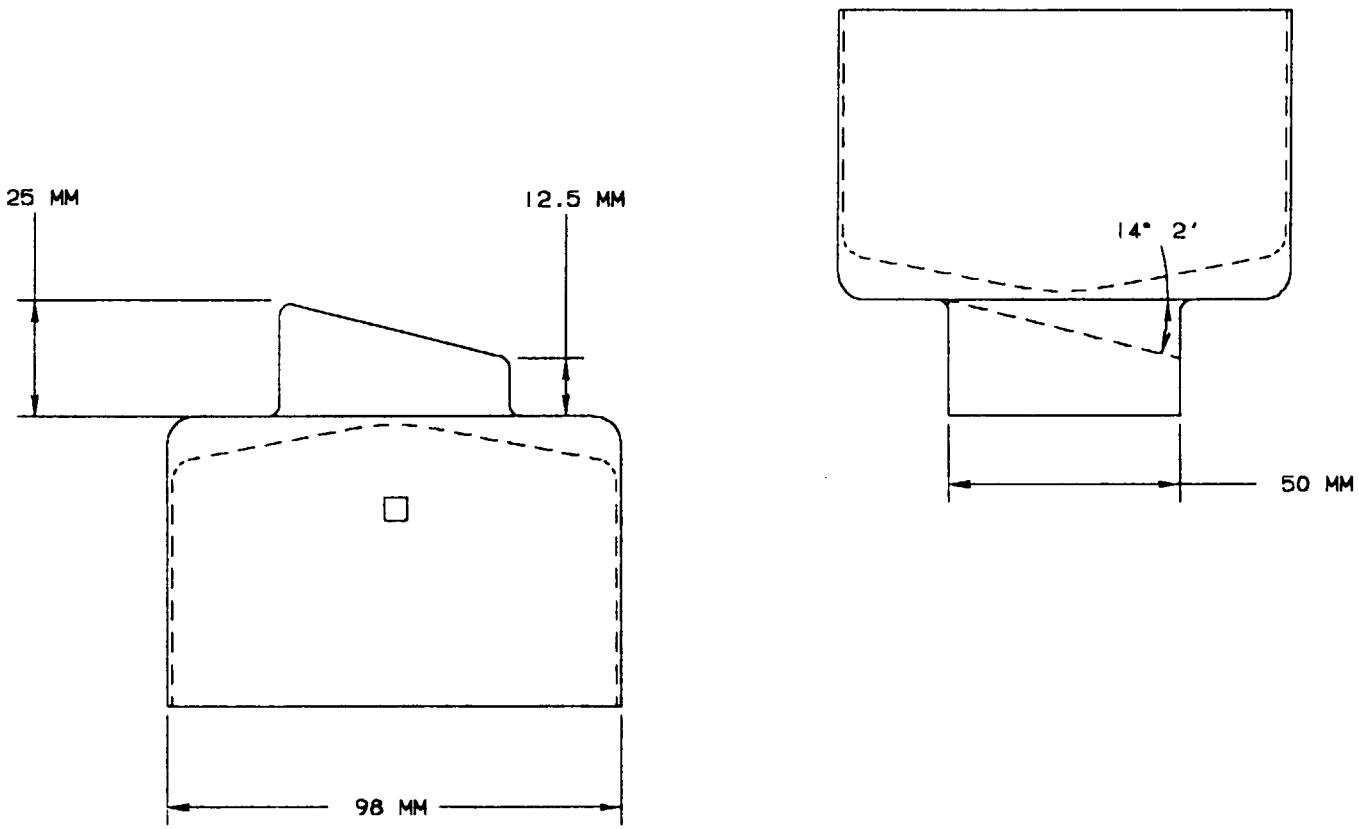

FIGURE 4.2.4.2

TOP VIEW OF MALE INTERFACE AND BOTTOM VIEW OF FEMALE INTERFACE

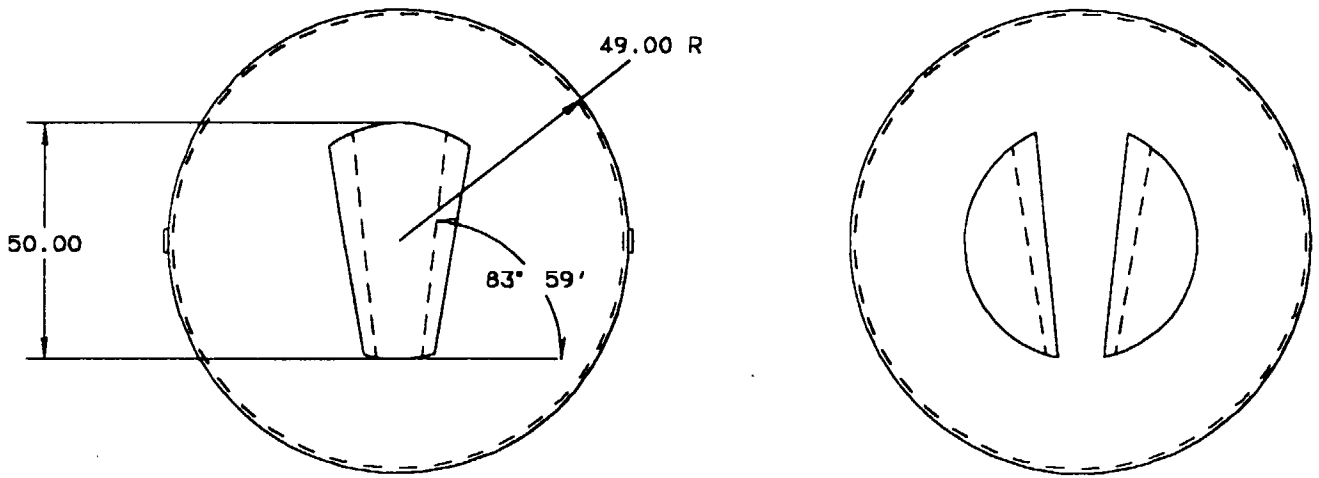

FIGURE 4.2.4.3

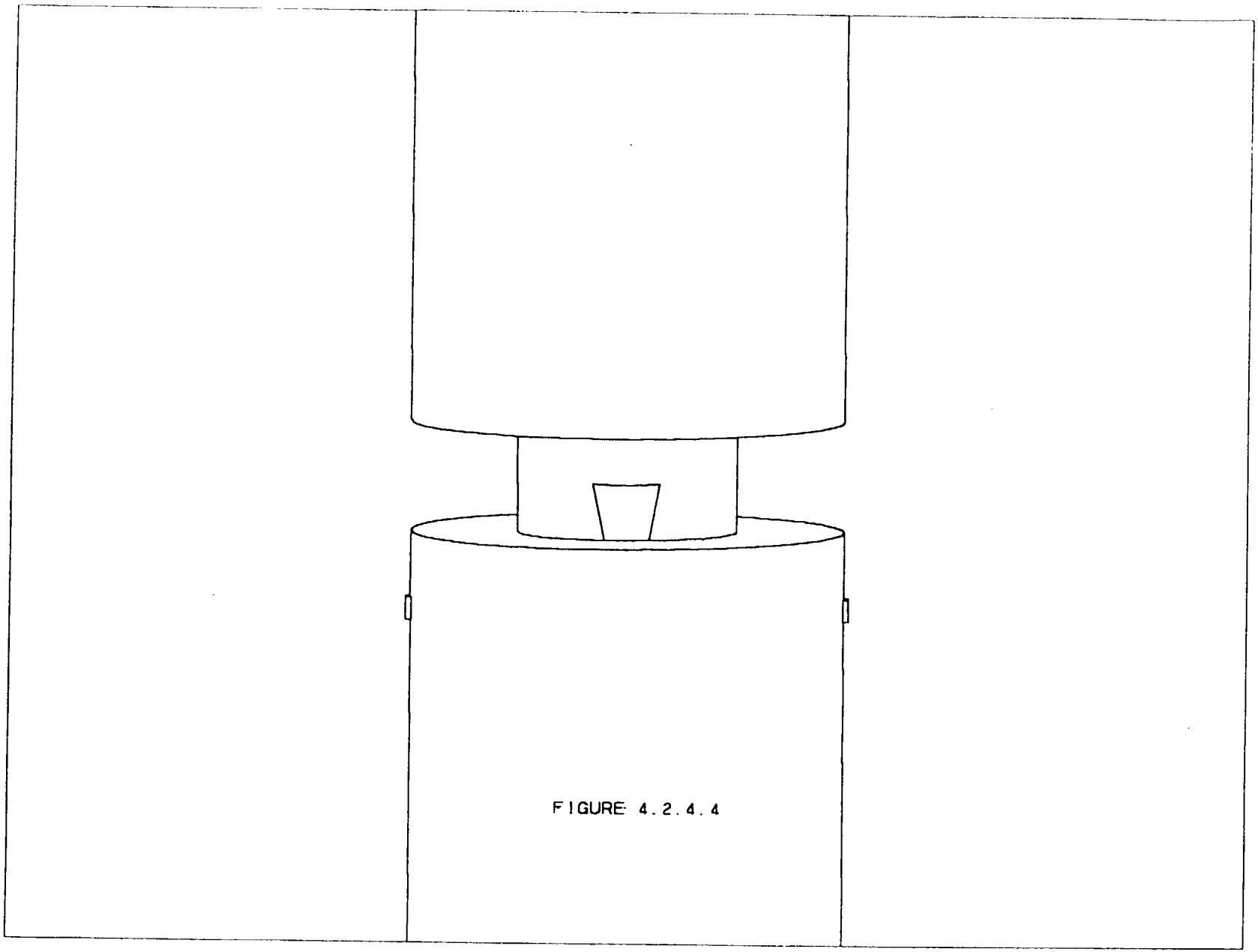

FIGURE 4.2.4.4

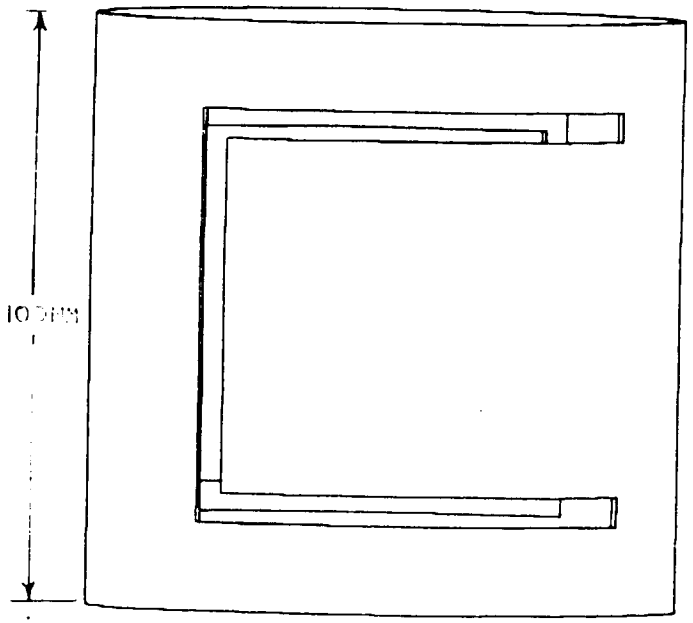

FIGURE 4.2.4.5

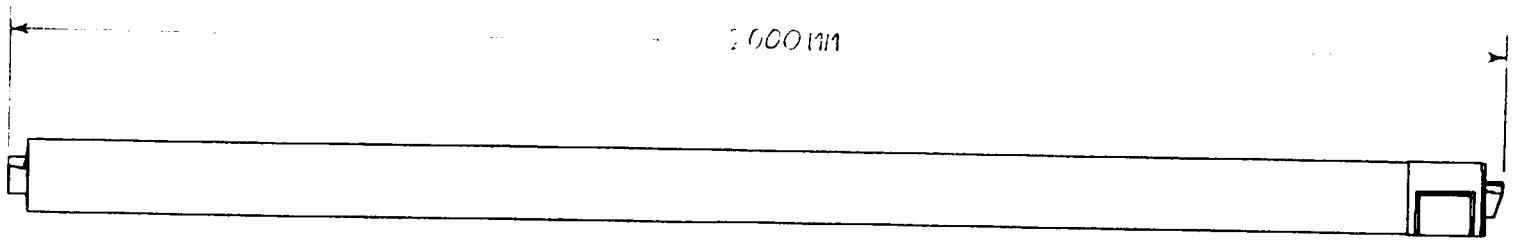

FIGURE 4.2.5.1

MAGNETIC MOTOR INTERFACE

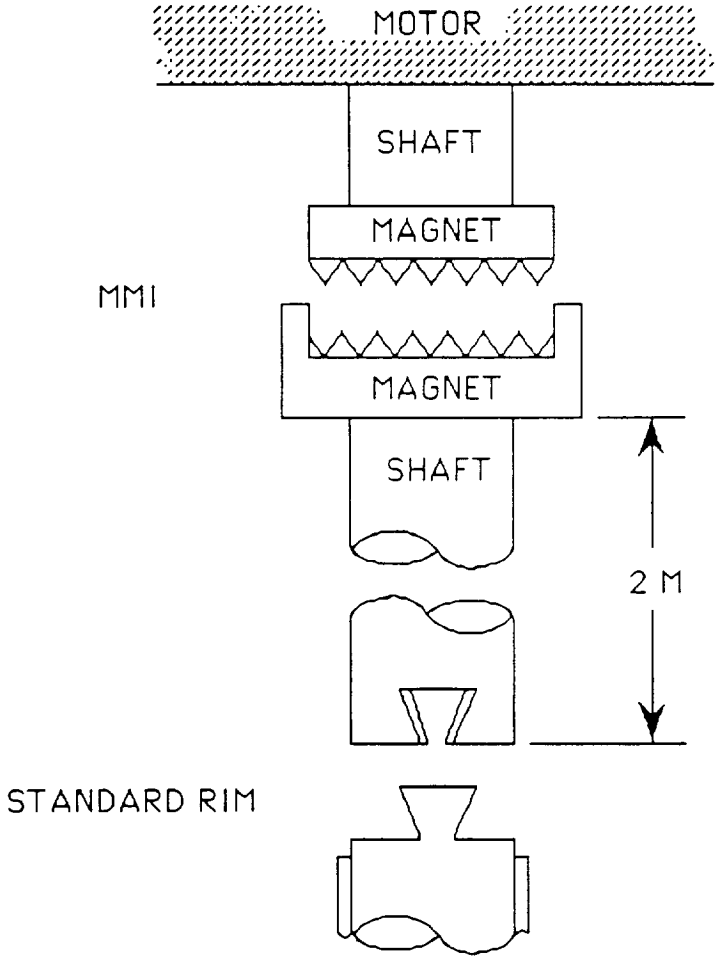

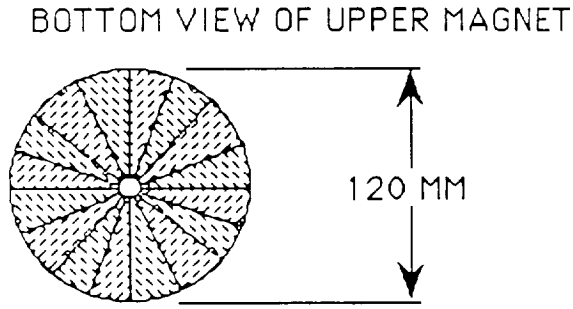

FIGURE 4.2.6.1

FIGURE 4.2.8.1

STEPPED AUGER SEGMENT

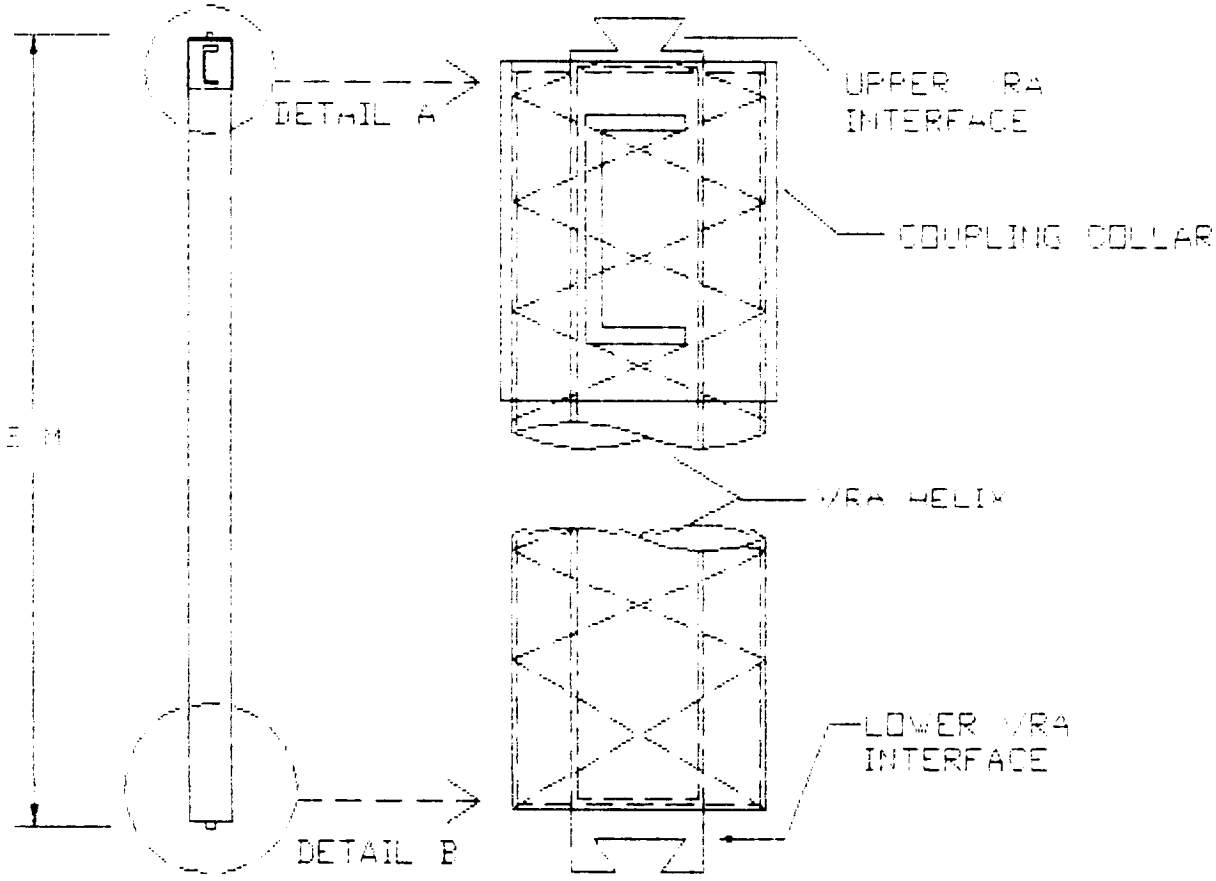

FIGURE 4.2.8.2

CUTAWAY OF STEPPED AUGER (VRA)

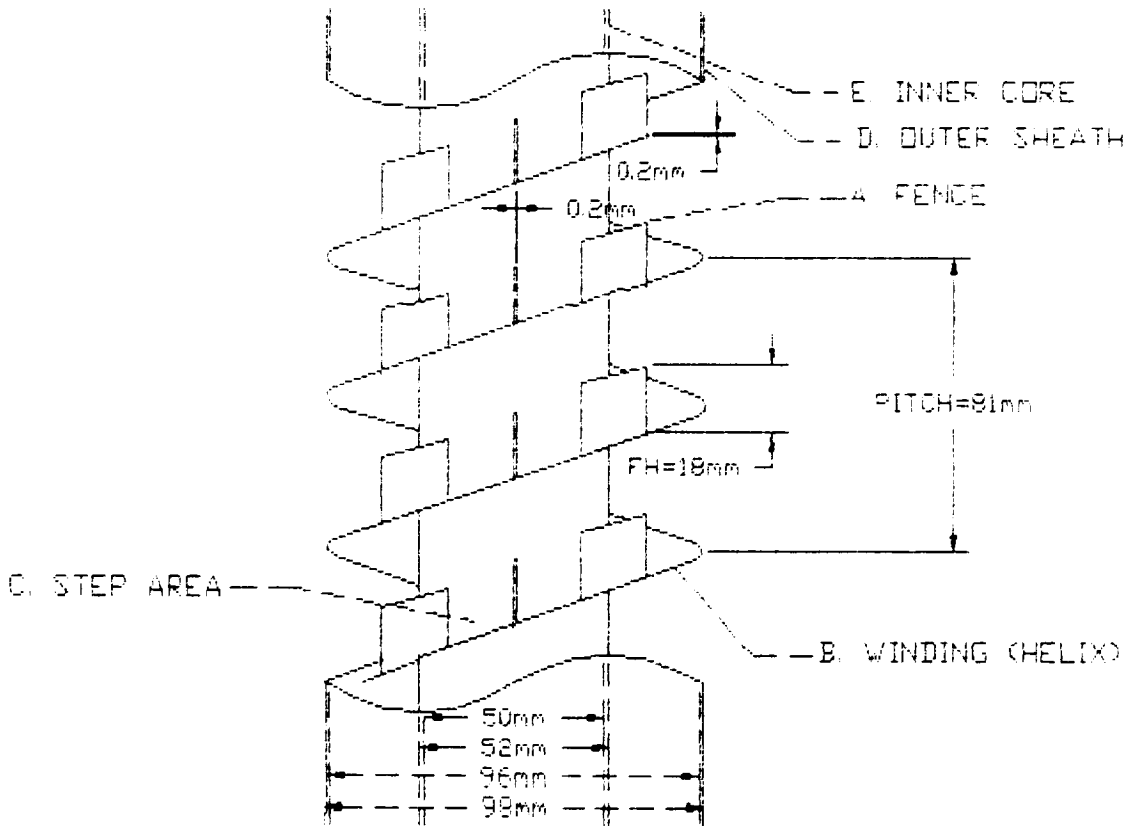

FIGURE 4.2.8.3

OVERVIEW OF A SINGLE ARA WINDING

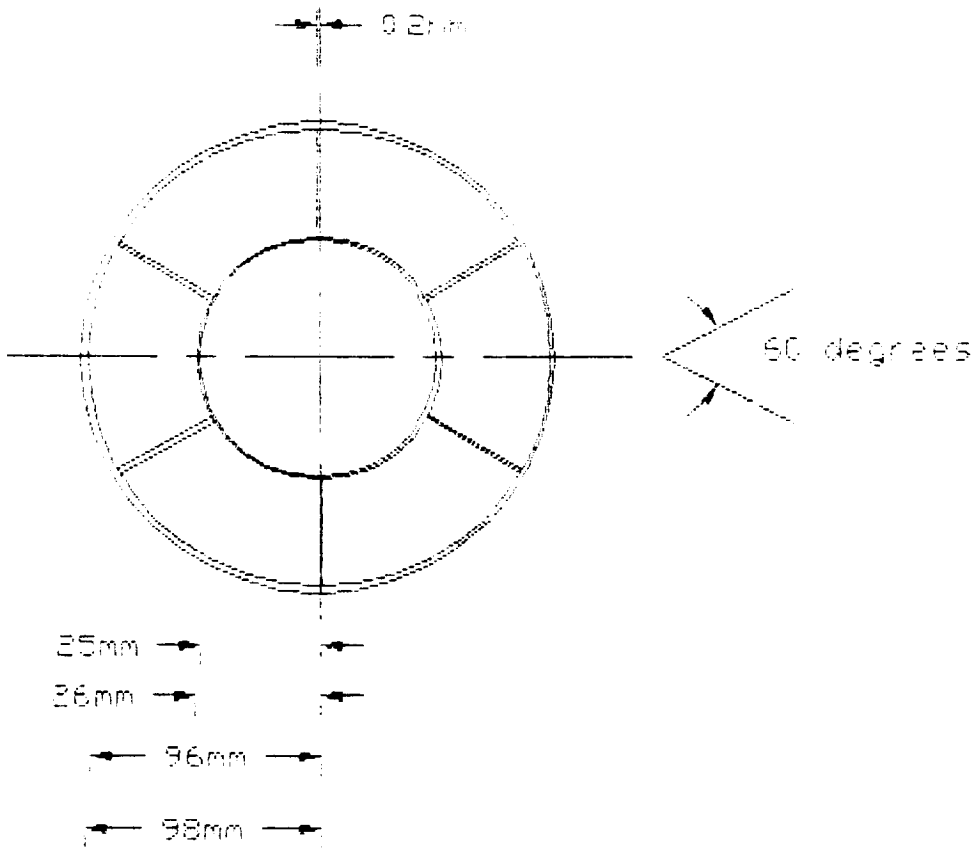

FIGURE 4.2.9.1

UPPER WRA INTERFACE

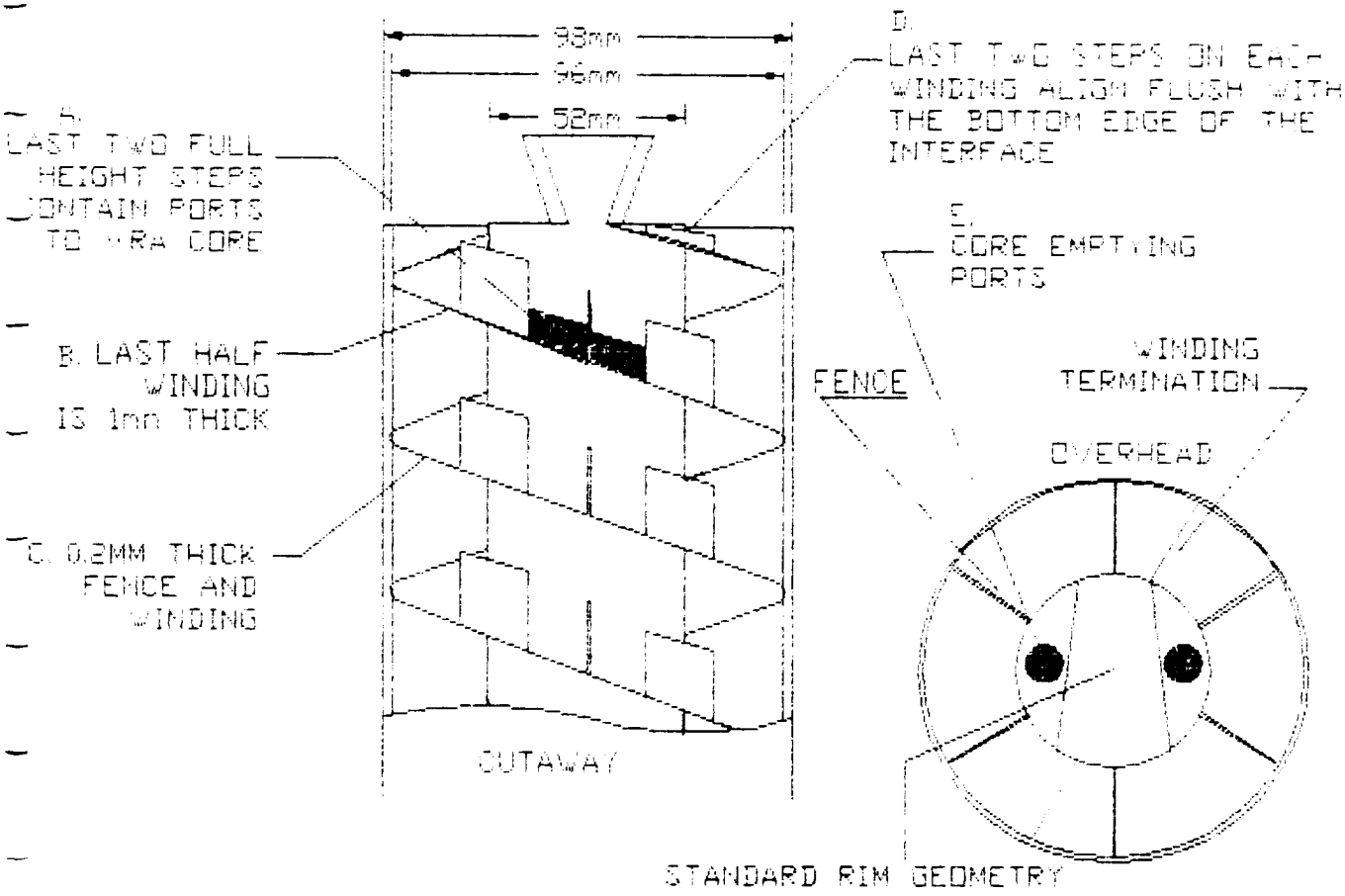

FIGURE 4.2.9.2

LOWER VRA INTERFACE

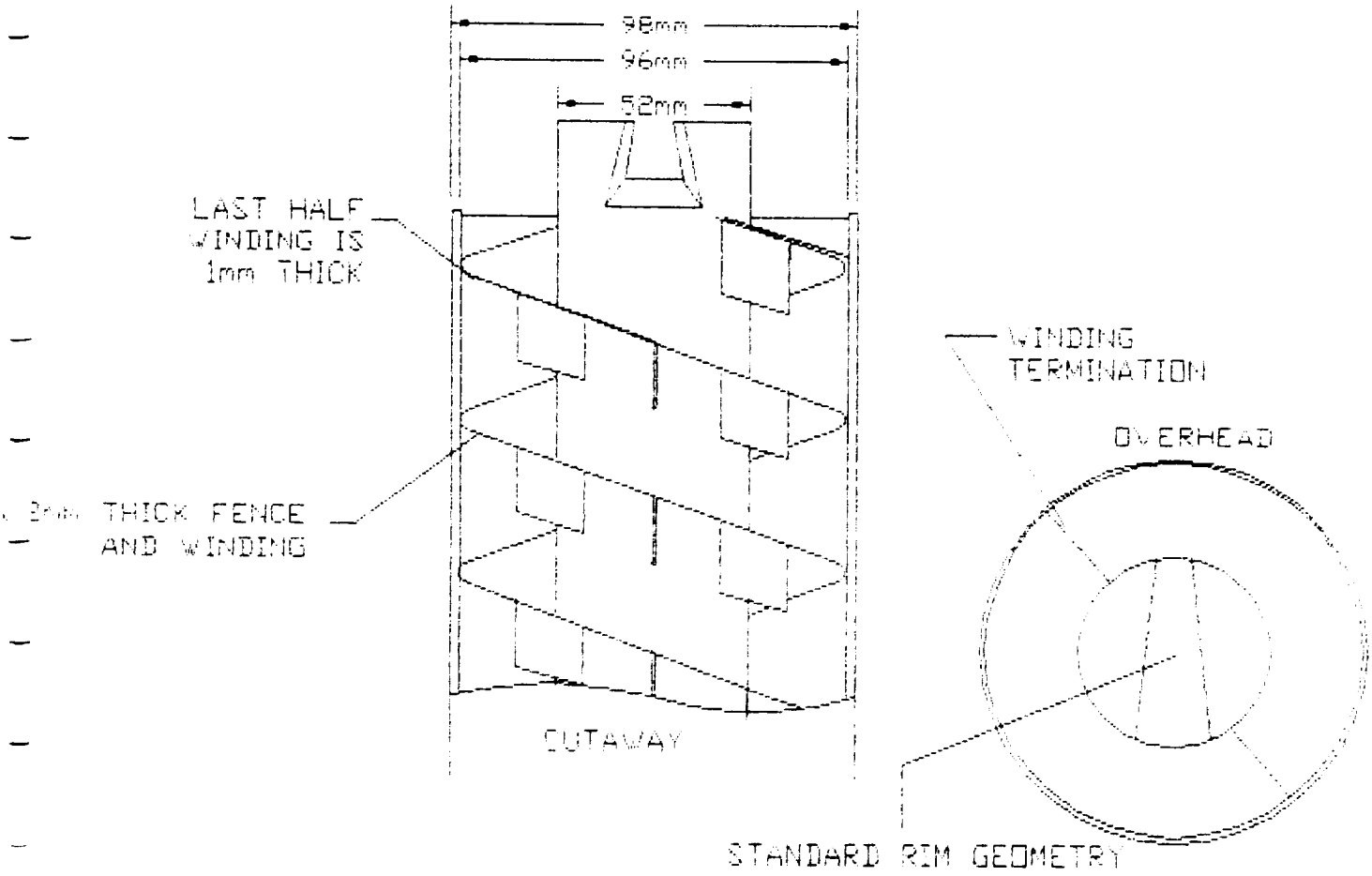

FIGURE 4.2.10.1

AUGER SEGMENT

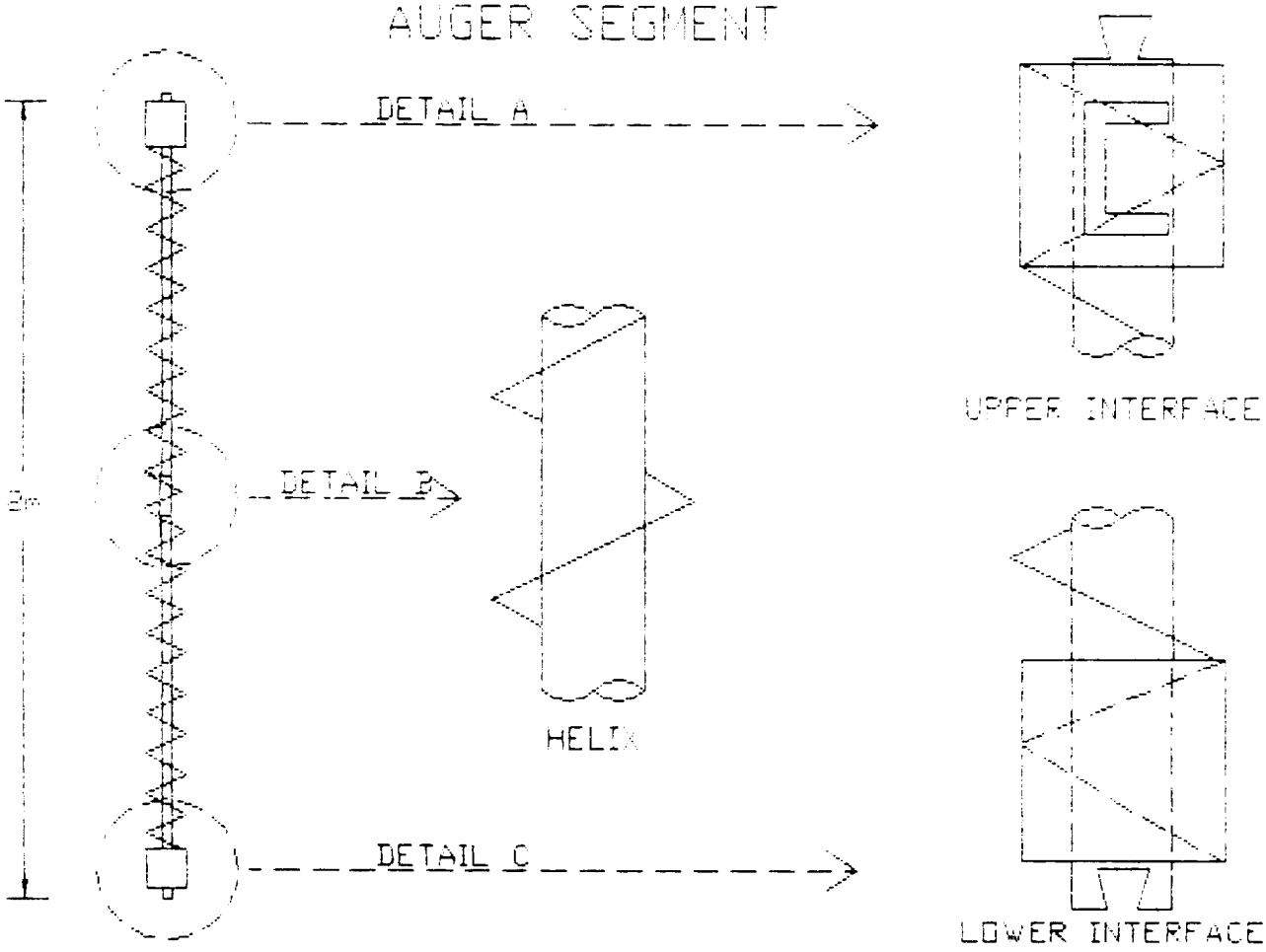

FIGURE 4.2.10.E
AUGER HELIX

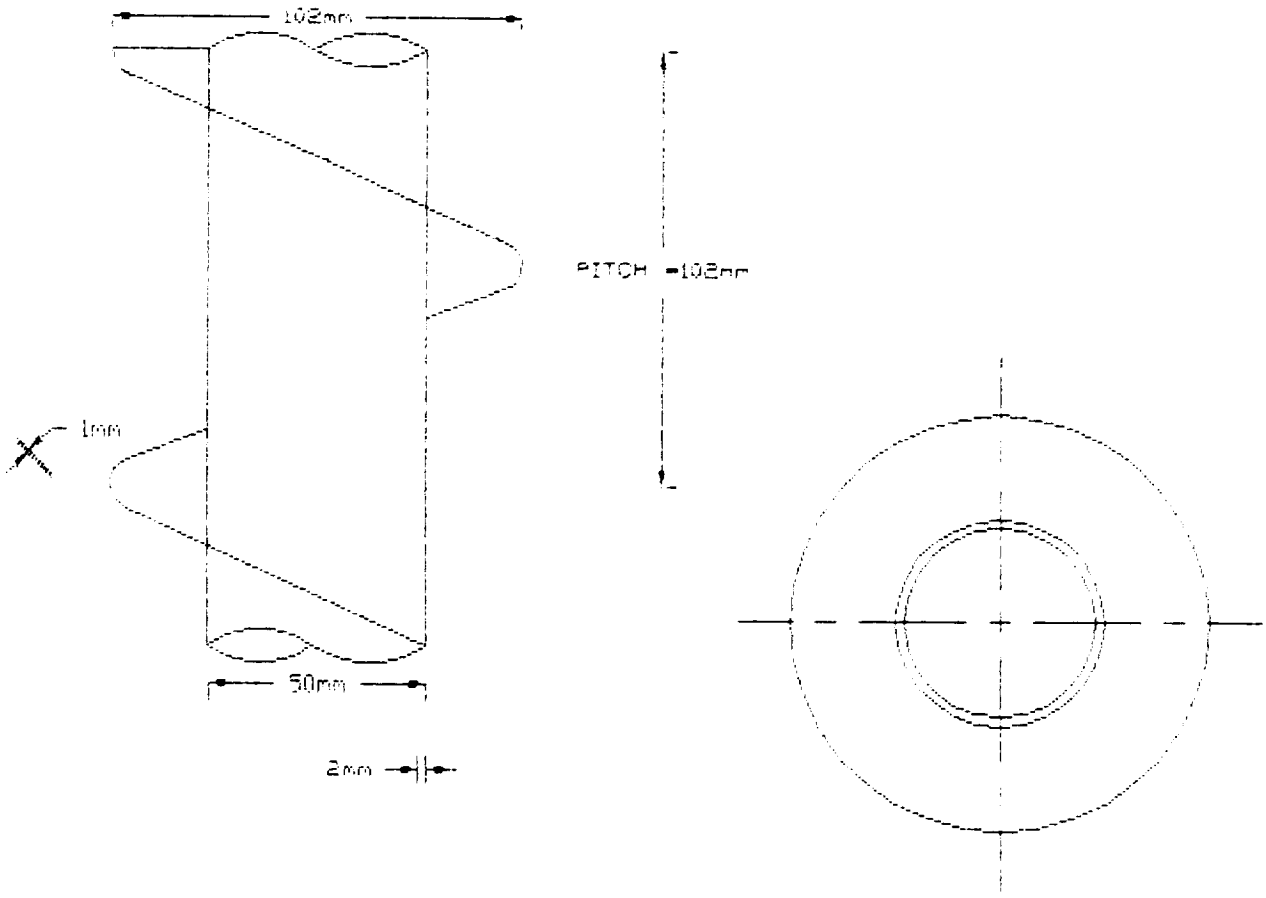

FIGURE 4.2.10.3

LOWER AUGER INTERFACE

CUTAWAY

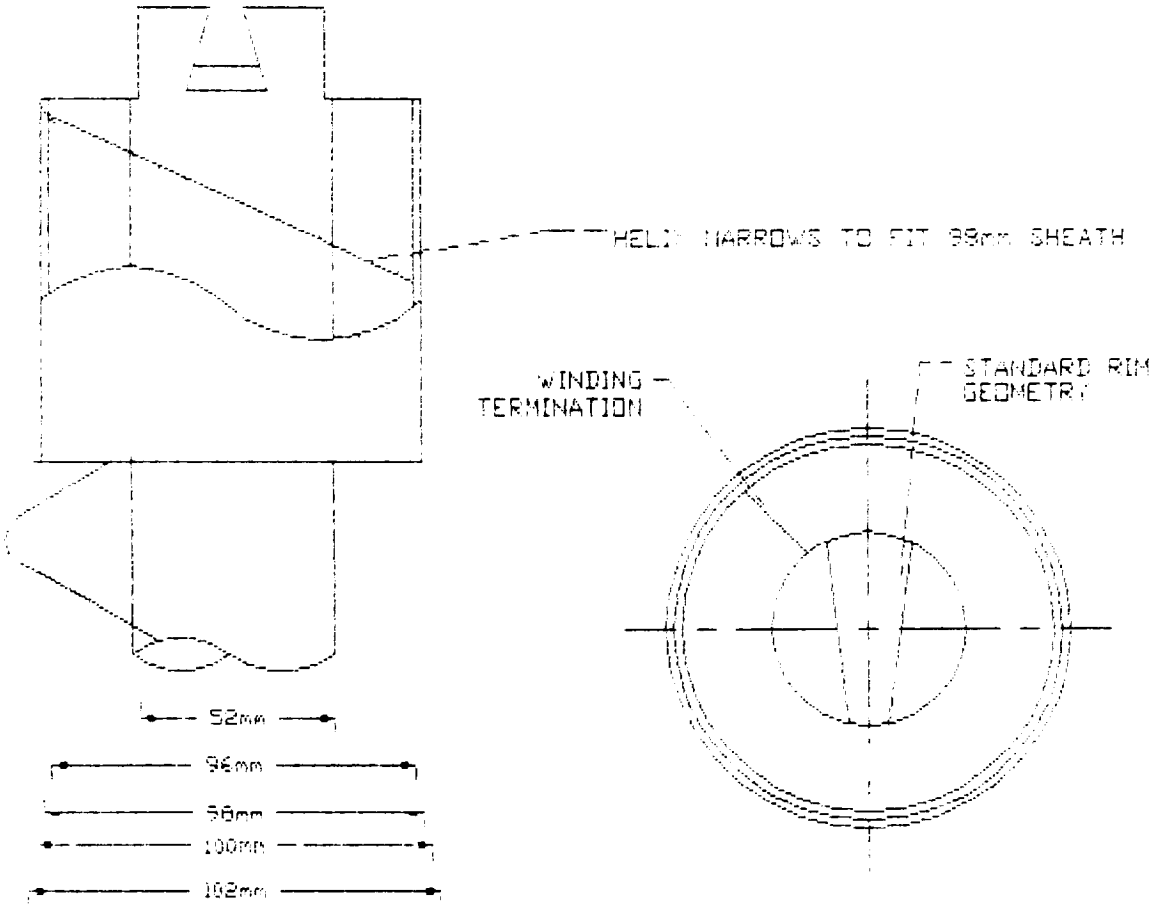

FIGURE 4.2.10.4

UPPER AUGER INTERFACE

CUTAWAY

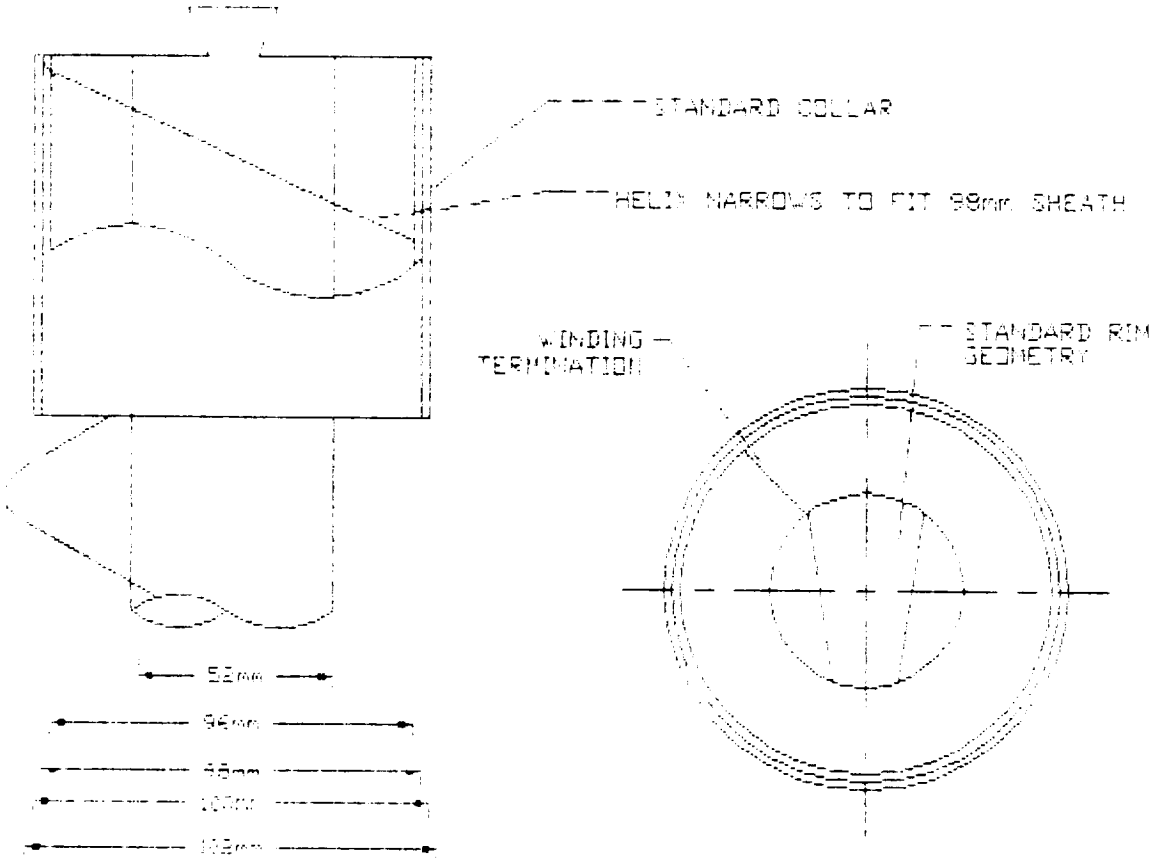

4.3 FOOTPLATE

4.3.1 System Operation

The footplate provides a stable platform for supporting the drill string during rod string addition or removal. For the following description of operation procedure, it will be assumed that the footplate will be stored in the ground with an adaptor rod attached. (This adaptor rod provides the interface between the drill drive and the footplate.) Initially, the adaptor rod with footplate will be attached to the drill drive. SKITTER will squat down on the adaptor rod connected to the footplate to drive the serrated casing as far down into the ground as possible. SKITTER will then screw the footplate counterclockwise into the ground. The serrated casing eases the torque requirements while the base fins on the bottom of the footplate provide torsional stability. Once the footplate has been completely driven into the ground, SKITTER will turn the drill drive 1/2 turn clockwise to release the adaptor from the footplate. The rod changer places the adaptor into the storage rack, retrieves a drill string and connects it to the auger. Drilling may then begin.

As each drill string is driven its length into the ground, a signal is sent to unlock the drive, causing the spring to clamp closed around the drill string. It is the tension in the spring which causes the clamping to occur; no motor power is required in this motion. Once the next string has been added, another signal causes the lifters, operated by a battery-powered motor, to rotate the spring open. The procedure for removal of drill strings is similar. Once drilling operations have been completed, all drill strings and auger sections are removed and the adaptor is reconnected to the footplate by the rod changer. The drill drive will engage with the adaptor and unscrew the footplate from the ground. SKITTER can then walk to the next anticipated drill site and the drill drive can screw the footplate into the ground again. SKITTER can leave the footplate in this position for storage until the new drilling operation is set to begin.

4.3.2 Base

The base houses all working mechanisms of the footplate. Made of aluminum-lithium, it is 550 mm in diameter and 855 mm in height and is welded together. Additional pieces are welded onto the base unless otherwise specified. See drawing 4.3.2.1 for footplate plan and elevation views.

4.3.2.2 Casing

The casing prevents loosely-packed regolith near the surface from collapsing into the newly drilled hole. Originally, variable depth casing which could be cut to size was to be used. After further investigation, however, it was determined that only the regolith 200 mm from the surface was loose enough to pose a problem, so a fixed casing was designed. This casing, 200 mm in length and 120 mm in diameter, is made from aluminum-lithium, like the base, to minimize thermal expansion differences and is permanently attached to the footplate. The bottom of the casing is serrated with four equally-spaced teeth to ease the torque requirements needed while rotating the footplate into the regolith. These four teeth have bottoms to prevent shear failure under torsion. Finally, the exterior of the casing has a double helix thread to further ease the torque requirements necessary to screw the footplate into the ground.

4.3.2.3 Fins

The four fins on the bottom of the footplate are designed to prevent the footplate from being forced out of the ground while drilling operations are in progress. The four fins, equally spaced and triangular in shape, and welded to the footplate base at their top and join the casing at their bottom. (Approximately 10 cm from the bottom of the casing.) These fins provide the torsional stability and are cut out to reduce their total weight..

4.3.2.4 Adaptor

The interface with the drive will be similar to the interface of the drill string. This adaptor will have a special connection to the footplate that will be able to withstand the amount of torque needed to drive the footplate into the ground. The adaptor will be made of aluminum-lithium and will be of the same diameter as the rods (98 mm) so that it may be stored in the rod rack. The interface to be attached to the footplate will be of the pin-groove type. The footplate will contain the grooved (female) section while the adaptor contains the male end, a pin which runs through the diameter of the adaptor rod. The pin will enter the grooved section, rotate through a slot, and lock. This mechanism will allow for the footplate to be suspended from the drive without allowing the footplate to fall. Drawing 4.3.2.2 shows the design of the adaptor.

4.3.2.5 Signalling

A flexible antenna, 500 mm in length, will be mounted to the outer perimeter of the footplate. This antenna can withstand bending motion and will be able to function even while covered with regolith. Accompanying the antenna will be a transmitter box with two relays. The relays, manufactured by Opto, will be solid state, single-pole, single-throw. One relay will turn the motor on and off; while the other relay will enable and disable the locking mechanism in the motor/gear box. A radio frequency signal from the controls group will operate the relays.

4.3.3 SPRING

The spring is the device that grips the drill string or auger while other drill strings are being added or removed. The spring is actually composed of a section of aluminum-lithium which is deflected upward and outward by lifters. It is shaped like a leaf spring with a hole cut in the center and slits cut along both sides of the hole and is similar in operation to a speed washer. (A drawing of this can be seen in the appendix as Figure 4.3.) The spring is 1.5 mm thick, 200 mm wide, and 500 mm long. In the closed position,

the two sections of the spring are flat and separated by a distance of 100 mm so the drill string can be tightly gripped. Figure 4.3.2 shows an elevation view of the spring in the closed position holding a drill string. In the fully open position, the two sections of the spring are separated by a distance of 120 mm allowing a 1 cm leeway on either side of the opening to account for stray drill string motion. Figure 4.3.1 shows a side view of the footplate with the spring in the open position. The upper section of the spring is reinforced by aluminum-lithium ribs to help prevent buckling and fatigue failure.

4.3.3.1 Grippers

Grooved aluminum-lithium pads on the ends of the spring grasp grooved sections on the drill string couplings to increase gripping capability. These pads are rounded to follow the contour of the strings and the auger and are 25 mm in length so that the auger can be held in a stable position. The grippers are welded to the center tongue of the spring.

4.3.3.2 Spring Support

In addition to spring stops, the spring will be supported by ribbing which runs the whole length of the deflecting flanges. Two equally-spaced lengthwise ribbings will reinforce the flanges and will help prevent the spring from overflexing.

4.3.3.3 Spring Stops

The base contains aluminum-lithium stops underneath the spring to provide additional support to the spring material and to help prevent the spring from overdeflecting. These stops, rectangular in cross-section and 20 mm in width, are placed at the lip of the spring opening and are welded to the base structure. They are curved in shape to closely fit to the spring opening. The stops are placed 5 mm from the grippers creating a cantilever arrangement.

4.3.4 Lifters

The lifters are the mechanisms which cause the spring to deflect open and, therefore, release the drill string. The deflection mechanism for the spring will be similar in operation to a camshaft in an internal combustion engine. The lifter lobes are actually arms connected to a shaft with a roller at the end which is in contact with the spring. These lobes will act on each side of the drilling hole. There will be a dry sealed roller bearing at the end of the lifter. The roller bearing reduces the amount of torque required to turn the lifters because the sliding motion is replaced by rolling motion. The two lifters will be connected by a solid shaft which runs just outside the radius of the drilling hole. The shaft will be mounted in brass bushings at each end. One end of the shaft will be connected to a motor with a sealed internal gear reduction mechanism. The force required to lift the spring was calculated to be 41.95 N and the lifter must raise the spring 38.3 mm up at the center.

4.3.5 Motor

A motor will be used to turn the shaft that lifts the spring to release the rod string. The motor will be a Micro Mo Electronics, Inc. Gearhead Series 34PG. Within the motor's sealed casing is an internal gear reduction set which reduces the torque and size requirements of the motor itself. There will be a sealed output shaft from the gearbox that is connected to the shaft. The operating temperature range of the motor is from -55 C to 125 C, so a molybdenum blanket will be used to insulate the motor. Also, the footplate will be covered in insulating regolith soon after drilling operations begin, further protecting it from extremes in temperature.

The motor and gear set, weighing a total of 451 grams, can provide a maximum torque of 3.5 N-m at the output shaft. The gear ratio is 1080:1 and the motor assembly is 87.33 mm long. The motor

will be connected to the base by mounting threads which are on the front of the gear reducer.

4.3.6 Power Storage

It is assumed that the power required to operate the transmitter and relays is relatively negligible compared to the power required to operate the motor. To power the motor, four Whittaker-Yardney #LRO5 Silvercels were chosen. These will be connected in series to provide a total of 0.5 Amp-hrs. At 6.0 V (1.5 V each), these cells are suitable for long life and low-rate use. A recharge will not be required in 50 holes. The total mass of the four cells is 0.0817 kg and the cells will occupy a space of 1505 mm^2 at a maximum height of 39.62 mm (including terminals). The batteries will also require an insulating molybdenum blanket to protect them from temperature extremes.

4.3.7 Materials

Aluminum-lithium alloys are best known for their low density and corrosion resistance. Electrical conductivity, ease of fabrication, and appearance are also attractive features. Aluminum-lithium alloys are part of a class of alloys known as high modulus alloys, isotropic metallic materials having a specific modulus higher than that of conventional aluminum, titanium, or iron base alloys. The weight saving potential of aluminum-lithium is now widely recognized and significant improvements in production capabilities and mechanical properties of alloys produced on a commercial scale have been achieved in the last two years.

In a solution treated condition, some aluminum-lithium alloys have low strength but high ductility which allows considerable cold forming. Strength can be increased substantially by aging, especially if the material has been cold worked before aging. Al-Li castings with good surface quality can be made under controlled conditions.

The particular aluminum-lithium alloy chosen was aged Weldalite, an alloy produced by Martin-Marietta. This alloy has suitable properties for the footplate design and can be welded to satisfaction, a problem with some of the aluminum-lithium alloys. See Table 2 for the range of properties of this alloy.

4.3.8 Analysis

See following pages for analysis.

4.3.9 Mass Analysis

See Table 1 for weight calculations.;

4.3.10 Regolith Protection and Removal

The drilling of a 50 m deep hole will involve removing 0.29 m^3 of regolith and depositing it upon the footplate. This amount of material would weigh about 465 kg and posses a lunar weight of 760 N. This volume and mass of cuttings could severely impair the operation of the footplate. The dirt could all pile on top of the spring mechanism either crushing it or rendering the motor useless under the weight. These cuttings may also find their way beneath the spring causing it to remain partially open and reducing the effectiveness of the grippers clamping ability. To avoid this problem a cylindrical bellows will be utilized between the base plate and the spring to keep the cuttings from getting underneath the spring. The bellows will be made of a high nickel alloy such as Mech metal with properties maintained in temperature ranges of -350 C to 250 C. Furthermore, a structural cover will be used to support the cuttings over the spring device and keeping the footplate operational.

4.3.11 Failure Analysis

Unfortunately, there are few parts on the footplate that can fail and still allow the footplate to continue operating properly. No

redundant systems have been incorporated into the design. Should any part of the motor or gearbox fail drilling operations would come to an abrupt halt. If the shaft, a lifter, a roller, a relay, the transmitter, or the spring fail, the result will be the same. If a fin breaks off of the bottom of the base there would only be a slight balance problem, but drilling can continue. If the casing should break in some way the extent of the setback will depend on the severity of the damage, and the footplate might again be slightly unbalanced. If the adaptor breaks drilling can not continue past the hole that the footplate is currently in. Should a cell in the battery go bad the voltage output will be reduced by 1.5 volts, and more power will be drawn out of the battery . If a cell goes bad early enough in the drilling operations, a dead battery might bring a premature ending to the operation of the footplate, and, therefore the drilling.

FIGURE 4.3.1

SIDEVIEW OF FOOTPLATE WITH

SPRING OPEN

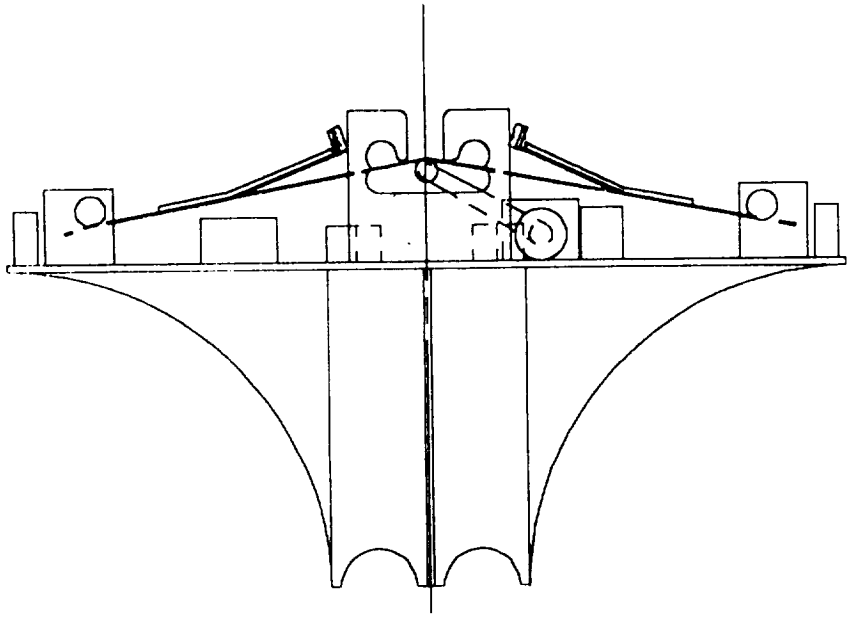

FIGURE 4.3.2

ELEVATION VIEW OF SPRING

CLOSED ON DRILL STRING

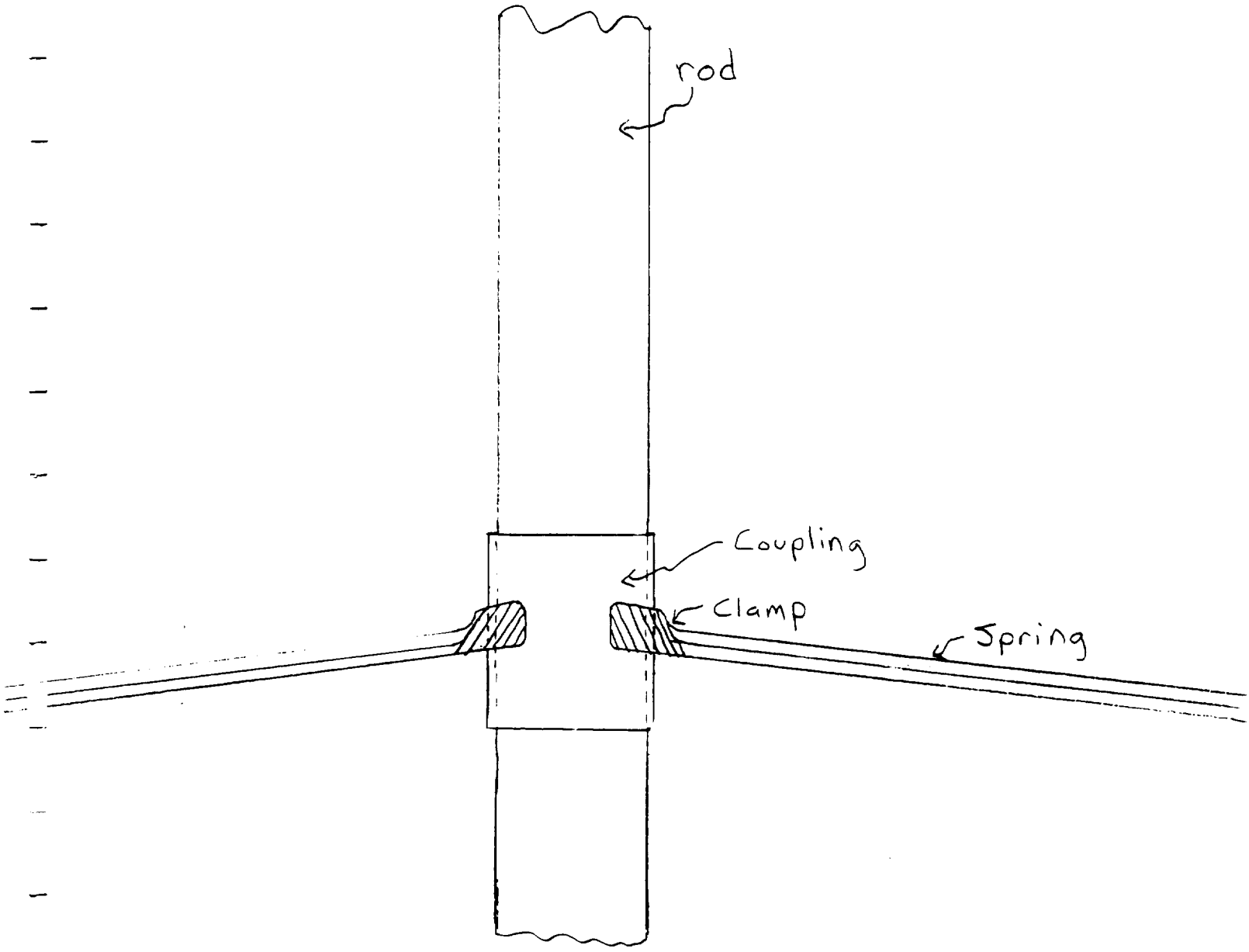

4.4 POWER SUPPLY, ROTARY DRIVE, AND HEAT MANAGEMENT

This section addresses the power supply, motor, and heat management requirements of the lunar deep drill. Figure 4.4.a is an outline of the design process used for these elements. Power will be supplied by a hydrogen-oxygen fuel cell. This system, which has been used on the Space Shuttle Orbiters, has an output range of 2 to 12 kilowatts. This will adequately supply the maximum of 10 kilowatts necessary for the worst case scenario; however the fuel requirements were designed for a normal operating point of 4 kilowatts of power output since the drill motor was designed to operate at 2.81 horsepower and 300 RPM. This design point may be too low for successful operation of the drill due to a lack of communication between design groups regarding power requirements near the end of the project. The on-board hydrogen and oxygen supplies will be contained in external cryogenic tanks which will be re-filled between drilling operations. Excess heat generated by the power supply will be conducted away by two heat pipes and dissipated to deep space by two radiator panels located on the periphery of the implement.

The drive mechanism for the drill will be the newly-developed Curvo-Synchronous Motor (CSM), which has only one moving part, operates at temperatures up to 350 degrees F, and has an efficiency of 91.3%. Heat generated by the motor will be transferred to a thermal radiator by a single heat pipe. The heat pipe will also act as a thermal diode to protect the motor if the radiator panel should overheat. The radiator panels will be oriented toward deep space by the positioning of SKITTER at the drilling site. Finally, a torque-limiting friction disc clutch has been incorporated into the design to protect the motor in the event of drill bit lock-up. This clutch will "run free" at an overload torque of 80 ft-lbs and will automatically re-engage when the overload has been removed. Two different 3-

dimensional views of the components from this section are shown in Figures 4.4.b and 4.4.c, and a plan view is included in Figure 4.4.d.

4.4.1 Power Supply

The design of the power supply system for the lunar deep drill apparatus (LDDA) involved fulfilling many of the general design criteria for the implement as a whole such as minimum weight, manageable volume, durability, and ability to operate in the lunar environment. The basic concept of the power supply system as a whole was that the power supply on-board the implement would serve as a temporary source which would be recharged or replaced by an external source, such as a solar array or some other outside source. The specific requirements of the on-board power supply were that it be compact enough to fit into the implement, be light enough to be portable, and that it be able to supply enough power to drill at least one complete 50 meter hole without needing to be recharged or replaced. A hydrogen-oxygen fuel cell power plant was the device chosen to provide the necessary power to the LDDA. Its relative light weight, durability, low maintenance requirements, and operating characteristics made it the obvious choice. The only other feasible alternative was the use of rechargeable batteries, which ultimately proved to be far in excess of the weight limitations of the project.

By summing all of the power requirements of the various groups, the capacity of the power supply system was set at 100 kilowatt-hours. The fuel cell power plant design chosen was one that has already seen extensive use on the Space Shuttle Orbiters. This system, manufactured by United Technologies, is capable of delivering power from a minimum of two kilowatts to a peak output of twelve kilowatts, and has physical dimensions and weight that are suitable for use in such an application. The total power output requirement during the entire drilling operation occurs during the

actual drilling of the hole when the motor will require four kilowatts of power. The length, width, and height of the power plant are 35 cm x 38 cm x 101 cm, and it weighs 91 kilograms. These dimensions and weight apply only to the power plant; the fuel for the power plant will be contained in external cryogenic tanks, and the by-product water will be collected in its own tank.

The fuel cell power plant that will be used essentially involves a reaction between hydrogen and oxygen which can be characterized as reverse hydrolysis wherein the reactants are combined to produce electrical energy and water as a by-product. In addition to producing the desired power for the drilling operation, the power plant will produce roughly 1500 watts of excess heat that must be dissipated. This heat will be conveyed through heat pipes to radiator panels for dissipation. The power plant and the necessary tanks are shown schematically in Figure 4.4.1.1 inside the skeletal structure of the implement. The power plant consists of three basic parts: the fuel cell stacks, the control and electrical components, and the necessary plumbing to convey the fuel and water to and from the plant, respectively. The heart of the power plant is a pair of two parallel stacks of fuel cells in which the hydrogen-oxygen reactions occur. At the operating point of four kilowatts, the cells are capable of producing 31.5 volts. This particular power plant is designed to operate as an unregulated direct current source and any necessary power conditioning must be done on the output of the power plant before it is used. Recent developments in power semiconductors have made this requirement possible as the technology available to date allows for the conversion from a D. C. source to an alternating output if such output is mandated. However, for the purposes of operation of the LDDA, only an increase in the output voltage of the power supply is required.

The capacity of the power supply depends solely on the quantity of fuel available on-board the LDDA at any given time. Therefore, by adjusting the reactant tank sizes, a similar adjustment of the capacity of the power system results. At an operating point of

four kilowatts of output, the power supply will consume 0.087 pounds of hydrogen per kilowatt-hour, 0.69 pounds of oxygen per kilowatt-hour, and will produce a maximum of 3 pounds of water per hour of operation. For the complete drilling of one hole, the total fuel requirements will be 17.4 pounds of hydrogen, 69 pounds of oxygen, and the amount of by-product water will be 75 pounds of water. Using this data, the necessary tank capacities were determined to be 0.5585 cubic meters for the hydrogen tank, 0.0275 cubic meters for the oxygen tank, and 0.034 cubic meters for the by-product water tank.

Using the given tank capacities and the space limitations of the structure, cryogenic tanks for the reactants were designed as well as a holding tank for the by-product water. Since little information was available on cryogenic tank design, a rigorous design for the reactant tanks was not possible; however, some recommendations on the tank design are in order. First, a selection of materials is necessary for the actual pressure vessel. Probably the leading choice is a Kevlar composite or due to its high strength, and its light weight. The insulating material should be a multi-layered reflective coating such as mylar with a metallic coating such as aluminum. One way to gain the best insulating characteristics for such a material would be to fabricate corrugated sheets and alternate the orientation of successive sheets. In this manner, the highly desirable insulating properties of a vacuum can be used to an advantage. Finally, the layout of the pressure vessel should be designed so as to minimize any stress concentrations that might occur because of improper geometry. Bearing these requirements and considerations in mind, an effort was made to calculate a rough estimate of the size required for each of the reactant tanks. In order to minimize both space limitations and possible stress concentrations within the tank, a cylindrical tank geometry with hemispherical ends was chosen. It was assumed that three inches radially would allow enough space for both the pressure vessel and the mylar insulation. In addition, it was decided that when the tanks were filled to desired capacity, that an additional five percent of tank capacity should be left to allow for

venting of reactants in gaseous form for emergency temperature maintenance if necessary. Using these requirements, the sizes of the reactant tanks were calculated as follows. Since the size of the tanks and hence the structure that contains them should be minimized, a minimum diameter was sought which would allow this minimization of space within the structure. The dimensions of the base of the structure were predetermined by the structures group (See Section 5). Using these dimensions, it was seen that a maximum length for the tanks was 1.23 meters or slightly more if the tanks were going to fit between the motor and one side of the structure. Using this length as a constraint for the larger tank size, a determination of the diameter was made using the following relation between the tank volume and the size of the tank which was characterized by the length of the cylindrical section and the radius of the cylinder and hemispheres.

$$V = (\pi)(R^2)(L) + (4/3)(\pi R^3)$$

After successive iterations, the final hydrogen tank dimensions were determined to be

L = 31.24 inches
R = 8.86 inches.

Once the radius of the cylindrical section was set, the length of the oxygen tank was determined by simply rearranging the equation to solve for the length. The resulting dimensions of the oxygen tank are therefore

L = 14.40 inches
R = 8.86 inches

Finally, the minimum volume for the water tank which was given earlier calls for an tank size which will include the necessary insulation and heating capability to maintain the waste water in a liquid state. It is recommended that the water reservoir be insulated in the same fashion as the reactant tanks and that heating of the tank to avoid freezing of the water be accomplished by resistive heaters built into the tank. In this manner, temperature

management can be closely monitored and adjusted by the on-board PLC (See Section 8). Based on this recommendation a cubic tank 45 cm on a side should be large enough to accommodate both the required capacity as well as the insulation and heat controls.

4.4.2. Motor

When choosing a motor to operate the drill string, several aspects had to be considered. First, the efficiency of the motor was crucial. Low efficiency means that much excess heat will need to be dissipated. Due to the negligible lunar atmosphere, this heat cannot be convected away. With only conduction and radiation left, a highly inefficient motor would pose serious problems. In addition to thermal considerations, physical limitations also had to be taken into account. The motor fits onto the supporting structure attached to the bottom of SKITTER. Weight is minimized so the LDDA can easily be picked up and transported by the walker. The power was determined by finding the torque necessary for successful drilling. The normal operating torque, assuming that there is no friction on the sides of the drill string, is :

$$T = (f)\ (W)\ (r)$$

where: T is in ft-lbs
W is in lbs
r is in (ft)

Therefore ...

$$T = (1.5)\ (200\ \text{lbs})\ (1.96/12\ \text{ft}) = 49.21\ \text{ft-lbs}$$

and at the normal operating speed of 300 RPM...

$$HP = (49.21\ \text{ft-lbs})\ (300\ \text{RPM})/(5252)$$
$$HP = 2.81\ \text{horsepower}$$

Considering these parameters, the choice was the recently-developed Curvo-Synchronous Motor (CSM). This motor was developed by Dr. Kent Davey from the Electrical Engineering Department at the Georgia Institute of Technology. The CSM has many desirable characteristics. The motor has only one moving part so that inertia and friction losses are small. The innovative winding scheme is such that the flux path between the magnets is minimized. See Figure 4.4.2.3 for a schematic of the CSM. Due to the radial positioning of the magnets, a large number of thin magnets can be used thus providing a thin disc-like shape. Efficiencies of 95% to 98% are not uncommon and the motor runs at temperatures up to 350 degrees F. Conventional permanent magnet motors were rejected for the same reasons that the CSM was chosen. They usually have a low efficiency of 30% to 50%, weigh a lot, take up more room, and are less tolerant of heat.

The particular motor that will be used is a 5 horsepower CSM. The 5 horsepower will accommodate some of the extreme values seen in Appendix A yet provide smooth operation at the normal operating speed and torque of 300 RPM and 49.21 ft-lbs, respectively. A torque limiter set at 83.3 ft-lbs will prevent motor overload, see 4.4.5, Friction Clutch, for details. Because the CSM is a direct drive system, a thrust bearing is included in the the design to transfer applied loads to the frame of the motor. A diagram of this thrust bearing is shown in Figures 4.4.2.6 and 4.4.2.7. The CSM's load characteristics appear in Figure 4.4.2.1 and its current characteristics appear in Figure 4.4.2.2. See calculations in Appendix A for the details of these two graphs. The motor has a diameter of 18 inches, a thickness of 2 inches, and weighs approximately 40 pounds according to Dave Ross, a CSM specialist from the VA Hospital in Decatur, Georgia. The efficiency of this motor was found by multiplying the winding resistance, R, by the square of the current, I. In this case, 933 volts and 4 amps are required. So ...

Heat loss = (22.135 ohms)(4 amps^2) = 354 Watts

The efficiency is then ...

n = (3730 Watts)/(3730 + 354 Watts) = .9133 = 91.33 %

where:

3730 Watts is input power
354 Watts is power loss

To dissipate the 354 Watts of excess heat, we employ a "sheath" of a highly conductive aluminum alloy which covers the sides motor. A heat pipe is then used to transfer this heat to a radiator panel. This motor mount and flange can be seen in Figures 4.4.2.4 and 4.4.2.5 and also provide for the mounting onto the supporting structure. The materials used for the "sheath" were an Aluminum alloy, 1199, and a Titanium Beta alloy. The justification for this choice is simple. First, no heat should be radiated to SKITTER; it should all be conducted to the heat pipe for proper disposal. With this in mind, a material with a low thermal conductivity and emmisivity value was needed for material "B" and a highly conductive material, Aluminum, was needed for material "A", refer to Figure 4.4.2.4. Secondly, the materials must have similar coefficients of thermal expansion to permit welding. The two materials that satisfied these criteria are AA 1199 O and Ti Beat Alloy. The Aluminum alloy has a linear coefficient of thermal expansion of 13.3/deg F x 10^6 and a thermal conductivity 1540 BTU/ft^2(h)(in.)(deg F) while the Titanium alloy has 10.1/deg F x 10^6 and 119 BTU/ft^2(h)(in.)(deg F). This arrangement will inhibit heat radiation towards SKITTER's under-belly, with the help of a coating on the Titanium alloy, and promote conduction to the heat pipe. Dissipation of heat is crucial because the CSM is not operable at temperatures exceeding 350 degrees F. For further details, see sections 4.4.3, Heat Pipes, and 4.4.4, Heat Radiation.

4.4.3 Temperature Management

Three heat pipes will provide proper temperature control of the CSM and the fuel cell power plant.

Heat Pipe Concept

The heat pipe is a device with an effective thermal conductivity of as much as 500 times that of copper. This property makes it especially suited for applications in which a large amount of heat must be transferred from one area to another. Figure 4.4.3.1 illustrates the basic concept for a standard heat pipe. The three basic elements are the working fluid, the porous capillary wick, and the outer pipe structure. The wick is saturated with the liquid phase of the working fluid and the remaining volume of the tube contains the vapor phase. Heat applied at the evaporator vaporizes the working fluid in that section. The resulting difference in pressure drives the vapor from the evaporator through an adiabatic section to the condenser where it condenses thus releasing heat and energy. The liquid enters the wick surface where a capillary pressure is developed. This capillary pressure pumps the condensed liquid back to the evaporator where the process can begin again. This passive heat exchange process can continue indefinitely if the heat pipe is properly designed.

Some of the advantages of utilizing heat pipes to regulate the temperatures of the motor and the power supply are:

a. Heat pipes are able to transfer high heat fluxes with small temperature gradients. A heat pipe is therefore very nearly isothermal and close to the saturated vapor temperature at all times.

b. Heat pipes do not require any external pumping power. Fluid movement is due solely to capillary forces rather

than gravitational forces in returning the condensed liquid to the evaporator.

c. The heat pipe can act as a thermal diode (i.e. operation in one direction only). This allows for the heat pipe to "shut off" if the heat sink or condenser side becomes hotter than the heat source side. This can be achieved by an adequate design of the wick configuration such that the liquid capillary pumping exists in one direction only.

d. The heat pipe can be manufactured into many common shapes (i.e. rectangular and circular) and can be bent or flexed to accommodate unusual geometries. The flexibility feature will be used in this design.

e. The absence of gravity allows it to be more efficient lending it to be advantageous in space applications.

A limit to its heat transport capabilities is the largest disadvantage of a heat pipe. These limitations are due to:

a. capillary pumping ability,

b. choking of the vapor (i.e. sonic limitation),

c. tearing of liquid off the liquid-vapor interface by vapor flowing at high velocity (i.e. entrainment limitation), and

d. the disruption of the liquid flow by nucleate boiling in the wick (i.e. boiling limitation).

These limitations will determine the requirements for the optimal design of the three basic elements of the heat pipe; the working fluid, the wick, and the pipe structure.

Design of the Heat Pipe

The design procedure used is outlined below:

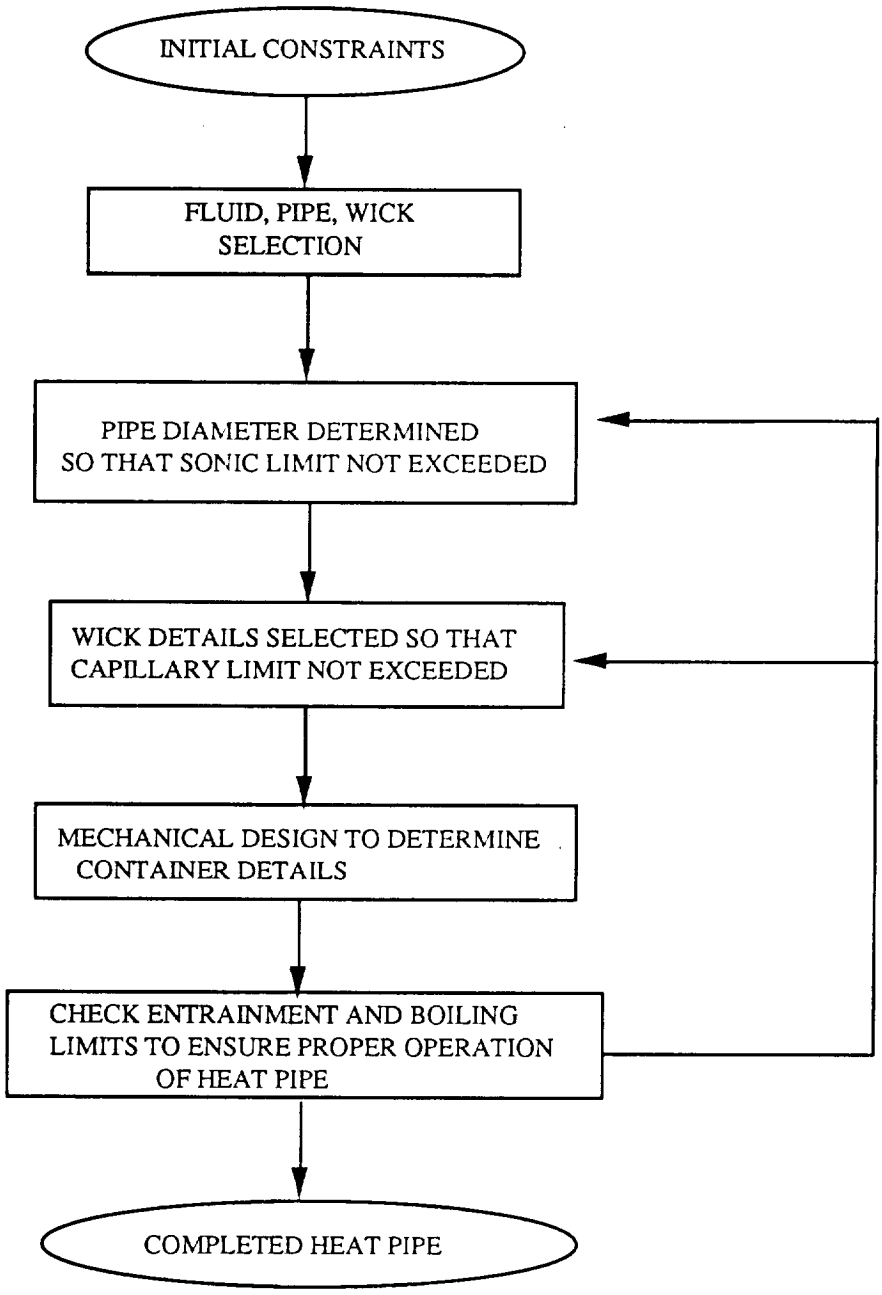

The geometry of the heat pipe will be the initial constraint for its design. A circular cross section with flat circular end caps is the chosen geometry for this design. It is the most common and easiest to manufacture. The first heat pipe to be designed will be the one which removes the excess heat developed by the motor. Then by simply following the same steps, the two heat pipes for removal of waste heat from the power supply will be accomplished. Figure 4.4.3.2 illustrates the space requirements for the heat pipe for the motor. The heat pipe will be wrapped around the motor so that temperature management over the entire surface of the CSM will be properly controlled. The peak power output of the CSM's power cycle will not exceed 5 horse power. With an efficiency of 91.33 %, 346 Watts must be adequately dissipated. The temperature of the CSM will be operated at 212F to ensure safe operation. We have assumed that the heat will be generated uniformly by the CSM so that the required dissipation of heat is shown below:

(346 Watts) x factor of safety of 2 = 692 Watts

The heat pipe will be 173 inches long so it may work in coordination with the radiator located 59 inches away in the rod rack. The radiator will be used as a heat sink which will be discussed in more detail in the next section. The evaporator and condenser section will have a length of 61 inches and 56 inches, respectively. Because of the width of the radiator, the overall diameter of the heat pipe cannot exceed 1.5 inches. Three U brackets with corresponding pop rivets will be used to connect the heat pipe to the sheath of aluminum about the CSM. Similarly, two such brackets will hold the heat pipe to the radiator panel.

For the successful operation of a heat pipe, its working fluid must have a melting point temperature below and a critical point temperature above the pipe operating temperature. For a pipe

operating at 212F, water, methanol and ammonia are suitable working fluids. The capillary limitation equation will be used to determine the most suitable liquid. The capillary limitation represents the required pressure balance at the liquid side of the liquid-vapor interface in the wick. An expression for capillary limitation on the heat transport factor $(QL)_{c,max}$ is represented by:

$$(QL)_{c,max} = 2\left(\frac{\sigma\rho_l\lambda}{\mu_l}\right)\left(\frac{k}{r_c}\right)(2\Pi r_v t_w)$$

$\sigma\rho_l\lambda/\mu_l$	– liquid transport property
k/r_c	- wick property
$2\Pi r_v t_w$	- wick cross sectional area

The larger value of the heat transport factor will thereby give a larger upper capillary limit. The heat transport factor is directly proportional to the the liquid transport factor. Water has a larger liquid transport factor and has higher conductance properties than methanol or ammonia. Therefore water has been chosen as the working fluid. According to Professor Gene Colwell at the Georgia Institute of Technology, freezing of the water during the lunar night will not pose a problem to the heat pipes performance. The heat pipe will act as a heat sink when the temperature falls below 32F. As the temperature rises due to the operation of the CSM, normal operation of the heat pipe will resume.

Selection of the pipe and wick material depend largely on their compatibility with the working fluids. Two major concerns of incompatibility are corrosion and the generation of noncondensable gas. Solid particles from corrosion may be transported with the flowing liquid to the evaporator region leading to an increased resistance to fluid flow. The generation of gas will have the effect of inactivating a portion of the condenser. Copper, nickel, and titanium are compatible materials for a water pipe. Copper is chosen because of its superior conductance properties to nickel and titanium and to its relative low cost.

The size of the pipe diameter necessary for a given application should be determined so that the vapor velocity is not excessive. At high Mach numbers, the compressibility of the flow of vapor may cause choking to occur. Therefore, the heat pipe will be designed so that its maximum Mach number does not exceed 0.2. Incompressible and laminar flow can now be assumed and the sonic limitation is immediately satisfied. Under these conditions the required vapor core diameter is determined by:

$$d_v = \sqrt{\frac{(20\ Q_{max})}{(\Pi \rho_v \lambda \sqrt{\gamma_v R_v T_v})}}$$

The vapor core diameter is:

$$d_v = 0.10 \text{ inches}$$

with a sonic limitation of:

$$Q_{s,max} = 4.27 \times 10^6 \text{ Watts.}$$

The capillary limitation is the most common of the four limitations. During normal operation of the heat pipe, vapor and liquid flow past each other separated only by the wick. There exists a pressure gradient called the capillary pressure along this liquid-vapor interface. The capillary limitation on the heat transport factor was determined by:

$$(QL)_{c,max} = \frac{Pcm}{F_l - F_v}$$

and represented by Figure 4.4.3.4, Figure 4.4.3.5, and Figure 4.4.3.6 of Appendix A. This relationship yielded the following wick dimensions:

Mesh number (N) = 250 $inch^{-1}$
Wick area (A_w) = 0.9818 $inch^2$
Wick diameter (d) = 0.0016 inches

with a capillary limitation of:

$$Q_{c,max} = 700 \text{ Watts.}$$

The container tube dimension can now be determined. The maximum hoop stress subject to internal pressure is given by:

$$f_{max} = \frac{P(d_o^2 + d_i^2)}{(d_o^2 - d_i^2)}$$

d_i = 0.1.12 inches
d_o = 0.1.25 inches
t_1 = 0.13 inches

A factor of safety of 2 was used in the calculation. For the most common circular heat pipes, a flat circular end cap is used. Assuming a thickness of less than 10% of the diameter, the wall thickness of the end cap can be determined by:

$$f_{max} = \frac{Pd_o}{4t_2}$$

$$t_2 = 0.06 \text{ inches}$$

Again, a factor of safety of 2 was used. The remaining space between the vapor core and the inside of the heat pipe wall will be left for the wick and liquid flow.

The basic parameters of the heat pipe have now been designed. The entrainment and boiling limitations must be checked to ensure

the proper operation of the heat pipe. The entrainment limit ensures that the wick will not dry out. Since the vapor and liquid move in opposite directions, a shear force exists at the liquid-vapor interface. If the vapor velocity is high enough, the liquid may be torn from the surface of the wick causing the wick to dry out. The entrainment on the axial heat flux is determined by:

$$Q_{e,max} = \lambda A_v \sqrt{\frac{\sigma r_v}{2 r_{hs}}}$$

and represented by Figure 4.4.3.7 of Appendix A. The value of Q/A_v for the designed heat pipe is 1.78 x 10^5 Btu/hr-in^2. The entrainment limit, $Q_{e,max}/A_v$, of 2 x10^5 Btu/hr-in^2 will not be exceeded.

The boiling limit is associated with the formation of vapor bubbles in the wick structure at the evaporator section. This formation can cause hot spots and obstruct the circulation of the liquid. The boiling limitation can be represented by:

$$Q_{b,max} = \frac{2\Pi L_e k_e T_v \frac{2\sigma}{r_n}}{(\lambda \rho_v \ln(\frac{r_i}{r_v}))}$$

and represented by Figure 4.4.3.8 of Appendix A. A boiling limitation of 1.5 x 10^4 Btu/ft-hr is above the operating value of Q/L_e for this pipe at 464 Btu/ft-hr.

Figure 4.4.3.3 illustrates the final design specifications of the heat pipe for the motor. In designing the heat pipes to convey waste heat from the fuel cell power supply, approximately 1500 watts must be dissipated at the normal operating point for the supply. Like the heat dissipation scheme for the motor, the excess heat will be radiated to deep space with the use of radiator panels. Two panels identical to the one used for the motor's excess heat will be

used; therefore, each heat pipe which feeds a radiator must carry 750 watts of heat.

In the design of the heat pipes for the temperature control of the power supply, an assumption has been made that the heat generated by the power supply is localized in a region near the center of the power supply since no actual heat sink location information is currently accessible. Furthermore, an assumption that a 10 inch evaporator length for the heat pipes is possible. Since the radiator panels for the power supply will be identical to the one for the motor, the condenser length will also be the same. The total length of the heat pipes was determined to be 96.5 inches: 56.5 inches for the condenser section, 10 inches for the evaporator section, and 30 inches for the adiabatic section. Using the same series of calculations and the same material selection as for the heat pipe for the motor, the final dimensions of the heat pipes for the power supply were determined to be as follows:

di = 1.45 inches
do = 1.30 inches
t1 = 0.15 inches
t2 = 0.065 inches

4.4.4 Heat Radiation

If we had a perfect motor there would be no excess heat generated. Unfortunately there are no perfect motors. Our motor design is very efficient, however we still will have up to 350 watts of waste heat to remove from the drill assembly. The power source generates another 1500 watts of waste heat. This gives us a total of 1850 watts or 6310 Btu/hr or waste heat.

The lack of atmosphere in the lunar environment models a virtual vacuum. The presence of the vacuum precludes energy loss

from any surface of a solid by conduction or convection. Cooling is only available in the form of thermal radiation from the surface.

One radiator will be connected to the motor and two radiators will be connected to the power sorce by heat pipes that will run along the length of the radiators as was described in section 4.4.3. This is shown in figure 4.4.3.2. This radiator will be welded to the rod rack along one side. Heat dissipation by radiation is controlled by the equation:

$$q = A\varepsilon\sigma\ (T_S^4 - T_{sur}^4)$$

where:

q = Heat dissipated in Btu/hr
A = Area of the radiator
σ = $.1714 \times 10^{-8}$ Btu/sq ft hr $^{o}R^4$
ε = Emissivity
T_S = Temperature of radiator
T_{sur} = Temperature of sink

The emissivity of the radiator depends on the material on the surface. The radiator can be coated with an enamel to give it the greatest possible emissivity and the lowest possible absorptivity. The low absorptivity will prevent the radiator from absorbing heat. Because of the heat pipe in our design there should not be a problem of the radiator absorbing heat. If the radiator becomes hotter than the motor the heat pipes will simply shut off. The heat pipes will only work one way. Enamel coatings that are currently in use will give the radiator a emissivity of 0.9 and an absorptivity of 0.3. (I&D) By coating the radiator with a very smooth enamel the affects of lunar dust will be minimized. The radiator should be highly polished after the enamel is sprayed on.

The maximum heat rejection will occur when the motor is at its maximum operating temperature of 212F. In order to keep the

radiator at a uniform temperature across its surface a material with a high thermal conductivity should be used for the internal part of the radiator. Aluminum is an excellent choice because it is light as well as highly conductive. Keeping the radiator thin will also help the radiator remain at a uniform temperature. Due to the size constraints of the positioning of the radiator in the rod rack, the radiator will be 1.5 inches in width.

The sink temperature will be the temperature of deep space which is -400F. Care will have to be taken so that the radiator is pointed toward deep space. This may be accomplished by the proper positioning of SKITTER so that the radiator will face towards deep space at all times during the normal drilling cycle.

Using the above equation to determine the required area of the radiator panel yields:

$$6310 = \text{Area} \times 0.9 \times 0.1714\text{x}10^{-8} \times (710^4 - 60^4)$$

$$\text{Area} = 16 \text{ ft}^2$$

With three radiators that would mean that each radiator would need a surface area of 5.36 ft^2. This would be the ideal radiator size. Lunar dust and changing sink temperatures are just a few of the places where error could occur. For this reason a factor of safety of at least 2 should be included. This would result in an area of:

$$\text{Area} = 2 \times 5.36 \text{ ft}^2 = 772 \text{ square inches}$$

The radiators will be able to radiate off of both sides. This gives us another factor of safety of two, but introduces additional error. As shown in figure 4.4.4.1 the radiator is 50.45 inches in height and 15.3 inches in length. The volume of each aluminum radiator would be:

$$\text{Volume} = \text{length} \times \text{width} \times \text{height}$$

$$V = (50.45)(15.3)(1.5) = 1157.8 \text{ inch}^3$$

The weight of each aluminum radiator can then be determined as:

mass = density x volume
$m = \rho \times v$
$m = (0.098 \text{ lb/inch}^3) \times (1157.8 \text{ inch}^3)$
$m = 113.5 \text{ lb}$

The height along which the heat will be applied to the radiator is 3.7 times the length. Therefore, the above calculations assumed an isothermal temperature gradient along the radiator as is shown in Figure 4.4.4.1.

4.4.4.1 Alternate Equation in SI Units

In si units the value of σ is 4.876×10^{-8} kcal/sq m hr $^{o}K^4$. 346 watts is equal to 297.8 kcal/hr Changing our values to si units we get the following equation:

$$297.8 = A*.9*4.876 \times 10^{-8}*(394^4-33^4)$$

Solving this equation we find the area to be .28 square meters. With the factor of safety of two this gives us a radiator with an area of .56 square meters. The radiator is 1.44 meters wide. This means that the radiator is .32 meters long.

.32 meters is approximately 12.6 inches the error in this term is due to very inaccurate conversion factors. This section is to help readers more familiar with si than English units. The design should be based on the English calculations.

4.4.5. Friction Clutch

In the event of a bit lock-up, a shut-off safety device was required to prevent damage to the drill motor, the supporting structure, and possibly SKITTER. This torque limiter can be used in this case and should be set at a shut-off torque which is high enough to allow for effective drilling, yet low enough to protect the drilling device. This will act as a backup to the control shut-off which senses a maximum current value as an indicator for a bit lock-up.

A disc friction clutch is an effective tool in torque overload protection. This clutch will transmit torque up to a predescribed value, after which it will "run free". It resets itself automatically once the overload is removed and speed reduced. Friction forces and a normal force provided by a spring are responsible for the transmission of power. See Figure 4.4.5.1 for a schematic of a standard friction clutch. The general formula governing the size of the clutch is as follows:

$$T = 0.5\ (i)\ (f)\ (Fa)\ (Dm)$$

where:

T = transmitted torque
i = number of pairs of contact surfaces
f = applicable coefficient of friction
Fa = axial engaging force
Dm = mean diameter

Higher torques mean larger diameters unless more than one pair of contact surfaces is employed. For this reason, multiple plate friction clutches are popular. Since there are torque limiters on the market today which suit our needs, design for such a device is not necessary. The Helland R&D Company offers a wide array of friction clutches known as Torq-Tenders. The model compatible with our needs is the

TT4X Standard Torq-Tender. The torque available is 1000 in-lbs (83.3 ft-lbs) which will well protect our system at an assumed overload torque of 960 in-lbs (80 ft-lbs). See Figure 4.4.5.3 for specifications. The bore size chosen was 1.75". Although incompatible with our drill string diameter, it was the largest diameter offered by the TT4X. To correct this, a variable diameter shaft interface was designed to accommodate the torque limiter and the upper-most end of the drill string, see Figure 4.4.5.2 and calculations.

The advantages of such a system are many. In addition to protecting our Lunar Deep Drill Apparatus, it requires no additional power, generates no heat, and is unobstructive. The Torq-Tender also makes up for improper alignment. It accepts up to 1.5 degrees misalignment and up to .015" of parallel misalignment. The system requires no maintenance and resets itself automatically. A torque limiter such as this makes for a good addition to our LDDA.

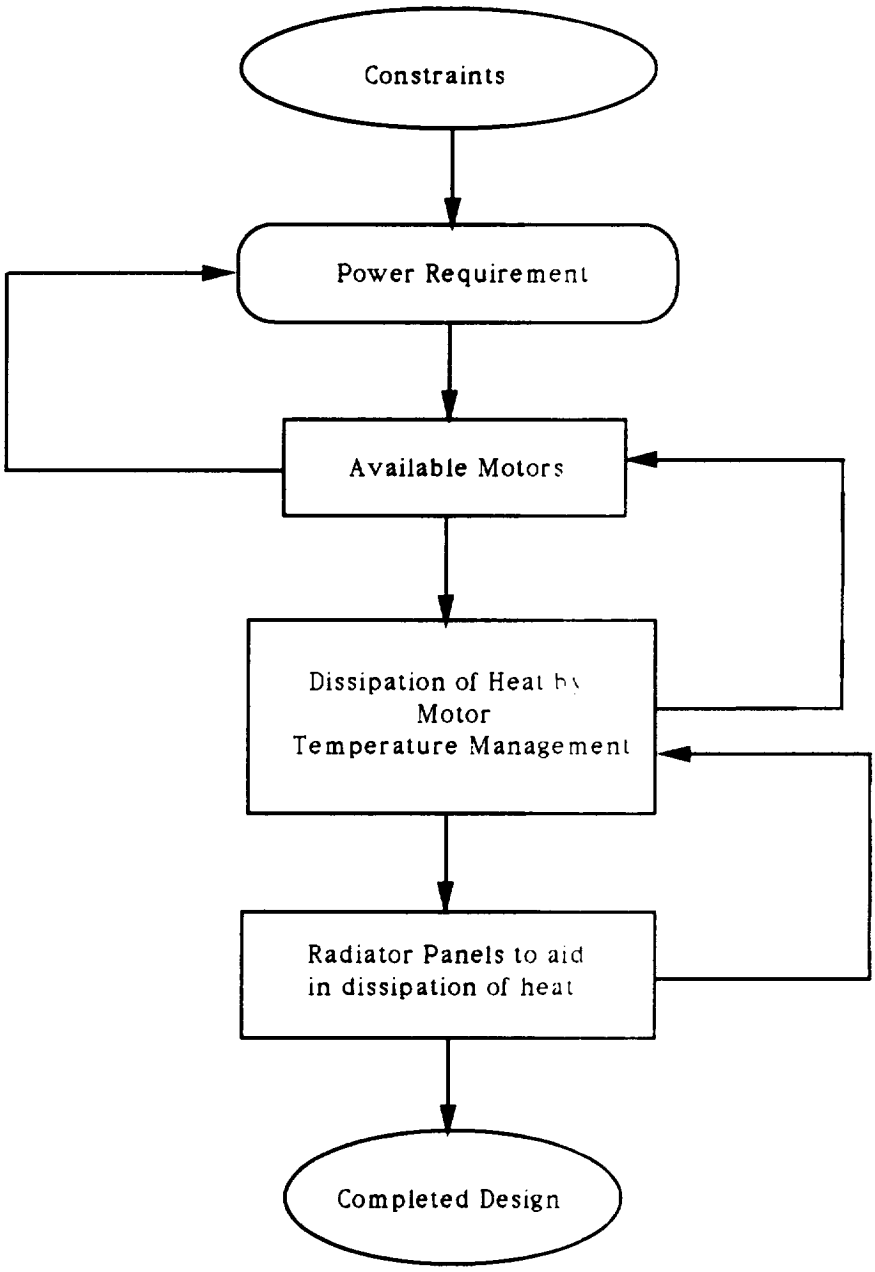

Figure 4.4.a Design Process for Power, Motor, and Temperature Management

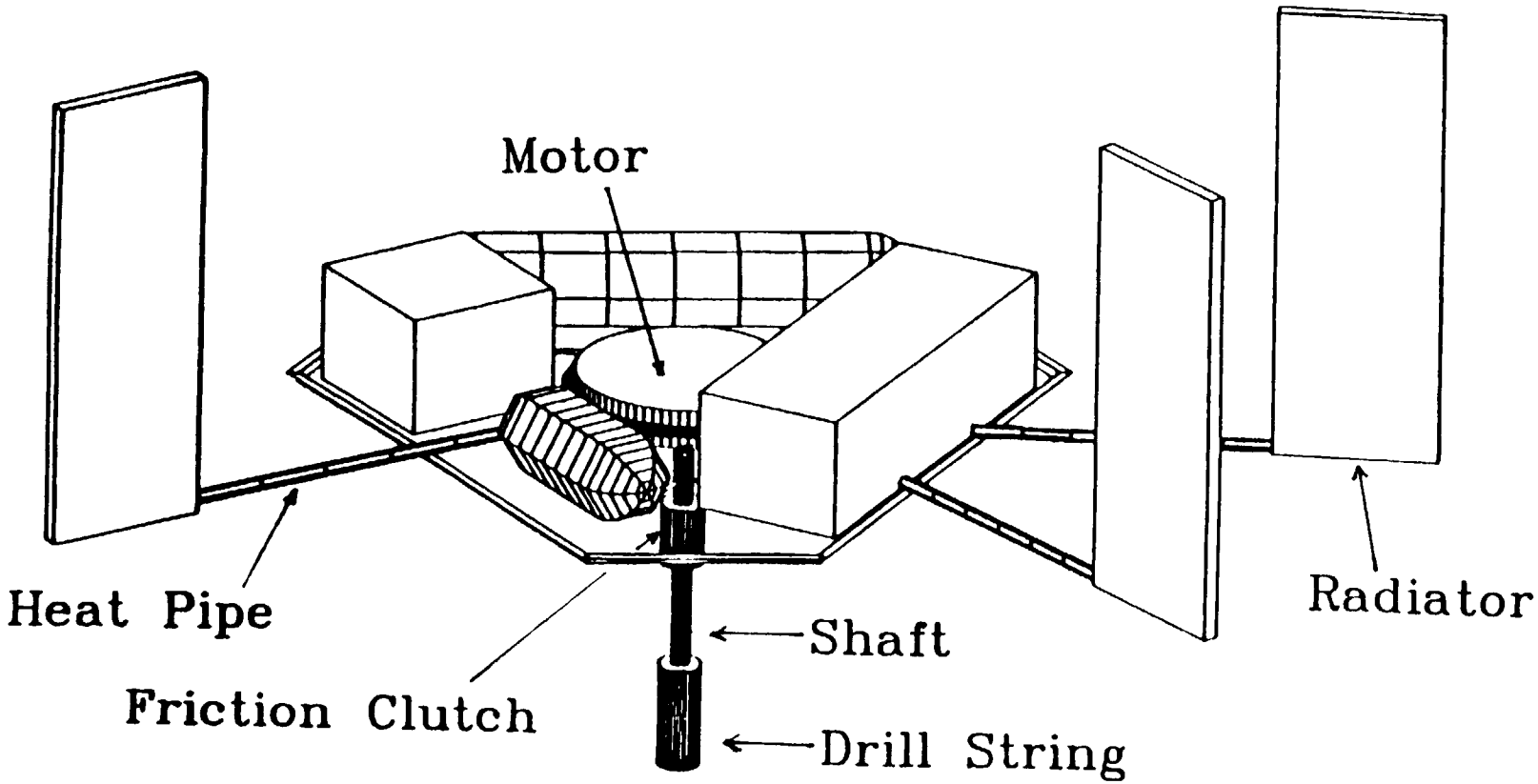

Figure 4.4.b
Overall Arrangement
Top View

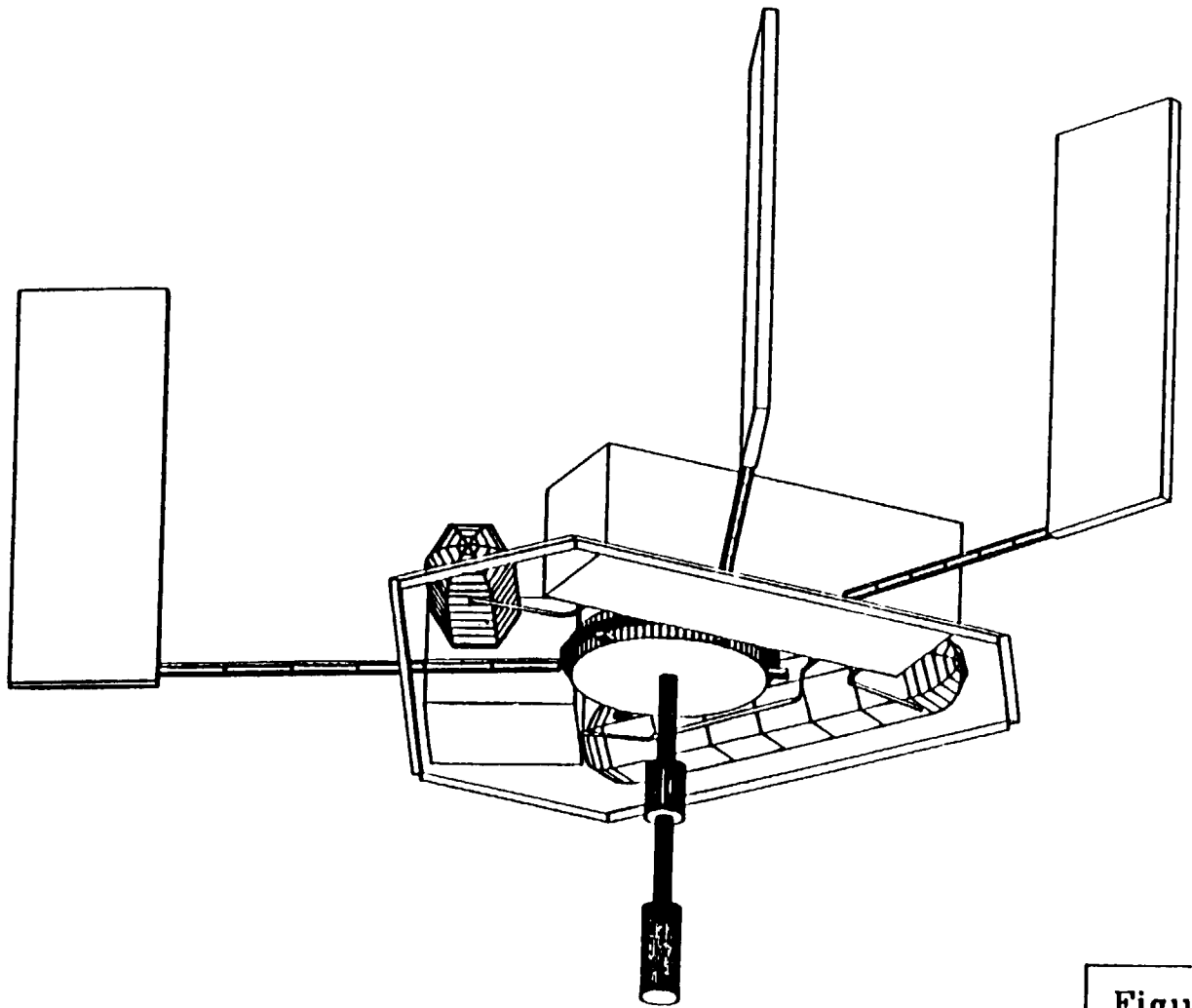

Figure 4.4.c
Overall Arrangement
Bottom View

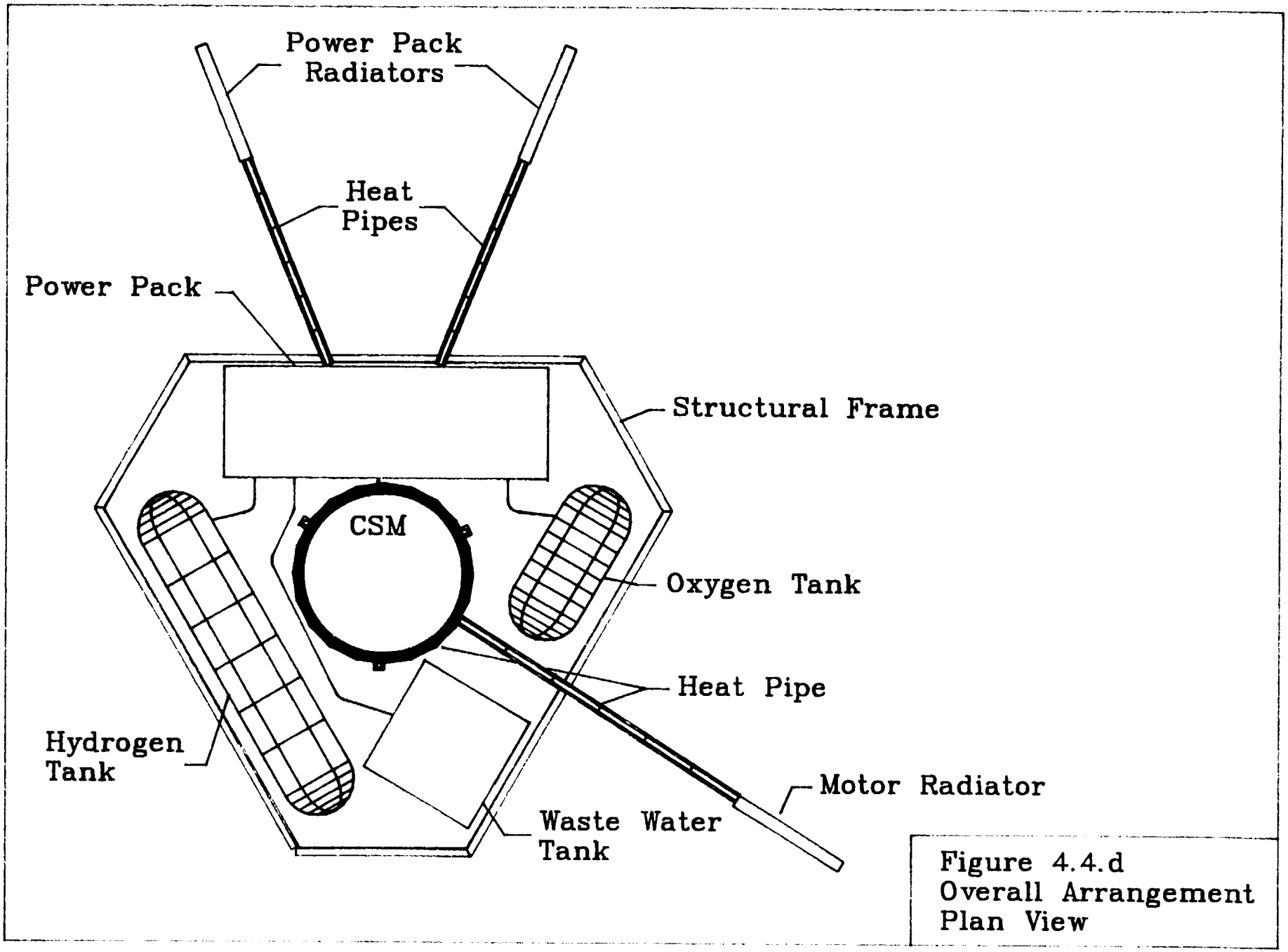

Figure 4.4.d
Overall Arrangement
Plan View

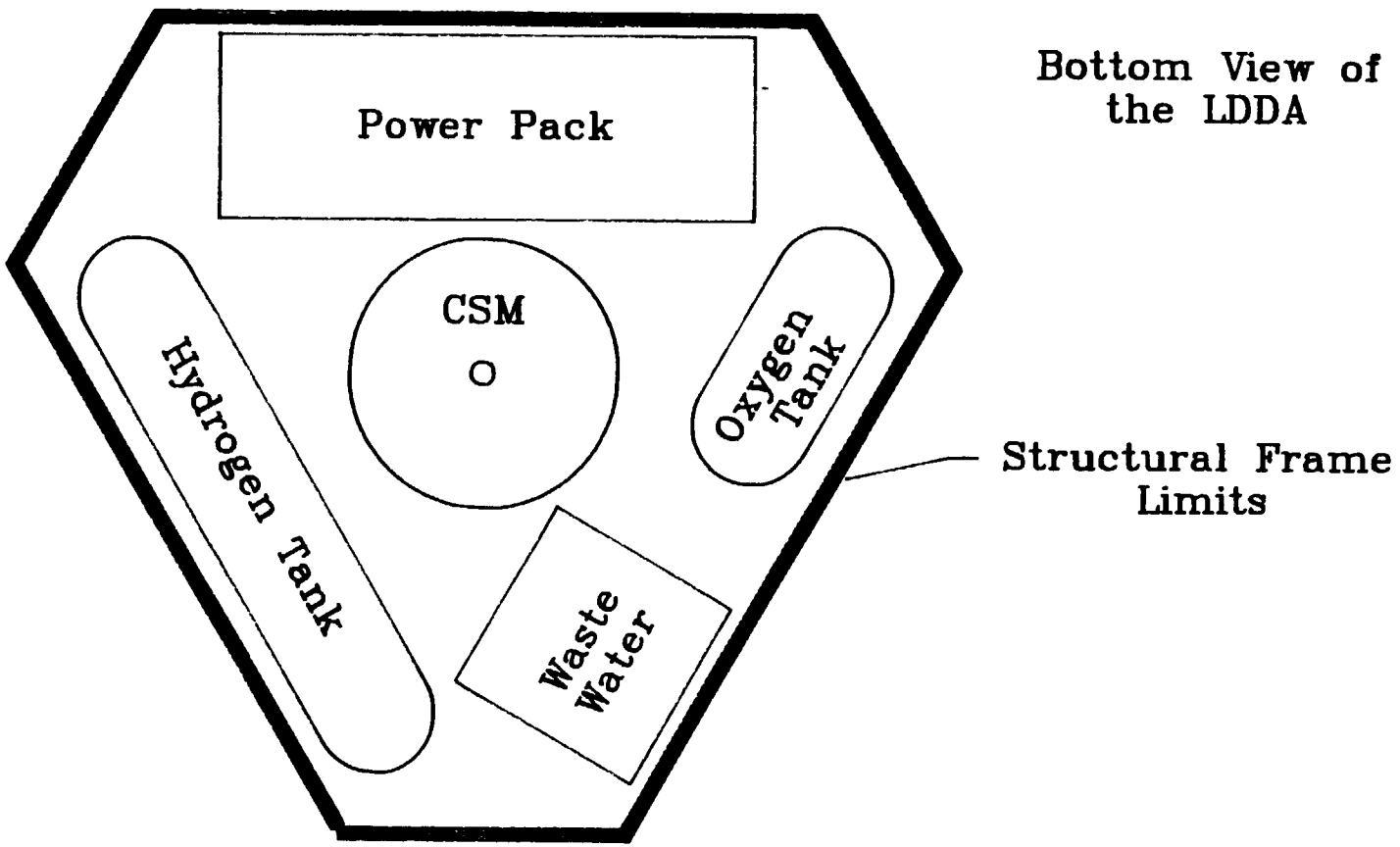

Figure 4.4.1.1
Power System Arrangement

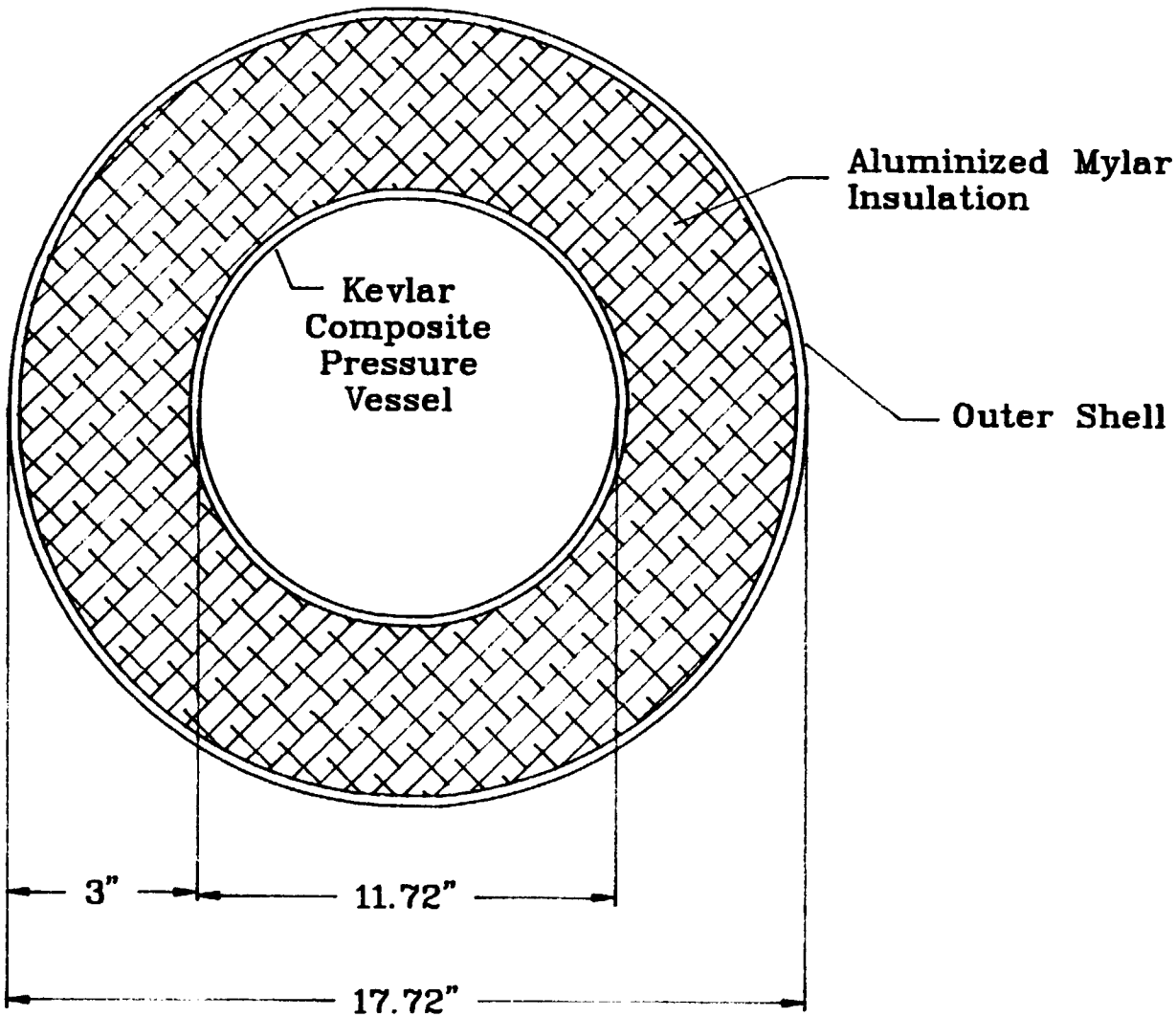

Figure 4.4.1.2
Tank Cross Section

Figure 4.4.2.1 Curvo-Synchronous Motor

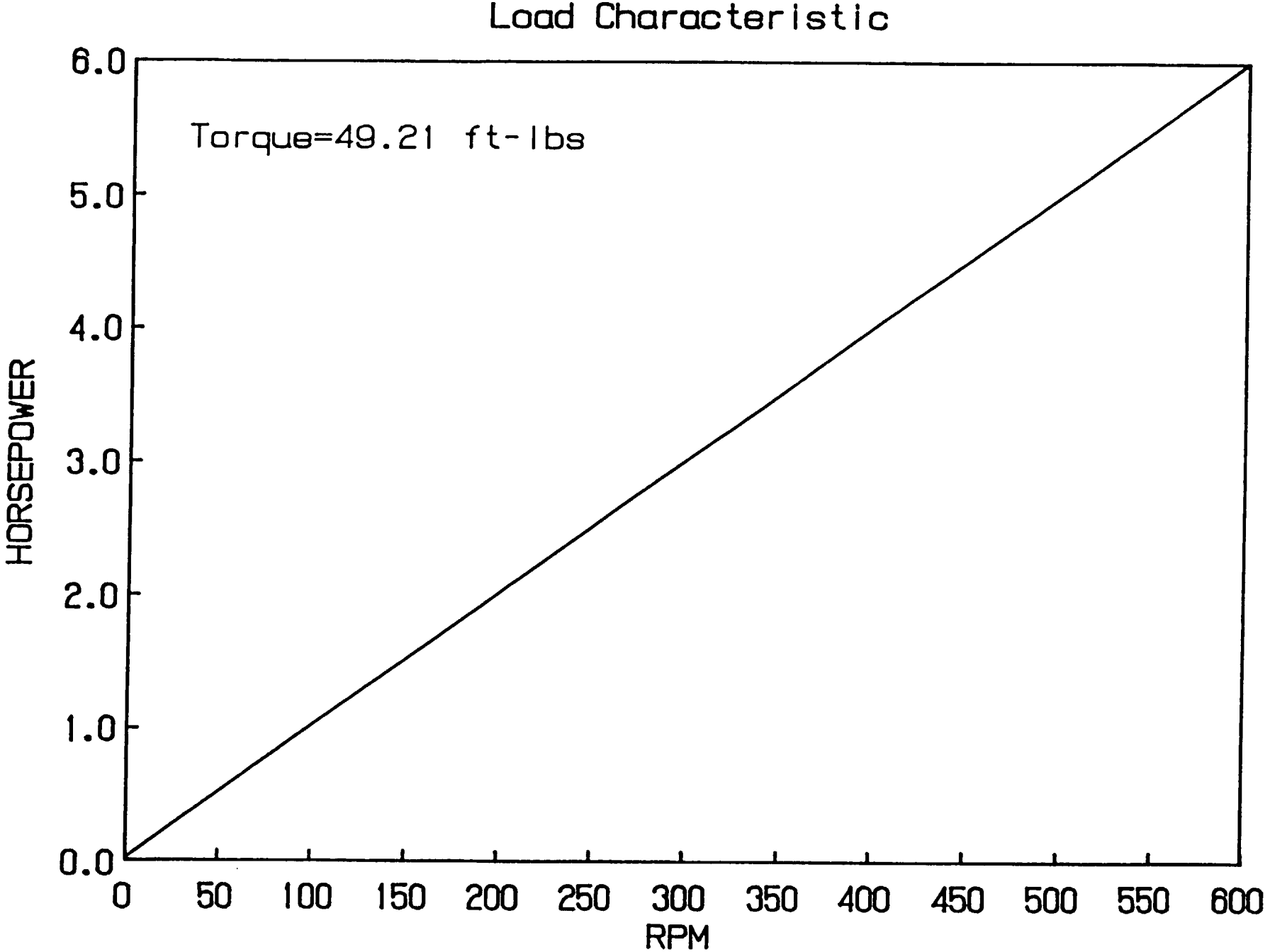

Figure 4.4.2.2 Curvo-Synchronous Motor Current Characteristic

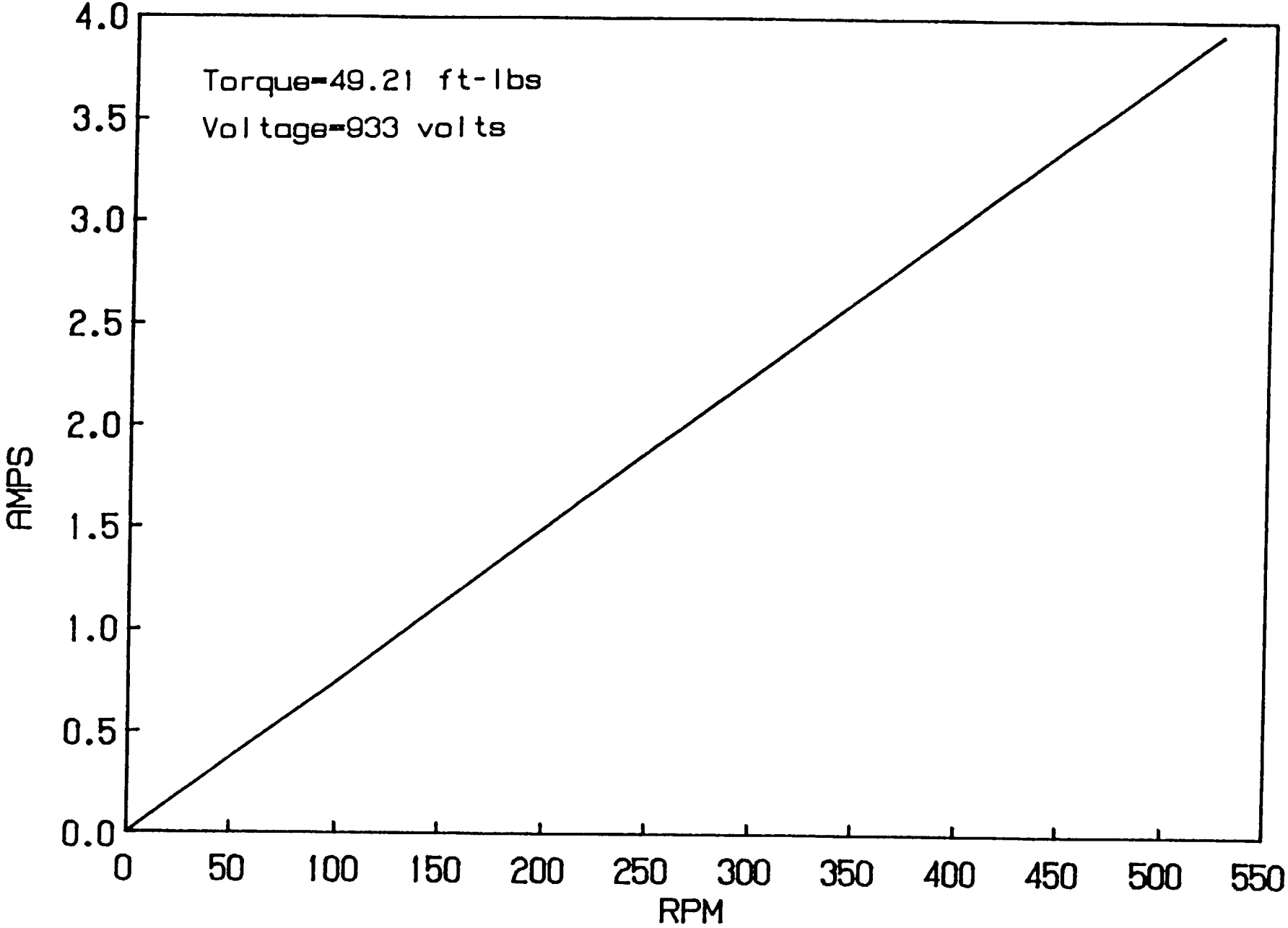

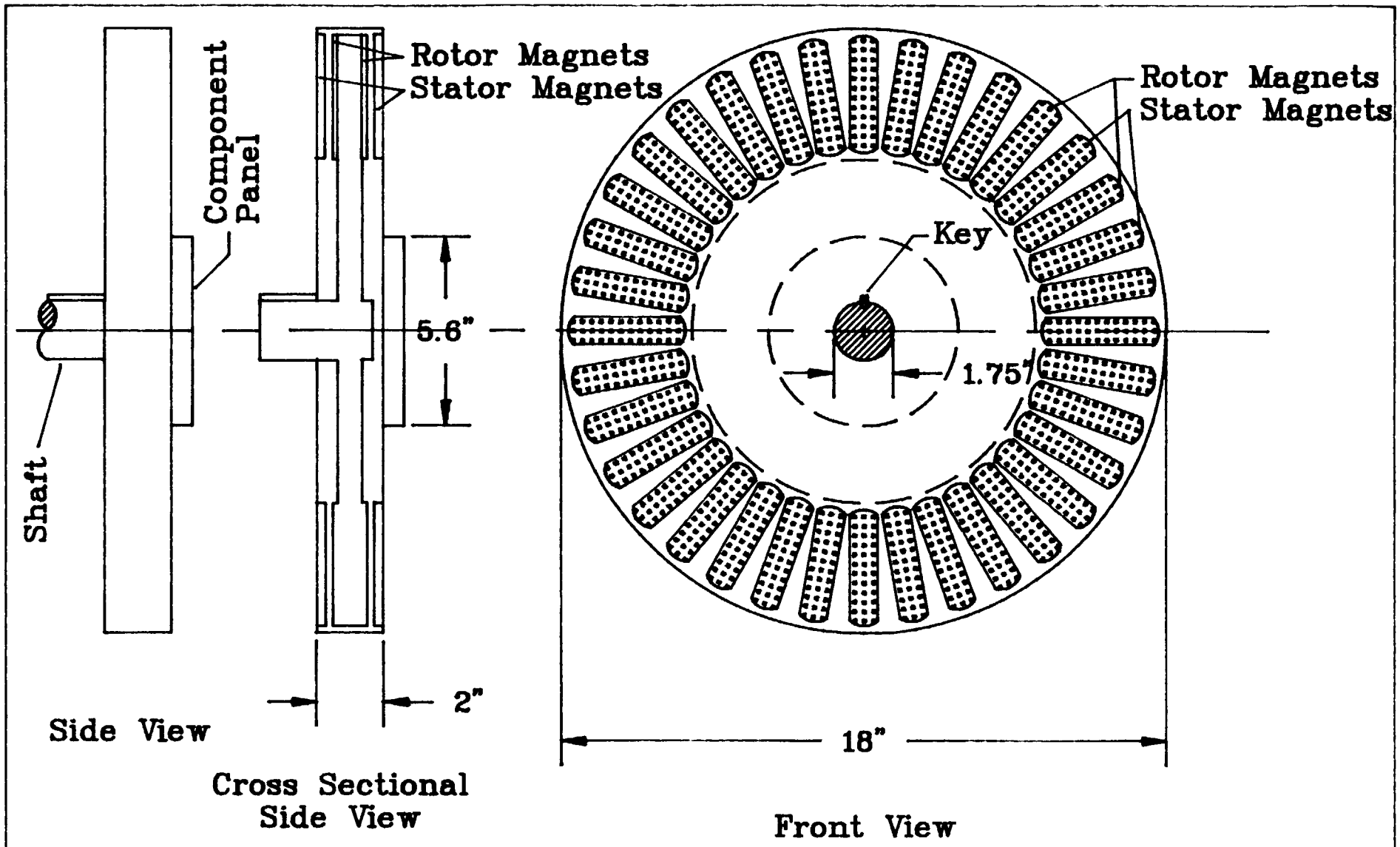

NOTE: Flange and Casing shown Figure 4.4.2.5

Figure 4.4.2.3
CSM Schematic

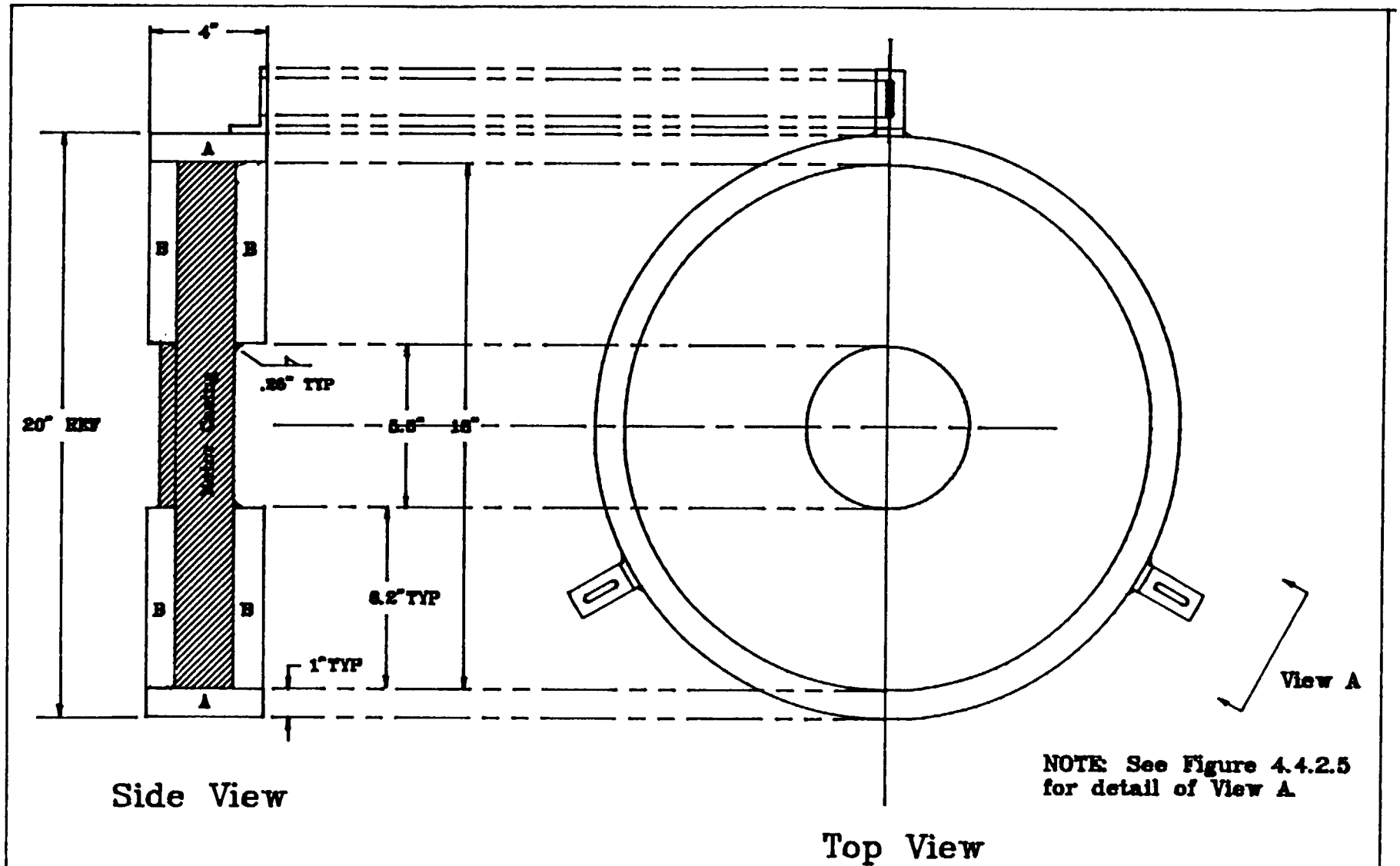

NOTE: Welded attachement to CSM

Materials
A – 1199 O Al alloy
B – Ti Beta alloy

Figure 4.4.2.4
Motor Mount and Flange

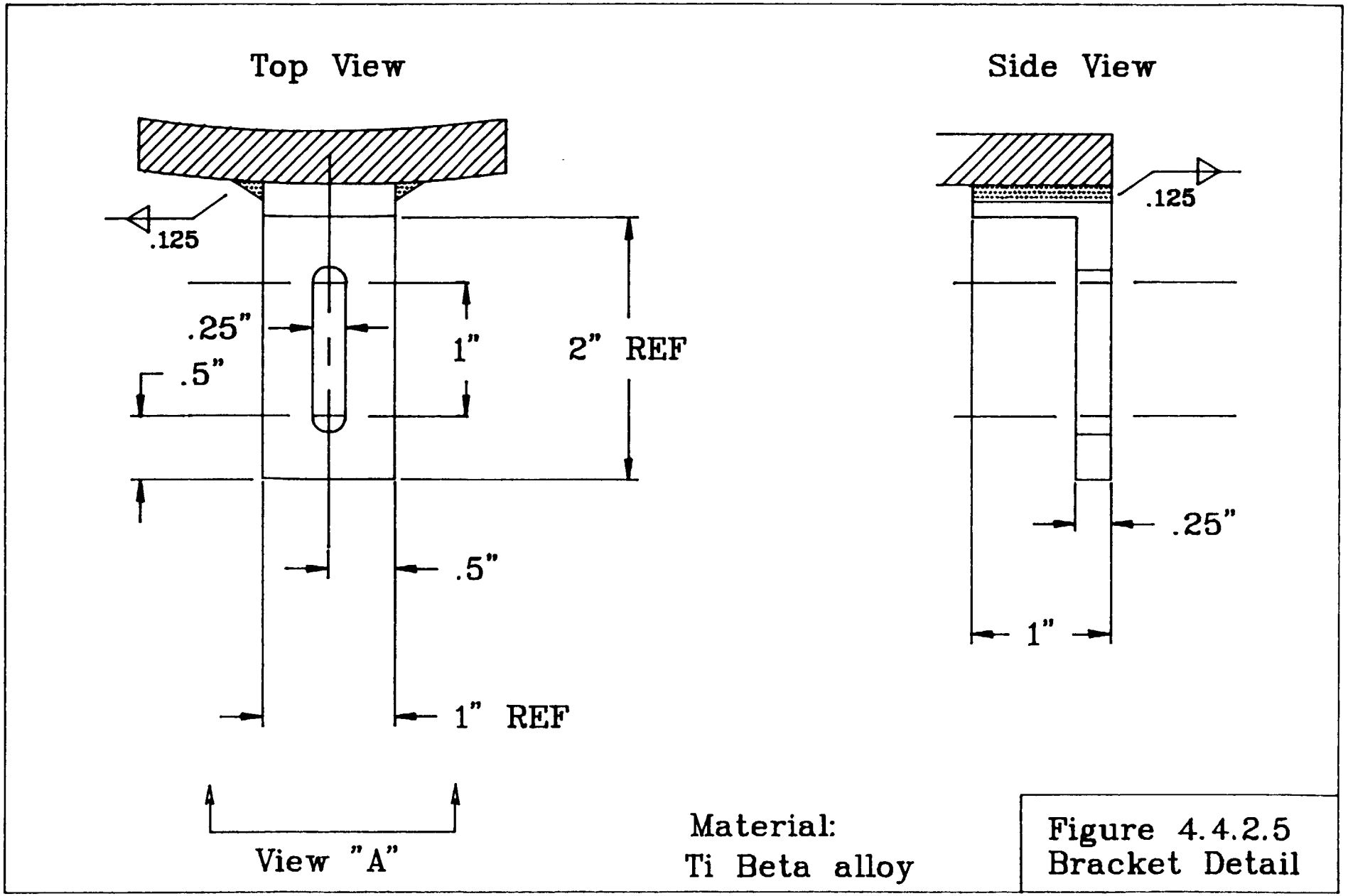

Figure 4.4.2.5
Bracket Detail

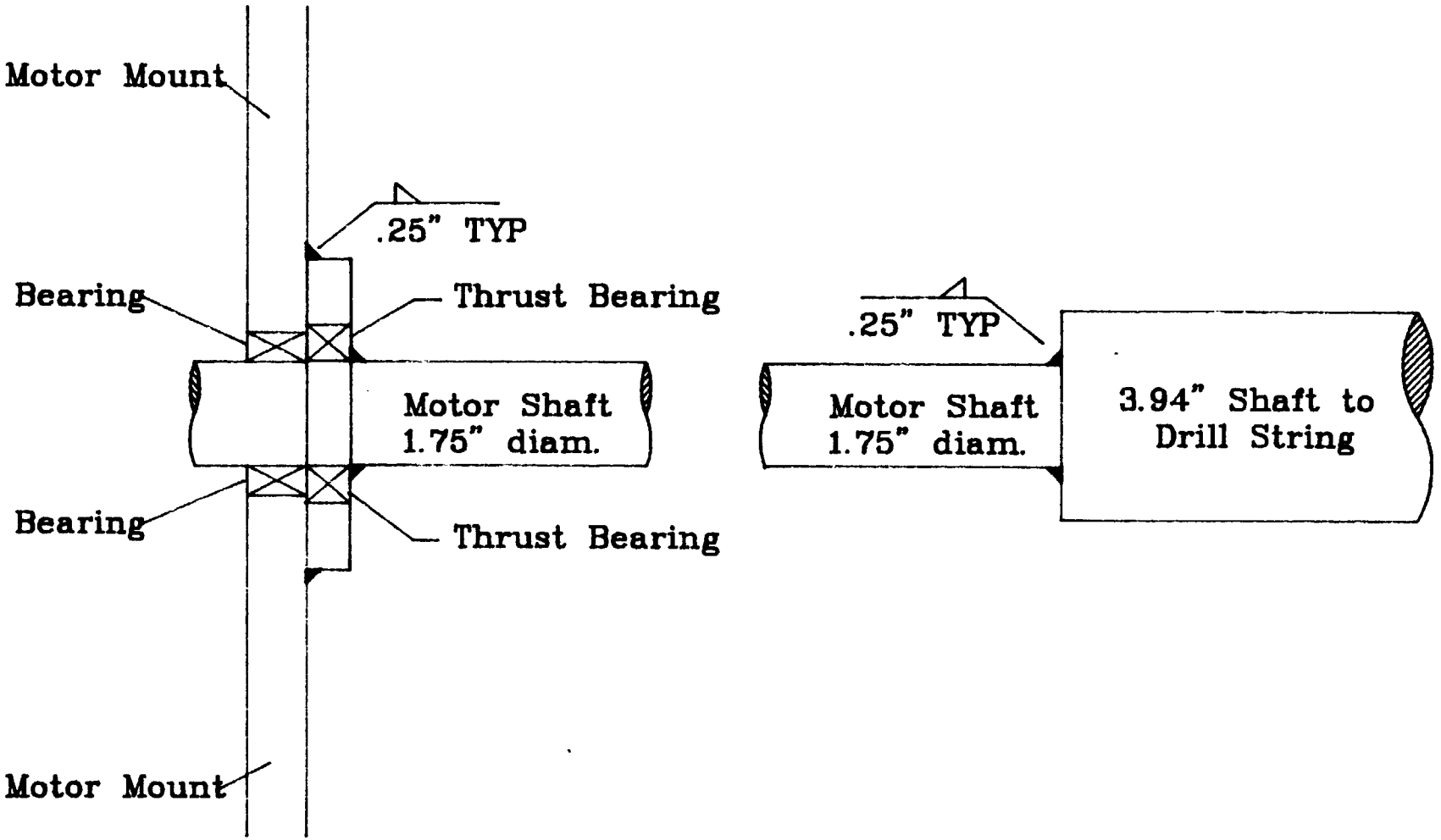

NOTE: Thrust Bearings resist Upward and Downward Motion.

Figure 4.4.2.6
Thrust Bearing

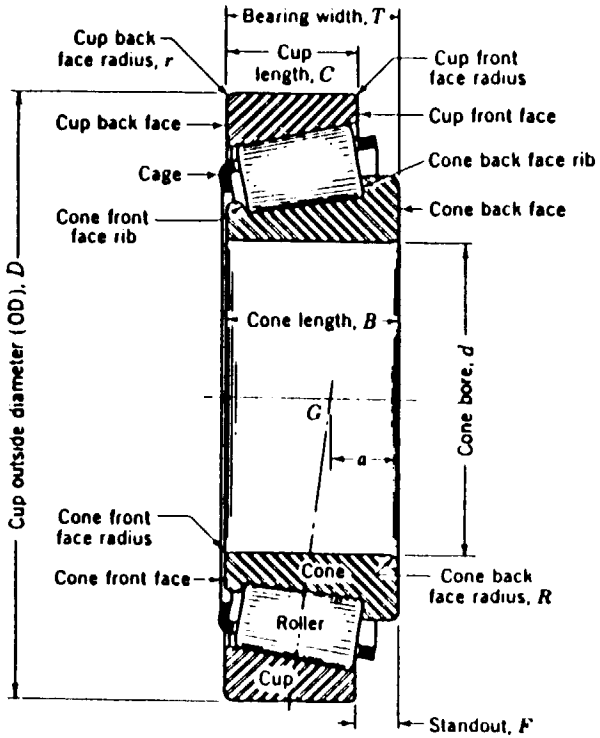

Figure 4.4.2.7
Thrust Bearing Detail

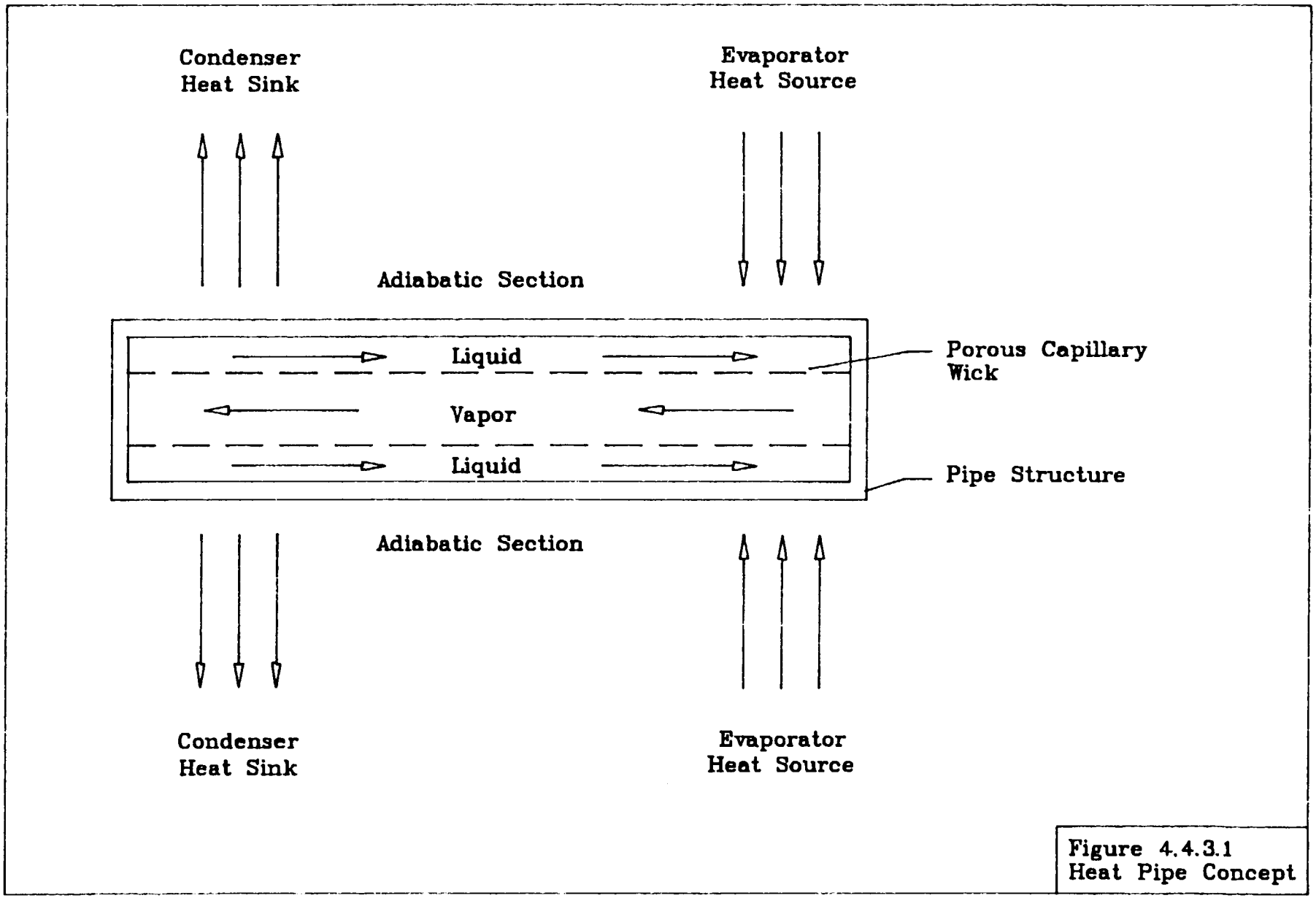

Figure 4.4.3.1
Heat Pipe Concept

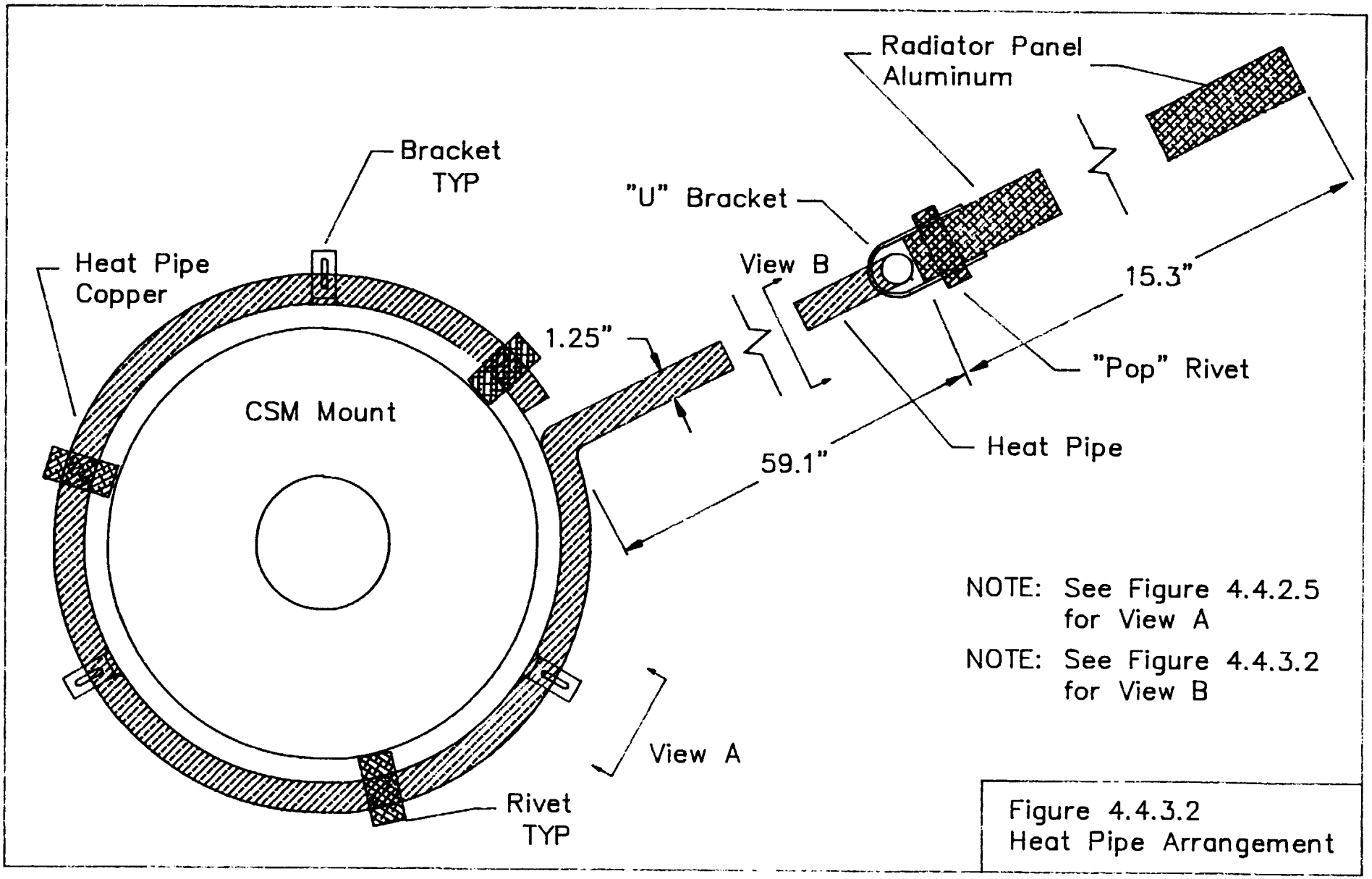

Figure 4.4.3.2
Heat Pipe Arrangement

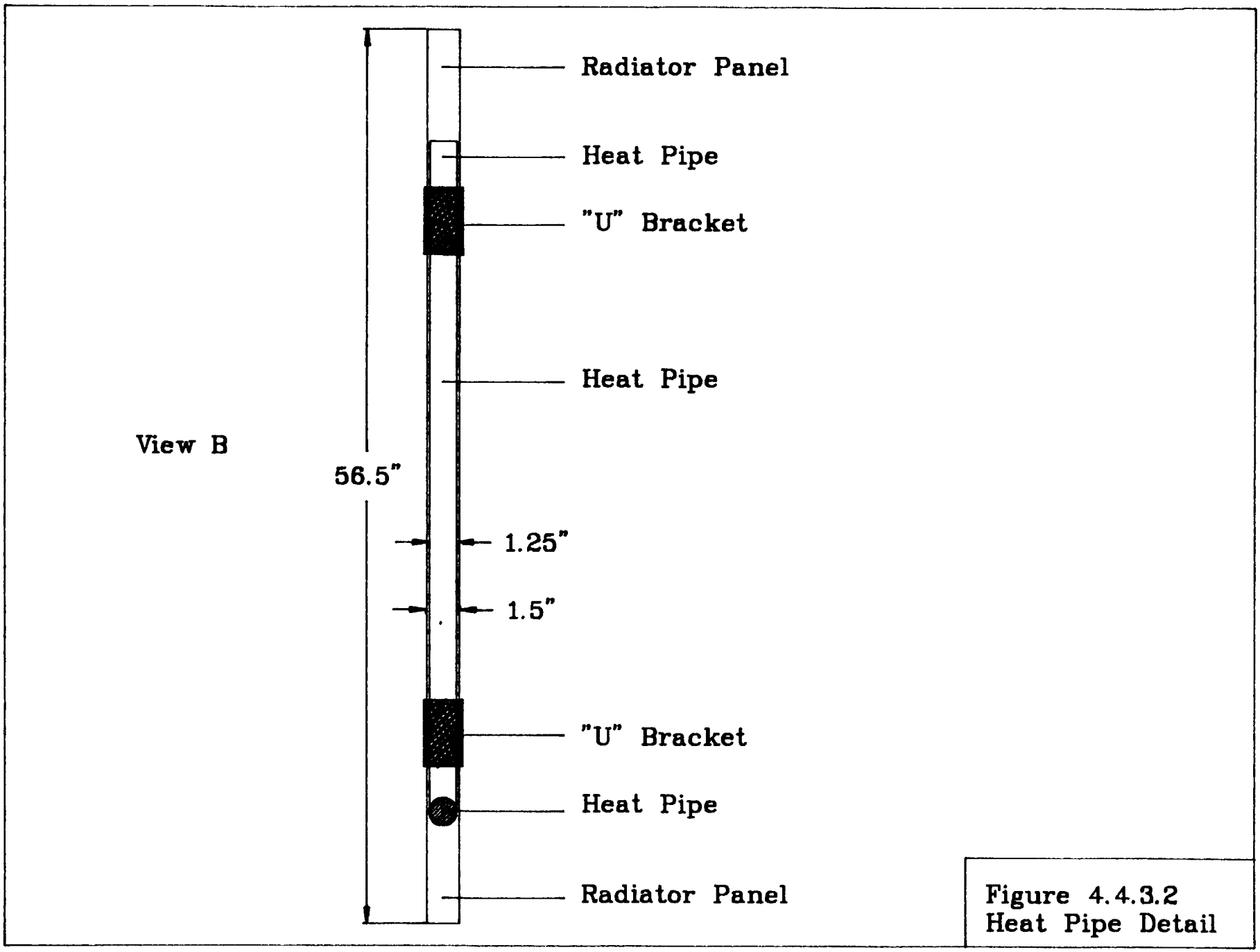

Figure 4.4.3.2
Heat Pipe Detail

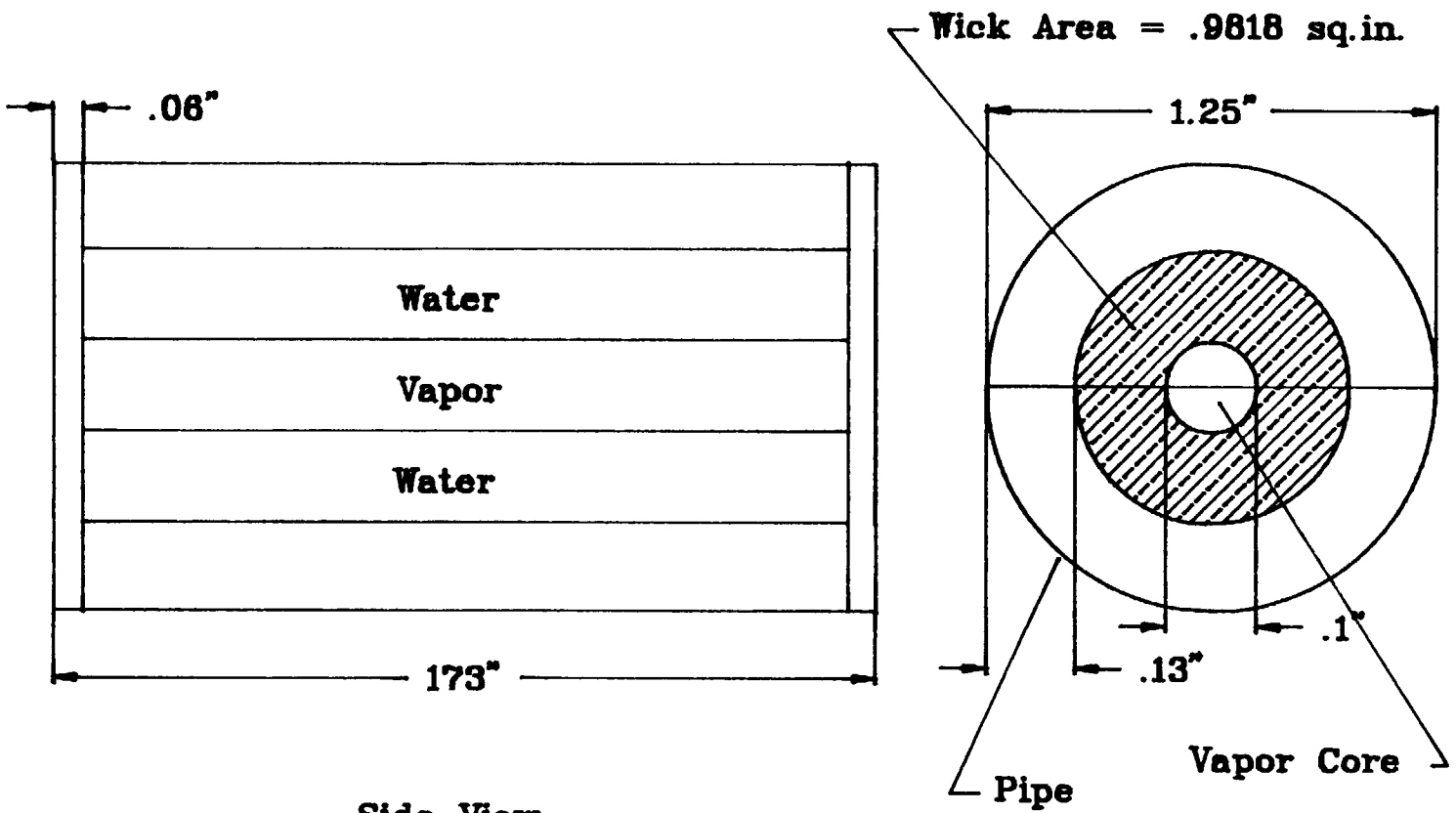

NOTE: Not drawn to scale.

Materials:
Pipe – Copper
Wick – Copper
Working Fluid – Water

Figure 4.4.3.3
Heat Pipe Specifications

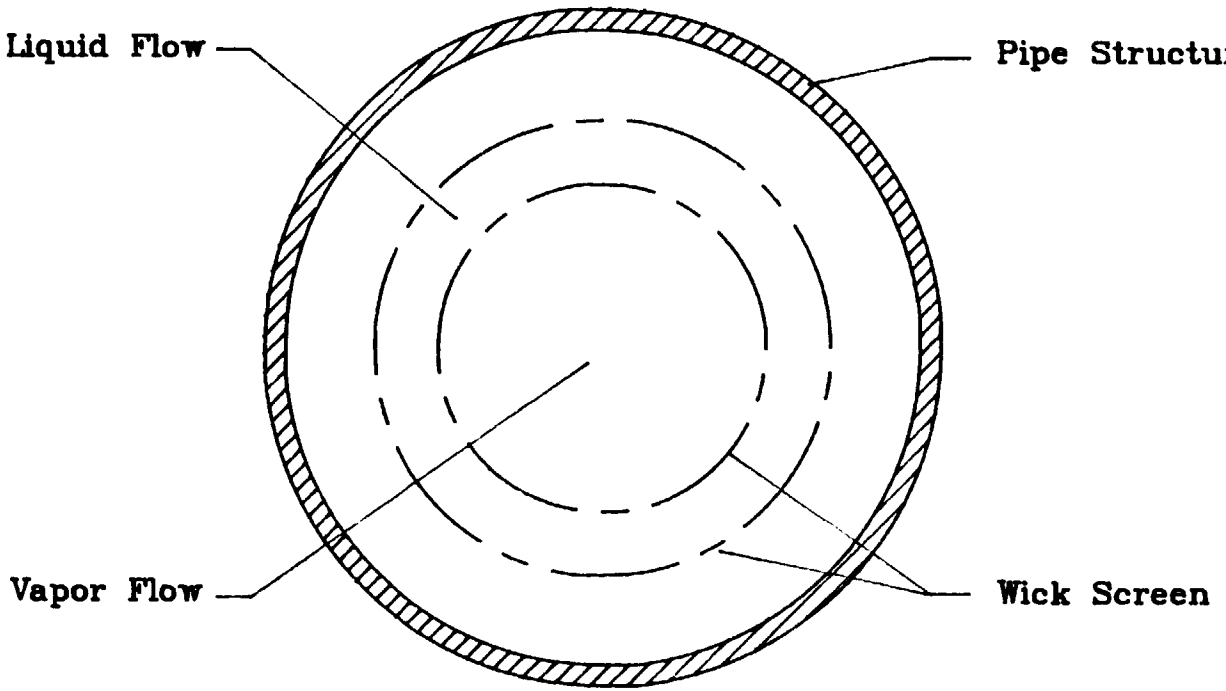

Cross Sectional View of
Heat Pipe Endpoint

Figure 4.4.3.4
Typical Wrapped
Wick Screen

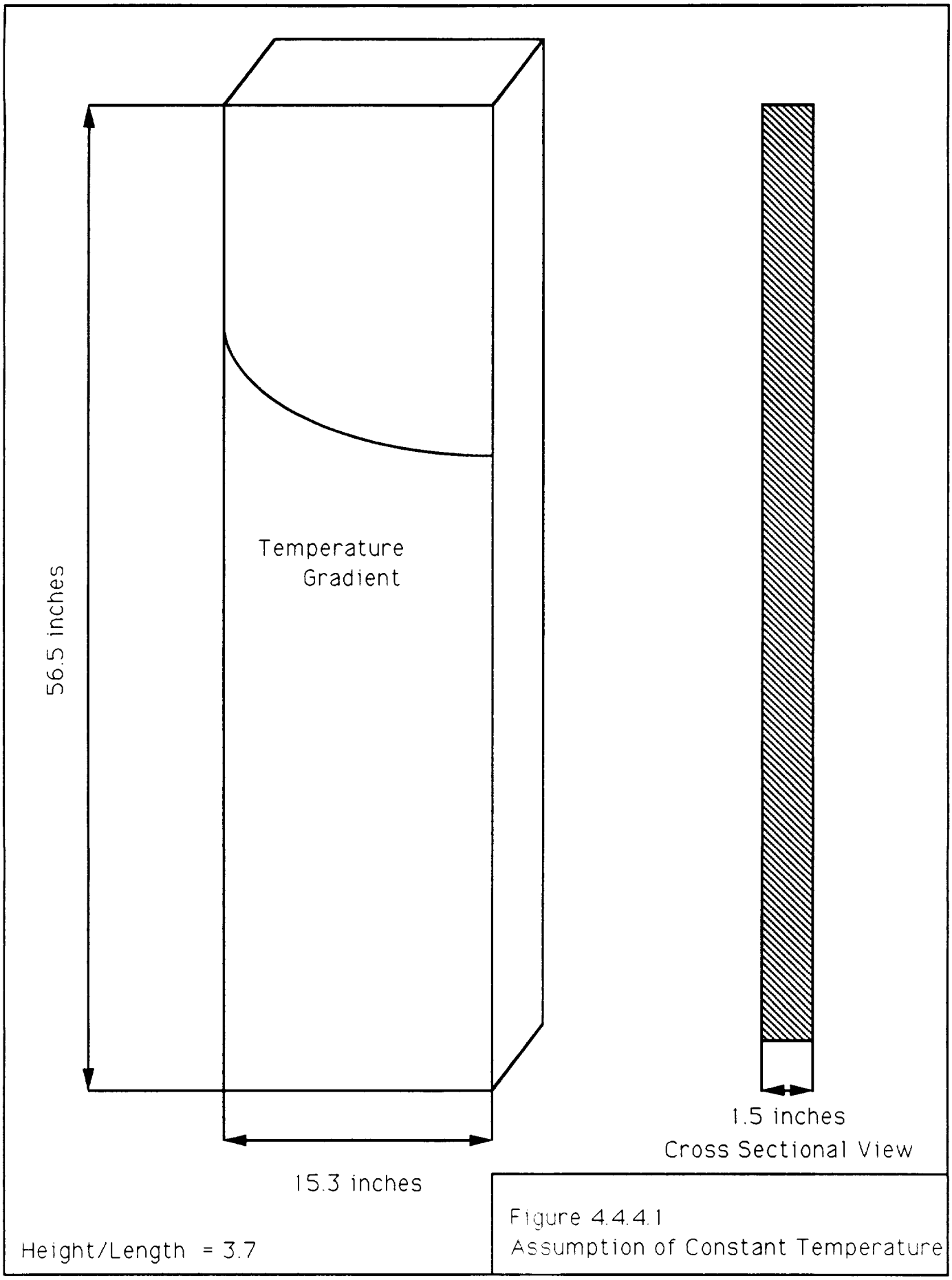

Figure 4.4.4.1
Assumption of Constant Temperature

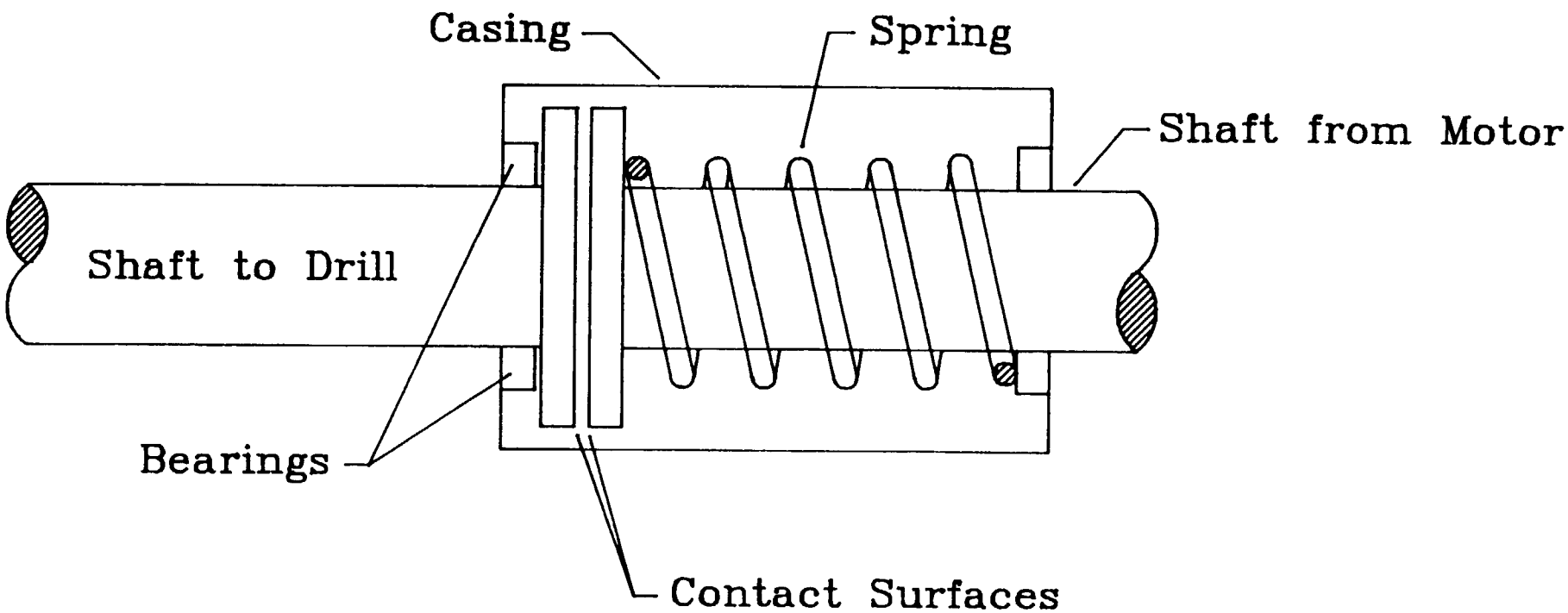

Figure 4.4.5.1
Friction Clutch

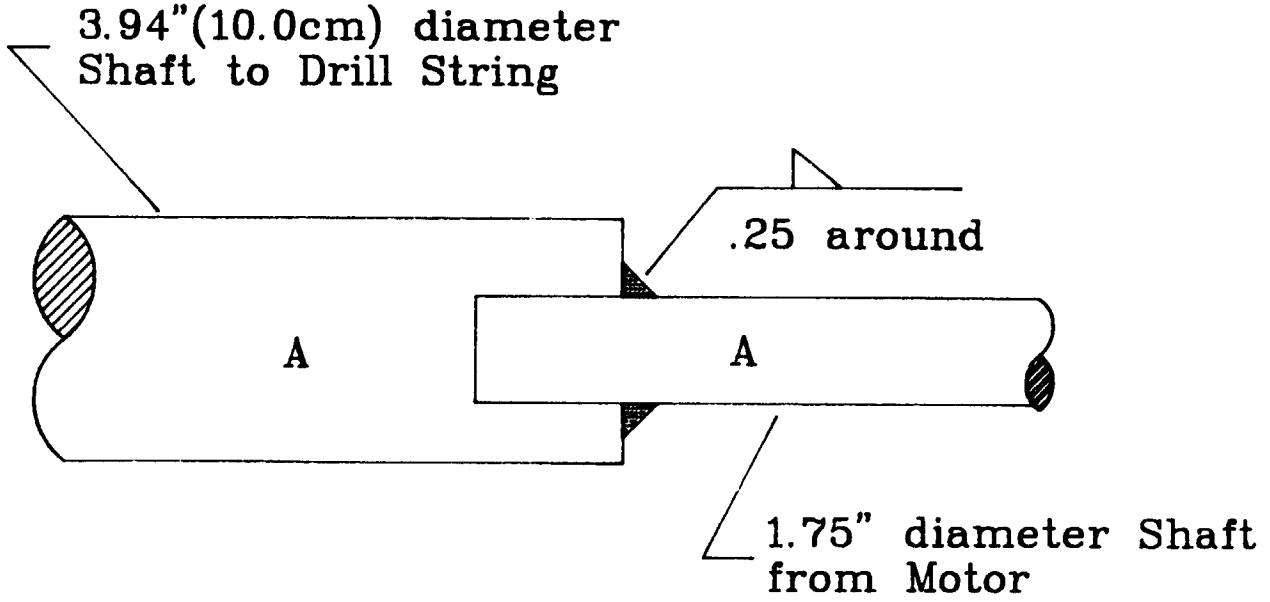

Material A – AISI 1045 Steel

Figure 4.4.5.2
Shaft Interface

TT4X STANDARD MODEL

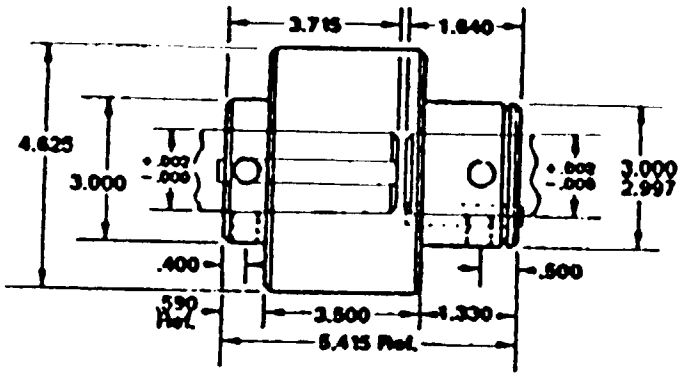

Figure 4.4.5.3 Friction Clutch Specifications

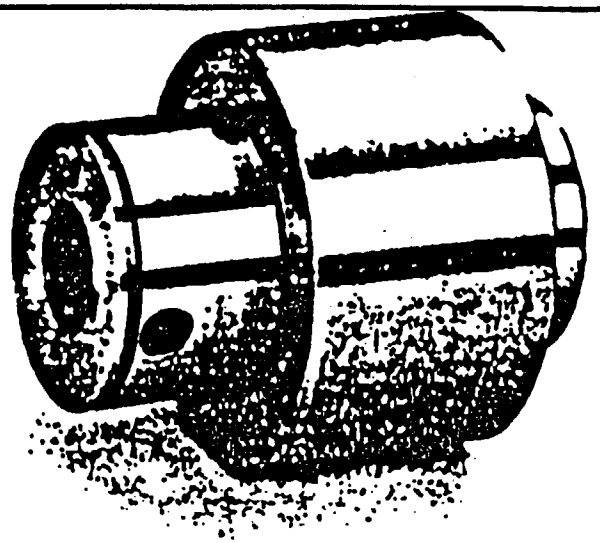

Model **TT4X** STANDARD
Helland Torq-Tender

- Standard torques available (in. lbs.): 750, 1000, 1250, 1500, 1750, 2000, 2250, 2500, 2750, 3000
- Standard bore and keyway sizes: 1", 1⅛", 1¼" bore with ¼ x ⅛ keyway; 1⅜" bore with ⅜ x 3/32 keyway; 1½", 1⅝", 1¾" bore with ⅜ x ⅛ keyway
- Bi-directional automatic reset.
- Tamper resistant design. Once installed, torque ratings cannot be changed unless springs of a desired new rating are substituted. The change can be made quickly and easily.
- Available in stainless steel, plated and sealed models for adverse operating environments.
- Installs quickly and easily as any simple coupling. Accepts up to 1.5 degrees misalignment and from .005" to .015" parallel misalignment.
- Optional automatic shut-off indicator pin, disc.

4.5 STRUCTURE AND MECHANICAL INTERFACE DESIGN FOR SKITTER DRILLING IMPLEMENT

4.5.1 Introduction

This section describes the design of the implement base structure and mechanical interface of the soil drilling mechanism which will be attached to the bottom surface of SKITTER. The implement base structure will be referred to as either the structural interface or platform throughout this section. This structural interface will accommodate the rotary drill drive, rod rack and changer arm to handle drill string rod elements, fuel cell power source, control module, antennae, and heat dissipation devices.

4.5.2 Constraints

Certain conditions found on the moon warrant special consideration during design to eliminate potential performance failures. Some of the possible problem conditions are lunar dust, radioactivity and extreme temperature ranges. A slightly smaller problem encountered on the lunar surface is micrometeorite bombardment.

The moon is covered with a layer of very fine dust which acts almost magnetic in nature due to the lack of gravity and atmosphere. This dust tends to cause friction and lubrication problems in moving parts and bearings. This played a large role in the mechanical interface design which is detailed in Mechanical Interface Design and Operation section.

The moon, as with most planets lacking an atmosphere, is subjected to intense solar winds, gamma rays and ultra-violet radiation. This radiation can cause weakening, embrittlement and creep in most metals without some kind of protection. Solar wind consists of hydrogen and helium nuclei and is the dominant source of the lunar atmosphere. Solar radiation is not the cause of the most harmful effects. Galactic cosmic radiation contains gamma and ultraviolet rays which are most harmful to the materials. The protection used on the structural interface is described in Material Selection and Treatment section.

The temperature extremes on the moon range from -130 deg. C to 158 deg. C. This is very detrimental in the areas where different materials are mated together. Tolerances must be closely monitored to avoid seizing of moving parts.

The bombardment by micrometeorites on the structural interface surfaces could cause microscopic scratches which could lead to crack propagation over an extended period of time. The polymer sealant used for radiation protection is also very effective in minimizing the microscratches from the micrometeorite bombardment.

4.5.3 Performance Criteria

There are three major performance criteria which are required of the structure during operation: it must provide a stable work platform; it must have mechanical simplicity to allow remote operation without human help; and it should have commonality of parts for standardization of repairs and compatibility of other implement devices designed in the future.

In order to be a stable work platform, the structure was designed to take all possible forces generated during operation

without significant deflections occurring which may disrupt or interfere with the drilling process. Deflections cannot be allowed to introduce bending in the drill string or cause vibration which may damage attachments which are fragile such as the heat dissipation panels or control module. The fact that it should not catastrophically fail is quite obvious since this would abruptly end the entire operation.

Mechanical simplicity is required to allow for the remote operation from the earth ground control base. The easiest way to insure simplicity is to use the smallest number of moving parts. In the design of the mechanical interface, which is the connection between the structural interface and SKITTER, the general idea was to use basic mechanical cams and springs which require no lubrication or maintenance. The few components which required separation from the dusty environment were enclosed in a self-contained cavity.

Since there will be other other implements designed for use by SKITTER, a universal latch design was chosen which could be easily used for all of these tools. It would have been short-sighted to design the mechanical interface as a unique connection which could not be adapted to all of the other implements.

4.5.4 Geometry

The geometry design evolved as a result of the SKITTER configuration and the outside surface area required by the rod holder attachments. The structure is a six-sided figure of symmetrical shape with three of the alternating sides longer than the other three. Figures 4.5.4.1 through 4.5.4.3 display the geometrical dimensions and angles of the structural interface.

The three sides which are shorter are located under the legs of SKITTER and are in effect "dead" space. Any objects placed in these areas would interfere with the motion The other three sides are the attachment points of the rod racks. These attachments required as much length as possible which resulted in the unequal side lengths. The height of the structure was determined by the power plant and accompanying fuel storage cylinders which supply electricity to the drill drive. A height of .5 meters was required mainly for the hydrogen, oxygen and waste water storage cylinder capacity requirements.

The top panel of the structure has a large opening in order to allow changing of damaged equipment such as the drill drive motor or control module. The bottom platform has more structural members to support the equipment and to provide a point of attachment for the drive motor. The side panels consist of cross framing to resist the torsional stress applied by the drilling operation. The side panels also contain vertical members to resist the upward force of the vertical acceleration used to reject the drill cuttings from the hole.

4.5.5 Construction and Assembly

The structure was analyzed using FEM (Finite Element Method) to find the highest stressed member. The rod diameter which was chosen to withstand buckling, stress and fatigue loading over the design life of the implement, is 25.4 mm. All the members are specified to be the same diameter to avoid a large number of different rod extrusion diameters and sleeve configurations. A later study to minimize individual diameters is recommended if the weight constraint is critical enough to warrant such a diverse number of rod diameters and sleeve configurations. The existing mass resulting from these dimensions is 71.1 kg. which is 697.5 earth pounds and 116.3 moon pounds.

The members are to be extruded using a matrix of 6061 aluminum with continuous beta silicon carbide fibers. This composite is described in the Materials Selection and Treatments section.

The sleeve connections are to be cast in parts with the number of parts depending on the geometry of the joint. The sleeves are to be cast using the same material as the structural members are extruded from. Joints joining members which are all in the same plane only require two halves, while three or four parts will be needed for three-dimensional joints. The joint construction will follow the following sequence:

1) One part or half of the sleeve is placed down on a flat surface
2) All structural members are glued into the sleeve part or half
3) The other half or parts of the sleeve are glued over the members
4) The sleeve halves or parts are bolted together through flanges provided on the perimeter of the sleeve

The sleeve recess which receives the structural members is sinusoidally machined at the edges to lessen the stress concentration applied at the end of the sleeve. A typical sleeve arrangement is shown in Figure 4.5.5.1. The insertion length of the member into the sleeve is 25 mm, which is the member diameter.

4.5.6 Connections to Attachments

One of the important duties of the structural interface is to do just that, interface. We had to be sure that the structure would not only withstand the moon environment and rigors of drilling, but that it could also accommodate the various apparatus for the operation.

This meant that we had to keep our design flexible until the final designs of the other groups were established. Figure 4.5.6.1 shows the different components that the platform must hold and the general location of each. Figure 4.5.6.2 shows the corresponding location of the fasteners and mounts for the components. The assumption was made that the platform and its attachments make up a self-contained, permanent apparatus. That is, there won't be a need for removeable fasteners between members and attachments.

The power generation equipment was placed inside the platform because it was large, awkward and sensitive. The power design group specified the dimensions of the plant and the three pressure vessels, as well as the brackets they will be mounted in. Since the vessels and power plant aren't stressed laterally, these fasteners won't need any critical design. They merely need to hold the vessels plant in place. Because large forces are transferred through the motor it was placed in the center of the structure so as not to create adverse moments on the structure due to the large forces transmitted through it. The power design group specified the sizes and geometry of the fasteners needed to secure the motor. Heat pipes used to transfer motor heat to the rejection panel are small and are easily placed inside. The control box is also placed inside the interface since it needs to be protected from unnecessary contact with moving parts.

The rods will be placed on racks around the perimeter of the platform. The interface will hold three racks consisting of 10 rods each. Each rack lies on the long sides of the interface in between the legs as seen in Figure 4.5.6.1.

The heat rejection panel is small(area = .016 sq. meters) compared to the racks and will fit easily between any of the rod racks. It will be attached similar to the rod racks.

According to the rotary disc design group, the disc will be connected to a bearing which will in turn be connected to the

structure. The bearing geometry and fastener locations haven't been specified. Consequently, we are designing under the assumption that a U-bolt arrangement will be adequate.

4.5.7 Fastener Considerations

As stated above, each of the objects attached to the platform, with the possible exception of the motor, are permanently affixed. We have specified locations and beam sizes and the other groups are designing their fasteners accordingly. We have informed them to use U-bolts. These type of "wrap around" fasteners are preferred because drilling holes into the beams will introduce stress concentrations.

4.5.8 Description of Loads

The rotary motor produces and transfers the largest forces on the platform. As mentioned above, the motor will be attached with three fasteners on the 'floor' of the structural interface. The torque and drilling force will be transferred at these fastener locations.

The motor design group used a torque of 68 N•m (50 ft.lbs.) as a maximum for drilling into the basalt of the moon. However, the drill bit group didn't confirm this figure and didn't specify a different one. Accordingly, we decided to use the maximum load torque of the motor itself, 271 N•m (200 ft.lbs). Thus, if the drill string jams and forces the motor up to its limiting torque, the structure will remain intact. Dividing this torque by the effective radius of the fasteners (.23 meters), we obtain a force of 395 N (89 lbs.) acting tangent to lines intersecting the fasteners and the center of the motor.

The vertical drilling force will also be transferred through the motor connections. Estimates by the drill-bit design group indicated a 890 N (200 lbs) force was necessary to successfully drill into the moon basalt. For our analysis, an assumed drill force of 300 N (75 lbs) will act vertically at each of the three motor fasteners.

The rod holders and associated rods create flexural bending at the sides of the platform. Figure 4.5.8.1 shows how the shear forces will subject the top and bottom members to flexural bending. The maximum weight of a rod holder set is 22.1 lbs (98.1 Newtons = 10 rods/set X 9.81 Newtons/rod). The rod holders and the length of the rods constitute the moment arms. The rod holder design group specified the geometry shown in Figure 4.5.8.1. The rod holders extend the rods' center of mass approximately 2 meters. From these values and the geometry of the figure, we calculated the reaction magnitudes at the structure interface/brace attachments to be 214 N (48 lbs.) for the lower fastener and 200 N (45 lbs) for the upper fastener for each brace.

The motor design group also needs to house a mini-power plant inside the structure. This plant will consist of a main generating facility, three pressure vessels (one fuel tank, one oxygen tank and one waste water tank). The main generating facility weighs 149 N, (33 lbs), and is located along one of the structural interface's three longer sides, as shown Figure 4.5.6.1. A resulting moment of 80.5 N•m is produced on the structure. The total weight of the three pressure vessels is approximately 65 N, (14.5 lbs), and they will be located along the remaining two long sides. The vessels produce a resulting moment of 15.3 N•m. The downward forces will be transmitted through the fasteners described in the previous section.

The vertical accelerator will create a vibratory force translated by the drill string, through the motor, and into the platform at the motor connections. The vertical accelerator design group indicated that maximum force of 533 N (120 lbs) will be generated as the rock is accelerated up the auger. Since this force occurs at a different

time and in a different direction than the drilling load, we created a separate analysis for it. Thus, we have two cases for the stress analysis.

The robot arm, rotary disc, motor weight, heat rejection panel and control box all amount to very little in the moon environment. Together, they constitute less than 5% of the drill, accelerator, and rod loads. Consequently, we neglected them in our analysis.

4.5.9 Structural Analysis

The integrity of the structures' design was evaluated by utilizing SDRC I-DEAS finite element software package. Preparation of the analysis included setting parameters, defining the boundary conditions, loads, and making some assumptions. Parameters for the physical and material properties were derived in the Material Selection and Treatment section. Two load cases where analyzed due to the different loading conditions.

The boundary conditions of the structure consisted of the latch/structure connection. It was assumed that when the structure is connected to Skitter, the latch positions would remain fixed. Therefore as the loads were applied to the structure, reaction forces occurred at these locations that could be used to design the mechanical interface.

4.5.9.1 Case One

The first case included the motor, rod and power plant loads. From this analysis, the maximum principle tensile and compressive stresses were determined, 545 kPa and 597 kPa respectively. These values where then compared to the corresponding maximum stress values for Silicon Carbide Aluminum, 458 MPa and 49.25 MPa. The

dramatic difference indicated that failure due to tensile or compressive yielding was highly unlikely.

Of equal concern was the possibility of failure due to buckling. A critical slenderness ratio of 9.11 was determined in order to confirm the consideration of buckling over yielding. When compared to the slenderness ratio for Silicon Carbide Aluminum, 193.7, it was determined that if failure would occur it would indeed occur by buckling, and the Euler Column formula was used to determine the critical load. A value of 27,591 N was calculated for the critical load using the following equation:

$$Pcr = A\frac{p^2E}{(l/k)^2}$$

where A = 5.067e-4
l = 1.23 m
k= d/4 = .0254 m/4
E= 207e9 Pa

Pcr = 27,591 N

This value was then compared to the maximum load of 276 N, which was determined from the analysis as occurring on a member of length 1.23 m. Here again, by a considerable difference, the analysis indicates that failure due to buckling is improbable.

Another concern is the possibility of fast fracture. At the maximum tensile stress of 545 kPa, the critical crack length was calculated using the following equation:

$$Kc = s(\sqrt{pa})$$

where Kc = 91 MN/m^3/2
a = critical crack length

solving for a, the number is on the order of a hundred meters. This indicates that fast fracture is not going to be a factor at this stress level.

Another consideration is the strength of the adhesive used to join the structures' members. Evaluating the maximum shear stress equation below:

$$T,\ max = \sqrt{\frac{h}{2}}\ x\ \coth\sqrt{\frac{h}{2}}$$

h = (G) (l^2) / ((E) (t1) (t2))

t1 = adherend thickness

t3 = glue thickness

It was found that the shear strength of the adhesive is 5.77 MPa. From the FEM analysis, the maximum shear stress component was determined to be .53 MPa. This indicates that the weak link in the overall design is at the joints where a factor of safety was determined to be approximately 11.

4.5.9.2 Case Two

A second load case was run in order to analyze the vertical accelerator operation. The second case consisted of the loads resulting from the vertical accelerator, rods and the power plant. Because of the vertical accelerators' cyclic operation, fatigue loading was a prime concern. In order to determine whether the existing fatigue was either high or low cycle fatigue, the maximum stress for the cyclic loading was calculated. This value was found to be 1.05 MPa. When compared to the yield strength of the aluminum matrix, 169 MPa, it was obvious the loading is in the high cycle fatigue regime. Therefore, any scratches, nicks or dents introduced onto the structure can reduce the fatigue life by orders of magnitude. In order to determine the number of cycles to failure at this stress level, Basquin's law will be evaluated.

In the steady state regime the crack growth rate is described by:

$$\frac{da}{dN} = A(\Delta K)m$$ where ΔK is the cyclic stress intensity

A and m are material constants

Solving for the number of cycles to failure, Nf :

$$Nf = \frac{1}{A(\Delta s)^4 p^2}(1/a0 - 1/ac)$$

Since ac is much larger than a0, it will be ignored. Performing the calculation with A = 4 e-13 and m = 4, the number of cycles to failure are 18e12.

Considering the maximum number of cycles in one day, the number of days in a year and the service life of the structure, the number of cycles expected is approximately 100,000. Compared to the number of cycles to failure, the material has an infinite life at this stress level.

4.5.10 Material Selection and Treatments

The space environment is such a hostile work space that demands on materials are rigorous. Ordinary structural materials such as steels and irons are inadequate when subjected to the harsh conditions in deep space. Materials used in this environment must be designed according to the following criteria:

1. High strength to density and stiffness to density ratios.
2. Long useful life at the operating temperatures.
3. High creep resistance.
4. Resistance to thermal and mechanical fatigue.
5. Low thermal expansion coefficients.
6. High fracture toughness.
7. Resists outgassing.

Although this list appears to exclude all known materials, potential does exist for the following space-age materials:

1. Aluminum alloys
2. Titanium alloys
3. Aluminum-Lithium alloys
4. Metal matrix composites

Aluminum and titanium were considered because of the extensive use of these alloys in previous space applications. Aluminum-Lithium alloys and metal matrix composites are new materials that are specifically designed for space applications. These promising materials are on the forefront of the space age materials technology. In order to choose the proper material to build the structure, each candidate's mechanical properties were evaluated and based on the seven criteria and a suitable material was chosen. In addition to the mechanical properties, another important factor was evaluated, fatigue strength. Since the structure will be subjected to cyclic stresses, and since numerous scratches will be inflicted onto the structure, the ability to withstand fatigue loading is paramount. The following sections present an analysis of each candidate.

4.5.10.1 Aluminum Alloys

Aluminum alloys have been used in space applications for the past 30 years. By possessing a low density, approximately 2.7 Mg/m^3, and a high modulus, 71 Gpa, these alloys are very attractive materials. However, because most alloy elements have a very low solubility in aluminum they are segregated to the dendrite cell boundaries. The dendritic structure, side branches growing from crystals in the metal, usually are formed from second phase iron particles. The iron particles are large and add only small increments to strength, however they do reduce the fatigue strength of the alloy. The fatigue strength can be improved with certain alloys, however aluminum alloys with good fatigue properties typically have poor

thermal or cryogenic properties. Since the temperature on the moon will cycle between -130 degrees C. and 160 degrees C., the structure will be subjected to thermal as well as mechanical cycles. Over the period of ten years, it must be able to resist fatigue failure.

4.5.10.2 Titanium Alloys

Titanium alloys, unlike their aluminum counterparts, have good fatigue properties. The alloy Ti-6Al-4V exhibits the best all around characteristics. This material is especially promising at very low temperatures. Since the temperature on the moon will drop to near -130 degrees C, a material must withstand the rigors of the extreme cold. The unnotched strength, fatigue crack propagation rate and fatigue strength are surprisingly maintained at temperatures as low as -253 degrees C. However when notched specimens were tested the results indicated that the fatigue strength decreased dramatically in this alloy.

Another problem with titanium alloys is their density. Titanium alloys usually have a density of 4.5 Mg/m^3 or a density that is twice that of most aluminum alloys. With the cost of space flight proportional to the weight of the payload, any savings in weight will reduce the cost of the planned mission.

4.5.10.3 Aluminum - Lithium Alloys

In recent years, a number of aerospace metals firms have been placing a great deal of research into the area of aluminum alloyed with lithium. A major reason is because each weight percent of lithium, up to 4 wt.%, added to aluminum results in a reduction of density of 3 percent and an increase in elastic modulus of 6 percent. The potential for weight savings and an increase in stiffness have been the primary reasons for the heightened expectations of this alloy.

Although this alloy has received a lot of attention one major drawback is that, it does not possess good structural properties. In particular, the fatigue properties of aluminum-lithium are not promising. This is a result of the impurities contained in lithium which tend to be cites of microcrack initiation. Current research at the Alcoa Research Center is centered on the removal of the impurities, however a time frame for a high fracture tough alloy has not been set.

4.5.10.4 Metal Matrix Composites

Materials composed of metals reinforced with fibers have demonstrated unparalleled mechanical properties. When compared to metals, metal matrix composites have the following advantages:

1. Major weight savings due to higher specific mechanical properties
2. Dimensional stability for space structures
3. Strength retention at higher operating temperatures
4. Improved fatigue characteristics

With respect to organic matrix composites, MMC offer;

1. Higher operating temperatures
2. Does not outgas or degrade in space
3. Radiation survivability, laser, nuclear , UV, etc.
4. Improved joining characteristics
5. Better transverse properties

The main reason for the introduction of fibers into the metal instead of traditional work hardening methods is that precipitation or dispersion hardening result in dramatic increases in the yield strength with little influence in the modulus. However, when fibers

are placed into the metal-matrix they increase the stiffness and because of there light weight an increased stiffness to density ratio is achieved. A high stiffness to density ratio is sought for structural purposes involving compression or flexural loading, which are two of the prime loading mechanisms expected in the structure. The following mathematical analysis demonstrates the effect of a high stiffness to density ratio on material selection.

Consider a round bar loaded in axial tension:

l = length d = diameter P = applied force

p = density m = mass A = area

total deformation: $d = Fl/AE$

$m = \text{Volume} \times p = (p)(d^2)(l)(p)/4$

$A = (p)(d)(l)$

$m = (A)(d)(p)/4$

$A = 4(m)/(dp)$

$d = Fldp/(4mE)$

therefore mass $= Fldp/(4dE)$

$= F/d \times ld/4 \times p/E$

From the final equation it can be seen that for a given rigidity F/del a minimum mass is achieved for maximum E/p (stiffness to density ratio). In other words, it makes sense to use high modulus fibers that are lighter that the metallic matrix for reinforcement in structural applications.

Although it has been established that metal matrix composites are the materials of choice for structural applications, an important question arises, which MMC should be selected? From research and conversations with various vendors aluminum 6061 reinforced with 47 percent continuous beta silicon carbide fibers will be used to design the structure. In order to have made a selection, a number of areas were examined. These include micomechanical properties such as transverse stresses between fibers and matrix, composite thermal

expansion coefficient and macromechanical properties such as strength, toughness and fatigue.

4.5.10.5 Micromechanical Properties

When a metallic composite is used with fibers a problem that can arise is that of poisson's ratio mismatch. This imbalance is caused by having a metal with an extremely different modulus compared to the fibers. An imbalance of this sort can have a dramatic impact on the overall properties of the composite. Specifically, the transverse stresses and the pressure that results at the fiber-matrix interface can cause enormous residual stresses in the composite. The residual stresses can cause the ductile metal to deform plastically near the interface which results in a weaker composite. The following mathematical analysis demonstrates how poisson's ratio can influence the composite.

HOOKES LAW: (cylindrical coordinates, see Figure 4.5.10.1)

$$\begin{vmatrix} er & 0 & 0 \\ 0 & eq & 0 \\ 0 & 0 & ez \end{vmatrix} = \frac{(1+n)}{E} \times \begin{vmatrix} sr & 0 & 0 \\ 0 & sq & 0 \\ 0 & 0 & sz \end{vmatrix} - n \times \frac{(sr+sq+sz)}{E} \times \begin{vmatrix} 1 & 0 & 0 \\ 0 & 1 & 0 \\ 0 & 0 & 1 \end{vmatrix}$$

equilibrium condition: $d(sr)/dr = (sr-sq)/r = 0$

plane strain condition in terms of displacements:

$er = d(ur)/dr$ $\qquad$ $eq = ur/r$

ur = radial displacement $\qquad$ $ez = \text{const}$

$$so/k = (1-n) \times eq + n \times (er+ez)$$
$$sr/k = (1-n) \times er + v \times (eo+ez)$$
$$k = E/((1+n) \times (1-2n)$$

Substituting the plane strain equations into the above two equations:

$$so/k = n \times d(ur)/dr + (1-n) \times ur/r + n \times ez$$
$$sr/k = (1-n) \times d(ur)/dr + n \times ur/r + n \times ez$$

Substituting the above two equations into the equilibrium condition:

$$d^2(ur)/dr^2 + (1/r) * d(ur)/dr - ur/r^2 = 0$$

The solution to the differential equation takes the form of:

$$ur = Cr + B/r$$

The constants can be found by applying known boundary conditions at the interface.

By denoting the matrix as component 2 and the fibers as 1 and letting sr,2 = -p. An expression for the radial pressure at the interface can be derived.

$$p = (n,2 - n,1) \times 2(ez) \times V,2 / (V,1/kp,2 + V,2/kp,1 + 1/G2+,2)$$

V = volume fraction
$kp = E/((2(1+v) \times (1-2v)$

The stress components at the interface are:

Fibers: $sr,1 = qo,1 = -p$
$sz,1 = E,1 \times ez - 2 \times (n,1) \times p$

Matrix: $sr,2$ = function of p
$sq,2$ = function of p
$sz,2 = E,2 \times ez$ + function of p

From the above analysis it can be seen that when the poisson's ratio difference (n2 - n1) goes to zero the radial pressure goes to zero and takes with it most of the stress components.

Of the metal matrix composites examined, the aluminum composite that was chosen possesses a very low poissons ratio difference. Aluminum 6061 has a n of .36 and the fibers have a ratio of .25, the difference being .11.

As discussed in the previous section the dissimilar poissons ratios can be attributed to the different modulus of elasticity for each component. In the case of Silicon Carbide Aluminum the moduli are of the same order of magnitude, which indicates why the poisson's ratios are similar. In order to calculate the modulus of the composite, the theory of elasticity should be used instead of the rule of mixtures. Generally, the often used rule of mixtures will only give an order of magnitude approximation of the desired value. The only draw back with there use is that the should be solved numerically or with the aid of complex variable techniques. For equally precise calculations without the complicated theory of elasticity equations, K.K. Chawla in COMPOSITE MATERIALS suggest using the the Halpin - Tsai Equations. These equations take the form of:

$$p/pm = (1 + xnVf) / (1-nVf)$$
$$n = (pf/pm - 1) / (pf/pm + x)$$

Values for x:

E	longitudinal	2(l/d)	
	E	transverse	.5
	G	longitudinal	1.0
	G	transverse	.5
	K		0

Where p and pm are the desired quantities and the matrix value respectively.

Using the above values the composite modulus in the longitudinal direction is 207 Gpa and in the transverse direction it is 159 Mpa.

Another micromechanical area is the thermal expansion coefficient. Just like a large difference in poisson's ratio can create residual stresses so too can dissimilar a's. When a choice is made to combine a metal and its reinforcing fiber careful thought is used so as to preserve a thermodynamic equilibrium when the composite is formed.

From the mechanical data available, the aluminum composite discused is comprised of components with similar a's. Aluminum 6061 has an a of 20 exp(-6)/K. The fibers have an a of 5.7 exp(-6)/K. Because the matrix and fibers have am order of magnitude similarity, the residual stresses in Silicon Carbide aluminum will be minimized.

An often used method of calculating the thermal expansion coefficient of the composite is the rather simple rule of mixtures formula. However, the use of the formula will overestimate the expansion because it does not take into account the restriction that the stiff fibers impose on the matrix. The fibers by restricting the movement of the matrix produce a composite that has a cte much less than a weighted average formula can predict. If the assumption is that the poisson's ratio differences are slight, as was shown earlier, then R.A. Schapery has demonstrated in the book COMPOSITE MATTER the validity of the following formulas:

a longitudinal: Vf Ef af + Vm Em am / (Ef Vf + Em Vm)
a transverse: af (Vf)^.5 + am(1-(Vf)^.5)(1 + K)

K = Vf nm Ef / (Ef Vf + Em Vm)

using the following values:

Vf = .4 Vm = .6 Ef = 430 Gpa
Em = 71 Gpa am = 20 exp (-6) / K
af = 5.7 exp (-6) / K
nm = .36

The thermal expansion coefficient of the composite in the longitudinal direction is 7.94 exp(-6) / K. The thermal expansion coefficient in the transverse direction is 12.1 exp(-6)/K. Notice that the composite will tend to expand more in the transverse direction. This is caused by the continuous fibers restraining the matrix more in their principal direction, longitudinal.

4.5.10.6 Macromechanical Properties

The macromechanical properties that will be of most concern are, compressive and tensile strengths, toughness and fatigue. The compressive strength of a unidirectional composite cannot not be predicted by examining both the compressive strength of the matrix and then the fiber because the main failure mode in compressive loading is buckling of columns. More specifically, fiber composites fail in compression by periodic buckling of the fibers. In order to determine the compressive strength of the composite, two buckling modes were examined. The first, in phase buckling, is characterized by the fibers buckling with the same alignments. In such a case the composite strength in compression is proportional to the matrix shear modulus, Gm. Whereby:

$$s,c = Gm/Vm$$

For an isotropic matrix, of which aluminum 6061 is;

$$Gm = Em/(2)(1+n,m)$$

Therefore;

$$s,c = Em/(2)(1+n,m)(Vm)$$
$$= 71(Gpa) / (2)(1+.36)(.53)$$
$$= 49.25\ Gpa$$

The other failure mode is out of phase buckling. This buckling mode involves transverse compressive and tensile strains. Here the compressive strength is given by the geometric mean of the fiber and matrix Young moduli:

$$s,c = 2/3 \quad (Vf)\ ((Vf\ )(\ Em)(\ Ef)\ /\ (Vm)^{\wedge}\ .5\ )$$
$$= 51.56\ Gpa$$

The particular mode of buckling is primarily dependant upon the volume fraction of fibers. In phase buckling is noticed at higher volume fractions because the fibers exert more influence on each other and tend to couple in phase. Since Silicon Carbide Aluminum uses 47 percent fibers, the upper bound on compressive strength is 49.25 Gpa.

The tensile strength can be similarly calculated with the following results:

Tensile Strength	(0 degrees)	1458 MPa
	(90 degrees)	86 MPa

High fracture toughness is one of the most attractive characteristics of composites. Because of the crack blunting effect of the fibers, these materials can resist crack propagation both statically and dynamically. In the particular case of Silicon Carbide Aluminum, the continuous fibers act as roadblocks to any crack that is propagating in the longitudinal direction. The fracture toughness of Silicon Carbide Aluminum is compared with Silicon Carbide particles and unreinforced aluminum in the following table:

MATERIAL	NOTCHED TENSILE STRENGTH % OF UNOTCHED STRENGTH	APPARENT K (KSI SQRT(in))
SCS2/AL	100	73
FP/AL	65	36
SiCp/AL	65	24-28

As illustrated in the table, Silicon Carbide Aluminum has a far superior fracture toughness compared to unreinforced aluminum and Silicon Carbide Aluminum with whiskers, a rival material.

Fatigue is an area of composites that has received a great deal of attention. Fatigue failure mechanisms in composites are quite different than in metals. Fatigue failure in metals occurs as a result of initiation and growth of a crack. Fiber composites, on the other hand, can withstand a variety of subcritical damage (matrix cracking, fiber fracture, fiber/matrix decohesion, and ply cracking). The biggest difference in fatigue failures is that in metals the critical factor is crack length while in composites it is crack density.

The various forms of damage mentioned above result in a reduction in the load carrying ability, which in turn causes a reduction in stiffness and strength. Fatigue, in composites, is characterized by two distinct stages. In the first stage, non-interactive cracks appear in isolated piles. In the second stage, the damage becomes localized in areas of crack interaction.

Just as the micro and macromechanical properties of Silicon Carbide Aluminum were evaluated, so were the elevated and cryogenic temperature properties. As mentioned in the opening of this section, the lunar environment is severe. In fact, the lunar temperature will cycle between 160 degrees C and -130 degrees C within one lunar day. Typical mechanical properties evaluated at room temperature may become meaningless at the range of temperatures expected on the moon.

Figure 4.5.10.2 illustrates that the strength of Silicon Carbide Aluminum, in the fiber direction, is far superior to other reinforced aluminum composites or even unreinforced aluminum 6061 at elevated temperatures. Figure 4.5.10.3 is an another example of the excellent high temperature capabilities of this composite. From the figure, it can be determined that the composite retains it stiffness up to approximately 300 degrees C.

Another area of prime concern with the use of materials on the moon is thermal fatigue. In metal matrix composites, thermal fatigue can have devastating effects on the material. More specifically, if the fiber and matrix have vastly different thermal expansion coefficients, the interface can be weakened causing the fibers to pullout of the matrix. The end result can be catastrophic failure of the structure. However, as discussed earlier, aluminum and the silicon carbide fibers have similar cte's which results in a composite that is not easily susceptible to thermal fatigue.

Some of the cryogenic properties of Silicon Carbide Aluminum are illustrated in Figure 4.5.10.4. The plots of composite strength versus temperature indicate that the material is not expected to loose any strength or modulus at subzero temperatures. Although the data was obtained down to -50 degrees C, these values should not change radically at the expected moon low temperatures. In fact the only problem that might arise is with the fatigue properties of the composite. Since the matrix of aluminum alloy 6061 becomes less ductile at these temperatures, the possibility of matrix failure could arise. Examining Figure 4.5.10.5, the fatigue properties are evaluated at high and low temperatures. From this data, it can be determined that the fatigue data corresponds favorably at these temperatures.

4.5.10.7 Treatment

An area that has not received any attention as of yet is the performance of the material when exposed to high levels of radiation for an extended period of time. Since the moon does not have an atmosphere that can filter the immense amount of radiation flux, any material used on the moon must withstand radiation from all sources. These include solar wind, solar flares, cosmic rays and ultraviolet radiation. Silicon Carbide Aluminum has a superior resistance to radiation degradation, however after a period of time

the radiation bombardment can attack the fiber-matrix interface causing a catastrophic failure. In order to prolong the life of the structure, a number of alternatives have been examined. One of these is to coat the entire structure with a radiation absorbing polymer. This polymer would act as a shield to protect the composite. One serious flaw with this approach is that the polymer would have to a near identical thermal expansion coefficient as the composite. If the polymer did not expand and contract as the composite does, the coating would loose its adhesiveness to the composite and peel off.

The other approach considered is of applying a sealant to the composite. The sealant would be similar to sealants used on wood to prevent water damage. By using a sealant the thermal expansion coefficients would not play as significant of a role because the composite would tend to allow the sealant to penetrate the first few microscopic layers. The sealant that has been used quite extensively is polydimethylsiloxane (PDMS). This thermoset polymer has as its backbone the high strength Silicon-Oxygen combination and methyl groups (CH3) as the side groups. This sealant is characterized by the following;

1. Glass transition temperature of 150 K.
2. Maximum operating temperature of 250 degrees C.
3. Thermal stability due to high bond energy of the backbone.
4. Good adhesive bonding with composites in the thermal cycling environment.

From the list it is evident that PDMS possesses excellent lunar properties. One particular advantage is that the glass transition temperature is so low that it will retain its' elastomeric properties at very low temperatures. In order to make the sealant provide UV as well as other forms of radiation protection, a UV absorber will be added to PDMS. The UV absorber, 2-hydroxybenzophene, will make

the sealant opaque thereby preventing the radiation from penetrating into the composite.

One additional problem must be addressed at this time. The point has already been made that the composite does not outgass, however PDMS does. In order to prevent the outgassing of the polymer research has shown that the following measures can be taken:

1. Curing the polymer at temperature well above the conventional curing levels.
2. Vacuum purification of the polymer.
3. Solvent extraction.

4.5.10.8 Adhesive Analysis

In order to build a rigid structure, the individual members must be connected in some permanent manner. Bolts and rivets can be used with composites, but it is often necessary to have load spreading inserts bonded into the structure, in order to reduce the stress concentrations. One particularly attractive bonding method is the use of adhesives. Adhesive bonding allows for a more gentle diffusion of the load into the structure, thus reducing the localized stresses encountered with the use of rivets and bolts.
The stress analysis for an adhesive bond is very complex. In fact, most of the methods used to determine the exact stress and strains on a joint are solved by numerical methods. Although this may make the calculations too complex, the tubular lap joint stresses and strains can be approximated by the ordinary double lap joint. Utilizing the double lap joint, the resulting stresses will be rough approximations to the actual values.

Since the adhesive joint will be subjected to high temperatures, an elasto-plastic analysis will be used to determine the stresses. The analysis was completed in detail in Structural Adhesive Joints in

Engineering by Robert D. Adams. The following section is a condensed version of his analysis.

Adhesive joints are typically subjected to three forms of stresses; shear stresses, bending moments, and tearing stresses. The analysis has shown that the maximum stress is a shear stress and occurs at the end of the joint. The stress is approximated by the following equation:

T, max = sqrt(h/2) x coth(sqrt(h/2))
h = (G) (l^2) / ((E) (t1) (t2))
t1 = adherend thickness
t3 = glue thickness

The tearing stresses or bond peel stresses cannot be ignored because their magnitude is less than the shear stress. The bond peel stress is much higher at the end of the joint and decreases to a minimum near the midsection of the joint. These stresses are caused by a high stress concentration at the edge of the adhesive joint. In order to reduce the stress concentration and to provide for a smoother transition of stresses into the otherwise unstressed regions of the joint-adherend interface, the overlap will be machined into a sinusoidal pattern to a distance of roughly one half of the overlap length. This pattern will enable a greater amount of shear energy to be transferred uniformly between the adherend and the adhesive.
In order to determine the glue thickness and the overlap length, a set of graphs for adhesives are employed. These graphs indicate for a certain glue thickness the optimum strength and for a overlap length the optimum strength. However, for a first order approximation the overlap length can be set to the diameter of the adherend. The glue thickness can be found from the graph of a typical adhesive to be approximately .15 mm.

The choice for an adhesive is similar to the choice for a material, it must be capable of withstanding the rigors of outer space. In the previous section it was mentioned that siloxanes are well suited to

the lunar environment and after much research, it was discovered that a form of PDMS can also be used as a space adhesive. This material, methacrylate-siloxane with 25 percent silica reinforcing filler(Whacker HDK 2000), possesses excellent physical properties. The properties were evaluated at both high and low temperatures and are summarized in the table below.

PROPERTIES	
Tensile Strength	2.86 MPa
Modulus	.48 MPa
Tear Strength	8.9 KPa

4.5.11 Mechanical Interface Design and Operation

The mechanical interface refers to the latch system which connects the drill implement to SKITTER. A very important aspect of the design was to conceive a connection arrangement which has the following properties:

1) Simplicity
2) Self-aligning movement
3) Self-closing operation
4) Small number of moving parts
5) Dependability

The latch design was kept simple in order to insure remote operation and robot control. Only one command is needed from ground control during the entire drilling process. This command is sent when the drilling task is complete and the implement is to be detached from SKITTER.

The closing of the latch was designed to be completed without any mechanical actuation required other than the force of SKITTER

lowering itself onto the implement. An involute cup with flat sides with an attachment rod in the center is the target of the latch claw. Both the claw and receiving cup are made with involute profiles. An involute curve is generated by tracing a point on a cord as the cord is unwrapped from a cylinder. This allows a smooth closing action between the mating surfaces. As the claw enters the cup, it is forced to close because the involute shape gets narrower towards the bottom and forces the two claw halves towards each other. The involute surfaces cause the claw to close until it reaches a point where the vertex of the claw hits the attachment rod. At this point, a lateral force is required to fully push the claws together. This is accomplished by placing one cam on each of the claw halves at a point where the attachment rod will contact the cams and create a moment about the claw pivot pin. This moment completely closes the claw and allows a spring-loaded lock pin contained on one half of the claw to extend into a mating hole on the other half of the claw which will keep the claw locked until implement detachment is desired. When drilling is complete, an electrical actuator is activated which pulls the lock pin out of the mating hole. The two halves of the claw are automatically pulled apart by two extension springs which cause the normal position of the claw to be open. Once the claws are open, SKITTER raises off of the implement. The latch mechanism remains open until SKITTER lowers onto another implement which operates on the same attachment basis. Figure 4.5.11.1 shows a typical latch with each part labeled.

The number of moving parts was kept to three. The two claw halves and the lock pin are the only moving parts, except for three springs. The lock pin-actuator mechanism can be separated from the environment by a dust cover to prevent interference. This design should insure a dependable mechanism which is not dependent on automated control.

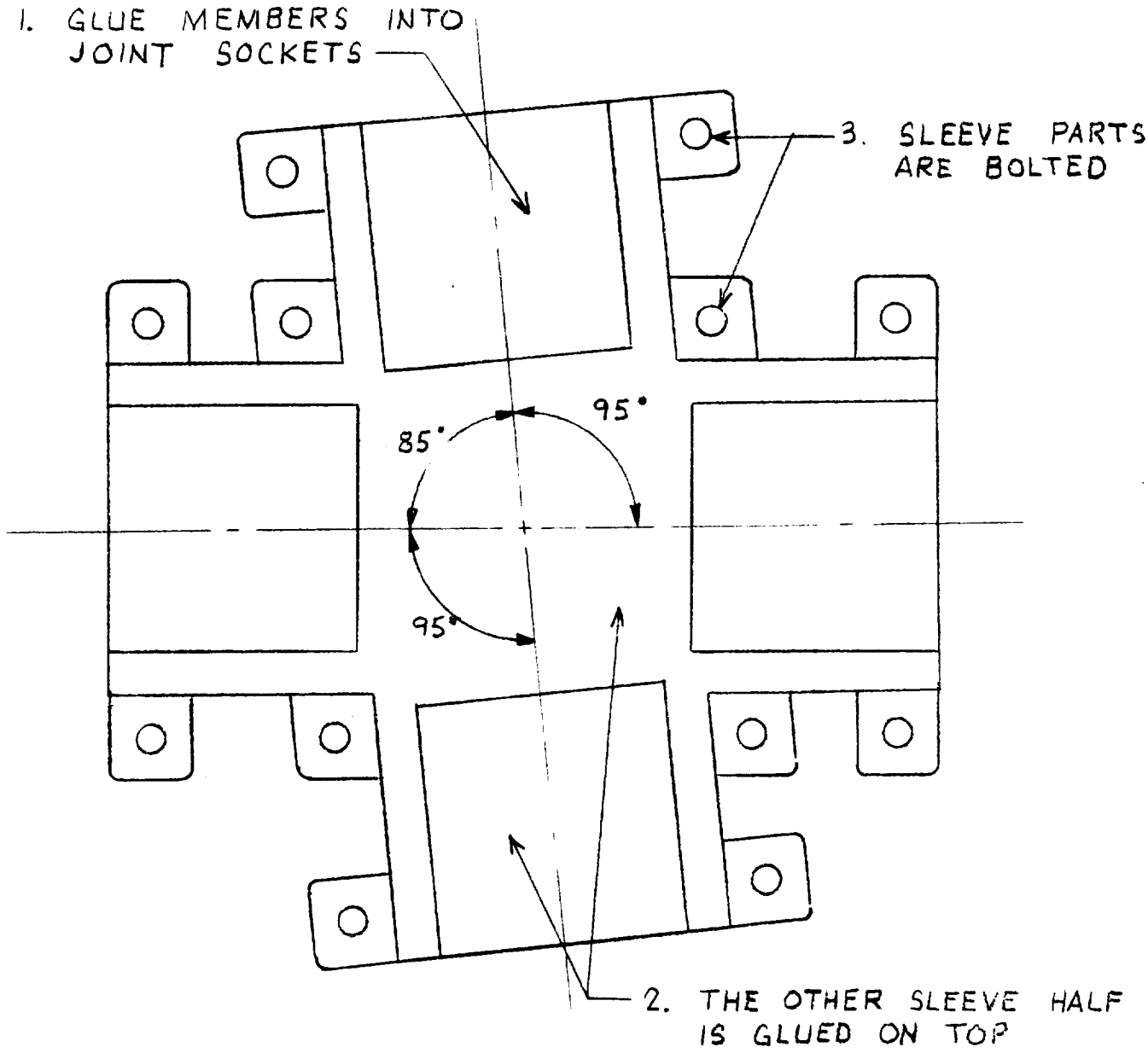

TYP. SLEEVE DETAIL

NOT TO SCALE

FIGURE 4.5.5.1

General Layout

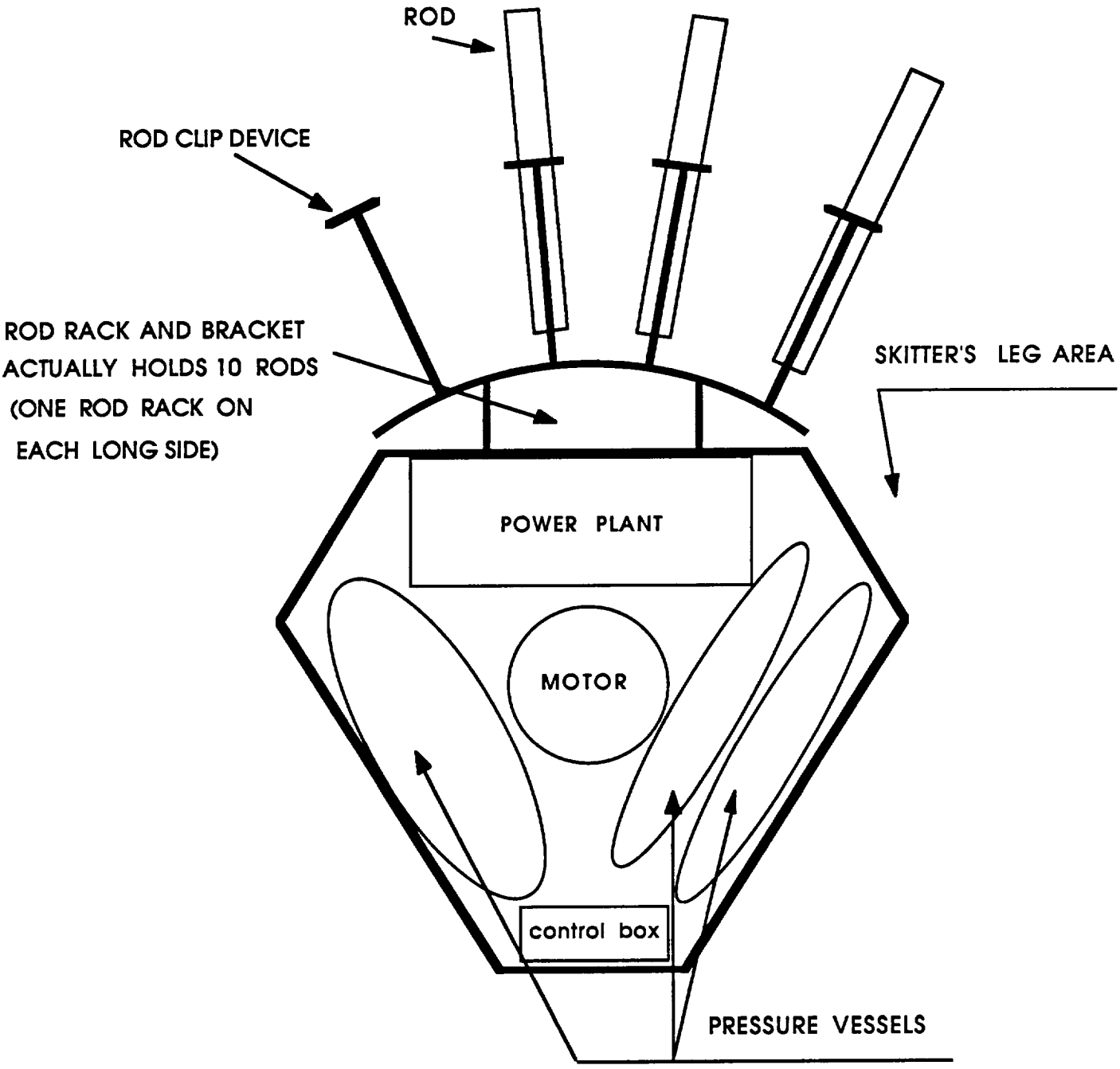

Figure 4.5.6.1

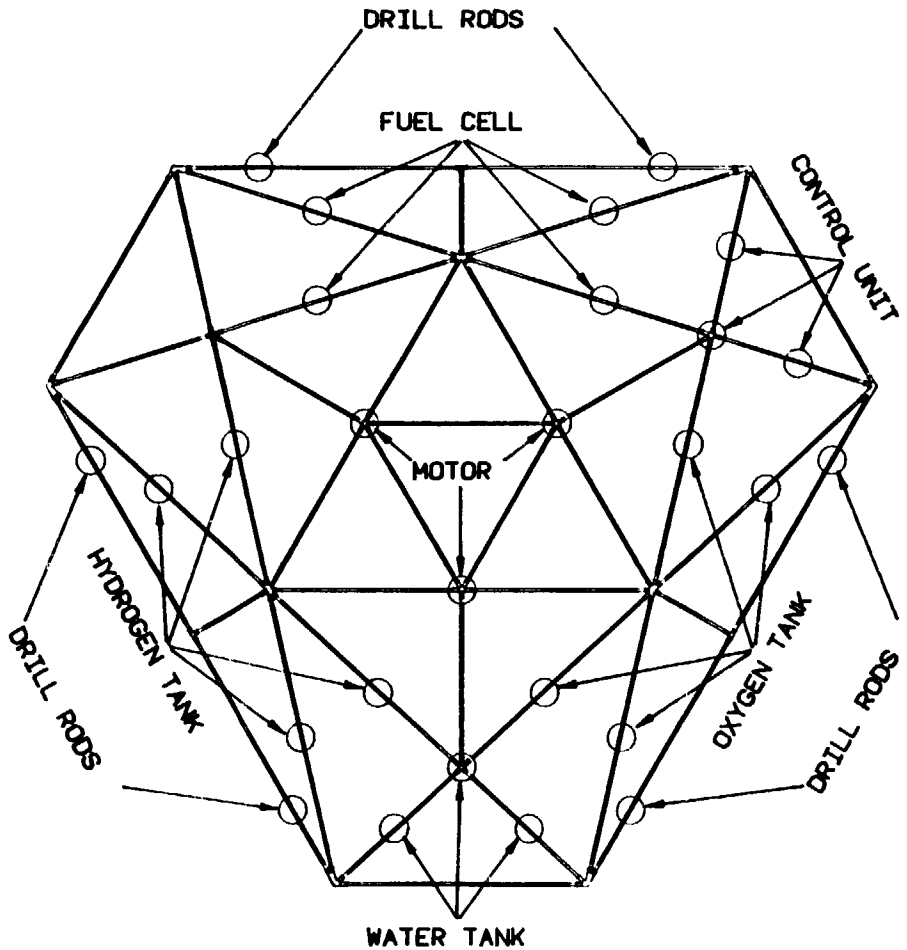

BOTTOM PANEL

ATTACHMENT LOCATIONS

NOTE: BALLOONS DENOTE ATTACHMENT LOCATIONS

GEORGE W WOODRUFF SCHOO OF MECHANICAL ENGINEERING
TITLE: ATTACHMENT LOCATIONS
DESIGN: STRUCTURAL INTERFACE
DATE: 5/28/89
FIGURE: 4.5.6.2

Shear Induced By Flexural Bending Due To Rod Weight

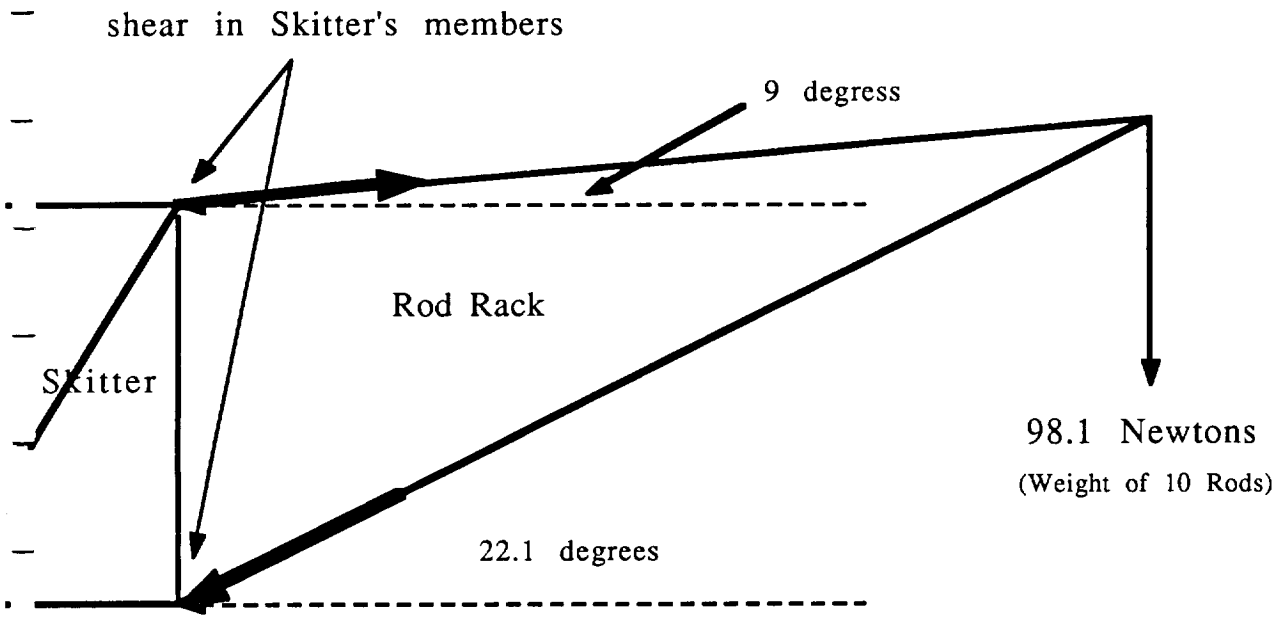

Figure 4.5.8.1

Fiber/Matrix Interface

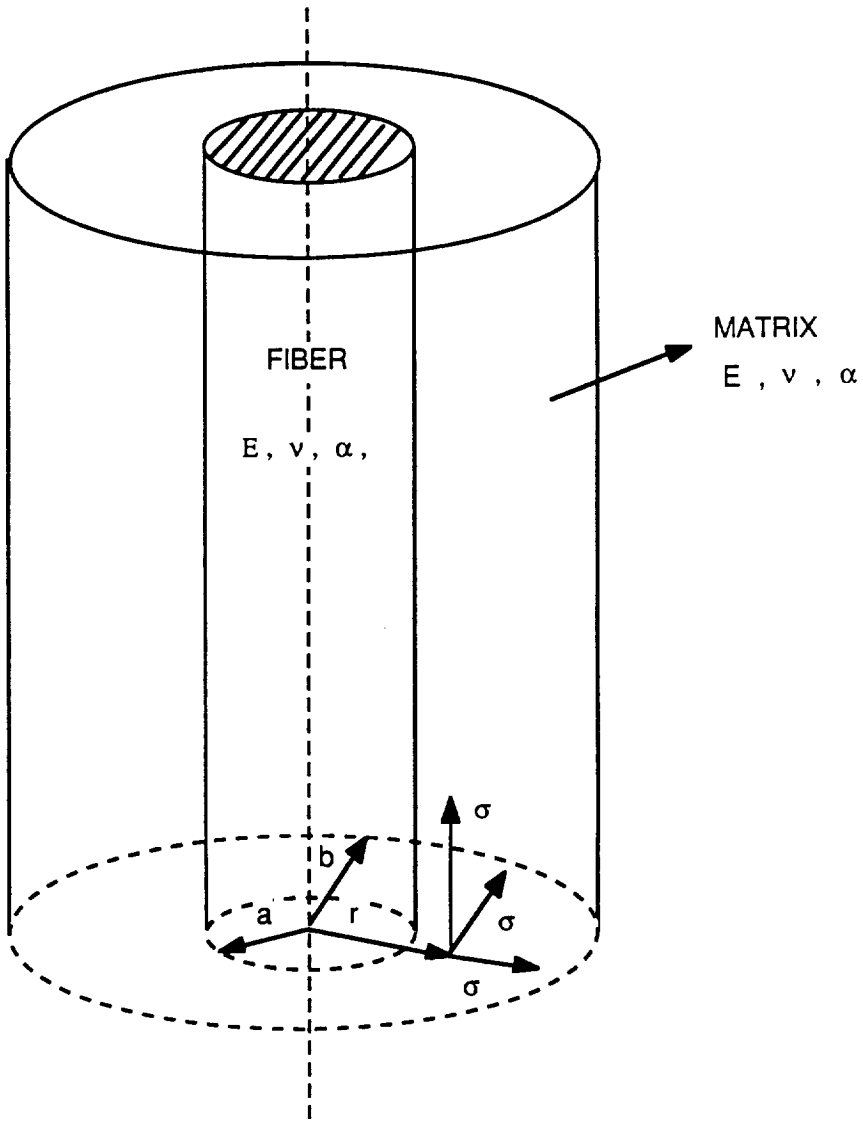

Figure 4.5.10.1

STRENGTH AT TEMPERATURE FOR CANDIDATE COMPOSITE MATERIALS

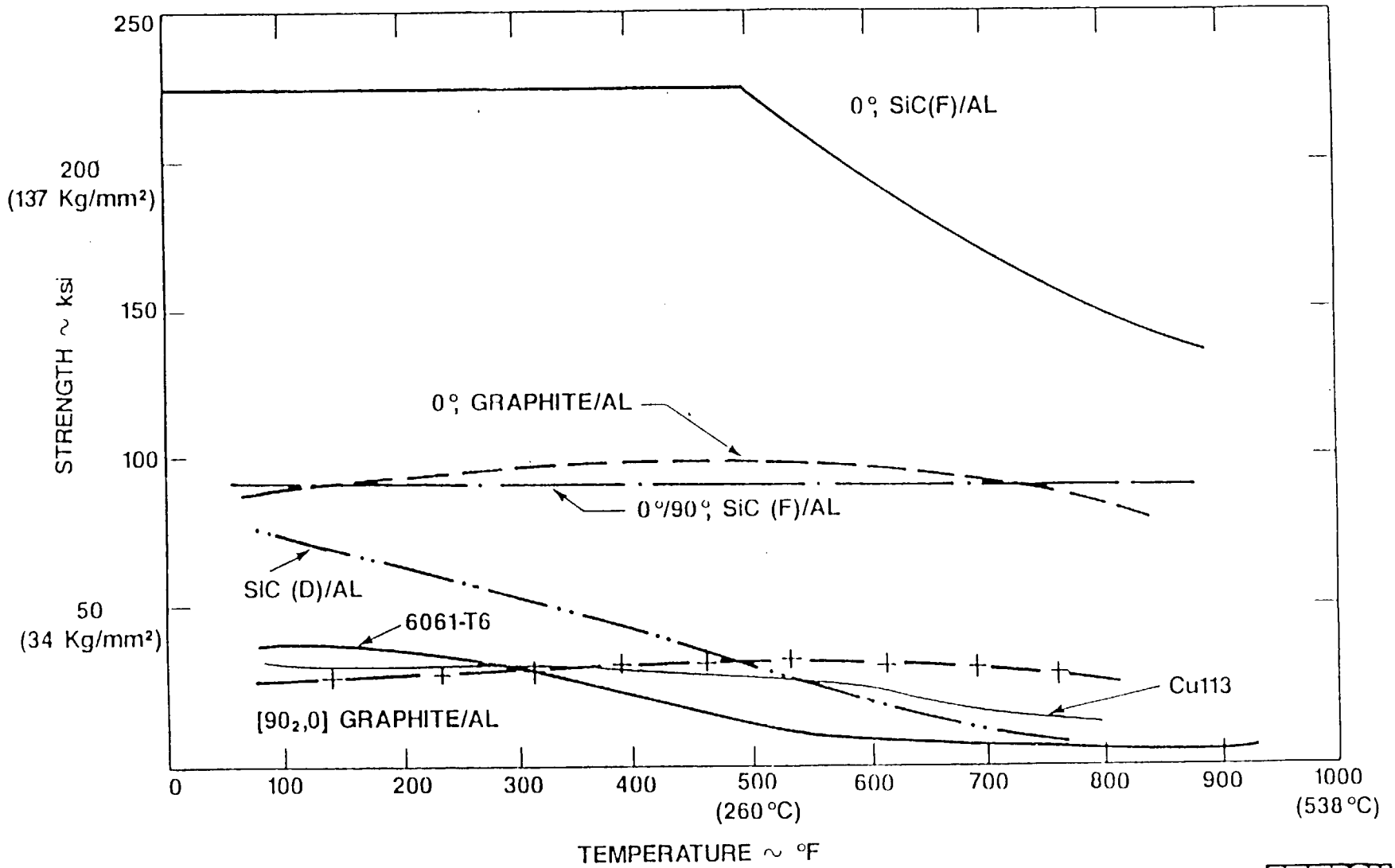

46-0527

Avco Specialty Materials TEXTRON

FIGURE 4.5.10.2

MODULUS AT TEMPERATURE FOR CANDIDATE COMPOSITE MATERIALS

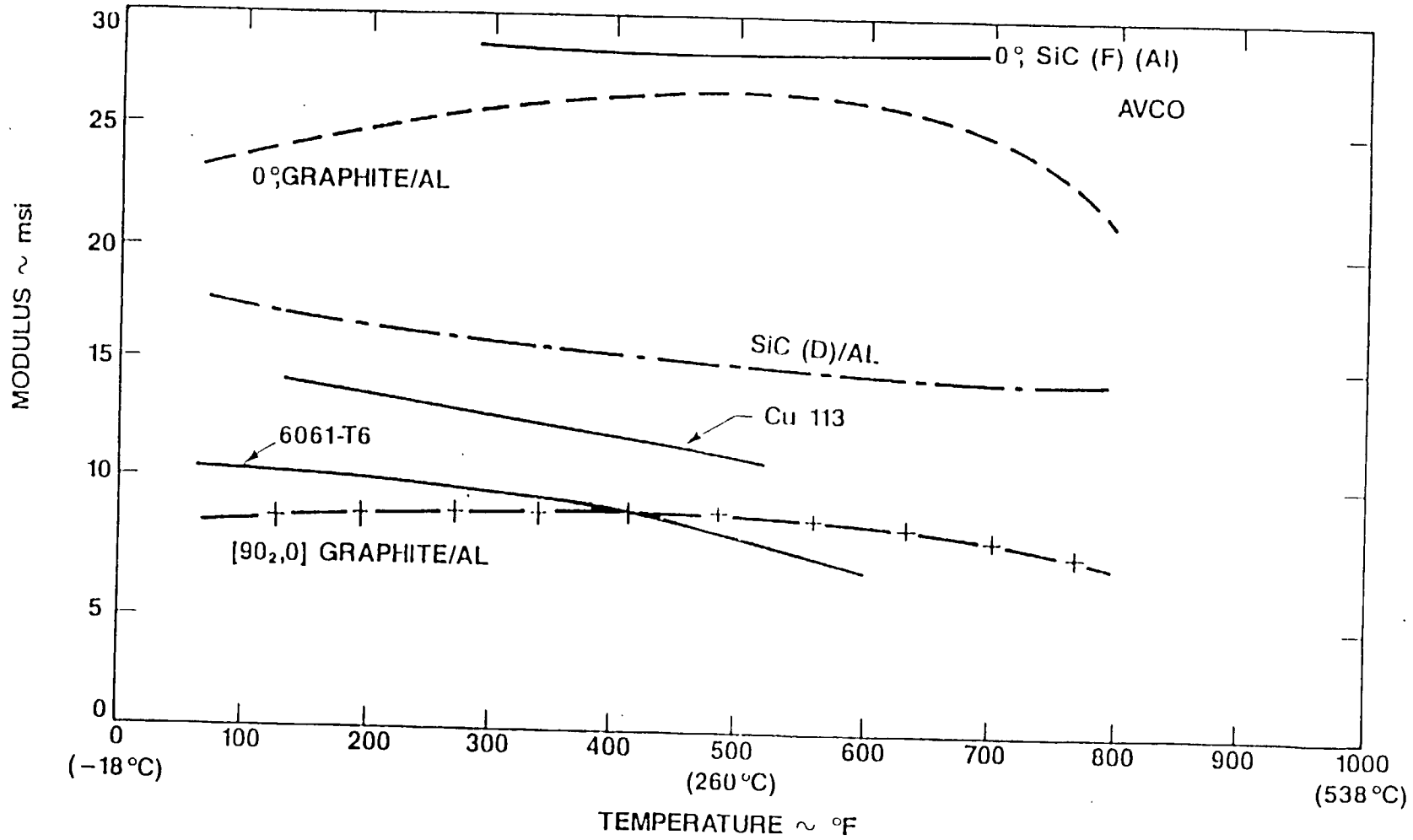

46-0528

Avco Specialty Materials TEXTRON

FIGURE 4.5.10.3

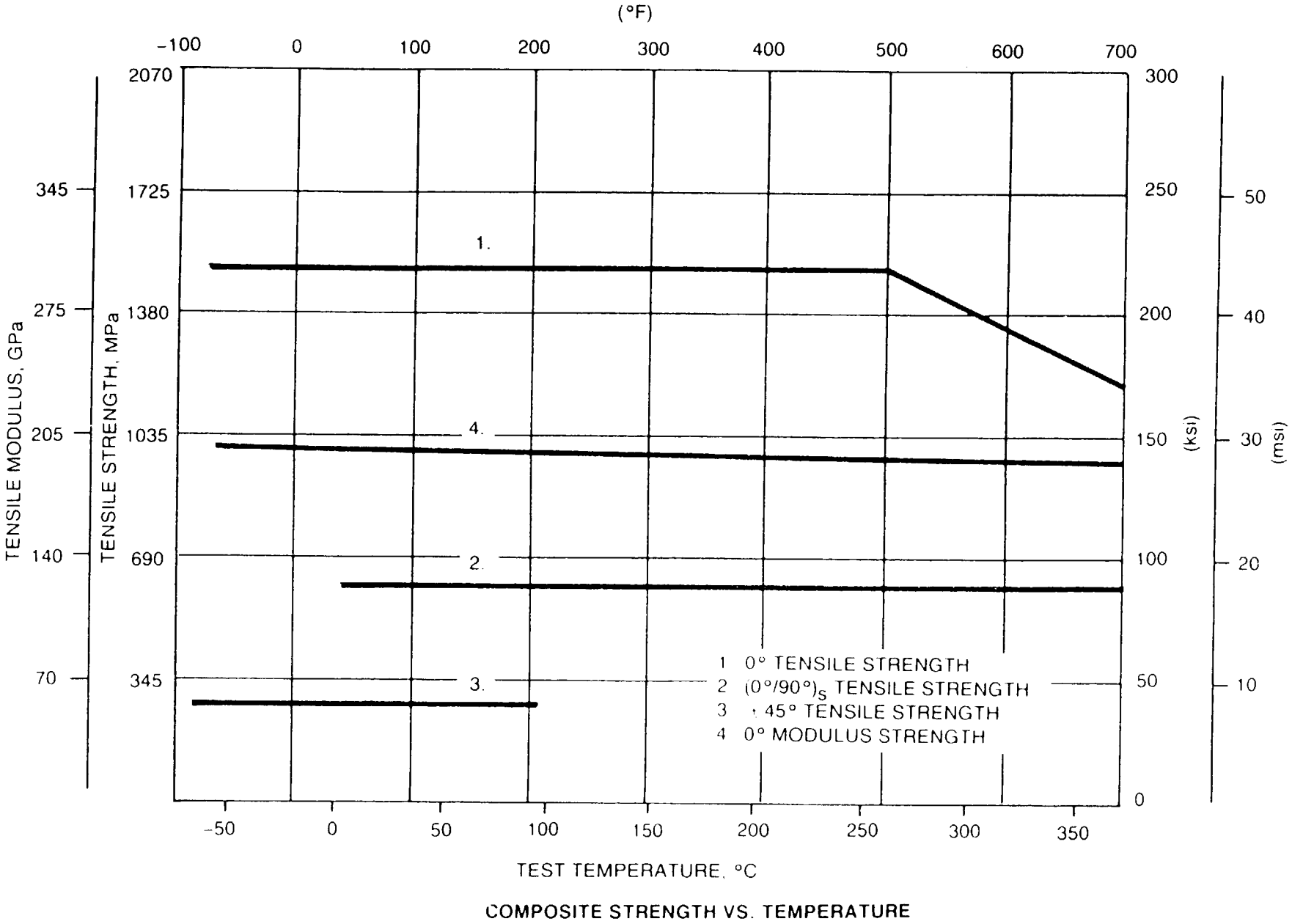

COMPOSITE STRENGTH VS. TEMPERATURE

86 2084

FIGURE 4.5.10.4

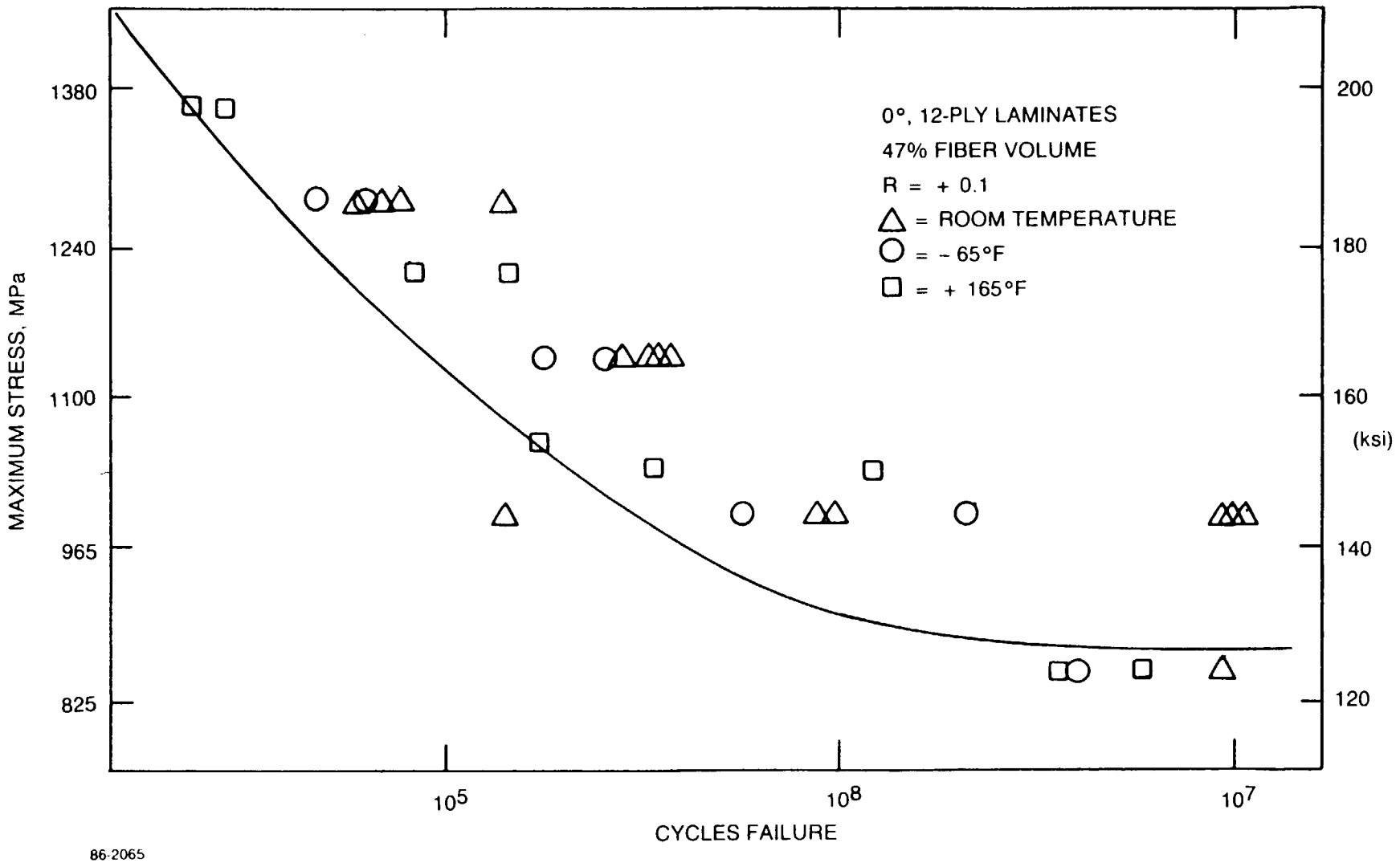

. SCS/ALUMINUM TENSION-TENSION FATIGUE

FIGURE 4.5.10.5

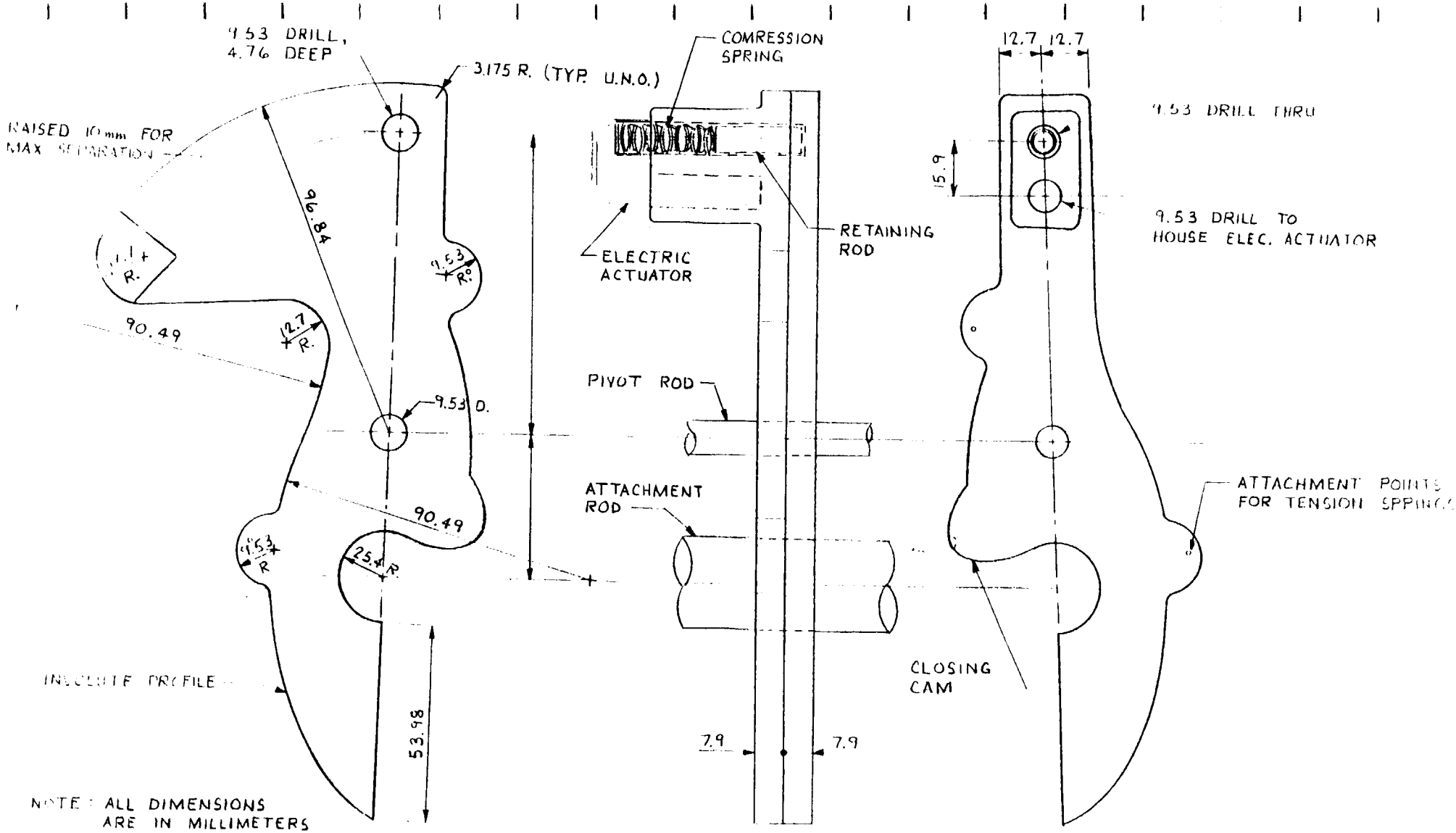

MECHANICAL INTERFACE LATCH

FULL SCALE

FIGURE 4.5.11

4.6 ROD CHANGER AND STORAGE RACKS

4.6.1 Gripping Mechanism

Since the end effector is responsible for the handling of the rods and other drilling implements, it's design and employment is vital to the success of the robotic system. These are the characteristics needed to define a gripping system:

1. Characteristics of the arm and especially the maximum transport load capacity of the arm.
2. Characteristics of the object, including
   - weight
   - range of specifications
   - nature of material (roughness)
   - geometry, dimensions and structure
   - contact forces
   - forces acting on object
   - environmental conditions
3. Maintenance

The gripping mechanism for the robot arm will be a bilateral gripper. This type of gripper was chosen over a unilateral design because of the gripping needed to grasp a rod. A magnetic unilateral gripper would not function as well as the bilateral. Unilateral grippers use only one surface to grip while bilateral grippers have two finger-like jaws. The multilateral gripper was determined to be too complex and unnecessary for our application. With our bilateral gripper, the degrees of freedom of the arm are reduced to three. This keeps the overall design of the arm simple and easier to maintain.

Considering various powering means, electric power use is light in weight and simple in maintenance for robotic arms. Electric power

is simpler to maintain versus an oil pressure system because it does not use any fluids that have to be sealed. All plastic or rubber seals would have to be covered to prevent them from being damaged by radiation. While the electrical method is inferior to the oil pressure method in output power, the electrical method is more suited to our design needs. Reliability in terms of maintenance is more important in our application versus output power. A large amount of output power is not needed since the heaviest object to lift is 16.67 lbs. on the moon. The fact that electric power is light in weight and simplistic was the determining factors in choosing it for gripper power requirements.

The gripper will be made of aluminum. For discussion on the choice of aluminum, please refer to the materials section, Section 4.6.2. The gripper has five main components. These include the motor, leadscrew, leadscrew nut, main rectangular bar, pinned bar, and the jaw part of the main rectangular bar. Please see Drawing 4.6.1.1 for the gripper design.

The jaw section of the gripper mechanism will be 81 mm tall. This will enable the jaws to grasp the 100 mm auger over two helix sections because of the double helix design, offering flexibility in grasping the auger. The gripper can grasp the auger on any part of its length. The main rectangular bar will connect to the jaw section at the middle of its 81 mm height. This will reduce the moment the object causes on the connection between the gripper and the robotic arm. The jaw section is 170 mm of the main rectangular bar length.

The gripper has to be designed to grasp both 100 mm augers and 50 mm rods. A V-type gripper jaw was chosen for its ability to accommodate both the 100 and 50 mm diameter digging implements. This design will enable the jaws to grip both size objects on the centerline of the gripper, considered to be a key design parameter. Therefore, the robot arm will only have to be programmed to go to one position for each rod storage and retrieval location.

The gripper design of a screw-driver has been chosen. Screw-driven grippers are operated by turning the screw uniformly through a motor. Our design is operated by turning the screw in a right handed direction to force the threaded block to shift to the left, thereby tightening the jaws through the action of the toggle links. This gripper was designed as a non-overrunning device. If the motor loses power the gripper will not open and drop the object it was holding.

The leadscrew, 5 mm in radius, is made out of tempered steel. It is 110 mm in length, with a pitch of 50 threads per inch. Acme screws with metal nuts range in efficiency from 35% to 55%. A median value of 40% was chosen for our application. The steel screw will be lubricated to reduce the coefficient of static friction. The lead screw nut will have pins on it for the pinned rectangular bar connection. The lubricated leadscrew will be covered by a tubular cover that will be connected to the nut. The cover will slide with the nut. It will have ball bearings on its ends to help it slide and offer protection from the atmosphere. We realize that the cover needs to protect the lubricated leadscrew, although we have not engineered the cover because of time constraints.

The gripper will have a rectangular bar, 53.41 mm in length, that is pinned at both ends. This rod will be connected to the leadscrew nut. The bar rests at 86.3 degrees from the horizontal when the gripper is closed. The bar then moves to the right with the nut when the leadscrew turns. The bar rests at 90 degrees from the horizontal when the gripper is fully open.

Each gripper main rectangular bar will be pinned respectively at the left end. This is the pivot point upon where the gripper system rotates. The gripper mechanism will be welded to the robotic arm at a downward angle of 16.5 degrees. The angle enables the gripper horizontal access to the vertical rods, held by the footplate, while the robot arm is off center. By free body diagram, the force

required by the gripper is equal to the product of the coefficient of static friction and the weight of the heaviest object to lift.

$$F = \mu W$$

A total factor of safety was chosen by the product of the factor of safety for uncertainties in regard to the load and the factor of safety for uncertainties in the strength of the gripper.

$$n = n_1 n_S$$

$$n_1 = \frac{F_u}{F}$$

$$n_S = \frac{S}{\sigma_p}$$

Where:

F_u is the limiting value of F
S = yield strength
σ_p = permissible stress

The max load of the gripper was then computed using the factors of safety.

$$F_u = n_1 F$$

An assumption was made in the calculation of the maximum bending moment. The main rectangular arm of the gripper that has a bend of 159.68 degrees is approximated as a straight rectangular arm.

The maximum stress was then computed.

$$s_p = \frac{M}{Z}$$

The section modulus for a rectangular section is:

$$Z = \frac{I}{c}$$

$$Z = \frac{b\ h^2}{6}$$

The maximum stress is then reduced to:

$$\sigma_p = \frac{6\ M}{b\ h^2}$$

The depth of the rectangle can then be computed by solving for b:

$$\frac{S}{n_s} = \frac{6\ M}{b\ h^2} \qquad b = \frac{6\ M\ n_s}{S\ h^2}$$

Calculations for b:

$n_1 = 2.0$
$n_s = 2.0$
$n = 4.0$
$\mu = 0.4$, aluminum on aluminum

$$F = \frac{(100/6)}{0.4}\ (\ 4.448\ ) = 185.3\ N$$

$F_u = (\ 2.0)\ (\ 185.3\ ) = 370.6\ N$
$M_p = (\ .210\ )\ (\ 185.3\ ) = 38.9\ N\text{-}m$

The yield strength of aluminum was approximated to be 49 kpsi.

$$b = \frac{(\ 6\ )\ (\ 38.9\ )\ (\ 2.0\ )}{(\ .012\ )^2\ (\ 49k\ )\ (\ 6890\ )}$$

$b = 9.6\ mm$

The height of the rectangular arm is 12 mm, while the base has been calculated to be 9.6 mm. Therefore the thickness of the rectangular gripping arm needs to be 9.6 mm to achieve a total safety factor of 4.0. All rectangular bars of the gripper will have

these dimensions. The gripper jaws will have at least 9.6 mm at the smallest part of the base. Other areas of the gripper jaw base will be wider.

The clearance for the gripper to move between two adjacent rods of 100 mm is 168 mm. The gripper may be holding a 100 mm object. For the gripper jaw, 9.6 mm of material is required to prevent yielding. Each jaw only requires 20 mm to open fully and slip by the rod that was just stored. This leaves approximately 2 mm of clearance between each side of the gripper jaw and the rods it passes by. To achieve this 20 mm of opening for the gripper jaws, 3.45 mm of horizontal translation of the leadscrew nut is required.

The gripper will have to go to a preset position for the jaws to grasp the rod properly. The gripper can not move forward toward the rod and then be stopped by the rod. The rod would come in contact with the lead screw. The controls for SKITTER will have to preset the forward movement of the gripper to grasp the rods.

The torque needed to close the gripper with a force of 185.3 N must be designated. F_1 will be the 185.3 N force required by the gripper. F_2 will be the vertical component of the force on the pin at 100 mm point along the length of the gripper, as measured from the left end. The relationship between the two forces is:

$$F_2 = F_1 \left(\frac{0.310}{0.100}\right)$$

F_2 is then calculated as:

$$F_2 = 185.3 \left(\frac{0.310}{0.100}\right) = 574.5 \text{ N}$$

The pin is at an angle of 3.7 degrees when the gripper is fully closed. The component of F_2 that is the force on the leadscrew, along

the pinned rectangular bar, will be F_3. This force is then calculated as:

$$F_3 = \frac{574.5\ N}{\cos(3.7)} = 575.7\ N$$

The force acting as a weight along the horizontal length of the lead screw is a component of F_3:

$$W = 575.7 \sin(3.7) = 37.2\ N$$

The torque required to drive the load W using a lead screw with pitch, p, and efficiency, e, has the following components:

$$T_{Total} = T_{Friction} + T_{Acceleration}$$

$$T_{Friction} = \frac{F}{2\pi p e}$$

Where:

F = frictional force in ounces
p = pitch in threads/inch
e = lead screw efficiency

$F = \mu_s W$ for horizontal surfaces where μ_s is the coefficient of static friction and W is the weight of the load.

$$T_{Acc} = \frac{1}{386}\left(\frac{J_{Load}}{e} + J_{Leadscrew} + J_{Motor}\right)\frac{\omega}{t}$$

$$\omega = 2\pi p v$$

$$J_{Load} = \frac{W}{(2\pi p)^2}$$

$$J_{Leadscrew} = \frac{\pi L \rho R^4}{2}$$

Where:

J = inertia, oz-in^2
ω = angular velocity, radians/sec
t = time, seconds
v = linear velocity, in/sec
L = length, inches
R = radius, inches
ρ = density, ounces/in^3

The formula for the load inertia converts linear inertia into the rotational equivalent as reflected the motor shaft by the lead screw. The following assumptions where made in the calculations for the required torque:

μs = 0.15, for lubricated aluminum on steel
e = 0.4, for acme lead screw with metal nut
p = 50 threads per inch, a fine pitch is needed to move only 3.45 mm
L = 110 mm
R = 2.5 mm
ρ = 1.54 oz-in^3
v = 4 in/sec
ω = 100 milliseconds
J_{Motor} = 0.08 oz-in^2

The torque calculations are as follows:

$$F = (0.15) (37.2 \text{ N}) = 5.58 \text{ N}$$

$$F = (5.58 \text{ N})\left(\frac{1 \text{ lb}}{4.45 \text{ N}}\right)\left(\frac{16 \text{ oz}}{1 \text{ lb}}\right) = 20.1 \text{ oz}$$

$$T_{Friction} = \frac{20.1 \text{ oz}}{2 \pi (50 \text{ rev/in}) (0.4)} = .160 \text{ oz-in}$$

$$J_{Load} = \frac{37.2\ N\ (\frac{4.45\ N}{1\ lb})\ (\frac{16\ oz}{1\ lb})}{(\ 2\pi\ (50)\ )^2} = 1.36 \times 10^{-3}\ oz\text{-}in^2$$

$$J_{Lscrew} = \frac{\pi\ (\ 11\ cm\ )\ (\frac{1\ in}{2.54\ cm})\ (\ \frac{1.54\ oz}{in^3}\ )\ (\ \frac{.25\ cm}{2.54\ cm/in}\ )^4}{2}$$

$$J_{Leadscrew} = 9.83 \times 10^{-4}\ oz\text{-}in^2$$

$$T_{Acc} = \frac{1}{386}\ (\ \frac{1.36 \times 10^{-3}}{0.4} + 9.83 \times 10^{-4} + 0.08\ oz\text{-}in^2)$$

$$\frac{2\pi\ (\ 50\ rev/in\ )}{0.1\ sec}\ \frac{4\ in}{1\ sec}\ \frac{oz\text{-}in\text{-}sec^2}{oz\text{-}in^2}$$

$$T_{Acc} = 2.681\ oz\text{-}in$$

$$T_{Total} = 0.160 + 2.681 = 2.841\ oz\text{-}in$$

The torque required by the gripper is 2.841 oz-in. The torque of the motor will be controlled by regulation of the supply amperage. A plot of current versus torque can be generated from experimental procedures. An interpretation of the current pattern will enable the correct current to be supplied for the needed torque. Experimentation with current versus torque is needed to prevent too much torque being supplied. This design helps to protect the gripper system. If the pinned rectangular bar jammed, the current would increase as the gripper would try to close. The system would be programmed to decrease the current at a determined value. This would prevent the gripper from continuing to close on the jammed bar.

The gripper motor will be discussed in the motor section of the paper, Section 4.6.5. The weight of the gripper motor and gripper mechanism is 3.33 N.

4.6.2 Materials

Materials Selection

Many areas must be examined when choosing a material for any engineering application. These areas include indemnification of material requirements, analysis of the environmental capability of the material and whether such a material has been used in a given application successfully. In the case of space exploration, the environmental capabilities of the materials becomes the most important factor. Three factors that will affect material selection are:

Temperature - A chosen material must withstand the moon's temperature gradient which ranges from -158 C to 130 C during the two week lunar day. Creep and brittleness of material can occur.

Vacuum Environment - This type of environment causes loss of material by volatilization of diffusion. Many materials experience cold welding in this environment.

Radiation - Damage can occur by formation of lattice defects which cause loss of strength. Chain scissors and cross linking of organic materials develop.

Weight is also an important factor. A material chosen should have a high strength to weight ratio.

In considering a material for the arm, gripper, rotating plate and rack and passive gripper system, environment considerations are of great importance. Plastics can be eliminated due to off gassing

and radiation induced decomposition. Both of these mechanisms cause an increase in brittleness and a decrease in strength. Ceramics cannot be used because they can not handle loads in tension. They are also brittle and have extremely low coefficients of expansion making ceramic -metal combination difficult to design. It necessary that the mechanical are gripper, arm and rotating disk be of the same material so as to avoid having to design for differing expansion coefficients. High-strength alloys based on magnesium, aluminum, titanium, beryllium and steel are used in aircraft application and appear to be most appropriate for moon use. Of these alloys, titanium and aluminum appear to demonstrate the best properties in the moon environment.

Aluminum has several properties which are particularly advantageous to moon use. First, the alloys have a high strength to weight ratio. Second, they are highly reflective. Third, they are good thermal conductors. Fourth they are corrosion resistant and fifth, have a high melting point. The 2000 and 7000 series aluminum alloys are high strength alloys used for structural components. These alloys have been heat-treated and age-hardened making them capable of withstanding a large temperature gradient without deterioration of mechanical properties. The alloy 2219-T37 is particularly attractive. This alloy's major alloying element is copper. Copper provides increased strength and improves elevated temperature properties and machinability. It has been heat-treated solution treated and cold worked to an almost full hard state. Therefore it is strong but still retains some ductility. This alloy has structural use at high temperatures up to 600 F. It has also been used in cryogenic applications and aircraft parts. 2219-T37 is available in sheets, tubing, bars, extrusions and forgings. The mechanical properties are as follows:

ultimate tensile strength = 414 MPa

yield strength = 338 MPa

$$\text{density} = 2.99 \frac{Mg}{m^3}$$

Young's modulus = 71 GPa

Brinell Hardness = 117

Endurance limit of infinite at 500,000,000 cycles

Titanium alloys have properties much like aluminum. The alloy, Ti-6Al-4V, physical properties make it the best titanium alloy for the moon. This alloy is used for cryogenic applications and has excellent corrosion and creep resistance. Its mechanical properties are as follows:

ultimate tensile strength = 1000 MPa

yield strength = 900 MPa

$$\text{density} = 4.4 \frac{\text{M g}}{\text{m}^3}$$

Young's modulus = 115 GPa

Titanium,s performance in a vacuum environment is slightly better than than of aluminum. Aluminum cold welds at temperatures above 300 C while titanium cold welds at temperatures above 500 C. Considering all properties aluminum and titanium are almost equal in mechanical performance. Therefore it necessary to compare the cost, weight, weldability and commercial forms of the materials in question. Aluminum is much cheaper, weighs less, is easily weldable and is readily available is more commercial form than titanium. Further, aluminum has been used successfully in the moon environment previously. Considering these factors Al 2219-T37 is the material of choice. The arm, mechanical gripper and rotating plate will be made of this material.

The rack system will be constructed of the same composite used in the structural interface. This decision was made because the rack must directly attach to the structural interface. Thus, providing good continuity between these two parts. The rack can be attached with the same type of connection which is used to hold the members of the structural interface together.

All passive grippers, pins, bolts and lead screws will be made of tempered steel to ensure a long fatigue life. Tempered steel has been used previous for equipment clips on the lunar rover.

The differences in materials between the rack and the passive grippers leads to the question of how will the different thermal expansion coefficients affect the design. Because metals generally have expansion coefficients which are relatively similar, the design should not be effected. However, this should be tested.

Although it is traditional to use metals for bearings, plastics have been considered for their light weight and "self-lubrication" features. The problems using plastics in space environments that were previously mentions will no be in effect because the bearings will be enclosed and not subjected to the damaging radiation. Plastics can be made self-lubricating be adding graphite, molybdenum disulfide, or silicone oil to the forming process. The polymer that has the best characteristics for this application is polyimide. Polyimide can take a maximum load of 10000 psi, operate continuously at 5000 $\frac{ft}{min}$ at a critical temperature of 316° C. It is one of the strongest polymers for this application having a modulus of 0.45 x 10^6 psi . Plastics have already proven themselves superior to other engineering materials and have been used successfully on the moon for interior structural purposes.

Lubrication

Several modes of lubrication are available that can be used on the moon. Again the environment must be taken into consideration. The regolith presents a special problem when dealing with lubrication. The regolith has the consistency of flour and tends to accumulate on all parts exposed. If an oil or other liquid system is used it would soon become gummy due to the regolith and lose its effectiveness. Liquid lubricants are also subject to evaporation, become unstable due to radiation exposure and lose oxidation

stability. A solid lubrication system is the other form that can be explored. The advantages of solid lubrication are listed as follows:

1. Shearing takes place more easily when high loads are applied.
2. Can be used at low speeds because it prevents the stick-slip action of asperities on mating surfaces.
3. Operate under extreme temperatures.
4. Can be used in dirty and abrasive environments.
5. Prevent fretting wear.
6. Simplify design.
7. No maintenance or unreliable parts.
8. Intermittent action with long periods of disuse.
9. No reaction with environment.
10. Stability under nuclear radiation.

From this list, it is apparent that solid lubrication is very appropriate to moon use. The only disadvantage with this system is that it is not renewable. Therefore the amount of lubricant film placed on the parts exceed the required amount for safety purposes. Resin-bonded molybdenum disulfide would be the lubricant of choice. It has a wear life of 9,869,000 cycles at 35,000 psi. It also has the lowest coefficient of friction at 0.036.

4.6.3 Rack and Passive Gripper System

Rack

The rack structure contains three sections, one between each of the legs of SKITTER. It is made of the same composite that the structural interface group has chosen. The reason for this selection is for continuity between the two structures. Both structures will thermally expand the same and they can both be fastened with the same connectors and glue.

The rack's members are circular rods. The top rods are 17 mm in diameter. These two rods are 1 meter apart and extend 868 mm out from the top of the structural interface beneath SKITTER. These rods are supported by two other rods that are 36 mm in diameter and extended from the bottom of the structural interface. These rods support the center of the top rods and are at an angle of 49 degrees from the horizontal. These rods are 662 mm long. The actual storage area has to be in an arc because the arm is on a rotating bar. This arc enables the rod to be grasped in the same place every time by a spring clip . The arc has a radius of 1.51 meters and an arc length of 2.1 meters. The arc has spring clips connected to it that hold the rods. These clips are at a 61.5 degree angle from the horizontal. The placement of the clips at an angle is used to compensate for the angle of the rods when the are placed in the rack by the rod changer arm. There are 14 clips on each of the three rack sections. The rack has a space in the center to allow the arm to move from behind the rack to retrieve another rod or implement. Ten of the clips are for 50 mm rods and the other four clips are for 100 mm implements. The clips are placed symmetrically with respect to the support rods. There is 140 mm between the center of each of the clips which allows room for the gripper to release the rod and move behind the rack.

When a rack section is completely loaded, the two support structures must support 227 kg each. The diameters stated above were calculated with a factor of safety of 2 and the actual calculations are shown in Appendix A.6. The stress calculations for the arc were done by approximating it as a straight beam. The top beams are experiencing shear while the rods extending from the bottom of the structure are in compression. The force to place a rod into the rack is only 34 N for the 100 mm rods and half that for the 50 mm rods. This force was insignificant in the calculations done.

In addition to force and stress calculations, deflection of each of the beams were found. The greatest deflection was in the support structure. It was found to be 5 mm. The arc was found to only

deflect 2 mm. The total weight of the a single section of the rack is 5.65 kg.

Passive Gripper

The passive gripper design is based on the principle of spring clips. This idea was discovered after examining the methods used to store tools on the lunar rover and in ordinary household situations. To determine the holding force required by each clip a simple friction calculation was used:

$$\mu N = F$$

μ will be set at 1 for simplicity. The inner surface of the clip will be roughened during processing to meet this criterion. It is assumed that the roughening will not cause significant stress concentrations in the clip. To solve for F the limiting weight of 16.7 lb. was resolved into x and y components using the 61.5° as shown in Drawing 4.6.3.1.

$$Fx = \sin 61.5(16.7) = 14.68 \text{ lb}$$
$$Fy = \cos 61.5(16.7) = 7.97 \text{ lb}$$

the requirement of the largest component must be satisfied, therefore the holding force must meet or exceed 14.68 lb per clip. A clip made by De-stat-co fit the design criterion. This clip is made of tempered steel which eliminates the calculation for fatigue. This material has an infinite fatigue life up to 500,000,000 cycles. Fatigue would be the main failure mode as the clips can be considered to be cyclically loaded. The final dimensions of the clip are shown in Figure 4.6.3.1.

4.6.4 Mechanical Arm and Rotating Bar

Mechanical Arm

In the design of the mechanical arm it was essential to simplify the mechanisms involved to maximize reliability and minimize weight. The final accepted design was that of a three degree of freedom system including the following:

1. A rotating bar to select rack position and change side to grip drilling implement if needed.
2. A jointed arm to move between the drill string and storage racks.
3. A bilateral gripper to grasp the various drilling implements.

The jointed arm was designed to grasp the drilling implement at a point 0.3 meters from the top. The joint will be powered by a brushless DC motor and will be attached through a double reduction worm gear from Boston Gear. This motor and speed reduction system will be attached to the stable upper part of the arm and will be covered by a small aluminum structure to protect it from the harsh environment of the moon. The housing will guide the output shaft with a ring of sealed bearings.

The upper arm will consist of two 0.5 meter long rectangular cross section beams projecting directly down from the rotating beam. This connection could be welded or, the rotating beam and upper arm could be manufactured as one piece. The cross section of the two rectangular portions of the arm will be 50 mm by 15 mm (See Figure 4.6.4.1).

The lower cylindrical section of the arm goes between the two upper arm sections. They are connected by a 20 mm shaft that is part of the lower arm. The shaft is also surrounded by sealed

bearings in the upper arm. The lower arm is 25 mm in diameter, 1.02 meters long, and the opposite end is attached to the mechanical gripper. The total weight of the arm will be 6.1 N moon weight. From the deflection calculations in Appendix A.2.6 the total deflection of the arm and rotating bar is not more than 10 mm.

Rotating Bar

The purpose of the rotating blade is to eliminate one degree of freedom from the mechanical gripper. The blade will consist of a simple beam which will be attached to the underside of the SKITTER. Power will be provided by a motor as specified in the motors section. The blade will rotate on a ring of sealed ball bearings. A counterbalance will be used to remove stresses from the bearings.

The calculations for the beam are based on the superposition of a cantilever beam with an intermediate load and a cantilever beam with an intermediate moment. Using formulas for maximum resulting stress in terms of loading for the Handbook of Formulas of Stress and Strain for the loading situations above and setting the maximum resulting stress at the yield strength of the aluminum with a factor of safety of 1.5, the dimensions of the beam were found to be:

height = 3.4 cm
thickness = 1.7 cm
length = 0.5 m

The end deflection was calculated using the superposition of the two different cantilever beam loading situations with formulas from the Handbook of Formula of Stress and Strain. The deflections were found to be:

y(point load) = .0052 m
y(moment) = .0094 m
y(total) = .0146 m = 14.6 mm

The weight of the bar is 0.838 kg. The calculations for all values can be found in Appendix A under A.6 Rod Changer and Rack, Rotating bar calculations.

4.6.5 Motors and Speed Reducers

Brushless Electric Servomotors

Brushless servomotors were chosen for their high efficiency, high power to weight ratios, and their durability. Also, motors with brushes will produce significant arcs in a vacuum, an undesirable side effect. To increase service life, vacuum sealed bearings will be used. A controller box, containing power control electronics will be necessary to run each of these three phase motors.

Three motors are used to actuate the rod changer system. One is used to rotate the beam on which the arm is mounted, another motor drives the elbow joint on the arm, and a third powers the gripping mechanism.

Speed Reducers

Speed reducers were chosen based on required torque and weight considerations. Worm gears were chosen for the arm's elbow joint and the for the rotating blade, to eliminate backdrive. In the case of a power failure the locking action of the worm gears will insure that the rod changing system does not swing uncontrollably under SKITTER. The gripping mechanism employs a power screw driven by a harmonic speed reducer and a brushless motor. The power screw locks the gripping mechanism if power is lost, so as not to drop a rod or drill implement.

Rotating Beam: motor and speed reducer

For the rotating beam, a relatively moderate torque, low output rpm is necessary. An Alling-Lander double reduction worm gear was chosen that provides a 5000:1 gear ratio. The torque necessary to rotate the beam is:

$$T = (\text{load}) \times (\text{arm}) \times (\text{safety factor}).$$

$$T = (96\ N)(1.02\ m)(1.5) = 147\ N\text{-}m.$$

This means that an input horsepower of 0.0012 is required of the drive motor. At a speed of 10,000 rpm, a Kollmorgen Co. model A714 brushless motor can provide 1.2 oz-in of torque. The worm gear weighs 67 N, and the motor weighs 15 N.

Arm elbow joint: motor and speed reducer

A high torque at a low speed is necessary to swing the arm from directly beneath SKITTER to the side mounted rod racks. This move is to be accomplished in about 30 seconds. The maximum torque necessary is calculated in Appendix A.2 at 140 N-m. A double reduction worm gear such as Hub City's 1300 series, style UR-R provides a 3000:1 reduction in speed. A Moog model 303-002 brushless motor with an input horsepower of 0.0112 at 1750 rpm provides the gear with the required power. Output from the gear is at 0.583 rpm and 160 N-m. The worm gear weighs 98 N, and the motor weighs 11 N. These elements can be seen in drawing 4.6.4.1.

Gripping Mechanism: motor and speed reducer

A power screw is driven to open and close the gripping mechanism. Torque is transferred to the screw from a brushless motor thru a harmonic drive. A harmonic drive was chosen for its' compactness, high efficiency, and low weight. Quincy Technology manufactures a 2000:1 ratio unit, that is 75 mm in diameter, and 60

mm long. The torque required to drive the grippers' power screw is 2.841 oz-in. The harmonic drive requires 0.0098 hp to provide 3.0 oz-in. An Inland Co. brushless motor provides 0.02 hp at 6500 rpm; a sufficient amount to power the gripper. The harmonic drive weighs 12 N, and the motor weighs 6 N. The configuration and approximate dimensions of these elements can be seen in drawing 4.6.4.1.

The weight of the three motors and three speed reducers total to 209 N.

4.5.6 Conclusions

This system has been design with the following consideration in mind:

1. high reliability
2. simplicity, with few moving parts
3. low maintenance requirements
4. minimum degrees of freedom
5. light weight
6. functionality with other SKITTER components
7. withstand extreme temperature ranges
8. high strength to weight ratio materials
9. durability for long life
10. regolith contamination

The design was limited to three degrees of freedom. The arm joint, gripper and rotating bar each represent one degree. Several materials were used in the design so that each application uses the material with the highest strength to weight ratio possible. This design can be incorporated well with other systems that need its use. For this design, the total weight was as follows:

Three racks:	166.28 N
Motors and speed reducers:	209 N
Arm:	6.1 N
Mechanical gripper:	3.33 N
Total weight:	384.71 N

FIGURE 4.6.1.1 ROBOT ARM WORK CELL

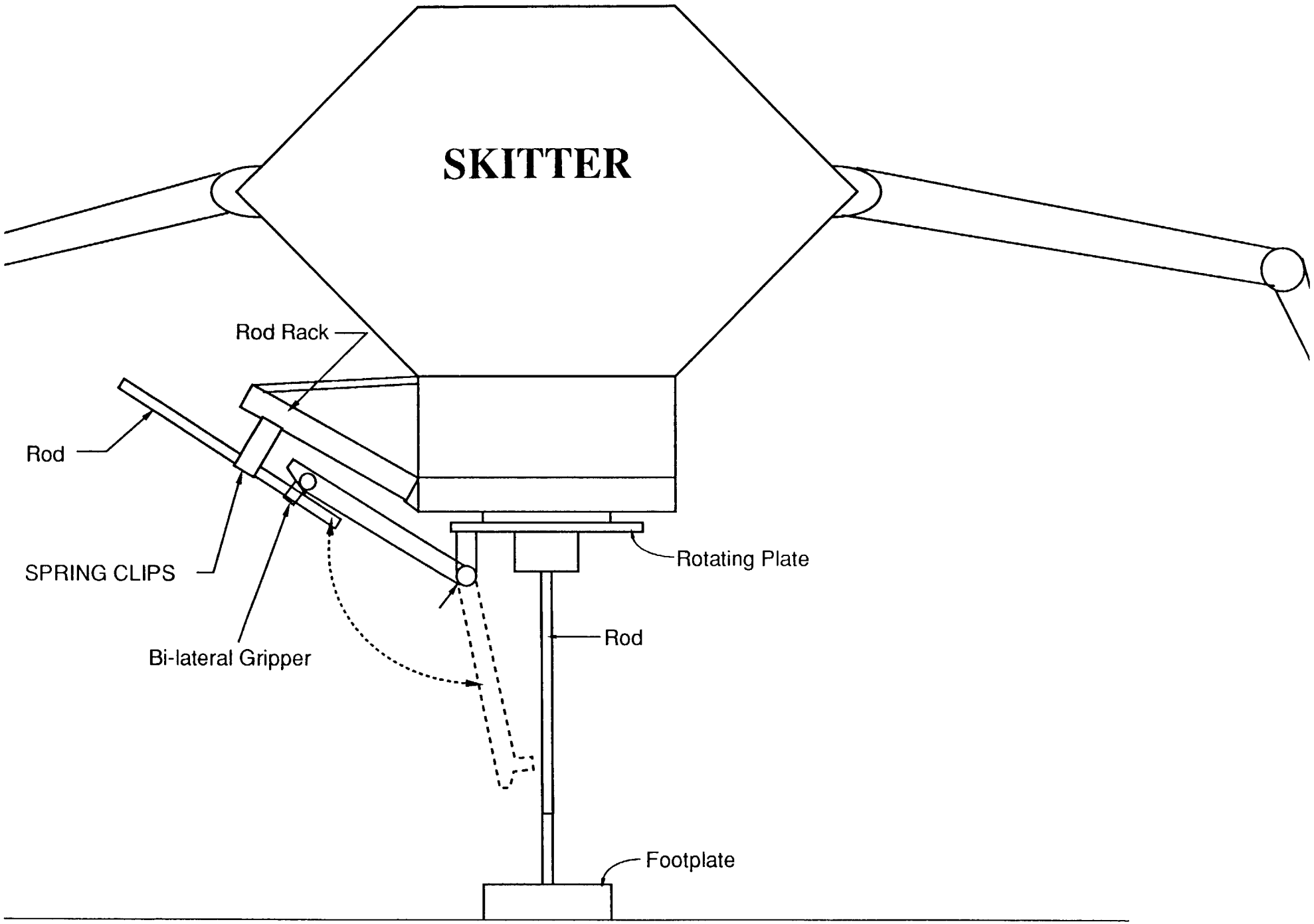

FIGURE 4.6.3.1 SPRING CLIP FOR ROD MOUNTING

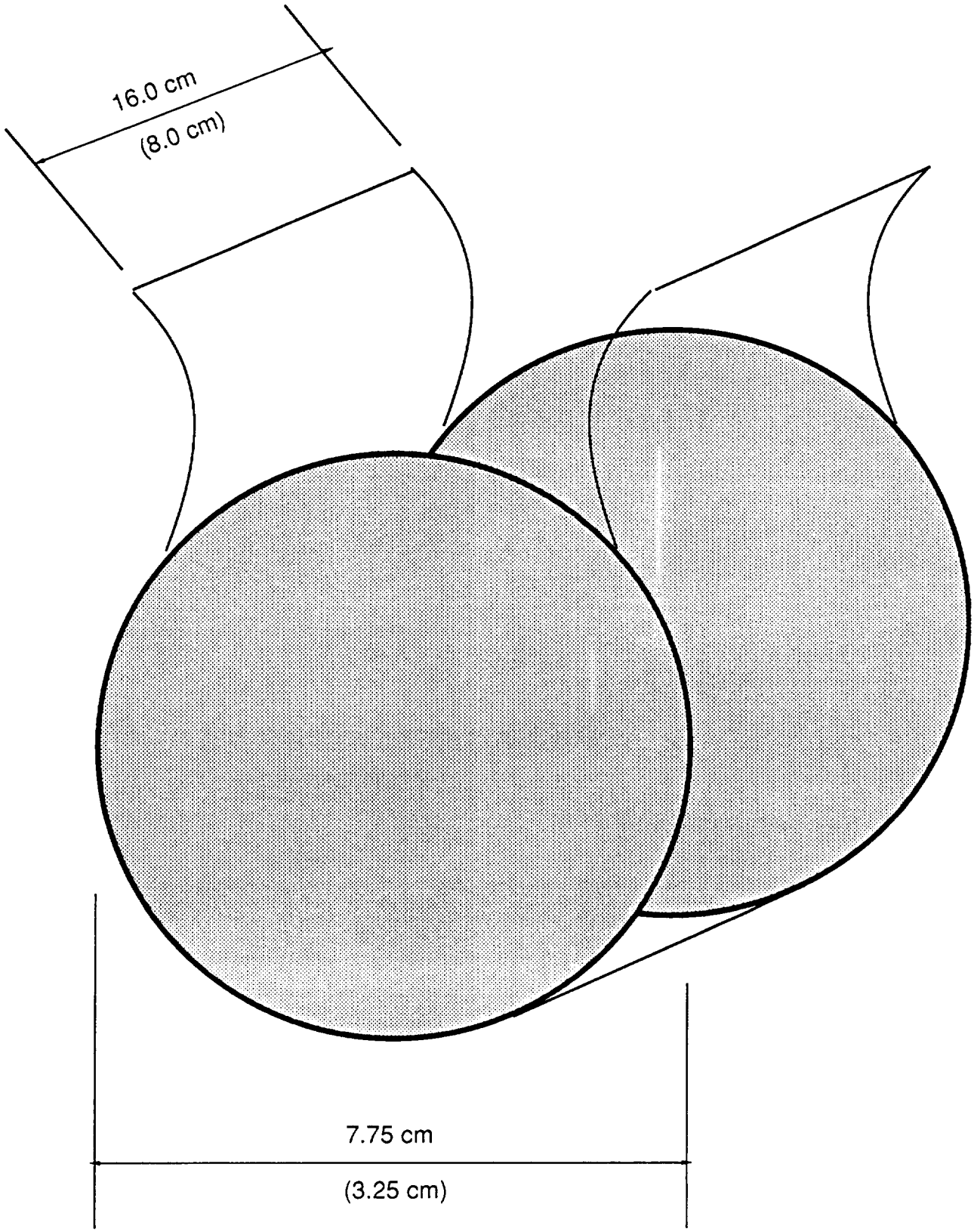

FIGURE 4.6.3.2

ROD RACK AND ARM - SIDE VIEW

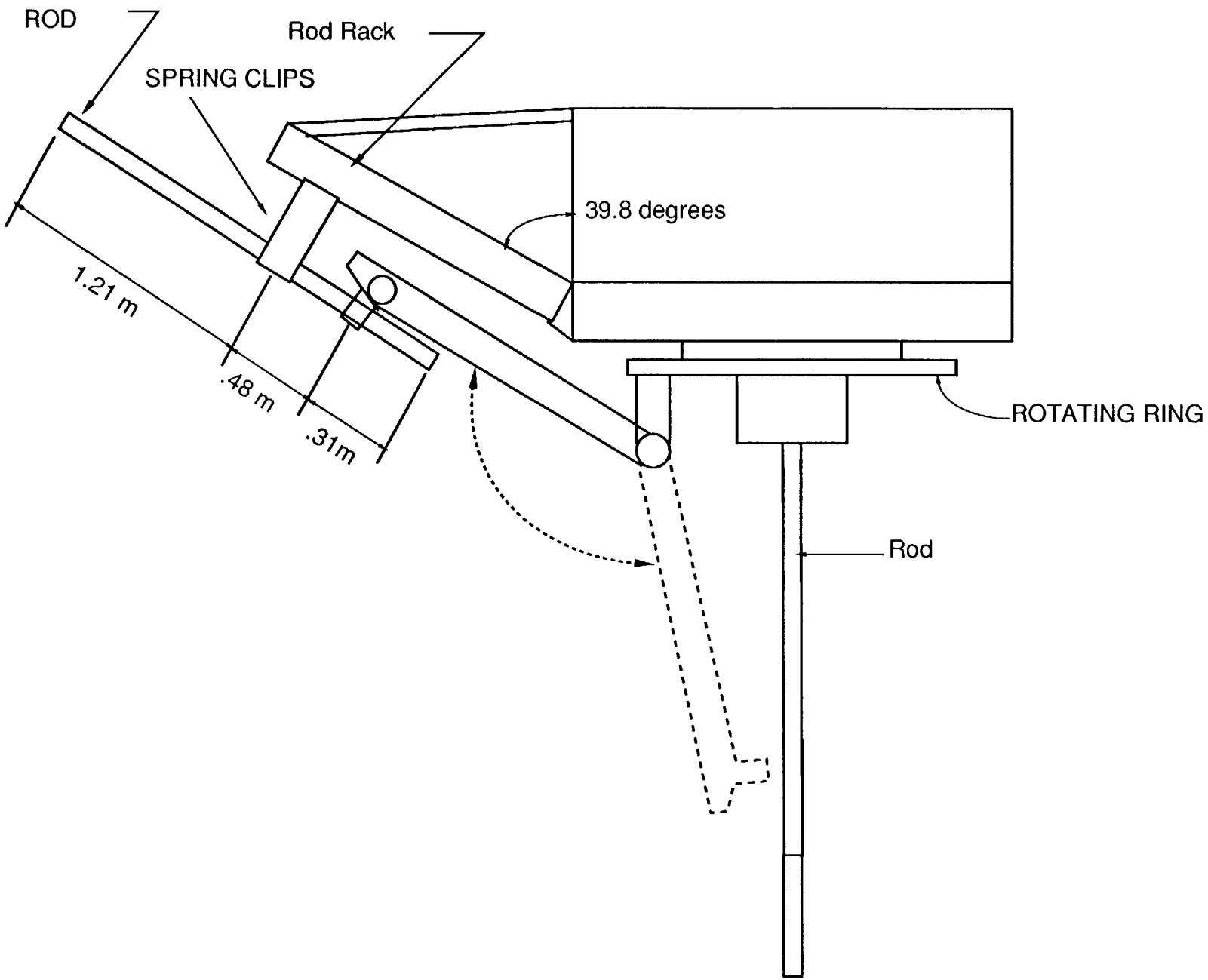

4.7 MACROCORE RETRIEVAL AND STORAGE SYSTEM

4.7.1 Explanation of Core Removal Process

After the drill and stepped auger are removed from the drill hole, a device will be sent down the drilled hole to extract the core. The retrieval device will be attached to the drill string and slowly lowered down into the drill hole. When the core retriever gets within two meters of the core, the core retriever is lowered at a slower pace. If the core is broken and lying against the wall of the drill hole, the core retriever may need to be rotated to properly feed the core into the retriever and allow the retriever to continue lowering. Upon reaching the desired depth the device will discontinue its descent and rotate a small increment around the sample to release the cutters and grippers. The device will then be rotated in the same direction around the core. After several revolutions, the core will be severed. The grippers will be engaged, and the core will be lifted out of the drill hole. Once on the surface of the moon, the core will be released from the core retriever and put into a storage cell. The core retriever will then be set aside so that drilling can be resumed.

4.7.2 General Overview of Equipment

Once the core retriever is placed around the core sample, it is necessary to cut the core. The sample can then be lifted to the lunar surface. The method which is employed for this task is modeled after a pipe cutter.

A pipe cutter employs a sharp circular disk to cut pipes. This disk is attached to a screw such that as the screw is turned, the pressure applied from the disk to the pipe is increased. The disk is spun around the pipe and tightened at certain intervals to cut through the pipe.

The same general principle is used in the lunar core sample case. However, rather than cutting through the core sample, three disks are used to propagate a crack across the core and severe it. The propagation is caused mainly by the shape of the disks. The disks will be thicker at its center than at its edges. Therefore, the disks also act as a wedge. These wedges are the main driving force behind the crack propagation.

The wedges propagate the crack because the material of the core is rock which is very brittle and experiences little to no elastic deformation. As the wedges are driven further into the core, the rock simply separates.

Heat dissipation is not a major concern for the mechanism will be moving slowly, not unlike a pipe cutter. However, since human assistance is unavailable to tighten the cutter, small springs are activated by rotating the top of the device and used to drive the disks very slowly into the rock as the entire apparatus is spun around the core sample.

After the core is separated, it will be gripped so that the core can be lifted to the surface. It is important that the grippers apply a uniformly distributed load across the cross section. Any type of point loading would run the risk of damaging the specimen. After gripping the core, the retriever containing the core sample will be lifted to the surface of the moon. When the specimen is ready for storage, the grippers and cutters will be reset using a gear. The gear will be rotated and reset by pressing it against the top of the storage device. The core sample will then slide out and be deposited into a storage cell.

4.7.3 Introduction

After the drill bit and stepped auger are removed from the hole, a core retrieval device must be sent down to bring the core to the surface.

4.7.4 Core Sample

The core sample will be 50 millimeters in diameter and up to 2 meters in length. Maximum mass will be 46 kilograms. It must be removed from a hole which has a 100 millimeter diameter and can be up to 50 meters deep. The core should be brought up to the surface and stored in a storage device that will protect it from the lunar environment.

4.7.5 Constraints

Various environmental and equipment constraints must be considered in the design of the macro-core retrieval and storage system. Moving parts must be kept to a minimum due to abrasion and wear caused by lunar dust and rock fragments. Temperature extremes and cosmic radiation must be considered when deciding upon materials. Reduced gravity and near vacuum conditions must also be taken into account.

Since little human supervision or maintenance will be available, the mechanism should be self automated and highly reliable. A fully mechanically operated system would be ideal due to power requirements. Transportation of the system puts restrictions on the size and weight of the retriever.

Restrictions are also put on our design by other parts of the drilling device. The connection device between the drill string and the motor attached to SKITTER limits our pulling force to 200 pounds. The motor provides a maximum torque of 50 ft-lbs.

4.7.6 Design Considerations

Several different ways of severing the core were explored. The methods that were researched included tension, torsion, bending, cutting, or a combination of these.

The properties of basalt, which is a lunar rock with high tensile and torsional strength, were used to compute the forces needed to break the core. Using pure tension to break a 50 millimeter core of basalt would require a force greater than 54 Mega-Newtons, which is much more than the 890 Newton (200 pound) restriction (Table 4.7.6.1). The pure torsional force required to severe the 50 millimeter core is also greater than 1353 Newton-meters (Table 4.7.6.2). Thus, pure torsion was not a feasible consideration in breaking the core.

The force needed to cut the core by pure bending is approximately 340 Newtons applied at the top of the core (Table 4.7.6.3). Although this method is realistic a sleeve would have to fit tightly over the core to prevent it from breaking. For a softer rock, clearance at the top of the sample may not be sufficient to break core.

Cutting or scoring the bottom of the core could be used in conjunction with one of the above methods to break the sample. The core could be scored creating a stress concentration which significantly reduces the force needed to break the sample (Table 4.7.6.4). The core could also be completely severed using a cutting device stored in the bottom of the core retriever. The core could then be held with a gripping device and raised to the surface.

The macro-core retriever uses a pipe cutting device to cut the core. By spinning a rotating cutting wheel around the core, the core

will be severed. The cutting wheel is very thin at the initial contact point, and gets larger towards the center of the wheel. The geometry of the wheel causes an outward force at the cut, pushing the core apart. The outward force, along with the compression force of the cutter, causes the core to break with a relatively small cut. The core breaks because of crack propagation, caused by the concentrated stresses at the point of contact of the cutter.

4.7.7 Design

The macro-core retrieval is a cylinder 2 meters high with a 100 millimeter diameter (Drawing 4.7.7.1). It is lowered into the hole by the drill string, and is stopped 2 meters from the bottom of the hole. At this time the retriever is lowered slowly over the core. The bottom of the device is conically shaped in case the core is broken. This will feed the broken core into the inner tube. The retriever will be spun counterclockwise if it gets hung up on a broken core.

When the retriever gets to within 3 centimeters of the bottom of the hole, its descent is stopped. The cutters are then activated by rotating the retriever 30 degrees clockwise. There are three cutters in the device. Each is spaced 120 degrees apart at the bottom of the core retriever. They are activated by a pin placed at the top of the cutter. The rotation of the top of the retriever pulls a chain that raises the pin (Drawing 4.7.7.2). The cutters are then pressed against the core by a tension spring. The device is rotated counterclockwise around the core while the spring presses the cutters into the sample. When the cutting blade is compressed 5 millimeters into the core, the core should be broken. A plate made to the contour of the core will then make contact with the core.

The plate will grip the core, and the retriever will be raised out of the hole by the drill string. When the core and retriever reach the surface of the moon, the rod changer will grab the core retriever and take it over to the core storage device. The storage device will

facilitate the resetting of the retriever. A reset gear is contained in the helical section at the bottom of the retriever. It is cut such that it is flat against the helical section when the cutters are not activated and swings out when the cutters are activated (Drawing 4.7.7.3). The storage device has a ridge on its top that will push the gear flat against the helical section when the retriever is pressed against it. This releases the core. The core will then slide out of the retriever into the core storage device.

4.7.8 Retriever Shell

The shell of the retriever will be 2 meters long with an outer diameter of 100 millimeters and an inner diameter of 55 millimeters. It will consist of an inner and outer tube. The tubes will be 3 millimeters thick and will be connected by supporting bars placed between them. The shell will be made out of a titanium alloy, Ti-5Al-2.5Sn, which maintains its high strength under the temperature extremes which will be encountered.

4.7.9 Top Connection

The top connection will allow a slight rotation, with a male and female connection between the two parts of the shell. This connection will be made of the same titanium alloy as the retriever shell.

4.7.10 Pipe Cutter

To cut the core sample, a 10 millimeter disk cutter similar to a pipe cutter is employed (Drawing 4.7.10.1). The core retrieval device will use three disk cutters spaced 120 degrees apart (Figure 4.7.10.1). These cutters will be spring loaded with a force of 222 Newtons. They will be rotated around the core by rotating the entire retrieval unit within the hole.

This method of cutting the core sample is unusual. Therefore, no information about removing a core sample in this manner could be found. However, a similar type of cutting disk is used in some tunneling operations. As a result, the design of the disk cutters is based upon disks used to cut tunnels.

The disks within the core retrieval unit are rotated by the friction developed between the cutting edge of the disk and the core sample. Traditional steel and steel alloy disks have a tendency to slip while in contact with the rock. Slipping increases the wear on the cutting edge and thereby decreases its life. The use of tungsten carbide helps to prevent slipping on a rock surface. Additionally, tungsten carbide cutting edges have been shown to successfully cut through extremely hard rocks which traditional cutting edge metals do very poorly. For these reasons, tungsten carbide was chosen as the material to make the disk cutter from.

Another important parameter of the cutting disk is the angle of the cutting edge. Sharp edged disks are best for penetrating into hard rocks quickly, but usually need frequent replacement. Disks with blunt angles tend to penetrate rock more slowly. A cutting edge angle anywhere from 55 to 60 degrees has been found to offer the best compromise between effective penetration and wear. From available data the expected cutting life of the disk cutter is approximately 200 hours.

The principle by which this method of rock cutting works is kerfing and compressive spalling. With the kerf principle, the sharp edge of the disk cutter cuts a groove into the rock, and the wedge shape of the disk imparts a shearing force causing the rock to break. The sharp edge of the cutting disk also induces a very large stress concentration where it makes contact with the rock. This stress concentration can get as high as 5 times the unconfined compressive strength of the rock. The force of this stress concentration breaks through the rock by essentially crushing all of the rock in the path of

the cutting edge. This crushing of rock is referred to as compressive spalling.

The cutter disks are designed to penetrate the core sample to a depth of 5 millimeters if necessary. Realistically, the cutters should never have to penetrate anywhere near 5 millimeters. There are no formulas on which to base this statement. Rather, this statement is based on theoretical considerations from books and upon a solitary test conducted by Mr. James Brazell. In this test, Mr. Brazell used an ordinary pipe cutter to cut a granite core sample approximately 45 millimeters in diameter. With a very minimal amount of force, the core sample was separated in just one revolution.

4.7.11 Spring

The spring will be a simple tension coil spring (Drawing 4.7.11.1). It will have 8.5 coils, an outer diameter of .0832 meters, and have a wire diameter of .0019 meters. It will be grounded and squared at both ends. The spring constant (K) will be 2.32 Newtons/meter and exert a force of 222.5 Newtons when fully compressed. A 186.59 Newton force will be exerted at the end of the cutters stroke. A material for the spring has not been found that will give the characteristics needed on the moon.

4.7.12 Reset Gear

The reset gear, used to reset the cutters after the core has been extracted from the hole, will be a normal gear with 18 teeth. The pitch diameter is 2 centimeters, and the angle of incident is 20 degrees. The face width will be 2 millimeters allowing a 222.5 Newtons of tangential force. The gear will be cut so that it will be flush with the conical section of the retriever when the cutters are reset.

4.7.13 Pin

The pin will be cylindrically shaped with rounded ends. It will be made of tungsten carbide with 10 percent cobalt to insure good wear life.

4.7.14 Grippers

There will be three pads that will grip the core after it is broken. The pads will be located directly above the three cutters and are powered with the same spring that the cutters use. They are shaped at an arc that will enable them to grip the core with the entire pad (Drawing 4.7.14.1). The geometry of the pads prevent point loading, which could cause harm to the sample. The pads will be made out of tungsten carbide with 10 percent cobalt. This material has a good wear life and can be used at the temperature extremes that the retriever will encounter.

4.7.15 Protective Gear Cover

There will be a flexible material around the gear and spring to protect them from dust and dirt. The material will be made of polyester yarn of Dupont type 56 dacron and has a urethane coating system by Mobay Chemical Company. It has a cyclical life of 2 million cycles. This material is used for space suits.

4.7.16 Core Storage Device

The storage system is designed to facilitate the storage of up to 26 core samples from a single hole. Each core sample has an individual unit-cell storage cylinder 100 millimeters in diameter and slightly bevelled to 50 millimeters. These unit-cells, however, are located in an overall rectangular storage system (Drawing 4.7.16.1). Four alternating columns of 6 and 7 unit-cell cylinders respectively

are positioned at a 60 degree angle to enable the SKITTER arm to swing upward, release the core, and allow gravity to assist in depositing the sample. In addition, the inner two columns will be recessed to allow for the SKITTER arm's sideways motion.

The entire system will be positioned in a location away from the drilling area but within easy access of the SKITTER. The operator will guide the SKITTER arm from the hole to the storage cylinder group and position it over the correct, pre-determined unit-cell for deposit. A marker band will be stretched across the entrance of each unused cell to assist the operator in discerning where to place the core sample. The marker will be torn and broken upon core deposit into the unit-cell so that the operator will be better able to tell which cells are full. Also, each unit-cell will be pre-labeled to account for the core sample's position in the hole and the particular hole from which it came. A circular ridge lining the bevelled area of each unit-cell will facilitate the macro-core retriever resetting process. As the core sample is deposited into the unit-cell, the ridge provides resistance to the pressure applied by the macro-core retriever and the gear is reset.

The storage system and unit-cells will be constructed of Ti-5 Al-2.5 Sn alloy. This material has an extremely low coefficient of thermal expansion (9.4 micro-in./in/C), and all material properties remain essentially the same at both high operating and low environmental temperatures.

Positioning of Cutters

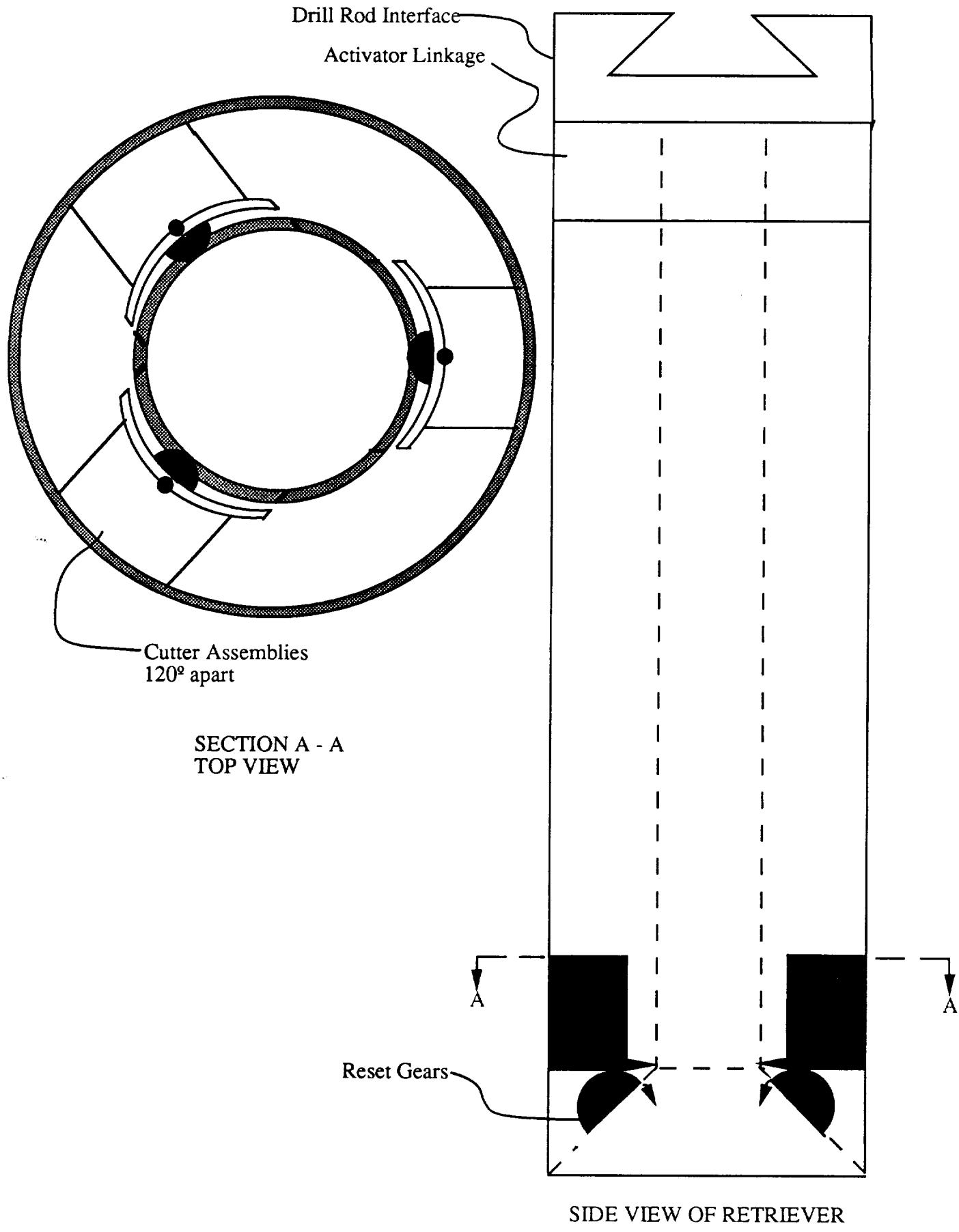

Figure 4.7.10.1

4.8 CONTROLS FOR ENTIRE DRILLING OPERATION

4.8.1 Task Definition

The initial step of designing the controls for this operation was to define the tasks that were to be performed to complete the drilling operation. The entire operation was broken into five basic routines that appear in the main flowchart. Each of the specific activities of the drilling operation was then specifically determined in flowchart form. The flowcharts and a discussion of the methods needed to read them appear in section 4.8.2. Each routine is uploaded to an onboard Programmable Logic Controller, PLC, on the drilling apparatus as the routine is needed. When the specified task has been completed that routine is then down loaded and the routine for the next task is then uploaded. This process allows maximum autonomy for the drilling apparatus while maintaining consistent contact for the operator.

After the tasks to be performed were defined and organized, it was determined where the operator would have input into the drilling operation. This involved careful consideration of the current design as well as the operation of other components of the drilling operation and SKITTER in general. Since there is approximately a 2.6 second communications delay between the Earth and Moon and back, full operator control is not possible without risking damage to the equipment; also, the time required to complete the drilling procedure would be significantly increased. Fully automating the process, however, would lock out human input and possibly prove as damaging as full operator control. In addition, the task of operating the equipment would cause the operator to become distracted due to lack of involvement. It was therefore decided that that a semi-automatic approach was more suited to the problem. Human input would be placed at critical points in the routines where decisions on

options must be made as well as to allow the operator to monitor the operation and intervene when a problem develops.

4.8.2 Drilling Operations

4.8.2.1 Operational Flowcharts

In the course of designing the control methodology for the drilling operation, it was found that the most efficient way of illustrating the steps in an operation was to construct a flowchart. In this section, each significant operation has been reduced to a flowchart that illustrates the complete sequence of events needed to complete a task.

Initially, the drilling operation was broken down into its major activities; these are referred to as routines. In each case these routines will be uploaded and downloaded to the onboard PLC to reduce the size of the required RAM memory areas. The five basic routines and the overall operating sequence for the drilling operation are illustrated in Fig. 4.8.2.1.1.

Once determined, the routines were written as the design process was completed for the respective areas. Each routine is designated in its own flowchart and appears in Figures 4.8.2.1.2 through 4.8.2.1.11. Each flowchart specifies the action of the integral operation and refers to the operational subroutines.

The subroutines were developed as areas of operation that are necessarily repeated frequently. The appropriate subroutines are appended to each routine that utilizes them and uploaded and downloaded as a set. Each subroutine appears as a separate figure in this section and are organized to be near those routines using them most often.

In reading the flowcharts, there are a few standards of which the reader must be made aware. Boxes represent specific system

commands that are acted upon directly by system hardware. Diamonds are decisions that are integral to the routine and are a answered affirmatively or negatively by logical iterative procedures in the routines. Ovals represent subroutine calls. In each subroutine call, the machine returns to the original routine at the same point it exited to the subroutine and continues forward from there. The unwritten understanding here is that SKITTER and movable hardware is always left in the same standard position as it was found upon entering a routine or subroutine. SKITTER is always in the "normal" position at the beginning and end of an operational segment, and the rod changer arm is always in the indexed position.. These positions are discussed in the next subsection.

4.8.2.2 Operational Positions

The specific areas that must have operational positions defined for SKITTER is the actual drilling operations and the vertical accelerator. These positions are defined in relative terms since quantitative information was not available at the time of writing. The specification of these positions is noted as a recommendation for further study as it may prove a good troubleshooting method in evaluating operations. These positions are illustrated in order of discussion in Figures 4.8.2.2.1 a,b,c,d.

SKITTER begins the drilling operation in the "normal" position. This position is the maximum working height that will be used in the drilling operation and will serve as the standard indexed reference position for SKITTER. At the "normal" position the rod changer arm has clearance to operate while carrying a rod, auger, bit, and the various devices used in other operations. When the desired component has been placed in position over the hole or drill string, SKITTER lowers into the "chucking" position at which the footplate can grasp the component. In the "chucking" position the rod changer arm has clearance to move only when not carrying a component. Generally, the rod changer will then be indexed to its standard position after releasing the component. SKITTER then lowers to the "motor lock" position which allows the motor to engage the drill string directly. The drill motor would then start and SKITTER would lower through the drilling procedure ending finally in the "drilling" position. At this point, components other than those in the hole must be stowed or in their standard indexed position as this is the point of least clearance between SKITTER and the lunar surface.

It must be noted that these positions are used as standards for automatic operation. Operation of the routine requires that specific positions be defined to ensure the smooth transition from routine to subroutine. Specifying these positions by no means disallows the

operator from moving SKITTER or the various components manually. In fact, this will certainly be the required action in an error situation or when damage occurs.

4.8.3 Human Factors Design

In the design of the control system for the lunar deep drill, considerable analysis of the interface between the operator and the drill were made. The first part of the analysis dealt with dividing the control tasks between operator and computer. The second part was to design the optimal control console to be used from Earth.

4.8.3.1 Workstation Design

Several criteria were used to determine the optimal means of human-to-hardware interface. The console had to be easy to use, keep the operator's attention, allow the operator to monitor the drill's systems and the drilling operation's progress, allow simple but complete control over the drill, and meet NASA specifications. After careful consideration of the requirements and alternative solutions, it was decided that a computerized system utilizing both a touch-sensitive screen and a normal computer keyboard would be used. On-screen menus would be the primary means of input from the operator.

As well as the visual feedback provided by animation of the menu screens, the operator will be able to monitor the operation through audio signals. A computer generated "whirr" will imitate the sound of the motor that the operator would hear if he were at the drilling site. This system will be analogous to the driver of a manual transmission automobile. Accompanying the motor simulation will be an audio simulation of the grinding of the bit into the rock, giving the operator a sense of how hard the drill motor is working and when it is approaching a stall. This sound will correlate to the motor torque much as the motor "whirr" will correlate to the motor rpm.

These two audio signals will enhance the operator's sense of the state of the drilling operation.

4.8.3.2 Menu Screens/Animation

The touch-screen computer system will use a number of different screens to allow access into the computer system, monitor the operations, give the operator visual feedback, and allow the operator to input decisions. The screens are multicolored with simple animation gauges and animated sketches showing the functions Skitter is carrying out. They are sequentially ordered according to the decisions made by the operator. The operator must touch the green "CONTINUE" area to advance to transmit the instructions to Skitter and advance to the next screen. They were designed in accordance with NASA-STD-3000 9.3.3.4.7. Touch-sensitive areas in use are outlined to show the operator what his choices are. On any given screen, there are few enough active touch areas to space them adequately to prevent accidental or erroneous activation. During normal operation, the keyboard is only needed to enter identification/password/access code and to enter the target drilling depth. Touch area activation is indicated by a color change in the activated area, except in the case of the "CONTINUE" area which will result in a new screen appearing. Examples of these screens can be found in Figures 4.8.4.1.1 - 4.8.4.1.14, with explanations and instructions following each screen layout.

4.8.3.3 Console Design

The primary criteria in the design of the control console was NASA-STD-3000. The console will be textured matte grey, which is in accordance with NASA-STD-3000 9.2.2.2.4. This color reduces reflections from illumination sources in the immediate environment. The touch-screen shall be positioned directly in front of the operator,

within arm's reach, and tilted back 10 degrees from vertical (NASA-STD-3000 Figure 9.2.4.2.2-1). The edges of the screen will be near the optimal $\pm$15 degree vertical and horizontal eye movement ranges (NASA-STD-3000 Figure 9.2.4.2.2-2). This orientation of the screen will allow the operator to easily see the screen with a minimal range of eye motion. Standard display controls (intensity, contrast, etc.) will be below the screen. Speakers for the audio feedback will be placed at the top of the console on either side of the screen. The computer keyboard is retractable, since its use is limited, so as not to inconvenience the operator. Armrests will be provided on each side of the console, to help prevent operator fatigue while operating the touch-screen. The Touch-Screen Disable toggle switch shall be placed on the right side of the screen; this switch will disable the touch-screen capability, allowing the screen to be cleaned of smudges and dirt without accidental actuation. The Emergency Stop button shall be located on the right side of the screen, positioned to provide immediate activation capability. The console will stand at a height such that the operator's knees will be free from contact with the console. Shelving for operation manuals, etc. will be available within arm's reach of the operator to his/her left. The design developed based on these criteria can be found in Figure 4.8.3.3.3-.4 as well as an artists rendering in Figure 4.8.3.3.5.

4.8.4 Menu Driven Operational Displays

As discussed in the previous section, the method of direct interaction between operator and apparatus will be through the touch screen control console. Approximations of the actual screens appear in order of operation in the following figures. These screens illustrate, generally, what the operator will see while running the apparatus through its various operations. The following are comments on the screens themselves.

4.8.4.1 Earthbound Control

Initially control will transfer from the SKITTER control console to the DRILLING OPERATIONS console when SKITTER seats the drilling operations rig, thereby activating it through passive sensors in the bomb latches securing the operation. The operator will move to the DRILLING OPERATIONS console and go through a series of entry requests shown in Fig. 4.8.4.1.1. Once into the system, Fig. 4.8.4.1.2, the operator will choose the pre-operation check so that all the systems on the drilling operation can be verified to be ready. If the operator has specific programming or editing that must be done he would choose system access. At this point, notice that the screen has a continue arrow at the bottom right and a stop figure at the bottom left. These are utilized by the operator to proceed after a decision has been made or return to the previous screen or system access to manually resolve a problem.

Choosing the pre-operation checklist brings up the screen in Fig. 4.8.4.1.3. As the system performs its checks the screen highlights those areas being checked with a box and highlights those areas that do check out with a green check mark. Those systems that fail the check are indicated with a red "X" mark. If a system has failed, the operator can strike the stop sign and go to system access or accept the failure if trivial and continue. Assuming all systems are operational, the operator will strike "go" and the screen in Fig.

4.8.4.1.4 will appear. At this point the drilling operation has been checked and is prepared to begin drilling. Control is then returned to the SKITTER console so that the operator can move SKITTER to the drilling site. Fig. 4.8.4.1.5 remains on the screen while SKITTER is moving to the drilling site, at which point control will revert back to the DRILLING OPERATION console and the operator will strike continue.

At this point the drilling operation can begin and the DRILLING OPERATION console has nominal control over SKITTER movement vertically. The Set Footplate screen, Fig. 4.8.4.1.6, comes up and the appropriate routine is uploaded. As the routine completes the task, the animated figure of SKITTER and the footplate go through a rough analogy of the motions that SKITTER is actually completing. The box at the bottom of the screen will show in words the current stage of the routine, similar to the corresponding flowchart points. The vertical bar on the left side is a graphic representation of completion of the routine and goes from top to bottom as the routine is completed.

The Drill Segment screen, Fig. 4.8.4.1.7, asks the operator to input the depth to which the hole will be drilled. This sets the markers at the left, which will be maintained to give the operator constant update as to the level of completion of the drilling operation. Upon entering the desired depth, the operator will strike continue and the Drilling screen, Fig. 4.8.4.1.8, will appear. The appropriate routines are uploaded and downloaded, the bit is positioned and drilling begins. Again the screen animation illustrates the actions of SKITTER as the operation progresses. Throughout the drilling process the screen is updated as to depth, motor rpm, motor amperage, SKITTER position, and rod changer arm position, as well as the ongoing depth update on the left.

Macro-coring animation is shown on the screen as in Fig. 4.8.4.1.9. Again the operation is animated and the operator can monitor the flowchart through the bottom box. At the completion of

the macro-coring the operator is asked to decide whether micro-coring is desired or not on the screen shown in Fig. 4.8.4.1.10. Here the choice is made and is indicated by a lighted box on the screen. If "Continue Drilling" is chosen, the screen reverts to that shown in Fig.4.8.4.1.8 and the process is iterated. If "Micro-coring" is chosen, the screen in Fig. 4.8.4.1.11 is revealed and the animated process is monitored by the operator once he sets the desired depth. Again the decision screen in Fig. 4.8.4.1.10 appears and the operator selects the next option. The drilling complete option is not available until the desired depth has been reached so that the operation can only be halted by the manual interdiction of the STOP button on the console or through system access. Once the desired depth has been reached and all coring is complete, the drilling complete option can be selected and the screen in Fig. 4.8.4.1.12 appears. The footplate is then retrieved and the screen in Fig. 4.8.4.1.13 is shown. At this point the system can be accessed for other work or control is reverted to the SKITTER console so another site can be selected.

These screens are not all inclusive of the detail that will be necessary in operating SKITTER. A great deal more detail will be required, but the direction chosen appears to be the most efficient and interesting to the operator. Further activities are reported in the Recommendations for consideration in design.

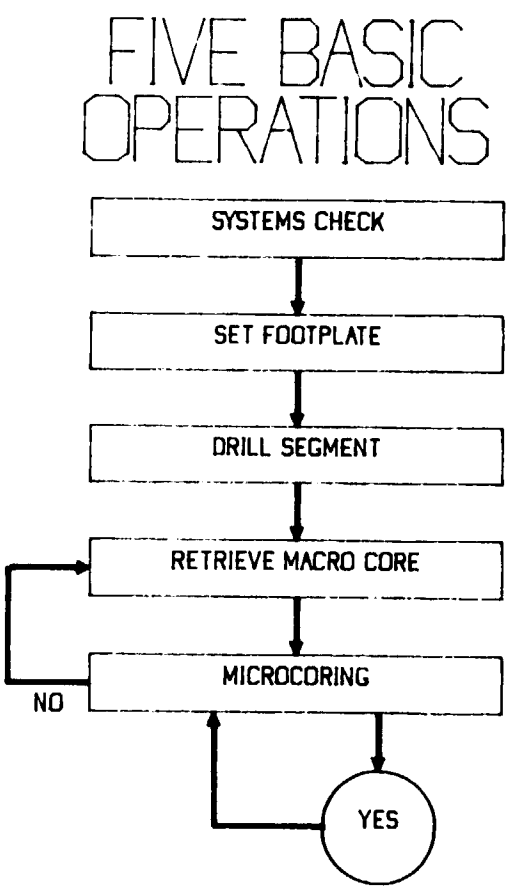

FIG 4.8.2.1.1

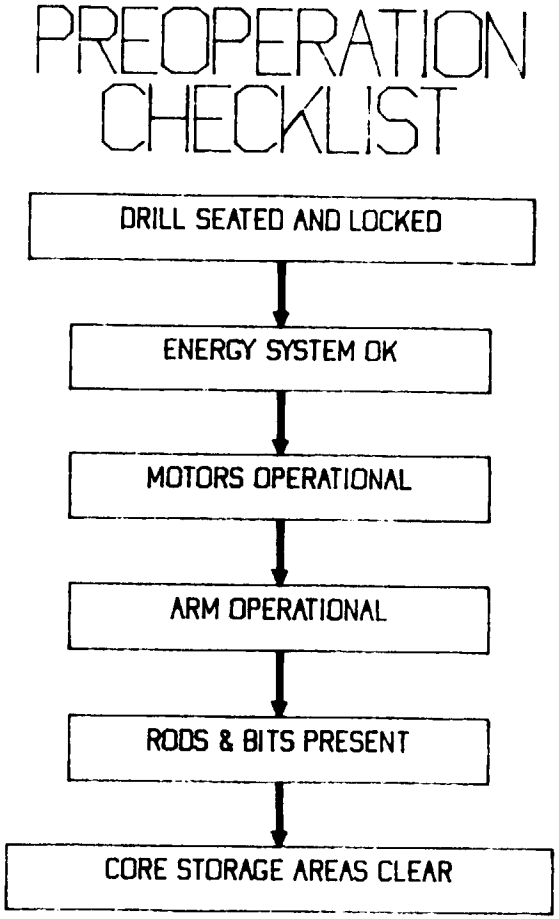

FIG 4.8.2.1.2

SET FOOTPLATE SUBROUTINE

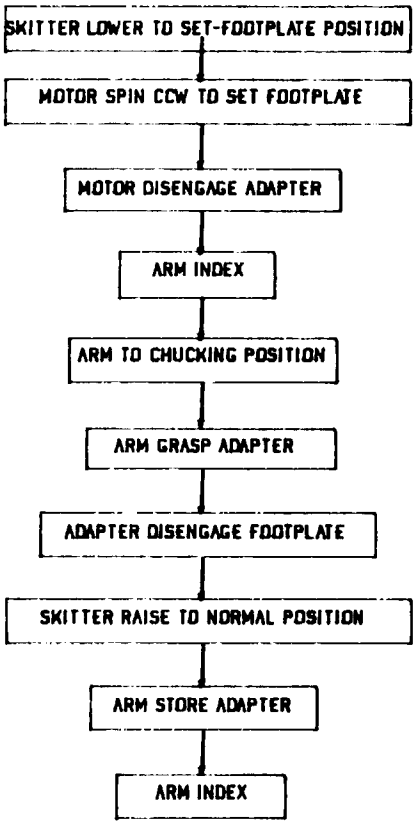

FIG 4.8.2.1.3a

REMOVE FOOTPLATE SUBROUTINE

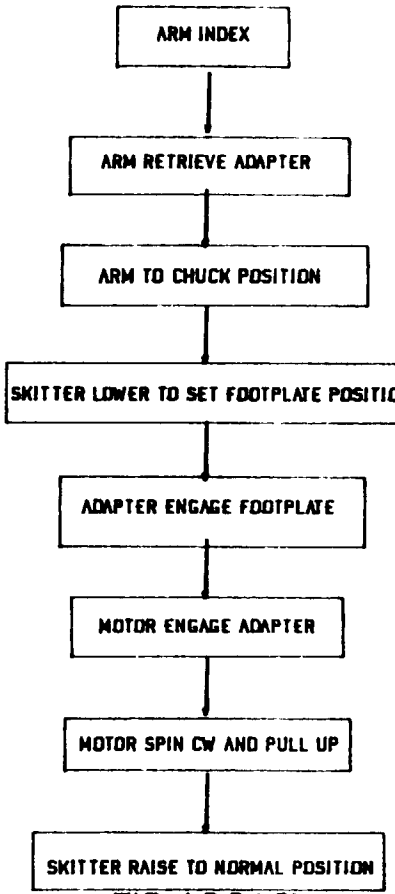

FIG 4.8.2.1.3b

DRILL SEGMENT ROUTINE

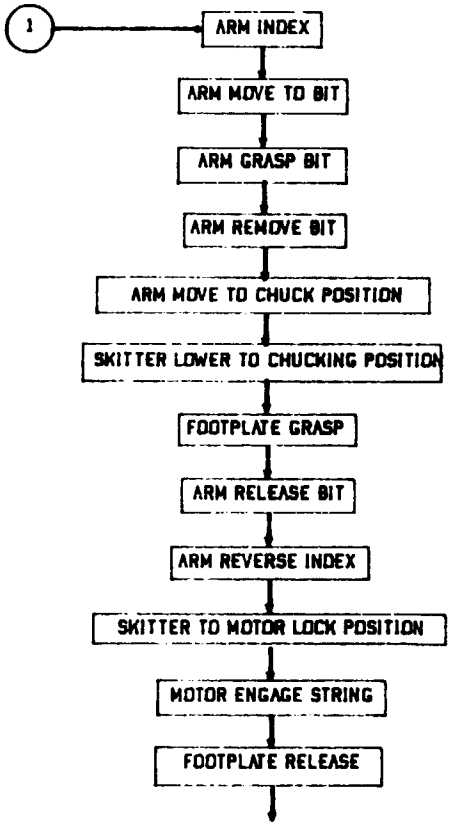

FIG 4.8.2.1.4

DRILL SEGMENT ROUTINE (CONTINUED)

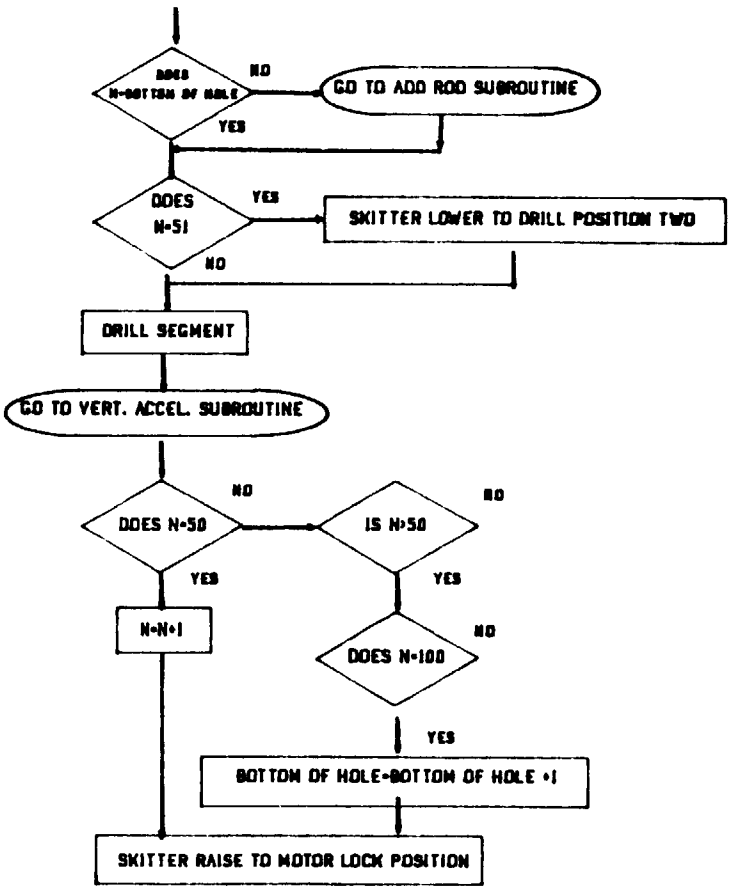

FIG 4.8.2.1.4 CONT.

DRILL SEGMENT ROUTINE (CONTINUED)

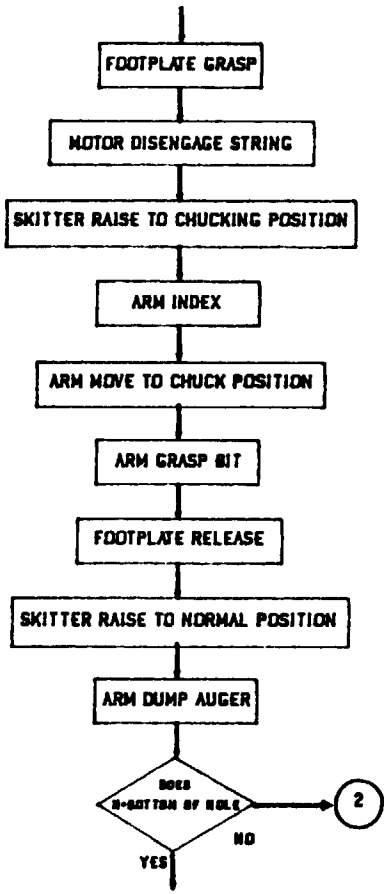

FIG 4.8.2.1.4 CONT.

DRILL SEGMENT ROUTINE (CONTINUED)

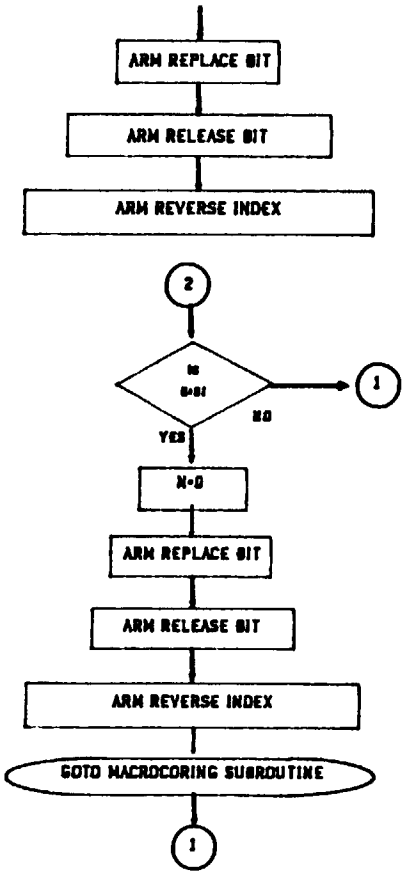

FIG 4.8.2.1.4 CONT

MACROCORING ROUTINE

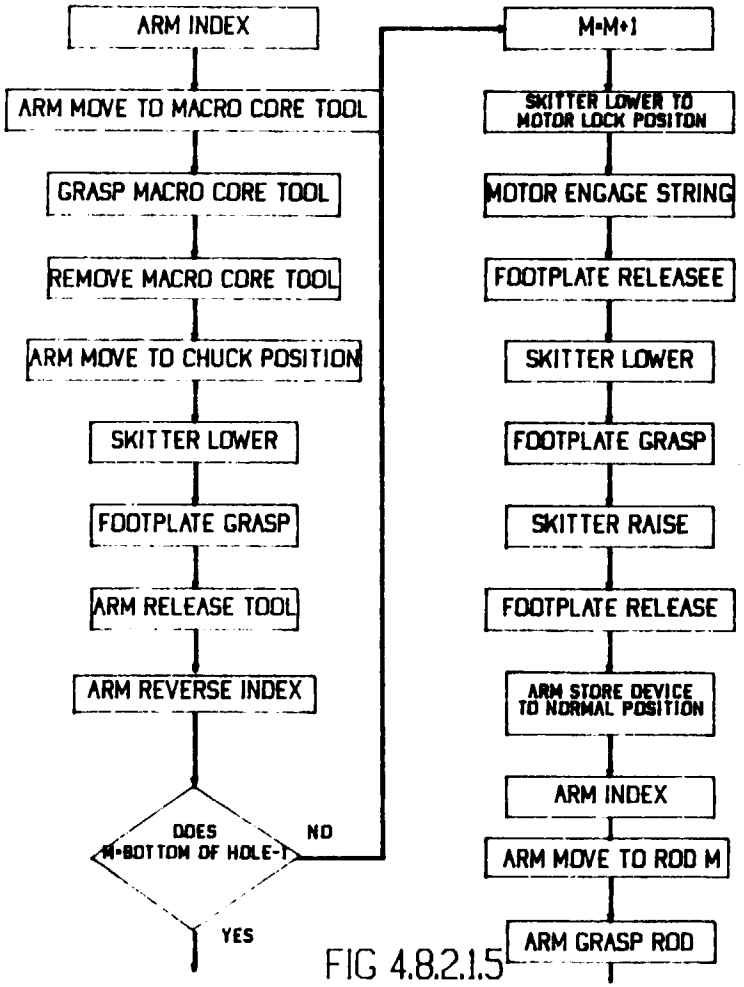

FIG 4.8.2.1.5

MACROCORING ROUTINE (CONTINUED)

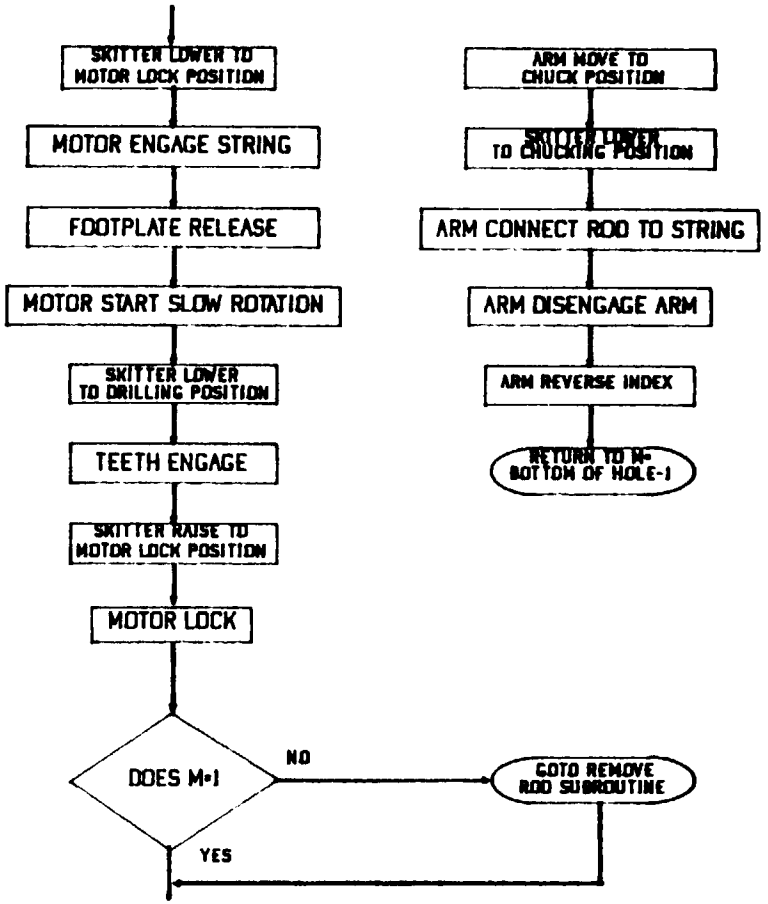

FIG 4.8.2.1.5 CONT.

MICROCORING ROUTINE

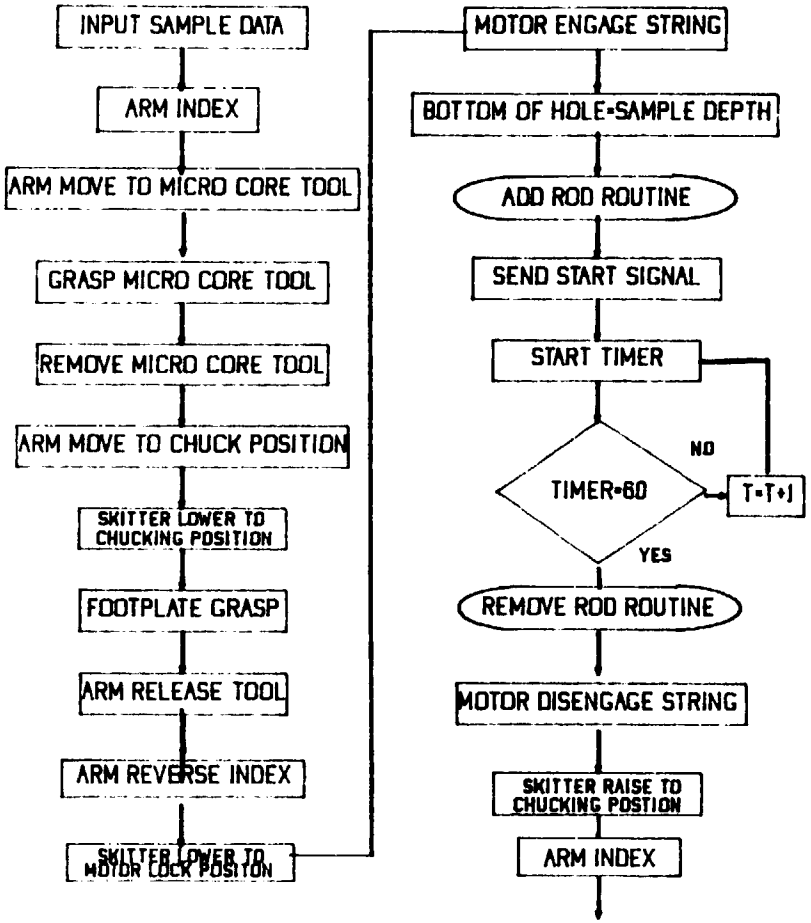

FIG 4.8.2.1.6

MICROCORING ROUTINE (CONTINUED)

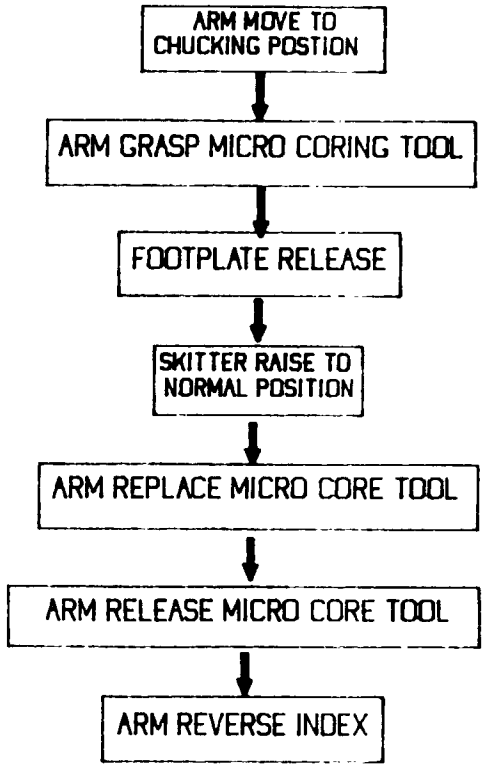

FIG 4.8.2.1.6 CONT.

MICROCORING ROUTINE (CONTINUED)

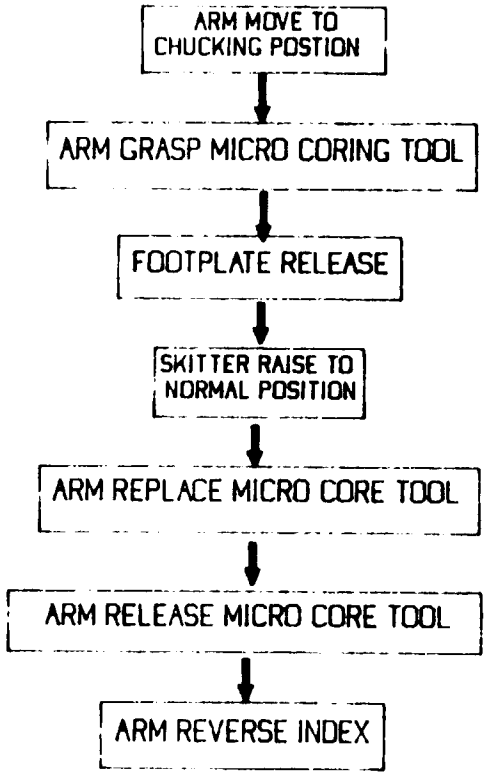

FIG 4.8.2.1.6 CONT.

VERTICAL ACCELERATOR SUBROUTINE

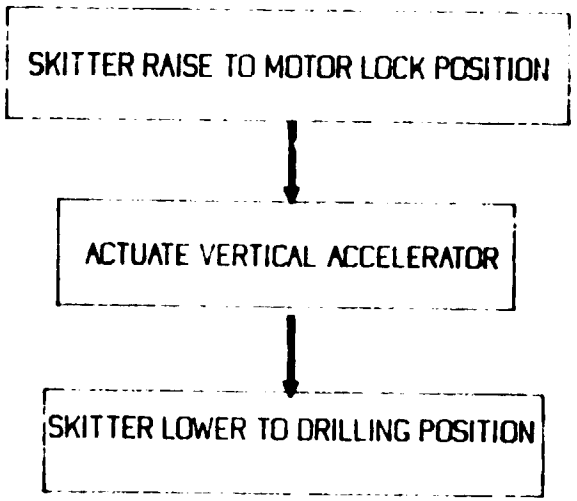

FIG 4.8.2.1.7

ADD ROD SUBROUTINE

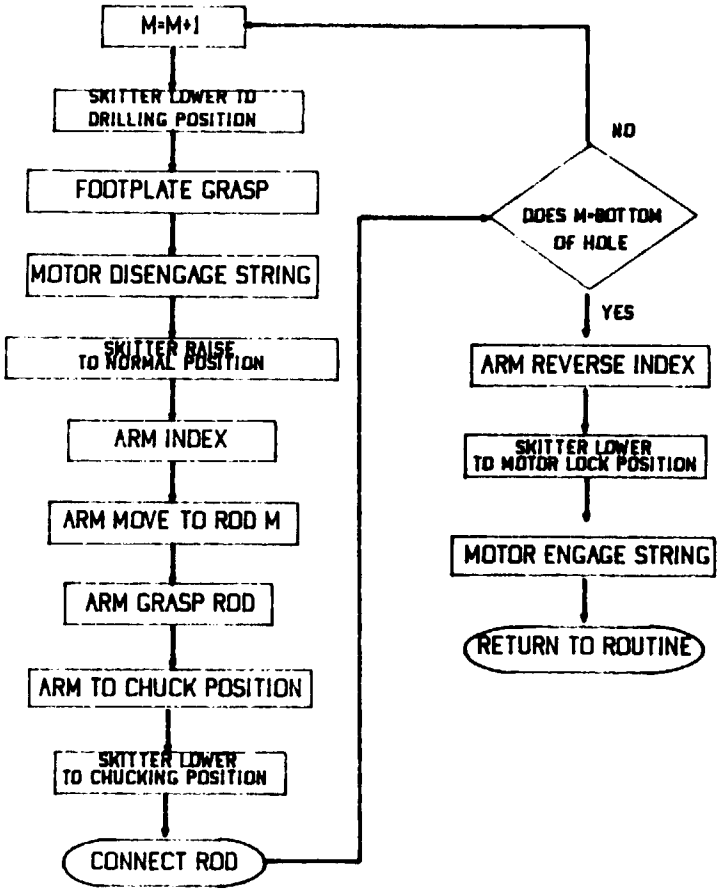

FIG 4.8.2.1.8

CONNECT ROD SUBROUTINE

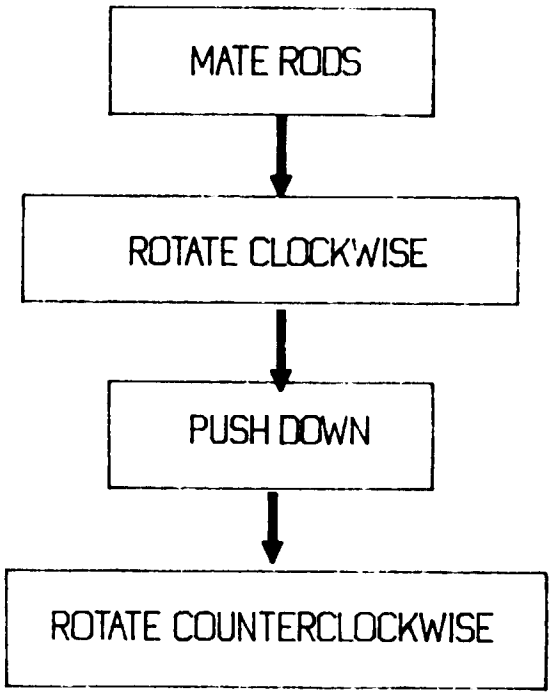

FIG 4.8.2.1.9

REMOVE ROD SUBROUTINE

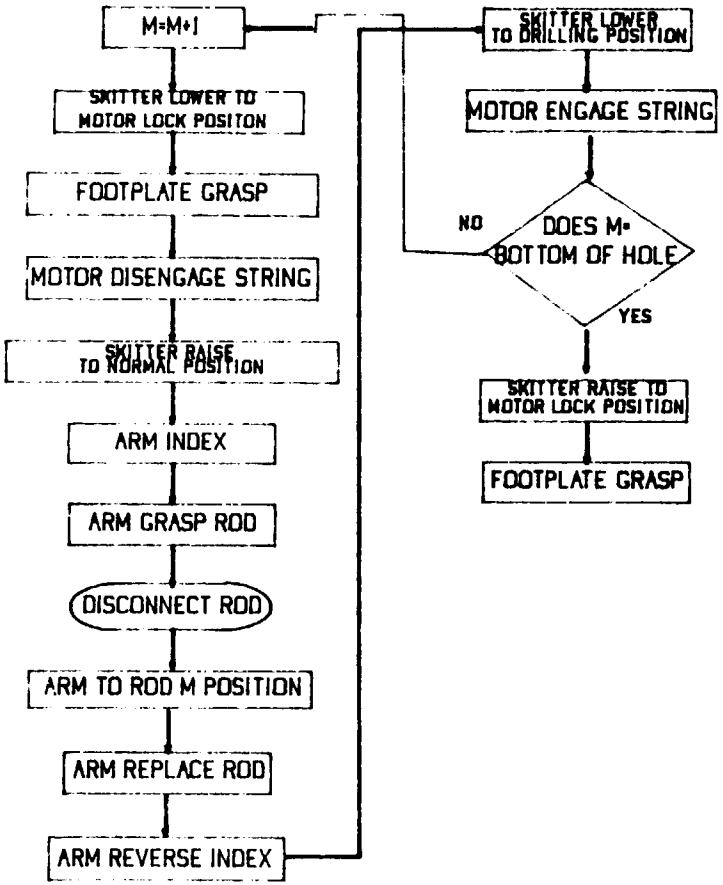

FIG 4.8.2.1.10

DISCONNECT ROD SUBROUTINE

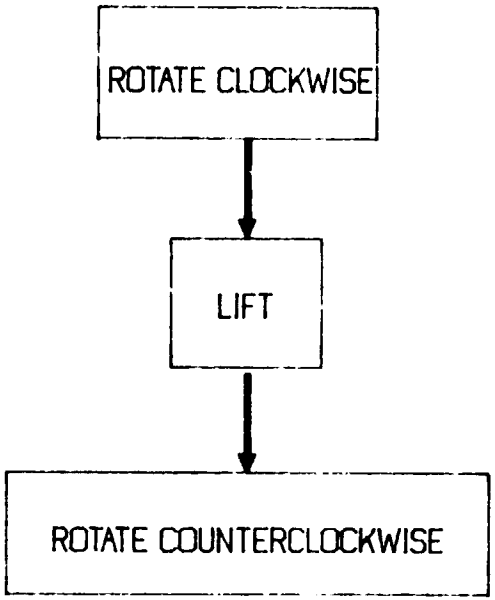

FIG 4.8.2.1.11

SKITTER DRILLING OPERATIONS POSITIONS

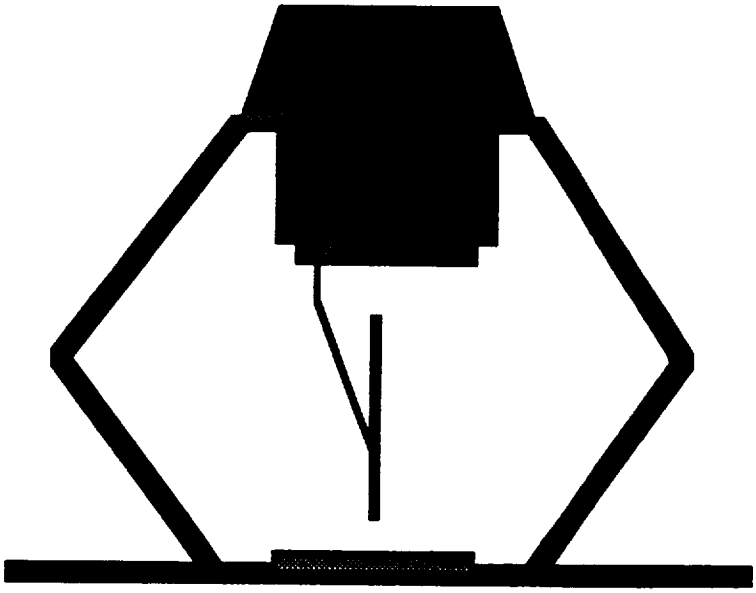

SKITTER NORMAL POSITION

(a)

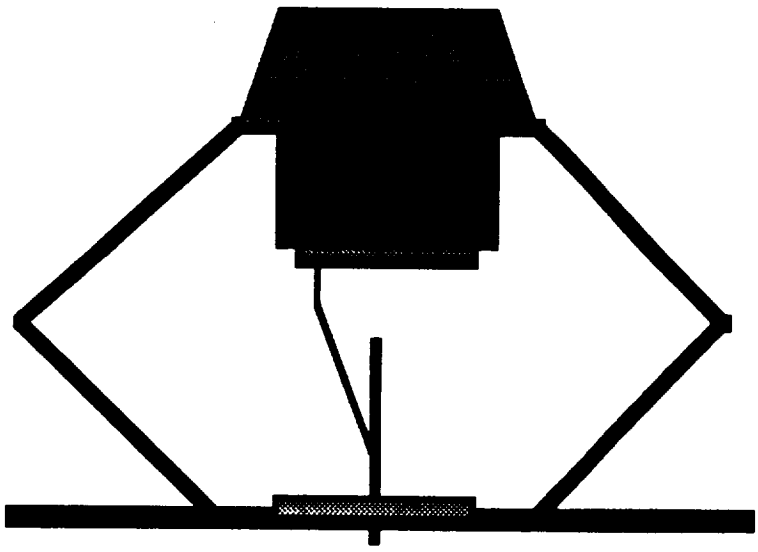

SKITTER CHUCKING POSITION

(b)

Figure 4.8.2.2.1

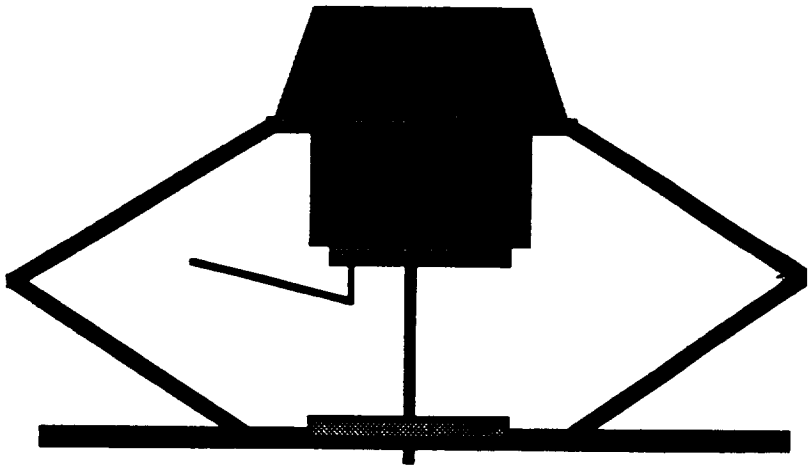

SKITTER MOTOR LOCK POSITION

(c)

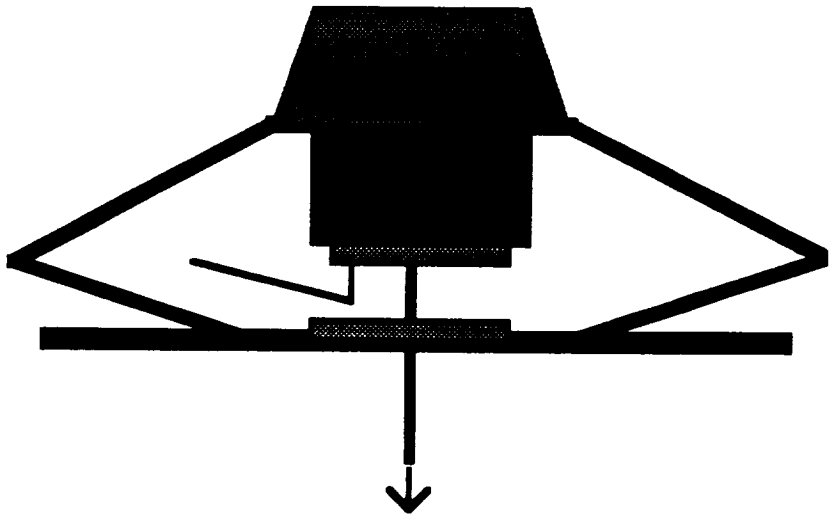

SKITTER DRILLING POSITION

(d)

Figure 4.8.2.2.1 cont.

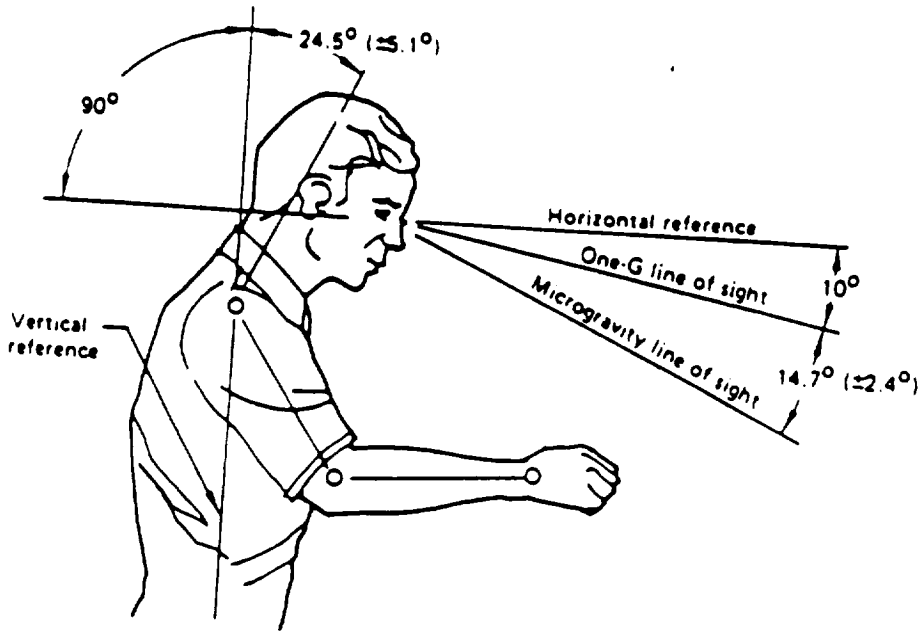

Figure 4.8.3.3.1 NASA-STD-3000 Fig. 9.2.4.2.2-1

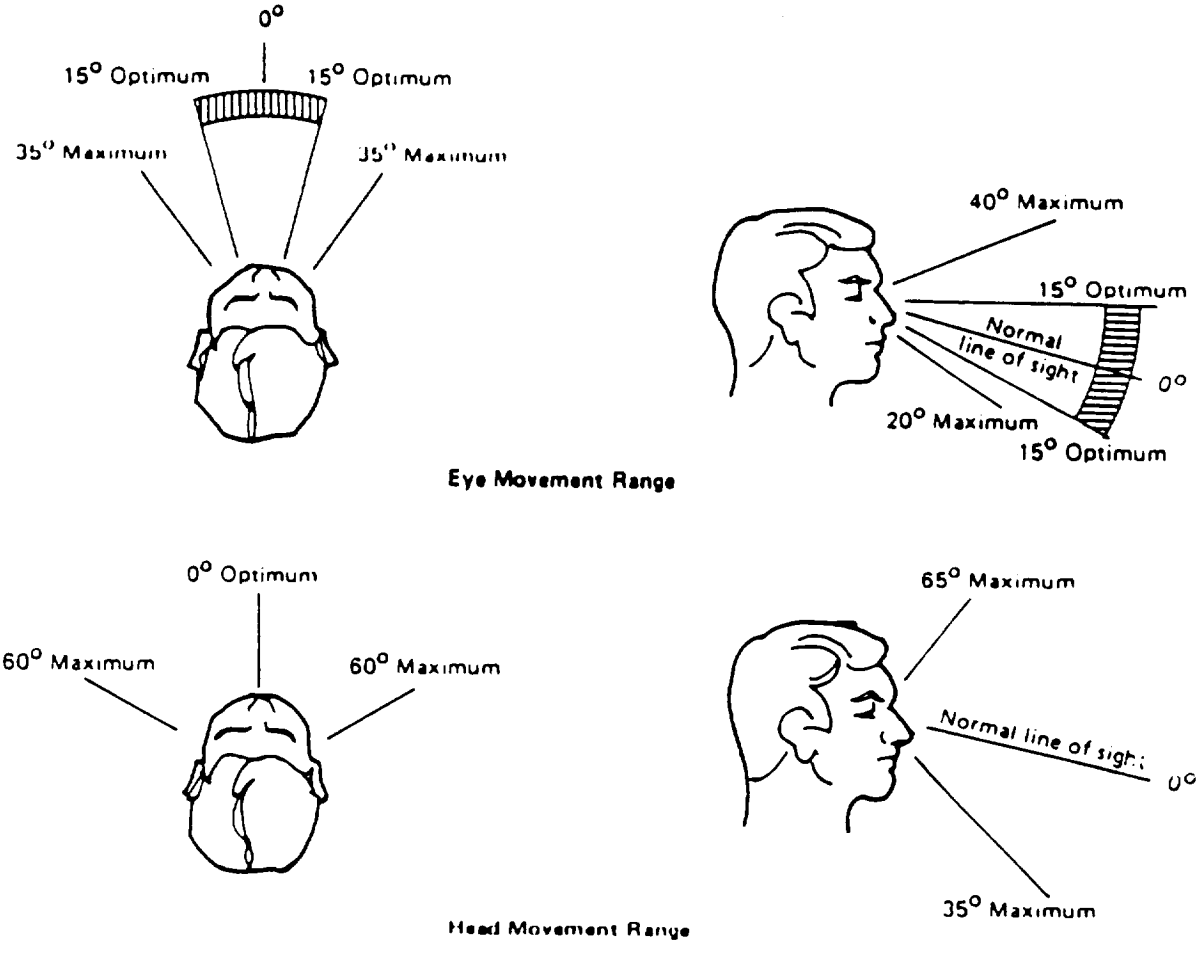

Figure 4.8.3.3.2 NASA-STD-3000 Fig. 9.2.4.2.2-2

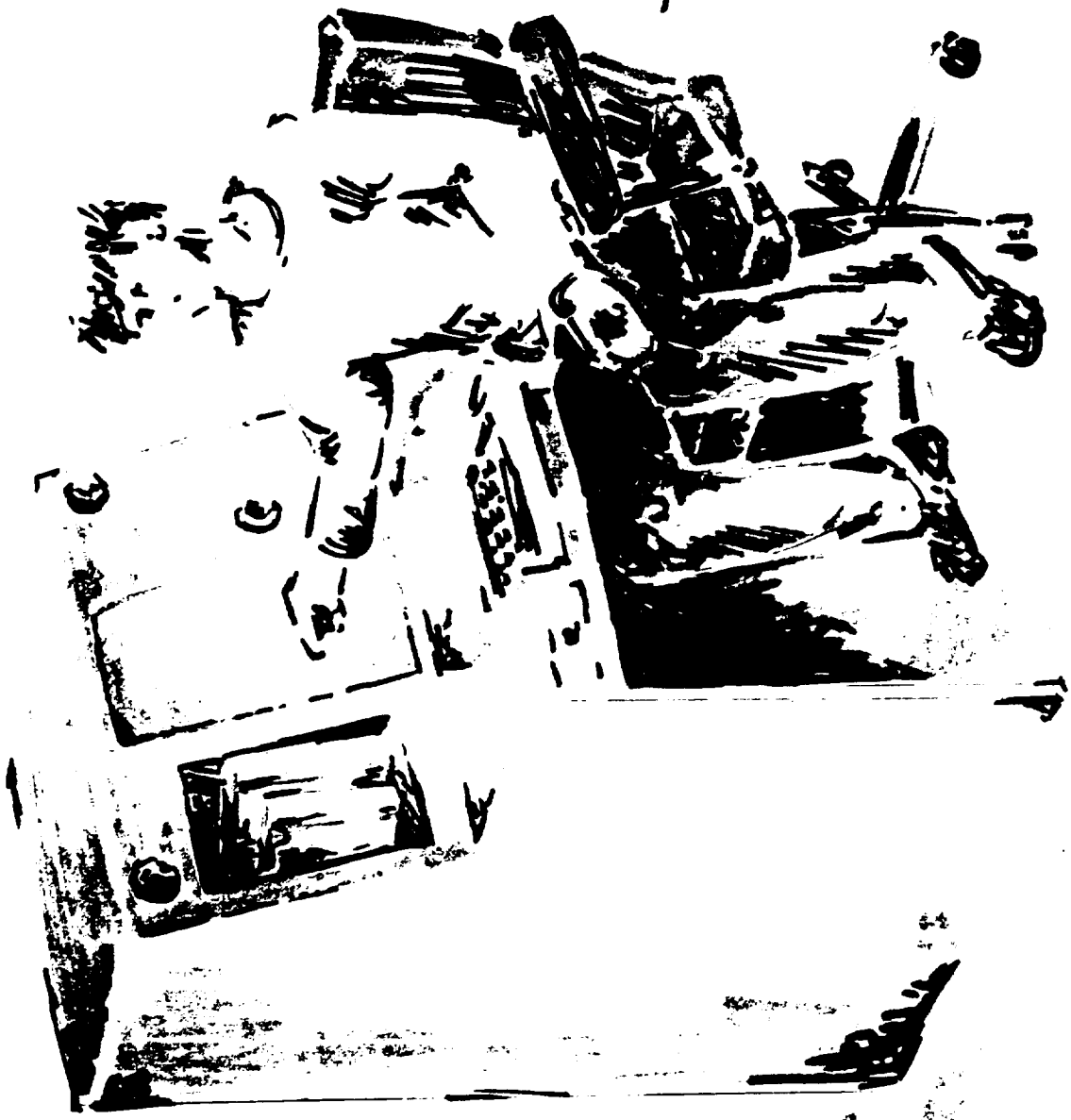

FIG. 4.8.3.3.5.

LUNAR DRILLING OPERATION

LOG ON

Name: _____

Password: _____

FIG 4.8.4.1.1

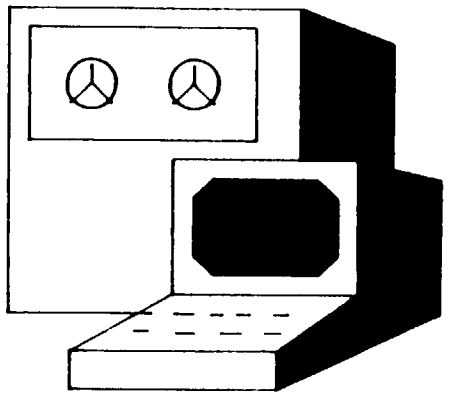

☐ System Access

☑ Preoperation Check

FIG 4.8.4.1.2

PREOPERATION CHECKLIST

- [x] Drill Seated and Locked
- [ ] Energy System at Proper Level
- [ ] Motors Operational
- [ ] Arm Operational
- [ ] Inventory
  - Rods and Bits Present
  - Core Storage Areas Clear

FIG 4.8.4.1.3

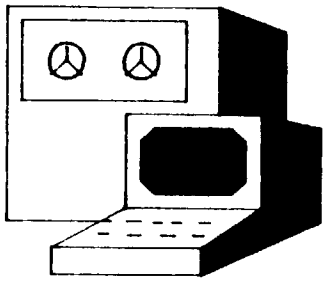

Return Control to Main Console

FIG 4.8.4.1.4

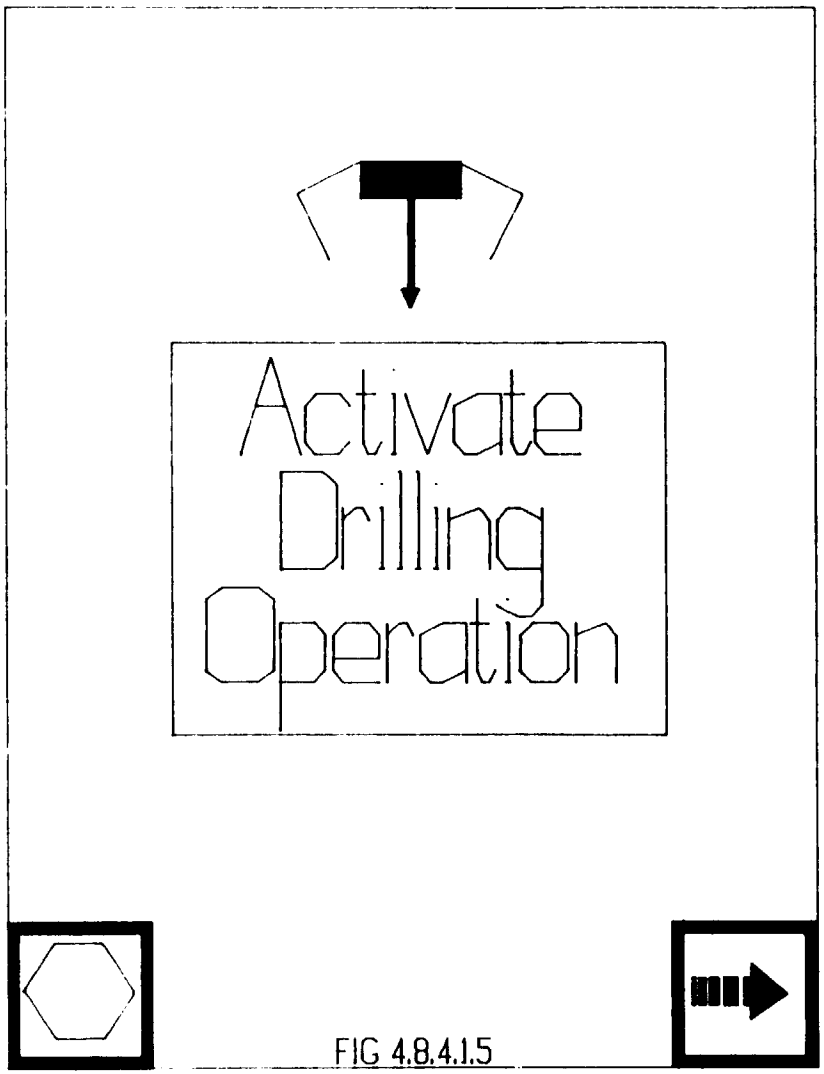

FIG 4.8.4.1.5

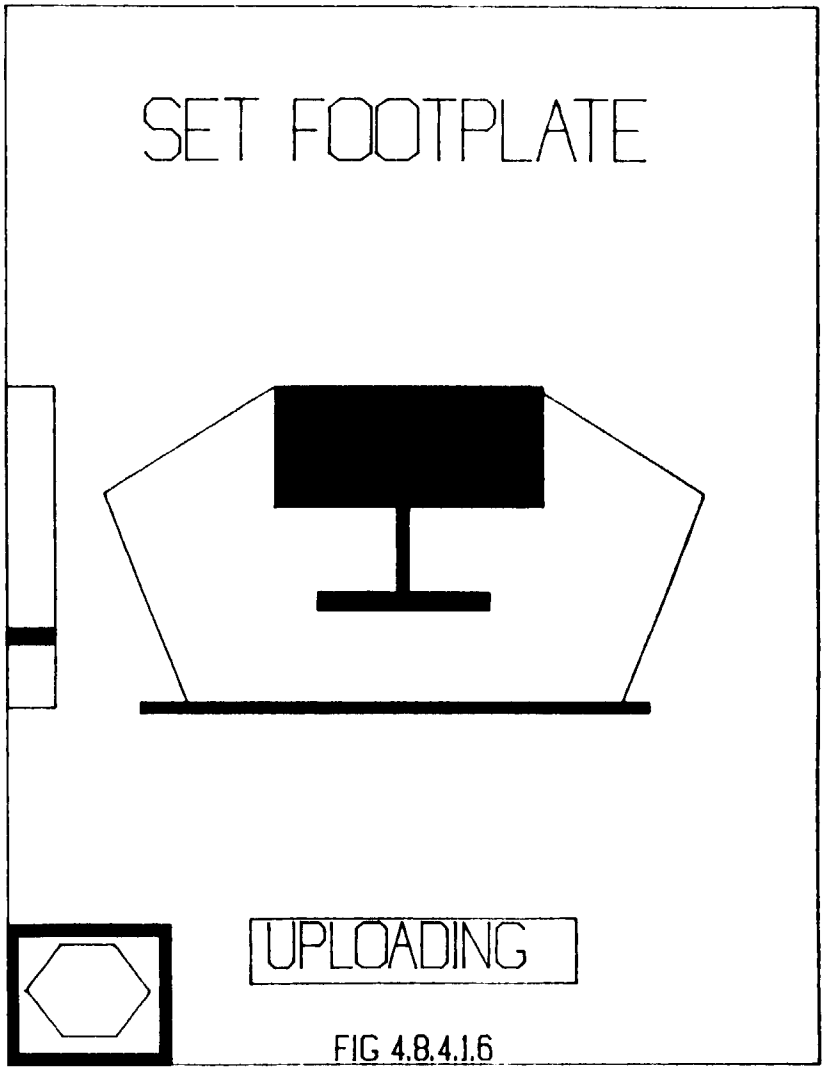

FIG 4.8.4.1.6

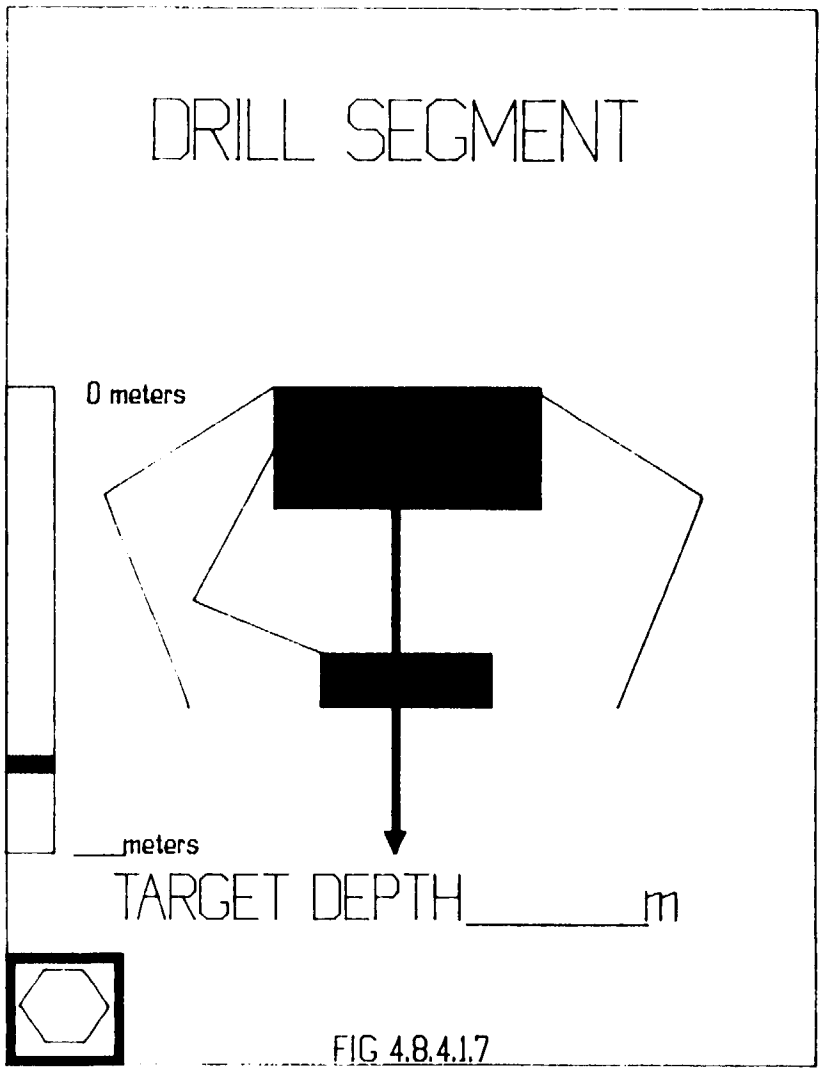

FIG 4.8.4.1.7

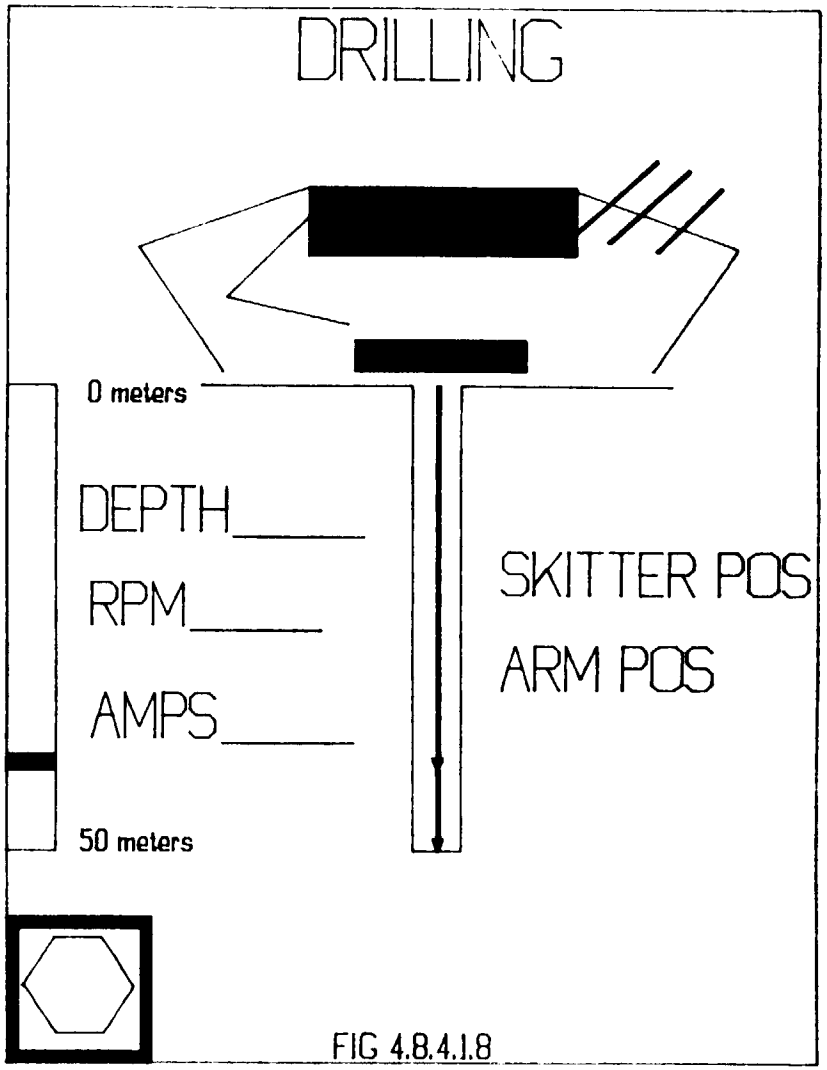

FIG 4.8.4.1.8

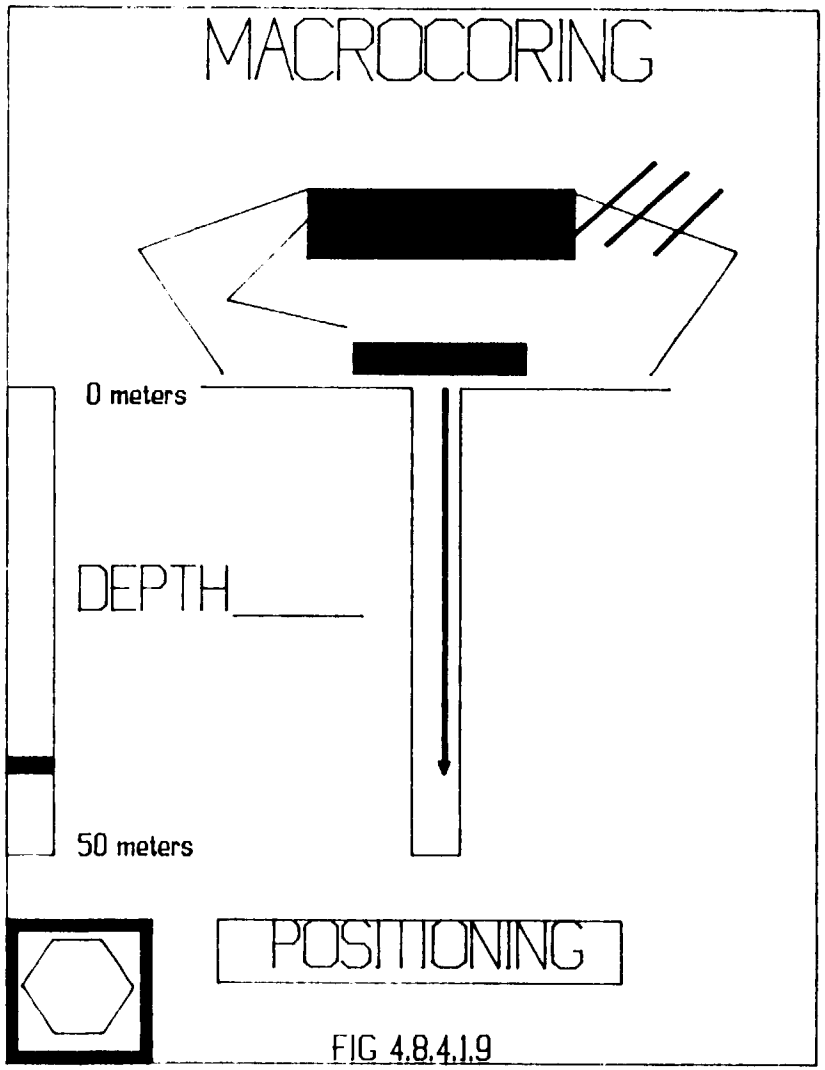

FIG 4.8.4.1.9

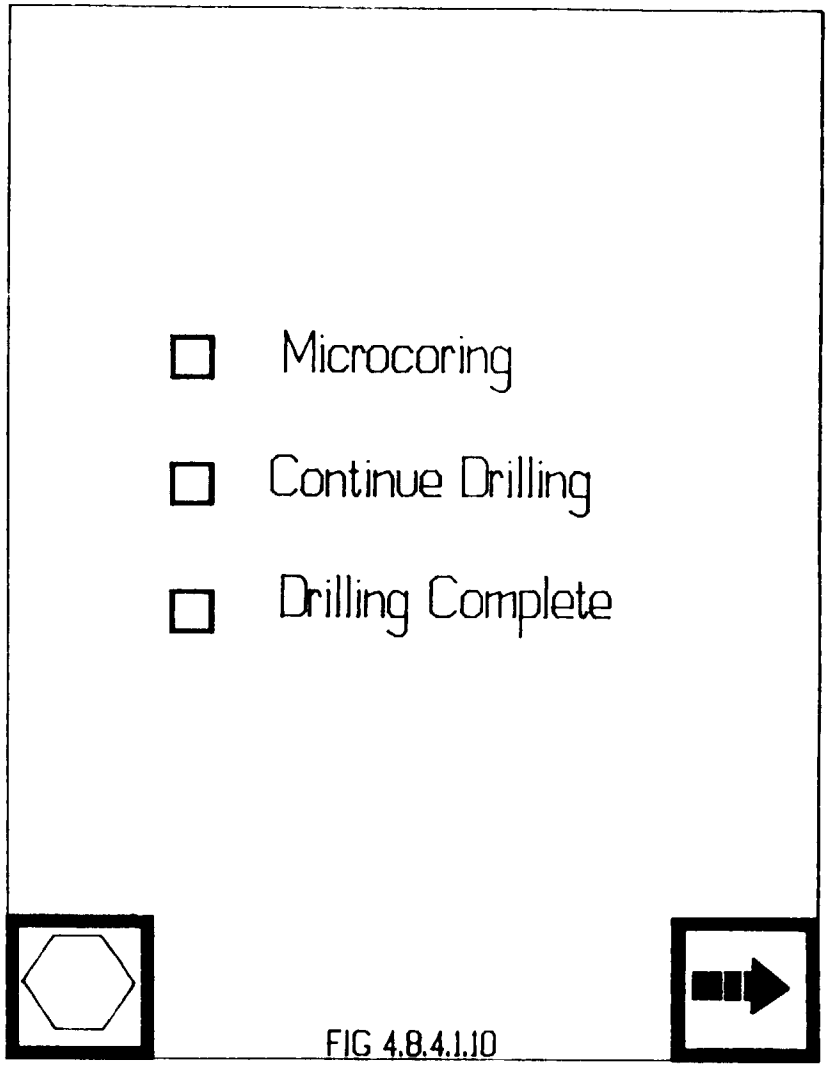

FIG 4.8.4.1.10

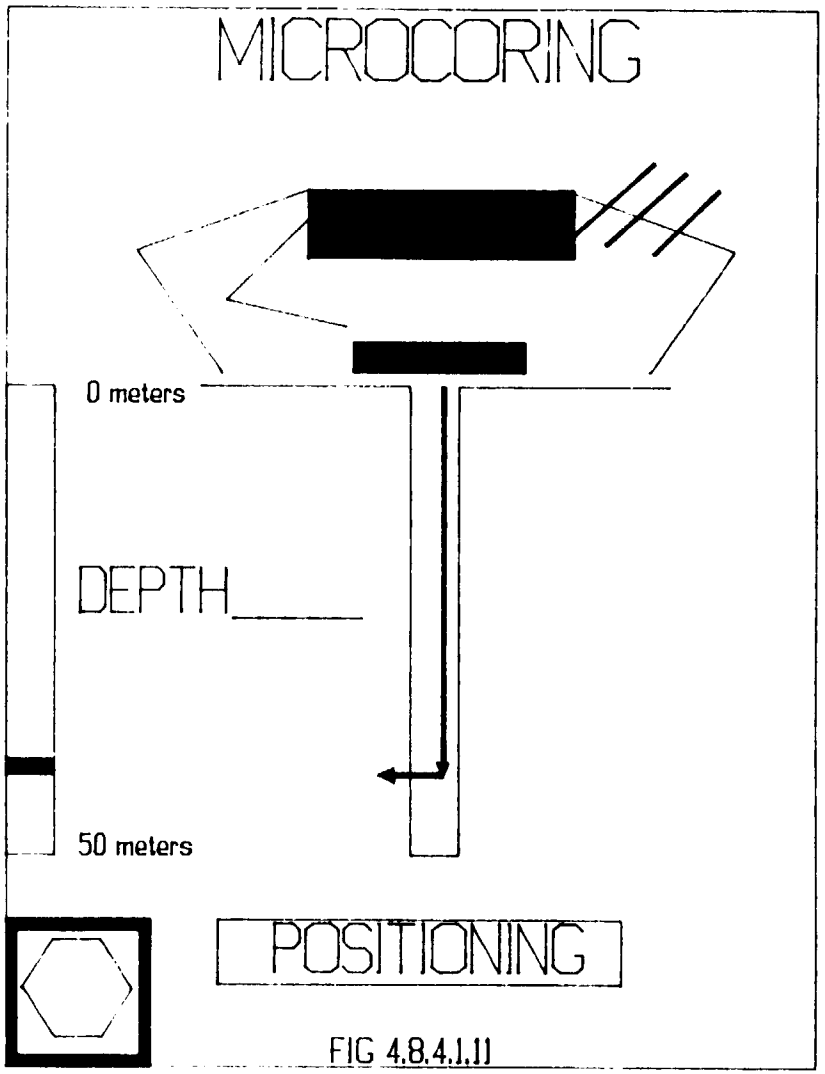

FIG 4.8.4.1.11

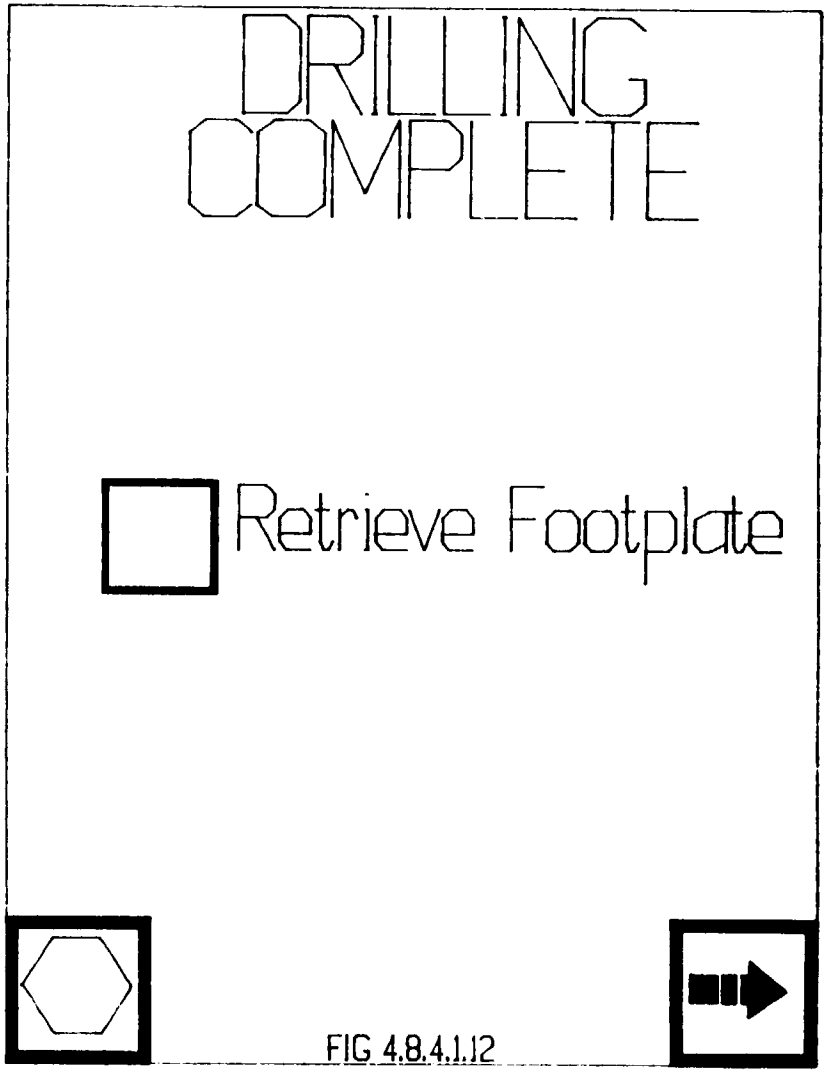

FIG 4.8.4.1.12

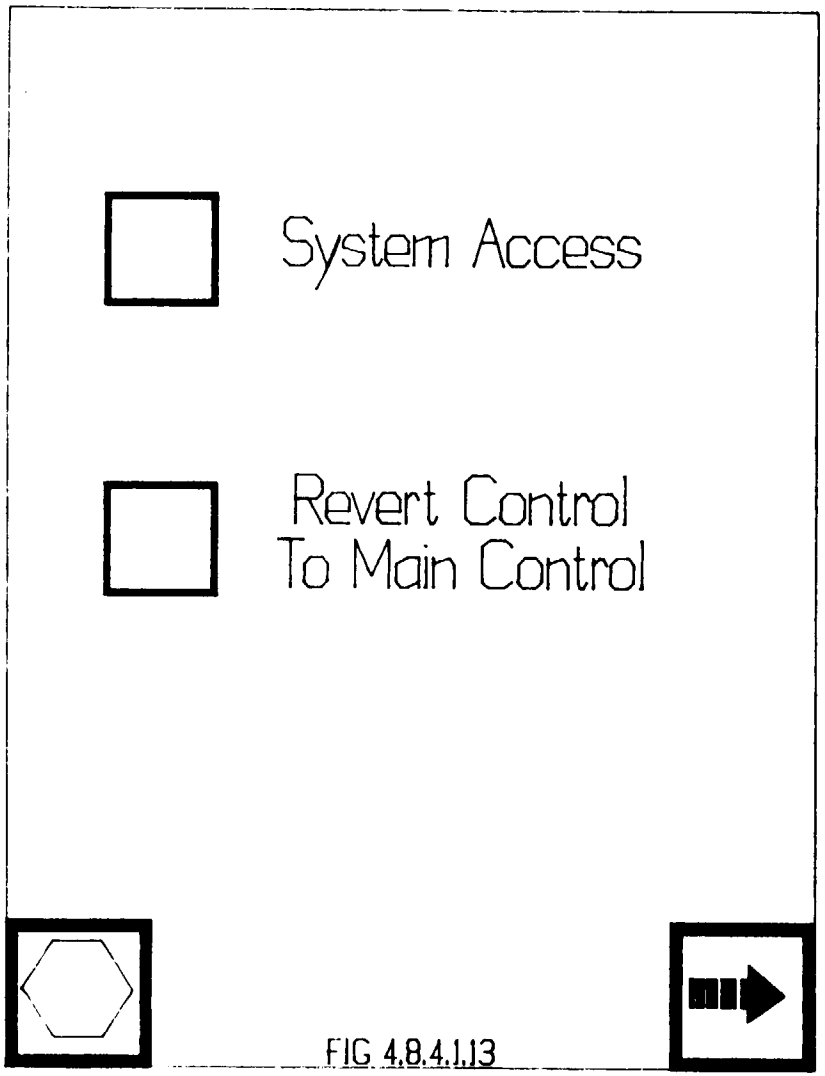

FIG 4.8.4.1.13

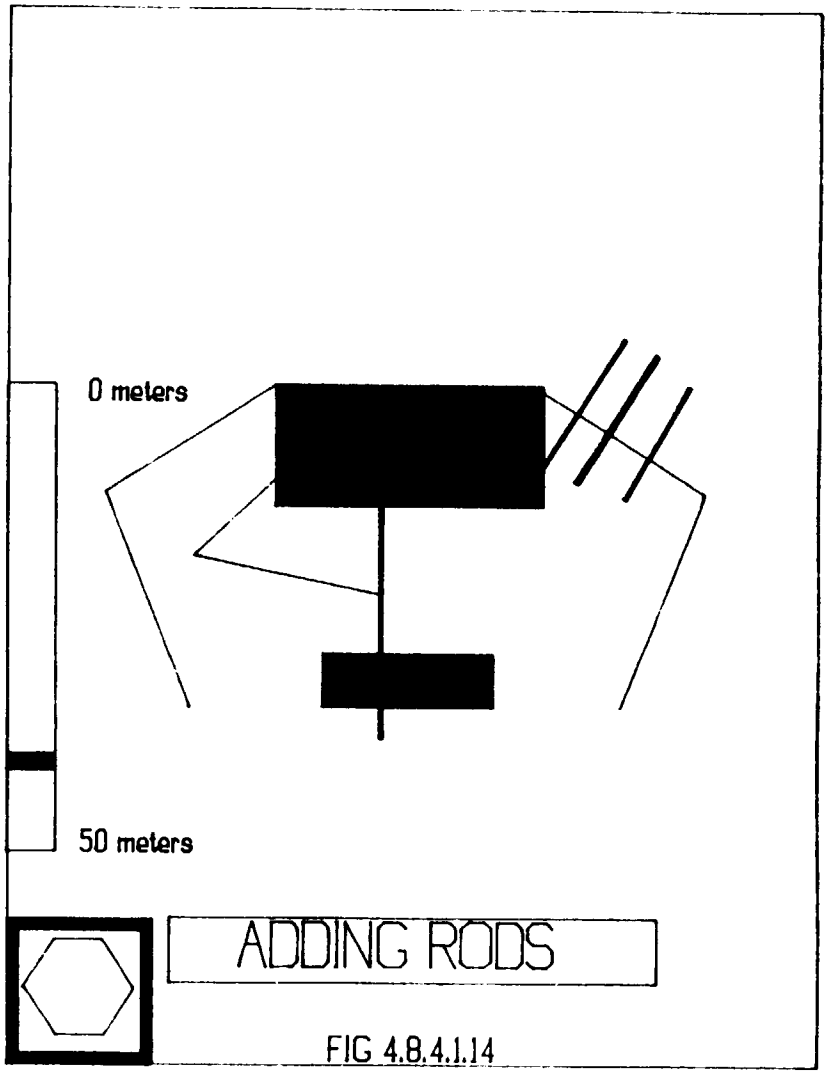

FIG 4.8.4.1.14

4.9 VERTICAL ACCELERATOR

4.9.1 Introduction

In order to remove the hot particles from the drilling chamber and the bit, a vertical reciprocating stepped auger must be implemented, as discussed earlier. These particles will collect in the bit collection chamber until it is full. A vertically reciprocating device can now be used to cause the particles in the collection chamber to advance up the small steps of the stepped auger. Therefore, this vertically reciprocating device will be able to induce a certain amount of volumetric throughput of particles per stroke. This volumetric throughput is mainly a function of the design parameters of the stepped auger and the upward applied force of the reciprocating device.

The final design for the vertical accelerator for the stepped auger is one which uses a sinusoidally shaped cam and a cam follower. This cam converts the rotational mechanical energy of the rotary drive into vertically reciprocating mechanical energy. The motion supplies the necessary acceleration to the drill string and the stepped auger to cause the particles in auger to advance. Illustrations of the accelerator are shown in the following figures: 4.9.1, 4.9.2, 4.9.3, 4.9.4 and 4.9.5.

The cam-follower idea was chosen over the others because of its simplicity and reliability. This method does not need a secondary motor which would add weight and complications to the overall system. This idea also has only two degrees of freedom, the rotating sinusoidal cam and the reciprocating cam chamber which attaches to the drill string.

The accelerator runs for 20 seconds at 50 rpm for a period of time, T_{run}. This time duration is only a function of the amount of soil

moved per stroke of the accelerator, through the stepped auger, and the amount of soil contained in the lower soil collection chamber. T_{run} should be long enough to completely empty the bit collection chamber (193,000 mm^3 of soil). Two accelerator strokes occur per revolution so the stroke frequency is 1.67 strokes per second. For the mathematical analysis of the advancement of the particles up the auger and component designs, see subsequent sections.

4.9.2 Detailed Operation Description

When the bit collection chamber is full of moon regolith the goes into auger mode. The rotary drive cuts off and the SKITTER stands up 152 mm to disengage the jaw clutches (A & B). Refer to figures 4.9.1-4.9.5. Now no torque is transmitted to the drill string, but the telescoping shaft still transmits torque to the cam (H). The rotary drive begins to turn the cam, and the cam housing (F) will also turn until the rollers on the outside of the cam housing hit against the vertical stops. As the rotary drive now continues to turn the cam, the cam roller followers roll on the cam, accelerating the cam housing up and down and in turn shaking the entire drill string. The cam housing rollers roll up and down the vertical stops keeping the cam housing from rotating. When the bit collection device is empty, the rotary drive stops, and the SKITTER goes back into drill mode by squatting back down engaging the jaw clutches and releasing the cam housing rollers from the vertical stops allowing it to rotate. This process is then repeated every 13 mm of drilling.

4.9.3 Specifications

Parts List

(A) Upper jaw clutch
(B) Lower jaw clutch
(C) Telescoping shaft - upper shaft - outer splines
(D) Telescoping shaft - lower shaft - inner splines
(E) Cylindrical vertical accelerator housing
(F) Cylindrical cam housing
(G) Vertical stops
(H) Sinusoidal shaped cam

4 Cam roller followers with needle bearings (25 mm dia., 13 mm thick)
2 vertical stop roller followers (25 mm, 13 mm thick)

Operational Requirements

Stroke distance	56 mm
Frequency	1.67 strokes/sec.
motor speed	50 rpm
Power	300 watts
Distance SKITTER lifts to aug	152 mm

Material

The entire accelerator is made of titanium alloy : Ti-6Al-4V
at 204° C (400°F) yield strength = 4.88 MPa
at 24° C (75°F) yield strength = 5.74 MPa
Roller follower and bearings: McGill Camrols-case hardened steel for smooth rolling and low wear.
Roller follower: Case hardened steel
Needle bearings: silver nitride ceramic; recommended by Torrington.

Because no lubrication is necessary, they can be manufactured to our specifications.

4.9.4 Control Operation Sequence

1). SKITTER squats engaging the jaw clutch which will transmit torque to the drill string.

2). The rotary drive drills down thirteen millimeters into the lunar surface, then drive stops.

3). SKITTER stands up 152 millimeters disengaging the clutch so that the drill string will not turn.

4). The rotary drive begins to turn at 50 rpm which means two strokes per revolution or 100 strikes per minute. The drive should run for 20 seconds.

5). When the auging is completed, the motor stops and the SKITTER squats back down engaging the jaw clutch and begins drilling another thirteen millimeters.

4.9.5 Math Model for the Vertical Accelerator

The advancement of the particles through the stepped auger requires that the particles be given an upward velocity great enough such that if the stepped auger were abruptly stopped, the particles would continue upward until they would impact with the underside of the helix above them. This velocity of impact must be great enough such that the particles would be "knocked" into the steps further up the stepped auger helix. The maximum distance that the particles could be knocked would be a perfectly symmetrical rebound path off the underside of the helix. However, due to the gravitational pull of the moon and the inelastic particle-particle and

particle-auger collisions, this overall advancement will be somewhat less than a symmetric rebound. This non-ideal rebound path would therefore be somewhat parabolic rather than a straight line as shown on the following page (Figure 4.9.1).

Due to the complexity of the analysis, a few assumptions have been made. The assumption that gravitational effects on the particle's rebound path will be small when the applied force is large was made. Also, the assumption that all particle-particle and particle-auger collisions will be elastic due to the difficulty in measuring these quantities without experimentation was made.

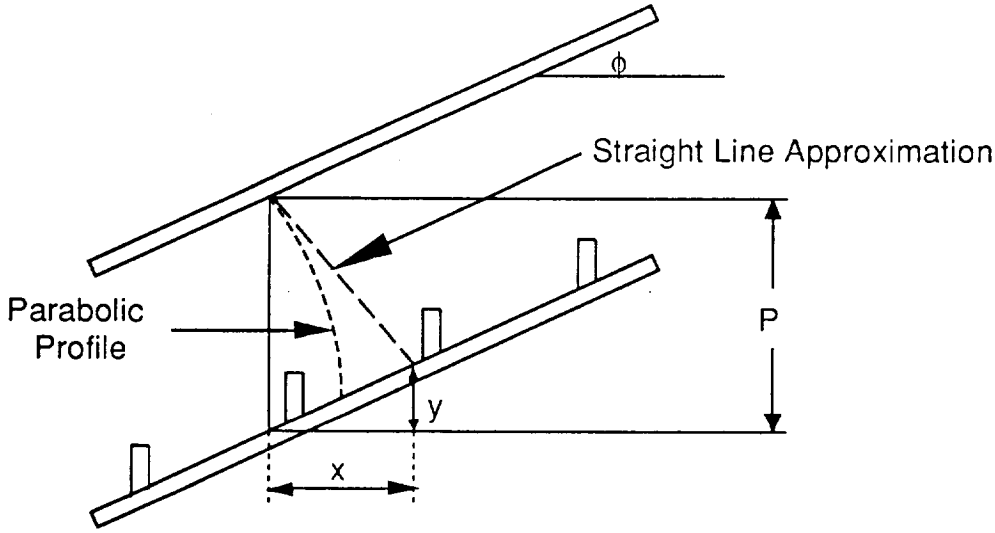

Figure 4.9.6

Therefore, the particle's advancement will only be a function of the applied upward force, and its rebound path will be linear and symmetric with a trajectory of impact when the upward force is sufficient.

The particles must be given a certain velocity in a certain distance, so they must be accelerated. The velocity required to be

sufficient to impact the helix adequately was determined from an energy balance on the particle's path, letting V_1 be the particle's velocity when it leaves the auger and V_{IMP} be the velocity of the particle when it impacts the underside of the helix, or the roof. Applying the concept that the particle's increase in potential energy will be approximately equal to its decrease in kinetic energy, and then solving for V_1 yields the relationship shown below.

$$V_1 = [\, g_{moon} \cdot P + \left(\frac{V_{IMP}^2}{2}\right)]^{1/2} \qquad [4.9.1]$$

In the above equation, P represents the distance that the particle must travel upward. This is the equivalent to the stepped auger pitch for single-helix augers and one-half of the pitch for double-helix augers.

The vertical reciprocating device must be capable of achieving V_1 in a certain distance, h_1, which will be determined by the space constraints of the overall design. Using the following relationships,

$$V_1 = \left(\frac{h}{t}\right) \qquad [4.9.2]$$

$$a = \left(\frac{V_1}{t}\right) \qquad [4.9.3]$$

the acceleration of a particle will be given by the following relationship after the expression for V_1 has been substituted into it.

$$a_1 = \left(\frac{g_{moon} \cdot P}{h}\right) + \left(\frac{V_{IMP}^2}{2h}\right) \qquad [4.9.4]$$

Therefore, the required force to produce this acceleration will be a function of the total mass, m_{tot}, of the drill string. This includes the masses of the drill bit, the stepped auger (empty and full), and the drill rods which vary from one to twenty five lengths. This force will also have to compensate for any frictional effects that the stepped auger encounters on the sides of the hole. It will be assumed that the diamond tip coated drill bit will produce rather smooth walls in the hole. The hole diameter also allows for some clearance between the stepped auger and the hole walls. Therefore, frictional effects will be considered negligible. The required upward force is shown below.

$$F_{up(min)} = m_{tot} * \left[\left(\frac{g_{moon} \cdot P}{h} \right) + \left(\frac{V_{IMP}^2}{2h} \right) \right] \quad [4.9.5]$$

In order to complete the model, it becomes necessary to derive an expression for the required impact velocity, VIMP, to provide the assumed straight line rebound approximation. The analysis of the dynamics of the stepped auger will be simplified somewhat as it will be treated as if the helices of the auger were simply unwrapped. Therefore, we are dealing with a ramp, rather than a helix . This assumption is not a poor one considering the fact the particles furthest away from the center of the auger advance the least anyway. Therefore, the outside radius is used as the basis for the VIMP model. The particle-wall collisions, again, were assumed elastic, therefore, the path of the particles up the auger steps in the helix will not vary much from the path of the particles in the unwrapped ramp, except for the absence of induced vorticity in the bulk particle motion in the helix. The parameters involved in the stepped auger to be used are the vertical pitch, P, the number of helix turns, N, the number of fences per turn, FT, the fence height, FH, the outer radius of the stepped auger, R_o, the angle of inclination of the helix, ϕ, and the advancement of the particles, A. The inclination angle is shown below and given by the following relationship.

Therefore;

$$\phi = \tan^{-1}\left(\frac{P}{2\pi R_o}\right) \qquad [4.9.6]$$

It is also necessary to analyze the vector dynamics of the velocities involved in the paths of the particle, both before and after the impact with the roof. This geometry is shown in the figure.

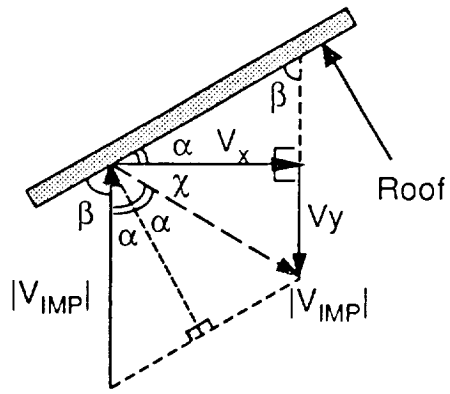

Figure 4.9.8

In the above figure, the quantity α represents the angle (ϕ), β represents (90 - ϕ), and χ represents (90 - 2ϕ). Therefore, the following relationships represent V_x and V_y.

$$V_x = |V_{IMP}| \cos (90 - 2\phi) \qquad [4.9.7]$$
$$V_y = |V_{IMP}| \sin (90 - 2\phi) \qquad [4.9.8]$$

Using the following equations of motion for a particle in a gravitational field;

$$x = V_x \cdot t \qquad [4.9.10]$$
$$y = \left(\frac{-g_{moon} \cdot t^2}{2}\right) + V_y \cdot t \qquad [4.9.11]$$

The impact velocity relationship was then determined. Eq. [4.9.10] was solved for t and substituted into Eq. [4.9.11]. Eqs. [4.9.7] and [4.9.8] were then substituted in to yield the following relationship.

$$y = -\left(\frac{g_{moon}}{2}\right) \cdot \left(\frac{x}{|V_{IMP}| \cos(90-2\phi)}\right) + x \tan(90-2\phi) \quad [4.9.12]$$

In Eq. [4.9.12] the variable x represents the horizontal component of the advancement shown in figure 4.9.1 and y represents the vertical component. Therefore, Eq. [4.9.12] can be satisfied by the x and y components of the position at which the rebound leaves the particle, shown below.

$$x = A \cos \phi \quad [4.9.13]$$

$$y = A \sin \phi - P \quad [4.9.14]$$

Substituting Eqs. [4.9.13] and [4.9.14] into Eq. [4.9.12] and solving for the impact velocity yields the following relationship.

$$V_{IMP} = \left(\frac{-g \cdot (A \cos\phi)^2}{2(\cos(90-2\phi))^2 \cdot (A\sin\phi - P - (A\cos\phi)\tan(90-2\phi))}\right) \quad [4.9.15]$$

The expression for the overall upward force required for the reciprocator to accelerate the particles enough to advance up the stepped auger is found by substituting Eq. [4.9.15] into Eq. [4.9.5].

The parameters which now need to be quantified are P, h, m_{TOT}, ϕ, and the advancement, A. If the rebound trajectory is assumed to be a straight line, the maximum advancement would

result. From the geometry of the stepped auger, this would result in an advancement shown below.

$$A_{max} = 2P \sin[\tan^{-1}\left(\frac{P}{2\pi R_o}\right)] \qquad [4.9.16]$$

$$A_{min} = FH \sin\phi + \left(\frac{2\pi R_o}{FT}\right) \qquad [4.9.17]$$

Eq. [4.9.17] was used to check the stepped auger design to be sure that the particles would make it to the next step and over the fences given the calculated upward force. The parameters P, N, FH, FT, R_o, and ϕ are all design parameters of the stepped auger. The vertical accelerator for the stepped auger will therefore be designed to optimally supply the auger with the required force. The only parameter left to be determined is the vertical displacement of the auger, h, which will be discussed in the next section.

The maximum upward force which can be tolerated must also be considered. The vertical accelerator will pull on the drill string with a force, F_{up}. When the stepped auger is abruptly stopped, the force required to stop the drill string from continuing upward must be considerably less than the weight of the drilling apparatus so that SKITTER will not hop around.

4.9.6 Cam-Follower Analysis

In order for the rotational mechanical energy from the rotary drive to be adequately converted into vertically reciprocating mechanical energy for the drill string, a sinusoidal cam and follower system will be used.

From the math model discussed earlier, the velocity that the particles must have to impact on the underside of the helix and then

rebound with a straight-line approximation is approximately 427 mm/sec. This value was determined after calculating the necessary impact velocity to be 368 mm to have the particles follow a straight line approximation given the design of the stepped auger and all of its parameters. Therefore, the cam must accelerate the drill string and the stepped auger such that the final velocity of particles in the stepped auger, when it is abruptly stopped, will be about 427 mm/sec.

The cam-follower design is basically a contoured disk mounted to a shaft which extends through the top casing of the accelerator which attaches to the motor. The cam itself has a "hill" profile which the weight of the drill string, supported by the rollers, must travel along. In the course of this motion, the follower must ride smoothly and properly over the cam's hill profile. The rotary drive rotates the cam with a certain angular velocity, and, in conjunction with the heights of the hill profile and the cam radius, $R_{cam,}$ will determine the velocities and accelerations of the drill string, stepped auger, and in turn, the particles will be determined.

Certain initial constraints had to be set when the motor speed, cam profile, and cam size were being determined. To support the weight of the drill string, two followers, 180° apart, are used so that the reciprocating motion occurs smoothly without any horizontal movement or moments caused by using only one roller follower. Therefore, for the weight of the drill string to be reciprocated smoothly, the entire hill profile of the vertical motion must occur in 180° of rotation in the cam. The cam virtually has the exact same hill profile repeated twice in 360° of the cam. This is so that the same heights of the hill profile will coincide with the follower supports at the same time.

The hill profile can be be broken down into three different periods of consideration: the rise section, the settling section, and the dwelling section. This was when the next constraints came into play. The rise section must induce a final velocity of V_1 = 427 mm/sec to

the drill string as discussed earlier. Also, the settling section must allow the particles sufficient time to travel up off of the auger, impact with the helix, and rebound into the next steps. Finally, the falling section must allow the drill string, the stepped auger, and the particles on the auger to lower to the starting position with an acceleration equal to or less than that of the gravity of the moon. This was done to minimize the amount of particle chaos in the stepped auger. In addition to these time constraints, t_{rise}, t_{settle}, and t_{fall}, the size of the cam and the necessary vertical displacement, h, were constrained by their magnitudes to keep the accelerator light and easy to handle. A 30° maximum pressure angle was also implemented.

The design of the settling time was first considered. It was found that a settling time of 0.2 seconds was appropriate for the particles to rebound and land in their final destinations. With this time known, the t_{rise} and t_{fall} must be split up from the remaining time for 180° of rotation of the cam.

The value of t_{fall} was considered next. It was found that this time was a function of the height, h, that the drill string had been displaced. The relationship is shown below:

$$t_{fall} = \left(\frac{2h}{g}\right)^{1/2} \qquad [4.9.19]$$

Therefore, the determination of the value of h was necessary before the natural necessary falling time for the drill string could be determined and compared to the amount time for falling which had been allowed.

In order to determine the height, h, and t_{rise} the initial constraint that V_1 must be at least 427 mm/sec was employed as shown below:

$$t_{rise} = \left(\frac{h}{V_1}\right) \qquad [4.9.20]$$

Many iterations were done to test all of the constraints of the final cam design.

It was finally decided that a 113 mm radius cam can be used at 50 rpm with 55 mm of overall vertical displacement. This design creates the necessary velocity required for particle advancement in the auger and satisfies all of the mentioned constraints. The final cam hill profile for 180° of rotation is shown below with the vertical displacement as a function of time, induced by the motor speed, the angle, and the actual horizontal displacement of the cam if the 180° of cam were unwrapped into a line instead of a semi-circle.

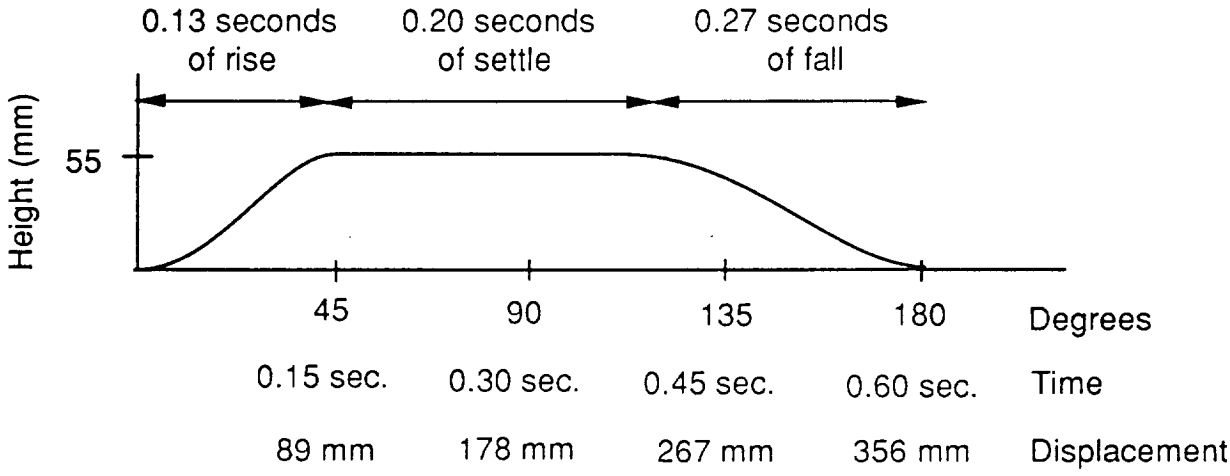

The thickness of the edge of the cam changes slightly on the exterior of the cam. This is necessary so that the smooth passage of the cam through the roller supports on each side will not be impeded. During the transitions from rise to settle or settle to fall, the cam will become thicker or thinner respectively to compensate for the change in cam angle. A modeled cantilever beam analysis could be performed to determine the minimum thickness of the cam with the

given radius, but the maximum thickness will be specified as 20 mm. This corresponds to a minimum thickness of about 17 mm.

4.9.7 Component Analysis

Bearing Analysis

The following is the analysis of the maximum load on the cam bearings:

Weight of full drill string = 245 N (on moon)
Acceleration of drill string (maximum) = 3277 mm/s^2
Maximum force to accelerate drill string

$$F = ma = \left(\frac{245\ N}{1646\ \left(\frac{m\ m}{s^2}\right)}\right) \cdot \left(3277\ \frac{m\ m}{s^2}\right)$$

$F_{max} = 487\ N$

Because the roller follower is being pushed at a maximum of a 30 deg. pressure angle it actually reacts to a larger force.

$$F_{max} = \frac{487\ N}{\cos(30^o)} = 562\ N$$

Maximum force on any one roller is then half of this total force.

$F_{roller} = 281\ N$

Load rating:

$$C_R = F_{roller} \cdot \left(\left(\frac{L_D}{L_R}\right) \cdot \left(\frac{n_R}{n_D}\right)\right)^{1/a}$$

Using an L_{10} life of 5000 hr and design rpm of 450:
$L_R = 3000$ hr
$n_R = 500$ rpm

L_D = 5000 hr

n_D = 450 rpm

a = 10/3

$$C_R = 281\ N \cdot \left(\left(\frac{5000}{3000}\right) \cdot \left(\frac{450}{500}\right)\right)^{3/10}$$

C_R = 317.5 N

The roller followers have a much higher load rating than the computed one estimated by Torrington; so the roller follower life should last through about 450 fifty meter holes, but we oversized the follower for about ten times that amount. Since there are extreme operating temperatures on the moon going as low as -158 °C at night, lubricants would just evaporate, therefore, the bearings used are designed without the need for any lubrication.

Shaft Analysis:

$Diameter_{min}$ = 25 mm

T_{max} = 28.6 N-m

Moment = 0

S_y = 827 MPa

n = ? (factor of safety)

Using a basic static failure analysis and solving for n (factory) gives,

$$d = \left(\frac{32n}{\pi}\left(\frac{M_a}{S_y} + \frac{0.866T}{S_y}\right)\right)^{1/3}$$

$$n = \frac{d^3 S_y \pi}{0.866(32)T}$$

$$n = \frac{(1)^3(827\ MPa)(3.14)}{0.866(32)(28.6)}$$

n = 645 Factor of safety

The reason for this high factor of safety on the smallest diameter shaft is because our design uses the same size rods as the rods in the drill string, and the vertical accelerator does transmit the required torque to the drill string during the drilling process. Thus, the shafts designed in the vertical accelerator are consistent with the drill string design and not designed based on factor of safety.

4.9.8 Design Development

Prior to the derivation of a satisfactory Vertical Accelerator, very in-depth analyses of design options were accomplished. Initially, various notions for oscillating the control rods and the stepped auger were conceptualized and recorded. These various methods of operation were divided up into specific categories and developed as a Version 1 design. The categories were as follows: Reciprocating Cam Mechanisms, Spring Actuated Devices, Gear Powered Devices, Secondary Motor Configurations, and a Miscellaneous section for designs which did not fit into one of the preceding areas. Next, a full evaluation was performed on each Version 1 design. The evaluation emphasized design effectiveness with respect to initial constraints. A final recommendation for each design was rendered. Unsatisfactory designs were discarded and the remaining feasible designs were developed further into subsequent versions. Following these versions, a more critical in-depth evaluation was performed with a more significant emphasis placed on initial constraints and a final design was brought forth (see table 4.9.1).

Table 4.9.1

DESIGN A (CAMS)	DESIGN B (SPRINGS)	DESIGN C (GEARS)	DESIGN D (2nd MOTOR)	DESIGN E (OTHER)
Version 1	Version 1	Version 1	Version 1	Version 1
Version 2	Version 2	Stop Here	Stop Here	Version 2
Stop Here	Version 3			Final
Design				
	Stop Here			

Design E (Version II) will be the final configuration choice for the report

Final design provides effective means of oscillating Auger to raise particles. If the pitfalls in following designs (A through D) could be overcome, these alternative designs could prove useful. Their difficulties are as follows:

Design A (Cams) -

Cam designs incurred complexities regarding controlling and secondary motors. Space constraints and cam alignment posed minor obstacles as well.

Design B (Springs) -

Although simple in design, spring options were exhausted due to poor precision, minimal oscillations, and abrupt motion.

Design C (Gears) -

Gear Configurations posed significant space interference problems. Secondly, the presence of lunar dust on the exposed gears gives rise to a demand for lubrication. A more in-depth study on these items could possibly solve discrepancies and lead to a satisfactory gear device.

Design D (External Motors) -

External Motors incur additional controlling and power requirements. Supplemental maintenance and high operational costs greatly minimize the feasibility of an accelerator requiring this added power.

For a more in-depth analysis of the design alternatives refer to Appendix B9.

Present Design -

The present design omits need for external motors and controlling. This accelerator fits onto the rod changer table. It is activated by the SKITTER raising up and down.

Fig. 4.9.1 - Vertical Accelerator

(General Arrangement)

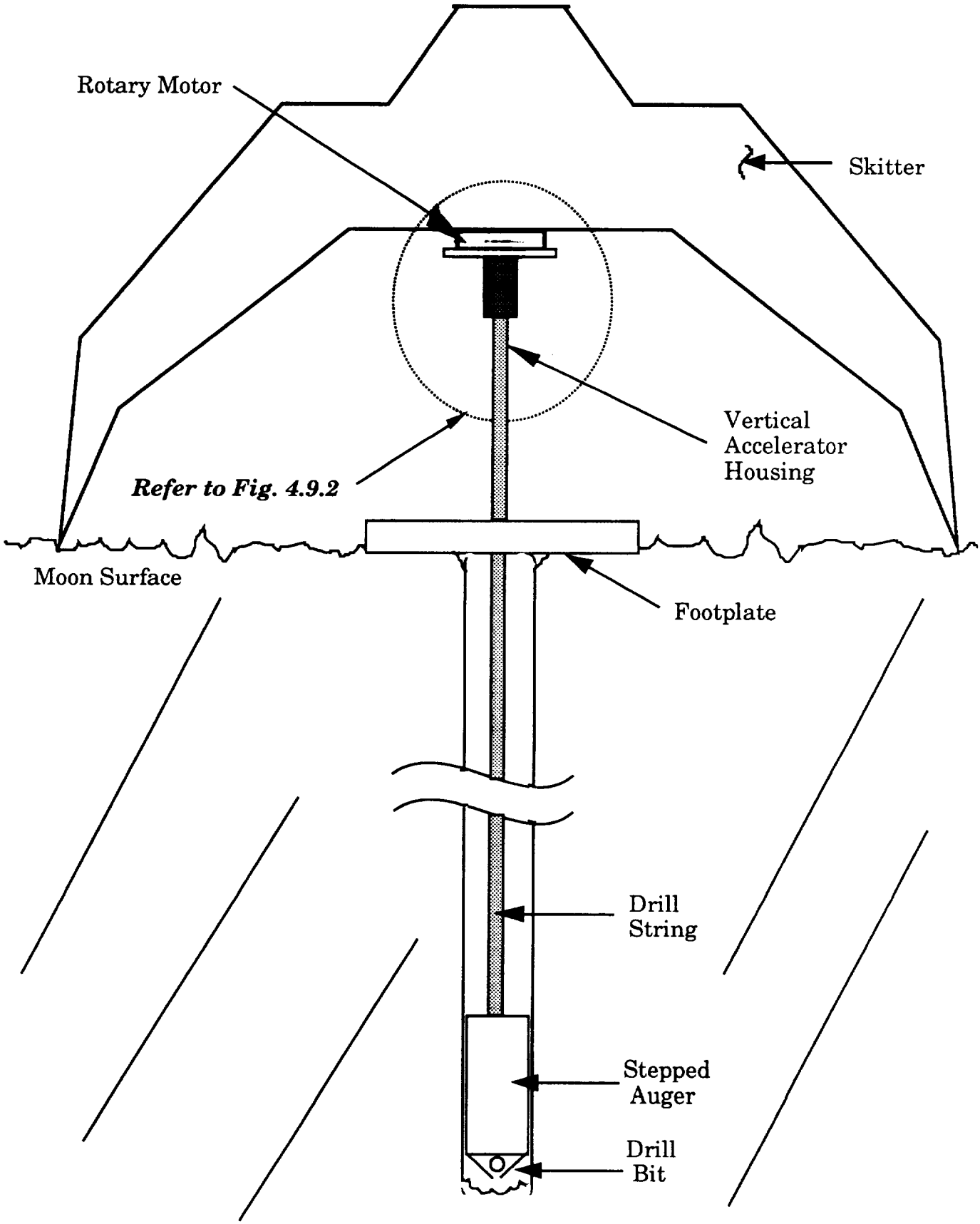

Fig. 4.9.2 - Vertical Accelerator

(Internal View)

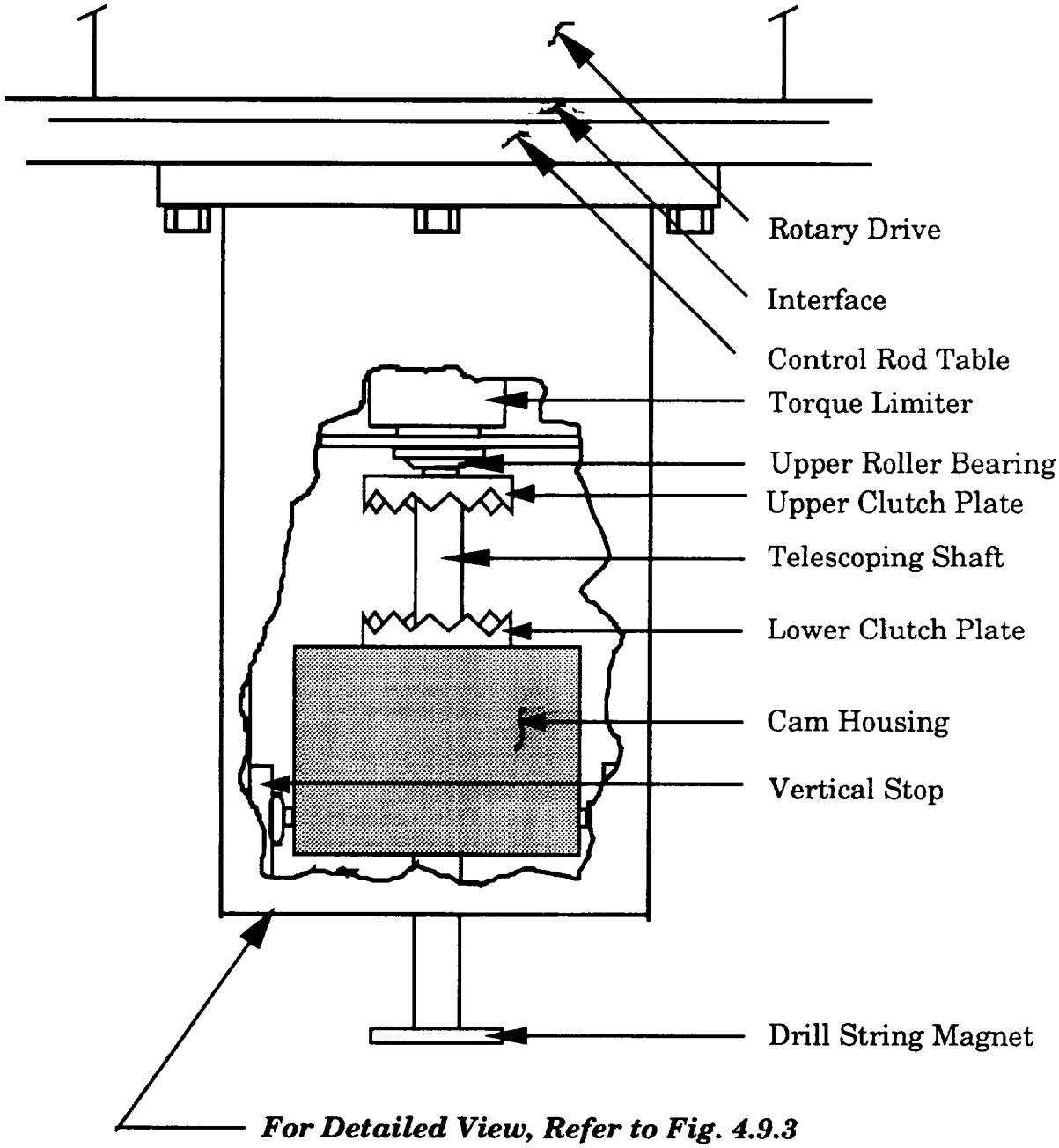

For Detailed View, Refer to Fig. 4.9.3

Fig. 4.9.3 - Vertical Accelerator

(Detailed View)

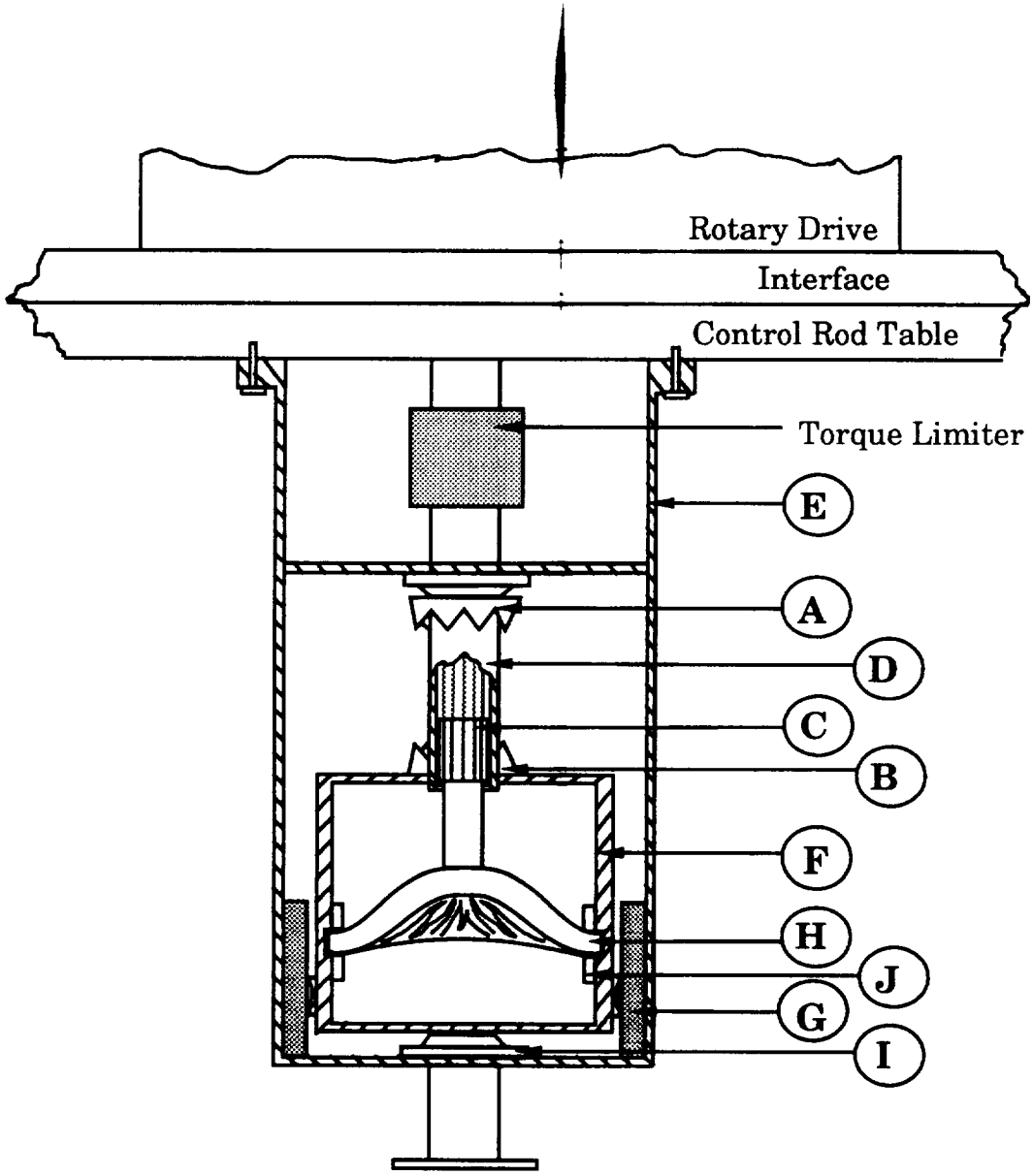

Fig. 4.9.4 - Detailed Specifications

(Clutch and Shaft Details)

A Upper Clutch Plate

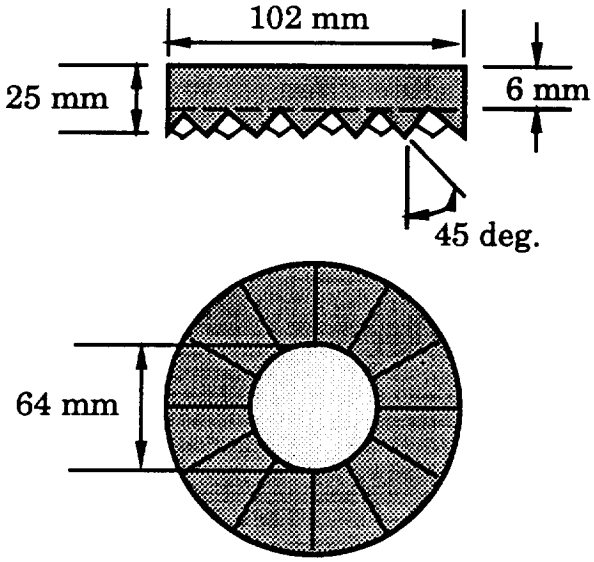

B Lower Clutch Plate

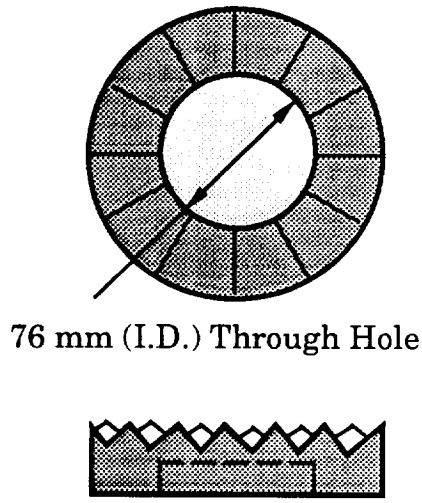

C Inner Shaft

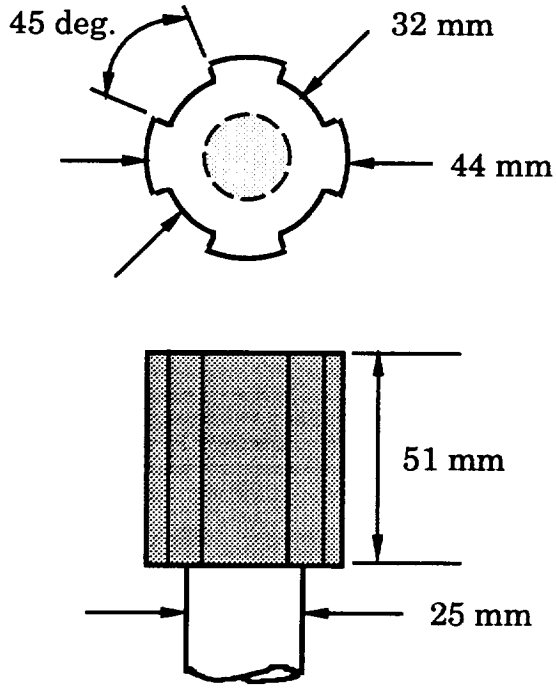

D Outer Shaft

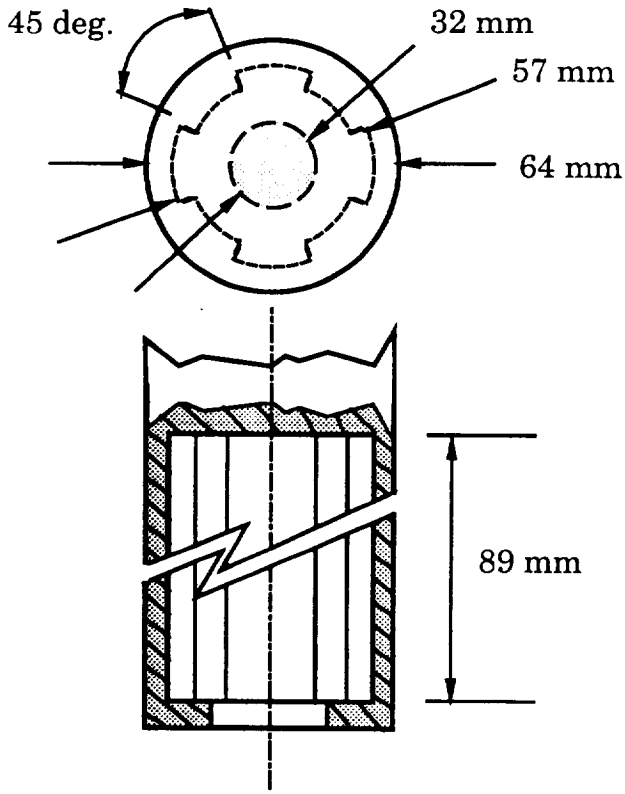

Fig. 4.9.5 - Detailed Specifications

(Housing Details)

(E) Vertical Accelerator Housing

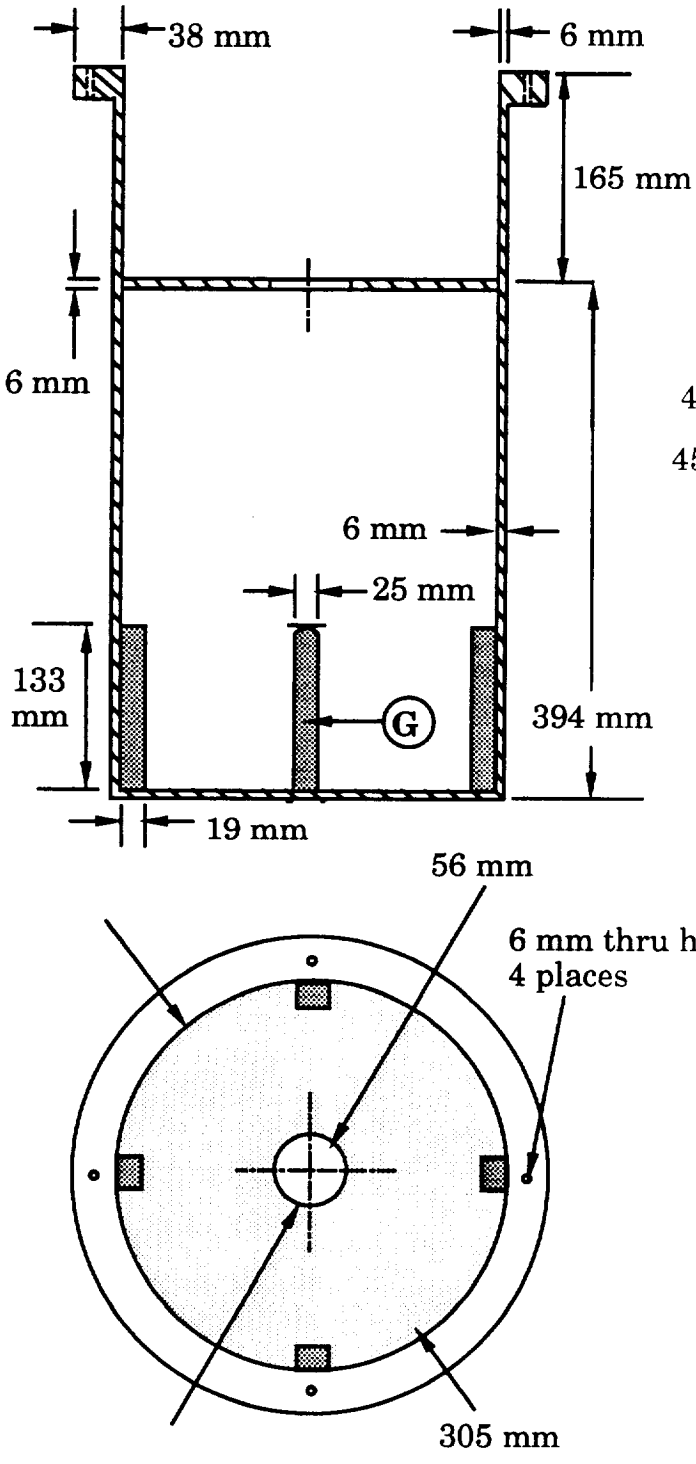

(F) Cam Housing

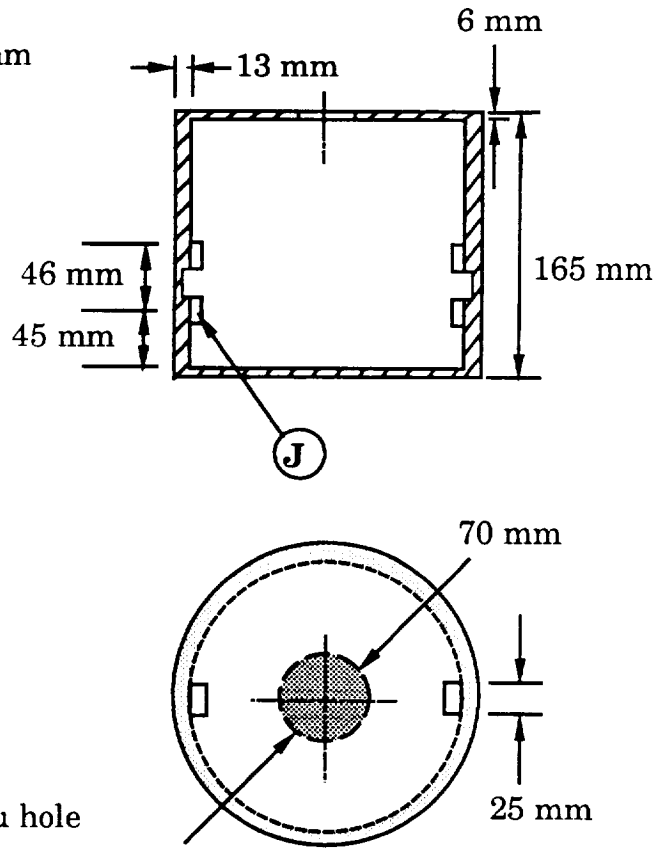

4.10 MICRO-CORING DRILL

4.10.1 Controls Requirements

Once the drill has been lowered to the required depth, an acoustical signal will be sent through the rod. This signal will be generated by a vibration induced in the rod by the impact from an object . This impact must produce a vibration with an amplitude larger than that of the noise that will be associated with the process of connecting and moving the rods. Experimental analysis of the entire project will be necessary to determine the amplitude and frequency of the vibration produced by the motion of the rods and the strength of the impact needed to produce a vibration that will have a greater amplitude than the above mentioned noise. The results of the experiments should take into account the damping of the vibration due to the length of the rods and the interface at which the rods are connected.

The vibration will be sensed by a piezoelectric accelerometer placed on the inner surface of the rod. At this point an impulse will be sent to a motor that controls a camshaft. A set of two cams will be used to rotate the bracing device (see 4.10.3) into position. This 180^{o} rotation will also rotate two more cams that will lower the sliding door used to protect the drill bit and the sample. This camshaft rotation will trigger a limit switch that will initiate the drilling process. The drill will translate 54 mm with a positive inclination of 20^{o} in order to remove the pristine sample. At the end of the translation the sample will displace a plug and the bit will clamp down on the sample. At this time two limit switches will be stuck in order to reverse the translation and stop the rotation, one by the motion of the plug, and the other by the drill bit.

The rotation will not be stopped immediately, but be allowed to continue for about 5 seconds in order to cut a grove into the sample.

cams will be rotated 180°, locking the bracing pads into the lunar basalt surrounding the micro-coring drill rod.

Upon completion of the core retrieval process, the micro-controller will send a signal to the bracing motors to rotate the cams to their original positions, allowing the spring-loaded bracing pads to retract away from the lunar rock surrounding the drill rod.

(3) The Speed of the Rotational Drive Motor - The rotational speed of the drill will be monitored through the use of photodiodes. The photodiodes will send a digital signal which will be analyzed by the micro-controller and converted to an analog signal by a D/A converter. This analog signal will be used to control the duty cycle of the power source of the rotational drive motor to maintain an angular velocity of 400 rpm (300 rpm if the bit becomes too hot) during the coring process.

(4) The Temperature of the Drill Bit - The drill bit temperature will be monitored by the use of thermocouples attached to the bit. If the temperature of the drill bit exceeds 290° K, the rotational speed of the micro-coring drill will be reduced to 100 rpm (to allow the bit to cool) until the temperature of the bit drops below 280° K. If the temperature of the bit exceeds 300 ° K, the rotational motor will be turned off until the bit cools by 25° K. Through these control functions, the core sample obtained will not be contaminated by excessive heat.

4.10.1.2 Microprocessor Selection

The microprocessor-based control system for the micro-coring drill will utilize a *Motorola* HCMOS MC68HC11A8 8-bit micro-controller. The hardware features of this device include:

- 8K Bytes of ROM memory
- 512 Bytes of EEPROM
- 256 Bytes of RAM
- 8 Channel, 8-Bit Analog-to-Digital Converter
- Enhanced 16-Bit Timer System

Assembly language programs to control the processes listed in section 4.10.4 of this report will be written by *Control Dynamics Corporation* in Huntsville, Alabama. This company has vast experience in the field of controls and currently is working on several NASA projects. *Control Dynamics* will interface with *Motorola* for pattern generation of these programs on the chip.

Data from the photodiodes and LED's used to control the rotational speed of the motor will be inputted to the micro-controller through pin A1 (located on serial port A of the device) into a pulse accumulator. By comparing the accumulation of pulses with a known internal clock speed for the micro-controller, the rotational speed of the motor can be determined.

Signals from the thermocouples located in the drill bit and from the piezo-electric accelerometer will be processed by the analog to digital converter for the micro-controller through pins on general input port E. Communications to the device controlling the duty cycle of the power source for the rotational drive motor will take place general I/O port D. A schematic of the microprocessor-based control system for the lunar micro-coring drill is shown in Figure 1.

4.10.1.3 Piezoelectric Accelerometer

The micro-coring operation will begin once a signal is sent through the rods in the form of a vibration. The vibration will be sensed by an accelerometer located near the drill bit, on the inner surface of the rod. In an accelerometer a coil-in-magnet arrangement is used between the mass and the base and this forms an electrodynamic system. At frequencies above the natural frequency of the mass on the spring, the voltage output from the coil is almost directly proportional to the velocity of the base of the transducer.

Piezoelectric accelerometers can measure accelerations in a range of 2×10^{-6} g to 10^{5} g in a frequency range of 0.1Hz to 60kHz. Bruel and Kjaer (UK) Ltd. is the manufacturer that produces the best piezoelectric accelerometers. After experimentation the frequency range of the vibration associated with the micro-coring operation will be determined, and the accelerometer that is best designed for this application may be selected. The sensitivity of commercially available piezoelectric accelerometers ranges from 1.5 mV g^{-1} to 10 V g^{-1} and the weight of the accelerometer from 0.5 g to 500 g.

4.10.1.4 Rotational Speed Control

From previous calculations (see Appendix A.10.1b), the optimal rotational speed for the micro-coring drill was determined to be 400 rpm. Due to the inherent nonhomogenous cross section of the lunar rock (into which the coring will take place), it would be nearly impossible to
power the drill at this velocity by a constant speed motor. Therefore, a feedback control system will be used to maintain the drill speed at a nearly constant value.

The light beam from a light emitting diode (LED) will be passed through a slit cut into the drill bit (near the rotational drive motor).

This light signal will be be collected by a photo-diode which transforms the optical signal to a series of digital pulses. These pulses will then be read into pin A1 of the microprocessor, where it will be fed to the pulse accumulator of the chip. By comparing the rate of pulse accumulation with a known internal clock speed for the micro-controller. By comparing the actual motor speed to the desired motor speed, the microprocessor will adjust the duty cycle of the nickel-cadmium batteries powering the rotational drive motor. Triggering devices and opto-isolators will be needed to interface the micro-controller to the motor and photo-diode, thus completing the motor control circuit.

4.10.1.5 Drill Bit Temperature Control

Since the core sample cannot have a cross-sectional temperature gradient of greater than 50°, it will be critical to closely monitor the surface temperature of the drill bit. To accomplish this purpose, thermocouples from the *Omega Corporation* will be placed in the crown of the drill bit 0.010 inch from the bottom of a face diamond.

Westinghouse Electric Company had success using this type of set-up in simulated lunar drilling tests conducted in 1967. Analog signals from the thermocouples will be fed through operational amplifiers (to increase signal strength) into general input port E of the microprocessor. The thermocouple input is then passed through the micro-controller's A/D converter and is processed by the chip as a digital signal.

The temperature from the thermocouples will be sampled every second. If the average sampling temperature from the thermocouples exceeds 290° C (corresponding to a temperature gradient of 40° C for the core sample), the desired rotational speed for the drill bit will be reduced from 400 rpm to 300 rpm. If the mean temperature of the thermocouples exceeds 300° C (corresponding to a temperature

gradient of 50° C for the core sample), the rotational power to the drill will be cut off for a period of ten seconds. After this ten second delay period, the temperature will be analyzed again. If the temperature gradient of the sample is small enough at that point, drill rotation will be continued.

4.10.1.6 Limit Switches

Limit switches are electromechanical devices which must be in contact with the object sensed and usually have a digital output. There are several possible actuators, such as rods, levers, or cams, and the selection of the actuators depends on the object to be sensed and its direction of approach to the limit switch. Because of the application, limit switches are recommended over the more sensitive but more delicate photoelectric sensors. Limit switches are low cost devices designed for industrial applications and, because of their dependability and resistance to wear, are indicated for the rugged lunar environment. For our application, we will use limit switches from *Micro Switch Company* located in Charlotte, North Carolina.

4.10.2 Drill Protecting Device

The drill rod is divided into different sections. The actual drill is contained in the bottom section of the rod. The core sample obtained from the drilling process must be kept safe from contamination. This is accomplished by raising and lowering a protective cylinder over the drill. When the drill rod is lowered to a specific depth the drilling process will take place. The protective cylinder will be lowered out of the way. When the drilling is completed, and the sample is retrieved into the rod, the cylinder will be raised over the drill. The movement of the cylinder is accomplished by the use of the same camshaft that drives the bracing system. The cylinder is attached to a set of connecting rods which are driven by the camshaft. The protective cylinder needs to be lowered far enough so that the drill bit can be translated outward.

The drill bit is 22 mm. in diameter, therefore the protective casing must be lowered at least 22 mm. if not a few more, in order to provide adequate room for the drill to translate out into the surrounding rock.

* NOTE - The bracing system and protective cylinder will rely on the same control system.

4.10.3 Bracing Mechanism

The micro-coring rod is designed to obtain a rock sample from the lunar surface. The sample will be obtained by the use of a coring drill. It is desired that the drill remain stationary while the drilling operation is taking place. For this to happen the drilling rod must remain relatively fixed. This is accomplished by a bracing system. The bracing system will consist of a motor and camshaft configuration. A set of bracing pads will be extended from the micro-coring rod. These pads will be rectangular in shape and will be bent to conform to the side of the main hole. The pads will be equipped with an abrasive surface. The bracing pads are attached to a set of connecting rods which are manipulated by a camshaft. The camshaft will be rotated by a chain drive or a set of gears. The power will be supplied by a D.C. motor.

4.10.3.1 Cams

The main objective of the camshaft is to provide translational motion to the bracing pad rods. Since the camshaft will only rotate once every drilling mission, the cam does not have to be designed with a high degree of precision, therefore a simple harmonic rise and return motion was chosen to design the cam lobes. A cam mechanism with reciprocating roller follower was chosen for this design. The motion of the bracing pads are described or detailed by a displacement diagram. A displacement diagram relates a known input motion (in this case the rotation angle) to the output motion,y. The diagram is divided into three regions; the rise, where the motion

of the follower is away from the center of the cam, the dwell, where the follower is a rest, and the return, where the motion of the follower is back towards the center of the cam. The displacement diagrams for simple harmonic rise and full-return motion are shown in Figures 2a. and 2b. The equations for simple harmonic motion are:

$$\text{(rise)} \qquad y = \frac{L}{2}\left(1-\cos\frac{pq}{b}\right)$$

$$\text{(return)} \qquad y = \frac{L}{2}\left(1+\cos\frac{pq}{b}\right)$$

The micro-coring drill rod has a diameter of 90 mm. , therefore the pads must be translated radially outward a distance of 5 mm. The cam will rotate 180 degrees, at this point the bracing pads will be fully extended. When the drilling operation is completed the cams will rotate another 180 degrees to return the pads to there original positions. When the rotation has been completed the drilling rod is ready to be raised. The camshaft used for our bracing system was designed to achieve a maximum lift of 5 mm. . When the bracing pads are in there extended position a force , due to the drilling, will be exerted on the cams. To stop the cam from slipping once the pads are in place a dwell was placed in our cam design. Various dwell angles were considered including 30, 45, and 60 degrees (see Figures 3, 4, and 5 for the displacement diagrams). A dwell angle of 45 degrees was chosen after consulting with various individual involved in this field. This means that for a cam rotation of plus or minus 22.5 degrees from the maximum lift angle, the lift will remain 5 mm. . This dwell should keep the cam from slipping due to any forces. The actual cam profile is given in Figure 6.

4.10.3.2 Bearings

The camshafts will be supported by a pair of roller bearings. The life of an individual bearing is defined as the total number of revolutions, or the number of hours at a given speed before failure occurs. Since the camshafts in our rod only rotate once per drilling operation, bearing life should not be a major problem. Therefore, a set of bearings should be picked which are light weight. Due to the lack of an atmosphere the bearings can not be lubricated using traditional means. Instead, a dry lubrication system will have to be employed.

4.10.3.3 Bracing Pads

The drill rod will be kept firmly in place, during the drilling operation, by a set of four bracing pads. The pads will be positioned flush against the drill rod's outer surface. When the drill rod is in the correct position the pads will be extended outward. To insure a stable base for the drilling operation, the pads must be contoured to fit to the surrounding wall. The pads must also have an abrasive surface to make sure that the drilling mechanism does not rotate. If the drill rod rotates the drill bit could be misaligned and the drilling operation would have to be cancelled. Various abrasive surfaces would have to be tested in order to determine the optimum design.

4.10.3.4 Bracing Pad Return Assembly

The bracing pads are connected to the camshaft by the use of connecting rods. The connecting rods or cam followers must remain in contact with the cams at all times. Furthermore, the pads must return to there original position before the drilling rod can be raised. This is accomplished by a retaining spring. The springs will be placed around the connecting rods, see Figure 7 . A spring rate must be chosen to insure that the cam follower remains in contact with the cam. Testing on such a cam system would have to be done before the correct spring rate can be determined.

4.10.3.5 Selection of Materials

The bracing pads will be constructed from high strength steel, this is also the case for the connecting rods. The cam shaft will be machined from a steel similar to the one used for the bracing pads. Since none of the bracing operation entails a high degree of reciprocation, fatigue life should not be a major concern. All mechanisms should be constructed as light as possible due to the high cost of space transportation.

4.10.4 Rotational Movement of Drill Bit

4.10.4.1 Heat Transfer Analysis

Since the core sample is to undergo a series of selenological tests, including carbon dating, it cannot be contaminated with excessive heat. Thus, the amount of power that can be used to rotate the drill bit in the process of obtaining a micro-core sample is limited by the amount of heat generated during the drilling process. The ambient temperature of lunar basalt (into which the micro-coring process will take place) is -23° C and the temperature of the lunar selenological lab will be 27° C. Thus, we chose 50° C, the temperature difference between these two locations to be the maximum allowable temperature gradient across the sample during the micro-coring process.

Through the use of Fourier's conduction law, the maximum allowable temperature gradient for the sample was used to calculate the maximum permissible amount of heat generation for the coring process. This value was set as the upper limit for the rotary power input into the micro-coring drill. Ideally, a two-dimensional, transient heat transfer analysis of the region near the drill bit should be carried out to relate the heat generation from the drilling process to the temperature profile of the core sample. However, by making several reasonable assumptions, we simplified the heat transfer problem to a one-dimensional, steady state problem to meet the

time limitations of this project.

The assumptions and calculations performed to determine the maximum allowable rotational power input for the micro-coring drill are listed in Appendix A.10.1. From these calculations, we determined the maximum permissible input power for the drill (taking into account only thermal contamination) to be .242 HP. Since the one-dimensional heat transfer calculation included several assumptions, we chose a more conservative .12 HP as the maximum allowable input power.

4.10.4.2 Torque Requirements for Rotation of Drill Bit

The torque the bit requires to cut the lunar rock was determined by estimating the dry coefficient of friction between the diamond tipped drill bit and the lunar rock. The coefficient of friction was found from the experimental data of the Westinghouse lunar drill experiment discussed in the 1967 Industrial Diamond Revolution Conference in which basalt was substituted for lunar rock. The speed, thrust force, and power were recorded at various points in the experiment and were used to determine a value of .64 for the dry coefficient of friction at the rock-diamond interface. The experiment was performed using a drill bit larger than the micro-coring bit used in our design, but this size difference should not affect the value obtained in the Westinghouse test.

The thrust force driving the micro-coring drill was set at 50 lbs. The thrust force multiplied by the coefficient of friction gives a resultant force on the bit. A radius of 20 mm was used to calculate the maximum torque on the bit of 12.6 in-lbs. This value of torque is considered to be the maximum value since the the thrust force will usually be less than 50 lbs.

4.10.4.3 Rotational Motor Selection

From material property considerations at the diamond bit-basalt interface, the coring drill will be required to deliver a rotational torque of at least 12.6 in-lbs (see calculations in Appendix A.10.1.2). Taking a factor of safety into account, the rotational drive motor will be designed to deliver a minimum 14 in-lbs of torque over a speed range of 300 to 500 rpm. When inputting its maximum power at 500 rpm, the motor will still generate less than half the limiting horsepower of .242 (to prevent thermal contamination of the sample). To meet these design criteria, we will use an *Electrocraft* E-400 servo-motor which has the following features:

Peak Torque	15 in-lb
Thermal Resistance	4.0/Watt
Length	25.4 mm (1.0 in)
Weight	2 lb 2 oz
Maximum Oper. Temp.	155° C

This motor is a high performance permanent magnet servomotor which combines many of the characteristics of a "torque motor" with those of a low inertia moving coil type. It has excellent voltage regulation and low inherent ripple torque.

4.10.5 Drill Translation Mechanism

The translation mechanism for the micro-coring drill consists of a small motor attached to a rack and pinion drive system. The pinion measures one-fourth inch in diameter, and power necessary for motor is 0.1 Hp.

By using a drilling time of two minutes, a rock drilling rate of 26 mm per minute was obtained. The torque on the motor shaft was found to be 12.6 in-lbs by using a coefficient of friction of 0.64 between the rock and the diamond-tipped bit. In order to traverse the drilling distance in the two minutes, the speed of the pinion and thus the translation motor was found to be 1.3 rpm's. Operation of

small motors at speeds as low as 1 rpm is non-traditional, but can be done. Electrocraft, a manufacturer of these type motors has assured us that these specifications for a motor are feasible.

During the drilling process, the drill bit is guided by a bearing sleeve around the bit. This sleeve is mounted to the side walls of the rod chamber both at top and bottom. The rack used in translating the drill bit is supported by a series of support members. These members are anchored to the main support, a bulkhead mounted horizontally within the rod chamber.

4.10.6 Micro-Coring Drill Bit Design

4.10.6.1 Overall Description

The drill bit design is one that resembles many coring bits used on earth with a few modifications. The micro-coring bit is composed of natural West African Boartz Diamond cutters and a 4140-stainless steel body (see Drawing 4.10.6.1). There will be four longitudinal slits cut in the bit, dividing the face of the bit into four distinct sections. The four sections of the bit will be machined to provide an inward clamping angle of two degrees (see Drawing 4.10.6.3) to aid in breaking the micro-core sample. The longitudinal slits also direct cuttings from the micro-coring process away from the 6 mm diameter sample. Finally, the slits increase the flexibility of the body of the drill bit, allowing a teflon plug to be inserted inside the bit.

The inner diameter will be 10 mm for a majority of the length of the bit (it will have a 6 mm I.D. for the 3 mm of length closest to the diamonds. Located inside this diameter will be a 10 mm wide Teflon plug which will aid in the bit clamping mechanism. The entire bit will be mounted to a shaft which extends from the rotational drive motor.

4.10.6.2 Diamond Selection and Mounting

The diamond type and configuration on the micro-coring bit was determined by using the diamond bit recommendation chart located in a book written by the *Acker Drill Co.* and from the results from the *Westinghouse* simulated lunar drilling experiment. The lunar rock (into which the coring operation will take place) was classified as a medium hard, solid, abrasive material similar to granite or basalt. The recommendations are as follows:

1. Diamond size: 1/50 carat
2. Diamond pattern: Spiral Snow Plow Set
3. Diamond amount: 127 stones

There will be a total of 2.15 carats on the end of the bit. Since cost was not a parameter, the quality of the diamonds will be high commonly known as AAA diamonds. From the Westinghouse experiment, tests results showed that the arrangement referred to above effectively drill a core sample from basalt under high vacuum conditions of $1x10^{-6}$ torr.

4.10.6.3 Bit Clamping Mechanism

The mechanism will operate as normal drill bit. The bit will rotate and form a sample 6 mm in diameter. The significance of the Teflon plug comes in to play at this point. The drill bit will be translate inward and as the bit moves inward the sample moves deeper into the bit, thus pushing the Teflon plug backward. At a point 46 mm from the front of the bit, the I. D. will widen again to 10 mm. The plug will move into this area of greater diameter and release the four sections of the bit. The whole mechanism will be designed to stop rotating at this point and retract. The bit has firm grip on the sample and the retraction will break the sample off in

tension. In order to insure that the sample breaks, the bit will rotate a few addition times after the plug has released the sections and this rotation will cut a groove in the sample which creates a flaw. Also, the bit clamps will be pointed and this will increase the radial force. The increase in radial force has been shown to lessen the force in tension necessary to break the sample. The flaw and the concentrated radial force will insure that there is a clean break and this will provide a sample 46 mm long and 6 mm in diameter. The sample received is larger in diameter than required and this adjustment is necessary for two reasons. First, the outer surface of the sample will be contaminated with fragments from the drill bit so an additional .5 mm was added to account for this contamination. Secondly, the sections of the bit may begin to clamp inward and actually taper the sample so an additional .5 millimeter was added in order to insure that at the smallest end the sample would still be 6 mm in diameter.

4.10.7 Lubrication and Bearings

The bearings used for the rotational and translation motors and the guide bearing will be anti-friction bearings in which the retainer rings are made of a solid composite lubricant consisting of silver-mercury and teflon. This composite was used with great success in the Westinghouse lunar drill experiment. The gear and sliding mechanisms will be coated in a dry lubricant containing molybenum disulfide. Molybenum disulfide is not adversely affected by the vacuum conditions. The trade name for the dry lubricant that would be used is Surf-Kote. It is a molybenum disulfide-resin mixture. The lubricants will lessen the power requirements by reducing the friction loss.

4.10.8 Dust Jacket

The movement of the rods against the main coring hole will cause large amounts of dust and debris to fall downward towards the micro-coring drill bit rod (located at the bottom of the drill string), possibly jamming it. The best way to avoid this problem would be to insert a rubber-like barrier to isolate the bit from a majority of the dust. This barrier will attached to the outside of the micro-coring rod just above the top of the sliding door mechanism used to expose the bit to the lunar rock for drilling. The dust trap will be able to conform itself to the shape of the hole and will have a concave upward orientation as the drill string slides down the 100 mm diameter coring hole. This contour will allow the trap to catch a large amount of the dust falling from the upper regions of the main coring hole while the sliding door mechanism is open and drilling is in progress. The rest of the falling debris will pass around the outside edges of the trap (which is wide enough to protect the drill bit from this dust.)

Once the micro-coring operation is completed, the sliding door mechanism closes (with the drill and micro-core sample inside the micro-coring rod) and the drill string begins to move upwards. As the micro-coring drill rod begins to ascend, the rubber part will take on a concave downwards orientation, releasing the dust. To allow the dust trap to change contour without cracking in the extremely cold lunar environment, a low durometer rubber should be used for this application. However, the material must be hard enough to support the load of the debris falling onto the trap during the micro-coring process.

4.10.9 Failure Scenarios

Since the micro-coring drill is located in the bottom rod of the drill string (at a depth of up to 50 m from the surface of the moon), failure of the micro-coring drill bit must be considered. To prevent the whole micro-coring rod or even the whole drill string from being

lost if the bit becomes embedded into the lunar basalt, we developed methods of overcoming the following failure modes:

(1) Drill Bit Becomes Embedded - Can Be Retracted - If the microprocessor reads the actual drill speed to be 0 rpm for over ten minutes and the temperature gradient of the sample does not exceed 30°, the direction of the translational motor will be reversed in an attempt to pull the drill bit out of the lunar rock. If the bit can be retracted from the micro-coring hole, it will activate a limit switch which will close the micro-coring rod sliding door mechanism, retract the rod's bracing, and signal the surface to raise the drill string. When the micro-coring rod is brought to the lunar surface, the bit will then be inspected and corrections will be made to prevent future failures.

(2) Drill Becomes Imbedded - Cannot be Extracted - In the event that the drill bit cannot be extracted from the lunar rock, our design ensures that only the bit and the sliding door mechanism (as opposed to our whole rod or the whole drill string) is lost. If reversing the direction of the translational motor fails to free the drill bit from the lunar rock, a distress signal will be sent to the HCMOS micro-controller. This will instruct the controller to retract the micro-coring bracing and send Skitter a signal to lower the rod with a force of at least 100 lunar lbs and raise it with a force of at least 200 lunar lbs. The downwards force will break the bit off from the rotational motor at the motor shaft (actually, only 30 lunar lbs. of force are needed to do this), and the upwards force will break off the sliding door mechanism from the rest of the micro-coring rod. The removal of this door will allow the drill string to be raised even if the micro-coring bit remains locked in the lunar basalt (like a cantilever beam).

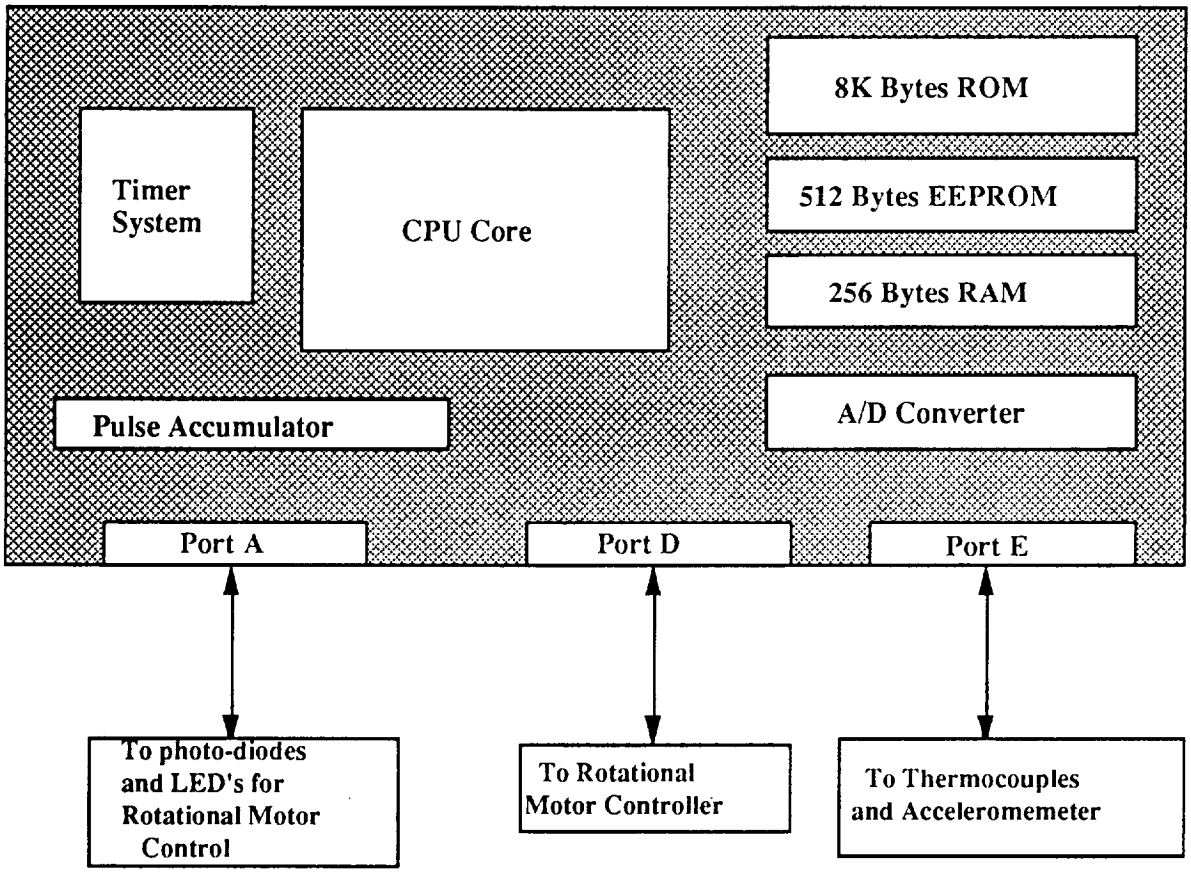
8K Bytes ROM
Timer System
CPU Core
512 Bytes EEPROM
256 Bytes RAM
Pulse Accumulator
A/D Converter
Port A
Port D
Port E
To photo-diodes and LED's for Rotational Motor Control
To Rotational Motor Controller
To Thermocouples and Accelerometer

Figure 4.10.1.

Figures 2a. and 2b.

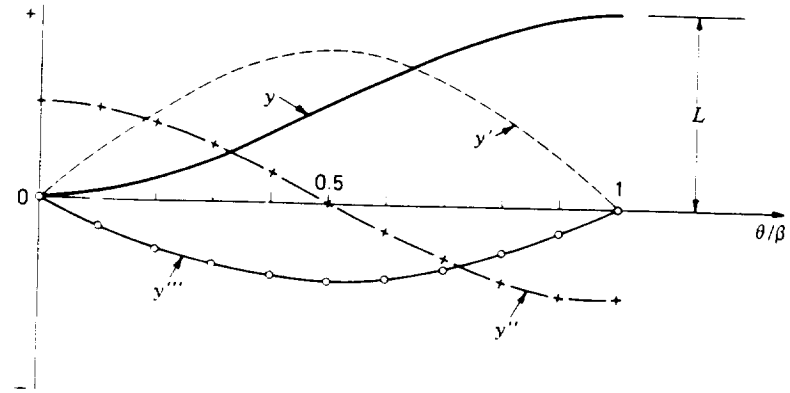

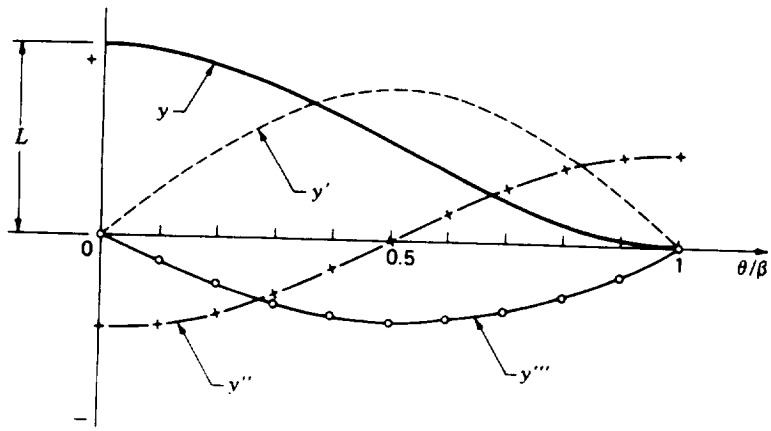

Figures 4.10.2a. and 4.10.2b

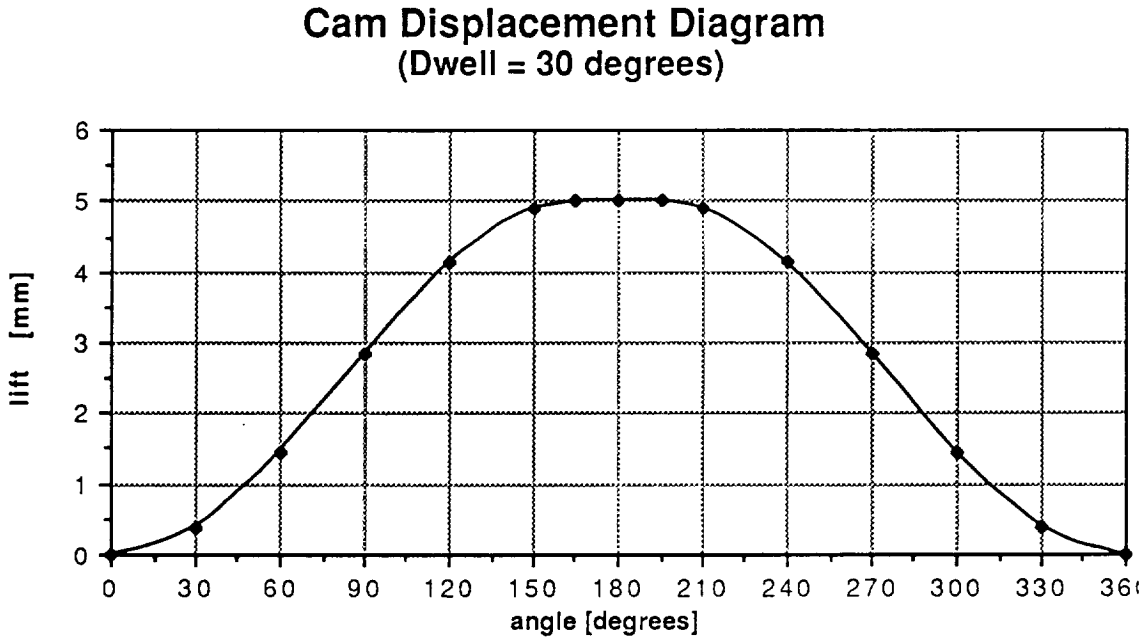

Figure 4.10.3

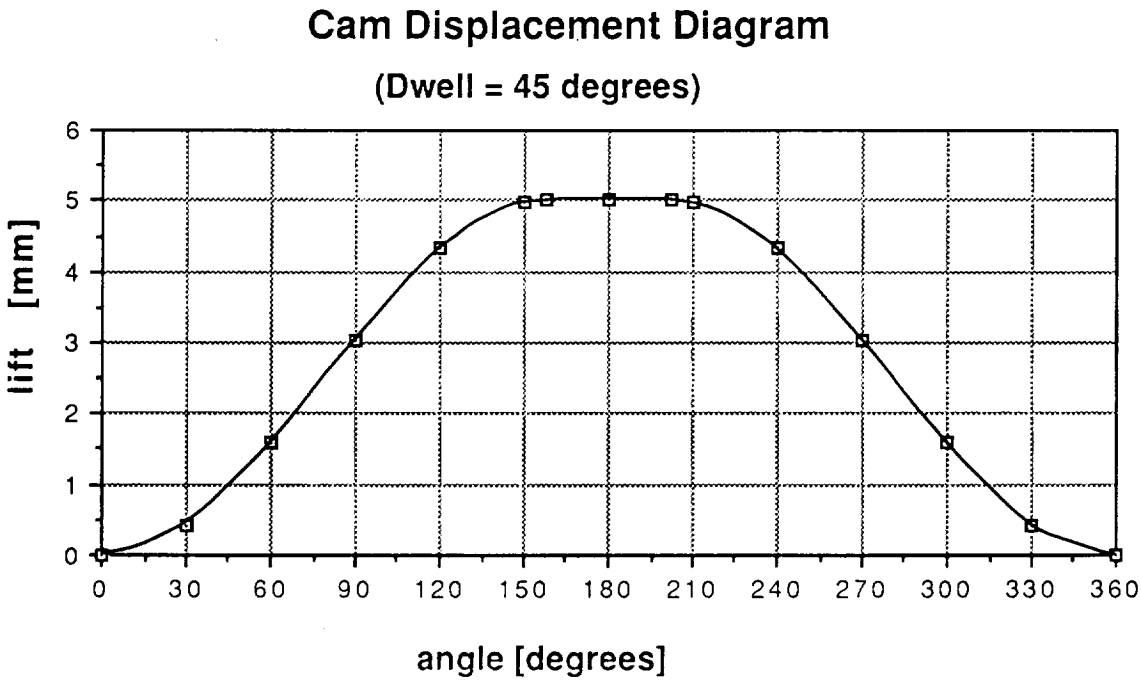
Cam Displacement Diagram
(Dwell = 45 degrees)
lift [mm]
0
1
2
3
4
5
6
0
30
60
90
120
150
180
210
240
270
300
330
360
angle [degrees]
Figure 4

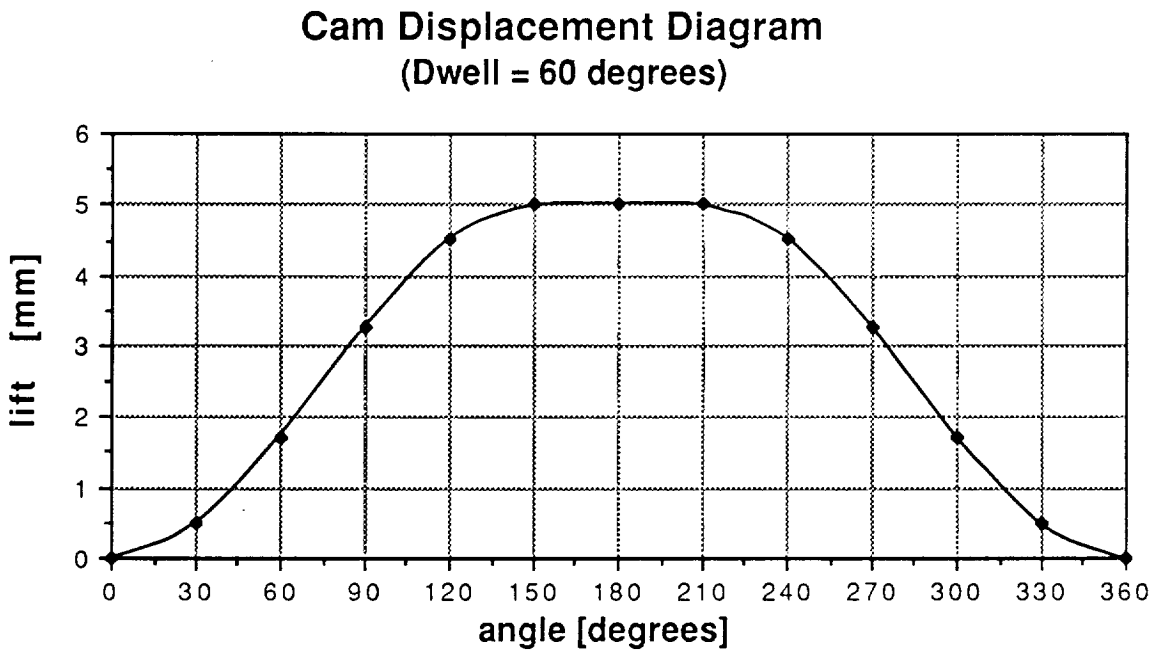
Cam Displacement Diagram
(Dwell = 60 degrees)
lift [mm]
0
1
2
3
4
5
6
0
30
60
90
120
150
180
210
240
270
300
330
360
angle [degrees]

Figure 5

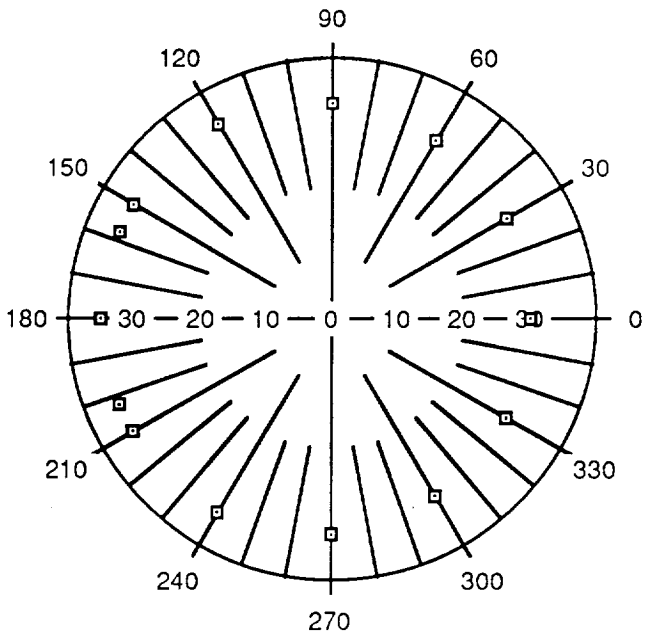
Cam Profile
90
120
60
150
30
180
30
20
10
0
10
20
30
0
210
330
240
300
270
Figure 6

Micro-Coring Drill Rod Chamber

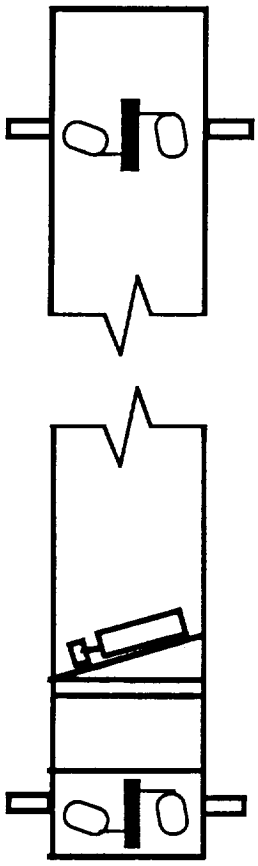

F i g u r e 7

Drilling Operation

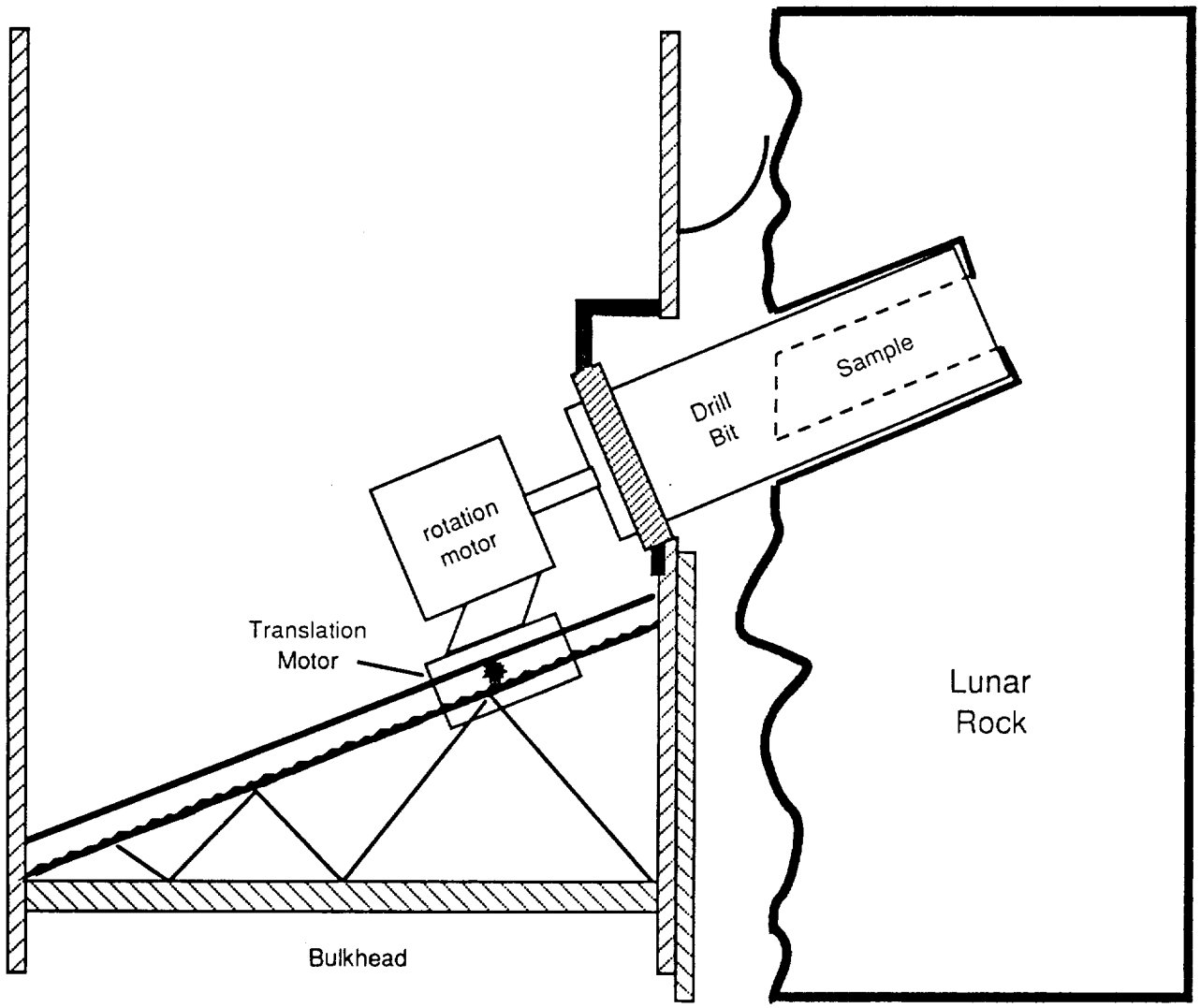

Figure 4.10.8

Drill Bit Translation Mechanism

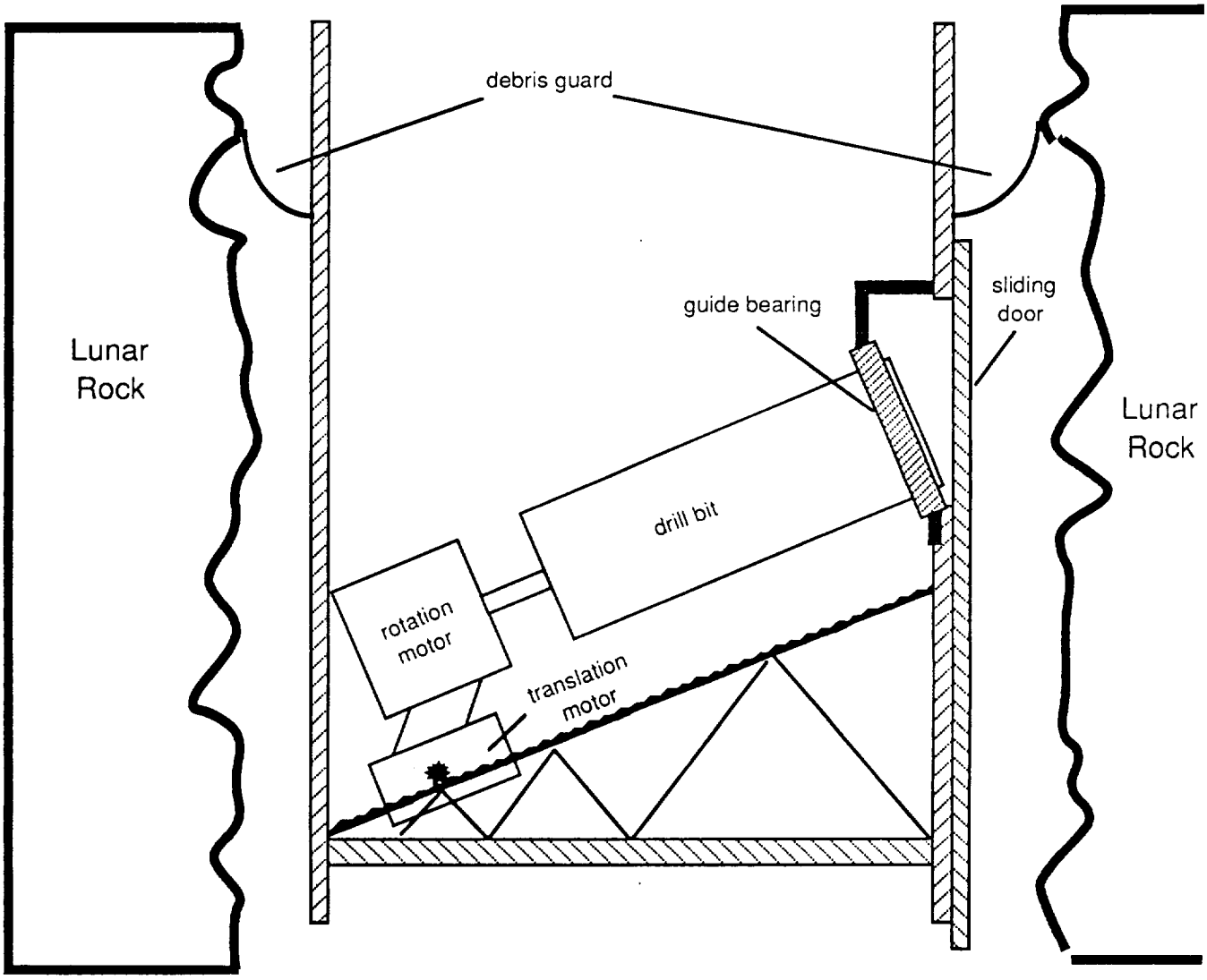

Figure 4.10.9

5.0 CONCLUSIONS

The entire drilling system was designed with three objectives; minimize weight, minimize moving parts, maximize reliability. The cost of transporting the implement to the lunar surface is directly related to weight. Therefore, when possible, light weight materials were chosen for all design elements. The control sequence from the earth incorporates an approximate 3 second time delay. To minimize control problems from complex design, the minimum number of moving parts was chosen. Also, maintenance on the lunar surface will be very difficult therefore minimizing the moving parts will help to increase the reliability of the machine.

The overall Deep Drill Design uses the SKITTER mobile platform to transport and help actuate the drilling process. The drill consists of a 100 mm coring bit, augers, rods, a footplate, rod changer, storage racks, a support structure, a macro-core retrieval tool, and a micro-coring apparatus. The control sequence described provides the automation and control necessary to produce 25 , 2 m core samples.

This design is an initial attempt to produce a mining or construction machine capable of drilling to such depths. The design indicates that a better material transport system from the bit to the top of the hole is needed. This would minimize the heat at the bit and allow for longer drilling periods. Also, the bit life would be greatly enhanced. The rods, which connect the bit to the rotary drive and transmit the power, are tubular with a simple connector which is easily handled by the rod changer. While this design is a good concept, initial interfacing suggests that a better design for the connection collar is needed. The auger and stepped augers are now being used primarily as a means to store the cuttings away from the bit. The auger interface is very similar to the rod interface. However, it causes a significant reduction in throughput. Therefore, a closer look at the interface is indicated. The driver for the stepped auger is a

cam which is located in one of the rods of the string. The cam changes the rotary motion of the motor shaft into an upward acceleration. The foot plate provides a very good working base for the lunar drill. The fins on the base of the footplate aid in the support of the hole along with the attached casing. The spring driven rod holders allow the rod changer ample time and space to add and remove rods to the drill string as needed. Storage racks are located between the legs of the SKITTER and hold all the drill implements necessary to complete one 50 meter hole. The power system is fueled by a hydrogen-oxygen fuel cell located in the supporting structure of the drill. The actual rotary drive for the drill is a curvo-synchronus linear motor. This motor has an efficiency rating around 95%. The fuel cells also power several other small motors on the implement. After the desired depth has been achieved, the micro-core retrieval unit is inserted to retrieve smaller core samples from the walls of the hole. The unit is housed inside a rod and controlled with a microprocessor.

The Lunar Deep Drill Apparatus design needs more work in the area of interfacing between the different systems. In the next section, numerous recommendations are made to improve upon the overall design.

6.0 RECOMMENDATIONS

The following is a list of suggestions to improve the functioning of the entire design. Specific recommendations are given for each section of the report. Overall improvements and observations follow the section recommendations.

6.1 Bit cutting loading into stepped auger

* A cooling system could be designed to transfer heat from the bit. This heat reduction would allow for a greater RPM to be used during drilling.

* Wear testing of the bit portion of the drill should be performed to determine and optimize cutter life, rake angle, and bit orientation.

6.2 Rods, Auger, and stepped auger

* Throughput and volume retention testing must be performed to evaluate the auger's capabilities. Pitch variations should be used to optimize the design.

* Fracture testing of the device should be performed under extreme lunar conditions.

* The AED should be redesigned to be compatible with the rod changer. Presently, the AED will not work as designed.

* The rod to motor magnetic connection should be redesigned. The design is not functional.

6.3 Footplate

* The design appears to be fully functional. A mechanical model should be built to analyze the footplate performance.

* Strength calculations and testing should be performed on the footplate.

* The storage procedure for the footplate should be re-evaluated.

6.4 Power source, rotary drive, and Heat Management

* The power of the motor has to be increased. The current power rating does not take into account non-ideal drilling conditions such as drilling uneven surfaces. Also, the effect of power dissipation due to friction from the drill string and lunar core has not yet been considered.

* Fuel cell testing should be performed to evaluate performance, especially at sub-zero temperatures. Possible freezing of the water could present a problem. Modifications will have to be made if freezing occurs.

* A refueling interface and a conversion location for the fuel waste must be designed.

6.5 Structure and Mechanical Interface with walker

* A new structural design should be considered. The construction of the present design does not appear to be possible due to the fastening method which is used.

6.6 Rod Changer and Storage racks

* The disk which provides the rotational movement of the arm does not provide a method to stop the rotation with any degree of accuracy. A device to accomplish this task must be designed.

* The model of the rod changer should be built, and a stress analysis should be performed at extreme operating temperature and conditions.

* The storage racks should be tested in conjunction with the rods, drill, auger, and core retrieval devices to determine the functionability. Also, the crushing capabilities that the racks supply should be tested.

6.7 Macro-core Retrieval tools and Storage

* Extensive testing must be performed to optimize the shape and size of the cutter. Performance should be rated on size, life, and overall cutting ability.

* The cutter should be placed on the centerline with the spring to prevent binding.

6.8 Controls for Operation and Console

* Components such as actuators need to be specified and designed where needed in the project.

* The procedures for the following possible failures must be addressed:
  - Bit jamming during drilling

- Rod drops
- Bit breaks
- Rod breaks
- Drill string falls into the drill hole
- Actuator fails
- Power fluctuations

6.9 Vertical Accelerator for stepped auger

* The accelerator model should be built and tested under lunar conditions (1/6th gravity). The design appears to be functional.

* A method to keep the dirt from entering the device as the rod moves up and down should be investigated.

* A bearing study for the cam should be performed.

6.10 Micro-coring Drill

* A heat transfer analysis should be performed on the bit.

* Detailed control and actuation for the micro-core needs to be developed.

* An optimum drilling angle should be experimentally determined.

6.11 Overall Recommendations

* The interaction (interconnection) among the different components of the lunar drilling device should be studied.

Once component modifications have been made, a model should be built to study this interaction.

* A detached study of materials for each component should be performed. Optimization of materials should include strength-to-weight ratios, overall strength, reliability, and life. Studies should consider the extreme temperature conditions.

7.0. References

7.1. Acknowledgements

We would like to thank the following individuals for there help and support in the completion of this project;

Mr. Bob Delauder of Brainerd-Killman, Inc.
Mr. Parks C. Stewart of Factory Automation Controls, Inc.
Mr. Anthony M. Aretakis of Whittaker-Yardney Power Systems
Mr. Gustav M. Geil of Micro Mo Electronics, Inc.
Mr. Dave Ross, VA Hospital Research
Dr. Kent Davey, EE Dept., Georgia Tech
Dr. Gene Colwell, ME Dept., Georgia Tech
Dr. Moussad Tavakoli, ME Dept., Georgia Tech
Mr. Dan Gibson, Good Tools
Dr. Robert Bachus, CE Dept., Georgia Tech
Dr. James S. Lai, CE Dept., Georgia Tech
Mr. Joe Chudecki of the Cerbec Corp.
Mr. Jim Kenedy of the Torrington Corp.
Dr. Johnson, ME Dept., Georgia Tech
Dr. Ferri, ME Dept., Georgia Tech
Dr. Black, ME Dept., Georgia Tech
Dr. Desai, ME Dept., Georgia Tech
Mr. Jaime Edwards
Dr. Mike Kelly of GTRI, Atlanta, Ga.
Mrs. Shannon Wolfe
Ack Electronics of Atlanta, Ga.
Franz Blam Racing of Atlanta, Ga.
Ms. Jill Harvey
and, of course, Mr. J.W. Brazell

7.2. Bibliography

7.2.1. Bit Cutting Loading Into Stepped Augur

Bensko, J.; Lindelof, L.; Paone, J.; and Woo, G. "A Lunar Drill Concept." Industrial Diamond Conference, 1967.

Hampe, W. R.; Simon, A. B.; Decker, W. E.; and Lundy, J. T. "The Moderate Depth Lunar Drill Programme - dry diamond drilling success: Part 1." Industrial Diamond Review April 1971: 132 - 140.

Maurer, William C. Advance Drilling Techniques, 1st ed. Oklahoma: The Petroleum Publishing Company, 1980.

Miner, Douglas F. and Seastone, John B. Handbook of Engineering Materials, 1st ed. New York: John Wiley & Sons, Inc., 1955.

Properties and Selection of Tool Materials. American Society for Metals, 1975.

Salisbury, John W. and Glaser, Peter E. The Lunar Surface Layer. London: Academic Press, Inc., Ltd., 1964.

Smith, Norman R. User's Guide to Industrial Diamonds, 1st ed. London: Hutchison Benham, Ltd., 1974.

7.2.2. Rods, Auger, and Stepped Augur

Budinski, K. G. Engineering Materials: Properties and Selection. Englewood Cliffs, New Jersey: Prentice-Hall, 1989.

Dieter, G. E. Engineering Design: A Materials and Processing Approach. New York: McGraw-Hill, 1983.

"Effects of Low Temperatures on Structural Materials." NASA SP-5012

December 1964.

Popov, E. P. Introduction to Mechanics of Solids. Englewood Cliffs, New Jersey: Prentice-Hall, 1968.

Shackelford, J. F. Introduction to Materials Science. New York: Macmillan Publishing Company, 1985.

Shigley, J. E. and Mitchell, L. D., Mechanical Engineering Design. 4th ed. New York: McGraw-Hill, 1983.

7.2.3. Lunar Footplate

Ashby, Michael and Jones, David R. Engineering Materials I & II. New York: Pergammon Press, 1980.

Crane, F. A. A. and Charles, J. A. Selection and Use of Engineering Materials. Boston, Massachusetts: Butterworth & Co., Ltd., 1984.

Dieter, George. Engineering Design. New York: McGraw-Hill Book Company, Inc., 1983.

Hall, Allen S., Jr.; Holowenko, Alfred R.; and Laughlin, Herman G. "Machine Design", Schaum's Outline Series. New York: McGraw-Hill Book Company, Inc.,1961.

Johnson, Stewart W. and Wetzel, John P., eds. Engineering, Construction, and Operations in Space. Proccedings of "Space '88". New York: American Society of Civil Engineers, 1988.

Marshek, Kurt M. Design of Machine and Structural Parts. New York: John Wiley & Sons, 1987.

Materials Processing in Space. Akron, Ohio: The American Ceramic Society, 1983.

Shigley, J. E. and Mitchell, L. D. Mechanical Engineering Design. New York: McGraw-Hill Book Company, Inc., 1983.

Taylor, Stuart Ross. Planetary Science: A Lunar Perspective. Houston, Texas: Lunar and Planetary Institute, 1982.

Whipple, Fred L. Earth, Moon, and Planets. Philadelphia, Pennsylvania: The Blakeston Co., 1941.

7.2.4.Power Source, Rotary Drive, and Temperature Management

ASM Metals Reference Book, 2nd ed. Metals Park, Ohio: American Society for Metals, 1983.

Avallome and Baumeister. Mark's Standard Handbook for Mechanical Engineers, 9th ed. New York: McGraw-Hill Book Company, Inc., 1983.

Chi, S. W. Heat Pipe Theory and Practice: A Sourcebook. Hemisphere Publishing Co., 1976.

Incropera, F. P. and Dewitt, D. P. Fundamentals of Heat and Mass Transfer, 2nd ed. New York: John Wiley & Sons, 1985.

Shigley, J. E. and Mitchell, L. D. Mechanical Engineering Design. New York: McGraw-Hill Book Company, Inc., 1983.

"Space Power Systems." Progress in Astronautics and Rocketry, Vol. 4. New York: Academic Press, 1961.

"Thermal Characteristics of the Moon." Progress in Astronautics and Rocketry, Vol. 28. Boston, Massachusetts: Alpine Press, 1972.

7.2.5. Structure and Mechanical Interface with Walker

Broadwell, R. G. and Hickey, C. F. "Toughness and Fracture Behavior of Titanium: a Symposium Presented at May Committee Week, American Society for Testing and Materials, Toronto, Canada, 1-6 May 1977." Philadelphia, Pennsylvania: The American Society for Testing and Materials, 1978.

Chawla, Krishan K. "Composite Materials." Science and Engineering. New York: Springer-Verlag, 1987.

Coyne, Edward James. "The Effect of Microstructure on the Fatigue Behavior of an Aluminum Alloy", Thesis. Atlanta, Georgia: Georgia Institute of Technology, 1979.

Hatch, John E. Aluminum, Properties and Physical Metallurgy. Metals Park, Ohio: American Society for Metals, 1984.

Heaney, John E. "Advanced Aerospace Materials." Aviation Week & Space Technology 12 October 1987: 69-106.

Heaney, John E. "Aerospace Materials." Aviation Week & Space Technology 3 October 1988: 45-74.

Donachie, Matthew J. Titanium, A Technical Guide. Metals Park, Ohio: ASM International, 1988.

Dervenis, Constantine P. "Microstructure, Deformation, and Corrosion-Fatigue Properties of Aluminum-Lithium Alloy." Thesis presented to Georgia Institute of Technology, 1986.

Hughes, David. "Textron Unit Makes Reinforced Titanium, Aluminum Parts." Aviation Week & Space Technology 28 November 1988: 91.

Irving, Robert. "Composites, Aluminum are Leading Space Station Materials Candidates." Metalworking News 7 December 1987: 4.

Irving, Robert. "Space Metals on the Horizon." American Metal Market 21 March 1988: 20.

Lee, Lieng-Huang. Adhesives, Sealants, and Coatings for Space and Harsh Environments. New York: Plenum Press, 1988.

Parkinson, Gerald. "Big Potential for RTM in Space." Chemical Week 16 March 1988: 20.

"Recent DSP Satellite Version Uses Graphite Epoxy Struts." Aviation Week & Space Technology 2 March 1987: 57.

Sanders, T. H. Aluminum-Lithium Alloys II. Warrendale, Pennsylvania: Metallurgical Society of AIME, 1984.

"Silicone Paint Identifies Space Shuttle Tiles." Modern Paint and Coatings February 1986: 44-45.

"Space-age Coatings Come Down to Earth." Design News 20 April 1987: 69-72.

"Space Polymer Identified." Design News 23 November 1987: 81.

Varma, Shailendra Krishna. "A Study of the Influence of Large Wire Drawing Plastic Strains on Dislocation Substructures and Mechanical Properties of Aluminum and its Dilute Alloys", Thesis. Atlanta, Georgia: Georgia Institute of Technology, 1977.

7.2.6. Rod Changers and Storage Racks

Ashby, Michael R. and Jones, David R. H. Engineering Materials 2 - An Introduction to Microstructures, Processing, and Design. New York: Pergamen Press, 1986.

Budinski, Kenneth G. Engineering Materials - Properties and Selection, 3rd ed. New Jersey: Prentice Hall, 1989.

Clauss, Francis J., ed. Surface Effects on Spacecraft Materials. New York: John Wiley & Sons, 1960.

Duffy, Joseph. Analysis for Mechanisms and Robot Manipulators. New York: John Wiley & Sons, 1980.

The Effects of Space Environment on Materials, Vol. II. SAMPE. Hollywood, California: Western Periodicals Co., 1967.

Gatland, K. W. and Thompson, G. V. E. Materials in Space Technology. London: Chapel River Press, 1963.

Griffel, William. Handbook of Formulas for Stress and Strain. New York: F. Ungar Publishing Company, 1966.

James, R. D. Using Robots to Assist Human Explorers on the Moon and Mars, IPRC 1985 Conference Proceedings. Phillips Petroleum Company, 1986.

Kalpakjian, Serepe. Manufactureing Processes for Engineering Materials. Massachusetts: Addison-Wesley, 1984.

Kato, Ichiro and Sadamoto, Kuni. Mechanical Hands Illustrated. Washington, D. C.: Hemisphere Publishing Company, 1987.

Kennedy, A. J. Materials Background to Space Technology. London: Newres International Monographs, 1964.

L'Hote, Francois; Kauffman, Jean-Marie; Andre, Pierre; and Talliard, Jean-Pierre. Robot Technology, Vol.4: Robot Components and Systems. London: Kogan Page, 1983.

Paker, Earl R., ed. Materials for Missiles and Spacecraft. New York: McGraw-Hill Book Company, Inc., 1963.

Pham, D. T., and Heginbotham, W. B., eds. Robot Grippers. Berlin: IFS Ltd., 1986.

Pugh, A., ed. Robotic Technology. London: Peter Peregrinus Ltd., 1983.

Rathmill, K.; MacConaill, P.; O'Leary, S.; and Browne, J., eds. Robot Technology and Applications. Berlin: IFS Ltd., 1985.

Roark, R. J. and Young, Warren C. Formulas for Stress and Strain, 5th ed. McGraw-Hill Book Company, Inc., 1966.

Sangveraphunsiri, Viboon and Dickerson, Stephen L. D. C. Moving Coil Motors for Robotic Applications. Atlanta, Georgia: MHRC Propriety, Materials Handling Research Center, Georgia Institute of Technology, 1983.

Shigley, Joseph E. and Mitchell, Larry D. Mechanical Engineering Design, 4th ed. New York: McGraw-Hill Book Company, Inc., 1983.

Staugaitis, Charles L., ed. Spacecraft Materials Guide. National Technical Information Service, 1975.

Zeldman, Maurice I. What Every Engineer Should Know About Robots. New York: Marcel Dekker, Inc., 1984.

7.2.7. Macro-core Retrieval Tools and Storage

Associated Spring Corporation. Mechanical Springs: Their Engineering and Design. Bristol, Connecticut: Wallace Barnes Co., 1944.

Bickel, John O. and Kwessel, T. R. Tunnel Engineering Handbook. New York: Van Nostrand Reinhold Company, 1982.

Brady, B. H. G. and Brown, E. T. Rock Mechanics for Underground Mining. London: George Allen and Unwin, Ltd., 1985.

Carlson, Harold. Spring Manufacturing Handbook. New York: Marcel Dekker, Inc., 1982.

Collie, M. J. Industrial Abrasive Materials and Compositions. Park Ridge, New Jersey: Noyes Data Corporation, 1981.

Franklin, John A. and Dusseault, Maurince B. Rock Engineering. New York: McGraw-Hill Publishing Company, 1989.

Gibbons, Robert C., ed. Woldman's Engineering Alloys. Metals Park Ohio: American Society for Metals, 1979.

Hellwege, K. H. ed. Numerical Data and Functional Relationships in Science and Technology, New Series, Vol. 1b. "Physical Properties of Rocks." Berlin-Heidelberg: Landolt-Bornstein, 1982.

Hellwege, K. H. ed. Numerical Data and Functional Relationships in Science and Technology, New Series, Vol. 2a. "Geophysics: Solid Earth-Moon-Planets." Berlin-Heidelberg: Landolt-Bornstein, 1982.

Metals Handbook - Properties and Selection of Metals, 8th ed. Metals Park, Ohio: American Society of Metals, 1979.

Metals Handbook - Properties and Selection: Stainless Steels, Tool Materials and Special Purpose Metals, Vol. 3, 9th ed. Metals Park, Ohio: American Society of Metals, 1980.

Olsen, L. Howard. Status Report on NSG-2356: Development of Molded, Coated Fabric Joints; Fabric Construction Criteria for a Spacesuit Elbow Joint. Atlanta, Georgia: Georgia Institute of Technology, School of Textile Engineering, August 1981.

Popov, Egor P. Introduction to Mechanics of Solids. Englewood Cliffs, New Jersey: Prentice-Hall, Inc., 1968.

Reynolds, Henry R. Rock Mechanics. New York: Unger Publishing Co., 1961.

Roberts, A. Geotechnology. New York: Pergamon Press, 1977.

Shigley, Joseph Edward and Mischke, Charles R. Mechanical Engineering Design, 5th ed. New York: McGraw-Hill Book Company, Inc., 1989.

Wahl, A. M. Mechanical Springs. McGraw- Hill Book Company, Inc.,1963.

Wiley, John & Sons. Rock Mechanics in Engineering Practice. London: K. G. Stagg and O. C. Zienkiewicz, 1968.

7.2.8. Controls for Operation and Console

NASA Standard 3000, 1988.

7.2.9. Vertical Accelerator for Stepped Augur

Mutch, Thomas A. Geology of the Moon: A Stratigraphic View. Princeton, New Jersey: McGraw-Hill Book Company, Inc., 1970.

Shigley, Joseph Edward and Mischke, Charles R. Mechanical Engineering Design, 5th ed. New York: McGraw-Hill Book Company, Inc., 1989.

Shigley, Joseph Edward and Uicker, Charles. Mechanical Design of Mechinisms. New York: McGraw-Hill Book Company, Inc., 1983.

7.2.10. Micro-coring Drill

Acker, W.L., Basic Procedures for Soil Sampling and Core Drilling, Acker Drill Co. Inc.,Scranton, Pa ,1974.

Anderson, Gene, Coring and Core Analysis Handbook, Petroleum Publishing Co., Tulsa, OK., 1975.

Grodzinski, Paul, Diamond Tools, Anton Smith & Co., New York, 1944.

Incropera, Frank P., DeWitt, David P., Fundamentals of Heat and Mass Transfer, Second Edition, John Wiley and Sons, Inc., New York, 1985.

McGregor, K., The Drilling of Rock, CR Books Ltd., London, 1967.

Shigley, Joseph Edward, Mitchell, Larry D., Mechanical Engineering Design, Fourth Edition, McGraw-Hill Book Co., 1988.

Shigley, Joseph Edward, Uicker, John Joseph, Jr., Theory of Machines and Mechanisms, McGraw-Hill Book Co., New York, 1980.

Shigley, Joseph Edward, Mischke, Charles R., Standard Handbook of Machine Design, McGraw-Hill Book Co., New York, 1986

Smith, Norman R., Industrial Applications of the Diamond, Hutchinson & Co., London, 1965.

Wilcox, Donald F., Boeser, Richard E., Bearing Design and Application, McGraw-Hill Book Co., New York, 1957.

DC Motors, Speed Controls, and Servo Systems, ElectroCraft Corporation, Hopkins, MN., 1975.

Motorola Semiconductor Technical Data, Advance Information HCMOS Single-Chip Microcontroller MC68HC11A8, Motorola Inc., 1988.

C 4

Proceedings of The Industrial Diamond Revolution, Advanced Technology Committee of the Industrial Diamond Association of America, Inc., 1967.

Proceedings of The Industrial Diamond Conference, Science and Technology of Industrial Diamonds, Oxford, England, Edited by John Burls, 1967.

Smorodinov, M.I., Lunar Rock and Soil Sampling, Drilling, and Testing for Physical Properties, NASA Document 72N12827, ppg. 406-413.

Crouch, D.S., Lunar Rock Coring Device Design Study - Final Report, NASA Document 66N15364.

Hickson, P.J., Modifications to the Apollo Lunar Surface Drill, NASA Document 78N79023.

7.3. Software

Autocad 9.02
Word Perfect, 1.0
Word Perfect, 5.0
Catia CAD software
Cadam CAD software
Versacad CAD software
McDraw II, Claris
Harvard Graphics 1.01
Cricket Draw
Microsoft Word, 3.01

APPENDIX A

SAMPLE CALCULATIONS

A.1 BIT

Power Requirements:

Definitions:

F = Downward force on bit
F_d = Drag force placed on tooth
μ = Drag coefficient
r = Radial position

Formulas:

$T = \Sigma F_d r_i$
$P = T\omega$
HP = (Tn)/63000

Calculations:

F = 250/54 = 4.629 lbs.
$F_d = \mu F = (1.0)(4.629) = 4.629$ lbs. = 20.6 N
T = 20.6(6)[0.025 + 0.03125 + 0.0375 + 0.04375 + 0.05 + 0.0281 + 0.0344 + 0.041 + 0.047]
= 20.6 N (6 starts)(0.3375)
= 41.7 N-m or 368.98 lbf - in

Power = $T\omega$ ω = 300 rpm = 31.14 $^{rad}/_{sec}$
= 1.37 kw

Horsepower = (Tn)/63000
= 1.757 Hp

Load = 375 lbs = 1668.075 N
(4 starts) = 11.25 lbs per tooth
T = 67.544 N-m = 597.81 lbf-in
Power = 2.2 Kw Hp = 2.85 Hp

Load = 500 lbs = 2224.1 N
(4 starts) = 15 lbs per tooth
T = 90.058 N-m = 797.085 lbf-in
Power = 2.8 Kw Hp = 3.8 Hp

Power Requirements due to friction against side of the hole:

bit diameter = 100 mm
hole diameter = 104 mm
clearance = 2 mm (all around)
downward force = 250 lbs
RPM = 300
Length of rod = 2 m

A. Bit leaning against wall:

(1) Find force (f_x) at the bottom of the bit by summing the moments about the end of the bit.

$f_x = 0.5$ lbs $= 2.224$ N

B. Entire bit touching the wall

(1) Find one constant force of 4448.2 N
(2) Torque = Force x Radius
$= 4448.2 \times 0.05$
$= 222.4$ N-m
(3) Add torque due to teeth.
(4) Find power and Hp.

$P_{tot} = T\omega$
$= (222.4 + 90.058)(31.4)$
$= 9.816$ Kw

$Hp = (Tn)/63000$
$= (2765.58)(300)/63000$
$= 13.169$ Hp

Intermediate Holding Device:

Due to size restrictions:

$L = 60$ mm : L = centerline length of holding device

Wall thickness (t) = 1 mm

$W = r_o - r_i - 2t = 50 - 25 - 2(1) = 23$ mm

Volume of solid rock cut (V_s):

$V_s = A_T d$: A_T = area of cutting teeth contact each revolution

d = depth cut

$A_T = \pi(49^2 - 26^2) = 5419$ mm^2

With an expansion factor of 3 (see section 4.1.3):

$C_s = 3V_s = 3A_T d$: C_s = volume of cuttings

Maximum capacity of the holding device (vmax):

$vmax = WLt = (23)(60)(18) = 24840$ mm^3

t = depth of device

The volume of cuttings cannot exceed this value.

$C_s = 3A_T d < 24840$

Solving for d:

$d = 24840/(3A_T) = 8280/5419 = (1.5 \text{ mm})(2) = 3$ mm

Although the above is very small, it does not determine the drilling depth restrictions since much of the cuttings will jump directly onto the auger.

TABLE 4.1.1

POWER REQUIREMENT CHART

RPM	LOAD (NEWTONS)	POWER (KW)	HORSEPOWER
300	1112.1	9.8	13.2
300	1334.5	9.9	13.4
300	1556.9	11.6	15.6
300	1779.3	13.3	17.8
300	2001.7	14.9	20.0
300	2224.1	16.6	22.3

** TEMPERATURE REQUIREMENTS **

At steady state for a cylinder straightened out as a wall :

$$q = \frac{KA}{L}(T_1 - T_2)$$

where: L = Length = 2m
A = Cross Sectional Area
$= \pi/4(.05^2 - .048^2) + \pi/4(.027^2 - .025^2) = .0024 m^2$
K = Thermal Conductivity K @ 520^0 K = 19.8 W/m-K
$T_2 = 0^0$ C = 273.15^0 K

$Q = K_f * W * \gamma = 1 * 1112.05 * (31.4 * .05) = 1746.804$ Watts

$Q' = 1746.804 * .2 = 349.361$ Watts

Also, 20% of the heat will remain in the cutting teeth.

** MODEL **

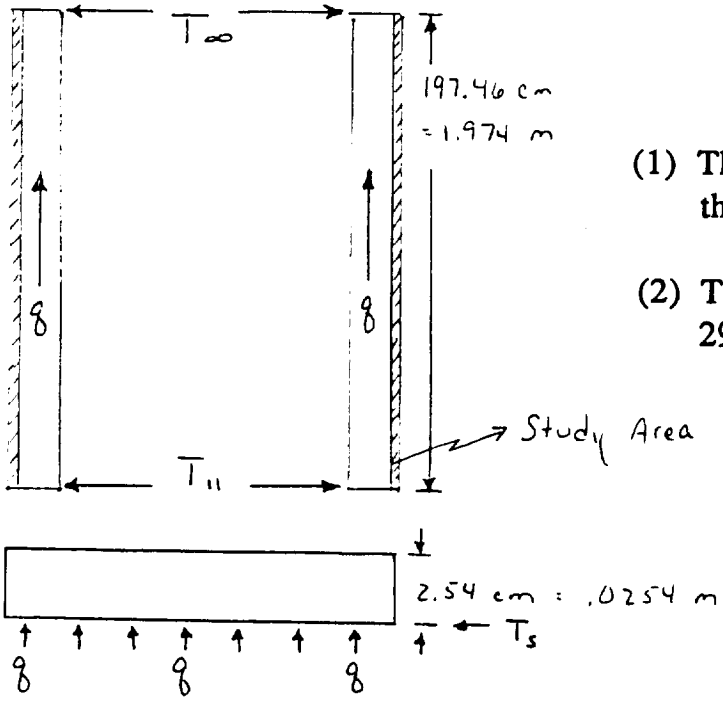

** MODEL ** (At steady state)

(1) There will be 12 diamonds so treat the model as 12 study areas.

(2) Therefore, 12 areas will dissipate 29.113 Watts each.

STEADY STATE HEAT :

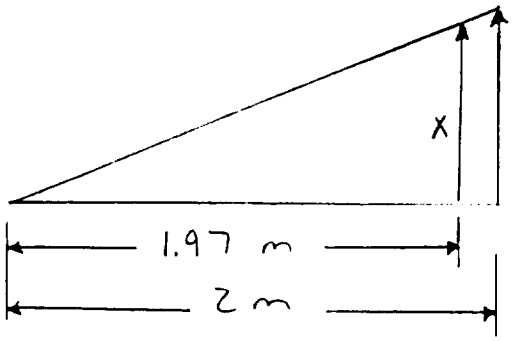

$$\frac{29.113}{2} = \frac{x}{1.97}$$

$x = 28.676$ Watts

$$28.676 \text{ Watts} = \frac{40\,(.0024)}{1.97}\,[T_1 - 273.15]$$

$T_1 = 861.62^0$ K $= 1091.24^0$ F

$A = \pi\,(.05^2 - .025^2) = .006 m^2$

$$29.113 \text{ Watts} = \frac{159\,(.006)}{.0254}\,[T_2 - 861.62]$$

$T_2 = 862.395^0$ K $= 1092.64^0$ F

Even though this temperature is above 952^0 F, the bit should still work because when calculating T_2, steady state was assumed. In order to reach steady state in this application, constant drilling must be done. This drill bit, however, will never be run constantly due to the shaking process that is needed to advance the cuttings up the auger. This will then lead to a temperature well below the calculated 1092.64^0 F.

STRESS ANALYSIS

All failing modes have same order of magnitude for similar calculations. Shown are those we estimated to be critical. We intend that resulting safety factors are large enough to account for discrepancies due to unknown information.

Mode 1

Description:

Normal stress in plane of smallest area in male interface.

Assumptions:

Curved edges taken as straight squared edges for area calculation.

Calculations:

$$\sigma_{max} = \frac{\text{total load}}{\text{normal area}}$$

$$= \frac{1{,}228.93\ \text{N}}{(10\ \text{mm})(50\ \text{mm}) + 2[0.5(5\ \text{mm})(50\ \text{mm})]}$$

$$= 1.64\ \text{MPa}$$

Safety factor:

$$\text{F.S.} = \frac{\sigma_y}{\sigma_{max}}$$

$$= \frac{827\ \text{MPa}}{1.64\ \text{MPa}}$$

$$= 504.71$$

Mode 2

Description:

Shear stress in plane of smallest area at interface of both male and female.

Assumptions:

Curved edges taken as straight squared edges for area calculation.

Calculations:

$$\tau_{max} = \frac{\text{total load}}{\text{parallel area}}$$

$$= \frac{1{,}228.93\ \text{N}}{2(25\ \text{mm})(20\ \text{mm})}$$

$$= 1.23\ \text{MPa}$$

Safety factor:

$$\text{F.S.} = \frac{\tau_y}{\tau_{max}}$$

$$= \frac{330.8\ \text{MPa}}{1.23\ \text{MPa}}$$

$$= 269.18$$

Mode 3

Description:

Shear stress in circular plane around male and female rod interface that intersects rod.

Assumptions:

None.

Calculations:

$$\tau_{max} = \frac{\text{total load}}{\text{parallel area around interface}}$$

$$= \frac{1{,}228.93\ \text{N}}{[2\pi(25\ \text{mm})][(9/48) + 9\ \text{mm}]}$$

$$= 571.59\ \text{KPa}$$

Safety factor:

$$F.S. = \frac{\tau_y}{\tau_{max}}$$

$$= \frac{330.8\ \text{MPa}}{571.79\ \text{MPa}}$$

$$= 578.74$$

Mode 4

Description:

Torsion in rod.

Assumptions:

None.

Calculations:

$$\tau_{max} = \frac{Tr_{max}}{J}$$

$$= \frac{(67.79\ \text{N-m})(49\ \text{mm})}{(\pi/32)[(98\ \text{mm})^4 - (96\ \text{mm})^4]}$$

$$= 4.63\ \text{MPa}$$

Safety factor:

$$F.S. = \frac{\tau_y}{\tau_{max}}$$

$$= \frac{330.8 \text{ MPa}}{4.63 \text{ MPa}}$$

$$= 71.39$$

Mode 5

Description:

Bending all around top of rod, below the interface due to axial load.

Assumptions:

None.

Calculations:

$$\sigma_{max} = \frac{Mc}{I}$$

$$= \frac{(1{,}228.93 \text{ N})[(1 \text{ mm})/(2\pi \cdot 48 \text{ mm})(48 \text{ mm})](6.67 \text{ mm})}{(1/12)(1 \text{ mm})(10 \text{ mm})^3}$$

$$= 15.66 \text{ MPa}$$

Safety factor:

$$F.S. = \frac{\sigma_y}{\sigma_{max}}$$

$$= \frac{827 \text{ MPa}}{15.66 \text{ MPa}}$$

$$= 52.83$$

Mode 6

Description:

Bending on one side of female interface.

Assumptions:

The cross-sectional area at the base of one side of the female interface was used instead of the one perpendicular to the moment arm. This approach is more conservative since the used area is smaller resulting in a higher critical bending stress. Also, this area was approximated as a parallelogram to simplify calculations.

Calculations:

$$\sigma_{max} = \frac{Mc}{I}$$

$$= \frac{(1{,}228.93\ \text{N})\sin(11.31^{\circ})\cdot [(25\ \text{mm})/\sin(78.69^{\circ}) + (5\ \text{mm})\tan(11.31^{\circ})]\cdot (4.33\ \text{mm})}{2(1/36)(10\ \text{mm})(15\ \text{mm})^3 + (1/12)(30\ \text{mm})(15\ \text{mm})^3}$$

$$= 2.68\ \text{MPa}$$

Safety factor:

$$F.S. = \frac{\sigma_y}{\sigma_{max}}$$

$$= \frac{827\ \text{MPa}}{2.68\ \text{MPa}}$$

$$= 308.58$$

Mode 7

Description:

Deflection of one side of the female interface due to tension allowing male interface to slip out.

Assumptions:

The cross-sectional area at the base of one side of the female interface was used instead of the one perpendicular to the moment arm. This approach is more conservative since the used area is smaller resulting in a higher critical bending stress. Also, this area was approximated as a parallelogram to simplify calculations.

Calculations:

$$y_{max} = \frac{F L^3}{3 E I}$$

$$= \frac{(1{,}228.93\ \text{N}) \sin(11.31^\circ) \cdot [(25\ \text{mm}) / \sin(78.69^\circ) + (5\ \text{mm}) \tan(11.31^\circ)]^3}{3(128{,}000\ \text{MPa}) \cdot 2(1/36)(10\ \text{mm})(15\ \text{mm})^3 + (1/12)(30\ \text{mm})(15\ \text{mm})^3}$$

$$= 1.13\ \text{mm}$$

Safety factor:

$$F.S. = \frac{\text{Common length of a side of male-female interface}}{y_{max}}$$

$$= \frac{5\ \text{mm}}{1.13\ \text{mm}}$$

$$= 4.42$$

Mode 8

Description:

Eccentric loading of one rod.

Assumptions:

None.

Calculations:

$P \equiv$ total load

$A \equiv$ rod cross-sectional area

$$k = \text{sqrt}[(1/16)[(98\ \text{mm})^2 + (96\ \text{mm})^2]$$
$$= 34.30\ \text{mm}$$

$$e = 1$$

$$c = 1$$

$$\frac{P}{A} = \frac{\sigma_y}{1 + (e \cdot c/k)\ \text{sec}[(1/k)\text{sqrt}[P/(4\ A\ E)]}$$

$$\frac{P}{\pi[(49\ \text{mm})^2 - (48\ \text{mm})^2]} = \frac{827\ \text{MPa}/\text{mm}^2}{1 + (2.04)\ \text{sec}[(2.33)(10)^{-3}\text{sqrt}(|P|)}$$

Iterating,

$$P = 82{,}895\ \text{N}$$

Safety factor:

$$F.S. = \frac{P}{\text{total load}}$$

$$= \frac{82{,}895\ N}{1{,}228.93\ N}$$

$$= 67.45$$

Mode 9

Description:

Buckling of one rod.

Assumptions:

None.

Calculations:

$C = 1$

$(L/k)_{cr} = \text{sqrt}[(2C\pi^2E)/\sigma_y]$

55.27

$(L/k) = 2\ m/34.30\ mm$

$= 58.31$

$(L/k) < (L/k)_{cr} \longrightarrow$ Euler column

$$P_{cr} = \frac{C\pi^2 E I}{L^2}$$

$= 112.21\ KN$

Safety factor:

$$F.S. = \frac{P_{cr}}{\text{total load}}$$

$$= \frac{112.21\ KN}{1{,}228.93\ N}$$

$$= 91.31$$

APPENDIX A.2 WEIGHT CALCULATIONS

ROD WEIGHT

Rod Volume = Hollow Cylinder + Top and Bottom Interface Support + Interface + Collar

$= (\pi/4)(98mm^2-96mm^2)(2000mm)$
$+ 2(\pi/4)(98mm^2)(2/3)(10mm)$
$+ (\pi/4)(50mm^2)(25mm)$
$+ (\pi/4)(100mm^2-98mm^2)(100mm)$

$= 7.903x10^5 mm^3 = 7.903x10^{-4} m^3$

Rod Mass $= \rho V = (4500\ kg/m^3)(7.903x10^{-4} m^3) = 3.6\ kg$

Earth Weight = 7.8 lb = 1.75 N
Moon Weight = 1.3 lb = 0.292 N

AUGER WEIGHT

Auger Volume = Sleeves + Tube + Helix + Interface + Collar

$= 3(\pi/4)(98mm^2-96mm^2)(100mm)$
$+ (\pi/4)(50mm^2-46mm^2)(2000mm)$
$+ (\pi/4)(50mm^2)(25mm)$
$+ (\pi/4)(100mm^2-98mm^2)(100mm)$
$+ \dfrac{(2000mm/10mm)(\pi/4)(100mm^2-50mm^2)}{(\cos 45)(1mm)}$

$= 9.42x10^5 mm^3 = 9.42x10^{-4} m^3$

Auger Mass $= \rho V = (4500\ kg/m^3)(9.42x10^{-4} m^3) = 4.24\ kg$

Earth Weight = 9.3 lb = 2.09 N
Moon Weight = 1.6 lb = 0.360 N

VRA WEIGHT

VRA Volume = Outer Tube + Inner Tube + Interface
+ 4 1/2 Windings + Windings + Steps + Collar

$= (\pi/4)(98mm^2-96mm^2)(2000mm)$
$+ (\pi/4)(52mm^2-50mm^2)(2000mm)$
$+ (\pi/4)(50mm^2)(25mm)$
$+ 4(\pi/4)(96mm^2-52mm^2)(1/\cos\ 39)(1mm)$
$+ 2((2000/81)-1)(\pi/4)(96mm^2-52mm^2)(0.2mm)$
$(1/\cos\ 39) + (2000/81)(6)(18.225)(22)(0.2)$
$+ (\pi/4)(100mm^2-98mm^2)(100mm)$

$= 1.11x10^6mm^3 = 0.00111m^3$

VRA Mass $= \rho V = (0.00111m^3)(4500\ kg/m^3) = 5.0$ kg

Earth Weight = 11 lb = 2.47 N
Moon Weight = 1.83 lb = 0.411 N

WEIGHT OF SOIL CUTTINGS

Volume = (Volume Drilled)(Expansion Factor)

$= (\pi/4)(100mm^2-50mm^2)(2000mm)(3)$

$= 4.5x10^7mm^3 = 0.045m^3$

Density of Cuttings = Density of MLS-1 Simulant
$= 0.108\ lb/in^3 = 3000\ kg/m^3$

Mass of Cuttings from 2m Worth of Drilling $= (.045m^3)(3000\ kg/m^3)$
$= 134$ kg

Moon Weight = 49 lb = 11.0 N

TOTAL STRING WEIGHT (LOADED AND ASSUMING NO AUGERS ARE USED AS RODS)

Mass = 9(VRA Mass) + 16(Rod Mass) + Soil Mass

= 9(5.0 kg) + 16(3.6 kg) + 134 kg
= 237 kg

Earth Weight = 520 lb = 117 N
Moon Weight = 86.75 lb = 19.49 N

Safety factor allows for 1.3 moon g's vertical acceleration (0.22 earth g's)

TOTAL SYSTEM WEIGHT ON EARTH

16 Rods at 7.3 lb each = 1.75 N each = 28 N total
9 VRA's at 11 lb each = 2.47 N each = 22.23 N total
3 Augers at 9.3 lb each = 2.09 N each = 6.27 N total

Total System Weight = 56.50 N

A.2 Failure due to Static Loads Calculations

FAILURE OF A ROD

Mode #1 Description: Rod yields in tension

Assumptions:

Tensile Force = 900 N (200 lb) *worst case*

Calculations:

Cross Sectional Area, $A = \frac{\pi}{4}(98\ mm^2 - 96\ mm^2) = 305\ mm^2$

$$\sigma = \frac{F}{A} = \frac{900\ N}{305\ mm^2} = 3\ \frac{N}{mm^2} = 2.95 \times 10^6\ \frac{N}{m^2}$$

Safety Factor, $n = \frac{\sigma_y}{\sigma} = \frac{827 \times 10^6\ N/m^2}{2.95 \times 10^6\ N/m^2} = 280$

Mode #2 Description: Rod yields in shear due to tension

Assumptions:

T_{max} = 50 lb-ft = 67.8 N-m = 6.78×10^4 N-mm (motor torque)

$\tau_y = 0.5\sigma_y = 414$ MPa

Calculations:

$$\tau_{max} = \frac{Tr}{J}$$

$$J = \frac{\pi}{32}(98^4 - 96^4) = 7.17 \times 105\ mm^4$$

$$r = r_{max} = \frac{98\ mm}{2} = 49\ mm$$

$$\tau_{max} = \frac{(6.78 \times 10^4 \text{ N-m})(49 \text{ mm})}{(7.17 \times 10^5 \text{ mm}^4)} = 4.63 \frac{\text{N}}{\text{mm}^2} = 4.63 \times 106 \frac{\text{N}}{\text{m}^2}$$

$$n = \frac{\tau_y}{\tau_{max}} = \frac{414 \times 10^6 \text{ N/m}^2}{4.63 \times 10^6 \text{ N/m}^2} = 89.3$$

Mode #3 Description: Rod buckles as a column under compressive force

Assumptions:

Both column ends pinned at interfaces (end constraint factor=4)
Force is purely axial

Calculations:

l = 2000 mm = 2 m
E = 127 x 10^4 MPa = 1.27 x 10^6 N/mm^2 (for titanium)
I = J/2 = 3.59 x 10^5 mm^4

Example:

$$P_{cr} = \frac{4\pi^2(1.27 \times 10^6 \text{ N/mm}^2)(3.59 \times 10^5 \text{ mm}^4)}{(2000 \text{ mm})^2} = 4.5 \times 10^6 \text{ N}$$

Example:

$$n = \frac{P_{cr}}{P} = \frac{4.5 \times 10^6 \text{ N}}{900 \text{ N}} = 5000$$

FAILURE OF AUGER

Mode #1 Description: Component yields in tension or compression
Assumptions: All axial forces are resisted by auger core alone. Worst case axial force = 900 N

Calculations:

Cross section area = A = $(\pi/4)((50mm)^2 - (46mm)^2) = 302\ mm^2$

$\sigma = F/A = (900N/302mm^2) = 3\ N/mm^2 = 3*10^2\ N/m$

eg. $n = \sigma_y/\sigma = 827*10^6/3*10^6 = 280$

Mode #2 Description: Component yields in shear due to torsion

Assumptions: All torsional loads resisted by core alone, maximum torque = 50 ft-lb = 67800 N/mm^2, $\tau_y = 0.5(\sigma_y) = 414$ MPa

Calculations:

$\tau_{max} = Tr/J$

$J = (\pi/32)((50mm)^4 + (46mm)^4) = 174000\ mm^4$

$r_{max} = 50mm$

$\tau_{max} = (67800\ N\ mm)(50\ mm)/(174000\ mm^4) = 19.5\ N = 1.95*10^7\ N/m^2$

eg.

$n = \tau_y/\tau_y = (414*10^6\ N/m^2)/(19.5\ *10^6\ N/m^2) = 21$

Stepped Auger Volume Retention Calculations

surface of soil arc length = 18.225 (sin(51)/sin(24)) = 34.8 mm = L
projection of L in XY plane = Lsin(75) = 41.88
angular subtense of soil arc = (41.8/(π*96))*360 = 50 degrees
Y projction of soil surface = Lcos(75)= 90 mm
volume of empty space above soil and below horizontal =
$(1/2)(49.9/360)(\pi/4)(96^2-52^2)(9) = 3190$ mm

volume of soil section per step =
$((1/2)(49.9/360)(\pi/4)(96^2-52^2)(90)-3190=28{,}700$ mm^3
number of steps = (2000/81)(2)(6) = 296
total retained volume in steps = (296)*(28,700) = $8.5*10^6$ mm^3
volume of core = $(\pi/4)(50^2)(2000) = 3.93*10^6$ mm^3
total volume that can be held by a VRA segment =
$(8.5*10^6 + 3.93*10^6)mm^3 = 0.0124$ mm^3

A.3. Footplate

PLACEMENT OF FOOTPLATE

Calculation for torque needed to overcome friction regolith. Assumed coefficient of friction of dirt to be C = 200 lb/ft^2. This simulates tightly packed soil on Earth. Torque calculation is as follows:

T = Area x C x Radius

where,

A = surface area of casing
r = radius of casing
L = length of casing
c = coeff. of friction

Area = 2 pi r L = pi d L

d = 120 mm = 4.724 in = 0.394 ft
L = 0.67 ft
r = 0.197 ft

A = pi(0.394 ft)(0.67 ft) = 0.83 ft^2
T = (0.83 ft^2)(200 lb/ft^2)(0.197 ft) = 33 ft-lb

Maximum torque available from the drive is 200 ft-lb.

A.3. Footplate

MASS CALCULATIONS

I. STRUCTURE

Part of Structure	Volume	
Base	$(3.14/4)(.55)^2(.005)$	$= 1.19 \times 10^{-3}$ m^3
Fins	$4(.5)(.21)(.215)(.005)$	$= 4.52 \times 10^{-4}$ m^3
Casing (est.)	$(3.14/4)(.130^2 - .120^2)(.3)$	$= 5.89 \times 10^{-4}$ m^3
Adapter (est.)	$[(.125^2 - .155^2)/2]\ (.1)(.873)$	$= 1.05 \times 10^{-4}$ m^3
Interface Roller, Shaft Supports (6) (est.)	$(6)(.01)(.025)(.04)$	$= 6.0 \times 10^{-5}$ m^3

Material Removal from Base

Square Sections	$(2)(.13)(.05)(.005)$	$= -6.5 \times 10^{-5}$ m^3
Triangular Sections	$(2)(.5)(.225)(.13)(.005)$	$= -1.46 \times 10^{-4}$ m^3

Total Volume of Structure $= 2.18 \times 10^{-3}$ m^3

Density of Aluminum-Lithium $= 2.6 \times 10^3$ kg/m^3

Mass $= \rho V_{tot} = 5.67$ kg

II. PARTS

Part	Volume	
Rollers (2)	$(2)(3.14/4)(.02)^2(.24)$	$= 1.51 \times 10^{-4}$ m^3
Shaft	$(3.14/4)(.015)^2(.24)$	$= 5.4 \times 10^{-5}$ m^3
Lifters (2) (est.)	$(2)(3.14/4)(.015)^2(.086)$	$= 3.0 \times 10^{-5}$ m^3
Spring (est.)	$(.5)(.2)(.0015)$	$= 1.5 \times 10^{-4}$ m^3

Total Volume of Al-Li Parts $= 3.85 \times 10^{-4}$ m^3

Mass = $\rho V_{tot,parts}$ = 2.6 x 10^3 kg/m^3 x V_{tot} = 1.00 kg

III. ADDITIONAL PARTS

Part	Mass	
Gear Reducer	0.39 kg	= 0.39 kg
Motor	2.18 oz. = 0.063 kg	= 0.06 kg
Batteries	(4 cells)(0.72 oz.)	
	2.88 oz. = 0.08 kg	= 0.08 kg
Transmitter &	1.0 lbf = 4.54 N	
Relays	= 0.46 kg	= 0.46 kg

Total Mass of Additional Parts = 0.99 kg

Overall Total Mass (Sum of Parts I, II, III) = 7.67 kg

The weight on Earth will be Mass times an acceleration factor of 9.81 m/s^2.
Earth Weight = 7.67 x 9.81 = 75.243 N.

The acceleration constant on the lunar surface is (9.81 m/s^2)/6 ;
a_L = 1.65 m/s^2,
therefore, Lunar Weight = (7.67)(1.635) = 12.54 N.

SPRING DEFLECTION CALCULATION

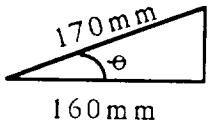

$\cos\theta$ = 160 mm/ 170mm

θ = 19.75°

need deflection of 19.75°

displacement of clamp lever = (170 mm) $\sin\theta$ = 57.45 mm

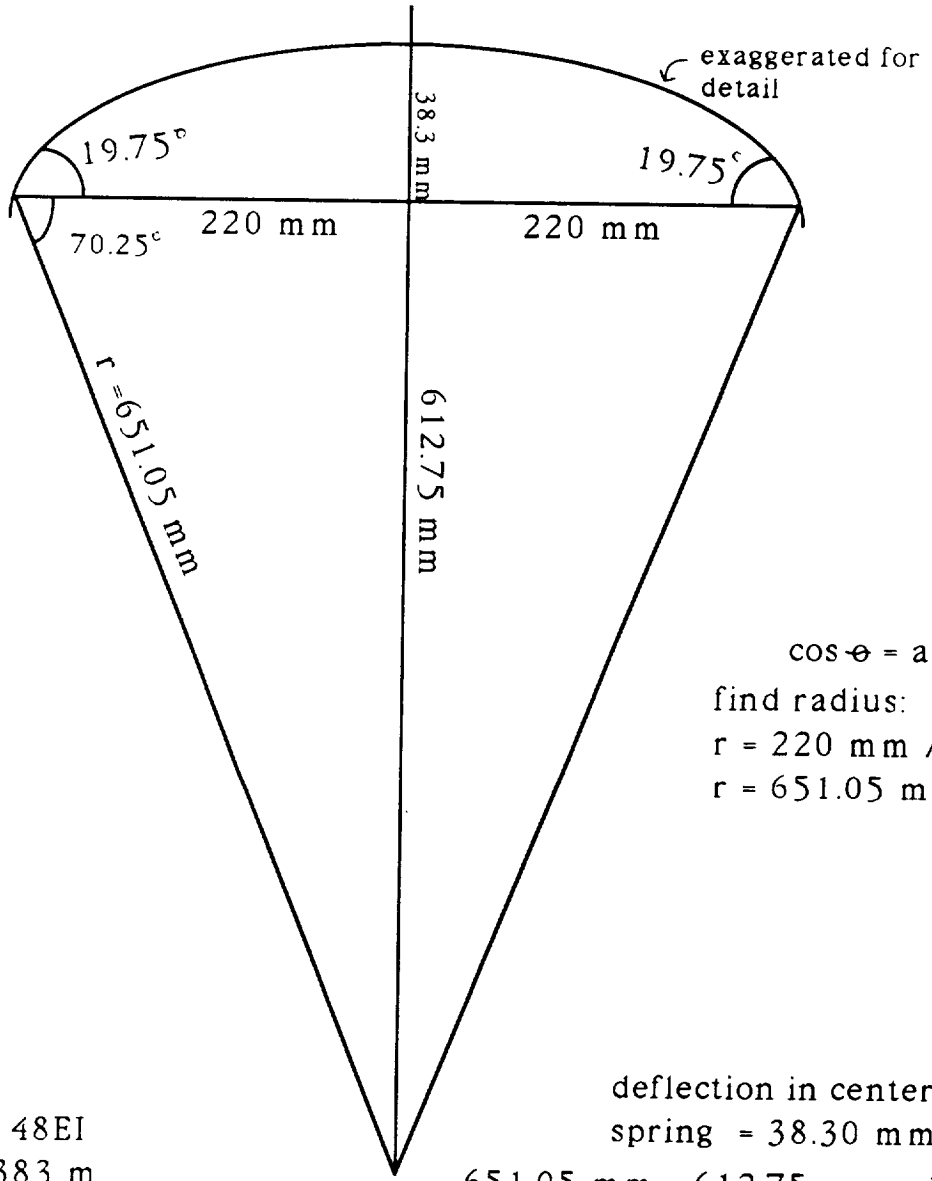

$\cos\theta$ = a/h

find radius:

r = 220 mm / cos 70.25°

r = 651.05 mm

deflection in center of spring = 38.30 mm

651.05 mm - 612.75 mm = 38.30 mm

y = Fl / 48EI

y = 0.0383 m

l = 0.440 m

E = 64 X 10 N/m

I = bh / 12

b = 0.108 mm

h = 0.003 mm (spring thickness)

A.3. Footplate

DEFLECTION OF LIFTER AND LIFTER LENGTH CALCULATIONS

F = (41.95 N) / 2 = 20.975 N

L = 0.084 m (ideal case, without bending)

$y_{max} = FL^3 / 3EI$; $E = 64 \times 109\ N/m^2$

$I = \pi d^2 / 64$

$d = 15\ mm = 0.015\ m$

$y_{max} = (20.975\ N)(0.084\ m)^3 (64) / 3 (64 \times 10^9\ N/m^2)(0.015\ m)^4 \pi$

$y_{max} = \underline{26.0 \times 10^{-6}\ m}$

1.) ideal

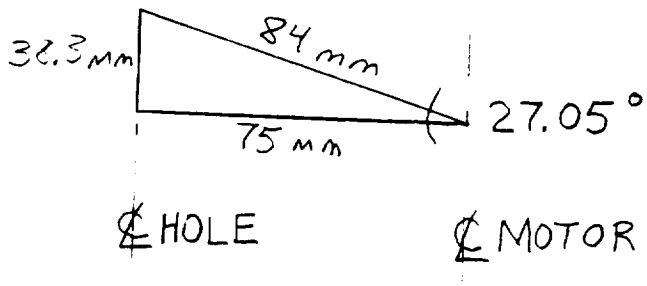

38.3 mm = deflection of spring required to open spring during drilling

2.) with bending

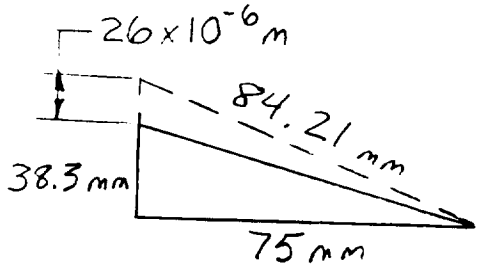

$\tan^{-1}$ (38.3 mm/ 75mm) = 27.05° = rotation required from the motor and the lifter length = 75 mm / cos 27.05° = 84.21 mm, where the arm

length is specified as the length from the centerline of the motor to the centerline of the roller.

A.3. Footplate

MASS ANALYSIS OF ADAPTOR

Adaptor diameter = .098 m
Material : AlLi, $\rho = 2.6 \times 10^3$ kg/m^3
Length = 1.75 m

The adaptor is an annular rod with inner radius of 44 mm and outer radius of 49 mm. The choice of an annular device was made to limit the weight requirements for transportation to the lunar surface.

Volume = $\pi(.049^2 - .044^2)(1.75) = .003$ m^3
therefore,
Mass = $\rho V = (2.6 \times 10^3)(0.003) = 6.65$ kg

A.3. Footplate

ANNULAR TUBE ADAPTOR

The following calculations are a force analysis to determine the strength of the annular adaptor rod.

$S_y = 6.67 \times 10^8$ Pa (Yield stress of Aluminum- Lithium)
$\tau = \tau_{max}\, \rho/c = T\rho/J$ (shear stress)
$J = (\pi c^4 - \pi b^4)/2$
$T_{max} = 200$ ft-lb
For positioning of footplate : T = 33 ft-lb
c = 49 mm = 1.93 in.

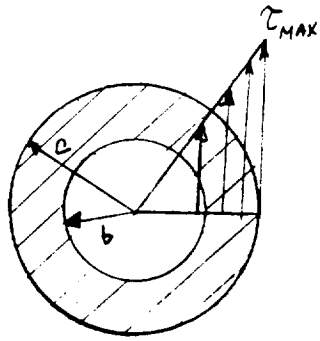

Case 1: Let b = 29 mm = 1.14 in.
$J = \pi(1.93^4 - 1.14^4)/2 = 21.79 - 2.65$
$J = 19.14$ in^4
$\tau_{max} = Tc/J = 200(12)(1.93)/19.14$
$= 242.01$ lbf/in^2 $= 1.67 \times 10^6$ Pa
so, $\tau_{max} < S_y$
therefore, this design is fine but it can still be reduced.
Volume $= [\pi(.049^2 - .029^2)/2](1.75) = 8.6 \times 10^{-3}$ m^3
Mass $= \rho V = (2.6 \times 10^3)(8.6 \times 10^{-3})$
$= 22.36$ kg

Case 2: Let b = 34 mm = 1.34 in.
$J = 16.73$ in^4
$\tau_{max} = 276.87$ lbf/in^2
$= 1.91 \times 10^6$ Pa
$\tau_{max} < S_y$
Volume $= 6.85 \times 10^{-3}$ m^3
Mass = 17.81 kg

Case 3: Let b = 44 mm = 1.73 in
$J = 7.72$ in^4

τ_{max}= 600 lbf/in^2

= 4.14 x 10^6 Pa

$\tau_{max} < S_y$

Volume = 2.56 x 10 $^{-3}$ m^3

Mass = 6.65 kg

Case 3 will be used due to its mass value and strength requirement.

A.3. Footplate

YIELD STRESS CALCULATIONS FOR LIFTER AND SHAFT

1.) Maximum torsion applied to the arm link at the motor hook-up is:

$$T = (41.95\ N) / (0.075\ m) = 3.15\ Nm$$

$= Tr / J$; $J = (pi)d^2 / 32$ = polar area moment of inertia

$= (3.15\ Nm)\ (0.015/2\ m)\ (32) / pi\ (0.015\ m)^4$

$= \underline{4.75 \times 10^6\ N/m^2}$

Since oy = $6.27 \times 10^8\ N/m^2$, the link is not in danger of failing and the factor of safety = $6.27 \times 10^8 / 4.75 \times 10^6 = 132$

2.) Maximum force applied (pure bending) to each lifter is:

$F = (41.95\ N)/ 2 = 20.975\ N$

and

$\sigma = Mc / I$; $I = J /2 = pi\ d^2 / 64$ = rectangular moment of inertia

$c = (0.015\ m) / 2$

$M = Fr$, where $r = 0.075$ m.

$\sigma = (20.975\ N)\ (0.075\ m)\ (0.015/2\ m)\ (64) / pi\ (0.015\ m)^4$

$\sigma = \underline{4.75 \times 10^6\ N/m^2}$

and $\sigma_y > \sigma$; so the lifters are not in danger of failing.

The factor of safety is $\sigma_y / \sigma = 132$.

A.3. Footplate

OPEN SPRING FORCE AND YIELD STRESS CALCULATIONS

Spring Force Calculation:

Spring Thickness = 1.5 mm = 0.0015 m

From previous page, y_{max} = 38.3 mm, and $F_{max} = 48EIy_{max}/L^3$.

E = 64 X 10^9 N/m^2 and $I = bh^3/12$.

I = (0.108 m) (0.0015 m)^3/12 = 3.0375 X 10^{-11} m^4

F_{max} = (48) (64 X109 N/m^2) (0.0383 m) (3.0375 X 10^{-11} m^4)/ (0.440 m)^3

= 41.95 N

F_{max}, per arm = (41.95 N)/2 = 20.975 N, per arm

T_{max} = (41.95 N) (0.075 m) = 3.15 Nm = 445.5 oz-in

Yield Stress Calculation:

$\sigma = Mc/I$ M = (41.95 N/2) (0.220 m) = 4.615 Nm

c = (0.0015 m) /2 = 0.00075 m

I = 3.0375 X 10^{-11} m^4

σ = (4.615 Nm) (0.00075 m) / (3.0375 X 10^{-11} m^4) = 1.140 X 10^8 N/m^2

and σ_y = 6.27 X 10^8 N/m^2. $\sigma_y > \sigma$ so the spring is not in danger of failing.

The factor of safety is:

σ_y/σ = 6.27 /1.140 = 5.5

A.3. Footplate

CLOSED - SPRING STRESS CALCULATIONS

From the rod group, the worst case maximum weight is 70 lb (318.2 N). We will assume the system to be a simple cantilever:

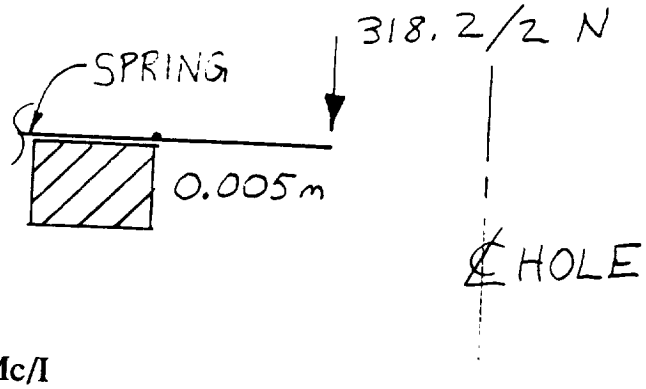

$\sigma = Mc/I$

$M = (159.1\ N)(0.005\ m) = 0.795\ Nm$
$c = (0.0015\ m)/2 = 0.00075\ m$
$I = 3.0375 \times 10^{-11}\ m^4$ (previous page)

$\sigma = (0.795\ Nm)(0.00075\ m)/(3.0375 \times 10^{-11}\ m^4)$
$\sigma = 0.196 \times 10^8\ N/m^2$

and $\sigma_{yield} = 6.27 \times 10^8\ N/m^2$

Factor of Safety $= \sigma_y/\sigma = 32$

A.3. Footplate

BALANCE CALCULATIONS

The unsymmetrical parts on the plate must not create a mass-moment about the center. The only movable parts are the batteries and the transmitter and relays box. Calculations for the combination that seems to be the best of several are shown below :

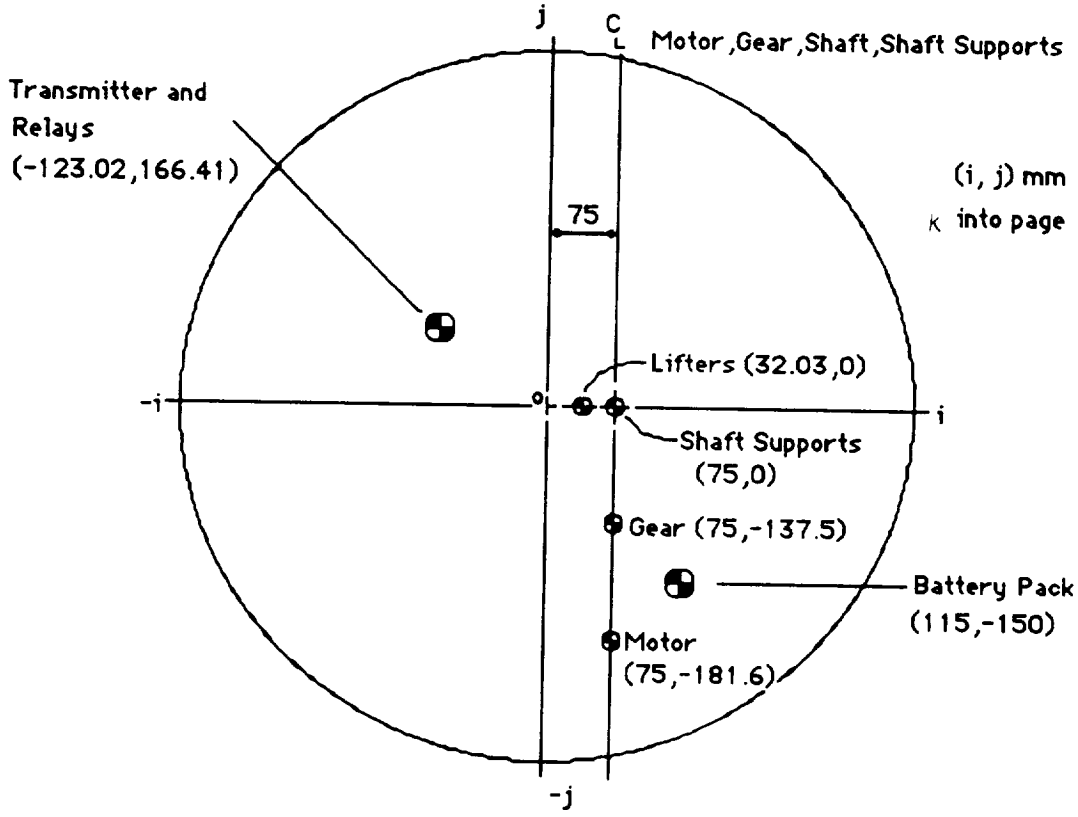

The moments created by the non-moving parts :

Part	Mass(kg)	x	Moment arm rel. to "0" (mm)		= Mom.(kg-mm)
Gear	0.39	x	75i-(100+10+55/2)j	=75i-137.5j	= 53.35i + 29.1j
Motor	0.06	x	75i-(100+10+55+33/2)j	=75i-181.6j	= 11.44i + 4.73j
Shaft	0.11	x	75i+0j	=75i+0j	= 0i + 8.25j
Lifters	2(.04)	x	(75-85.95/2)i+0j	=32.03i+0j	= 0i + 2.56j
Supts.	2(.02)	x	75i+ 0j	=75i+0j	= 0i + 2.93j

Total Moment of Non-moving Parts = 64.79i + 47.56j kg-mm.

The moments created by the batteries and the transmitter and relays must equal the total of (-64.79i - 47.56j) kg-mm for the structure to balance. The battery will be placed at location (115, -150) near the gear and motor. Its moment is :

$$64.79i + 47.56j$$
$$\underline{12.25i + 9.40j}$$
$$77.05i + 56.96j \quad \text{kg-mm}$$

or, $-77.05i - 56.96j$ kg-mm

$= M \times r = 0.46 \text{ kg } k \times r$

$r = (\text{moment } j / \text{mass})i$

$r_{\text{TO TRANSMITTER}} = (-123.02i + 166.41j)$ mm

A.3. Footplate

MOTOR POWER REQUIREMENTS

The motion of raising the spring will occur in one second. The lifter will traverse an arc of 29.24°.

$$\frac{29.24^\circ}{1\ \text{sec}} \times \frac{1\ \text{rev}}{360^\circ} \times \frac{60\ \text{sec}}{1\ \text{min}} = 4.87\ \text{rpm at gearbox output}$$

Since the maximum torque required is 444.5 oz-in, and occurs at maximum deflection, we will cut this figure in half to get an average, continuous torque for the means of calculating input power requirements.

$$T_{avg,cont} = 444.5\ \text{oz-in}/2 = 222.75\ \text{oz-in}$$

With a reduction of 1,080 and a gearbox mechanical efficiency of 55%, the motor output torque is:

$$T_{motor} = \frac{222.75\ \text{oz-in}}{(1080)(0.55)} = 0.375\ \text{oz-in}$$

According to the Micro Mo Catalog, torque in oz-in mutiplied by rpm and a conversion factor of 0.00074 gives mechanical power in watts:

$$P_{mech} = (0.375\ \text{oz-in})(4.87\ \text{rpm})(1080)(0.00074)$$
$$P_{mech} = 1.46\ \text{W}$$

And with a motor efficiency of 80%:

$$P_{mech} = 1.82\ \text{W}$$

Since we are dealing in DC voltages:

$$I = P/V \quad \text{Supply Voltage is 6 VDC}$$
$$I = 1.82\ \text{W}/6\ \text{VDC} = 0.303\ \text{Amps/raise motion}$$

5000 cycles will be required at 1 second per cycle. This gives battery power as:

$$(0.303\ A)(5000)(1\ s/cycle)(1\ hr/3600\ s) = 0.4213\ Amp\ hrs$$

It is assumed that the power required to operate the transmitter and relays is relatively negligable. Four Whittaker - Yardney #LR05 Silvercells connected in series will provide a total of 0.5 Amp hrs. At 6.0 V (1.5 V each), these cells are for long life and low rate use. A recharge will not be required in 50 holes.

The total mass of four cells is 2.88 oz or 0.82 kg.

The four cells will occupy a space of 2.33 in^2 (1505 mm^2) on the plate.

Cell base width = 0.54 in
Cell base length = 1.08 in
Cell height (inc. terminals) = 1.56 in = 39.6 mm

$$(4\ cells)(0.54\ in)(1.08\ in) = 2.33\ in^2 = 1505\ mm^2$$

A.4 POWER SOURCE

4.4.5. Friction Clutch.

These calculations were used to determine the required diameter for the motor shaft. Also, see Figure 4.4.5.2.

From Mohr's Circle...

$$Tmax = ((Ox/2)^2 + (Txy)^2)^.5$$

$$Tmax = 16(M^2 + T^2)^.5 / pi(d)^3$$

where:

M = moment = 0 (assumed)
T = torque = 83.3 ft-lbs (from Torq-Tender specifications)

$$Tmax = 16(83.3)/pi(d)^3$$

from Maximum Shear Stress Theory, Ssy = Sy/2
AISI 1045 Steel - Sy = 276 kpsi

with a factor of safety of 2

$$d = .42"$$

The d dictated by the maximum Torque-Tender shaft diameter to accommodate the 3.94" interfacing with the drill string is 1.75". This diameter is large enough. See Figure 4.4.5.2 for the shaft interface and Figure 4.4.5.3 for the Torq-Tender specifications.

4.4.3 TEMPERATURE MANAGEMENT CALCULATIONS

Heat Pipe Wall Thickness Calculation

At 212F, the water vapor pressure is 180 psi and the Copper Ultimate Tensile Strength is 18 kpsi. The maximum allowable stress on the container walls is one-quarter of the ultimate tensile stress. The maximum pressure stress is determined by:

$$f_{max} = P\,(d_o^2 + d_i^2) / (d_o^2 - d_i^2)$$
$$d_o^2 = [(-P/f_{max} - 1)/(P/f_{max} - 1)]\, d_i^2$$
$$d_o = [(-180/1.8 \times 10^3 - 1)/80/(1.8 \times 10^3 - 1)]\ (0.10)^2$$
$$d_o = 0.1.25 \text{ inches}$$

$$t_1 = 0.1.25 - 0.1.12$$
$$t_1 = 0.13 \text{ inches}$$

End Cap Calculation

For the most common circular heat pipes, a flat circular end cap is used. Assuming a thickness of less than 10%, the wall thickness of the end cap can be determined by:

$$f_{max} = P\, d_o / 4t_2$$
$$f_{max} = 1/4\ (UTS) = 1/4(18 \text{ kpsi}) = 4.5 \text{ kpsi}$$
$$4.5 \text{ kpsi} = 2(180 \text{ psi})(0.1.25 \text{ inch})/4t_2$$
$$t_2 = 0.06 \text{ inches}$$

A factor of safety of 2 was used.

Diameter of Vapor Core Calculation

$$d_v = [(20\ Q_{max}) / (\Pi \rho_v \lambda\, (\gamma_v R_v T_v)^{1/2})]^{1/2}$$

$$dv = \sqrt{\frac{20(4.3\ E6)}{(1.33)(462)(373.15)\quad\sqrt{(3.1415)(2.254\ E6)(0.58)}}}$$

$$d_v = 0.10 \text{ inches}$$

Properties of Water Vapor at 212F and Nomenclature

ρ_v = vapor density (3.62 E-2 lbm/ft^3)
λ = latent heat of evaporization (754.3 E3 ft-lbf/lbm)
γ_v = vapor specific heat ratio (1.33)
R_v = vapor gas constant (85.78 ft-lbf/lbm-F)
T_v = operating temperature
f_{max} = maximum hoop stress in the wall
P = inside pressure of heat pipe
d_o = tube outside diameter
d_i = tube inside diameter
d_v = vapor core diameter
t_1 = cylindrical thickness
t_2 = end cap thickness
A_w = wick cross sectional area
A_v = vapor core cross sectional area
σ = surface tension coefficient (0.8521 lbf/ft)
ρ_l = liquid density (59.97 lbm/ft^3)
μ_l = liquid viscosity (0.682 lbm/ft-hr)
Q_{max} = maxmimum dissipated heat per heat pipe
Q_e = entrainment limitation
Q_b = boiling limitation
Q_c = capillary limitation
r_c = screen wick capillary radius
t_w = screen wick thickness
L_e = length of evaporater section
L_a = length of adiatbatic section
L_c = length of condenser section
N = wire screen mesh number
d = wire screen wire diameter
F_v = vapor frictional coefficient
F_l = liquid frictional coefficient
P_{cm} = maximum capillary pressure

Capillary Limitation Calculation

The capillary limitation on the heat transport factor was determined to be:

$$(QL)_{c,max} = \frac{Pcm}{F_l - F_v}$$

where

P_{cm} = maximum capillary pressure
F_l = liquid frictional coefficient
F_v = vapor frictional coefficient

Using Figure 4.4.3.4 below with a Mesh number of 250 inch^{-1} at the operating temperature of 670R (212F), the maximum capillary pressure is:

$$P_{cm} = 47 \text{ lbf/ft}^2$$

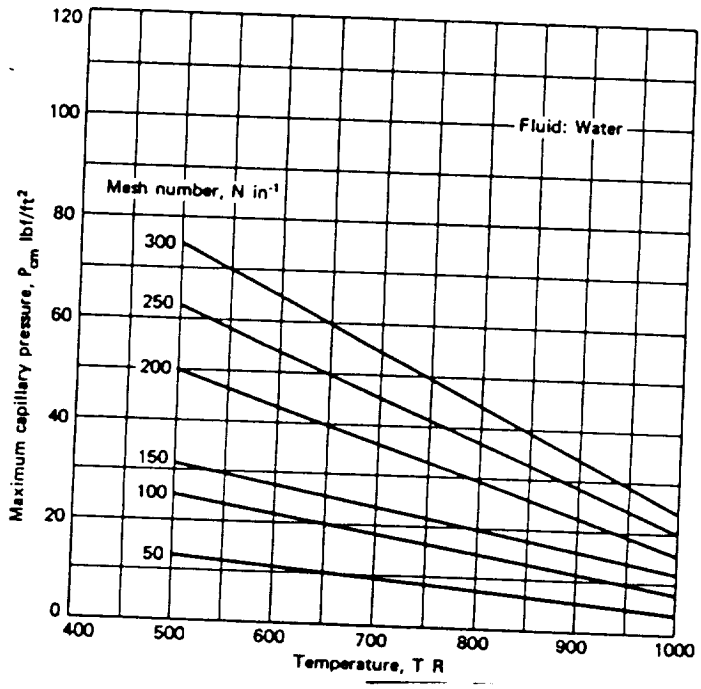

Figure 4.4.3.4 Maximum capillary pressure for screen wicks

Figure 4.4.3.5 shows the vapor frictional coefficient F_v at a vapor core diameter of 0.10 inches to be:

$$F_v = 2 \times 10^{-4} \ (lbf/ft^2) \ / \ (Btu\text{-}ft/hr)$$

$$Q_{c,max} = (QL)_{c,max} / [0.5(L_c) + L_a + 0.5(L_e)]$$
$$700 = (QL)_{c,max}/[(0.5)(0.1.55) + (1.50) + (0.5)(1.43)]$$
$$(QL)_{c,max} = 2076 \ \text{Watt-meters}$$
$$(QL)_{c,max} = \frac{Pcm}{F_l - F_v}$$
$$F_l = 0.0022 \ (lbf/ft^2) \ / \ (Btu\text{-}ft/hr)$$

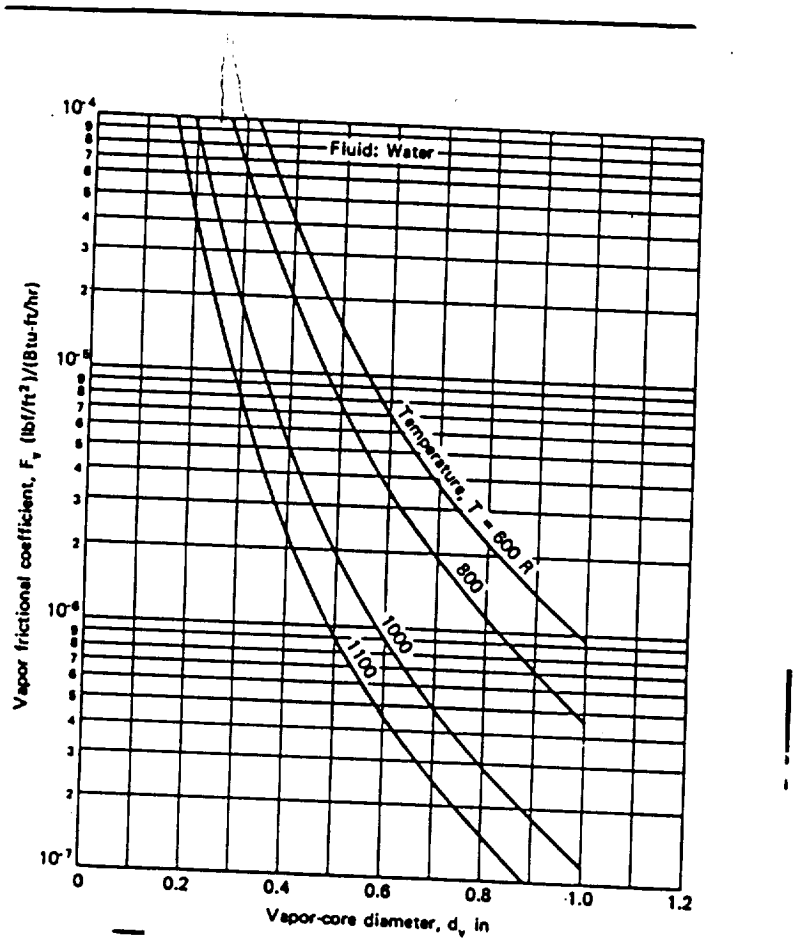

Figure 4.4.3.5 Vapor frictional coefficient for round tubes

By use of Figure 4.4.3.6, with a mesh number of 250 inch-1 at 670R (212F), a wick diameter d of 0.0016 is obtained. The liquid frictional coefficient can be determined:

$$F_l A_w = 1.5 \times 10^{-5} \text{ lbf / (Btu-ft/hr)}$$

$$F_l = 0.0022 \text{ (lbf/ft}^2\text{) / (Btu-ft/hr)}$$

$$A_w = F_l A_w / F_l$$

$$A_w = 1.5 \times 10^{-5} / 0.0022$$

$$A_w = 0.0068 \text{ ft}^2 = 0.9818 \text{ inch}^2$$

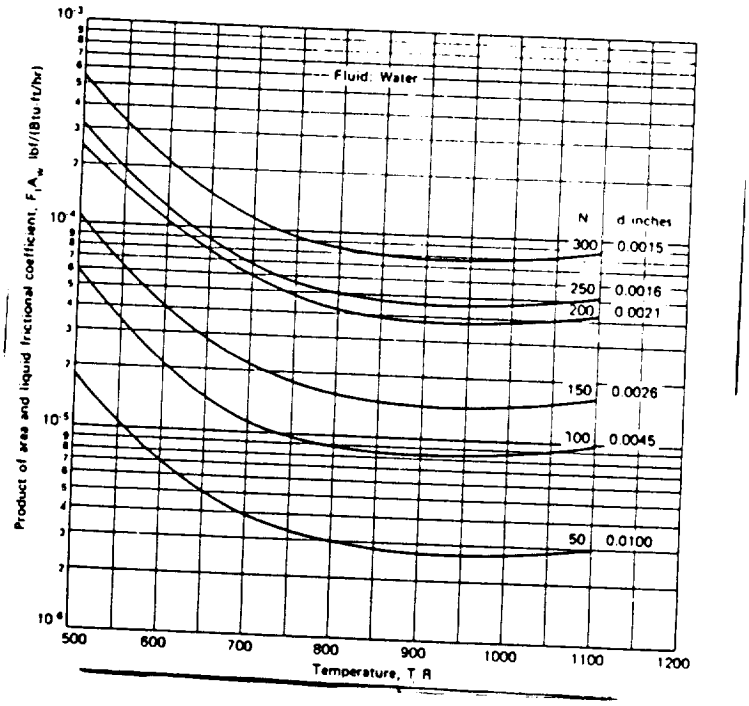

Figure 4.4.3.6 Liquid frictional coefficient for round tubes

Entrainment Limitation Calculation

The entrainment on the axial heat flux is determined by:

$$Q_{e,max} = \lambda A_v \left[(\sigma r_v) / (2r_{h,s})\right]^{1/2}$$

Figure 4.4.3.7 below shows a plot of the above relationship and is used to determine the value of $Q_{e,max}/A_v$ for the designed pipe. The operating temperature and wire mesh number are used as parameters. The value of Q/A_v for the designed heat pipe is 1.78 x 10^5 Btu/hr-in^2. At 670R (212F), a mesh number of 250 and a screen wire diameter of 0.0016 inches will yield a $Q_{e,max}/A_v$ of 2 x 10^5 Btu/hr-in^2.

$$A_v = \Pi\ d_v^2/4$$
$$A_v = \Pi\ (0.075)^2/4$$
$$A_v = 0.0044\ \text{inch}^2$$

$$Q/A_v = 746/0.0044$$
$$Q/A_v = 1.7 \times 10^5\ \text{Btu/hr-in}^2$$

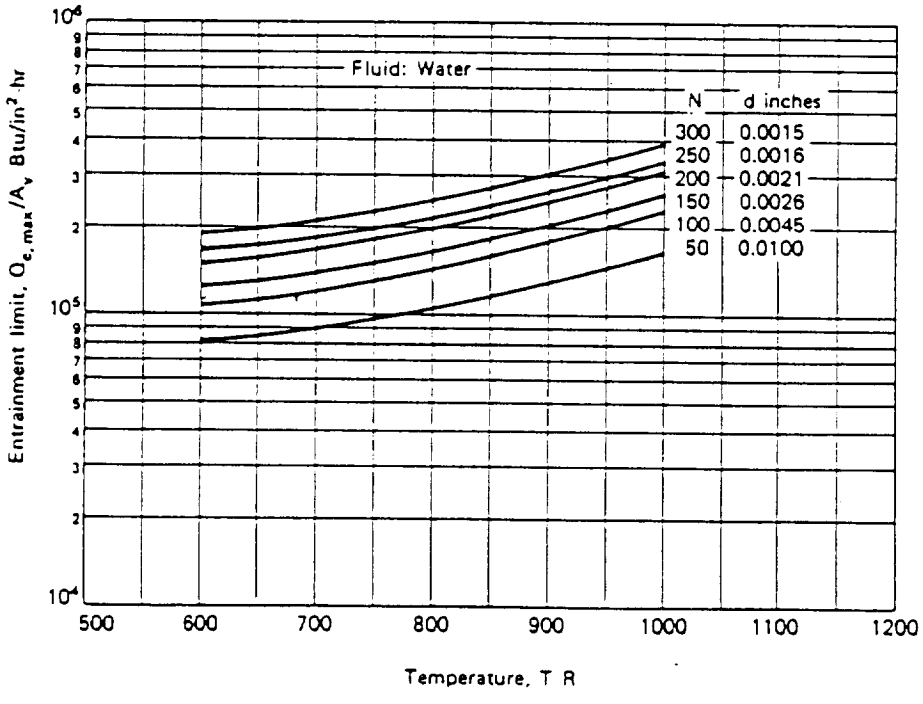

Figure 4.4.3.7 Entrainment limit on axial heat flux density

Boiling Limitation Calculation

The boiling limitation can be represented by:

$$Q_{b,max} = [(2\Pi\ L_e k_e T_v)(2\sigma/r_n)] \ / \ [(\lambda \rho_v\ \ln(r_i/r_v))]$$

Figure 4.4.3.8 below shows a plot of the above relationship to determine $Q_{b,max}/L_e$ for the designed pipe. Using the value of 0.896 for d_i/d_o as the controlling parameter for the plot shows a boiling limitation of 1.5 x 10^4 Btu/ft-hr. The operating value of Q/L_e for this pipe is:

$$Q/L_e = 2362.4/(61/12)$$
$$Q/L_e = 464.75 \text{ Btu/ft-hr}$$

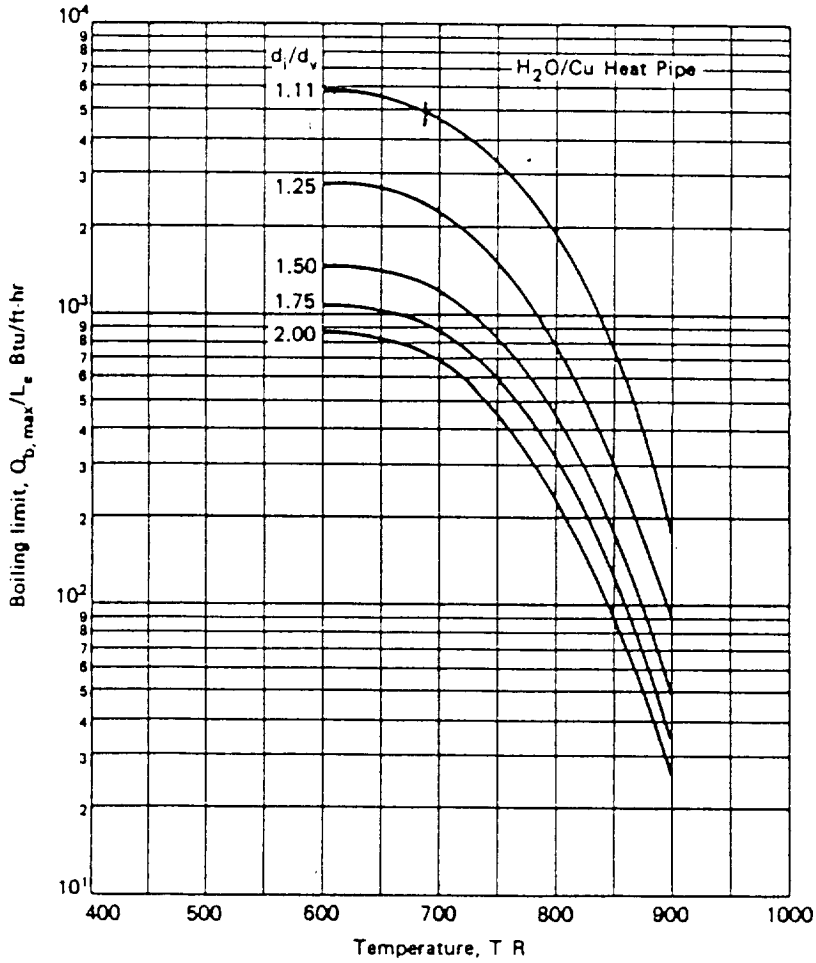

Figure 4.4.3.8 Boiling Limitation

A.5:

Refer to **figure 4.5.11.1**:

Summing Moments about A:

$\Sigma M_a = 0 = F_b(.0826) - (142.5)(.1223)$

$F_b = 210.9$ N

Summing Forces about B:

$\Sigma F_y = 0 = 210.9 - 142.5 - F_a$

$F_a = 68.5$ N

Moment of Inertia at smallest h:

$$I_b = \frac{bh^3}{12} = \frac{(.0095)(.0191)^3}{12} = 5.502e^{-9}\ m^4$$

Largest Moment:

$M_b = (68.5)(.0826) = 5.66$ N m

Largest Tensile Stress:

$$\sigma_{b(flexural)} = \frac{(M_b)(c)}{I} = \frac{(5.66)(.0191)}{5.502e\text{-}9} = 19.64 \text{ MPa} = 2.85 \text{ kpsi}$$

$$\sigma_{b(bearing)} = \frac{F_b}{A_b} = \frac{210.9}{.00009} = 2.34 \text{ MPa}$$

$\sigma_u = 42$ GPa >> 19.64 MPa ; therefore very good!!

This is obviously an over-design, but considering the fatigue loading over the life of the latch and relatively small weight this is justified.

TENSION SPRING DESIGN:

Desired Spring Forces: 8 N when claw is open
5 N when claw is locked

Material: Music Wire (UNS G10850)

Property Constants: m = .146
A = 2170 MPa
G = 79.3 GPa

Desired Geometry: O.D. = 5 mm; d = .8 mm

D = O.D. - d = 4.2 mm

Spring Index: $C = \frac{D}{d} = 5.25$

Shear Stress Mult. Factor: $K_s = 1 + \frac{.5}{C} = 1.095$

Alt. Force: $F_a = \frac{F_{max} + F_{min}}{2} = 3.5$ N

Mean Force: $F_m = \frac{F_{max} - F_{min}}{2} = 1.5$ N

CASE ONE: Static

Max. Shear: $\tau_{max} = K_s \frac{8F_{max}D}{\pi d^3} = 114.4$ MPa

Ult. Strength: $S_{ut} = \frac{A}{d^m} = 2.24$ GPa

Yield Strength: $S_y = .75S_{ut} = 1.68$ GPa

Using Dist.-Energy Theorem: $S_{sy} = .577S_y = 970$ MPa

Static Factor of Safety: $\eta_{static} = \frac{S_{sy}}{\tau_{max}} = 8.48$

CASE TWO: Fatigue
For peened springs from pg. 436 Shigley, 5th edition.

Endurance Limit: $S_{se} = K_a K_b K_c S_{e'} = 465$ MPa

Alt. Shear: $\tau_a = \tau_{max} \frac{F_a}{F_{max}} = 80.1$ MPa

Fatigue Factor of Safety: $\eta_{fatigue} = \frac{S_{se}}{\tau_a} = 5.81$

COMPRESSION SPRING DESIGN:

Desired Spring Forces: 8 N when claw is open
5 N when claw is locked

Material: Music Wire (UNS G10850)

Property Constants: m = .146
A = 2170 MPa
G = 79.3 GPa

Desired Geometry: O.D. = 10 mm; d = .9 mm

Spring Rate: $k = \frac{\Delta F}{\Delta Y} = 600$

Free Length: $L_f = L_1 + \frac{F_1}{k} = 38.3$ mm

$$ND^3 = \frac{d^4 G}{8k} = 1.084e\text{-}5$$

Total # Coils: $N_t < \frac{L_2}{d} = 25$

Active Coils: N = Nt - Nd = 23 ; Nd = # dead coils

Coil Diameter: $D = \left(\frac{ND^3}{N}\right)^{.33} = 1.084e\text{-}5$

Inside Diameter: I.D. = D - d = 6.9 mm

Outside Diameter: O.D. = D + d = 8.7 mm

Compressed Length: $L_s = N_t\, d = 22.5$ mm

Spring Index: C = D/d = 8.65

Shear- Stress Mult. Factor: $K_s = 1 + \frac{.5}{C} = 1.06$

Max. Force: $F_{max} = (L_2 - L_s)\, k + F_2 = 9.5$ N

Max. Shear: $\tau_{max} = K_s \frac{8 F_{max} D}{\pi d^3} = 273$ MPa

Ult. Strength: $S_{ut} = \frac{A}{d^m} = 2.2$ GPa

Yield Strength: $S_y = .75\, S_{ut} = 1.65$ GPa

Using Dist.-Energy Theorem: $S_{sy} = .577\ S_y = 953$ MPa

$\tau > S_{sy}$ therefore it's O.K. to use the .9 mm music wire with both ends ground and squared.

Static Factor of Safety: $\eta_{static} = \frac{S_{sy}}{\tau_{max}} = 3.5$

A.6 ROD CHANGER & STORAGE RACK

Calculations for the arm dimensions:

Constants:

$\rho_{Alum} = 2.99 \frac{Mg}{m^3}$ $\quad S_{sy} = 49{,}000$ psi $= 336$ MPa

$E = 71$ GPa $\quad G = 26.2$ GPa

with safety factor of 2.5: $\quad S_{sy} = 134.4$ MPa

Lower arm (cylindrical):

$$\sigma = \frac{F}{A} = \frac{94.17 \text{ N} + 10 \text{ N}}{134.4 \frac{MN}{m^2}} = 0.775 \text{ mm}^2$$

$$\sigma = \frac{Mc}{I} \qquad \frac{I}{c} = \frac{M}{s} = \frac{5.1 \text{ N m} + 18.06 \text{ N m} + 116.7 \text{ N m}}{134.4 \frac{MN}{m^2}}$$

$$= 1040.4 \text{ mm}^3$$

$$\frac{I}{c} = \frac{\pi d^3}{32} = 1040.4 \text{ mm}^3 \qquad d = 21.97 \text{ mm}$$

set $\quad d = 25$ mm

$$A = \frac{\pi d^2}{4} = 490.9 \text{ mm}^2 > 0.775 \text{ mm}^2$$

$$\text{Vol.} = \frac{\pi l d^2}{4} = 500{,}691 \text{ mm}^3 \qquad W = \rho g V = 14.67 \text{ N} = 2.44 \text{ N (moon)}$$

Pin: $\quad d = 20$ mm $\qquad J = \frac{\pi d^4}{32} = 15.71 \times 10^{-9} \text{ m}^4$

<u>torsion</u> $\qquad \tau_{max} = \frac{Tr}{J} = \frac{(136.86 \text{ N m})(0.01 \text{ m})}{15.71 \times 10^{-9} \text{ m}^4} = 89.03 \times 10^{-6} \frac{N}{m^2}$

<u>deflection</u> $\qquad L = 20$ mm

$$\theta = \frac{TL}{GJ} = \frac{(136.86 \text{ N m})(0.02 \text{ m})}{(26.2 \times 10^9 \frac{N}{m^2})(15.71 \times 10^{-9} \text{ m}^4)} = 0.007°$$

Upper arm (two rectangular sections):

$$A = \frac{F}{\sigma} = \frac{115.17\ N}{134.4\ x\ 10^6\ \frac{N}{m^2}} = 0.859\ mm^2$$

$$\frac{I}{c} = \frac{M}{\sigma} = \frac{139.86\ N\ m}{143.4\ x\ 106\ \frac{N}{m^2}} = 1040.4\ mm^3$$

set cross section 15 mm x 50 mm

$A = 2\ x\ 15\ (50) = 1500\ mm^2$

Vol. = AL = $1500\ mm^2$ (500mm) = $750{,}000\ mm^3 = 7.5\ x\ 10^{-4}\ m^3$

$W = \rho gV = 21.98\ N = 3.66\ N$ (moon)

Stress concentration:

d = 20 mm w = 50 mm h = 20 mm

A = (w - d)t = (50 mm - 20 mm) 15 mm = $450\ mm^2$

$$\sigma_0 = \frac{F}{A} = \frac{120\ N}{450\ mm^2} = 2.67\ x\ 10^5\ \frac{N}{m^2}$$

$$\frac{d}{w} = \frac{20\ mm}{50\ mm} = 0.4 \qquad \frac{h}{w} = \frac{20\ mm}{50\ mm} = 0.4$$

Look up $\frac{d}{w}$ and $\frac{h}{w}$ on stress concentration graph.
Resulting Kt = 3.5

$$\sigma_{max} = K_t\sigma_o = 3.5(2.67\ x\ 10^5\ \frac{N}{m^2}) = 9.34\ x\ 10^5\ \frac{N}{m^2}$$

Deflection:

Upper arm: $x_{max} = \frac{FL^3}{3EI} = \frac{(279.72\ N)(0.5\ m)^3}{3(71\ x\ 10^9\ \frac{N}{m^2})(312{,}500\ x\ 10^{-12}\ m^4)}$

$= 0.0005\ m = 0.5\ mm$

$$y_{max} = \frac{FL}{EA} = \frac{(115.17\ N)(0.5\ m)}{(71 \times 10^9 \frac{N}{m^2})(0.0015\ m^2)}$$

$$= 5.407 \times 10^{-7}\ m = 0.00054\ mm$$

Lower arm:

$$y_{max}\ (\text{when horizontal}) = \frac{FL^3}{3EI}$$

$$= \frac{(137.18\ N)(1.02\ m)^3}{3(71 \times 10^9 \frac{n}{m^2})(312{,}500 \times 10^{-12}\ m^4)}$$

$$= 0.0022\ mm = 2.2\ mm$$

$$x_{max}\ (\text{when vertical}) = \frac{FL}{EA}$$

$$= \frac{(104.17\ N)(1.02\ m)}{(71 \times 10^9 \frac{N}{m^2})(0.00049\ m^2)}$$

$$= 3.054 \times 10^{-6}\ m = 0.00305\ mm$$

ROTATING BAR CALCULATIONS

DIMENSIONS

$$S_{max} = \frac{W_{ac} + Mc}{I}$$

where:

Smax = maximum resultant stress = Ssy/1.5
a = distance from arm attachment to bearing attachment
W = the point load from the arm
M= the resulting moment from the arm
c= 1/2 the beam thickness
I = moment of inertia

$$I = \frac{bh^3}{12}$$

where:

b = 2c
h = 2b

therefore:

$$I = 16/12(c)^4$$

now:

$$c^3 = \frac{1.5}{Ssy} \frac{12(Wa + M)}{16}$$

where:

Ssy = 338 MPa
W = 115.17 N
M = 138.86 N
a = 0.425m

substituting values:

$c^3 = 6.2 \times 10^{-7}$m
$c = 8.5 \times 10^{-2}$m
b = 1.7cm
h = 3.4cm

DEFLECTION:

FORCE DEFLECTION:

$$ymax = \frac{-W}{6EI}(3a^2 - L - a^3)$$

where:

$$E = 71 \text{ GPa}$$
$$L = .5\text{m}$$

Note: all other values are the same as above

substituting:

$$y_{max} = (-1/6)(115.17/[(71x10^9)(6x10^{-8})](3(.425)^2-.5-(.425)^3)$$

y_{max} for force = 0.0052 m

MOMENT DEFLECTION:

$$y_{max} = (Ma/EI)(L - 1/2(a))$$

substituting:

$$y_{max} = [(138.86)(.425)]/[(71x10^9)(6x10^{-8})][.5 - 1/2(.425)]$$

y_{max} for the moment = .0094 m

TOTAL DEFLECTION = 1.4cm

STORAGE RACK

DIMENSIONS:

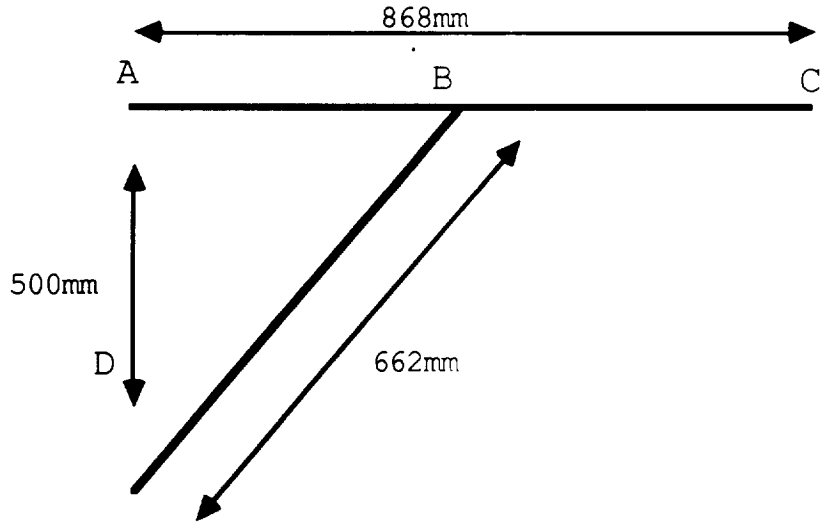

FORCE CALCULATIONS:

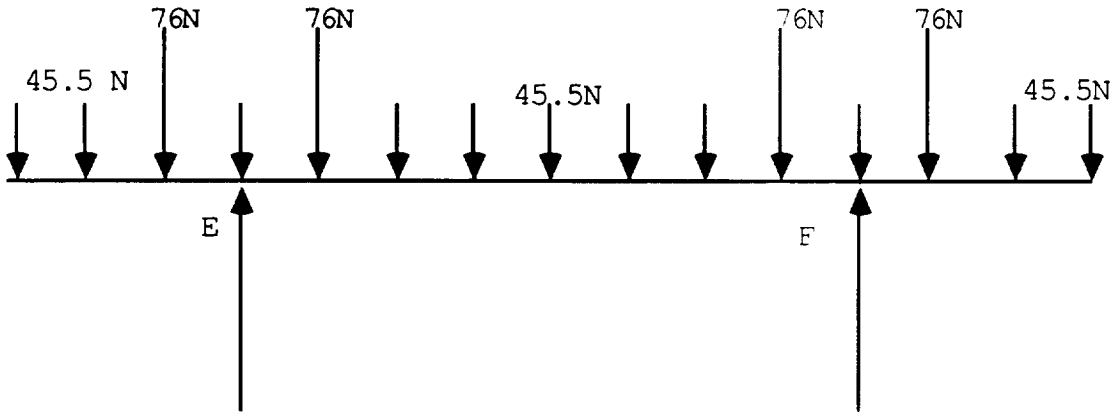

10 rods x 43.6 N/rod = 436N

4 impl. x 76 N/impl. = 304N

Total = 740N

Each of the two support rods must withstand 370N.

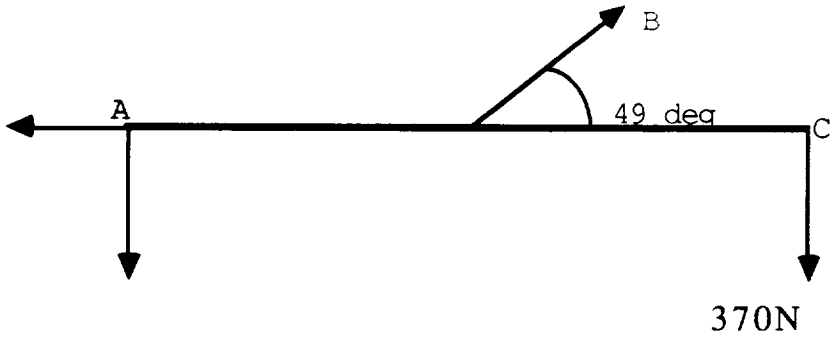

To find the forces at A and B, sum of moments and forces equations were used.

$$M_A = B(.434m)\ \sin(49) - 370N(.868m) = 0$$
$$B = 980.5N$$

$$F_y = B\ \sin(49) - A_y - 370 = 0$$

$$A_y = 370N$$

$$F_x = B\ \cos(49) - A_x = 0$$

$$A_x = 643.3N$$

Rod BD is a two force member in compression. The force on this rod is 980.5N. The forces in the members that counter the moment created by placing rods into the rack are are magnitudes smaller (34N) than the forces of the implements themselves that they are negliable.

Stress Calculations:

The arc was approximated as a straight beam for the stress calculations. The maximum bending stress will occur at the supports.

$$M_{max} = 45.5(.28 + .42) + 76(.14)$$

$$M_{max} = 42.49\ \text{N-m}$$

the shear stress is :

$$\sigma = 32(M)/\pi(d)^3$$

$$\sigma = 32(42.49)/\pi(d)^3$$

Set this shear stress equaton to the maximum shear stress divided by the safety factor (2) and solve for the diameter (d).

$$S = S_{sy}/2$$

$$S = 316 \text{ MPa}$$

$$316 = 32(42.49)/\pi(d)^3$$

$$d = 11 \text{ mm}$$

The moment created by placing a rod into a spring clip is 14.28N-m is much less than the moment created by the weight of the rods so the stress calculations have been neglected.

The maximum bending moment on the top beam of the support structure occurs at the center. And is calculated as follows

$$M_{max} = 340(.434)$$

$$M_{max} = 147.6 \text{ N-m}$$

The stress was calculated using the same technique as above and then d is solved for.

$$S = 32(147.6)/\pi(d)^3$$

$$S_{max} = 316 \text{ MPa}$$

$$316 = 32(147.6)/\pi(d)^3 \qquad d = 16.8\text{mm}$$

This beam is also in tension do to the angle of the support beam below it so a tension calculation must be done. The force on the beam is divided by the area of the beam.

$$\sigma = P/A$$

$$\sigma = 147.6/\pi(d)^2$$

The ultimate tensile stress is then divided by the safety factor(2) and the result is the maximum allowable tensile stress.

$$S_{max} = 1461 \text{ MPa}/2$$

$$S_{max} = 730.5 \text{ MPa}$$

This value is then pluged in the equation above and the diameter is solved for.

$$730.5 = 147.6/\pi(d)^2$$

$$d = 1\text{mm}$$

The diameter is taken to be 16.8mm because it is the greatest. the next diameter that is needed s the lower support beam. This beam is in compression and the greatest concern is with buckling. The beam is assumed to be a Johnson column and this will be checked later. The first calculation is for the constant 'b'.

$$b = (S_y/2\pi)^2/CE$$

C - end conditions constant
E - Young's Modulus
S_y - Yield strength

$$b = (1096/2\pi)^2/(1.2)(206000) = 0.123$$

This is then pluged in to the Johnson equation

$$S = S_y - b(l/k)^2$$

$$S = 1096 - .123(l/k)^2 \qquad k=d/4$$

The stress on this beam is then calculated by dividing the force by the area of the beam.

$$S = 980/\pi(r)^2$$

$$S = 1248.4/d^2$$

Plug this into the equation above and solve for the diameter.

$$.001248.4/d^2 = 1096 - (1.48/d^2)$$

$$d = 36.8mm$$

Deflection:

The curved beam was approximated to be a straight beam for the deflection calculations. The deflection of the ends of the arc were calaculated as follows.

$$y = (1/12)(SL^2)/(Ec)$$

S - shear strength
L - length of the bar
E - Young's Modulus
c - distance to the center of the bar

$$y = (1/12)(316)(.42)^2/(207000)(.011)$$

$$y = 2mm$$

The deflection at the cented of the beam is calculated using the same formula but the moment and the shear at the center must be calculated first.

$$M = 45.5(.14 + .28 + .56 + .84 + .98) + 76(.42 + .7) - 370(.56)$$

$$M = 5.32 \text{ N-m}$$

$$S = 32(5.32)/pi(.011)^3$$

$$S = 40$$

$$y = (1/2)(316)(40)(1.12)2/(207000)(.011)$$

$$y = 1.8\text{mm}$$

The support structure is next

$$y = (1/12)(316)(.868)^2/(20700)(.017)$$

$$y = 5.6\text{mm}$$

Weight Calculations:

		Volume
Curved beam:	$2.1(\pi(.011)^2/4)$	$= .0002\ m^3$
Top Beam:	$.868(\pi(.017)^2/4)$	$= 2(0.00019\ m^3)$
Bottom Beam:	$.662(\pi(.0368)^2/4)$	$= 2(0.0007\ m^3)$
		Total $= .00199\ m^3$

Weight = V(p)
= (.00199)(2840)
= 5.65 kg (per section)

A.7 MACROCORE RETRIEVAL

Mass of Core Sample

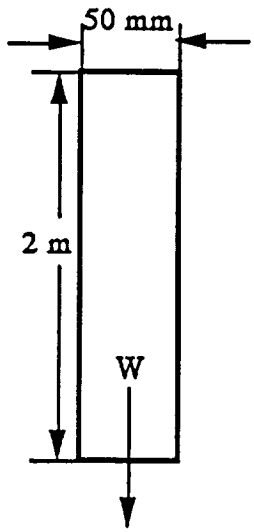

Basalt

ρ = #

V = π (r^2) L

m = ρ V

g = 9.8 m/s^2 (Earth)

W = m g (Earth)

W = m g / 6 (Moon)

ρ = 2.9 g/cm^3

V = π (5 cm)^2 (200 cm) = 15,708 cm^3

M = (2.9 g/cm^2)(15708 cm^3) = 45,553 g = **45.553 kg**

A.7 MACROCORE RETRIEVAL

Mass of Retriever:

Material: Ti - 5Al - 2.5Sn
$\rho = 4.46$ g/cm^3

Outer Shell:
$V = \pi (r^2) L = \pi [(5 \text{ cm})^2 - (4.7 \text{ cm})^2](200\text{cm})$
$= 1828.41$ cm^3
$M = \rho V = (4.46 \text{ g/cm}^3)(1828.41 \text{ cm}^3)$
$= 8154.69$ grams

Inner Shell:
$V = \pi (r^2) L = \pi [(2.8 \text{ cm})^2 - (2.5 \text{ cm})^2](200\text{cm})$
$= 999.03$ cm^3
$M = \rho V = (4.46 \text{ g/cm}^3)(999.03 \text{ cm}^3)$
$= 4455.66$ grams

Single Support Beam:
$V = Lwh = (200 \text{ cm})(1.9 \text{ cm})(.2 \text{ cm}) = 76$ cm^3
$M = \rho V = (4.46 \text{ g/cm}^3)(76 \text{ cm}^3)$
$= 338.96$ grams

Single Mechanism (Model as Solid Block):
$V = Lwh = (2.1 \text{ cm})(1.5 \text{ cm})(.2 \text{ cm}) = 6.3$ cm^3
$M = \rho V = (4.46 \text{ g/cm}^3)(6.3 \text{ cm}^3)$
$= 28.098$ grams

Total Mass of Retriever:
$= 8154.69 \text{ g} + 4455.66 \text{ g} + (3 \times 338.96 \text{ g}) + (3 \times 28.098 \text{ g})$
$= 13{,}711.52$ g
$=$ **13.71 kg**

A.7 MACROCORE RETRIEVAL

Simple Buckling of Outer Shell

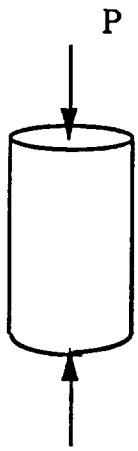

$I_o = J/2 = \pi r_{avg}^3 \tau = \pi (4.85 \text{ cm})^3 (3\text{cm}) = 1075.21 \text{ cm}^3$

$P_{cr} = \pi^2 E I_o / 4L^2 = \pi^2 (7.586 \times 10^7 \text{ Pa})(10.7521 \times 10^{-6} \text{ m}^4)/4(2 \text{ m})^2$
$= 503.14 \text{ N}$

A.7 Macrocore Retrieval

Spring Design:

Assumptions:

Cutting Force = 50lbs
Cutting Stroke = 1.0cm
Width of spring = 1.0cm

Material is UNS461500
m=.167
A = 167kpsi
$G=11.5 \times 10^6$psi

Ultimate and Shear Strength

$Sut = A/d^{.167}$
$= 169kpsi/d^{.167}$

$Sy = .75(Sut)$ $Ssy = .577Sy$
$Ssy = (.577)(.75)Sut$
$Ssy = 73.135kpsi/d^{.167}$

Diameter of wire(d) and spring(D)

$Ssy = \tau = 8FD/\pi d^3(1+.5/C)$

$C = D/d$
$D = 1.0/2.54 - d$
$C=(1.0/2.54 - d)/d$

$73.135/d^{.167} = [8(50)(1.6/2.54-d)/\pi d^3]\ [1+.5(1.0/2.54-d)/d]$

by iteration **d = .07379 in. = .0019 m**
D = 1.0/2.54 - d = 3.199 in. = .0813 m

Number of Coils in the Spring (N_t)

fully compressed $N = N_t + N_c$
$N_t = (1.6/2.54)/d$
N_t = 8.5 turns

Squared and Grounded ends
N_c = 2 turns
N = 6.5 turns

Minimum Forces during cutter stroke

$K = d^4G/8D^3N = (.07379)^4(11.5 \times 10^6)/8(.3199)(6.5)$

K= 20.5 lbs/in. = 2.32 N/m

force when gripper should touch

F= 50lb. - K(1.0/2.54)

Fmin = 41.93 lbs = 186.59 N

Conclusion

Diameter of coil (D) = 3.199 in. = .0813
Diameter of wire (d) = .0738 in. = .0019 m
Number of coils (N_t) = 8.5 turns
Spring Constant (K) = 20.5 lbs/in. = 2.32 N/m
Fmin = 41.93 lbs = 186.59 N
Fmax = 50.0 lbs = 222.5 N

A.7 Macrocore Retrieval

Reset Gear Design:

Assumptions:

Tangential Force:	W_t = 50 lbs = 222.5 N
Pressure Angle:	$\phi = 20^o$
Number of Teeth:	N = 18
Pitch Diameter:	d = 2 cm = .7874 in

Velocity Factor:

Assume V = 1 in/sec = 5 ft/min

$K_V = 50/(50 + V^{0.5})$ (Hobbed Gears)

$= 0.957$

Y = 0.29327 (From Shigley & Mitchell)

Face Width:

$$F = W_t P/K_V Y \sigma_p = (50 * 22.86)/((0.957 * 0.29327) * \sigma_p)$$

$3p = \text{Face Width}_{min} = 0.412$ in

$5p = \text{Face Width}_{max} = 0.687$ in

(σ_p: permissible bending stress = $S_y/4$

where 4 = safety factor)

A.7 Macrocore Retrieval

From Face Width Criterion:

S_{Pmax} = 9884.75 psi

S_{Pmin} = 5926.25 psi

Therefore, S_y range = 23705 psi to 39539 psi
= 163 MN/m^2 to 272 MN/m^2

Gear Properties:

N = 18 Teeth

P = 22.86

Φ = 20°

d = 0.7874 in = 2 cm

A.7 Macrocore Retrieval

Pin Design:

Contact Points:

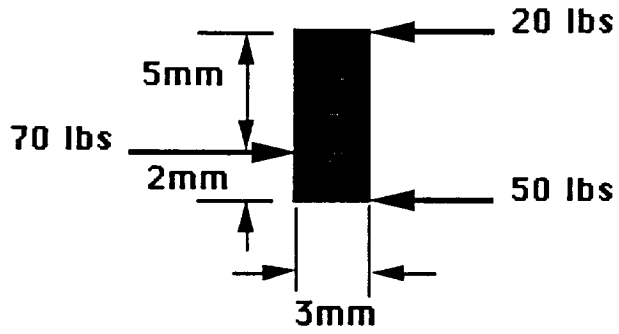

$I = \pi d^4/64 = \pi(.3/2.54)^4/64 = 9.5525 \times 10^{-6}\ in^4$

M_{max} = 50lbs x 5mm x (cm/10mm) x (in/2.54cm)
= 9.84in-lbs

$\sigma = Mc/I = (9.84in\text{-}lbs \times (.15/2.54)in) / 6.552 \times 10^{-6}\ in^4$
$= 6.083 \times 10^4$ psi = 419 MN/m^2

A.7 Macrocore Retrieval

Breaking the Core Sample:

Using Tension:

$F_{min} = \sigma_t \times A = (1kpsi)(3.043in^2) = 13.5kN$

$F_{max} = \sigma_t \times A = (4kpsi)(3.043in^2) = 54.1kN$

Using Torsion:

$T_{min} = (\tau \times \pi \times d^3)/16 = (2kpsi)(\pi)(.05m)^3/16 = 338.2Nm$

$T_{max} = (\tau \times \pi \times d^3)/16 = (8kpsi)(\pi)(.05m)^3/16 = 1352.9Nm$

Using Bending:

$Fmin = \sigma \times I/L*c = (2kpsi)(3.07x10^{-4})/(2m)(.025m) = 84.6N$

$Fmax = \sigma \times I/L*c = (8kpsi)(3.07x10^{-4})/(2m)(.025m) = 338N$

Table 4.7.6.1: FORCE NEEDED TO BREAK CORE SAMPLE
USING TENSION: F = St *A

Core Diameter (mm)	Area (m^2)	Fmin St = 1kpsi (N)	Fmax St = 4kpsi (N)
50	1.96E-03	13,528.52	54,114.06
45	1.59E-03	10,958.10	43,832.39
40	1.26E-03	8,658.25	34,633.00
35	9.62E-04	6,628.97	26,515.89
30	7.07E-04	4,870.27	19,481.06
25	4.91E-04	3,382.13	13,528.52
20	3.14E-04	2,164.56	8,658.25
15	1.77E-04	1,217.57	4,870.27
10	7.85E-05	541.14	2,164.56
5	1.96E-05	135.29	541.14

Table 4.7.6.2: TORQUE NEEDED TO BREAK CORE SAMPLE
USING TORSION: T = Tau*Pi*d^3 /16

Core Diameter (mm)	d^3 (m^3)	Tmin Tau = 2kpsi (N-m)	Tmax Tau = 8kpsi (N-m)
50	1.25E-04	338.21	1,352.85
45	9.11E-05	246.56	986.23
40	6.40E-05	173.16	692.66
35	4.29E-05	116.01	464.03
30	2.70E-05	73.05	292.22
25	1.56E-05	42.28	169.11
20	8.00E-06	21.65	86.58
15	3.38E-06	9.13	36.53

Table 4.7.6.3: FORCE NEEDED TO BREAK CORE SAMPLE USING BENDING: F = (Sb*I) / (L*c)

Core Diameter (mm)	Moment of Inertia (m^4)	Fmin Sb= 2kpsi (N)	Fmax Sb = 8kpsi (N)
50	3.07E-07	84.5532	338.2129
45	2.01E-07	55.4754	221.9015
40	1.26E-07	34.6330	138.5320
35	7.37E-08	20.3012	81.2049
30	3.98E-08	10.9581	43.8324
25	1.92E-08	5.2846	21.1383
20	7.85E-09	2.1646	8.6582
15	2.49E-09	0.6849	2.7395
10	4.91E-10	0.1353	0.5411
5	3.07E-11	0.0085	0.0338

A.7 Macrocore Retrieval

Failure $K = K_C$

$K_C = 3\ MN/m^{1.5}$ for Granite

$K = \sigma \times (\pi \times a)^{0.5}$

$\sigma = K / (\pi \times a)^{0.5} = (3\ MN/m^2)/(\pi \times .001m) = 53.52\ MN/m^2$

where $a = .001m$

$A = \pi \times r^2 = \pi \times (.025m)^2 = 1.96 \times 10^{-3}\ m^2$

where $r = .025m$

$F = \sigma \times A = 54MN/m^2 \times .00196m^2 = 105.8kN$

where $\sigma = 54MN/m^2$

Friction Force (Gripper)

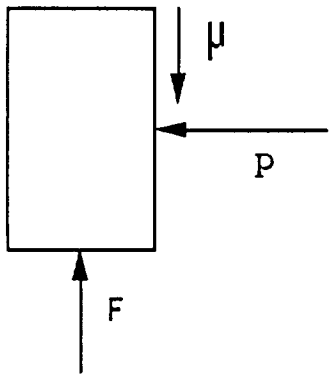

$P = F / \mu_S = (10\ lbs) / (0.1) = 100\ lbs = 445\ N$

Material - Granite (Westerly)
Kc = 3 MN/m^(3/2)
K = Sigma * (pi*a)^(1/2)
Failure K = Kc

a (mm)	Sigma (MN/m^2)
1	53.52
2	37.85
3	30.90
4	26.76
5	23.94

A = pi*r^2

radius (mm)	Area, A (mm^2)	Area (m^2)
25	1,963.50	1.96E-03
23	1,661.91	1.66E-03
21	1,385.45	1.39E-03
19	1,134.12	1.13E-03
17	907.92	9.08E-04

Table 4.7.6.4: Force Calculation with Varying Stress Concentration

F = Sigma * Area

Force (MN)		Area (m^2)				
		0.00196	0.00166	0.00139	0.00113	0.000908
Sigma (MN/m^2)	54	0.10584	0.08964	0.07506	0.06102	0.049032
	38	0.07448	0.06308	0.05282	0.04294	0.034504
	31	0.06076	0.05146	0.04309	0.03503	0.028148
	27	0.05292	0.04482	0.03753	0.03051	0.024516
	24	0.04704	0.03984	0.03336	0.02712	0.021792

Friction Force (Gripper)

P = Coefficient of Friction * Force

P (lbs)		Force (lbs)				
		10	11	13	15	17
Coef. of Fric.	0.1	100.0	110.0	130.0	150.0	170.0
	0.2	50.0	55.0	65.0	75.0	85.0
	0.3	33.3	36.7	43.3	50.0	56.7
	0.4	25.0	27.5	32.5	37.5	42.5
	0.5	20.0	22.0	26.0	30.0	34.0

P (N)		Force (N)				
		44.5	48.95	57.85	66.75	75.65
Coef. of Fric.	0.1	445.0	489.5	578.5	667.5	756.5
	0.2	222.5	244.8	289.3	333.8	378.3
	0.3	148.3	163.2	192.8	222.5	252.2
	0.4	111.3	122.4	144.6	166.9	189.1
	0.5	89.0	97.9	115.7	133.5	151.3

* 1 pound = 4.45 Newtons

A.8 CONTROLS

There are no sample calculations available from the controls group.

A.9 VERTICAL ACCELERATOR

Bearing Analysis

The following is the analysis of the maximum load on the cam bearings:

Weight of full drill string = 245 N (on moon)
Acceleration of drill string (maximum) = 3277 mm/s^2
Maximum force to accelerate drill string

$$F = ma = \left(\frac{245\ N}{1646\ \left(\frac{m\ m}{s^2}\right)}\right) \cdot \left(3277\ \frac{m\ m}{s^2}\right)$$

F_{max} = 487 N

Because the roller follower is being pushed at a maximum of a 30 deg. pressure angle it actually reacts to a larger force.

$$F_{max} = \frac{487\ N}{\cos(30^o)} = 562\ N$$

Maximum force on any one roller is then half of this total force.

F_{roller} = 281 N

Load rating:

$$C_R = F_{roller} \cdot \left(\left(\frac{L_D}{L_R}\right) \cdot \left(\frac{n_R}{n_D}\right)\right)^{1/a}$$

Using an L_{10} life of 5000 hr and design rpm of 450:
L_R = 3000 hr
n_R = 500 rpm
L_D = 5000 hr
n_D = 450 rpm
a = 10/3

$$C_R = 281\ N \bullet \left(\left(\frac{5000}{3000}\right) \bullet \left(\frac{450}{500}\right)\right)^{3/10}$$

$C_R = 317.5\ N$

The roller followers have a much higher load rating than the computed one estimated by Torrington; so the roller follower life should last through about 450 fifty meter holes, but we oversized the follower for about ten times that amount. Since there are extreme operating temperatures on the moon going as low as -158 °C at night, lubricants would just evaporate, therefore, the bearings used are designed without the need for any lubrication.

Shaft Analysis:

$Diameter_{min} = 25\ mm$
$T_{max} = 28.6\ N\text{-}m$
$Moment = 0$
$S_y = 827\ MPa$
$n = ?$ (factor of safety)

Using a basic static failure analysis and solving for n (factory) gives,

$$d = \left(\frac{32n}{\pi}\left(\frac{M_a}{S_y} + \frac{0.866T}{S_y}\right)\right)^{1/3}$$

$$n = \frac{d^3 S_y \pi}{0.866(32)T}$$

$$n = \frac{(1)^3(827\ MPa)(3.14)}{0.866(32)(28.6)}$$

$n = 645$ Factor of safety

A.10 Microcore Retrieval

CAM DESIGN

Simple Harmonic Rise $y = (1 - \cos \pi\phi/\beta) * L/2$

Simple Harmonic Full Return $y = (1 + \cos \pi\phi/\beta) * L/2$

$\beta = 150$ L = 5 mm $0 <= \phi <= 360$

Stations	f	y (mm)
0	0	0
1	30	.477
2	60	1.727
3	90	3.273
4	120	4.523
5	150	5.000
6	180	5.000
7	210	5.000
8	240	4.523
9	270	3.273
10	300	1.727
11	330	.477
12	360	0

$y = 2.5 * (1 - \cos 1.2\phi)$

$y = 2.5 * (1 + \cos 1.2\phi)$

Lift vs. Rotational Angle

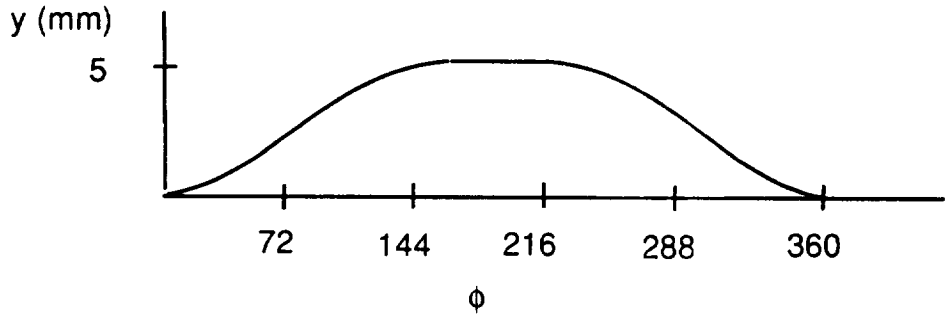

APPENDIX B

DESIGN ALTERNATIVES

B.1 BIT

There are no design alternatives available from the bit group.

B.2 Design Alternatives for Rod, Auger, and Stepped Auger

B.2.1 Rod

A solid rod cross section was considered for strength and fracture toughness but rejected because of weight considerations.

B.2.2 Rod Interface

A rod interface design which was identical for both top and bottom ends of the rod was considered (see drawing in progress report). This design was rejected because the collar required for the coupling could not be coupled by the rod changer (see Fig.D.4.2.1).

B.2.3 Vertically Reciprocating Auger Design

Several pitch and fence height configurations were considered but rejected to achieve a suitable balance between throughput and volume retention.

B.2.4 Vertically Reciprocating Auger Interface

An interface with a continuous helix was considered but rejected because no suitable method for coupling could be arrived at given the abilities of the rod changer. Ignoring the VRA interface by using only a single VRA incorporated in the bit segment was considered but rejected because the volume retention was much too low for 2 m of drilling.

B.2.5 Motor Interface

A motor interface which was identical to the rod interface but utilized a collar which was actuated from above was considered. Although rejected this design is probably more practical than the current MMI design.

Fig. D.4.2.1

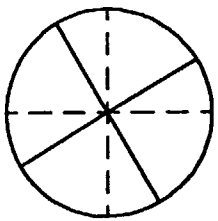

TOP VIEW

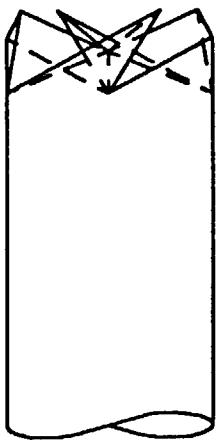

FRONT AND SIDE VIEW

GEORGIA TECH COLLEGE OF ENGINEERING
TITLE: ROD INTERFACE
DESIGN: DATE
CHECK: DATE
DRWG NO.

B.3 FOOTPLATE

A different design utilizing a tool chuck (like those on power drills) with rotary clock springs was also considered, but turned down. The outer housing is fixed to the plate while the center of the chuck rotates, opening and closing the chuck jaws on the drill string. A series of clock springs, acting independent of each other would provide opening and closing power for the chuck. Mechanical power for energizing the springs would be provided by the drive at the bottom of its stroke as it meshes with the rotating part of the chuck. A spring is de-energized by the flip of a lever, but does not cause the other springs to de-energize, hence the independence. The design would be very complex and difficult to seal from the lunar environment, but would have offered the advantage of not requiring a battery and motor to provide mechanical power. The design of the chuck, as it appears on the patent, is attached.

United States Patent [19]
Dietzen et al.

[11] 3,949,998
[45] Apr. 13, 1976

[54] TOOL CHUCK

[75] Inventors: William H. Dietzen, Fayetteville, N.C.; Stephen J. Ehrlich, Owings Mills, Md.

[73] Assignee: The Black and Decker Manufacturing Company, Towson, Md.

[22] Filed: May 2, 1973

[21] Appl. No.: 356,615

Related U.S. Application Data

[63] Continuation of Ser. No. 126,472, March 22, 1971, abandoned.

[52] U.S. Cl. ..... 279/62; 279/1 ME
[51] Int. Cl.² B23B 31/04
[58] Field of Search ..... 279/60, 61, 62, 63, 64, 279/65, 1 K, 1 ME

[56] References Cited

UNITED STATES PATENTS

3,162,164	8/1969	Wightman	279/62
3,810,642	5/1974	Derbyshire	279/62

FOREIGN PATENTS OR APPLICATIONS

435,216	5/1948	Italy	279/62
1,255,450	11/1967	Germany	279/62

Primary Examiner—Willie G. Abercrombie
Assistant Examiner—Z. R. Bilinsky
Attorney, Agent, or Firm—Joseph R. Slotnik; Edward D. Murphy; Leonard Bloom

[57] ABSTRACT

A tool chuck for drills and the like including a body having gripping jaws slideably supported in tapered ways formed in the body. A split nut rotatably supported on the body threadedly engages the jaws and is operable to engage and release the jaws from a bit. The nut and body are interfitted to rotatably support and axially retain the nut on the body. A cup is fitted on the nut to hold it together and on the body and, together with the interfitted body and nut, protects the internal chuck parts from dirt and other foreign material.

17 Claims, 4 Drawing Figures

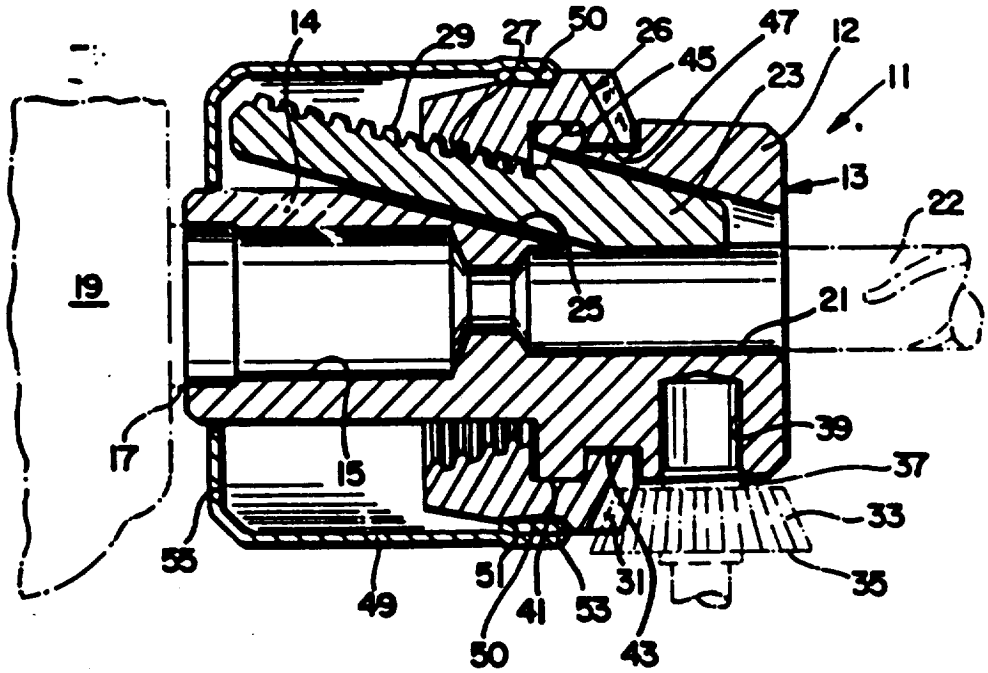

B.4 POWER SUPPLY, ROTARY DRIVE, AND HEAT MANAGEMENT

Design alternatives considered but discarded are listed below with a brief reason for their rejection.

1) Rechargeable Batteries: Silver-zinc batteries were considered for the application, but proved to be far too heavy for the design.

2) On-board Solar Panels: The power requirements made this alternative not feasible.

3) Gearing for the Motor: Gearing proved to be unnecessary since a motor could be designed which would meet all of the design requirements.

B.5 STRUCTURE AND MECHANICAL INTERFACE

There are no design alternatives available from the structure and mechanical interface group.

B.6 ROD CHANGER AND STORAGE RACKS

The first mechanical gripper to be used as a proposal was a gripper that had one jaw in a fixed position. The other parallel jaw would move by means of a lead screw towards the fixed jaw. This type of gripper could accommodate both size diameters of digging implements, 50 mm and 100 mm. The problem this design created was that these different shaped digging implements could not both be held on the center line of the gripper. The robot arm will have a fixed position to travel to for each individual clip. This position would not be the correct position for the rod storage if the rod was off center while in the grasp of the gripper. A control problem would arise if for every different size rod, the robot arm position would change. The design we chose held the different size rods on the center line of the gripper.

Another gripper design had parallel jaws with two lead screws. The gripper would be powered by a motor turning these right-handed and left-handed threaded lead screws. When the lead screws turned the two female threaded jaws, the rotating motion would be translated into linear motion. The two parallel jaws would approach each other in a clamping motion. This design was not chosen because of the fact that it has two lead screws. Our simplified design only has one lead screw. The width of this gripper design is wider than the chosen design. The smaller design in width will enable the rack to hold more rods. This is because the gripper requires clearance to move in between the rods.

Another gripper design used a fixed body and a rotating arm. The gripper had a U shape body that was stationary. The U shape had a radius of 50 mm to hold the 100 mm digging implements. The rotating arm was driven by gears. This gripper needed a curved slot cut into it for the 50 mm rods. This slot would position the smaller rods so that they were on the center line of the gripper. This design was not used because the chosen design was less complex. This gripper design would also drop whatever it was carrying because the gears would turn, reducing the force on the gripped object if there

was a loss of power to the motor. This design would not be a non-overrunning system.

These gripper designs originally had sensors to detect the force exerted by the gripper on the rods. A simpler way of measuring the amperage required by the gripper to detect when the gripper was closed with the proper force was used.

As stated in the materials section titanium, particularly the Ti-4V-6AL alloy was considered as a structural material. It has similiar properties to the aluminum alloy chosen. However it is heavier, and costs quite a bit more than aluminum. The titanium alloys are difficult to weld and are not readily available in many forms. The properties of the aluminum are sufficient for our design.

Two clip designs were considered, both based on clips made by Gibson Good Tools. The first design considered was a u-shape where each side bends back on itself. This design was refected because of excess material and the design used was easily approximated as a cantilever beam, thus simplifying the calculations required. Also the accepted design more easily accomodates for drilling implements of differing sizes.

Design Matrix

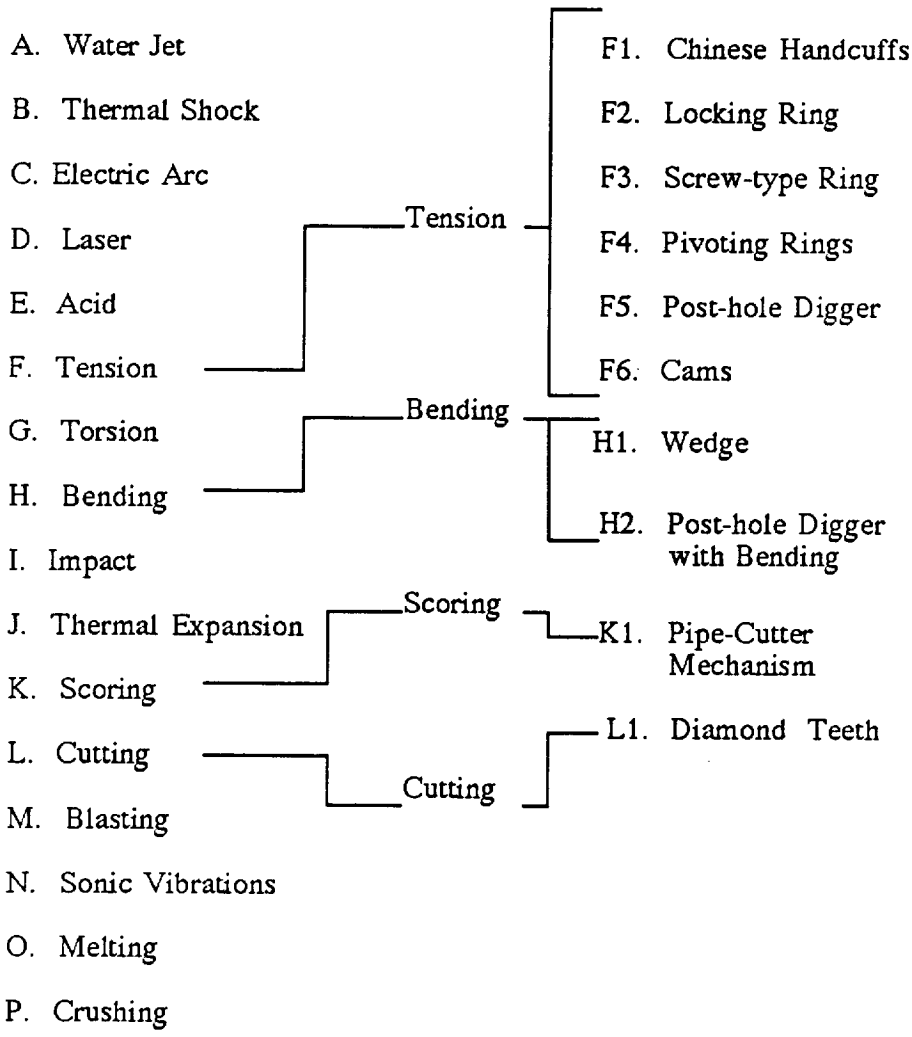

B.6 DESIGN ALTERNATIVES

Gripper

The first mechanical gripper proposed was a gripper that had one jaw in a fixed position. The other parallel jaw would move by means of a lead screw towards the fixed jaw. This type of gripper could accommodate both size diameters of digging implements, 50 mm and 100 mm. The problem this design created was that these different shaped digging implements could not both be held on the center line of the gripper. The robot arm will have a fixed position to travel to for each individual clip. This position would not be the correct position for the rod storage if the rod was off center while in the grasp of the gripper. A control problem would arise if for every different size rod, the robot arm position would change. The design we chose held the different size rods on the center line of the gripper.

Another gripper design had parallel jaws with two lead screws. The gripper would be powered by a motor turning these right-handed and left-handed threaded lead screws. When the lead screws turned the two female threaded jaws, the rotating motion would be translated into linear motion. The two parallel jaws would approach each other in a clamping motion. This design was not chosen because of the fact that it has two lead screws. Our simplified design only has one lead screw. The width of this gripper design is wider than the chosen design. The smaller design in width will enable the rack to hold more rods. This is because the gripper requires clearance to move in between the rods.

Another gripper design used a fixed body and a rotating arm. The gripper had a U shape body that was stationary. The U shape had a radius of 50 mm to hold the 100 mm digging implements. The rotating arm was driven by gears. This gripper needed a curved slot cut into it for the 50 mm rods. This slot would position the smaller rods so that they were on the center line of the gripper. This design was not used because the chosen design was less complex. This gripper design would also drop whatever it was carrying because the

gears would turn, reducing the force on the gripped object if there was a loss of power to the motor. This design would not be a non-overrunning system.

These gripper designs originally had sensors to detect the force exerted by the gripper on the rods. A simpler way of detecting this was to measure the amperage required by the gripper to close with the proper force.

Materials

As stated in the materials section titanium, particularly the Ti-4V-6AL alloy, was considered as a structural material. It has properties similar to the aluminum alloy which was chosen for the final design. The titanium alloy was not selected for many reasons. It is heavier, and it costs quite a bit more than the aluminum. Also, titanium alloys are difficult to weld and are not readily available in many forms. The properties of the chosen aluminum alloy are more than sufficient for our design criteria.

Clips

Two clip designs were considered, both based on clips made by Gibson Good Tools. The first design considered was a U-shaped clip where each side bends back on itself. This design was rejected because of excess material and the design used was easily approximated as a cantilever beam thus simplifying the calculations required. Also the accepted design more easily accommodates for drilling implements of differing sizes.

Rack

A first design for the rack was a free-standing rack. It held the rods in a cylindrical holder. This design resembled a vertical baseball bat holder. The holder was going to sit under SKITTER to permit easy access for the robot arm. This design became unfeasible when SKITTER would have to squat down. The cylindrical holder was then going to be placed out from under SKITTER. If the holder was placed away from SKITTER, the rod changer would need another

degree of freedom. Either the mechanical gripper would need a wrist of the robot arm would need a third section.

Another design for the rack involved a revolving pulley system between the legs of SKITTER. This design would allow twice as many clips as the design of a fix rack. This design was decided to be too complex. The spacing between the clips on the fixed rack was reduced to account for all the required clips. Because of this, we were able to use the fixed rack. Another problem with the revolving rack was the parameter of the rack needing to be in an arc shape. A revolving rack that traveled the path of an arc would be even more complex.

Arm

Many different types of arms were considered for this application with degrees of freedom from 2 to 6. To improve reliability and reduce complexity, the arm finally decided upon contained 3 degrees of freedom. This allowed us to maximize simplicity and yet be able to achieve all of our performance objectives. For the actuation of the arm, electric, hydraulic, and pneumatic driving system were examined.

B.7 MACROCORE RETRIEVAL AND STORAGE

I. Methods of Breaking Core

A. Water Jet:

DESCRIPTION: Water jet technology employs a narrow, high velocity stream to cut through a variety of hard materials.

DISCUSSION: Impractical in a lunar environment due to hard vacuum and lack of water supply.

B. Thermal Shock:

DESCRIPTION: Sufficient thermal stress in a localized region causes crack propagation. Application of liquid nitrogen or other supercooled liquids can accomplish this task.

DISCUSSION: Hard vacuum prevents application of any type of liquid bath. Also, if this method could be employed, the core could be destroyed.

C. Electric Arc:

DESCRIPTION: High energy path is produced between two electrodes in an electric arc which can be used to vaporize or melt rock.

DISCUSSION: Lack of atmosphere prevents formation of an arc.

D. Laser:

DESCRIPTION: Lasers can be used to cut through many materials including rock.

DISCUSSION: This would be an effective method, however, there is a high degree of complexity and relative lack of dirt tolerance involved.

E. Acid:

DESCRIPTION: Certain strong acids can eat through rock.

DISCUSSION: Hard vacuum prevents the use of volatile substances.

F. Tension:

DESCRIPTION: Sufficient tension will break a mineralogical specimen. Most rock cores on earth are broken by this method.

DISCUSSION: This is a good solution, but the force required in this situation may approach 4000 pounds per square inch. The skitter has the capacity of providing approximately 200 pounds of upward force. This limited force could be used in combination with some type of jacking device mounted on the footplate. The release of energy upon breakage could be potentially catastrophic and decrease the overall reliability of the system.

G. Torsion:

DESCRIPTION: Rock specimens can be broken by applying a torsional force.

DISCUSSION: Essentially the same problems and advantages exist as in tensional breakage.

H. Bending:

DESCRIPTION: Application of a bending moment can break a rock specimen.

DISCUSSION: This is a good method for it requires much less force than tensional or torsional breakage. However, due to the size of the outer annular diameter, there is little room to apply this force to the top of the core sample.

I. Impact:

DESCRIPTION: Sufficient impulse loading on a localized area can causes crack propagation and breakage.

DISCUSSION: Limited space makes this method impractical because a reasonable amount of room would be required to accelerate this impacted mass into the core. Also, excessive damage of the core could occur.

J. Thermal Expansion:

DESCRIPTION: Water in a confined, localized area of a specimen can an exert a large amount of pressure due to freezing, thus causing crack propagation.

DISCUSSION: Hard vacuum prevents the use of water in this application.

K. Scoring:

DESCRIPTION: Creating a local high stress area to assist in breaking by another method (eg. breaking glass).

DISCUSSION: Good concept, but must be used in conjunction with another method of removal.

L. Cutting:

DESCRIPTION: Grinding or cutting the specimen either partially or totally with some type of abrasive arm or wheel.

DISCUSSION: This is a good solution since it does not require large amounts of torque or lifting force. It would interact well with another method of core removal.

M. Blasting:

DESCRIPTION: Use of explosives will break rock.

DISCUSSION: Dangerous and catastrophic forces involved and lack of oxygen for burning make this method impractical.

N. Sonic Vibrations:

DESCRIPTION: High frequency sound waves resonant a local area to its natural frequency, thus weakening and breaking material.

DISCUSSION: This method would not be feasible due to its complexity and the varying types of strata encountered in the lunar regalyth.

O. Melting:

DESCRIPTION: Application of high heat source could be used to weaken and melt an area of the specimen.

DISCUSSION: Lack of oxygen makes this solution untenable.

P. Crushing:

DESCRIPTION: Application of a large load to crush a localized area of the specimen.

DISCUSSION: The necessity of applying incredibly large forces as well as the possible destruction of the sample makes this method undesirable.

II. Methods of Breaking Core using Tension

F1. Chinese Handcuffs:

DESCRIPTION: This method is a system of interlocking cables which come together locking down on the core when tension is applied to either end of the cylindrical cable network.

DISCUSSION: This is a good method for the network will hold the core intact. However, the interlocking cable network is statically indeterminate and hard to manage.

F2. Locking Ring:

DESCRIPTION: The bottom of the core retrieval device flairs out into several flanges. By forcing a ring down onto the flanged region, its inner diameter decreases locking onto the core for subsequent breakage in tension and removal.

DISCUSSION: This method would work, but several problems become instantly obvious. First, the ring sliding over the outer body of the retriever must overcome possible vacuum welding conditions. Second, this design requires a veritable plethora of moving parts. Finally, dirt could become lodged between the ring and the core retrieval body and result in wear problems.

F3. Screw Ring:

DESCRIPTION: This is an extension of the locking ring concept in which the locking ring moves down over the flanges by means of screw threads.

DISCUSSION: The mechanism of this system would provide an excellent steady increase of pressure on the core for gripping purposes. However, dirt tolerance creates difficulties in using any type of threaded device in the lunar environment.

Figure B.7.1 CHINESE HANDCUFFS

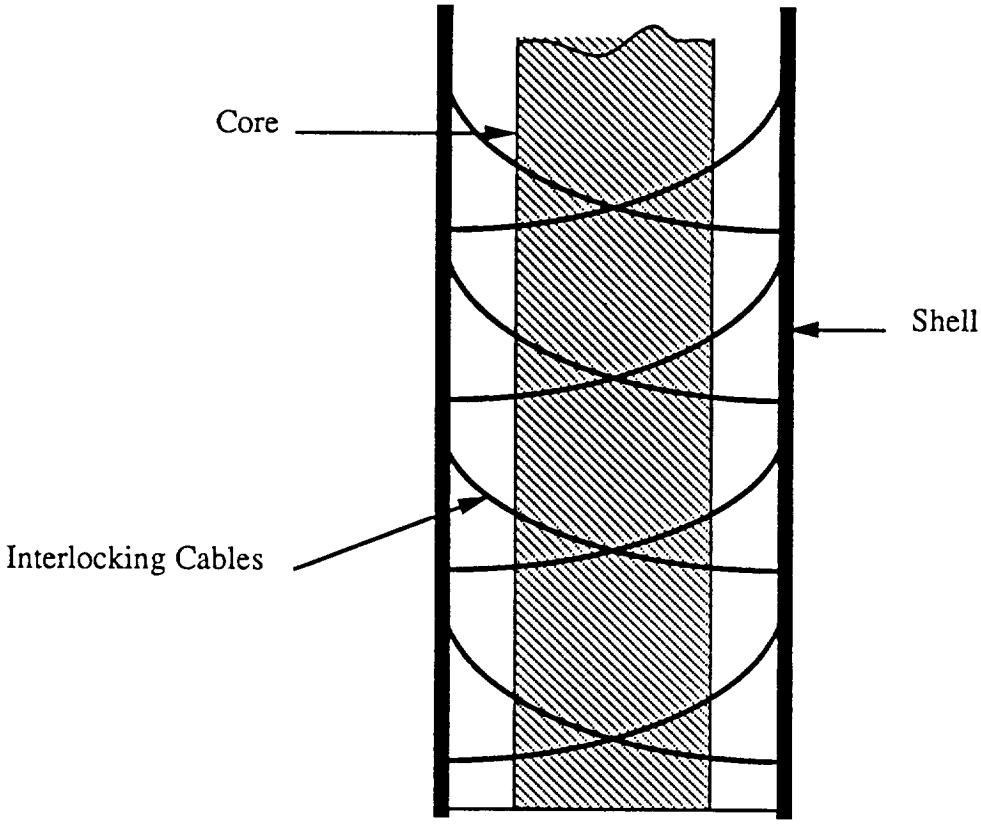

Figure B.7.2 TENSION RING

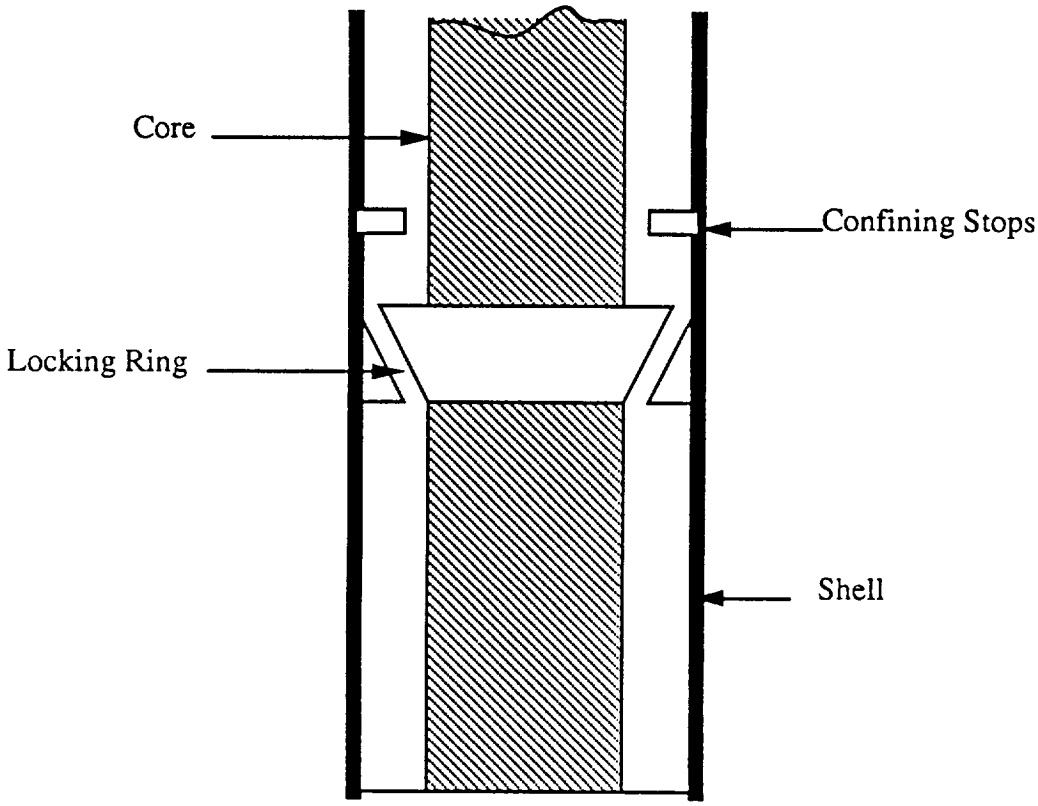

F4. Pivoting Rings:

DESCRIPTION: A pair of rings, hinged on an annular axis, is rotated such that each member is pulled in an opposing direction. Points of high stress are created at the contact area affecting eventual breakage for removal.

DISCUSSION: This mechanism will work, but it is not capable of optimum core retention.

F5. Post-hole Digger:

DESCRIPTION: The name of this design belies its description. Two half cylinders rounded at one end can descend to the core and tighten around it. The core can then be broken and removed by a tensile or bending action.

DISCUSSION: This method is well-adapted to the removal of broken cores. Problems arise in the areas of gripping and removing of core that is intact.

F6. Cams:

DESCRIPTION: The core retrieval body is a cylinder two meters in length lined on the inside with spring driven cam-shaped elements. These elements allow the retriever body to slide downward over the core, but force into the core with any upward movement. If sufficient upward tension can be applied to the core in tandem with this gripping action, the core can be broken and removed.

DISCUSSION: This would be an effective method of gripping the core in the hole. Problems arise in the area of loading stresses since the individual cams will contact the core and cause large point loads possibly crushing the core.

Figure B.7.3 PIVOTING RINGS

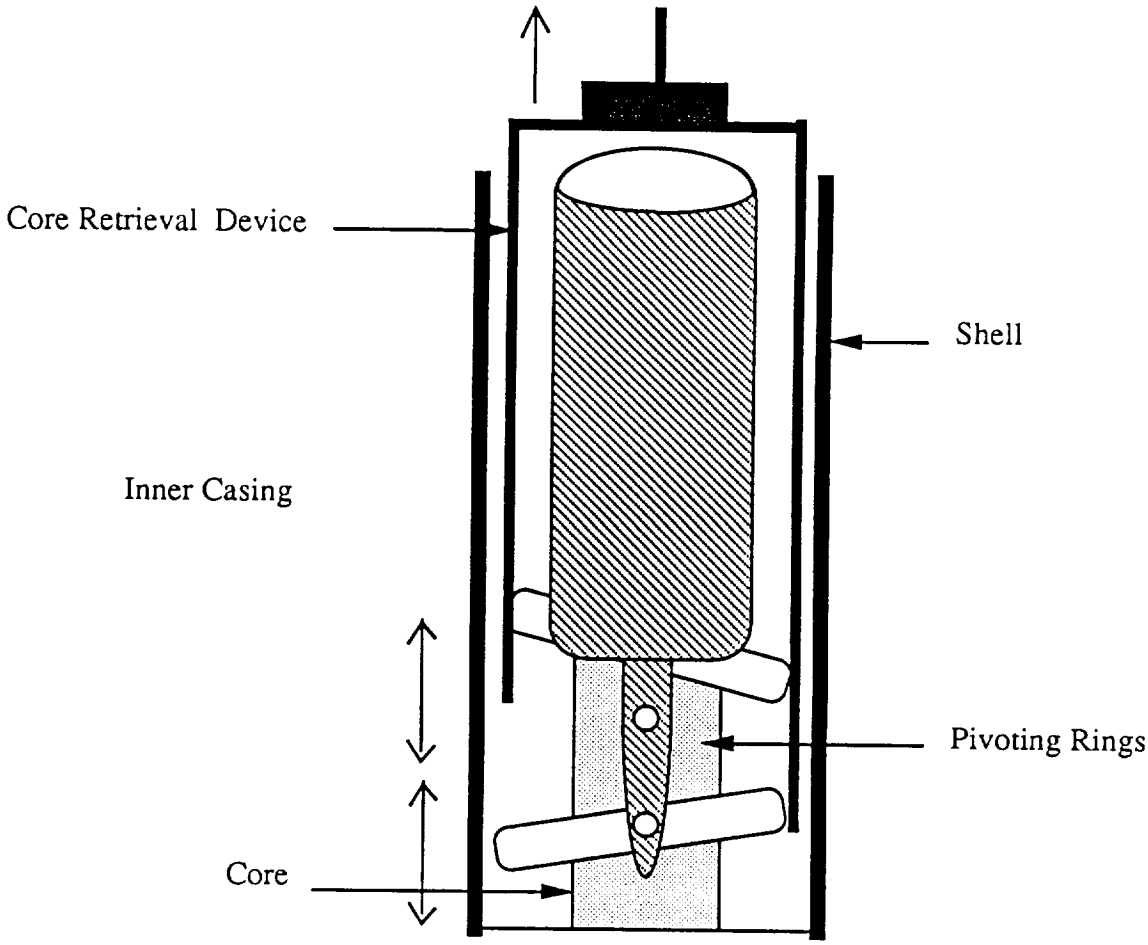

Figure B.7.4 TENSIONING ANNULAR REDUCER

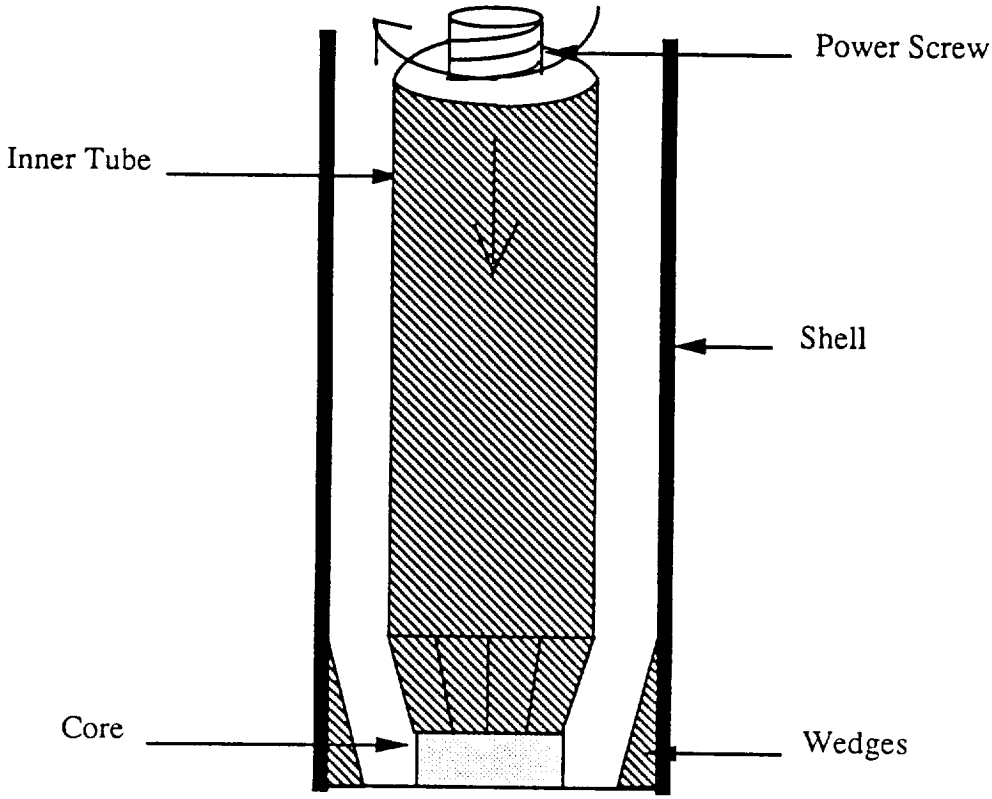

Figure B.7.7 MODIFIED WEDGED GRIPPER

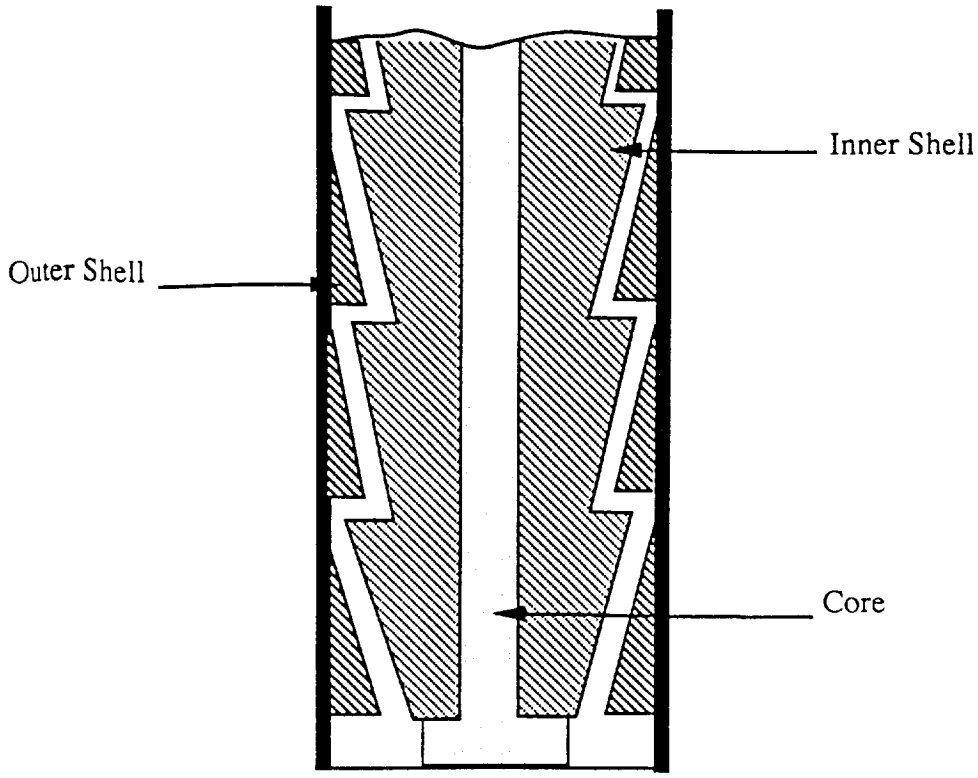

Figure B.7.8 CAMS

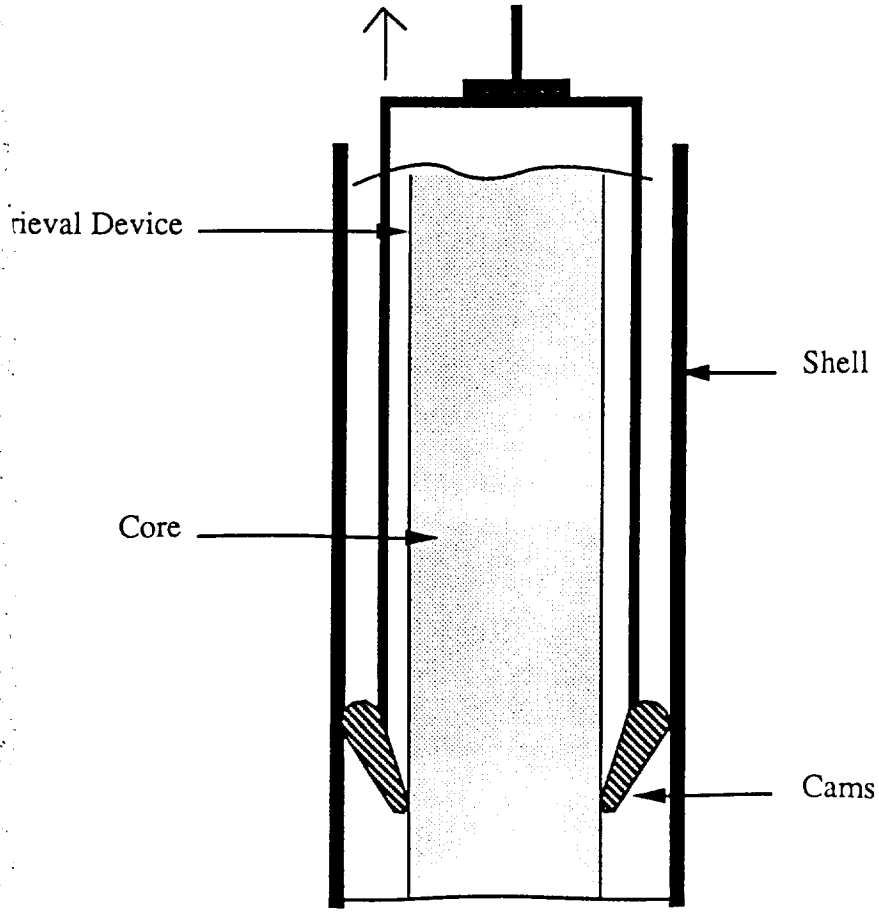

III. Methods of Breaking Core using Bending

H1. Wedge:

DESCRIPTION: The cylindrical retriever body would be equipped with a wedging device at its top. When the retriever is fully in place around the core, the wedge is forced down between the top of the core and the retriever body producing a bending moment on the core itself. This moment would break the core.

DISCUSSION: This is not a good way to break the core, since it will likely consist of varying strata with a vast range of yield strengths. Therefor the core would break at the weakest point and not necessarily the bottom. It is desired to retrieve the full core so this is not a good solution.

H2. Post-hole Digger with Bending Mechanism:

DESCRIPTION: This design is a post-hole digger concept combined with a method of applying a bending moment to the core once it is securely gripped. The bending moment breaks the core and the retriever is retracted from the hole.

DISCUSSION: Although this is a good design, there are problems in dealing with possible broken cores as well as with the mechanics of gripping the core. The mechanism is very long and the bottom sections of a broken core could dislodge and fall back into the hole.

IV. Methods of Breaking Core using Scoring

K1. Pipe Cutter Mechanism:

DESCRIPTION: A disk of hardened metal with a sharp wedge-shaped edge is forced into one side of the core while a rolling wheel is applied to produced an opposing contact force. The disk and wheel rotate in tandem around the core. This action produces a related stress field which follows the contact point force of the rotating disk. It is this stress field and the stresses induced by the wedge-shaped disk that causes the cylindrical core section to split apart.

Figure B.7.5 Post-hole Digger

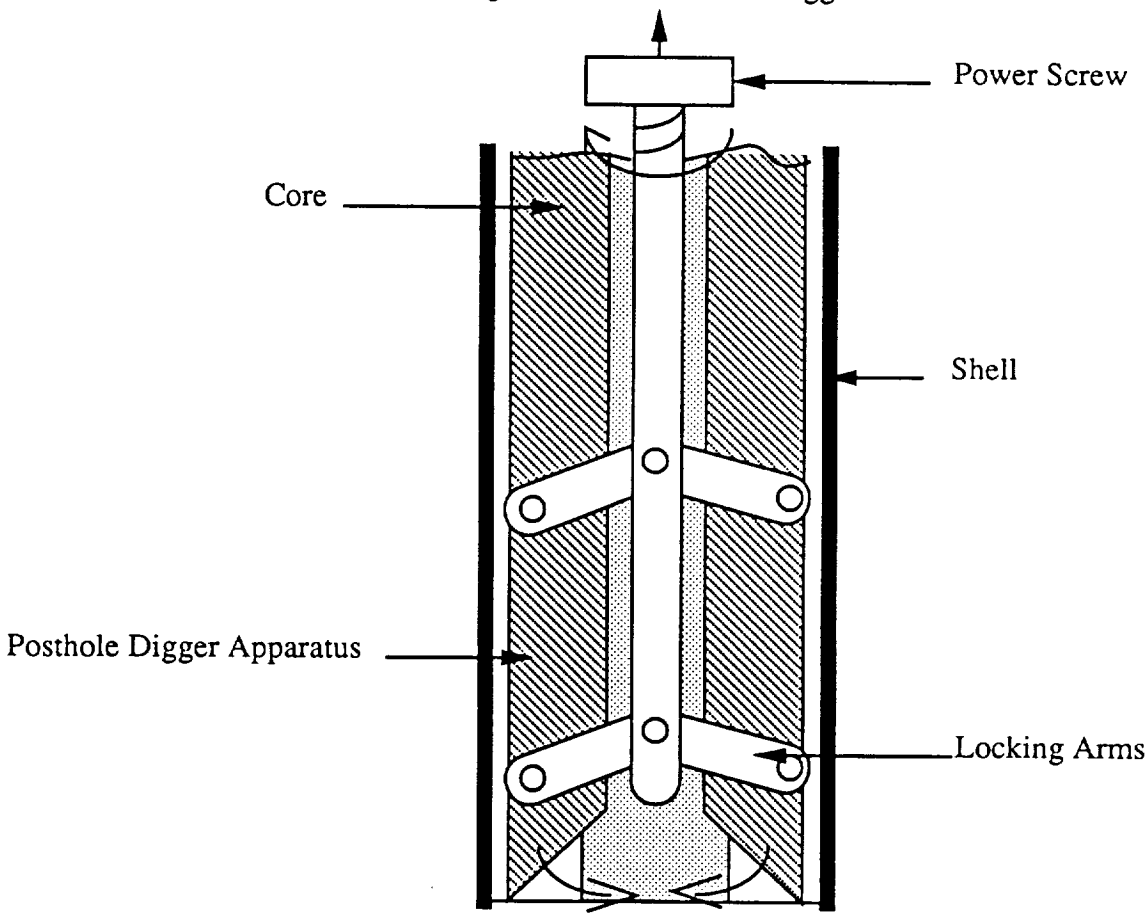

Figure B.7.6 WEDGE

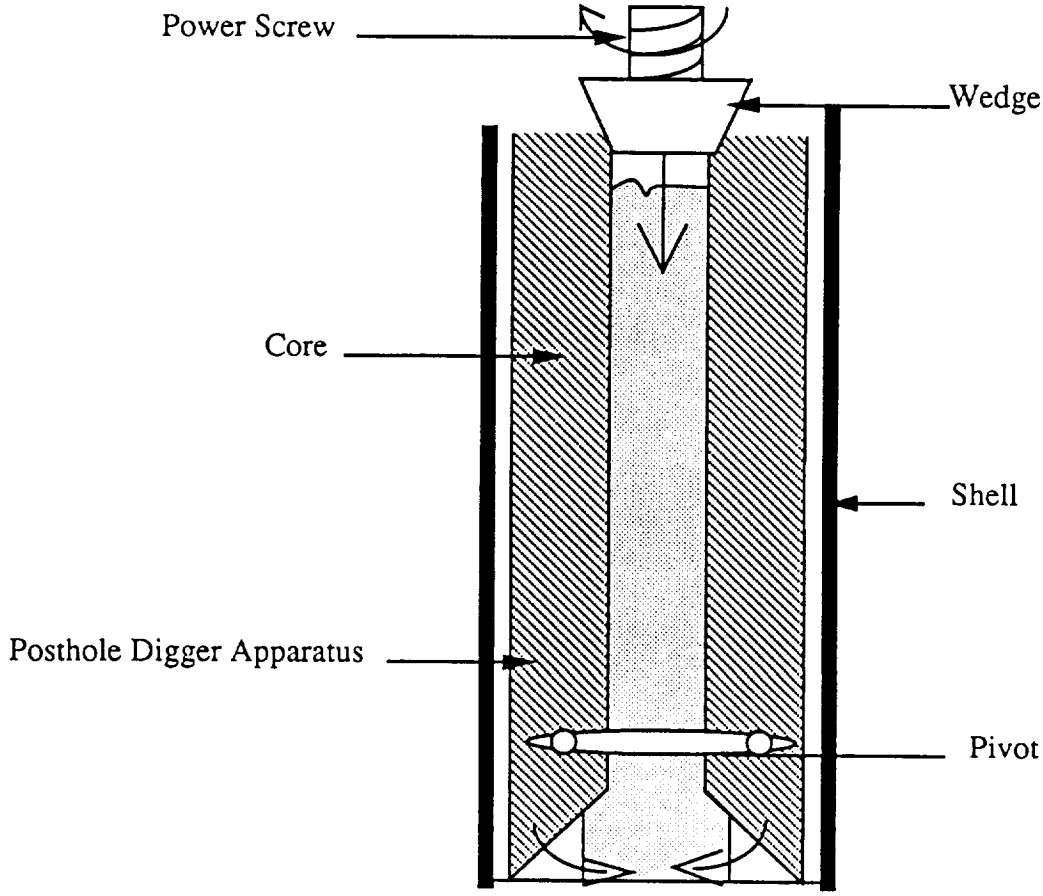

DISCUSSION: This is an excellent method because little penetration of the disk is required to actually break the core. The heterogeneous and brittle nature of a typical regalythic core assists in the fast fracture mechanics of this method. In addition, this method is relatively quick for the same reasons mentioned above. It must be used in conjunction with a device that will grip the core in a removal process.

V. Methods of Breaking Core using Cutting

1. Diamond Teeth Cutting Arms:

DESCRIPTION: Rocker arms inside of a gripping device are imbedded with diamond teeth. At the proper location on the core, the arms could be mechanically activated to contact the core under force of a torsional spring. The drill string is then rotated by the skitter and the arms cut into the core until it is broken and ready for removal.

DISCUSSION: This method creates a heat management problem in the cutting arms. These arms would be relatively small bodies of metal incapable of dissipating much heat. Also, there are possible problems with core chip removal and abrasion of the arms.

B.8 Controls

The alternative designs discussed for control of the drilling operation consisted of both a more traditional design as well as a more futuristic design.

The traditional design that was discussed consisted of the "typical" NASA space control panel common to the Apollo and earlier space missions. The panel contained analog gauges and solid state switching. Data entry and routine commands were executed through the use of a keyboard or specifically designated push-button controls. This system was not chosen because of its size, maintenence difficulty, and lack of concern for the comfort of the operator.

The futuristic design was not chosen due to the unknown reliability and expense of its leading-edge technology. This design would, however, result in the ultimate in operator comfort and control. The work site on the moon would be monitored by video cameras at three or more multi-occular positions. The views would be assimilated by a computer and a three dimensional projection would appear on a global screen about the operator. This would give the operator the sensation of witnessing the procedure in person. The benefits for the operator of such asystem are obvious, but incorporation of the technology would not be feasible at this time.

Design Alternatives

DESIGN A (CAMS)	DESIGN B (SPRINGS)	DESIGN C (GEARS)	DESIGN D (2nd MOTOR)	DESIGN E (OTHER)
Version 1	Version 1	Version 1	Version 1	Version 1
Version 2	Version 2	**Stop Here**	**Stop Here**	**Version 2**
Stop Here	Version 3			**Final Design**
	Stop Here			

Design E (Version II) will be the final configuration choice for the report

VERTICAL ACCELERATOR FOR STEPPED AUGER

TYPE : A **VERSION :** 1

TITLE OF DESIGN : Rotating Cam Mechanism

DESIGN COMPONENTS :
Secondary Motor and Support Brackets
Rotating Cam and Gearing Struts
Clutch and Internal Spring
Engaging Device for Rotating Cam

METHOD OF OPERATION : Following completion in drilling, clutch disengauges to allow for control rod separation. Rotating Cam is powered up by means of secondary motor. Stepped Auger is able to vertically oscillate downward due to the Cam and return upward due to compression spring.

DESIGN ADVANTAGES :
- Cam design provides method of jerking Auger particles in an abrupt fashion.
- Good Reliability
- Gear Simplicity

DESIGN DISADVANTAGES :
- External Motor and Power Up required
- Complexities involved in engaging motor and cam structure to control rod
- Difficulties for internal spring mount
- Addition controls required for clutching rods and engaging motor
- Continual Cam alignment with control rod
- Spacing availabilities with regard to rod changer and storage racks
- Rotating Cam to control rod lip contact yields metal to metal wear

COMMENTS : Due to complexities involving present location of Rotating Cam and difficulties regarding secondary motor and clutch controls, design is not feasible as shown.
However, if a cam was designed powered and located differently to control rod rotating cams may prove to be effective.

FINAL RECOMMENDATIONS :

Discontinue all futher developments regarding existing design

Design A.1 - Rotating Cam Mechanism

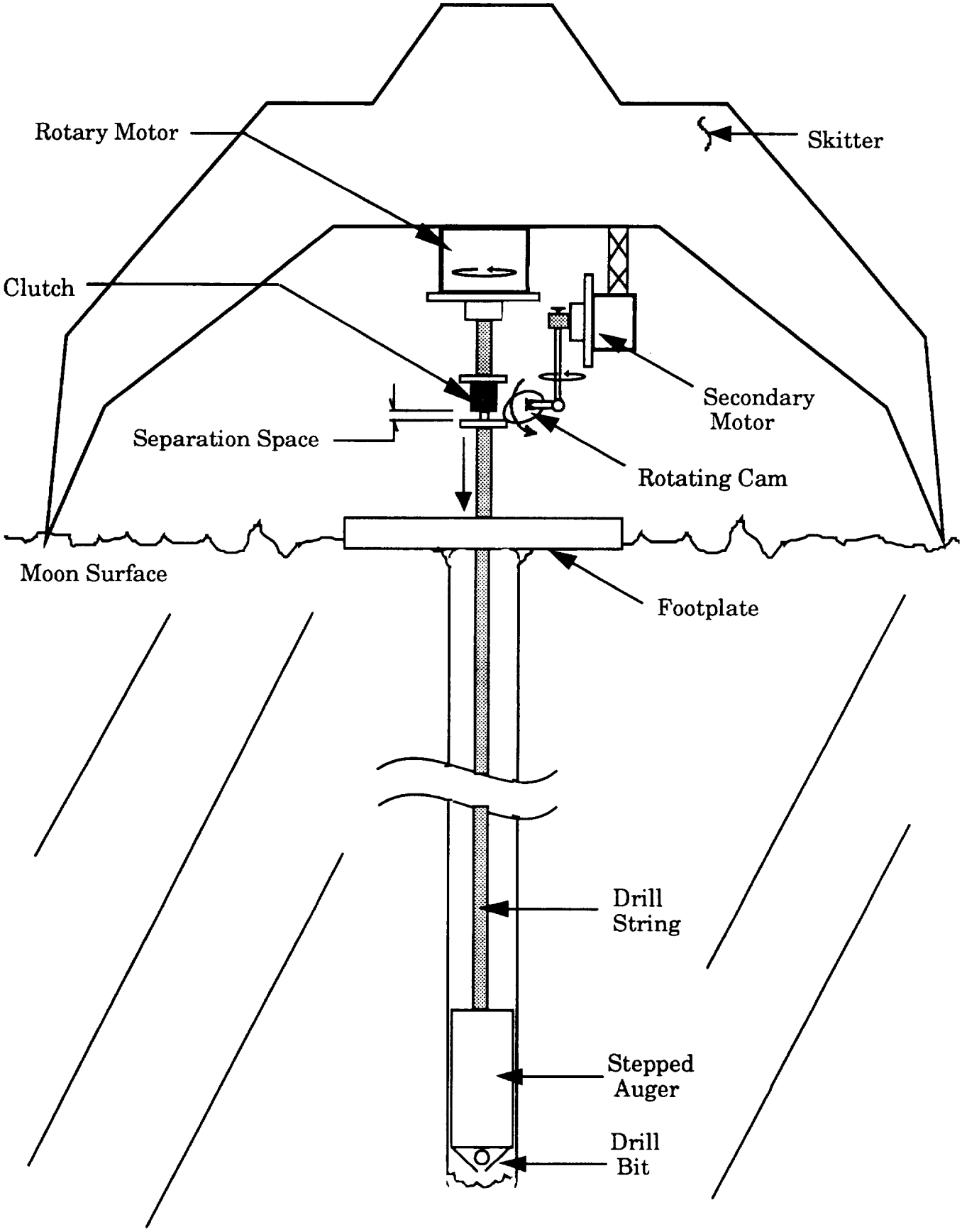

VERTICAL ACCELERATOR FOR STEPPED AUGER

TYPE : A **VERSION :** 2

TITLE OF DESIGN : Retractable Cam Mechanism

DESIGN COMPONENTS :
Secondary Motor and Motor Supports
Rotating Cam and Control Rod Clamp
Linkage and Retractable Strut Supports
Possibility of third motor to engage and disengage retractable cam mechanism

METHOD OF OPERATION : Following completion in drilling, control string is disengaged from motor and vertical accelerator extends inward to "snap" onto control rod. Rotating Cam is powered up by means of secondary motor. Stepped Auger is able to vertically oscillate due to inner configuration of cam track.

DESIGN ADVANTAGES :
- Cam design provides method of jerking Auger particles in an abrupt fashion.
- Good Reliability
- No crude springs or gear wearing
- No clearance difficulties or complex controlling
- Implements existing gripping present in footplate
- Maximum number of oscillations can be used as needed.

DESIGN DISADVANTAGES :
- External Motor(s) and Power Up required
- Possible friction occurring on inner cam track
- Potential difficulties could exist in alignment

COMMENTS : Although complexities are involved with additional motor(s) operation and controlling, cam design as shown will have good reliability and is a very feasible and realistic system.

FINAL RECOMMENDATIONS :

Develop existing design as a feasible vertical accelerator for the stepped auger

Design A.2 - Auxilliary Motor Driven Cam

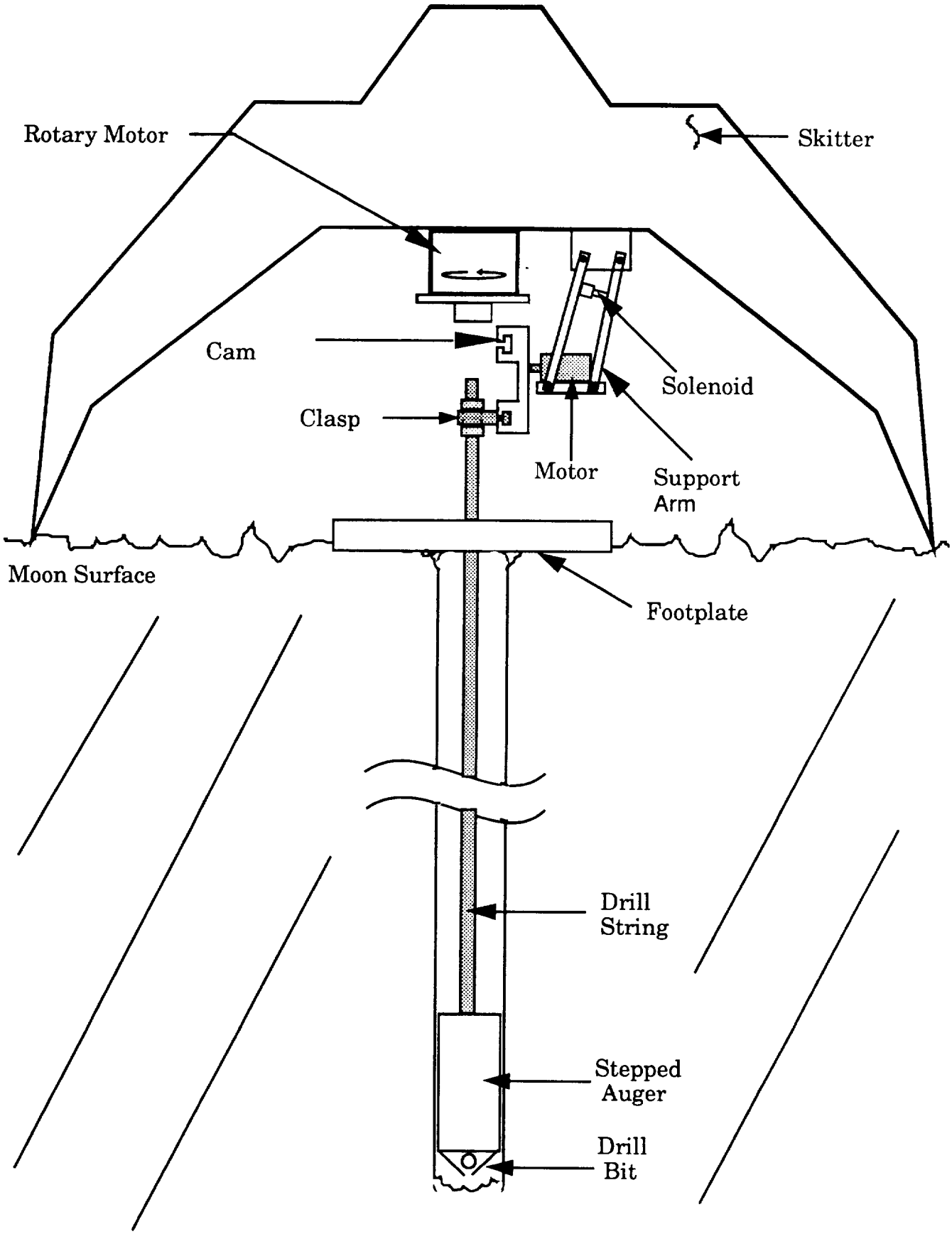

VERTICAL ACCELERATOR FOR STEPPED AUGER

TYPE : B (Springs) **VERSION :** 1

TITLE OF DESIGN : Above Ground Compression Spring Mechanism

DESIGN COMPONENTS :
100 mm Compression Spring
Spring Housing
Control Rod Piston

METHOD OF OPERATION : As Skidder lowers itself during drilling process, control rod piston will lower into spring housing compressing and turning spring under a reduced rotation with respect to control rod. After drilling is completed, footplate will grip control rod and Skidder will raise itself. When instructed footplate will release grip of rod and spring will extend rod down forcing particles upward through the Auger.

DESIGN ADVANTAGES :
- Few components and design simplicity
- No secondary motor required
- Single compression spring no gearing required
- Minimal controlling required
- Implements existing gripping present in footplate and forceable compression by means of Skidder

DESIGN DISADVANTAGES :
- Minimal vertical oscillations each time spring is enabled.
- Abrupt oscillations will minimize the number of particles jumping between steps.
- Low precision due to crudeness of spring design
- Spring housing and Piston interfere with rod changer
- Turning Spring during compression creates unnecessary spring stress

COMMENTS : Skidder and footplate operation benefits indicate potential for existing design. Try to eliminate space constraints imposed by rod changer and spring rotation.

FINAL RECOMMENDATIONS :

Continue to develop or modify the existing design as needed

Design B.1 - Above Ground Compression Spring

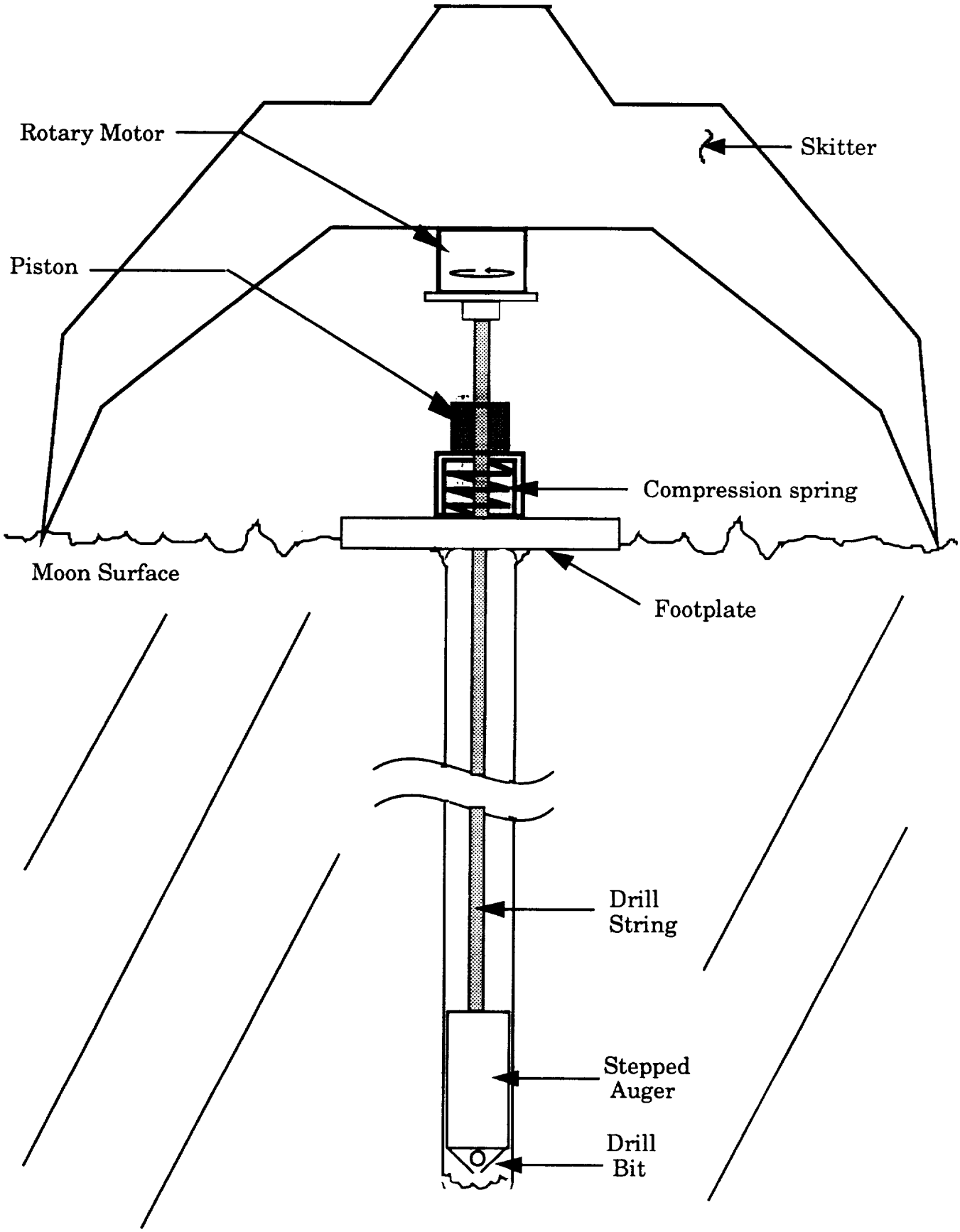

VERTICAL ACCELERATOR FOR STEPPED AUGER

TYPE : B (Springs) **VERSION :** 2

TITLE OF DESIGN : In-Ground Compression Spring Mechanism

DESIGN COMPONENTS :
80 mm Compression Spring
Spring Housing
Control Rod Piston

METHOD OF OPERATION : As Skidder lowers itself during drilling process, control rod piston will lower into spring housing compressing and turning spring under a reduced rotation with respect to control rod. After drilling is completed, footplate will grip control rod and Skidder will raise itself. When instructed footplate will release grip of rod and spring will extend rod down forcing particles upward through the Auger.

DESIGN ADVANTAGES :
- Few components and design simplicity
- No secondary motor required
- Single compression spring no gearing required
- Minimal controlling required
- Implements existing gripping present in footplate and forceable compression by means of Skidder
- No interference with rod changer
- No additional stress caused by twisting spring

DESIGN DISADVANTAGES :
- Minimal vertical oscillations each time spring is enabled.
- Abrupt oscillations will minimize the number of particles jumping between steps.
- Low precision due to crudeness of spring design
- Underground spring forces control rods downward thereby subjecting the drill bit to damage from lunar surface
- Minimal oscillations due to footplate interference
- Footplate damage resulting from impacted piston
- Additional controls required for a piston clutch

COMMENTS : Use of inground application for compression spring poses serious clearance problems. Existing compression spring design is not feasible either above or below footplate. Remaining alternatives leave only extension spring designs.

FINAL RECOMMENDATIONS :

Discontinue all further research regarding compression springs. Analyze opportunities involving extension springs.

Design B.2 - In-Ground Compression Spring

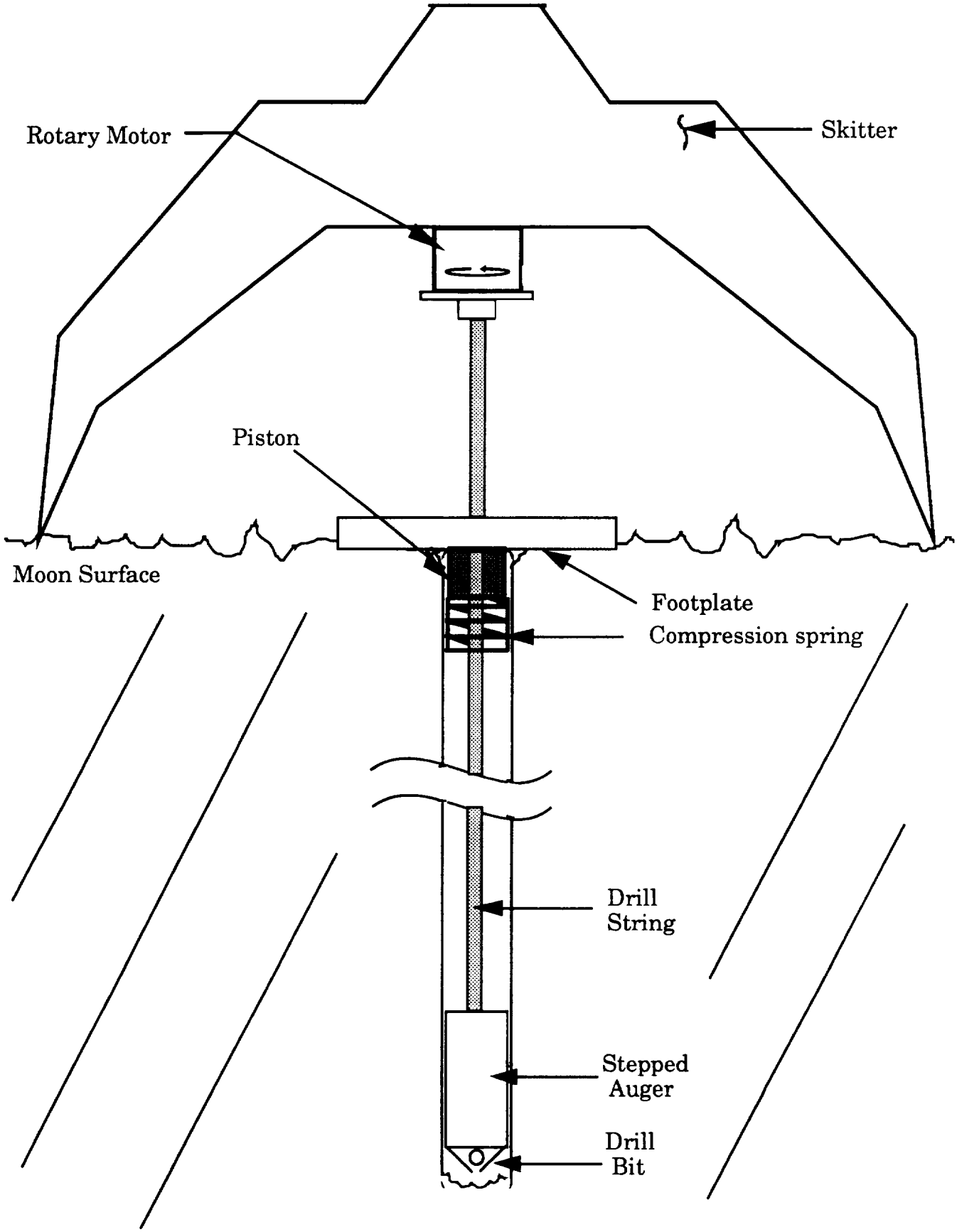

VERTICAL ACCELERATOR FOR STEPPED AUGER

TYPE : B (Springs) **VERSION :** 3

TITLE OF DESIGN : Extension Spring Mechanism

DESIGN COMPONENTS :
Extension Spring
Spring Housing
Threaded Shaft

METHOD OF OPERATION : After drilling is completed, Skitter raises up and footplate grips control rod. Motor reverses direction to unscrew rod assembly. Skitter raises again to extend spring. Footplate releases and rod oscillates.

DESIGN ADVANTAGES :
- Few components and design simplicity
- No secondary motor required
- Single compression spring no gearing required
- No addition stress caused by twisting spring
- No clearance difficuties
- Implements existing gripping present in footplate and forceable compression by means of Skidder
- No interference with rod changer
- No additional stress caused by twisting spring

DESIGN DISADVANTAGES :
- Minimal vertical oscillations each time spring is enabled.
- Abrupt oscillations will minimize the number of particles jumping between steps.
- Low precision due to crudeness of spring design
- Possible danager can exist in using extension springs
- Reversability of drill shaft required

COMMENTS : Research possibilty of implementing reversable drill motor. Continue further analysis of feasibility regarding extension spring

FINAL RECOMMENDATIONS :

Continue to develop existing design as needed.

Design B.3 - In-Ground Compression Spring

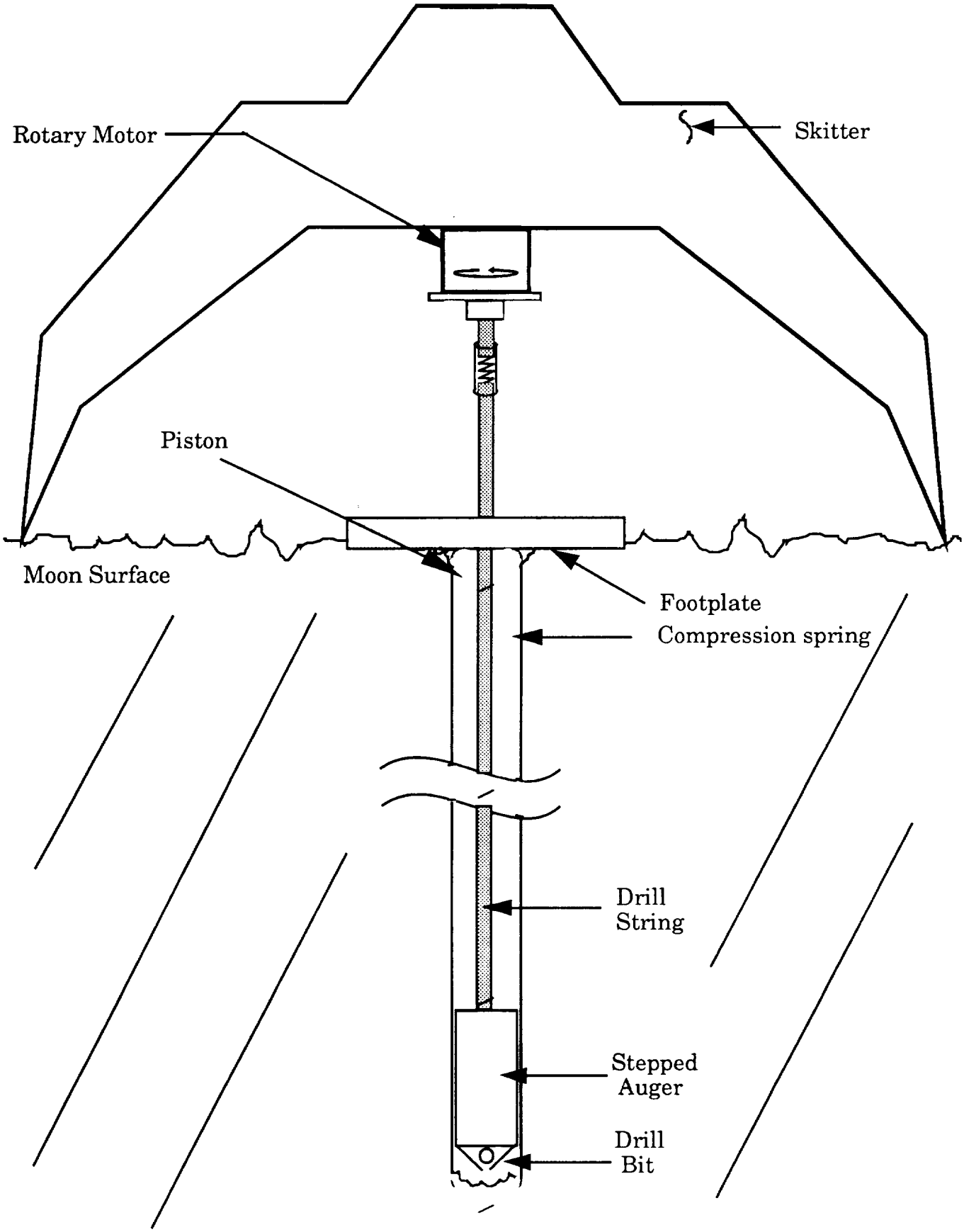

VERTICAL ACCELERATOR FOR STEPPED AUGER

TYPE : C (Gears) **VERSION :** 1

TITLE OF DESIGN : Bevel Gear Mechanism

DESIGN COMPONENTS :
2 Bevel Gears
2 Retractable Arms for Device
Control Rod Pivit and Guide
Link conecting Gear to Control Rod

METHOD OF OPERATION : Following completion of drilling, Skitter will raise itself to detach from control rods. Retractable arms will engage beveled gear device onto primary motor. Gears will be powered and will vertically oscillate conecting link quickly shaking Auger particles.

DESIGN ADVANTAGES :
- No secondary motor required
- Accuracy due to beveled gears
- No crudeness due to springs
- Good Reliability
- Maximum number of oscillations can be used as needed.

DESIGN DISADVANTAGES :
- A great number of controlling devices are required
- Simetrical Gear will cause difficultly in allowing enough time to force particles up the Auger
- Retractable arms will interfere will rod changer
- Lunar dust will cause excessive gear wear
- Torque overload exists on pivot
- Difficulties involving control link connection to gear

COMMENTS : Retractable arm interference and a great degree of controlling will be required. However, beveled gear design does pose many benefits of simplicity oscillatory motion.

FINAL RECOMMENDATIONS :

Modify the existing design as needed to achieve satisfactory gear device

Design C.1 - Bevel Gear Mechanism

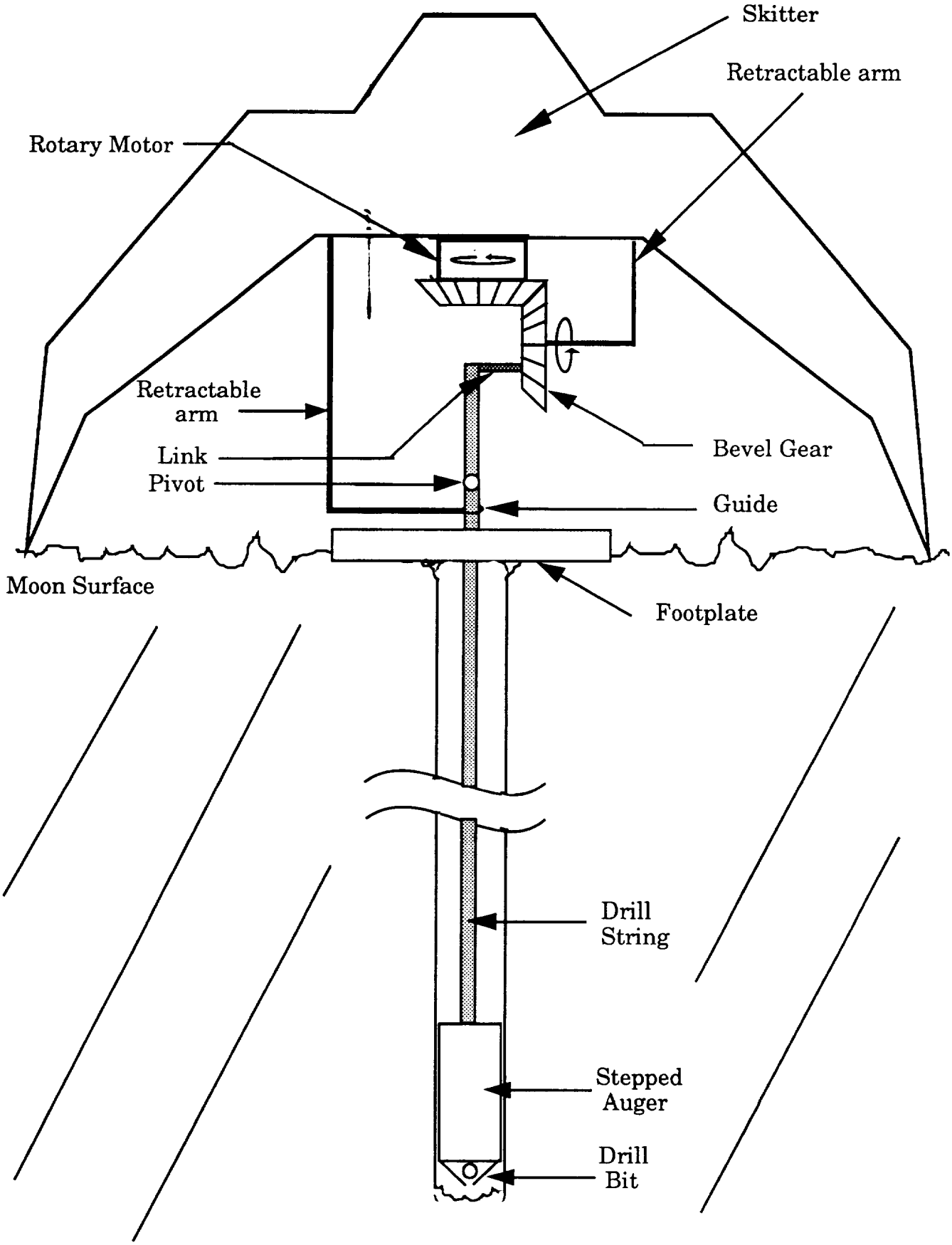

VERTICAL ACCELERATOR FOR STEPPED AUGER

TYPE : D **VERSION :** 1

TITLE OF DESIGN : Secondary Motor Configuration

DESIGN COMPONENTS : Secondary Motor and Support Brackets
Clutch and Detachable Housing
Link conecting Secondary Motor to Control Rods

METHOD OF OPERATION : Following completion of drilling, clutch disengauges to allow for control rod separation. Secondary motor and control link attach to lower control rod. Link will vertically oscillate Auger shaking particles.

DESIGN ADVANTAGES :
- Few components
- No strain on primary motor
- Secondary motor provides ability for accurate oscillations
- No crudeness due to springs
- Good Reliability
- Maximum number of oscillations can be used as needed.

DESIGN DISADVANTAGES :
- Additional control devices and maintenence are required for secondary motor
- Space limitations exist with external mounting of secondary motor
- Larger operational costs due to additional motor

COMMENTS : Without further analysis, mounting locations and control rod conections presently inhibit the effectiveness of the secondary motor. Secondary motor assembly dimensions and interconnection with regard to the control rods would have to be studied further in order to render a more accurate decision.

FINAL RECOMMENDATIONS :

Continue to develop the existing design as needed

Design D.1 - Secondary Motor Configuration

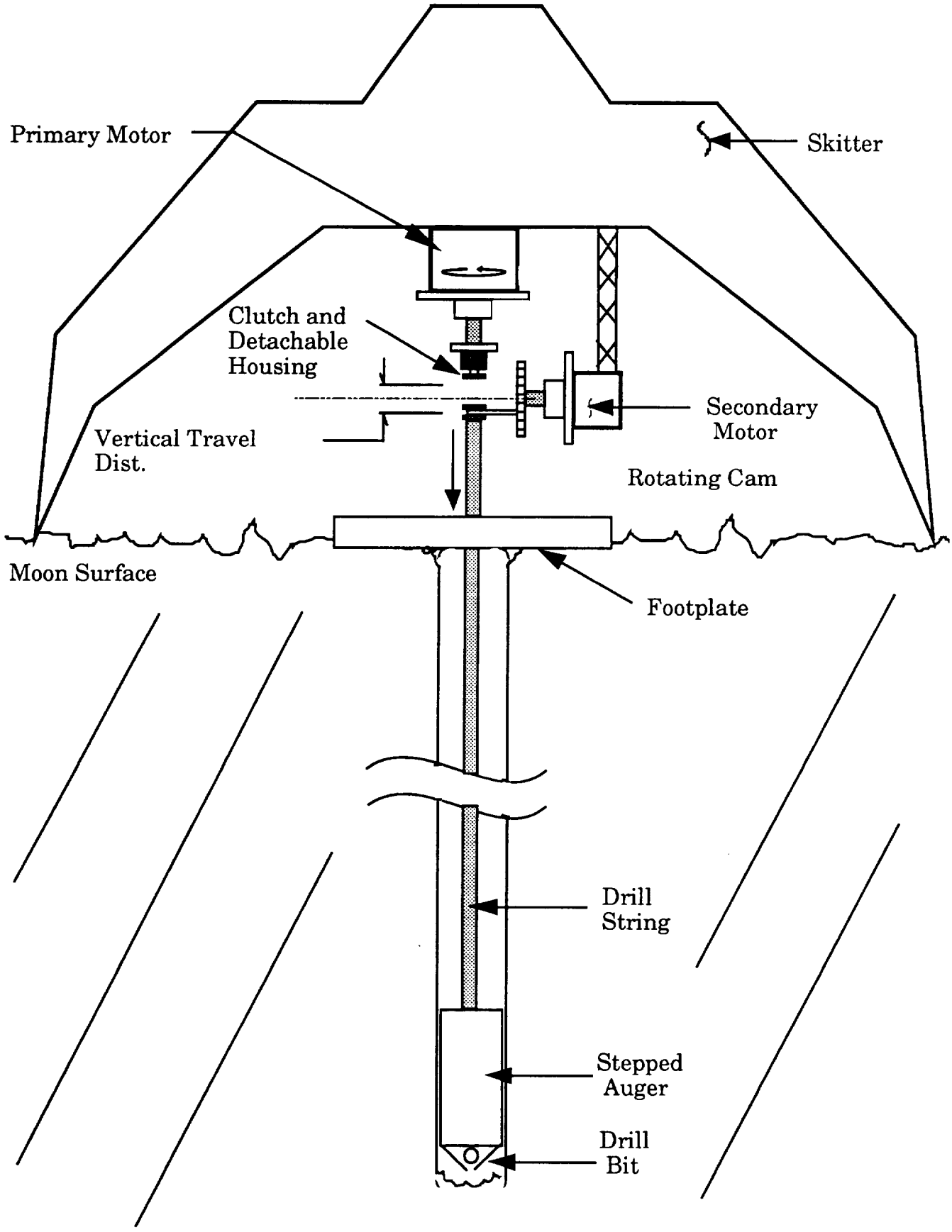

VERTICAL ACCELERATOR FOR STEPPED AUGER

TYPE : E **VERSION :** 1

TITLE OF DESIGN : Footplate Mountable Shaker Device

DESIGN COMPONENTS : Twelve Control Rod Cups per 2 meter rod
Clutch and Detachable Housing
Footplate mounted Roller Ball and Spring Device

METHOD OF OPERATION : Following completion of drilling, clutch disengauges to allow for control rod separation. As Skitter raises, control rods will be drawn upward through footplate. The roller ball mounted to the footplate link will catch each conrol rod cup as it travels upward through the footplate. After a critical point is achieved the roller ball will slip off each cup abruptly jerking rods causing Auger to shake.

DESIGN ADVANTAGES :
- No rotary of motor driven parts
- No strain on primary motor
- No maintenence
- No controls needed for shaking
- Consistent adjustable travel distance for rods

DESIGN DISADVANTAGES :
- Vast complications develop when altering design of control rods due to cups
- Oscillations are performed by Skitter lifting up, only minimal shakes will for each drilling cycle
- Control cups will affect rod changer and storage racks design
- Control cups will affect footpate design and pose potential gipping difficulties for the group
- Multiple cups will add significant weight to control rods and drill motor, especially at 50 meters

COMMENTS : Although simple in design, control rod cups and footplate shaker pose significant difficulties due to interaction with other groups and major design changes on existing parts.

FINAL RECOMMENDATIONS :

Discontinue all further developments regarding existing design

Design E.1 - Footplate Mountable Shaker Device

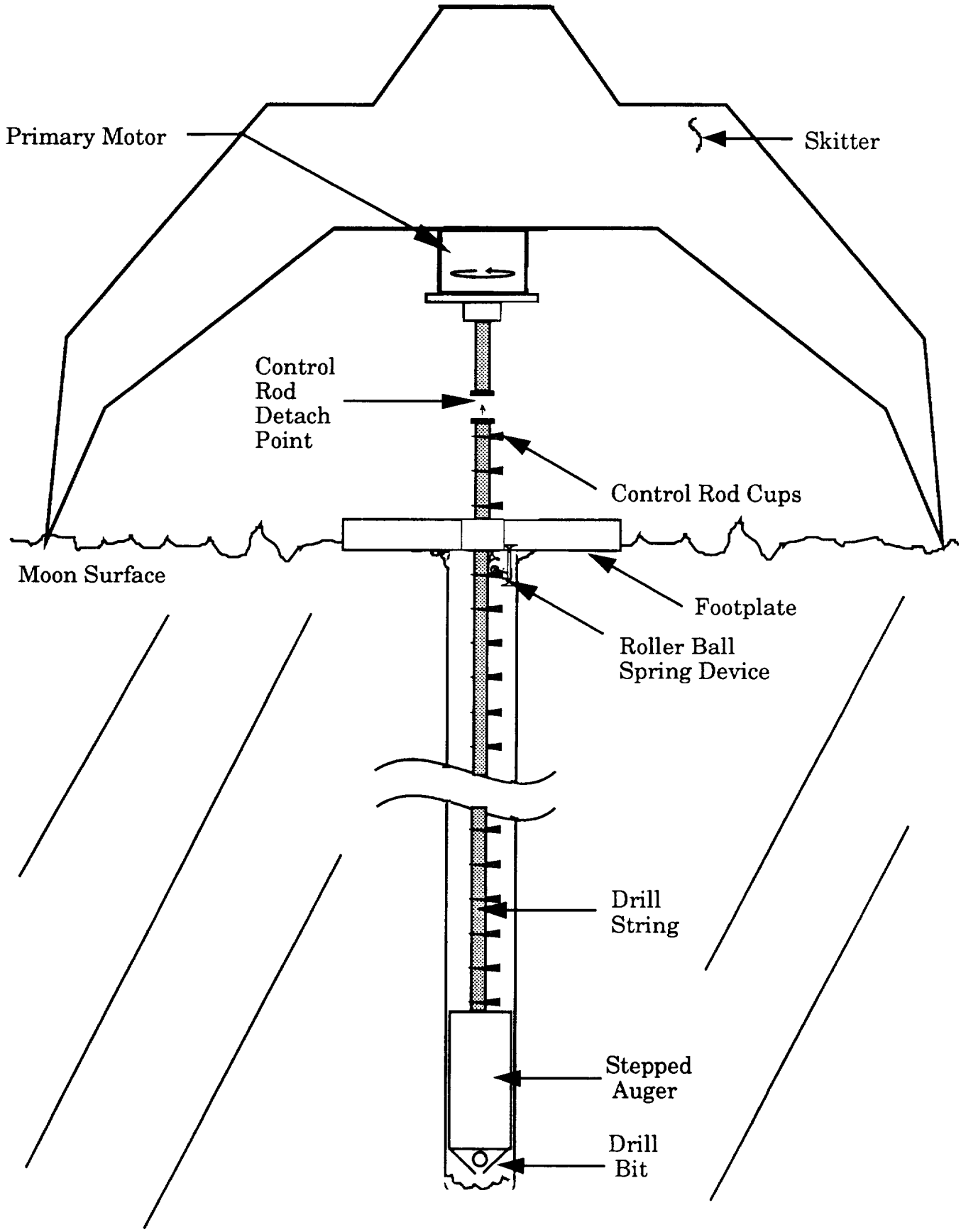

B.10 MICRO-CORING DRILL

B.10.1 Drilling mechanism

Several drilling mechanisms were considered before a decision was made to use the Diamond-Tipped coring bit. These alternative modes are listed below:

- Ultrasonic Drill: when the ultrasonic vibrations are applied to a solid at a certain point, plastic deformation will occur, and if the cycles continue at a high amplitude, the sample will break.
- Wedge Impact Sampling: this method uses a chisel like instrument to break of a sample. This method is very effective when ample space is available.
- Vibro Drilling: drilling by vibration involves the use of pulsations from a high frequency vibration source and the weight of the drilling apparatus to penetrate the soil.

B.10.2 Bracing system

Two alternative methods of bracing were considered but were deemed undesirable for this application. The first method would have used two screws on opposite sides of the rod, driven into the wall by a shaft powered by the main motor. The other bracing mechanism we considered was a truncated cone that would slide into the hole until its diameter was too large to slide any further, thus bracing the rods firmly at the top.

B.10.3 Power source

An alternative source of power for the drill bit could be the main motor from Skitter. The motor mould rotate a shaft, and a series of gears would be used to convert this rotational motion into rotational and translational motion for the drill bit.

A bevel gear attached to the drive shaft would mate with a spline to transmit the necessary power. Two spur gears, located on opposite sides of a separate motor, would rotate along two pairs of racks to translate the drill bit into the lunar rock.

B.10.4 **Sample protection**

The sample could be protected by a device similar to the one found in the final design. In this alternative case, an entire section of the cylinder would move down, but this would leave no place to mount the tracks for the translation.

APPENDIX C

PROGRESS REPORTS

WEEK OF APRIL 10, 1989

- The cutting teeth configuration for the main drill bit and a shovel-type mechanism to remove rock cuttings away from this bit were discussed.

- Commercially pure grade-5 titanium was selected as the rod material due to its good high temperature behavior and superior strength to weight ratio.

- A set of ring sleeve bearings was added to the rod deisgn to improve buckling resistance.

- Reliability and performance constraints for the lunar footplate were determined.

- Nuclear fission and hydrazine were ruled out as potential power sources for the lunar drilling apparatus. Employing a solar power source with a rechargeable battery was determined to be the most feasible method of providing power for this project.

- The materials selection and method of attachment for the drilling platform mechanical interface were discussed.

- Research was conducted on grippers and robot arms feasible for use in the rod changer.

- Martin Marrietta's Report on Lunar Apparatus and an Acker Drill Company catalog were examined to find a potential method of removing the macro-core produced by the main drilling process.

- Each member of the five man controls team took responsibility for interfacing with two of the groups designing the other sub-sections of the lunar drilling apparatus.

Continued

- The interaction of the vertical accelerator with the overall lunar deep drilling apparatus was discussed.

- Using a diamond-tipped coring bit was determined to be the best method of obtaining a pristine, micro-core sample. Ultrassonic drilling, drilling by vibration, and wedge impact sampling were alternatives that were eliminated.

WEEK OF APRIL 17, 1989

- It was determined that the main drilling operation needs to be continuous for depth increments of only one-half inch. This will make the removal of cuttings from the drilling process more reasonable.

- The rod interface and coupling collar were designed to isolate torsional and and tensional loads in separate elements.

- Rather than designing the footflate mechanism to handle an uneven surface, it was decided have Skitter smooth out a surface in the lunar regolith before the footplate is set down. A fishtail bit or a scraping mechanism will be employed to carry out the smoothing process.

- A CSM motor was obtained from the VA hospital on April 20,1989. This will be used to power the drill bit for the main coring operation, the macro-core removal process, and possibly part of the micro-coring process.

- Various alternatives for removal of the macro-core were considered. Most of these would employ a "post hole digger" type mechanism.

- A list of potential vendors for electrical sensors, temperature sensors, switches, actuators, velocity sensors, torque sensors, and force sensors was compiled by the controls team.

- Several potential methods for bracing the bottom rod for the micro-coring process were analyzed. It was determined that pads at the end of a spring loaded piston should be driven by an oval-shaped cam.

Continued

- The mechanical and thermal properties of basalt were researched by the micro-coring group to be used in a heat transfer analysis to determine the maximum power input to that drill.

WEEK OF APRIL 24, 1989

- The design of the cutting teeth and the inner stepped auger and core bit connection was begun this week. Contact was also made with several dry core drilling companies for information.

- A one-fourth scale model was built of the entire drilling operation. Preliminary drawings of the rod and interface mechanism were completed.

- A chuck-type mechanism was proposed for the design of the lunar excavation assistance foundation. An impeller type arrangement is also under consideration currently.

- Specifications for the CSM motor were obtained, and the sizes of heat pipes and radiators were calculated.

- Information on materials for the space environment was collected. Research is also under way for information pertaining to the method of attaching the platform to Skitter.

- From force analysis, the exertable force by the walker is estimated to be 450 lbs. in the upward direction, and 350 lbs downward. This will limit the size of the core that walker can pull up.

- Currently, five preliminary designs are being considered for the vertical accelerator.

- Three preliminary methods for bracing the micro-coring drill operation were presented during this week.

WEEK OF MAY 1, 1989

- A drilling increment of 0.4" was decided for the main drill bit.

- Possible materials for the rods are currently magnesium and titanium, or possibly some form of metal matrix composite. Final selection will depend on temperature requirements and strength.

- The chuck-type mechanism proposed last week has been replaced with a simpler, lighter design. The previous design was scrapped due to anticipated problems in sealing from dirt and dust and the complexity of the clamping device

- Batteries as a source of power for the drilling operation continue to cause problems due to the temperature limitations. Fuel cells are a possibility for an alternative power source.

- The interface shape was changed from triangular to hexagonal to accommodate the large rotary motor, power cells, and rod holders. The platform's depth was also increased.

- From the five preliminary designs for the vertical accelerator, the two most feasible are cams and locking ring mechanisms. Research is continuing of the properties of lunar rock.

- Issues in the control system of the lunar deep drilling operation were discussed this week with Dr. Mike Kelly of the Georgia Tech Research Institute.

- A mathematical model for the vertical accelerator is completed and can be implemented to optimize the required amount of force.

WEEK OF MAY 8, 1989

- The final dimensions of the cutting holders on the drill bit were completed. The core bit can drill to a depth of .43 in with out stopping for rock chip removal. Looking at the possible use of removable teeth. The implementation of heat pipes is being investigated.

- Force and deflection calculations for the clamping spring on the footplate were done. The selection of the micromotor that will provide a lifting motion for the spring. This motor will incorporate a built-in, sealed gear reducer and it will be insulated.

- The motor specifications were changed to a 5 hp CSM motor that will operate at 100 rpm. A clutch was incorporated into the design along with a solar radiator. The power supply will come from batteries stored in the rods that will last for 10 hours. The storage rack clips need to be modified for battery contacts.

- The height of the mechanical interface reduced due to only 2" of height needed for the motor.

- Cams or a locking ring mechanism will be used in the macrocore retrieval and storage process.

- A mathematical model of the vertical accelerator for the stepped auger is complete. This is capable of optimizing the force required in determining the design parameters

- The motor and cam system utilized in bracing the micro-coring drill are complete. The current design is also completed, using only one motor to drive the drill translation.

WEEK OF MAY 15, 1989

- Preliminary analysis of the heat developed at the cutting interface was developed and this will allow the calculation of the temperature at the teeth. The final problem was sectioned in smaller subsections.

- The rod interface was redesigned to accomodate the connection of two stepped augers. The selection of possible materials was narrowed to four.

- Calculations for the deflection of the foot plate were almost finalized. Modifications to the flat spring are still being discussed.

- A material was selected for the structural frame of the drilling platform. The material selected was aluminum reinforced with 40% silicon carbide fibers.

- The design of the rod changer and storage rack were almost completed. Al 2219-T37 was used as the main material and MoS_2 was selected for the lubrication.

- Computer operating screens were developed for the control console. Time calculations for the length of the entire drilling process were conducted.

- The bearings for the vertical accelerator were sized and designed.

- The micro coring drill will be powered by two seperate motors that are independent of the main motor. The drill will be protected by a sliding door.

WEEK OF MAY 22, 1989

The final week was almost entirely dedicated to the preparation of the final report and the models for the formal presentation of the project.

- A new method of power supply was adopted. Due to the excessive weight of a battery powered system, a hydrogen-oxygen fuel cell system was adopted.

- For the macro core retrieval a new system was designed. A cutting device similar to a pipe cutter, powered by a spring, will be used to cut the core. The device will no longer be attached to the drill bit, but be contained in a separate cylinder.

- The design of the rack clip was finalized and the force analysis was completed on the robot arm.

APPENDIX D

DRAWINGS

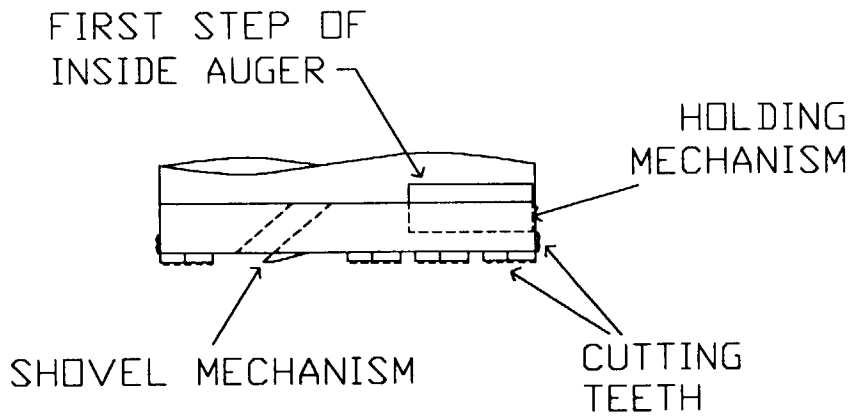

TEETH DESIGN

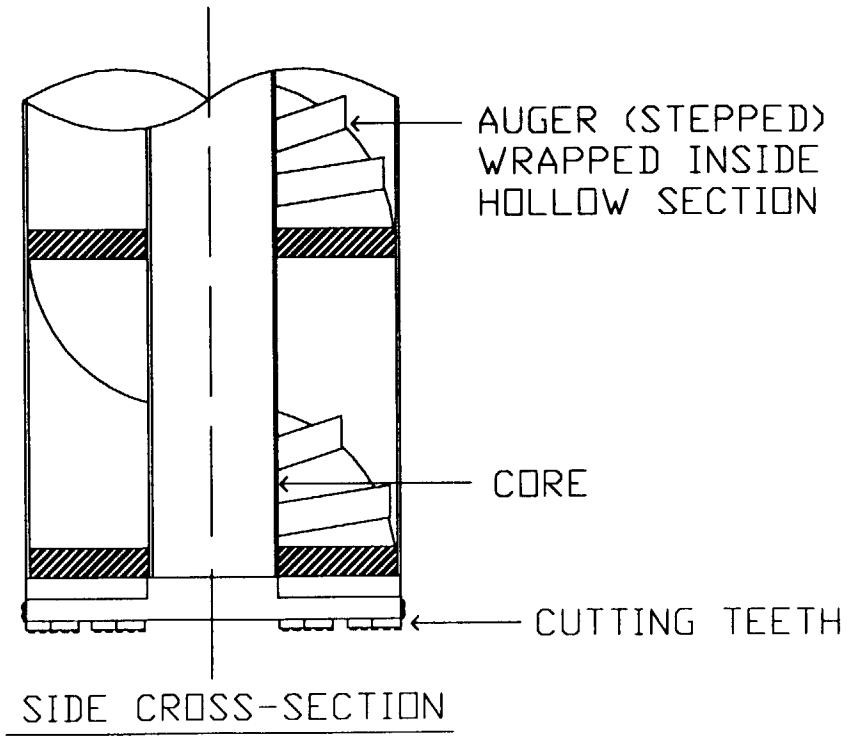

SIDE CROSS-SECTION

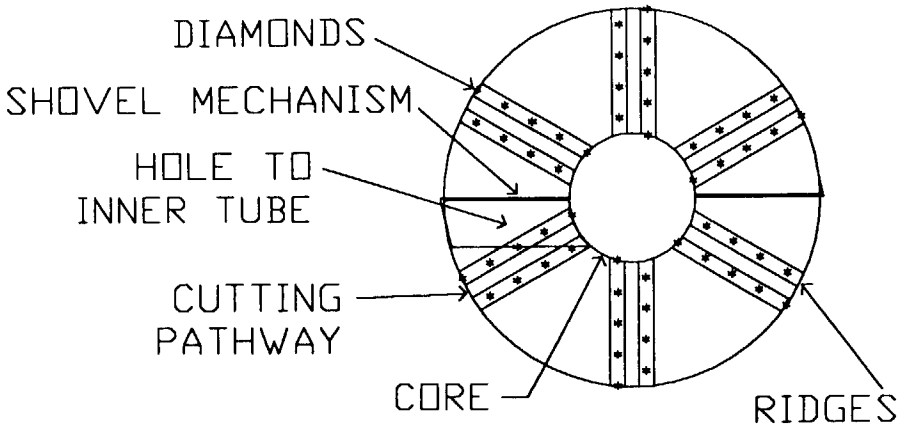

BOTTOM

PRELIMINARY DESIGN	GROUP #1
SPECIFICATIONS ON BIT	

BIT DIMENSIONS:

- LENGTH=2m
- OUTSIDE DIA=100mm
- CORE=50mm
- -DOUBLE HELICAL AUGER
- -SHALL BE A STEPPED AUGER
- -WILL BE CONNECTED TO THE ROD ABOVE THE BIT

TEETH DETAIL:

- -WILL BE DIAMOND COVERED AND RECTANGULAR
- -STAGGERED AS SHOWN IN BOTTOM VIEW
- -EACH SET HAS OWN HOLE AND SCOOP

ME4182 MECHANICAL DESIGN 4.1.4.1

BIT DESIGN - GROUP #1

OVERALL DESIGN AND DOCUMENTATION

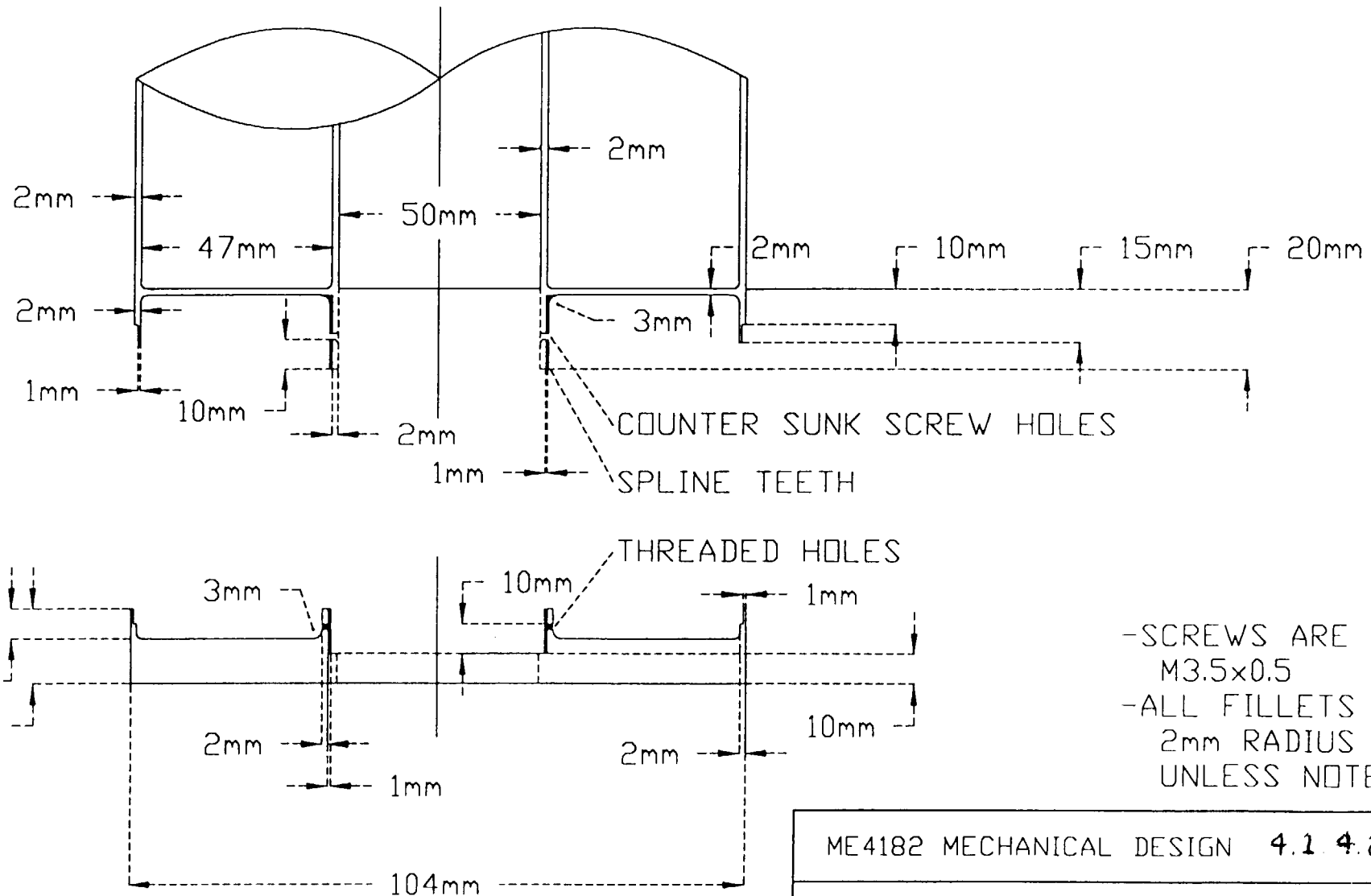

-SCREWS ARE M3.5x0.5
-ALL FILLETS ARE 2mm RADIUS UNLESS NOTED

ME4182 MECHANICAL DESIGN 4.1 4.2
BIT DESIGN - GROUP #1
SPLINE CONNECTION DESIGN

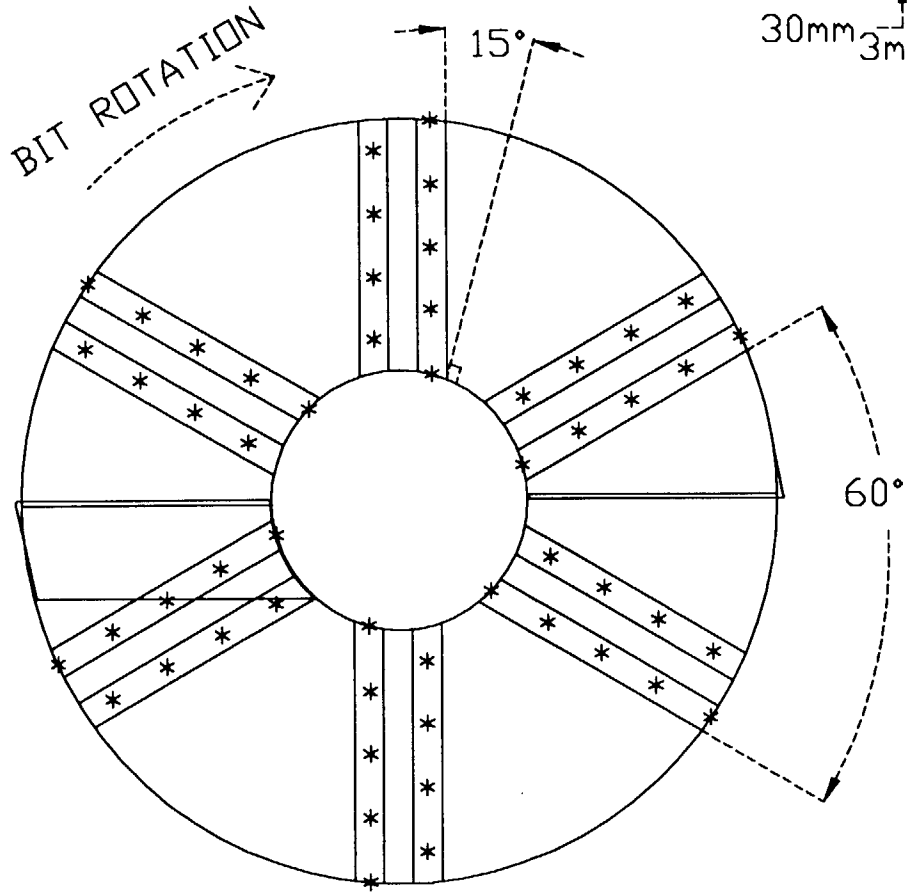

BOTTOM

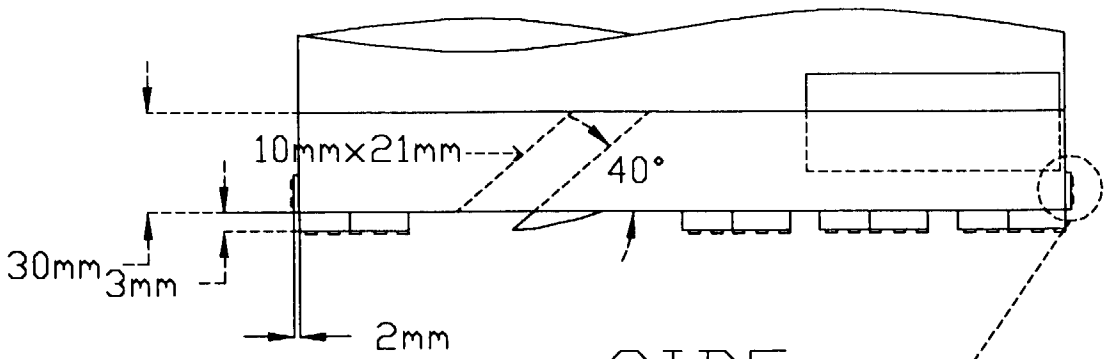

SIDE

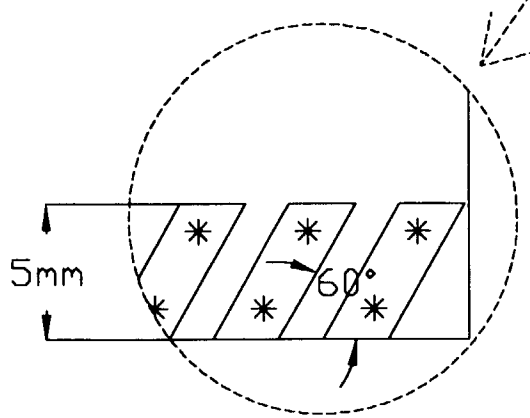

✳ SEE DRAWING 4.1.5.1 FOR PART DETAILS

ME4182 MECHANICAL DESIGN 4.1.1.1
BIT DESIGN - GROUP #1
TEETH DESIGN

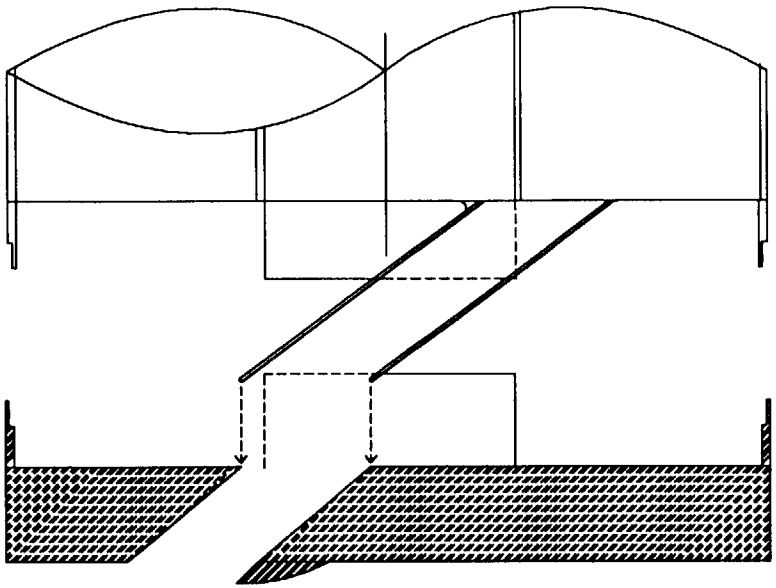

SCOOP BETWEEN UPPER AND LOWER BIT

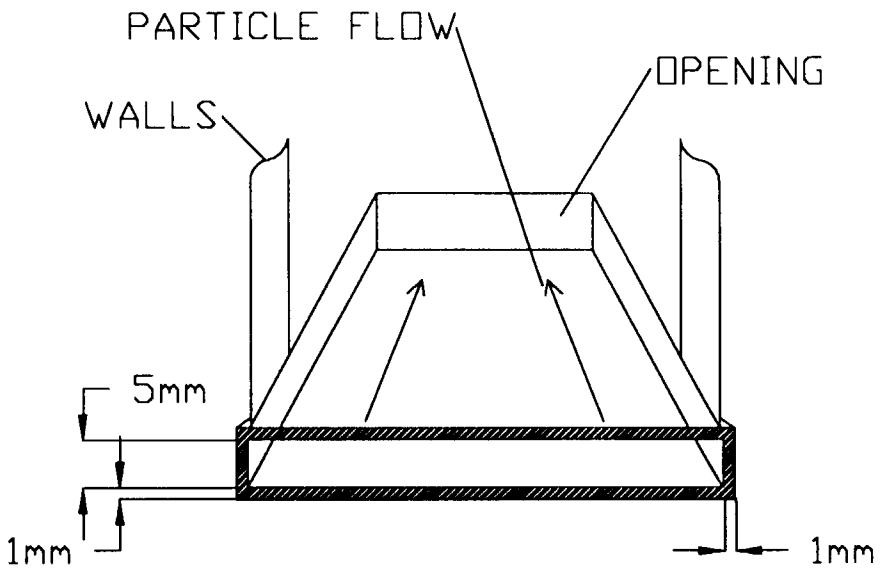

FRONT VIEW

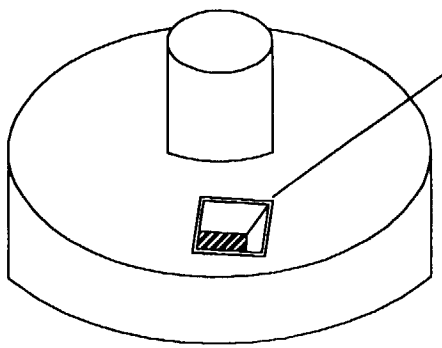

OVERALL VIEW

- NOTE: EXTENSION FROM THE UPPER BIT SURROUNDS THE RING EXTENDING FROM THE LOWER BIT SURFACE

✳ SEE DRAWING 4.1.1.1 FOR OUTER DIMENSIONS OF THE SHOVEL

ME4182 MECHANICAL DESIGN 4.1.2.1
BIT DESIGN - GROUP #1
SCHEMATIC OF SHOVEL DESIGN

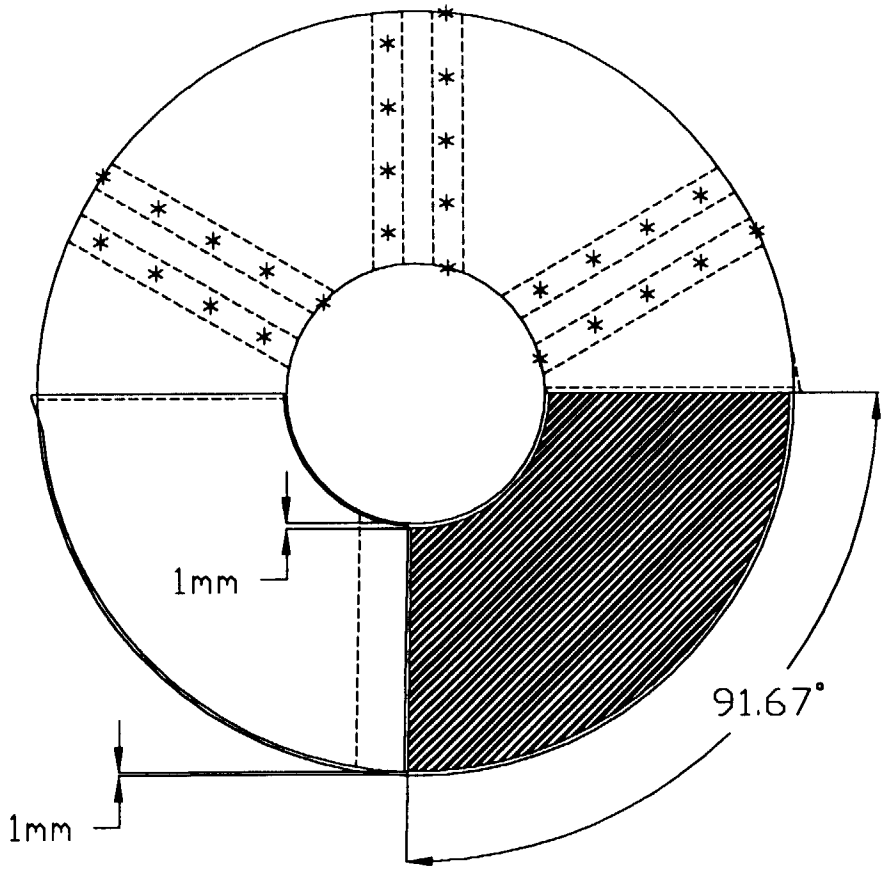

TOP VIEW

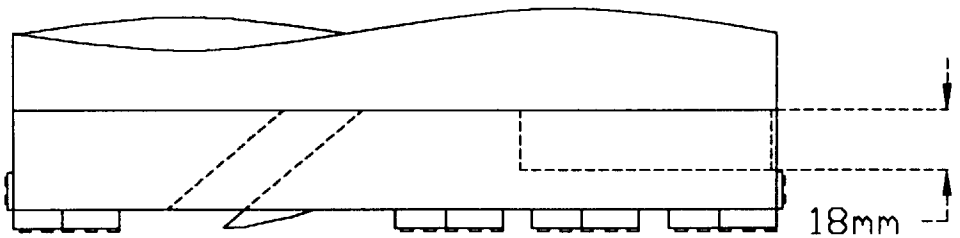

FRONT VIEW

ME4182 MECHANICAL DESIGN 4.1.3.1
BIT DESIGN - GROUP #1
HOLDING DEVICE DESIGN

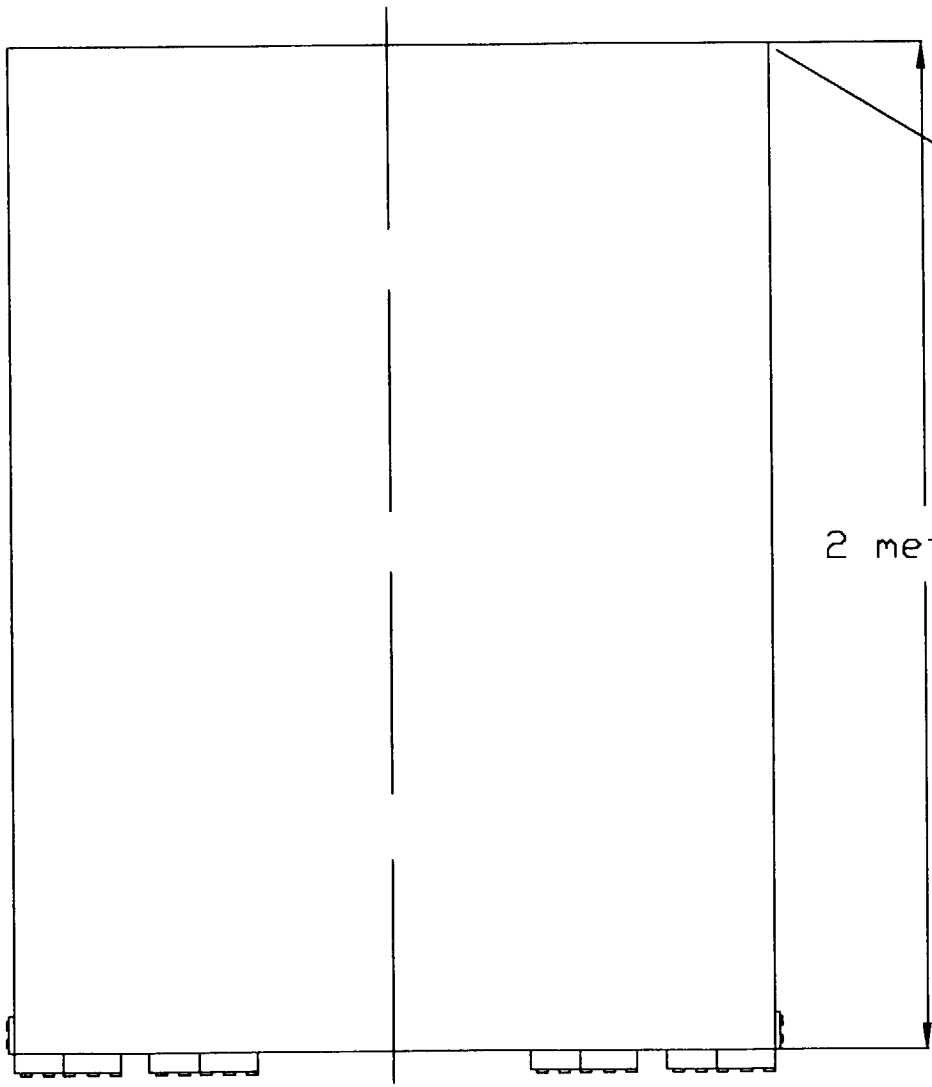

-NOTE: FOR A DIAGRAM OF THE ROD INTERFACE FOR THE BIT AND THE NEXT ROD, SEE DRAWING 4.2.4.1

ME4182 MECHANICAL DESIGN 4.1.8.1
BIT DESIGN - GROUP #1
SCHEMATIC OF BIT AND ROD CONNECTION

ROD ENDS

FRONT VIEW - MALE INTERFACE

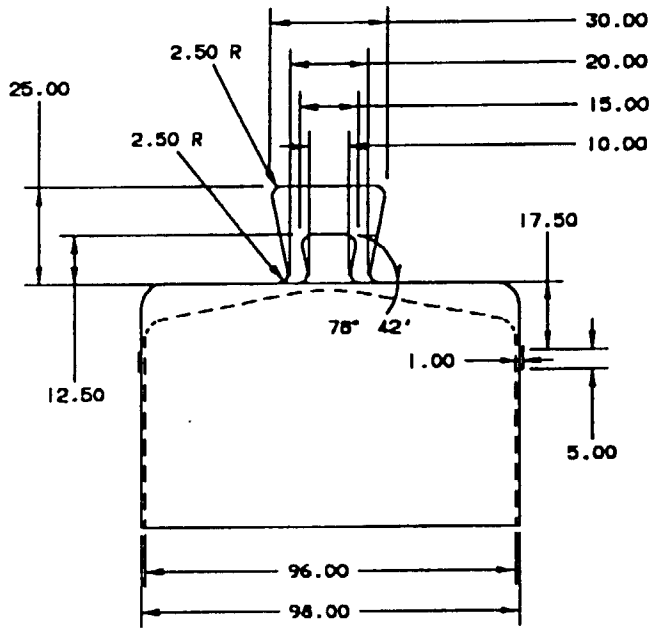

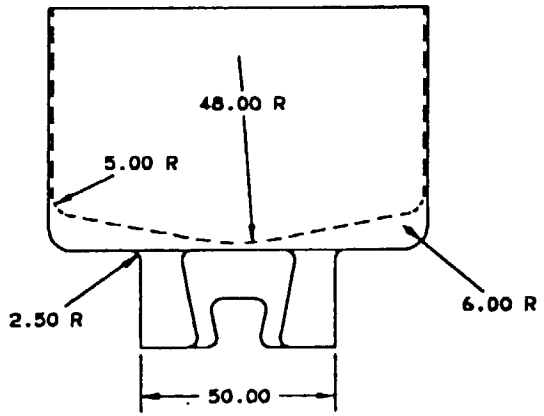

BACK VIEW - FEMALE INTERFACE

MADE OF TITANIUM-5-2.5

GEORGIA TECH COLLEGE OF ENGINEERING
MECHANICAL ENGINEERING DESIGN
ME 4182-A GROUP 2
APPENDIX A.2.4.1 ROD ENDS
UNITS: MM SCALE: 0.5/1

ROD ENDS

SIDE VIEW - MALE INTERFACE

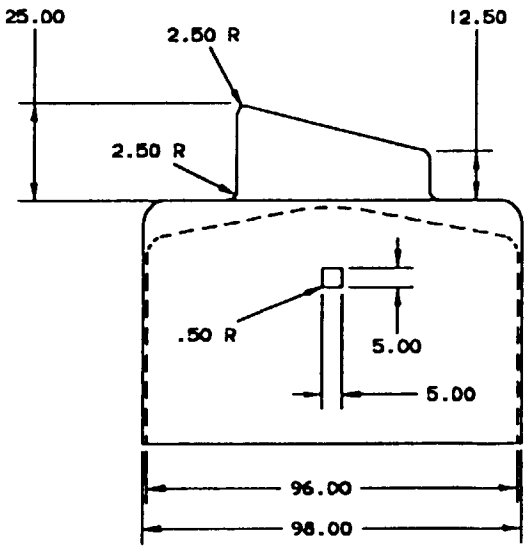

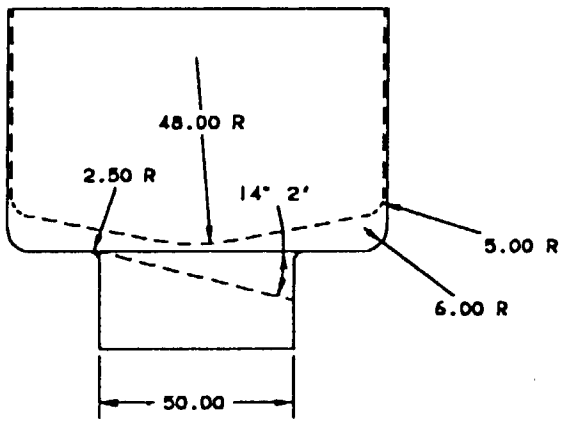

SIDE VIEW - FEMALE INTERFACE

MADE OF TITANIUM-5-2.5

GEORGIA TECH COLLEGE OF ENGINEERING
MECHANICAL ENGINEERING DESIGN
ME4182-A GROUP 2
APPENDIX .4.2.4-2 ROD ENDS
UNITS: MM SCALE: 0.5/1

ROD ENDS

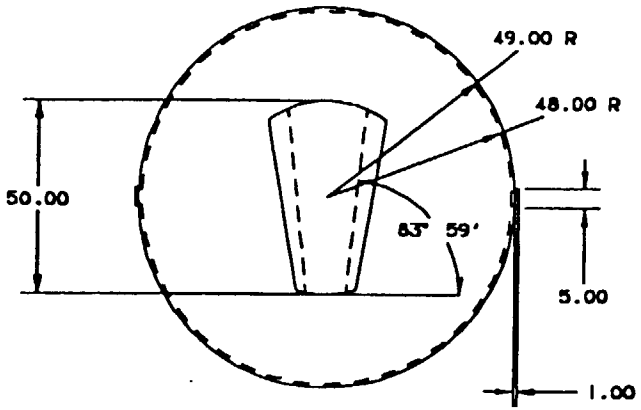

TOP VIEW - MALE INTERFACE

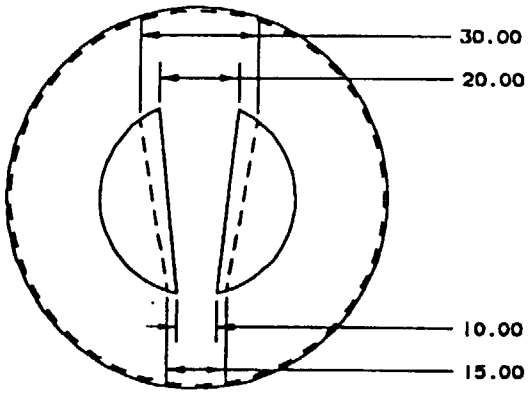

BOTTOM VIEW - FEMALE INTERFACE

MADE OF TITANIUM-5-2.5

GEORGIA TECH COLLEGE OF ENGINEERING	
MECHANICAL ENGINEERING DESIGN	
ME4182-A	GROUP 2
APPENDIX 4.4c 4.3	ROD ENDS
UNITS: MM	SCALE: 0.5/1

COLLAR

FRONT VIEW

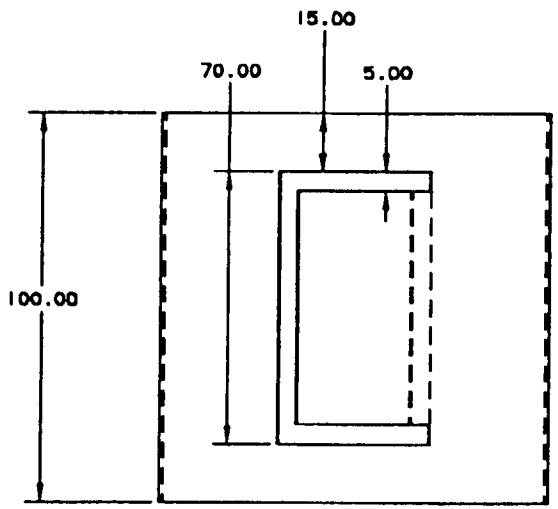

TOP VIEW

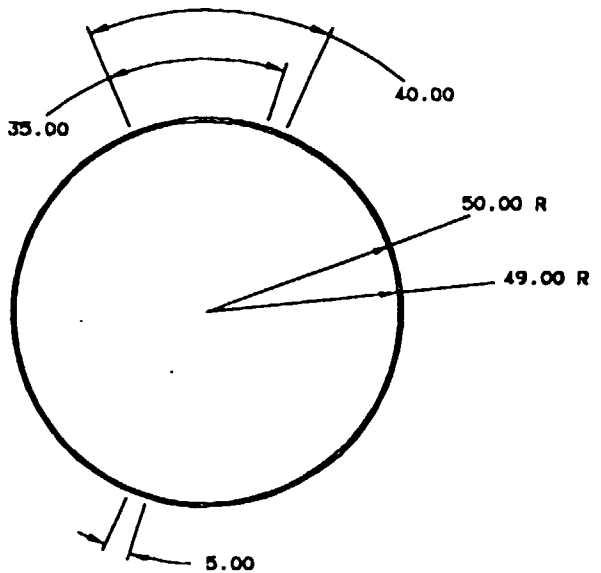

MADE OF TITANIUM-5-2.5

GEORGIA TECH COLLEGE OF ENGINEERING
MECHANICAL ENGINEERING DESIGN
ME4182-A GROUP 2
APPENDIX : 4.2.4.4 COLLAR
UNITS: MM SCALE: 0.5/1

DRAWING 4.3.2.1

FOOTPLATE PLANE AND ELEVATION VIEWS

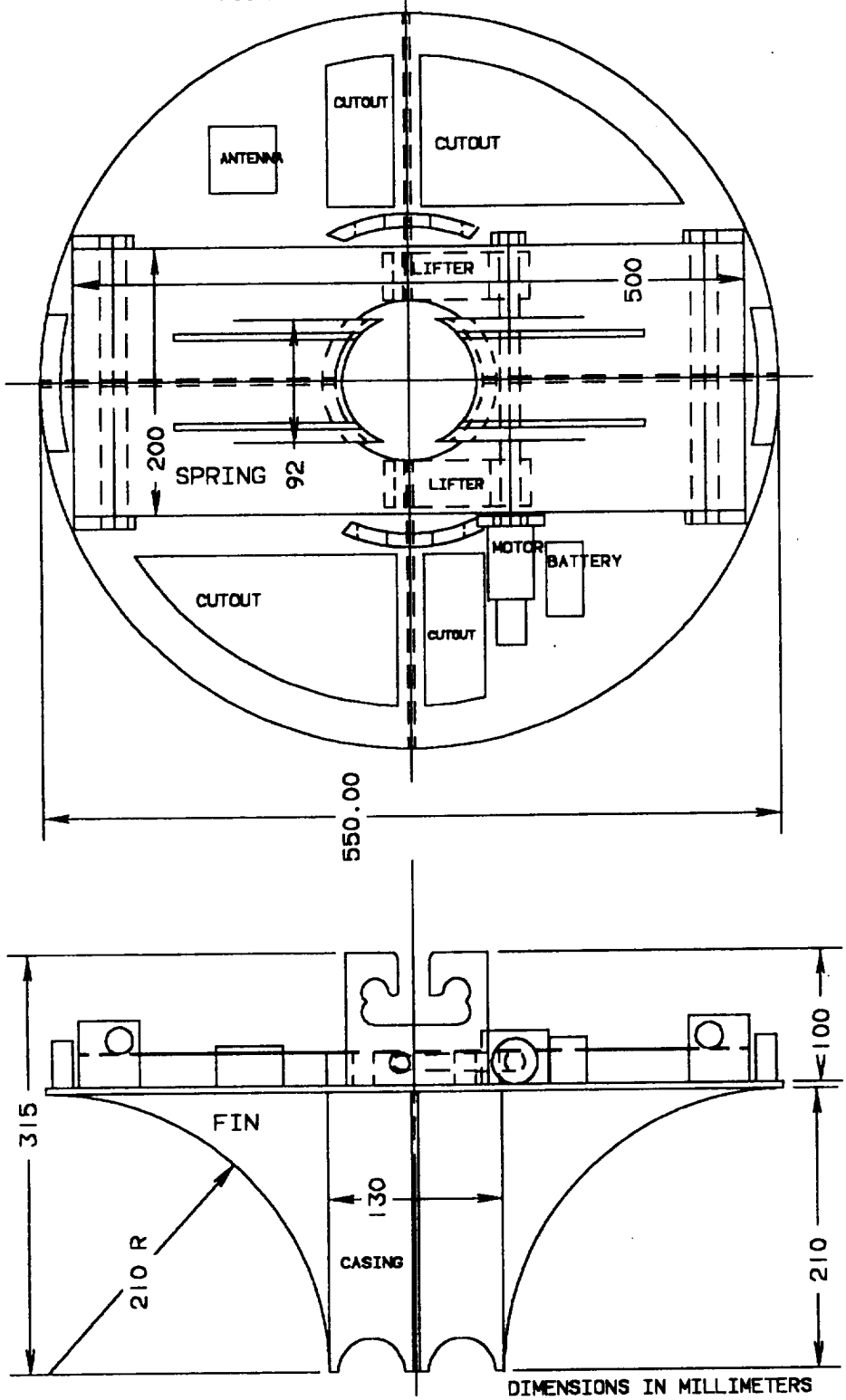

DIMENSIONS IN MILLIMETERS

DRAWING 4.3.2.2

FOOTPLATE DRIVE INTERFACE

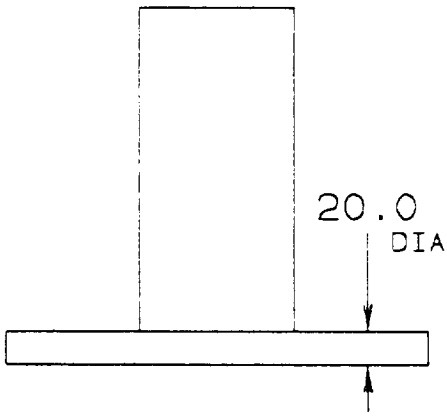

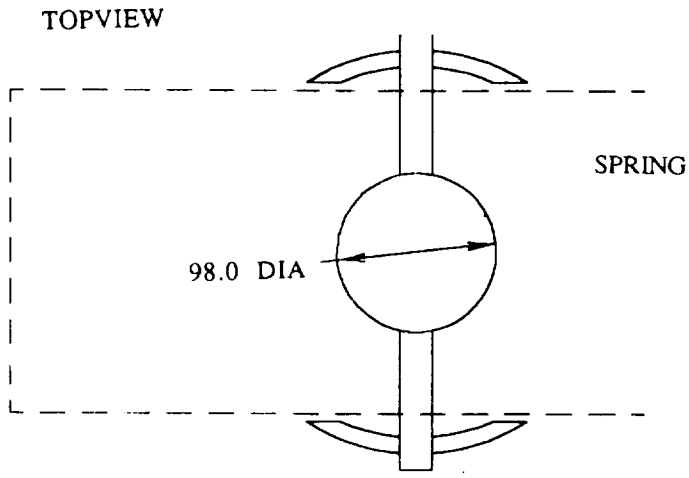

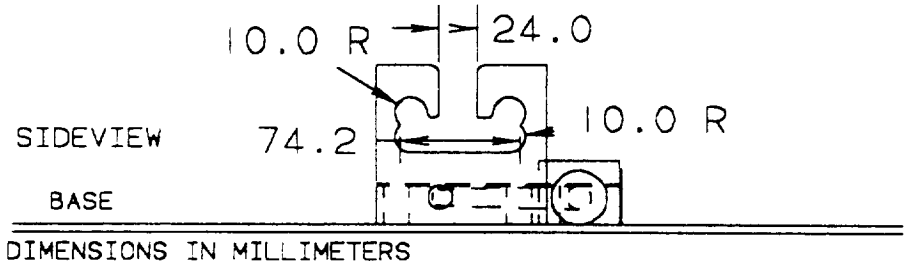

DIMENSIONS IN MILLIMETERS

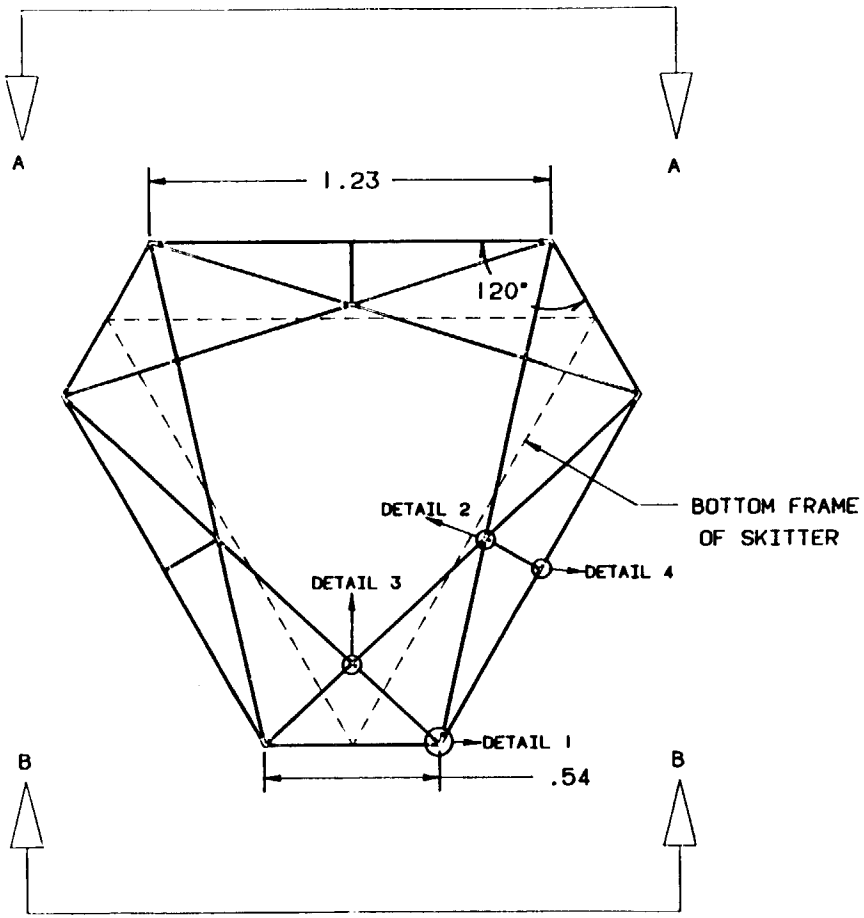

TOP PANEL OF

STRUCTURAL INTERFACE

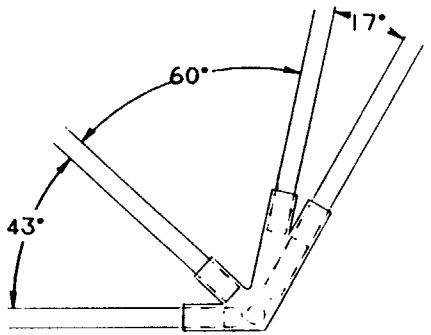

DETAIL 1

6 REQD. AS SHOWN

6 REQD. OPPOSITE HAND

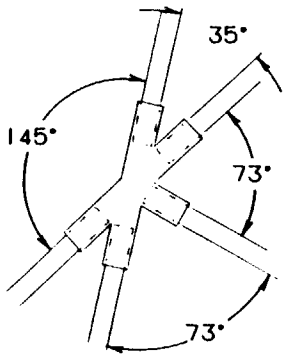

DETAIL 2

3 REQD. AS SHOWN

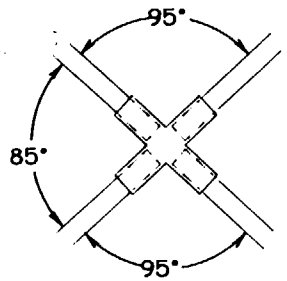

DETAIL 3

3 REQD. AS SHOWN

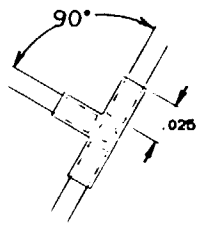

DETAIL 4

6 REQD. AS SHOWN

NOTE: SEE DRAWING 3 FOR SECTION A-A & B-B

GEORGE W. WOODRUFF SCHOOL OF MECHANICAL ENGINEERING
TITLE: TOP PLATFORM
DESIGN: STRUCTURAL INTERFACE
DATE: 5/28/89
DRWG NO. 4.5.4.1

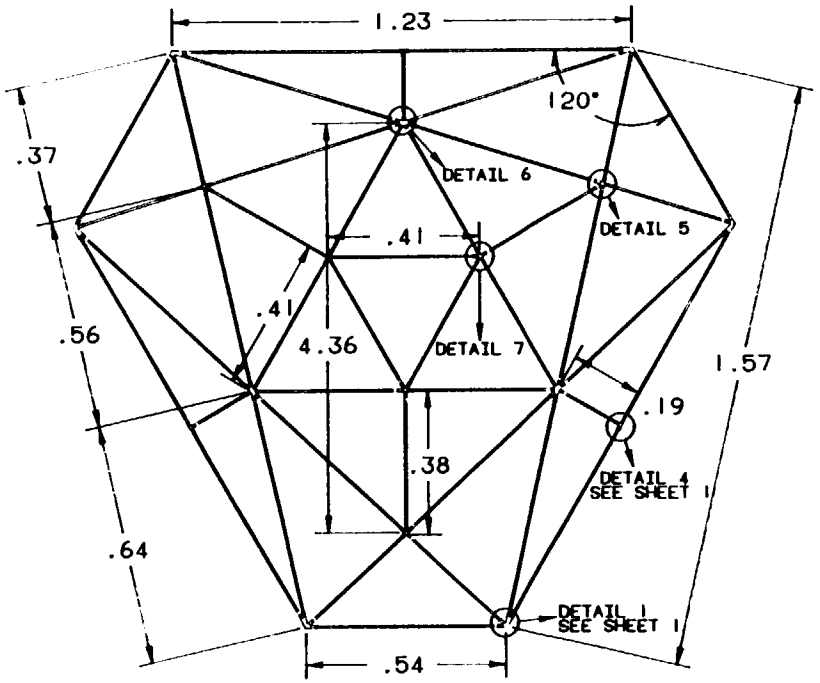

BOTTOM PANEL OF

STRUCTURAL INTERFACE

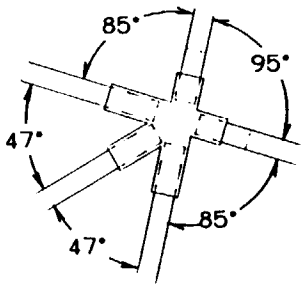

DETAIL 5

3 REQD. AS SHOWN

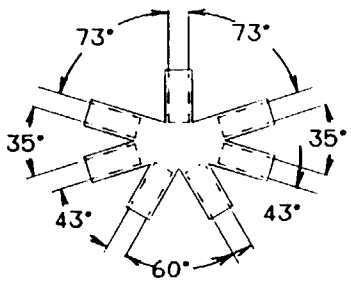

DETAIL 6

3 REQD. AS SHOWN

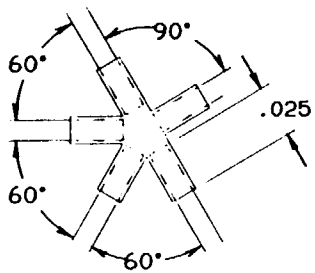

DETAIL 7

3 REQD. AS SHOWN

NOTE: SEE DRAWING 3 FOR SECTION A-A & B-B

GEORGE W. WOODRUFF SCHOOL OF MECHANICAL ENGINEERING
TITLE: BOTTOM PLATFORM
DESIGN: STRUCTURAL INTERFACE
DATE: 5/28/89
DRWG NO. 4.5.4.2

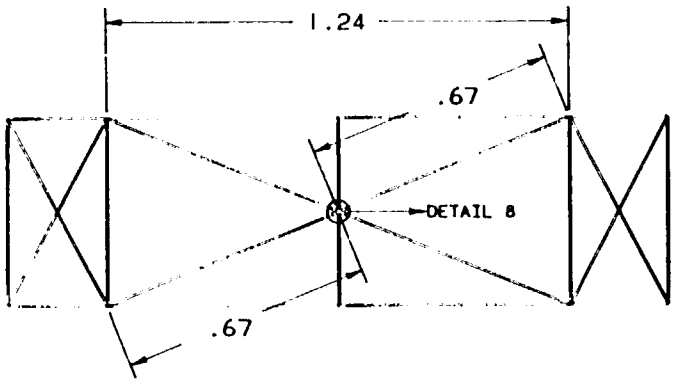

SECTION A-A

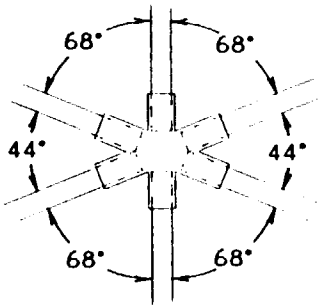

DETAIL 8

3 REQD. AS SHOWN

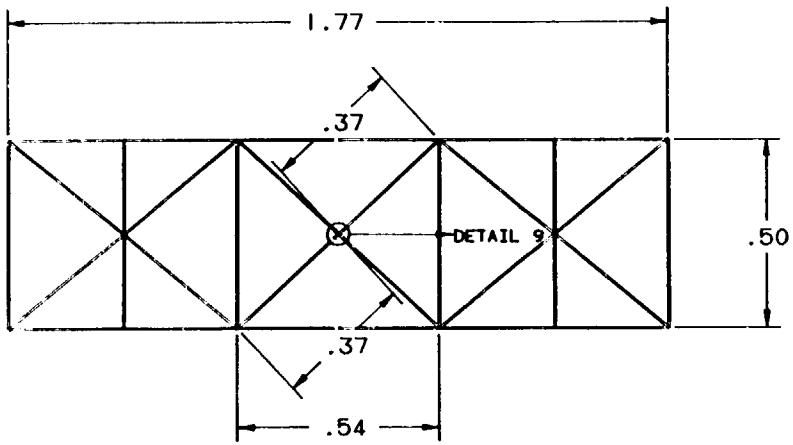

SECTION B-B

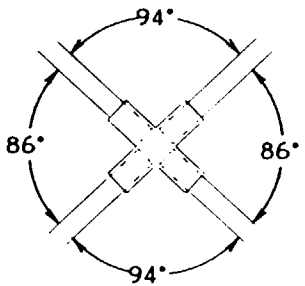

DETAIL 9

3 REQD. AS SHOWN

GENERAL NOTES:

1. ALL DIMENSIONS SHOWN ARE IN METERS
2. DRAWINGS ARE NOT TO SCALE
3. SLEEVES SHALL BE CAST USING AN ALUMINUM MATRIX WITH CONTINUOUS SILICON-CARBIDE FIBERS
4. ALL STRUCTURAL MEMBERS ARE TO BE .0254 M DIAMETER EXTRUDED ALUMINUM MATRIX WITH CONTINUOUS SILICON-CARBIDE FIBERS

GEORGE W. WOODRUFF SCHOOL OF MECHANICAL ENGINEERING
TITLE: SECTION VIEW
DESIGN: STRUCTURAL INTERFACE
CHECK: 5/28/89
DRWG NO. 4.5.4.3

Side view - Rod Rack Support members

Drawing 4.6.3.1

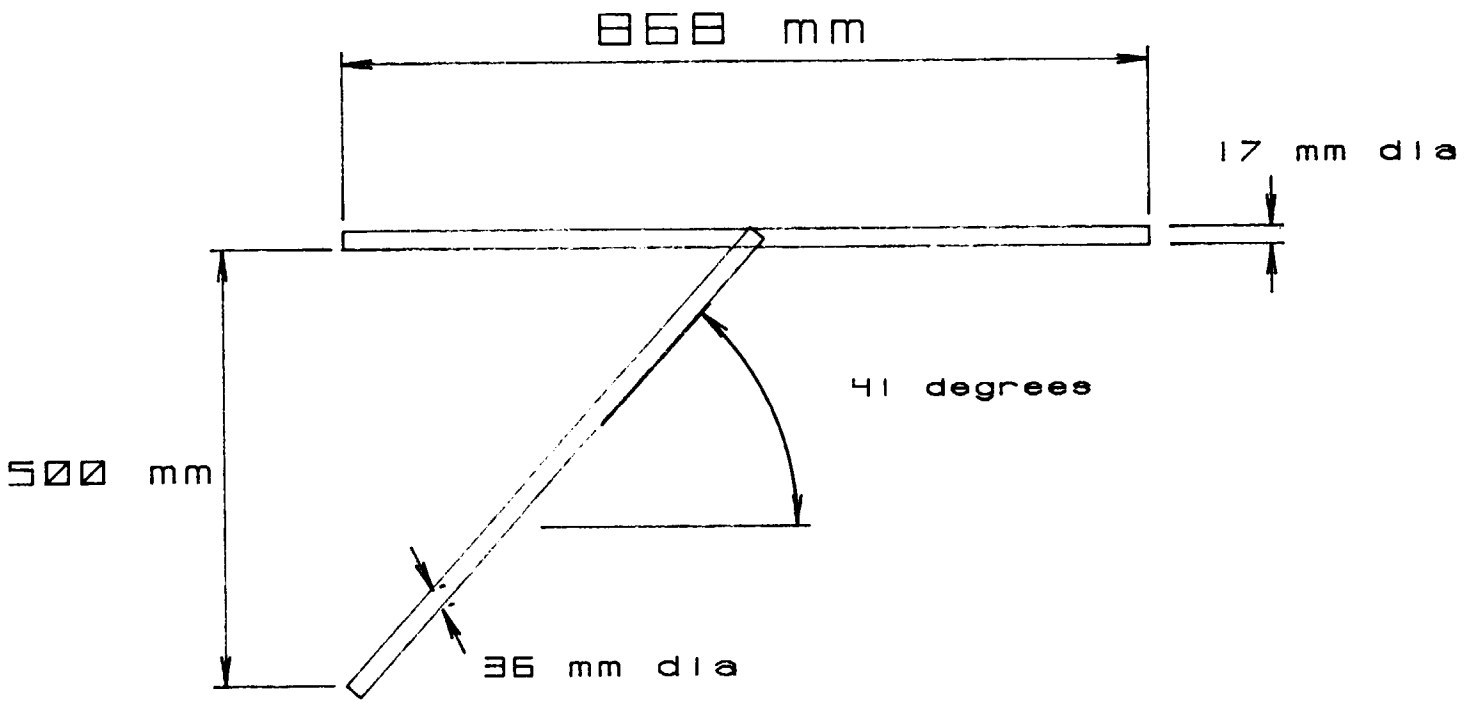

Drawing 4.6.4.1

Rod Changer Arm

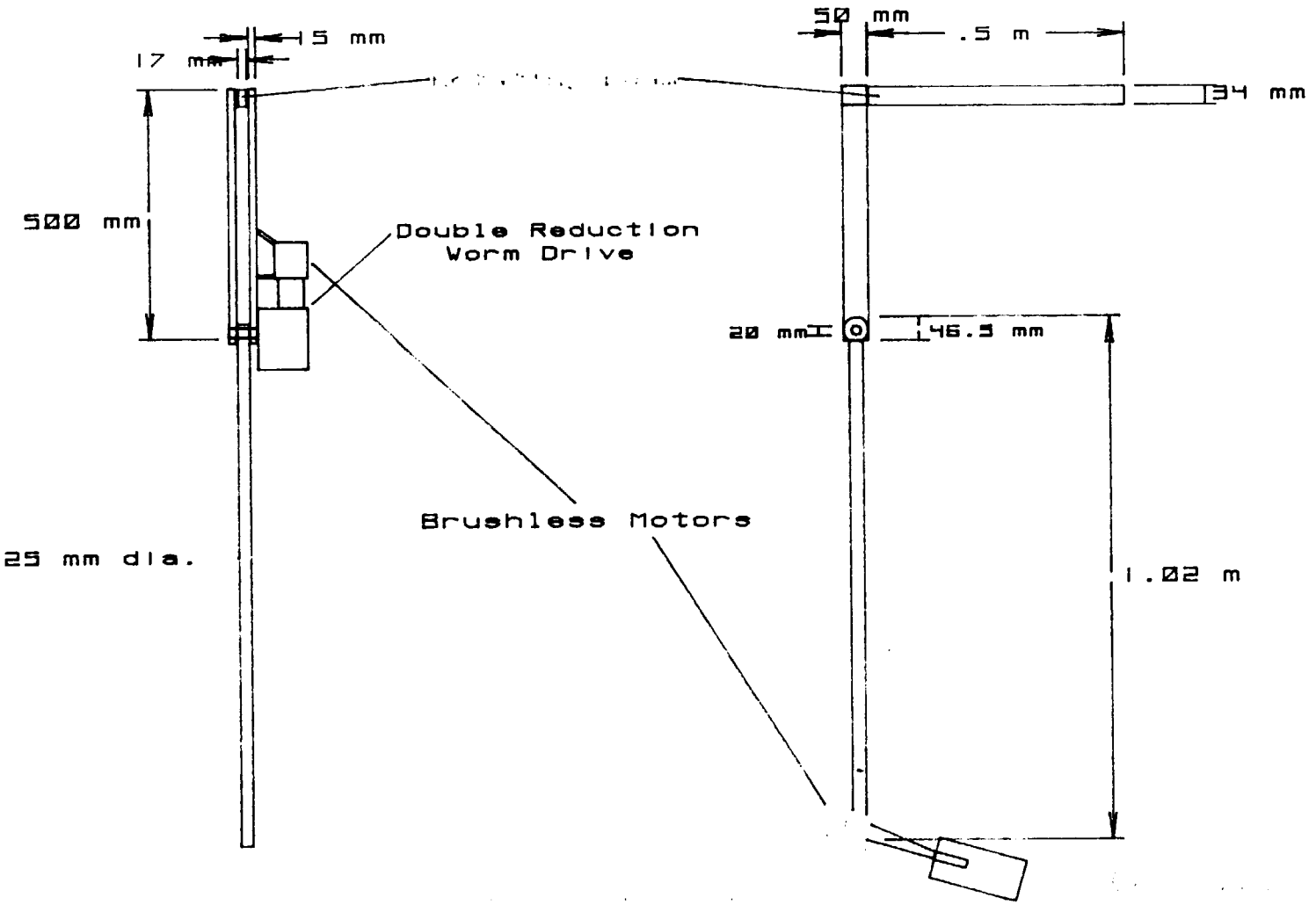

front view

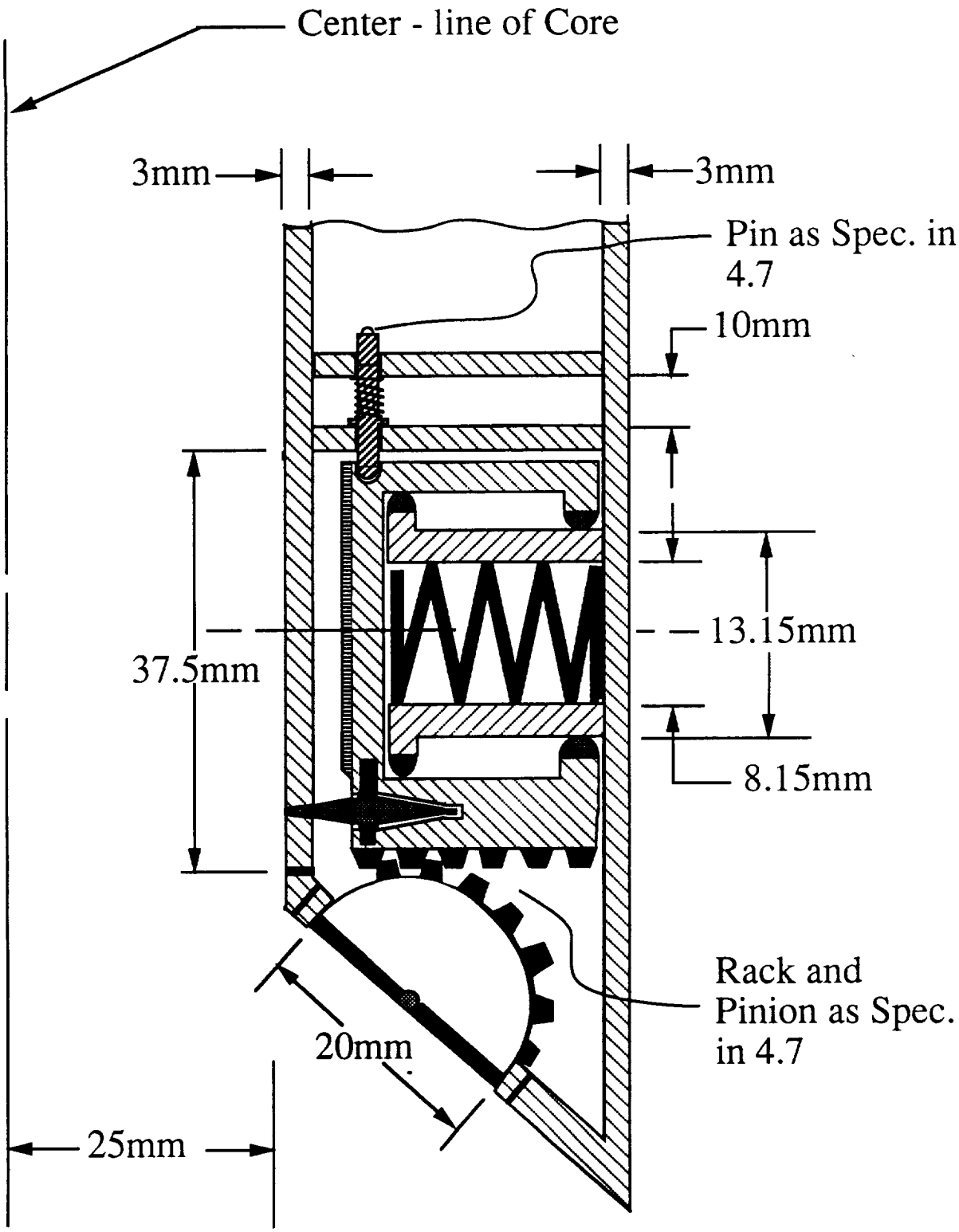

*DRAWING NOT TO SCALE

ME 4182 MECHANICAL DESIGN
MACRO-CORE RETRIEVER - GROUP 7
CUTTER WHEEL SECTION

Drawing 4.7.7.1

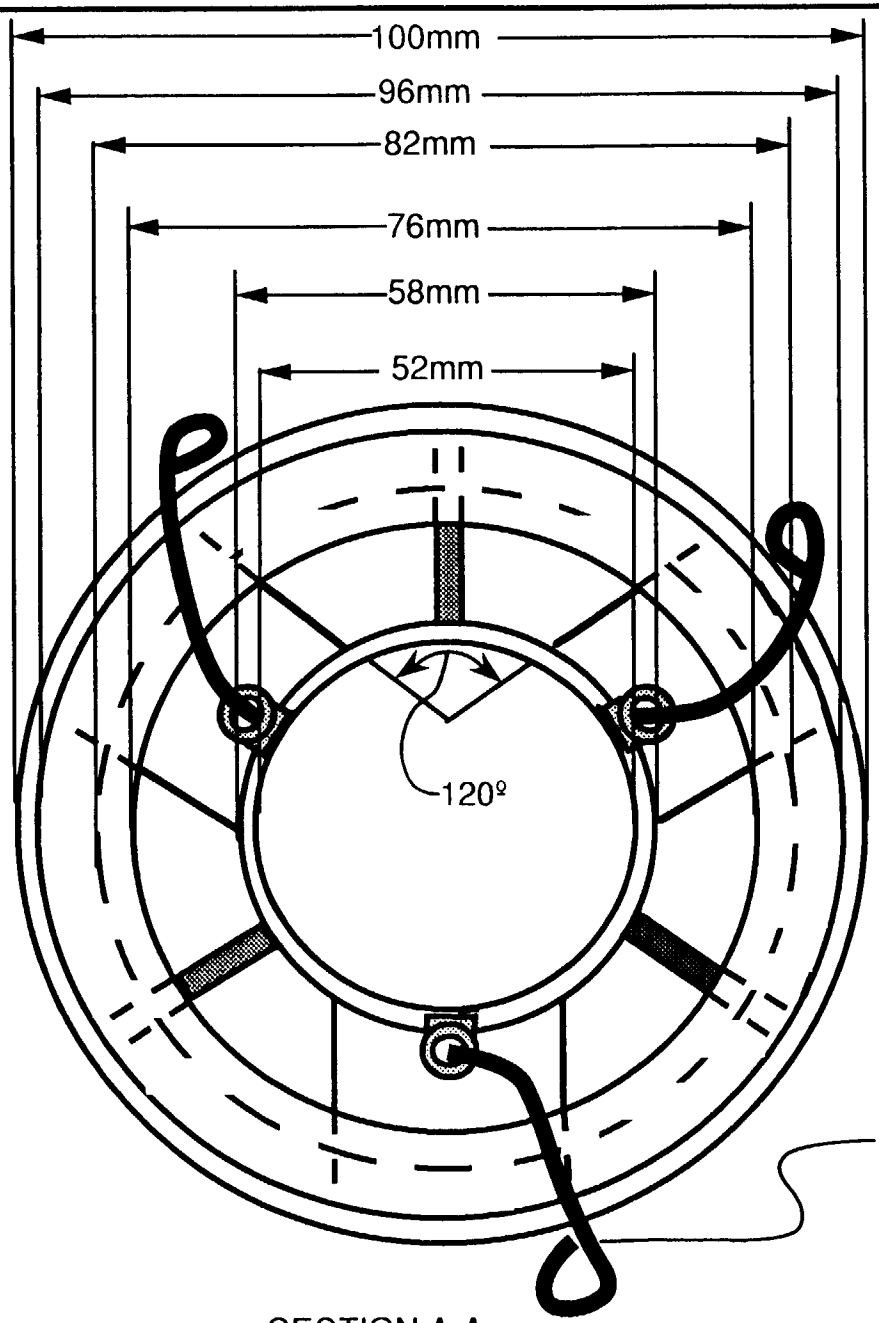

SECTION A-A

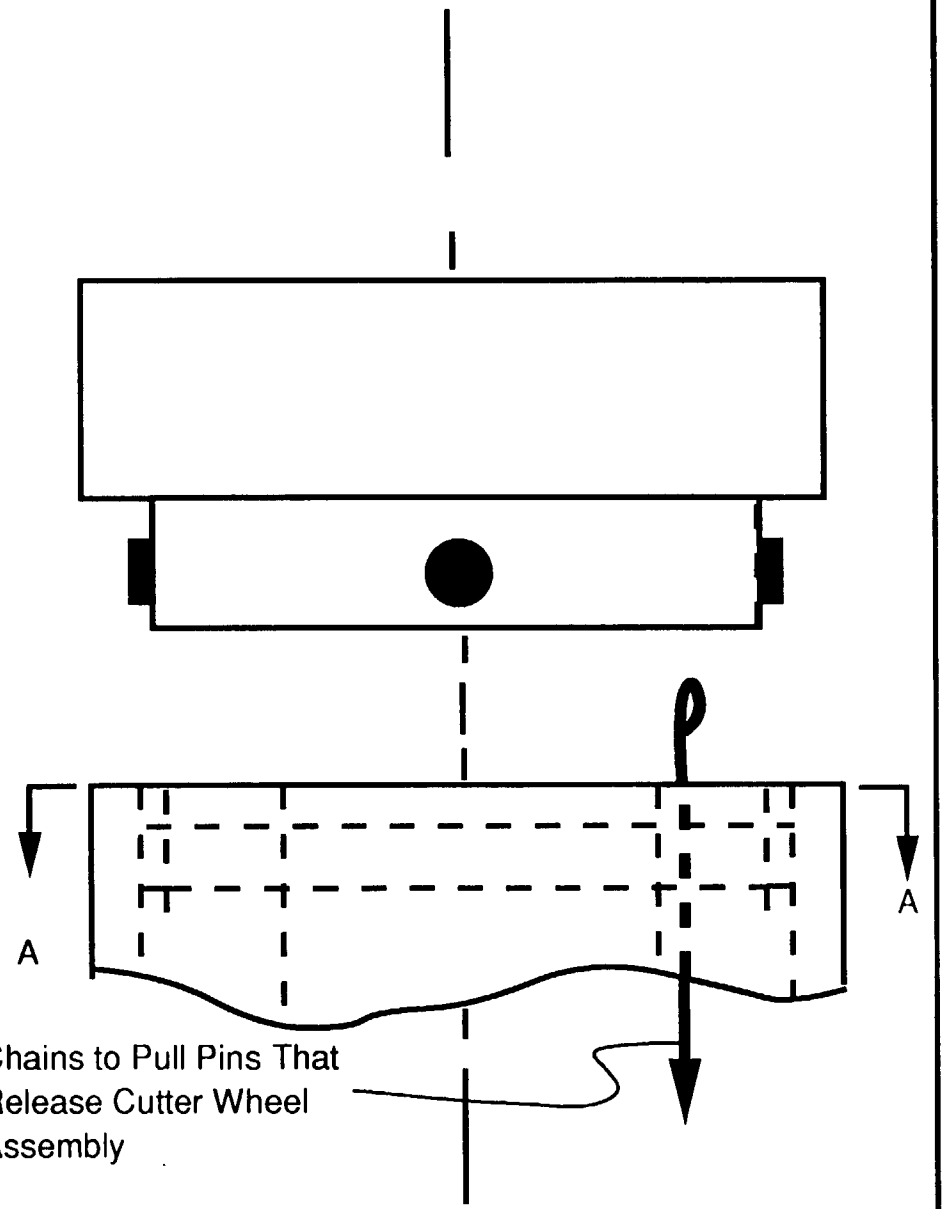

Chains to Pull Pins That Release Cutter Wheel Assembly

Drawing 4.7.7.2

ME 4182 MECHANICAL DESIGN
MACRO-CORE RETRIEVER - GROUP 7
TOP CONNECTION

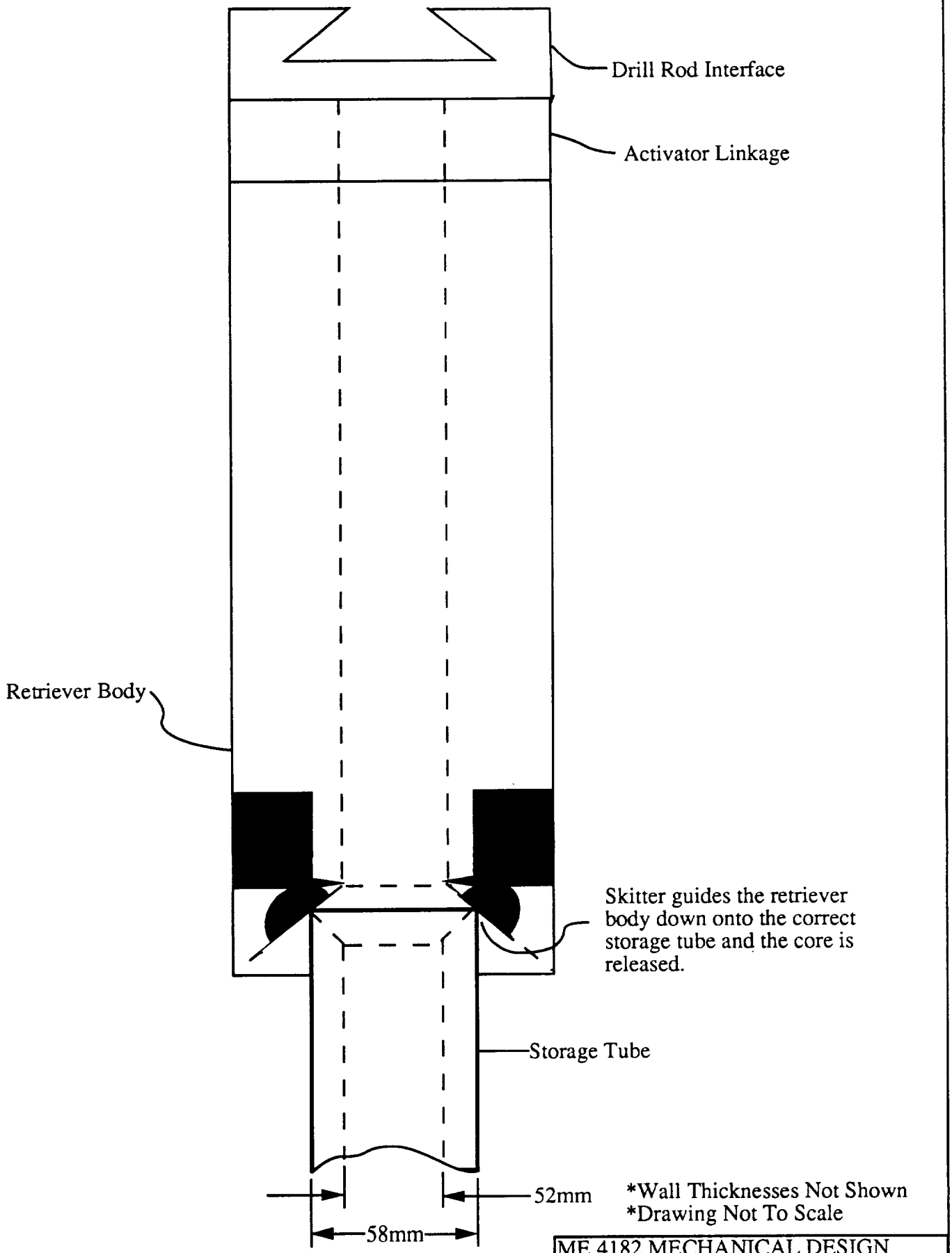

*Wall Thicknesses Not Shown
*Drawing Not To Scale

ME 4182 MECHANICAL DESIGN
MACRO-CORE RETRIEVER - GROUP 7
RESET OF CUTTERS

Drawing 4.7.7.3

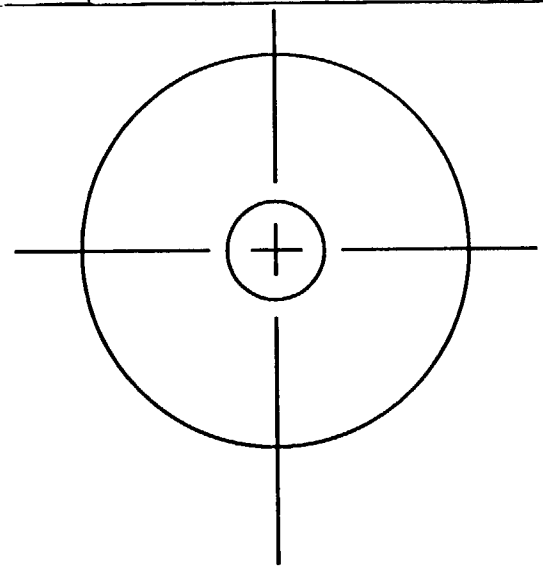

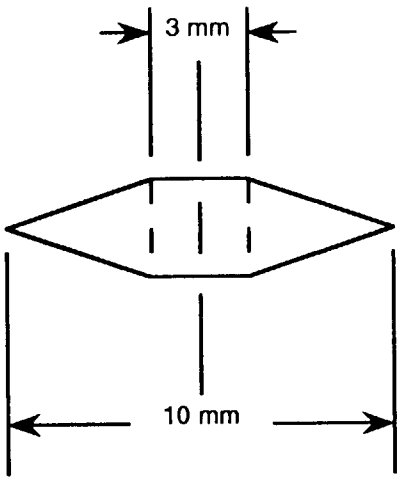

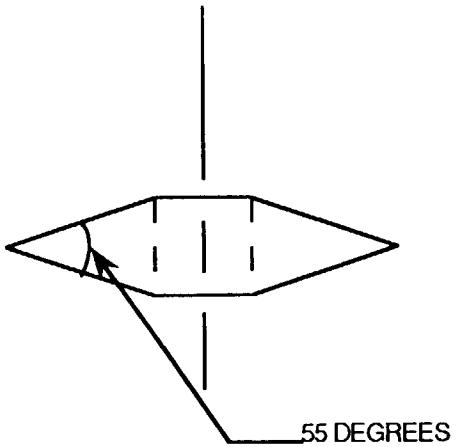

ME 4182 MECHANICAL DESIGN
MACRO-CORE RETRIEVER GROUP 7
DISK CUTTER
DRAWING 4.7.10.1

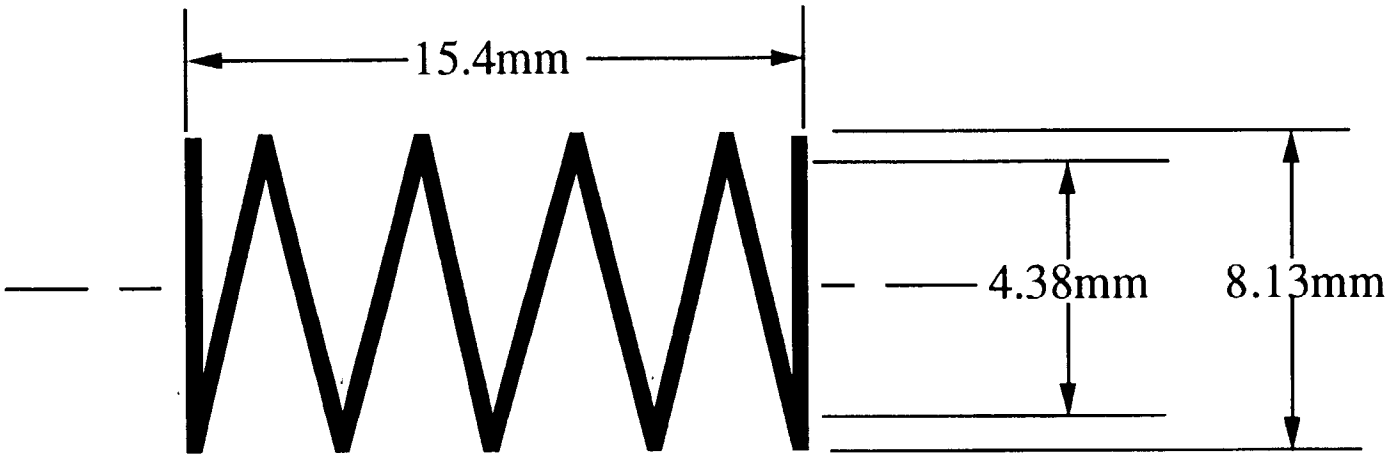

Main Spring for Cutter Wheel Assembly
D = 8.13mm
d = .12mm
Total Turns = 8.5
Spring Constant k = 20.5 lbs/in
Ends Squared

* DRAWING NOT TO SCALE

ME 4182 MECHANICAL DESIGN
MACRO-CORE RETRIEVER - GROUP 7
SPRING DESIGN

Drawing 4.7.11.1

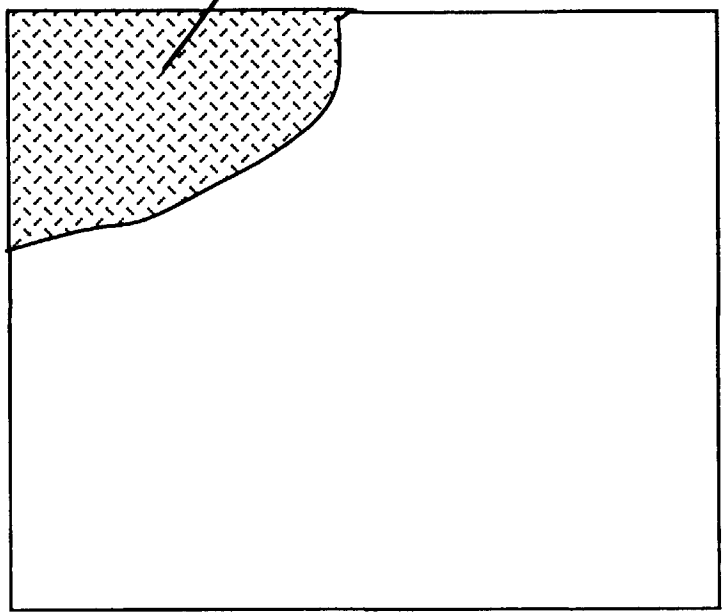

Front View

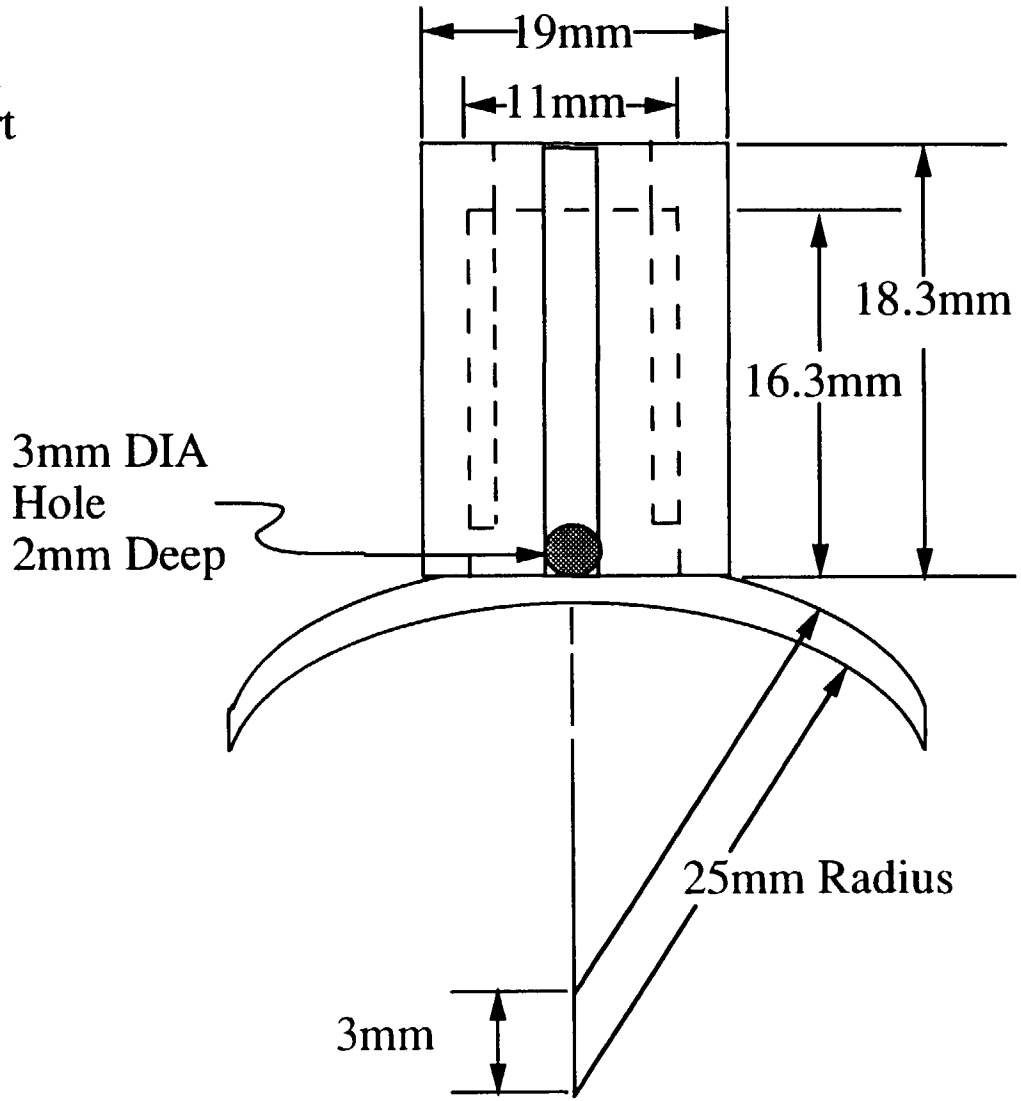

Top View

*DRAWING NOT TO SCALE

ME 4182 MECHANICAL DESIGN
MACRO-CORE RETRIEVER - GROUP 7
CORE GRIPPER ASSEMBLY

Drawing 4.7.14.1

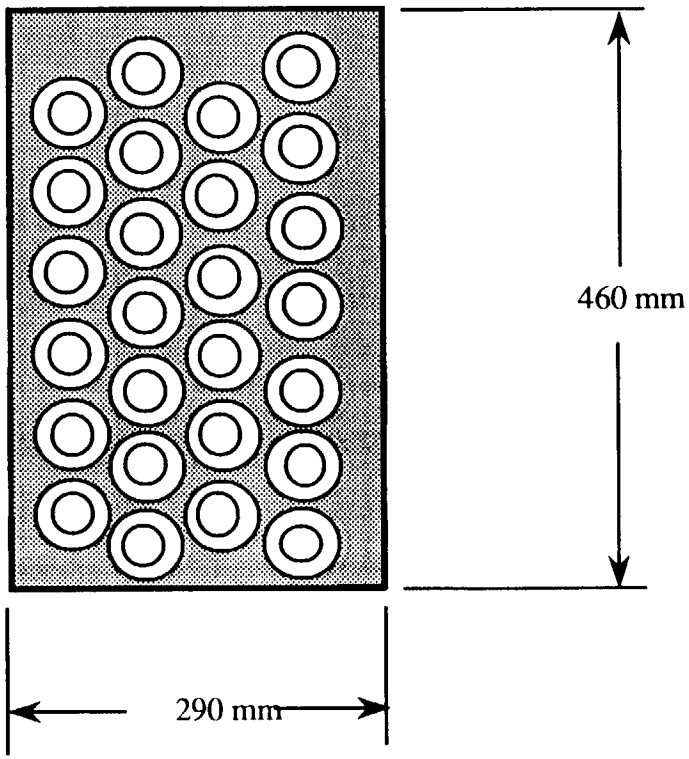

Section A - A

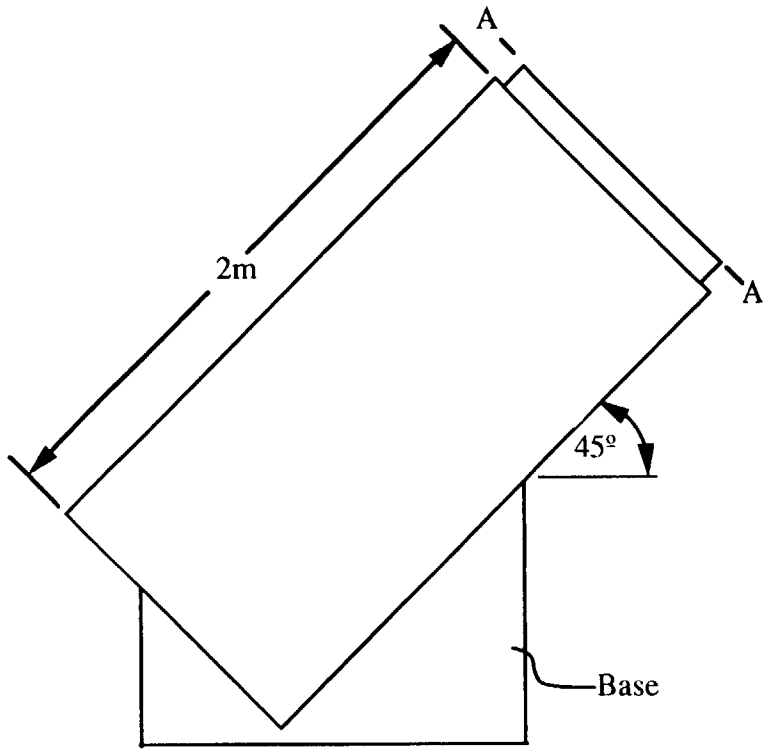

Side View

The Tube Storage Bank is positioned at a 45 º angle near Skitter to facilitate the deposit of retrieved cores.

*Drawing Not To Scale

ME 4182 MECHANICAL DESIGN
MACRO-CORE RETRIEVER - GROUP 7
STORAGE DEVICE

Drawing 4.7.16.1

Control Console
Side View

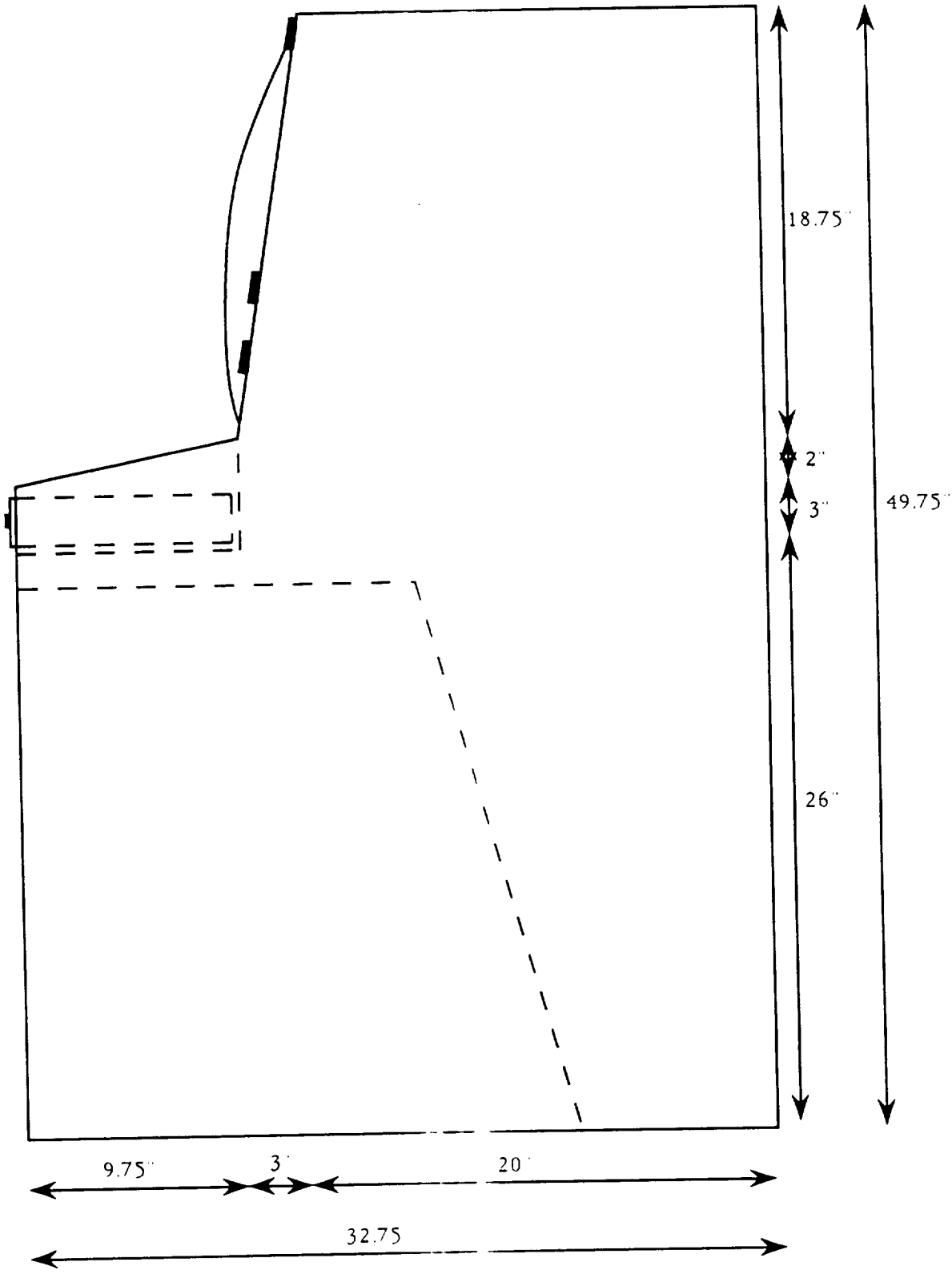

Control Console
Front View

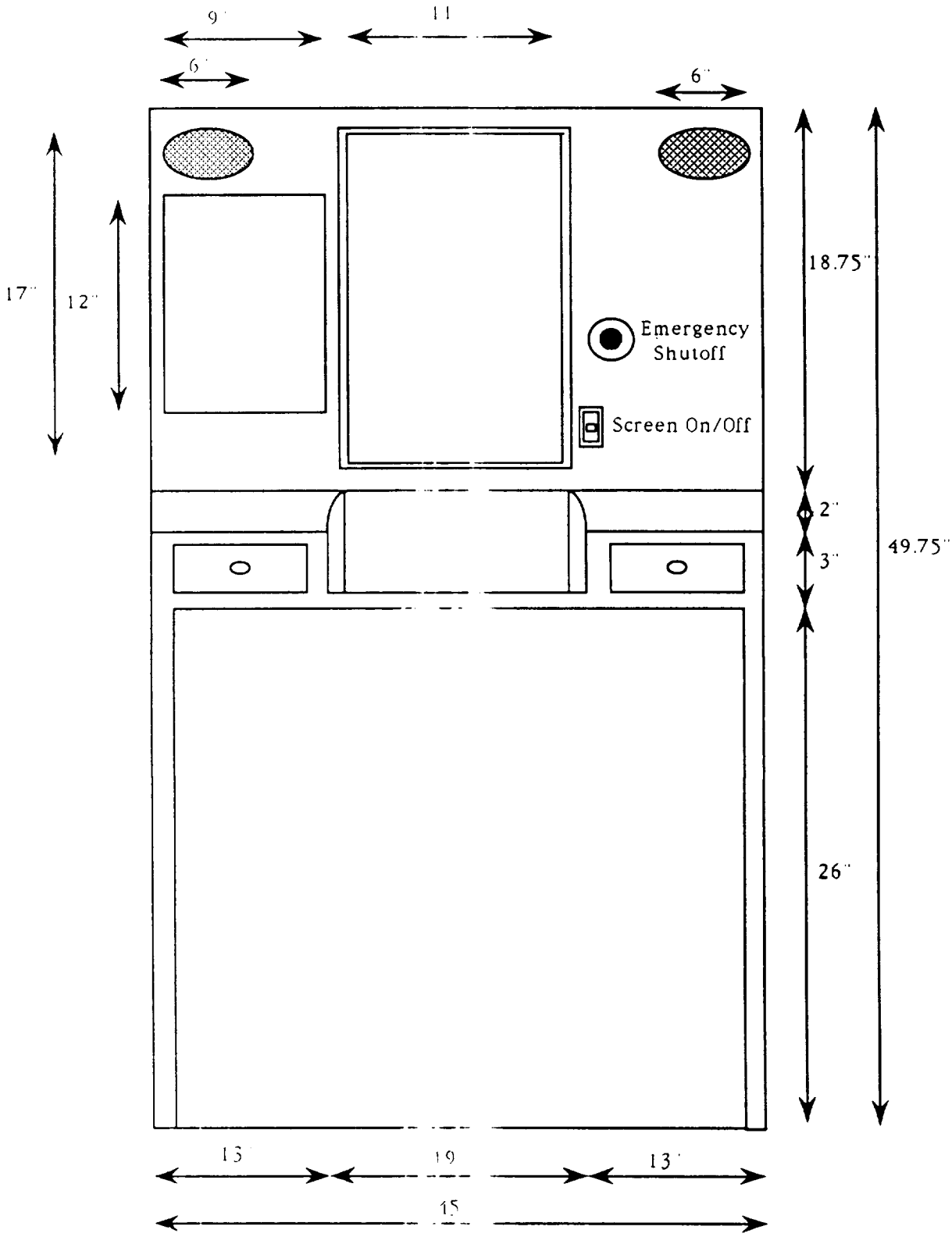

Drawing 4.9.1.1 - Vertical Accelerator

(Detailed View)

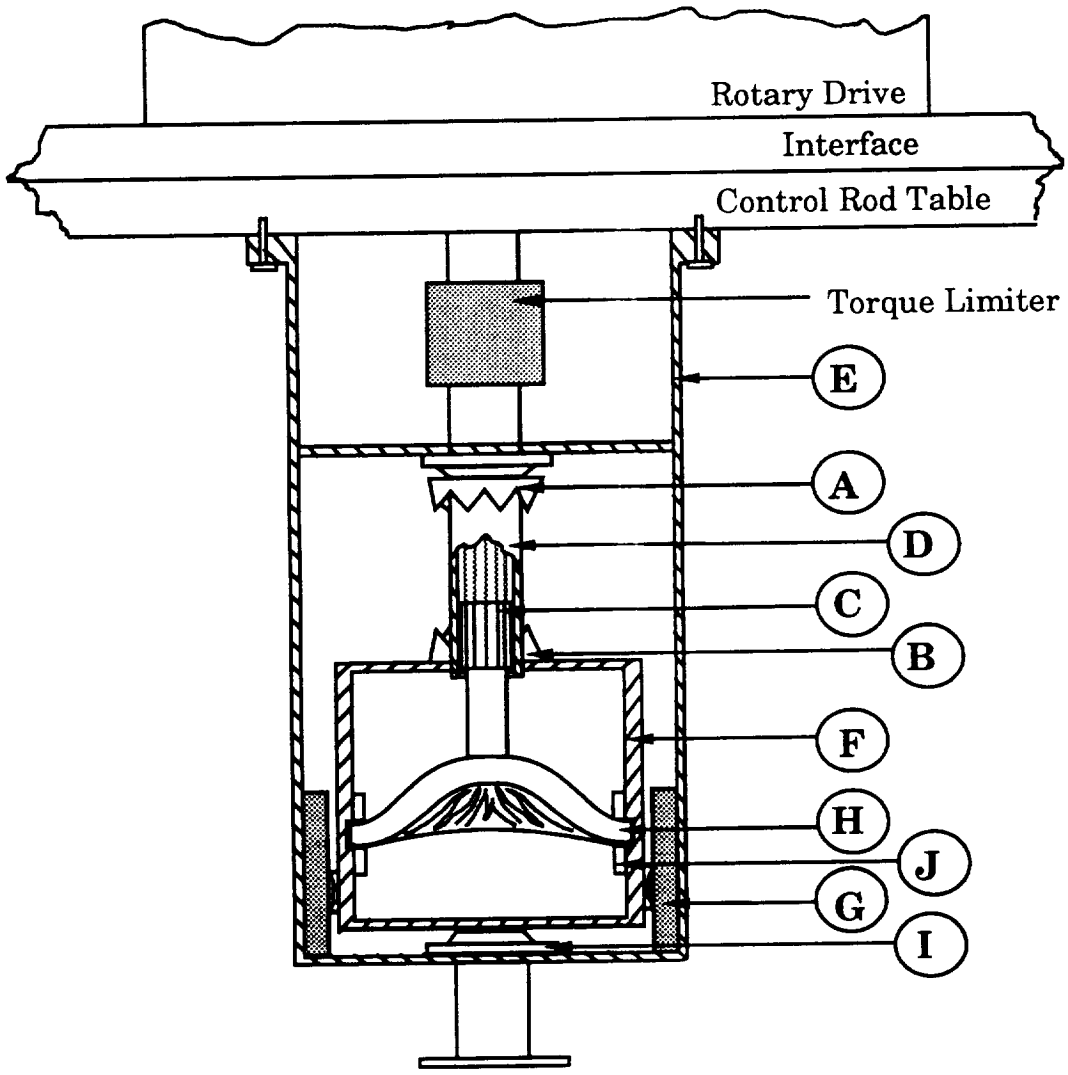

Drawing 4.9.1.2 - Detailed Specifications

(Clutch and Shaft Details)

(A) Upper Clutch Plate

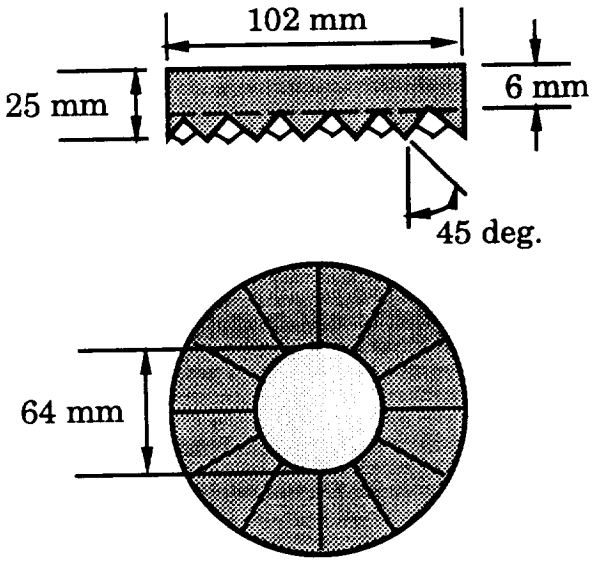

(B) Lower Clutch Plate

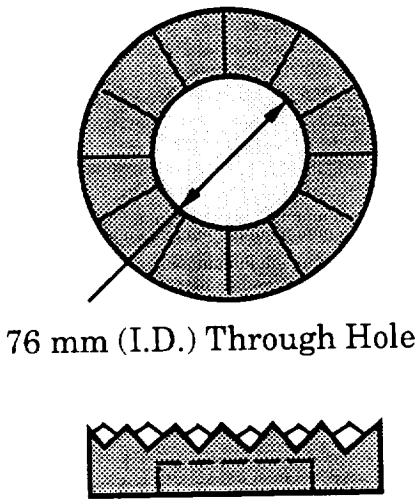

(C) Inner Shaft

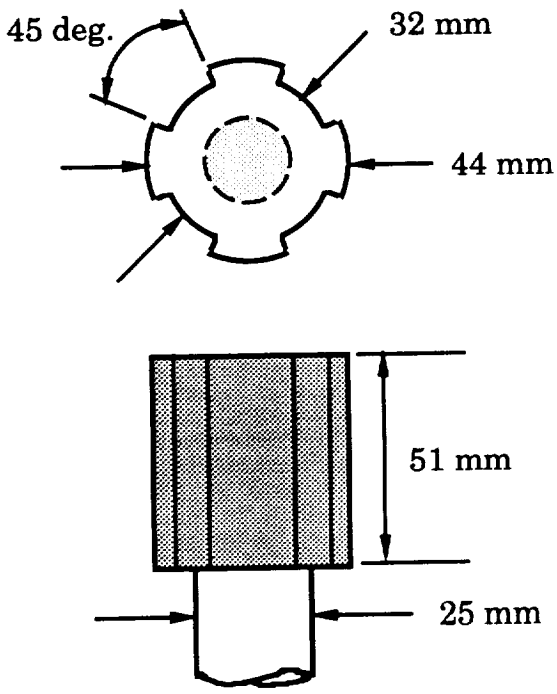

(D) Outer Shaft

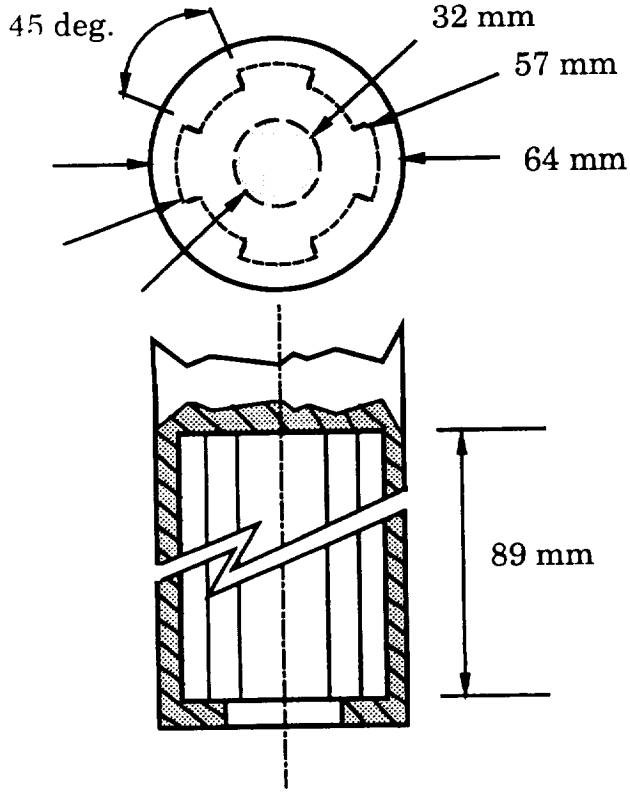

Drawing 4.9.1.3 - Detailed Specifications

(Housing Details)

(E) Vertical Accelerator Housing

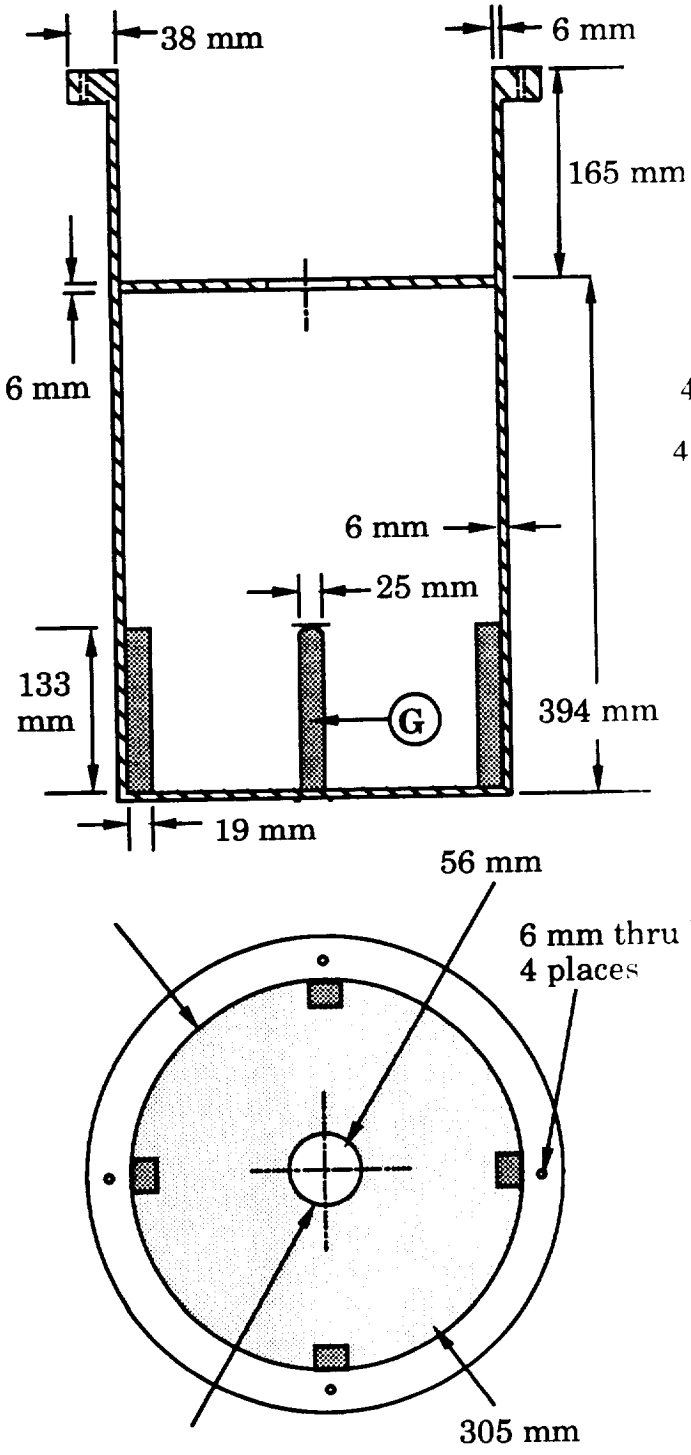

(F) Cam Housing

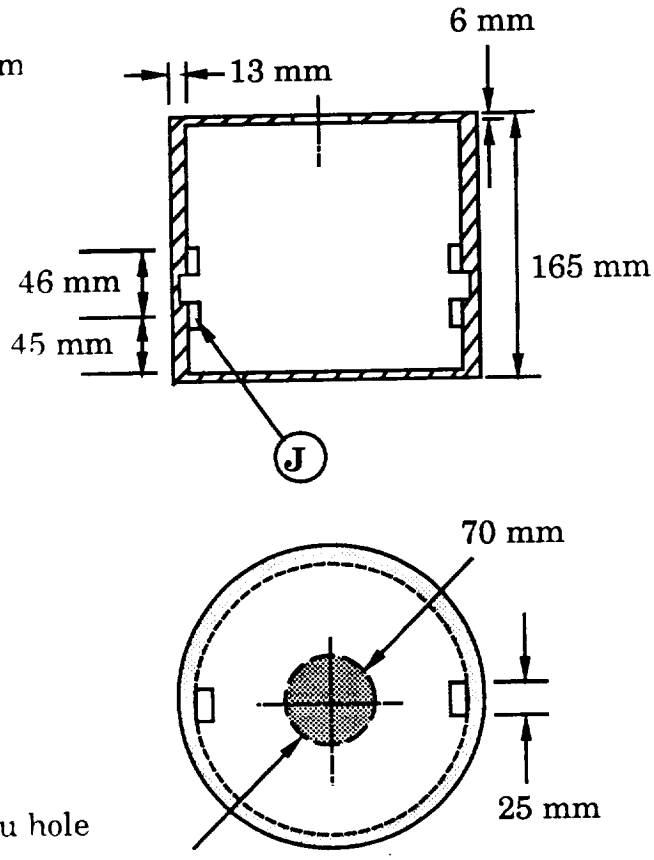

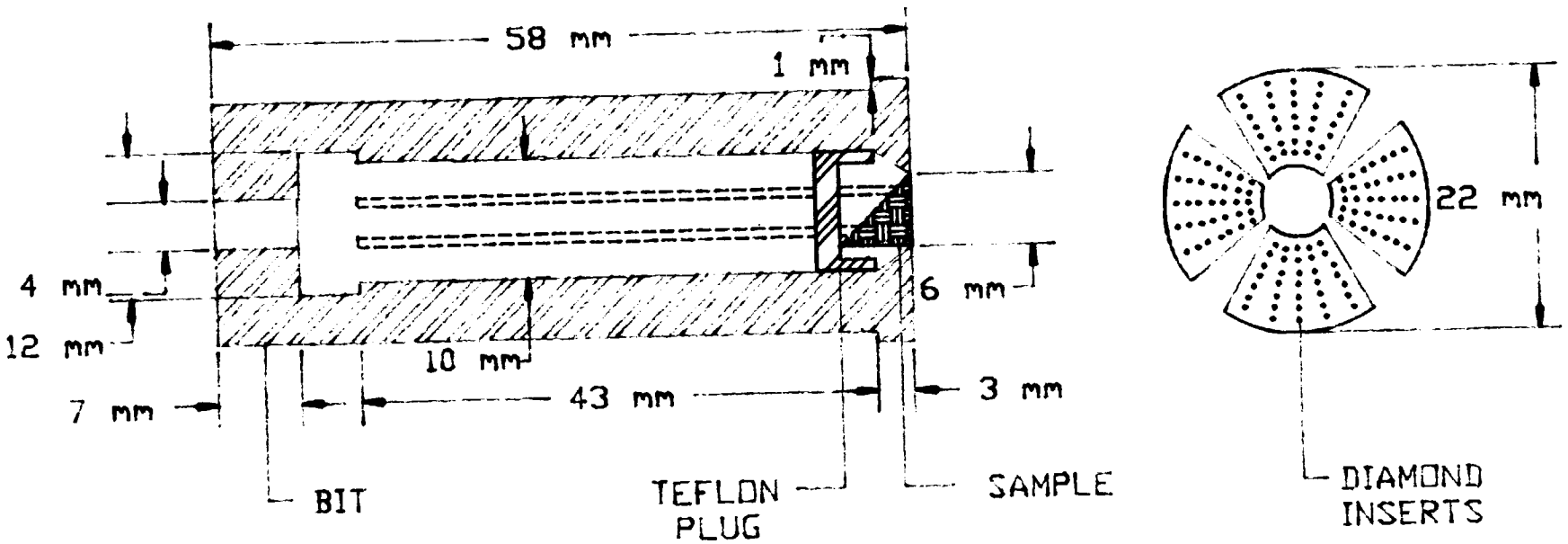

MICRO-CORING DRILL BIT

Drawing 4.10.6.1

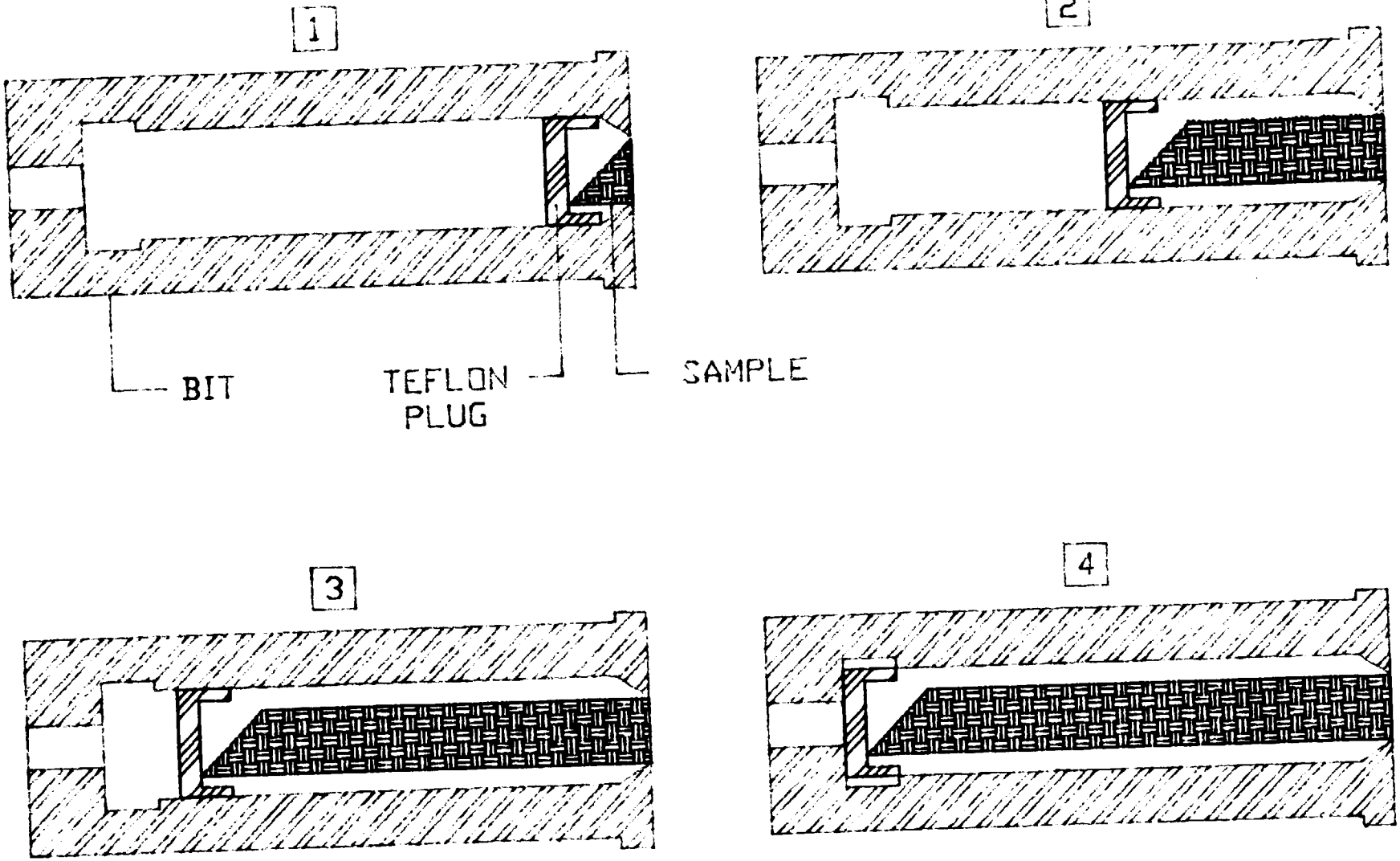

MICRO-CORING DRILL BIT MOVEMENT
Drawing 4.10.6.2

Drawing 4.10.6.3